

ANALYTICA CHIMICA ACTA

International journal devoted to all branches of analytical chemistry

EDITORS

A. M. G. MACDONALD (Birmingham, Great Britain)

HARRY L. PARDUE (West Lafayette, IN, U.S.A.)

Editorial Advisers

F. C. Adams, Antwerp
R. P. Buck, Chapel Hill, NC
G. den Boef, Amsterdam
G. Duyckaerts, Liège
D. Dyrssen, Göteborg
W. Haerdi, Geneva
G. M. Hieftje, Bloomington, IN
J. Hoste, Ghent
A. Hulanicki, Warsaw
E. Jackwerth, Bochum
G. Johansson, Lund
D. C. Johnson, Ames, IA
J. H. Knox, Edinburgh
P. D. LaFleur, Washington, DC
D. E. Leyden, Denver, CO
F. E. Lytle, West Lafayette, IN
H. Malissa, Vienna
A. Mizuike, Nagoya
E. Pungor, Budapest

W. C. Purdy, Montreal
J. P. Riley, Liverpool
J. Růžička, Copenhagen
D. E. Ryan, Halifax, N.S.
J. Savory, Charlottesville, VA
W. D. Shults, Oak Ridge, TN
W. Simon, Zürich
W. I. Stephen, Birmingham
G. Tölg, Schwäbisch Gmünd, B.R.D.
A. Townshend, Hull
B. Trémillon, Paris
A. Walsh, Melbourne
H. Weisz, Freiburg i. Br.
F. W. West, Baton Rouge, LA
T. S. West, Aberdeen
J. B. Willis, Melbourne
Yu. A. Zolotov, Moscow
P. Zuman, Potsdam, NY

ANALYTICA CHIMICA ACTA

International journal devoted to all branches of analytical chemistry
Revue internationale consacrée à tous les domaines de la chimie analytique
Internationale Zeitschrift für alle Gebiete der analytischen Chemie

PUBLICATION SCHEDULE FOR 1980 (incorporating the section on Computer Techniques and Optimization).

	J	F	M	A	M	J	J	A	S	O	N	D
Analytica Chimica Acta	113/1 113/2	114	115	116/1	116/2	117	118/1	118/2	119/1	119/2	120	121
Section on Computer Techniques and Optimization			122/1			122/2			122/3			122/4

Scope. *Analytica Chimica Acta* publishes original papers, short communications, and reviews dealing with every aspect of modern chemical analysis, both fundamental and applied. The section on *Computer Techniques and Optimization* is devoted to new developments in chemical analysis by the application of computer techniques and by interdisciplinary approaches, including statistics, systems theory and operation research. The section deals with the following topics: Computerized acquisition, processing and evaluation of data. Computerized methods for the interpretation of analytical data including chemometrics, cluster analysis, and pattern recognition. Storage and retrieval systems. Optimization procedures and their application. Automated analysis for industrial processes and quality control. Organizational problems.

Submission of Papers. Manuscripts (three copies) should be submitted as designated below for rapid and efficient handling:

Papers from the Americas to: Professor Harry L. Pardue, Department of Chemistry, Purdue University, West Lafayette, IN 47907, U.S.A.

Papers from all other countries to: Dr. A. M. G. Macdonald, Department of Chemistry, The University, P.O. Box 363, Birmingham B15 2TT, England.

For the section on *Computer Techniques and Optimization:* Dr. J. T. Clerc, Universität Bern, Pharmazeutisches Institut, Sahlstrasse 10, CH-3012 Bern, Switzerland.

American authors are recommended to send manuscripts and proofs by INTERNATIONAL AIRMAIL.

Information for Authors. Papers in English, French and German are published. There are no page charges. Manuscripts should conform in layout and style to the papers published in this Volume. Authors should consult Vol. 121, p. 353 for detailed information. Reprints of this information are available from the Editors or from: Elsevier Editorial Services Ltd., Mayfield House, 256 Banbury Road, Oxford OX2 7DE (Great Britain).

Reprints. Fifty reprints will be supplied free of charge. Additional reprints (minimum 100) can be ordered. An order form containing price quotations will be sent to the authors together with the proofs of their article.

Advertisements. Advertisement rates are available from the publisher.

Subscriptions. Subscriptions should be sent to: Elsevier Scientific Publishing Company, P.O. Box 211, 1000 AE Amsterdam, The Netherlands. The section on *Computer Techniques and Optimization* can be subscribed to separately.

Publication. *Analytica Chimica Acta* (including the section on *Computer Techniques and Optimization*) appears in 10 volumes in 1980. The subscription for 1980 (Vols. 113–122) is Dfl. 1390.00 plus Dfl. 160.00 (postage) (total approx. U.S. \$795.00). The subscription for the *Computer Techniques and Optimization* section only (Vol. 122) is Dfl. 139.00 plus Dfl. 16.00 (postage) (total approx. U.S. \$79.50). Journals are sent automatically by airmail to the U.S.A. and Canada at no extra cost and to Japan, Australia and New Zealand for a small additional postal charge. All earlier volumes (Vols. 1–112) except Vols. 23 and 28 are available at Dfl. 153.00 (U.S. \$78.50), plus Dfl. 11.00 (U.S. \$5.50) postage and handling, per volume.

Claims for issues not received should be made within three months of publication of the issue, otherwise they cannot be honored free of charge.

Customers in the U.S.A. and Canada who wish to obtain additional bibliographic information on this and other Elsevier journals should contact Elsevier/North Holland Inc., Journal Information Center, 52 Vanderbilt Avenue, New York, NY 10017. Tel: (212) 867-9040.

ANALYTICA CHIMICA ACTA

VOL. 121 (1980)

ANALYTICA CHIMICA ACTA

International journal devoted to all branches of analytical chemistry

EDITORS

A. M. G. MACDONALD (Birmingham, Great Britain)

HARRY L. PARDUE (West Lafayette, IN, U.S.A.)

Editorial Advisers

F. C. Adams, Antwerp
R. P. Buck, Chapel Hill, NC
G. den Boef, Amsterdam
G. Duyckaerts, Liège
D. Dyrssen, Göteborg
W. Haerdi, Geneva
G. M. Hieftje, Bloomington, IN
J. Hoste, Ghent
A. Hulanicki, Warsaw
E. Jackwerth, Bochum
G. Johansson, Lund
D. C. Johnson, Ames, IA
J. H. Knox, Edinburgh
P. D. LaFleur, Washington, DC
D. E. Leyden, Denver, CO
F. E. Lytle, West Lafayette, IN
H. Malissa, Vienna
A. Mizuike, Nagoya
E. Pungor, Budapest

W. C. Purdy, Montreal
J. P. Riley, Liverpool
J. Růžička, Copenhagen
D. E. Ryan, Halifax, N.S.
J. Savory, Charlottesville, VA
W. D. Shults, Oak Ridge, TN
W. Simon, Zürich
W. I. Stephen, Birmingham
G. Tölg, Schwäbisch Gmünd, B.R.D.
A. Townshend, Hull
B. Trémillon, Paris
A. Walsh, Melbourne
H. Weisz, Freiburg i. Br.
P. W. West, Baton Rouge, LA
T. S. West, Aberdeen
J. B. Willis, Melbourne
Yu. A. Zolotov, Moscow
P. Zuman, Potsdam, NY



ELSEVIER SCIENTIFIC PUBLISHING COMPANY

Anal. Chim. Acta, Vol. 121 (1980)

ANALYTICA CHIMICA ACTA
121 2521

© Elsevier Scientific Publishing Company, 1980.

All rights reserved. No part of this publication may be reproduced, stored in a retrieval system or transmitted in any form or by any means, electronic, mechanical, photocopying, recording or otherwise, without the prior written permission of the publisher, Elsevier Scientific Publishing Company, P.O. Box 330, 1000 AH Amsterdam, The Netherlands.

Submission of an article for publication implies the transfer of the copyright from the author to the publisher and is also understood to imply that the article is not being considered for publication elsewhere.

Submission to this journal of a paper entails the author's irrevocable and exclusive authorization of the publisher to collect any sums or considerations for copying or reproduction payable by third parties (as mentioned in article 17 paragraph 2 of the Dutch Copyright Act of 1912 and in the Royal Decree of June 20, 1974 (S. 351) pursuant to article 16 b of the Dutch Copyright Act of 1912) and/or to act in or out of court in connection therewith.

Printed in The Netherlands

Special Report

THE ANALYTICAL PERFORMANCE OF DIRECT CURRENT, NORMAL PULSE AND DIFFERENTIAL PULSE POLAROGRAPHY WITH STATIC MERCURY DROP ELECTRODES

A. M. BOND and R. D. JONES

Division of Chemical and Physical Sciences, Deakin University, Waurn Ponds 3217, Victoria (Australia)

(Received 18th April 1980)

SUMMARY

The recently developed static mercury drop electrode (SMDE) provides a fundamentally new approach to electrodes for polarography. An analytical evaluation of the electrode is presented. For a range of electrode processes, current-sampled d.c. polarography at the SMDE is useful down to at least the 10^{-7} M concentration level when short drop times and fast potential scan rates are used. The improvement in the limit of detection for d.c. polarography is therefore very substantial. Improvements in sensitivity associated with normal pulse and differential pulse polarography at the SMDE compared with the dropping mercury electrode (DME) are marginal. It is concluded that at the SMDE, the analytical performance and response characteristics of d.c., normal pulse and differential pulse polarography tend to converge.

The dropping mercury electrode (DME) has been essential to the polarographic method since it was developed by Heyrovsky over fifty years ago. Whilst substantial changes have been made at frequent intervals to the electronic instrumentation interfaced to the electrode, there have been no real fundamental changes to the DME itself aimed at providing increased sensitivity. Current–voltage curves are still routinely obtained at a mercury electrode continuously expanding under gravity control. The recent advent of the static mercury drop electrode (SMDE) [1] marks a new development of the DME, which could drastically alter many of the ideas commonly associated with d.c., pulse and other polarographic techniques [2–5].

The SMDE is related to the conventional DME, in that it incorporates a mercury reservoir and a capillary through which mercury flows to form a drop [1]. However, the electrode assembly incorporates a valve which allows the mercury flow to be stopped at selected time intervals to produce a stationary rather than a growing drop on the tip of the capillary. Current–voltage curves are obtained from data measured during this stationary period of the drop life. The use of a wide-bore capillary allows mercury drops to be grown very rapidly when the valve is opened so that relatively large electrode areas can be obtained rapidly during the drop life. Variable

valve opening times (of the order of 100 ms) allow drops of different size to be used. In a typical experiment, the valve opens to commence the drop growth and then closes while the stationary drop is held for a preset period. Finally, the current is measured immediately before the drop is mechanically dislodged. When this procedure is used, the SMDE retains all the advantages of the conventional DME [1–6], e.g., a renewable electrode of constant size with reproducible surface characteristics, but the problems of having to obtain data at an electrode with a continuously changing area are avoided.

The theory associated with this electrode is of course related to that for the DME but there are some very significant differences. Since the drop is stationary during the time when current measurements are made, the theoretical concepts developed for stationary electrodes [6, 7] can be employed as a first approximation. In particular, a diffusion-controlled current is expected to be approximately described by the Cottrell equation [7] rather than the Ilkovič equation commonly used for the DME [6]. The essential difference between these two equations is that an area growth term which is proportional to $t^{2/3}$ (t , time) is included in the Ilkovič equation, giving the diffusion-controlled current an overall $t^{1/6}$ dependence on time. In the absence of electrode growth, a $t^{-1/2}$ dependence of diffusion-controlled current on time is predicted via the Cottrell equation. Differences between the DME and SMDE are summarized diagrammatically in Fig. 1.

The new electrode design and mode of operation should essentially eliminate problems of charging current arising from area growth, shortly after the growth ceases. At the time when the area growth ceases, the faradaic current is close to its maximum value, and so the well established tradition that long drop times provided optimum sensitivity in d.c. and pulse polarography may have little theoretical validity when the SMDE is used. Limitations previously reported with short drop-life techniques [8–10] would then no longer apply. Furthermore, several refinements proposed in d.c. and pulse polarography have emanated from consideration of charging current arising from area growth terms [11–14] associated with a DME. Such refinements also would serve no purpose with a SMDE. Indeed, the question can be raised as to whether the potential step experiment associated with normal pulse voltammetry (chronoamperometry) and d.c. polarography at

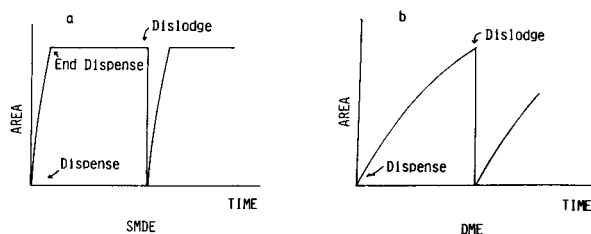


Fig. 1. Comparison of operation of the SMDE and DME. Schematic diagram of area vs. time curves for (a) SMDE and (b) DME.

the SMDE with stepped development of the electrode area are not very closely related and therefore very similar in performance.

All the above leads to interesting conclusions concerning the future role of d.c. polarography. In recent times, pulse and related methods have almost invariably been recommended for low concentration work [15] and d.c. polarography is rarely advocated. The prospect of performance characteristics equivalent to the pulse techniques might therefore lead to a renaissance of the instrumentally very simple technique of d.c. polarography in conjunction with the SMDE. The validity of these ideas is examined critically in this report by measuring the responses of a range of polarographic techniques near the limits of detection for several reversibly and irreversibly reduced species. Comparative results are presented for the SMDE and the conventional DME, and the importance and significance of the new electrode format are assessed from these data.

EXPERIMENTAL

Solutions and instrumentation

All chemicals used were of analytical-grade purity. Polarographic cells and all glassware were thoroughly cleaned in nitric acid, then washed prior to use. Distilled water was used for preparing all solutions. Blanks, containing only the supporting electrolyte, were run at frequent intervals to ensure that contamination was not a problem at the low levels investigated. Fresh standard solutions were prepared regularly. All solutions were degassed with high-purity nitrogen for a minimum of 4 min before each polarogram was recorded. The nitrogen used was passed through an oxygen-scavenging system containing vanadium(II) chloride and amalgamated zinc in 2 M hydrochloric acid [16].

A PAR Model 174A Polarographic Analyzer was used to record polarograms. All data were obtained at ambient temperature (20 ± 1)°C. Mechanically controlled drop times were obtained with the attachment described elsewhere [17]. The conventional DME electrode arrangement incorporated a PAR Model 172 Mechanical Drop Kicker and was used in the three-electrode configuration with a platinum wire as auxiliary electrode and an Ag/AgCl (satd. NaCl) reference electrode. The PAR Model 303 SMDE was employed with an Ag/AgCl (satd. KCl) reference electrode and a platinum wire auxiliary electrode, and was interfaced to the PAR 174A Analyzer as recommended by the manufacturer.

Constant vigilance and maintenance of the SMDE electrode was required to produce the results reported below. Continuous use of four of these electrodes over an extended period of time suggests that maintenance time requirements are higher than for a conventional DME.

Recording of data at the SMDE

The electrode area—time (Fig. 1) and therefore current—time curves for the SMDE and DME are very different. The rapid area growth early in the drop life of the SMDE produces a very large charging current spike in d.c. polarography (Fig. 2a); but once the drop growth ceases, the charging current decays rapidly (Fig. 2b). A small component of charging current from the application of an analog linear potential—time ramp could occur, but in d.c. polarography with slow scan rates (small potential increment per drop) the dE/dt term is negligible.

These large current spikes arising from rapid drop growth can be removed from the readout by using current-sampled d.c. polarography. In this method, the current is recorded only just before the drop is dislodged (Fig. 2b). With this readout form and a SMDE area growth period of 50 or 100 ms, a well defined background current or baseline with very low currents is obtained with d.c. polarography over a wide potential range at all drop times between 0.2 and 5.0 s at least. Background currents in the absence of dA/dt terms are very much lower than those usually associated with d.c. polarography at a DME, and flat baselines are obtained even when background currents are measured at the nA level (Fig. 3).

When a faradaic process occurs, the large current spike produced during drop growth still occurs (Fig. 4a) but now the measured current contains both faradaic and charging current components. The conventional d.c. polarogram is virtually unusable (Fig. 4a). However, when current-sampled d.c. polarography is used with an electrode growth time of 50 or 100 ms and drop times greater than 0.2 s, the charging current has time to decay to a very small value and the spikes are not evident, so that useful information on the faradaic current can be obtained (Fig. 4b). All subsequent d.c. polarographic measurements with the SMDE therefore refer to the current-sampled technique.

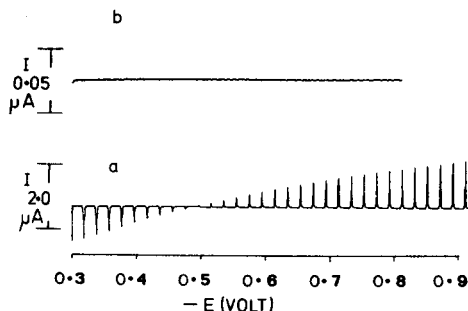


Fig. 2. Background current for a 1.0 M KCl solution at the SMDE. (a) D.c. polarogram; scan rate, 20 mV s^{-1} ; electrode area, $9.7 \times 10^{-7} \text{ m}^2$; electrode growth period, 50 ms; drop time, 0.5 s. (b) Current-sampled d.c. polarogram; scan rate, 5 mV s^{-1} , drop time, 0.5 s; electrode area, $9.7 \times 10^{-7} \text{ m}^2$; electrode growth period, 50 ms.

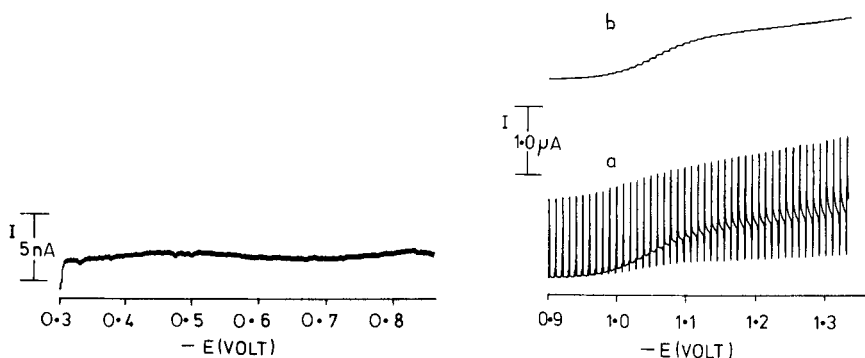


Fig. 3. Current-sampled d.c. polarogram of a 1.0 M KCl solution using the SMDE, recorded at high sensitivity. Scan rate, 5 mV s^{-1} ; drop time, 0.5 s; electrode area, $9.7 \times 10^{-7} \text{ m}^2$; electrode growth period, 50 ms.

Fig. 4. Reduction of $5 \times 10^{-4} \text{ M}$ nickel(II) in 1.0 M KCl at the SMDE. Electrode area, $9.7 \times 10^{-7} \text{ m}^2$; electrode growth period, 50 ms; drop time, 1.0 s. (a) D.c. polarogram; (b) current-sampled d.c. polarogram.

THEORY

If it is assumed that the current decay process occurs from the start of the drop life, then under conditions of planar diffusion the Cottrell equation for the limiting current region can be written as follows

$$i_d = nFAC (D/\pi t_d)^{1/2} \quad (1)$$

where A is the electrode area, i_d is the diffusion-limited current, t_d is the drop time, C is the concentration of the electroactive species, D is the diffusion coefficient, and F is the faraday constant. The implication of this approximate expression is that $i_d \propto t_d^{-1/2}$. The validity of this theoretical relationship was tested in part for the reduction of cadmium in 0.1 M NaNO_3 by plotting i_d vs. $t_d^{-1/2}$ (Fig. 5). A straight line plot was obtained at intermediate drop times. At short drop times, hydrodynamics from the rapid electrode growth, as partly accounted for by the Ilkovič equation, presumably contribute to the current. The use of t_d as the time term in the Cottrell equation is also clearly inaccurate at short drop times. At long drop times, depletion and other effects arise. Indeed, data at long drop times approach close to the polarogram obtained at a stationary hanging mercury drop electrode with the same area as the SMDE at a very slow scan rate. A rigorous theoretical treatment of the d.c. theory applicable to the SMDE is currently being considered, but the above approximate version is adequate for present purposes.

If eqn. (1) can be used to describe the diffusion-controlled limiting current in d.c. polarography at the SMDE, then it is immediately obvious that there is a close theoretical similarity between the d.c. and pulse techniques, since the equation for pulse polarography would be

$$(i_d)_p = nFAC(D/\pi t_m)^{1/2} \quad (2)$$

where t_m is the time at which the current is measured after application of the pulse and $(i_d)_p$ is the diffusion-controlled limiting current in pulse polarography. At the SMDE, for a constant value of t_m , the value $(i_d)_p$ will be independent of drop time. According to eqns. (1) and (2), the only difference between d.c. and pulse polarography at the SMDE is that a longer decay period is associated with measurements made under d.c. conditions and therefore faradaic currents measured are predicted to be smaller. However, the ratio of faradaic current to charging current should be superior, so that analytically the d.c. method could be superior, if noise associated with measuring small currents is not a problem.

LIMITS OF DETECTION

The reduction $\text{Cd(II)} + 2e^- \rightleftharpoons \text{Cd(Hg)}$ in 0.1 M NaNO_3 or 1 M NaCl was taken as a model of a reversible system, the reduction $\text{Ni(II)} + 2e^- \rightleftharpoons \text{Ni(Hg)}$ in 0.1 M KCl as a model of a quasi-reversible system, and the reduction $\text{Ni(II)} + 2e^- \rightarrow \text{Ni(Hg)}$ in 1.0 M KCl as a model of an irreversible system. The

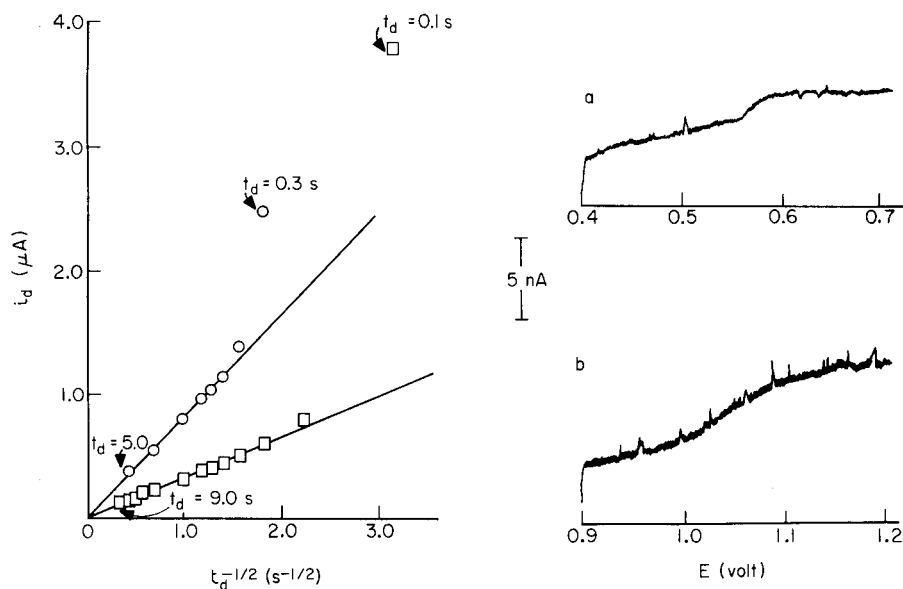


Fig. 5. Plots of i_d vs. $t_d^{-1/2}$ for reduction of 1.0×10^{-4} M Cd(II) in 1.0 M NaCl at the SMDE. (\square) Electrode area = 9.7×10^{-7} m²; electrode growth period = 50 ms. (\circ) Electrode area = 2.52×10^{-6} m²; electrode growth period = 200 ms.

Fig. 6. Current-sampled d.c. polarograms for reduction of Cd(II) and Ni(II) at the SMDE. (a) Reduction of 2.0×10^{-7} M Cd(II) in 0.1 M NaNO_3 ; drop time 0.2 s; electrode area 9.7×10^{-7} m²; electrode growth period = 50 ms. (b) Reduction of 5.0×10^{-7} M Ni(II) in 1.0 M KCl ; drop time 0.2 s; electrode area 9.7×10^{-7} m²; electrode growth period 50 ms.

nature of the nickel electrode processes has been summarized [6]. These systems were used to evaluate the performance characteristics of d.c., normal pulse (n.p.) and differential pulse (d.p.) polarography with respect to the SMDE. Results were also compared with the conventional DME. Detection limits using sampled d.c. pulse and differential pulse polarography were compared at each electrode. The detection limit or lowest concentration which gives a perceivable response is difficult to measure accurately, given the inherent problems associated with work at low concentrations; also the results obtained are often subjective. Only differences of a factor of two or more are therefore considered significant. Indeed, the detection limit is never recommended for routine analysis [17] and is usually not the parameter of interest. However, bearing in mind these difficulties, the "detection limit" is convenient here as a basis for comparison.

D.c. polarography

At the DME. Measurement of the electrode response for either the reversible cadmium or quasi-reversible nickel process is possible down to the 10^{-6} M level with the conventional DME (Table 1) and current-sampled d.c. polarography, provided that long drop times and slow scan rates are used. However, analytically useful results are obtained only at the 5×10^{-6} M level. The limit of detection for the irreversibly reduced nickel is 5×10^{-6} M under the same conditions at the DME. All results are summarized in Table 1. The higher detection limit for the irreversible nickel wave is predominantly due to its elongated nature. For each of these cases, the limit of detection is very dependent on drop time, and for the optimum results quoted above, drop times of 2.0–5.0 s must be used. The background (charging current and residual oxygen) at these levels slopes severely, hence quantifying the waves is difficult in the 10^{-6} M concentration range at a DME for all classes of electrode process.

At the SMDE. In contrast to the DME results, reversibly reduced Cd(II) and quasi-reversibly reduced Ni(II) can be detected at the 10^{-7} M concentration level using the SMDE with a drop time of about 0.5 s (Fig. 6). A readily usable response is obtained at the 2×10^{-7} M level for drop times as low as 0.2 s and a drop size of 0.97 mm^2 . The irreversibly reduced nickel(II) can be detected at the 2×10^{-7} M level under these conditions. Results are summarized in Table 1. The background at the 1×10^{-7} M Cd(II) level is still relatively small and the limit of detection with d.c. polarography at the SMDE for Cd(II) and Ni(II) is governed by electronic and mechanical noise rather than by background current. In principle, detection limits in the range of 10^{-8} M are feasible with the SMDE, if electronic noise could be suppressed; i.e., nanoamp currents need to be measured in d.c. polarography for the very much lower concentrations available at the SMDE rather than the microamp currents usually associated with the conventional DME. Little advantage is gained by using the option of larger drop sizes as the signal-to-noise ratio is not markedly enhanced. Limits of detection at long

TABLE 1

Performance characteristics of current-sampled d.c., normal pulse and differential pulse^a polarography at the SMDE and DME

Electrode process	Electrode	Technique	Drop time (s)	Limit of detection (M)
Cd(II) + 2e \rightleftharpoons Cd(Hg) (0.1 M NaNO ₃)	DME	D.c.	5.0	2×10^{-6}
		N.p.	2.0	4×10^{-7}
		D.p.p.	2.0	8×10^{-8}
	SMDE	D.c.	0.5 ^b	1×10^{-7} ^d
		N.p.	0.5 ^c	2×10^{-7}
		D.p.p.	0.5 ^b	1×10^{-7}
Ni(II) + 2e \rightleftharpoons Ni(Hg) (0.1 M KCl)	DME	D.c.	2.0	3×10^{-6}
		N.p.	2.0	3×10^{-7}
		D.p.p.	2.0	1×10^{-7}
	SMDE	D.c.	0.5 ^b	1×10^{-7} ^d
		N.p.	0.5 ^c	3×10^{-7}
		D.p.p.	0.5 ^b	1×10^{-7}
Ni(II) + 2e \rightarrow Ni(Hg) (1 M KCl)	DME	D.c.	2.0	5×10^{-6}
		N.p.	2.0	3×10^{-6}
		D.p.p.	2.0	7×10^{-7} ^e
	SMDE	D.c.	0.2 ^b	3×10^{-7} ^d
		N.p.	0.5 ^c	5×10^{-7}
		D.p.p.	0.5 ^b	5×10^{-7} ^e

^aPulse amplitude, 50 mV. ^bElectrode growth period, 50 ms. ^cElectrode growth period, 200 ms. ^dDetection limit governed by electronic noise and not background current. Detection limit if governed by background is slightly lower. All other detection limits governed by background current masking faradaic current. ^eVery broad elongated wave.

drop times with the SMDE (e.g., 5.0 s) are less favourable than at short drop times because of the inherent decrease in faradaic current and concomitant decrease in signal-to-noise ratio. Drop times less than 0.2 s suffer from problems associated with the drop growth period. Thus for d.c. polarography, the SMDE gives at least a factor of ten improvement in sensitivity compared to the conventional DME, when both electrodes are used under optimum conditions. However, at the SMDE, sensitivity is not critically dependent on drop time over the range 0.2–2.0 s. Thus, at the SMDE with 0.2-s drop times, high sensitivity at very fast scan rates (e.g. 50–100 mV s⁻¹) and short analysis times can be obtained; this offers great advantages over the equivalent experiment undertaken on the DME. Under these conditions, improvements in sensitivity up to two orders of magnitude are found.

Normal pulse and differential pulse polarography

Figure 7 provides examples of normal and differential pulse polarograms obtained at the SMDE. For the three electrode processes considered, only marginally more favourable limits of detection are obtained for differential pulse and normal pulse when the SMDE is used at drop times in the range 0.2–2 s compared with the conventional DME (Table 1) for long drop times in the range 2–5 s. In all cases, the differential pulse technique gives limits of detection lower by factors of 2–5 than the normal pulse technique. The normal pulse response near the limit of detection in all cases is superimposed on a severely sloping background, and the usable concentration level is generally much lower for differential pulse polarography. This is consistent with the results of Bond and Canterford [17] for the conventional DME. At the SMDE, the detection limit in normal and differential pulse polarography is not critically dependent on drop time; as for d.c. polarography, optimum results can be obtained with drop times as short as 0.2 s. This means that time saving by using short drop times and fast scan rates can be gained in pulse methods, but the spectacular gain in sensitivity associated with the d.c. method is not observed. The above considerations emphasize that replacement of the DME by the SMDE provides a major advance in the technique of d.c. polarography. The improvement in d.c. polarography is so great when the SMDE is used that it rivals differential pulse techniques and offers an improvement over the normal pulse method for the electrode processes examined.

Of course, the normal pulse method retains its advantages with respect to elimination of adsorption and other surface phenomena [18] arising from the different potential format used.

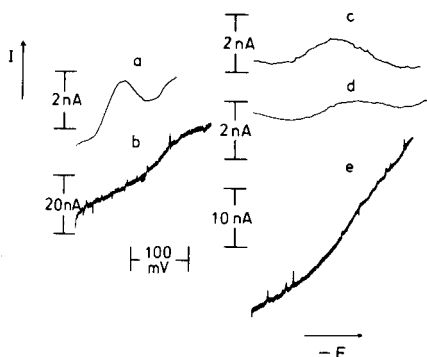


Fig. 7. Normal pulse and differential pulse polarograms for low concentrations of Ni(II) and Cd(II) at the SMDE. (a) D.p.p. of 2.0×10^{-7} M Cd(II) in 0.1 M NaNO₃; drop time 0.5 s; pulse amplitude -50 mV; electrode area 9.7×10^{-7} m²; electrode growth period 50 ms. (b) N.p.p. of 2.0×10^{-7} M Cd(II) in 0.1 M NaNO₃; electrode area 2.5×10^{-6} m²; electrode growth period 200 ms; drop time 0.5 s. (c) D.p.p. of 1.0×10^{-7} M Ni(II) in 0.1 M KCl; conditions as for (a). (d) D.p.p. of 5.0×10^{-7} M Ni(II) in 1.0 M KCl; conditions as for (a). (e) N.p.p. of 5.0×10^{-7} M Ni(II) in 1.0 M KCl; conditions as for (b).

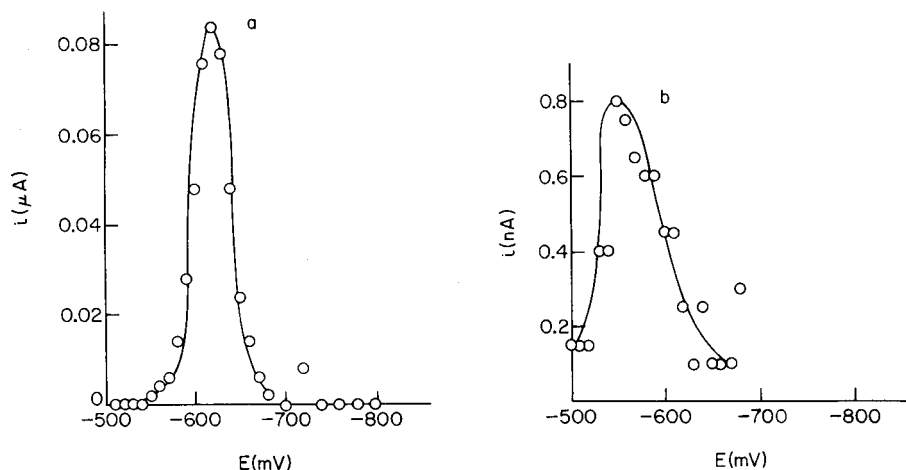


Fig. 8. Pseudo-derivative current-sampled d.c. polarograms at the SMDE. Drop time 0.5 s; drop area $9.7 \times 10^{-7} \text{ m}^2$; electrode growth period 50 ms; increment between data points 10 mV. (a) 10^{-4} M Cd(II) in 1 M NaCl; $E^{1/2} = -0.625 \text{ V}$ vs. Ag/AgCl (satd. KCl). (b) 10^{-6} M Cd(II) in 0.1 M NaNO_3 ; $E^{1/2} = -0.570 \text{ V}$ vs. Ag/AgCl (satd. KCl).

In view of the elimination of charging current arising from area growth terms, it is not surprising that there is little difference in detection limits between d.c.p. and d.p.p. at the SMDE (Table 1). Indeed, for elongated irreversible waves such as those for nickel, the d.c. technique at the SMDE is more sensitive than differential pulse polarography. The added complexity of the instrumentation required for differential pulse polarography may no longer be warranted. An advantage of the differential pulse technique is the peak-shaped response, but the use of a derivative or pseudo-derivative output technique for the d.c. response at the SMDE gives essentially equivalent results (Fig. 8).

Conclusions

The data obtained indicate that at the SMDE, d.c. polarography at short drop times in the range 0.2–2 s provides performance similar to, or better than, that associated with pulse techniques. The ability to use short drop times and rapid scan rates and still obtain optimum sensitivity suggests that current trends towards the ever-increasing use of pulse techniques should be reviewed. In view of the simpler instrumentation required for d.c. techniques, a renaissance in the use of d.c. polarography can be expected if the SMDE becomes widely adopted.

REFERENCES

- 1 W. M. Peterson, *Am. Lab.*, 11 (12) (1979) 69.
- 2 I. M. Kolthoff and J. J. Lingane, *Polarography*, Vol. I, Interscience, New York, 1952.
- 3 L. Meites, *Polarographic Techniques*, 2nd. edn., Interscience, New York, 1965.

- 4 H. Schmidt and M. Von Stackelberg, *Modern Polarographic Methods*, Academic Press, New York, 1963.
- 5 A. M. Bond, *Modern Polarographic Techniques in Analytical Chemistry*, M. Dekker, New York, 1980.
- 6 J. Heyrovsky and J. Kuta, *Principles of Polarography* Academic Press, New York, 1966.
- 7 R. N. Adams, *Electrochemistry at Solid Electrodes*, M. Dekker, New York, 1969.
- 8 A. M. Bond, *J. Electrochem. Soc.*, 118 (1971) 1588.
- 9 H. Blustein and A. M. Bond, *Anal. Chem.*, 48 (1976) 248.
- 10 A. M. Bond and R. J. O'Halloran, *J. Electroanal. Chem.*, 68 (1976) 257.
- 11 B. H. Vassos and R. A. Osteryoung, *Chem. Instrum.*, 5 (1973-74) 257.
- 12 J. G. Osteryoung, J. H. Christie and R. A. Osteryoung, *Bull. Soc. Chim. Belg.*, 84 (1975) 647.
- 13 N. Klein and Ch. Yarnitzky, *J. Electroanal. Chem.*, 61 (1975) 1.
- 14 W. P. Van Bennekom and J. B. Schute, *Anal. Chim. Acta*, 89 (1977) 71.
- 15 J. B. Flato, *Anal. Chem.*, 44 (1972) 75A (Sept.).
- 16 L. Meites and T. Meites, *Anal. Chem.*, 20 (1948) 984.
- 17 A. M. Bond and D. R. Canterford, *Anal. Chem.*, 44 (1972) 721.
- 18 E. P. Parry and R. A. Osteryoung, *Anal. Chem.*, 37 (1965) 1634.

THEORETICAL CONSIDERATIONS ON THE PERFORMANCE OF ELECTROCHEMICAL FLOW-THROUGH DETECTORS

H. B. HANEKAMP* and H. J. VAN NIEUWKERK

Department of Analytical Chemistry, Free University, de Boelelaan 1083, 1081 HV Amsterdam (The Netherlands)

(Received 24th March 1980)

SUMMARY

A survey of the equations on the limiting current in electrochemical flow-through cells is presented. For voltammetric detectors, a generalized equation for the limiting current is given. The conditions to be considered in designing an electrochemical flow-through detector for optimal signal-to-noise ratios are outlined for tubular, thin-layer, wall-jet and disk electrodes.

Electrochemical flow-through detectors have received much attention because of their application in liquid chromatography and continuous flow analysis. Various authors have proposed equations for the limiting current in electrochemical flow-through detectors. Although these detectors usually differ only in geometry or in the electrode material applied, the equations still seem to differ considerably for the description of similar phenomena. In the work reported here, the aim was to generalize these equations into a form applicable to all types of detectors. This should simplify investigations of the influence of different parameters, such as the geometry of the cell and fluid velocity, on the signal-to-noise (S/N) ratio. The S/N ratio has been chosen as a criterion since the usual feature of interest is improvement of the detection limit, which is commonly defined as the quantity causing a signal equal to three times the noise. Other features of a detector such as the time constant and correct electrode position will be briefly discussed.

The limiting current

The limiting current, i_l , can be written as

$$i_l = nFI_{\max} \quad (1)$$

where I_{\max} is the maximum diffusion mass flow towards the electrode surface; for convenience all symbols are listed in Table 1. In order to establish an equation for the limiting current, the diffusion towards the electrode has to be described. The problem of convective diffusion in liquids has been extensively treated by Levich [1]. Most of the equations published on the limiting current are based on his work or derived in a similar manner. To

calculate the diffusional flow towards an electrode, the following assumptions are generally made: the flow pattern is laminar, the reaction rate is infinitely large compared to the rate of mass transfer, and the electrode length and width are significantly larger than the hydrodynamic boundary layer.

FLOW-THROUGH DETECTORS

Flow-through cells can be divided into polarographic and voltammetric detectors according to the electrode material used. In the first type, mercury is used as the working electrode; in the second type, a solid-state material is used.

With the polarographic detectors, three types were considered as shown in Fig. 1 with the mercury flow parallel, opposite or perpendicular to the fluid flow. With the voltammetric detectors, four geometrical types were considered; these are tubular electrode cells, thin-layer cells, disk electrodes with perpendicular fluid flow, and cells based on the wall-jet principle.

Polarographic detectors (see Fig. 1)

In the case of parallel mercury and fluid flows (see Fig. 1a), Kimla and Stráfelda [2] obtained the following equation (their eqn. 20)

$$i_1 = 0.0605 nFC^*D^{2/3}(mt)^{4/9}v^{1/3}[1 + 1.86 D^{1/3}(mt)^{-1/9}v^{-1/3} + 0.00332 D^{-1/3}m^{4/9}t^{-5/9}v^{-2/3}] \quad (2)$$

(see Table 1 for definitions of symbols). At high linear fluid velocities (v), e.g., above 3.5 cm s^{-1} with a drop time of 1 s, this equation becomes

$$i_1 = 0.0605 nFC^*D^{2/3}v^{1/3}(mt)^{4/9} \quad (3)$$

Takemori and Honda [3] employed a detector constructed according to this principle.

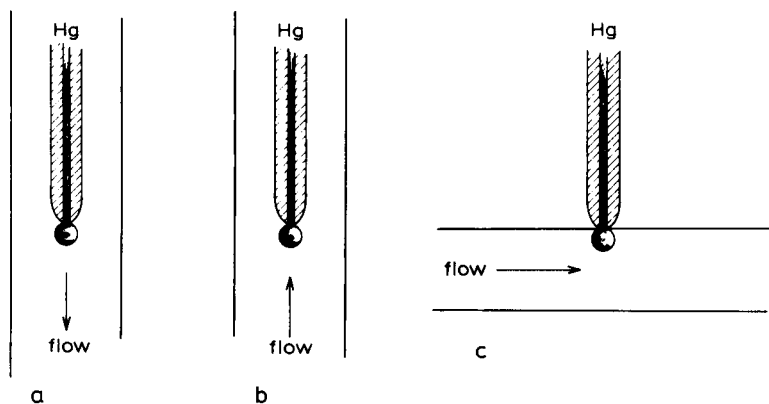


Fig. 1. Polarographic detectors: (a) parallel mercury and fluid flow; (b) opposite mercury and fluid flow; (c) mercury flow perpendicular to fluid flow.

TABLE 1

List of symbols

a	nozzle diameter	(cm)	r	radius	(cm)
A	surface area	(cm ²)	Re	Reynolds number	
α	exponent of Reynolds number		S	signal	(A)
b	width of electrode	(cm)	Sc	Schmidt number	
C^*	bulk concentration	(mol l ⁻¹)	σ_c^2	peak variance	(s ²)
d_h	hydraulic diameter	(cm)	t	droptime	(s)
D	diffusion coefficient	(cm ² s ⁻¹)	t_e	transference number	
F	Faraday constant	(96487 C mol ⁻¹)	t_R	retention time	(s)
ϕ	peak fidelity		τ	time constant	(s)
i_l	limiting (electrical) current	(A)	U	(maximum) linear fluid velocity	(cm s ⁻¹)
j_l	limiting current density	(A cm ⁻²)	V_o		
j_{\max}	maximum diffusional flux	(mol s ⁻¹ cm ⁻²)	v_{\max}		
I_{\max}	maximum diffusional flow	(mol s ⁻¹)	v	linear fluid velocity	(cm s ⁻¹)
k	numerical constant		\bar{v}	mean linear fluid velocity	(cm s ⁻¹)
l	length	(cm)	V	volume flow rate	(cm ³ s ⁻¹)
m	mercury mass flow	(mg s ⁻¹)	V_r	response volume	(cm ³)
n	number of electrons involved		w	width	(cm)
N	noise	(A)	γ	characteristic for electrode dimensions	(cm)
N_c	plate number				
ν	kinematic viscosity	(cm ² s ⁻¹)			

In the case of opposite mercury and fluid flows (see Fig. 1b), Stráfelda and Kimla [4] obtained their eqn. 16

$$i_l = 0.460 i_0 [\lambda / (1 + \gamma)]^{1/2} \{1 + 4.20 [1 + 0.85\gamma / (1 + \gamma)] \lambda^{-1/2} - 56\lambda^{-1} + 4.30 \mu [1 + 1.5\gamma / (1 + \gamma)] \lambda^{-1}\} \quad (4)$$

In this equation, $i_0 = 31600 nC^*D (mt)^{1/3}$; $\lambda = 0.026 (mt)^{1/3} v/D$; $\gamma = 1.5$ in aqueous solutions; and $\mu = 0.000226D^{-1} m^{2/3} t^{-1/3}$. Substituting these values into eqn. (4) and rearrangement yields

$$i_l = 0.0154 nFC^*D^{1/2} (mt)^{1/2} v^{1/2} [1 + 39.3 D^{1/2} (mt)^{-1/6} v^{-1/2} - 2154 \times D(mt)^{-1/3} v^{-1} + 0.0710 m^{1/3} t^{-2/3} v^{-1}] \quad (5)$$

Analogously to eqn. (2) this equation can be written for high fluid velocities as

$$i_l = 0.0154 nFC^*D^{1/2} v^{1/2} (mt)^{1/2} \quad (6)$$

Comparing parallel and opposite mercury and fluid flow, Stráfelda and Kimla [4] found that higher currents can be obtained with mercury and fluid flows in opposite directions.

For a mercury flow perpendicular to the fluid flow, Okinaka and Kolthoff [5] derived the equation (their eqn. 1)

$$i_l = 230 nC^*D^{1/2} [m^{2/3} t^{1/6} + 103 D^{1/2} (mt)^{1/3} + 7.45 v^{1/2} (mt)^{1/2}] \quad (7)$$

This can be rearranged to

$$i_l = 0.0178 nFC^*D^{1/2} v^{1/2} (mt)^{1/2} [1 + 13.8 D^{1/2} (mt)^{-1/6} v^{-1/2} + 0.134 m^{1/6} t^{-1/3} v^{-1/2}] \quad (8)$$

Analogously to eqns. (2) and (5), this yields at high fluid velocities

$$i_l = 0.0178 nFC^*D^{1/2}v^{1/2}(mt)^{1/2} \quad (9)$$

Examples of detectors based on this principle are those presented by Koen et al. [6] and Fleet and Little [7]. Comparison of eqns. (6) and (9) indicates that they differ only in the value of the constant, which is larger in eqn. (9). Hence, it can be concluded that the highest currents are obtained with the mercury flow perpendicular to the fluid stream.

Voltammetric detectors (see Fig. 2)

To describe the diffusion phenomena in the detector cell it is convenient to use the dimensionless Reynolds number $Re_x = \bar{v} l \nu^{-1}$ where \bar{v} is the average linear velocity of the fluid, l is a characteristic length of the electrode and ν is the kinematic viscosity. It must be noted that this is not the usual Reynolds number:

$Re = \bar{v}d_h/\nu$ where d_h is the hydraulic diameter defined as $d_h = 4$ (square surface)/(wetted perimeter). This number is used as a criterion for the existence of laminar or turbulent flow. Another useful dimensionless number is the Schmidt number: $Sc = \nu D^{-1}$.

For the tubular electrode (Fig. 2a) Blaedel et al. [8] derived an equation for the limiting current (their eqn. 2), according to the procedure of Levich [1]:

$$i_l = 2.01 nF \pi C^* D^{2/3} r^{2/3} l^{2/3} V_0^{1/3} \quad (11)$$

where r is the internal radius of the electrode, l its length and V_0 the maximum linear velocity. For a tube, with $\bar{v} = \frac{1}{2}V_0$, eqn. (11) can be rearranged to

$$i_l = 7.96 nFC^*D(Sc)^{1/3} l^{1/3} r^{2/3} (Re_x)^{1/3} \quad (12)$$

This result can also be obtained when the same procedure is applied to eqn. (22) reported by Matsuda [9]. Only a slightly different numerical

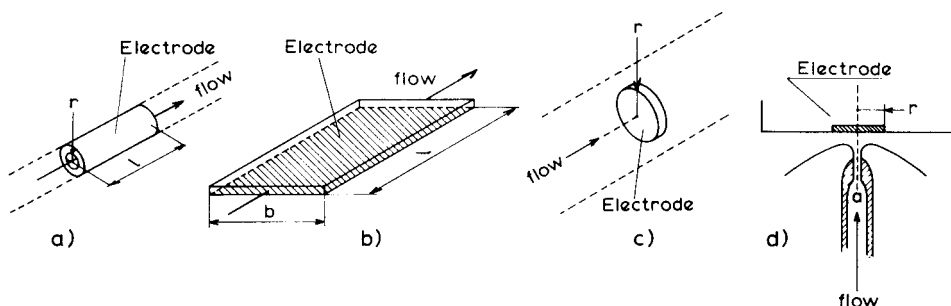


Fig. 2. Voltammetric detectors: (a) tubular electrode; (b) thin-layer cell; (c) disk electrode; (d) wall-jet electrode.

constant (8.05) is found. Examples of the use of this type of detector have been given by Blaedel et al. [10, 11] and by Armentrout et al. [12].

For the thin-layer cell (Fig. 2b), the equation for the diffusional flux to the surface of a plate as derived by Levich [1] (his eqn. 15.13) can be used. This procedure was followed by Brunt and Bruins [13] who gave the equation (their eqn. 6):

$$j_{\max} = 0.68C^*bD(Sc)^{1/3}(Ulv^{-1})^{1/2} \quad (13)$$

where U is the maximum linear fluid velocity, b the width and l the length of the electrode (Fig. 2b). Substitution of $U = v_{\max} = 3/2\bar{v}$ (which accounts for a laminar flow between two plates) in eqn. (13) gives the equation for the limiting current

$$i_l = 0.83 nFC^*D(Sc)^{1/3}b(Re_x)^{1/2} \quad (14)$$

Another type of solution for this problem has been presented by Wranglén and Nilsson [14]. They derived the following relationship for the limiting current density

$$j_l = 0.331 (nF(1 - t_e)^{-1}DC^*l_e^{-1}(Sc)^{1/3}(Ul_e\nu^{-1})^{1/2}[1 - (l_0/l_e)^{3/4}]^{-1/3} \quad (15)$$

where U is the maximum linear fluid velocity, l_0 is the distance from detector inlet to the electrode, l_e the length of the electrode, and t_e the transference number. It can be assumed that in the presence of a supporting electrolyte, $t_e \approx 0$ and with the usual detector design $l_0 \ll l_e$. Under these conditions and substituting $U = v_{\max} = 3/2\bar{v}$, the limiting current can be obtained by integrating j_l along the surface. After rearrangement this yields

$$i_l = 0.81 nFC^*D(Sc)^{1/3}b(Re_x)^{1/2} \quad (16)$$

Several examples of this type of detector design [13, 15–21] have been given in the literature. Swartzfager [18] and Ikenoya et al. [20] found 0.3 as the exponent of the Reynolds number, even though they applied a similar cell geometry. This would be more in agreement with eqn. (12) for the tubular electrode.

A solution for the description of convective diffusion to a disk electrode with perpendicular flow (Fig. 2c) has been given by Marchiano and Arvia [22]. Assuming mass transport only in the direction perpendicular to the electrode surface, they derived for the maximum diffusional flux j_{\max} to the electrode (their eqn. 20)

$$j_{\max} = 0.78 DC^*(Ur^{-1}\nu^{-1})^{1/2}(Sc)^{1/3} \quad (17)$$

After replacement of U by \bar{v} and integration along the surface, this yields for the limiting current

$$i_l = 3.27 nFC^*D(Sc)^{1/3}r(Re_x)^{1/2} \quad (18)$$

Here the Reynolds number is based on the electrode radius r .

In the solution of this problem, Matsuda [23] took into account that in the case of a flow perpendicular to the electrode surface, the pattern is not uniform. For the maximum current density on a disk electrode, the equation is (Matsuda's eqn. 30)

$$j_1 = 0.68 nFC * D^{2/3} \nu^{-1/6} U^{1/2} r^{-1/2} \quad (19)$$

After substitution of $U = v_{\max} = 2 \bar{v}$, the limiting current can be obtained by integrating along the surface. Matsuda obtained the limiting current by multiplication with the surface area. Integration and rearrangement gave

$$i_1 = 3.02 nFC * D(Sc)^{1/3} r(Re_x)^{1/2} \quad (20)$$

Hence this procedure results in a smaller value for the constant than that found in the solution of Marchiano and Arvia [22].

A special case of flow perpendicular to a disk electrode is the wall-jet electrode (Fig. 2d). Here a fluid stream from a nozzle impinges on a disk electrode. For the limiting current, Yamada and Matsuda [24] derived an equation (their eqn. 10)

$$i_1 = 1.38 nFC * D^{2/3} \nu^{-5/12} V^{3/4} a^{-1/2} r^{3/4} \quad (21)$$

where V is the volume flow rate of the solution issuing from the circular nozzle and a is the diameter of this nozzle. This volume flow rate is equal to the mean linear velocity of the fluid in the nozzle multiplied by the area of the nozzle outlet

$$V = 1/4 \pi a^2 \bar{v} \quad (22)$$

Introduction of eqn. (22) into eqn. (21) and rearrangement yields

$$i_1 = 1.15 nFC * D(Sc)^{1/3} a(Re_x)^{3/4} \quad (23)$$

Equation (21) has been confirmed by Yamada and Matsuda with a true wall-jet electrode, i.e., in a large vessel. In detectors based on this principle, such as the design of Fleet and Little [7] or the Metrohm EA1096 detector (Metrohm, Herisau, Switzerland), the exponent of the Reynolds number is not equal to 3/4. With a Metrohm EA1096 detector, an exponent of 0.44 was obtained from a log-log plot of the limiting current versus the volume flow rate during the present work. This value is more in agreement with the theoretical value of 0.5 for a thin-layer cell (eqns. 14 or 16).

Now, a comparison of eqns. (12), (14), (16), (18), (20) and (23) shows that for solid-state electrode detectors, the limiting current can be represented by the equation

$$i_1 = knFC * D(Sc)^{1/3} w(Re_x)^\alpha \quad (24)$$

where k is a dimensionless factor dependent on the cell geometry, w is characteristic of the electrode width, and the exponent α of the modified Reynolds number depends on the cell geometry. The values for these parameters are summarized in Table 2.

TABLE 2

Parameters for eqn. (24)

Detector type	k	w	l^a	α
Tube	8.0	$1^{1/3}r^{2/3}$	l	1/3
Thin layer	0.8	b	l	1/2
Disk	3.0/3.3	r	r	1/2
Wall-jet	1/2	a	r	3/4

^aCharacteristic of electrode length from $Re_x = \bar{v}l\nu^{-1}$.

OPTIMIZATION OF THE DETECTOR PERFORMANCE

In all electrochemical detectors, the signal (i.e., the output current) increases with the Reynolds number. This means that it is advantageous to build a detector with a small cross sectional area in order to increase the mean linear liquid velocity and to choose such a geometry that the highest value of α is obtained.

Another way to improve the signal would be to increase the electrode length, but this can cause problems when the input is considered as a Gaussian concentration profile. With the well-known equation for the chromatographic plate number: $N_c = (t_R/\sigma_c)^2$, where t_R is the retention time and σ_c^2 the peak variance any Gaussian peak profile can be determined for a given chromatographic column. To describe the desired detector performance, Sternberg [25] introduced the concept of peak fidelity, ϕ

$$(\tau/\sigma_c)^2 = 1/\phi^2 - 1 \quad (25)$$

where τ is the detector time constant. For the hypothetical case of $\phi = 1$, the peak is completely undistorted, which means that $\tau = 0$. The time constant τ is a characteristic of the detector and can be measured by injection of a large plug [26, 27]. The time constant can be related to a response volume V_{res} : $V_{\text{res}} = \tau V$, where V is the volume flow rate. This response volume is not necessarily equal to the geometrical volume, although these two volumes are of course related. In order to limit the peak distortion caused by the detector, it is necessary to limit the detector volume and hence the electrode length.

Another important parameter is the noise as this is related to the detection limit defined as the quantity causing a signal that equals three times the noise. The noise in electrochemical detection is proportional to the electrode surface area [16, 28], hence $N \approx A$. Combination of this approximation with eqn. (24) allows the S/N ratio to be given as a function of y (see Table 3 and Fig. 3).

From Fig. 3 it becomes clear that it is advantageous to keep y as small as possible. The limit for decreasing y is given by the amplification system. For a tubular electrode, this means a cell with a small radius and length, for a thin-layer cell a short but wide electrode, and for disk and wall-jet electrode

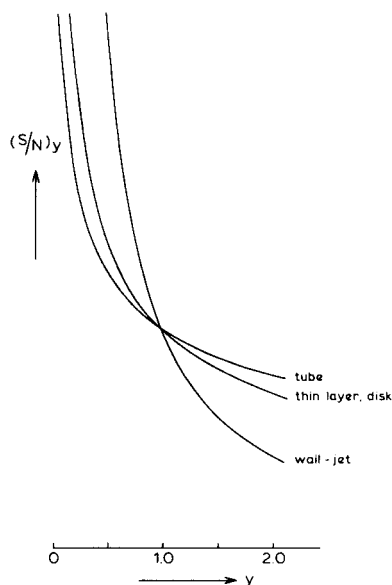


Fig. 3. Dependence of S/N ratio on y : tubular electrode, $y = r l$; thin-layer cell, $y = l$; disk or wall-jet, $y = r$.

TABLE 3

S/N ratio as a function of the electrode dimensions

Detector type	A	$S \approx$	$(S/N)y \approx$
Tube	$2\pi r l$	$r^{2/3} l^{2/3}$	$(rl)^{-1/3}$
Thin layer	bl	$b l^{1/2}$	$l^{-1/2}$
Disk	πr^2	$r^{3/2}$	$r^{-1/2}$
Wall-jet	πr^2	$r^{3/4}$	$r^{-5/4}$

cells an electrode of small radius. This conclusion is in agreement with findings of Weber and Purdy [29]. The advantage (in view of the S/N ratio) of employing a small electrode was experimentally verified by Hanekamp et al. [30]: when a polarographic detector with a horizontal dropping mercury electrode [31] was used, the best S/N ratio was obtained with small mercury drops at a fast drop rate. Another conclusion can be that, as far as the S/N ratio is concerned, there is no advantage to coulometric detection, but if required the best type of electrode for coulometric detection would be a tubular electrode.

The electrode position is another important feature in designing a good electrochemical flow-through detector. For best results, the electrodes have to be positioned in such a way that the cell resistance is low [20]. High cell resistance is probably also the reason why the differential pulse technique has not so far yielded increased sensitivity [18, 32]. Only McDonald and Duke

[33] have reported an improvement by using the differential pulse technique probably because of their close electrode position. The application of pulses is not only limited by the electrode position, but also by the electronics which have to have a fast response and be capable of handling the high currents resulting from the application of a pulse[34].

Conclusions

In designing a polarographic flow-through detector, the best signals can be obtained with a cell where the mercury flows perpendicularly to the fluid stream. Optimal S/N ratios can be expected with fast dropping mercury electrodes.

The performance of solid-state detectors can best be described by eqn. (24). The best results, with regard to the S/N ratio, can be obtained in tubular electrode cells with short narrow-bore electrodes, in thin-layer cells with short wide electrodes in a narrow flow channel, and in disk and wall-jet electrode cells with electrodes of small radius.

REFERENCES

- 1 V. G. Levich, *Physicochemical Hydrodynamics*, Prentice-Hall, Englewood Cliffs, NJ, 1962.
- 2 A. Kimla and F. Stráfelda, *Collect. Czech. Chem. Commun.*, 29 (1964) 2913.
- 3 Y. Takemori and M. Honda, *Rev. Polarogr.*, 16 (1970) 96.
- 4 F. Stráfelda and A. Kimla, *Collect. Czech. Chem. Commun.*, 30 (1965) 3606.
- 5 Y. Okinaka and I. M. Kolthoff, *J. Electroanal. Chem.*, 73 (1957) 3326.
- 6 J. G. Koen, J. F. K. Huber, H. Poppe and G. den Boef, *J. Chromatogr. Sci.*, 8 (1970) 192.
- 7 B. Fleet and C. J. Little, *J. Chromatogr. Sci.*, 12 (1974) 747.
- 8 W. J. Blaedel, C. J. Olson and L. R. Sharma, *Anal. Chem.*, 35 (1963) 2100.
- 9 H. Matsuda, *Electroanal. Chem.*, 15 (1967) 325.
- 10 W. J. Blaedel and D. G. Iverson, *Anal. Chem.*, 49 (1977) 1563.
- 11 W. J. Blaedel and Z. Yim, *Anal. Chem.*, 50 (1978) 1722.
- 12 D. N. Armentrout, J. D. McLean and M. W. Long, *Anal. Chem.*, 51 (1979) 1039.
- 13 K. Brunt and C. H. P. Bruins, *J. Chromatogr.*, 172 (1979) 37.
- 14 G. Wranglén and O. Nilsson, *Electrochim. Acta*, 7 (1962) 121.
- 15 Y. Takata and G. Muto, *Anal. Chem.*, 45 (1973) 1864.
- 16 J. Lankelma and H. Poppe, *J. Chromatogr.*, 125 (1976) 375.
- 17 P. T. Kissinger, C. Refshauge, R. Dreiling and R. N. Adams, *Anal. Lett.*, 6 (1973) 465.
- 18 D. G. Swartzfager, *Anal. Chem.*, 48 (1976) 2189.
- 19 C. Bollet, P. Oliva and M. Caude, *J. Chromatogr.*, 149 (1977) 625.
- 20 S. Ikenoya, T. Tsuda, Y. Yamano, Y. Yamanishi, K. Yamatsu, M. Ohmae, K. Kawabe, H. Nishino and T. Kurahashi, *Chem. Pharm. Bull.*, 26 (1978) 3530.
- 21 H. Hashimoto and Y. Maruyama, *J. Chromatogr.*, 152 (1978) 387.
- 22 S. L. Marchiano and A. J. Arvia, *Electrochim. Acta*, 12 (1967) 801.
- 23 H. Matsuda, *Electroanal. Chem.*, 15 (1967) 109.
- 24 J. Yamada and H. Matsuda, *Electroanal. Chem.*, 44 (1973) 189.
- 25 J. C. Sternberg, in *Advances in Chromatography*, Vol. 2, M. Dekker, NY, 1966.
- 26 M. Forina, *Ann. Chim. (Rome)*, 63 (1973) 763.
- 27 H. B. Hanekamp, P. Bos, U. A. Th. Brinkman and R. W. Frei, *Fresenius Z. Anal. Chem.*, 297 (1979) 404.

- 28 H. B. Hanekamp, W. H. Voogt, P. Bos and R. W. Frei, *Anal. Chim. Acta*, 118 (1980) 81.
- 29 S. G. Weber and W. C. Purdy, *Anal. Chim. Acta*, 99 (1978) 77.
- 30 H. B. Hanekamp, W. H. Voogt, P. Bos and R. W. Frei, *Anal. Lett.*, 12 (1979) 175.
- 31 L. Michel and A. Zatka, *Anal. Chim. Acta*, 105 (1979) 109.
- 32 W. A. McCrehan and R. A. Durst, *Anal. Chem.*, 50 (1978) 2108.
- 33 A. McDonald and P. D. Duke, *J. Chromatogr.*, 83 (1973) 331.
- 34 R. Kalvoda and A. Trojanek, *J. Electroanal. Chem.*, 75 (1977) 151.

THE CONTINUOUS REMOVAL OF OXYGEN FROM FLOWING SOLUTIONS

A. TROJÁNEK and K. HOLUB*

J. Heyrovský Institute of Physical Chemistry and Electrochemistry, Czechoslovak Academy of Sciences, Jilská 16, 110 00 Prague 1 (Czechoslovakia)

(Received 12th May 1980)

SUMMARY

An apparatus for continuous removal of oxygen or other dissolved gases from liquid samples is described; it is useful in continuous analyses. The gas diffuses through a semi-permeable membrane into a space with a lower partial pressure of the particular gas. The separation unit consists of two concentric tubes and is practical and efficient. The mathematical model for transport under conditions of stationary gas diffusion with laminar flow of the liquid in the tube did not correspond satisfactorily to the experimental relationship, probably because of turbulence in the flow.

In the application of electroanalytical methods, dissolved oxygen in samples frequently interferes. Oxygen dissolves in pure water which is in contact with the atmosphere at 25°C to form a solution about 0.5 mM; at this concentration, the marked current signal obtained on cathodic reduction may obscure the signal providing the analytical information. In precise coulometric determinations, the reduction of oxygen is an undesirable side-reaction which decreases the current efficiency during the determination of the required component. In unbuffered solutions, the reduction of oxygen leads to a pH decrease in the vicinity of the electrode, which may result in the precipitation of the salts of heavy metals present and thus lead to a decrease in their diffusion currents [1]. In stripping voltammetry, the oxygen present leads to partial dissolution of the metal accumulated by pre-electrolysis [2] and thus lower analytical results are obtained, etc.

It is almost always desirable to remove oxygen from test solutions, and various methods can be employed in batch arrangements. However, for work with continuous flow systems, only the methods which remove oxygen with high efficiency and speed are really viable although sometimes continuous removal can be replaced by a batch process. For example, in liquid chromatography, the eluents are often freed from dissolved gases before the beginning of the analysis by evacuation or boiling; with flow-through analyzers, suitable organization of work permits oxygen removal from the individual samples before their introduction into the analyzer [3]. Among the methods that really work continuously, the most widely used are those based on decreasing the partial pressure of the oxygen above the solution by using an inert gas.

Intimate contact between the liquid and the gas can be achieved in flow-through columns with particulate packings [4] or in columns consisting of a narrow tube [5], where turbulent flow is ensured at relatively low flow-rates. In another type of apparatus [6], a large-area glass frit is employed to ensure contact between the inert gas and the thin layer of flowing electrolyte.

This paper describes a method of removal of dissolved oxygen (or other dissolved gases) from test solutions, based on diffusion of gases through a semipermeable membrane.

EXPERIMENTAL

Apparatus

The process of continuous removal of oxygen from a flowing solution was studied quantitatively on the apparatus depicted in Fig. 1. The actual separation of the gaseous components was done in the separation unit consisting of a tube of silicone rubber (1 mm i.d., wall thickness 0.265 mm), placed concentrically in a polyethylene tube (4 mm i.d., wall thickness 2 mm). The test solution flowed through the silicone tube and nitrogen was passed through the space between the tube walls; in some tests this space was filled with air. The measuring procedure for the concentration of oxygen in the 0.1 M KCl electrolyte employed involved the use of a flow-through polarographic detector [7] at a constant potential of -0.45 V vs. a saturated Ag/AgCl electrode. The potassium chloride solution was pumped by a multichannel peristaltic pump (Type 340, Zalimp, Poland), the flow rate being measured by a flow meter with a calibrated tube. Before use, nitrogen was freed from traces of oxygen by bubbling through traps containing an acidic chromium(II) solution in contact with zinc amalgam, and thermostatted by passage through a copper tube (6 m long, 1-mm i.d.) placed in a thermostatted bath. The nitrogen flow rate was measured with a capillary

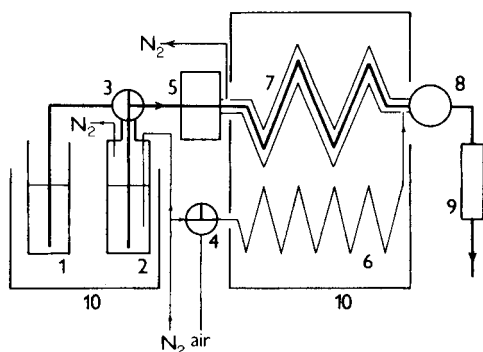


Fig. 1. Scheme of the experimental arrangement for measuring the efficiency of removal of oxygen from a flowing solution. (1, 2) Reservoirs R1 and R2 with the test solution; (3, 4) stopcocks; (5) peristaltic pump; (6) copper tube for thermostating the gas; (7) separation unit; (8) polarographic detector; (9) flow meter; (10) thermostat.

flow meter. Both the reservoir with the base electrolyte and the separation unit were placed in the thermostatted bath at 25°C.

RESULTS

In considering the dependence of the response of the detector on the electrolyte flow rate, the ratio $(i - i_B)/(i_0 - i_B)$ was employed as an indicator of the separation efficiency; here i_0 and i are the cathodic limiting currents of oxygen measured by the detector at the outlet of the separation unit. In measurements of i_0 , the pump provided a solution containing oxygen from the reservoir R1 to the separation unit, which was rendered non-functional by the presence of air between the walls. In the measurements of i , the air was replaced by a nitrogen flow, ensuring normal functioning of the separation unit. Both current values were corrected for the background signal, i_B , produced by the presence of electroactive impurities. In the measurement of i_B , the deaerated solution was led from reservoir R2 by a glass tube to the separation unit with a nitrogen atmosphere.

The value of the fraction was studied as functions of the average flow rate (\bar{v}) of the solution in the range 2.5–100 cm s⁻¹, and the length (L) of flow through the separation unit in the range 50–270 cm. As the fraction was found to be independent of the flow rate of nitrogen in the range 0.3–20 cm³ s⁻¹, all the measurements were carried out at a constant nitrogen flow rate of 1 cm³ s⁻¹. The semilogarithmic dependence plotted in Fig. 2 shows that the efficiency of oxygen removal in the apparatus is quite high but strongly dependent on the value of parameter L/\bar{v} . For example, on flow of the solution through a separation unit with a length (L) of 270 cm at a flow rate (\bar{v}) of 2.33 cm s⁻¹ (i.e., 1.1 cm³ min⁻¹), the value of the oxygen limiting current decreased more than 500-fold. When the length of the separation was decreased to 100 cm under otherwise identical conditions,

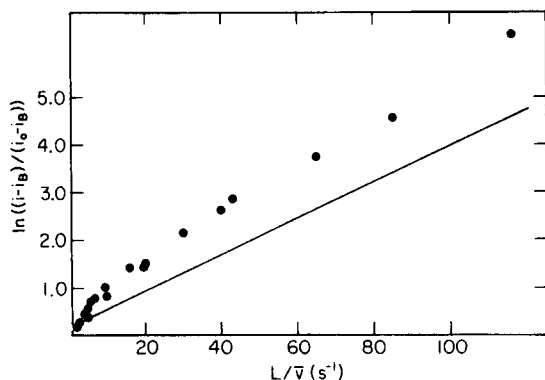


Fig. 2. The dependence $\ln[(i - i_B)/(i_0 - i_B)]$ vs. L/\bar{v} . The straight line represents the limiting case ($L/\bar{v} \gg 1$) of the mathematical solution for laminar flow. The diffusion coefficient of oxygen used in the calculation was $D = 2.6 \times 10^{-5}$ cm² s⁻¹ [8].

the decrease in the limiting current was only 17-fold. An attempt was made to characterize this dependence by solution of the transport problem connected with stationary diffusion in laminar flow in a tube.

THEORETICAL

The problem of removal of oxygen from a solution passing through a tube was formulated mathematically under the following four assumptions. First, the solution flows laminarily through a circular tube with internal radius R ; thus the flow rate is given by the relationship [9]

$$v = v_0(1 - r^2/R^2) \quad (1)$$

where v_0 is the flow rate in the direction of the z -axis, placed along the tube axis and r is the perpendicular distance from the tube axis. Secondly, in the stationary state, the concentration (C) of oxygen is described by $(v \cdot \text{grad}) \times C = D \text{ div grad } C$, where D is the diffusion coefficient of oxygen in the solution, and v is the flow rate of the solution given by eqn. (1). The first assumption means that the flow rate in a plane perpendicular to the tube axis is zero. Thirdly, when a laminarily flowing solution with an oxygen concentration of C_0 is introduced into the tube (where z is the distance from this point along the z -axis) where removal of oxygen occurs, then for $z = 0$ and $R > r$, $C = C_0$. Fourthly, in a tube with $z > 0$, oxygen disappears from the internal surface of the tube at a rate which is proportional to the oxygen concentration on the tube surface; thus the boundary condition is

$$z > 0, r = R: \partial C / \partial r = -\beta C \quad (2)$$

The use of this boundary condition is based on the following considerations.

The equation describing stationary diffusion $\partial^2 C / \partial r^2 + \partial C / r \partial r = 0$, for $R < r < R_0$ with the boundary conditions $r = R: C = C(R)$ and $r = R_0: C = C(R_0)$, where R_0 designates the tube external radius, has the solution [10]

$$C = k_1 + k_2 \ln r \quad (3)$$

where it follows for k_2 from the boundary conditions that

$$k_2 = [C(R) - C(R_0)] / \ln(R/R_0) \quad (4)$$

The diffusion flow at point $r = R$ is then given by the expression

$$D \partial C / \partial r = D' \partial C / \partial r = D' k_2 / R \quad (5)$$

where D' is the diffusion coefficient in the material of the tube. If we further assume that $C(R_0) \ll C(R)$, then eqn. (2) is obtained. This latter assumption can be considered justified as, in the external medium (gas), the diffusion coefficient of oxygen is several orders greater than in the solid or liquid phase.

The mathematical problem defined from eqn. (1) to eqn. (2) has been solved. It holds for the average concentration of oxygen \bar{C} at the outlet from the tube that

$$\bar{C}/C_0 = \sum_{k=1}^{\infty} A_k \exp(-W_k^2/\kappa) \quad (6)$$

where $\kappa = v_0 R^2/DL$, W_k^2 are the eigenvalues of the problem and A_k are constants. The eigenvalues W_k^2 and constants A_k depend on the magnitude of constant β in eqn. (2). Solution (6) is suitable for the calculation when κ is not much larger than unity. Then the first few terms of the series are sufficient for calculation of the decrease in the amount of oxygen in the solution, which is then considerable.

Expression (6) is not suitable for calculation of small decreases in the amount of oxygen. It is then possible to employ the solution obtained by a boundary layer method (for $\kappa \gg 1$)

$$\bar{C}/C_0 = 1 - [2DL\alpha/(R^2\bar{v})]F_a[1.089\alpha(DL/v_0)^{1/3}R^{-2/3}] \quad (7)$$

where \bar{v} is the mean flow rate of the solution in the tube, $\alpha = \beta R$ and function $F_a(u)$ is given by the expression

$$F_a(u) = [1 - \exp(-u^3)]u^{-3} - u\Phi(1, 7/3, -u^3)/\Gamma(7/3) + u^2\Phi(1, 8/3, -u^3)/\Gamma(8/3) \quad (8)$$

The following relationships hold for this function

$$\lim_{u \rightarrow 0} F_a(u) = 1 \text{ and } \lim_{u \rightarrow \infty} F_a(u) = 0$$

Consider the first case ($\kappa \rightarrow 0$). It can be seen from condition (2) that the rate of removal of oxygen by diffusion transport through the tube wall will be the greater the larger the value of constant β . For very large values of β the concentration at the internal surface of the tube is almost zero (analogously to electrode reactions, if the rate constant increases indefinitely, the concentration of the electroactive substance at the surface is zero, i.e. the limiting diffusion current is attained). Transport through the wall and thus removal will be maximal when the concentration of oxygen at the wall is zero

$$z > 0, r = R: C = 0 \quad (9)$$

This condition determines the constants (in our case, $R^2 \ll L^2$) A_k , W_k^2 ($A_1 = 0.82$, $A_2 = 0.098$, ... $W_1^2 = 2.70^2 = 7.31$, $W_2^2 = 6.68^2 = 44.6$, ...).

If the above assumptions are valid, then

$$\{[\bar{C}/C_0]_{(9)} \leq [\bar{C}/C_0]_{(2)}\} \equiv \{[C_0/\bar{C}]_{(9)} \geq [C_0/\bar{C}]_{(2)}\} \quad (10)$$

where the subscripts beside the square brackets indicate the boundary set conditions by expressions (2) and (9). It is then readily derived that, for $\kappa < 15$, the relative error resulting from the second term for boundary condition (9) is less than 1%. Then expression (6) can be rewritten in the form

$$\ln C_0/\bar{C} \approx 0.2 + 7.31/\kappa = 0.2 + 7.31 DL/(v_0 R^2) \quad (11)$$

This limiting dependence is designated by the straight line in Fig. 2. According to relationship (10), the experimental points should lie below this straight line; it follows from Fig. 2 that this condition is not fulfilled.

For boundary condition (9), the solution by the boundary layer method yields [9] $\bar{C}/C_0 = 1 - 4.07\kappa^{-2/3}$, and inequality (10) then leads to the relationship $1 - 4.07\kappa^{-2/3} < \bar{C}/C_0$. Considering the experimental points corresponding to the smallest removal, this inequality is fulfilled only for the first of them. This fact indicates that more oxygen is removed from the solution passing through the tube than corresponds to the theory based on the four assumptions stated initially. This disagreement is most probably caused by the invalidity of the assumption of laminar flow. Although the Reynolds number (R_e) here is less than 1000 (laminar flow can be assumed for $R_e < 2500$ [9]), the flow can be nonlaminar as a result of roughness on the inner surface of the tube and as a result of pulsations in the flow produced by the peristaltic pump. A certain contribution to the disagreement may result from the fact that the separation tube was wound in a coil.

Conclusions

The separation unit described for continuous oxygen removal is very efficient, the efficiency being increased by the presence of turbulent flow. The efficiency can be further markedly increased by using thinner membranes (0.265 mm here). For continuous analyses it is important that the oxygen be removed not only from the carrier solution but also directly from the analyzed sample. The deaeration apparatus does not require any special arrangement for removal of bubbles before entrance of the sample into the detector. The identity of the samples forming zones in the liquid flow is completely retained during the removal process. In continuous analyzers, the separation unit can act simultaneously as a reaction coil. The space with a low partial pressure of oxygen, into which the dissolved oxygen diffuses through the membrane walls, can be rinsed with a strongly reducing solution pumped in a closed circuit through a suitable regenerator using one channel of a multichannel peristaltic pump.

REFERENCES

- 1 A. M. Bond, *Talanta*, 20 (1973) 1139.
- 2 D. Jagner, *Anal. Chem.*, 51 (1979) 342.
- 3 W. Lund and L. N. Opheim, *Anal. Chim. Acta*, 79 (1975) 35.
- 4 R. L. Rebertus, R. J. Cappell and G. W. Bond, *Anal. Chem.*, 30 (1958) 1825.
- 5 W. J. Blaedel and J. W. Todd, *Anal. Chem.*, 30 (1958) 1821.
- 6 J. Wang and M. Ariel, *Anal. Chim. Acta*, 99 (1978) 89.
- 7 A. Trojáněk, unpublished results.
- 8 I. M. Kolthoff and C. S. Miller, *J. Am. Chem. Soc.*, 63 (1941) 1013.
- 9 V. G. Levich, *Physico-chemical Hydrodynamics*, Prentice-Hall, Englewood Cliffs, NJ, 1962.
- 10 H. S. Carslaw and J. C. Jaeger, *Conduction of Heat in Solids*, Oxford University Press, Oxford, 1959, p. 189.

ELECTROCHEMISTRY IN FLUOSOL-43, A PERFLUORINATED BLOOD SUBSTITUTE

The Influence of Pluronic F-68 Surfactant on some Polarographic Electrode Processes

J. GEORGES

*Laboratoire de Chimie Analytique III (E.R.A. 07 0474), Université Claude Bernard
Lyon I, 43 Boulevard du 11 Novembre 1918, 69622 Villeurbanne Cedex (France)*

(Received 10th April 1980)

SUMMARY

The inhibition of thallium(I), lead(II) and cadmium(II) reductions at the dropping mercury electrode is studied in Fluosol-43 and explained as a result of surfactant adsorption. The adsorption of Pluronic F-68 on the DME, examined by electrocapillary, tensammetric and current–time curves, is diffusion-controlled. The similarity established between aqueous solutions of Pluronic F-68 at concentrations near the critical micelle concentration and Fluosol-43 confirms that the adsorption depends only on the monomer form of the surfactant. The magnitude of the inhibitory effect, evaluated from charge-transfer coefficients and rate constants, decreases in the order $\text{Cd}^{2+} > \text{Pb}^{2+} > \text{Tl}^+$; for the same cation, inhibition depends on the nature of the anion of the supporting electrolyte, the adsorbability of which decreases in the sequence $\text{ClO}_4^- > \text{NO}_3^- > \text{SO}_4^{2-}$.

Fluosol-43 is an aqueous emulsion containing 25% perfluorotributylamine, the surfactant being Pluronic F-68 at a concentration of 3.2% (w/v) in distilled water [1]. Before it is used as a blood substitute, hypertonic Krebs–Ringer hydrogencarbonate solution containing hydroxyethyl starch is added to provide the emulsion with physiological osmolarity, oncotic pressure and buffer capacity. Previous work in this laboratory [2, 3] has shown that electrochemical reactions can proceed in this medium and that reductions of some cations at the dropping mercury electrode are strongly affected by Pluronic F-68, the surface-active properties of which are striking. The present work is concerned with these properties of Pluronic F-68: its adsorption behaviour under different polarographic conditions and its inhibitory effect on electrode processes in the presence of depolarizers such as Tl^+ , Pb^{2+} and Cd^{2+} are described.

EXPERIMENTAL

Direct current and normal pulse polarograms were obtained with a Princeton Applied Research Model 174 Polarographic Analyzer fitted with a drop-timer system, and recorded with a Sefram TRP X-Y recorder. Tensammetric

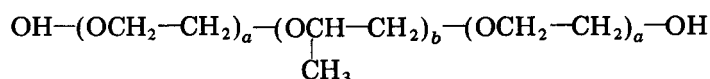
curves were obtained with a Solea—Tacussel PRG-3 polarograph. The applied alternating voltage was 5 mV, the frequency 200 Hz and the demodulation phase angle 90° . The working electrode was a dropping mercury electrode with a flow rate of 1 mg s^{-1} . Current—time curves were recorded at a lower mercury flow rate and a natural drop-time. The reference was a saturated calomel electrode (SCE) with an agar-agar salt bridge [2]. All experimental potentials are referred to the SCE.

Fluosol-43 was supplied by the Green Cross Corporation (Gamou-cho, Joto-ku, Osaka, Japan). Its pH is about 3. Stock solutions (1% w/v) of Pluronic F-68 were prepared by dissolution of the commercial product in distilled water. The reagents (analytical grade) were used without purification.

Dissolved oxygen was removed from the solution by bubbling nitrogen through a plain narrow glass tube for 15 min [2]. All experiments were done at 25°C .

SURFACE-ACTIVE PROPERTIES OF PLURONIC F-68

Pluronics are non-ionic surfactants, resulting from a mixture of polyoxyethylene—polyoxypropylene block copolymers [4] of general formula:



The ratio of the hydrophobic and hydrophilic groups varies throughout the series. Pluronic F-68 contains 80% ethylene oxide groups and has a mean molecular weight of 8350. It has been used as an emulsifying, dispersing, wetting and defoaming agent. Clinical and experimental studies have demonstrated that Pluronic F-68 is not toxic and may alleviate some of the adverse effects of extracorporeal blood circulation [1]. In the following paragraphs, the adsorption behaviour of Pluronic F-68 at the dropping mercury electrode is discussed and a comparison is made between an aqueous solution of surfactant and Fluosol-43 without Krebs—Ringer hydrogencarbonate solution.

Electrocapillary curves

The interfacial tension of any mercury/solution interface varies with the electrode potential [5]. A common method of recording an electrocapillary curve is to measure the drop life which is approximately proportional to the interfacial tension. Figure 1 shows the variation caused by the addition of Pluronic F-68 to an aqueous solution. The lower curve presents a marked degree of asymmetry with a shift of the electrocapillary maximum (e.c.m.) to more positive potentials. The interfacial tension decreases from 0.1 V to -1.8 V vs. SCE, which corresponds to the potential range of Pluronic F-68 adsorption. The curves corresponding to the emulsion and the aqueous solution of the surfactant (about $4 \times 10^{-5} \text{ mol l}^{-1}$) with the same supporting

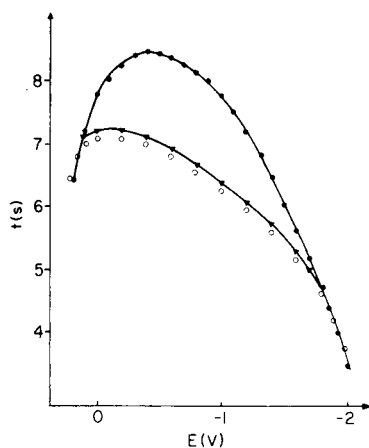


Fig. 1. Electrocapillary curves of mercury in (●) water + 0.1 M Na_2SO_4 ; (○) water + 0.1 M Na_2SO_4 + 4×10^{-5} M Pluronic F-68; (▼) Fluosol-43 + 0.1 M Na_2SO_4 .

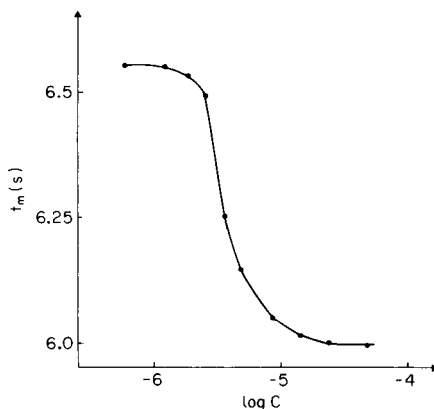


Fig. 2. Drop time at the e.c.m. (0.5 V vs. SCE) as a function of the Pluronic F-68 concentration in water.

electrolyte are practically identical. Figure 2 shows the variation of the drop time at the e.c.m. ($E = -0.5$ V vs. SCE) with surfactant concentration in aqueous 0.1 M LiClO_4 solution. The shape of the curve is very similar to that described for Triton X-100 [6]; an initial slow change is followed by a sudden sharp change until a characteristic concentration of approximately 2×10^{-5} mol l^{-1} is reached, when the drop times become constant. This concentration has been interpreted as the point of micelle formation or critical micelle concentration, CMC [7–10]. If it is recalled that this indirect estimate of the CMC must be lower than that given for a pure solution in the absence of supporting electrolyte, the value is reasonably close to the value 10^{-4} mol l^{-1} determined by the benzopurpurin and iodine methods [11]. Although the idea of CMC for Pluronics is a matter of dispute [11], it can be stated that the present value corresponds to a concentration beyond which the properties of the solution vary very slowly. This is the reason why in the first part of this work, comparison was done between the emulsion medium (Fluosol-43) and aqueous solutions of Pluronic F-68 at a concentration of 4×10^{-5} mol l^{-1} , i.e. near the CMC.

Tensammetry

Like many surface-active compounds, Pluronic F-68 exhibits tensammetric peaks under the conditions of alternating current polarography. Figure 3 shows again the similarity between the Fluosol-43 medium, and an aqueous solution (4×10^{-5} mol l^{-1}) of surfactant for which curve 2 is the same. The positive and negative tensammetric peaks, which reflect the periodic adsorption–desorption process [12] as a result of the superimposed alternating potential, define the adsorption range of Pluronic F-68 (+0.050 to -1.850 V

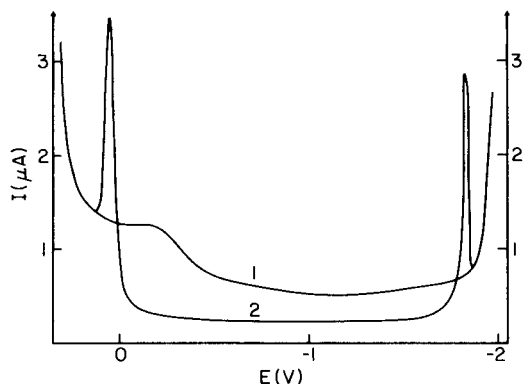


Fig. 3. Tensammetric curves in (1) water + 0.1 M Na_2SO_4 ; (2) water + 0.1 M Na_2SO_4 + 4×10^{-5} M Pluronic F-68, or Fluosol-43 + 0.1 M Na_2SO_4 .

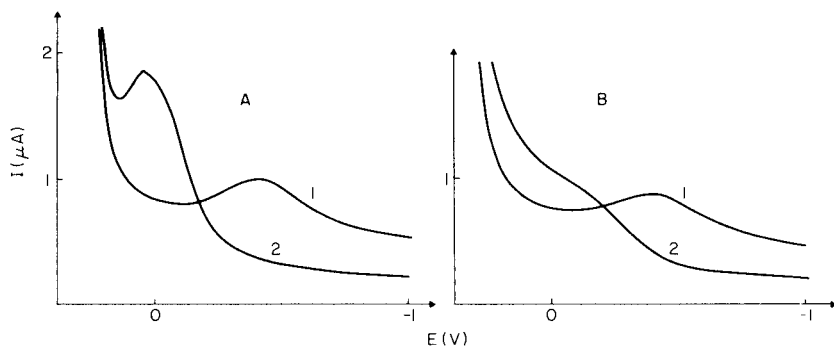


Fig. 4. Influence of the supporting electrolyte on tensammetric curves at anodic potentials: (A) water + 0.1 M KNO_3 ; (B) water + 0.1 M LiClO_4 . Curves (1) are in the absence of Pluronic F-68 and curves (2) in its presence.

vs. SCE). Figures 3 and 4 show that the anodic peaks are influenced by the nature of the supporting electrolyte, the interaction of the anion with the mercury electrode being different. From the curves obtained with and without Pluronic F-68, it appears that competitive adsorption between the electrolyte anion and surfactant is the greater with perchlorate; anion adsorbability was found to decrease in the order $\text{ClO}_4^- > \text{NO}_3^- > \text{SO}_4^{2-}$. In contrast, the cathodic peaks are only slightly affected by the nature of the supporting electrolyte because the cations are present in the double layer in their hydrated forms and their behaviour is quite similar [12].

Current-time curves

Current-time curves for cadmium ions in water in the presence of increasing amounts of Pluronic F-68 are similar in shape to those reported by Schmid and Reilley [13] in the presence of Triton X-100, and prove that the adsorption is diffusion-controlled. According to Koryta [14], the sudden decrease in current (Fig. 5) corresponds to full coverage of the electrode by

the adsorbate and must obey the equation $\tau = kC^{-2}$, where τ is the time at which the surface of the electrode is completely covered, k is a constant and C is the bulk concentration of the surfactant. Practically, τ is compared with t° , the time when the current reaches zero. An excellent linear plot was obtained between t° (0–5 s) and $1/C^2$ for the concentration range given in Fig. 5, which confirms that the adsorption is diffusion-controlled and that t° corresponds to full coverage of the electrode; the latter has been already reported by Ayabe [15]. Extrapolation of the straight line to $t^\circ = 0$ leads to a surfactant concentration of about $2 \times 10^{-5} \text{ mol l}^{-1}$, which is very near the characteristic concentration determined from the electrocapillary curve. From these results, it can be assumed that full coverage is obtained in aqueous solutions of Pluronic F-68 at $C \geq 2 \times 10^{-5} \text{ mol l}^{-1}$ and very likely in Fluosol-43 from the very beginning of the drop life. Figure 6 shows that the magnitude of the inhibitory effect of the surfactant in an aqueous solution ($4 \times 10^{-5} \text{ mol l}^{-1}$) of Pluronic F-68 and in Fluosol-43 emulsion is equal in the same conditions of supporting electrolyte and pH. In the two media, reduction of $5 \times 10^{-4} \text{ M}$ cadmium(II) at the DME occurs at the same potential and with the same irreversible character. The limiting current is less in Fluosol-43 than in the aqueous solution of Pluronic F-68, certainly because of a decrease in the diffusion coefficient in such an emulsion.

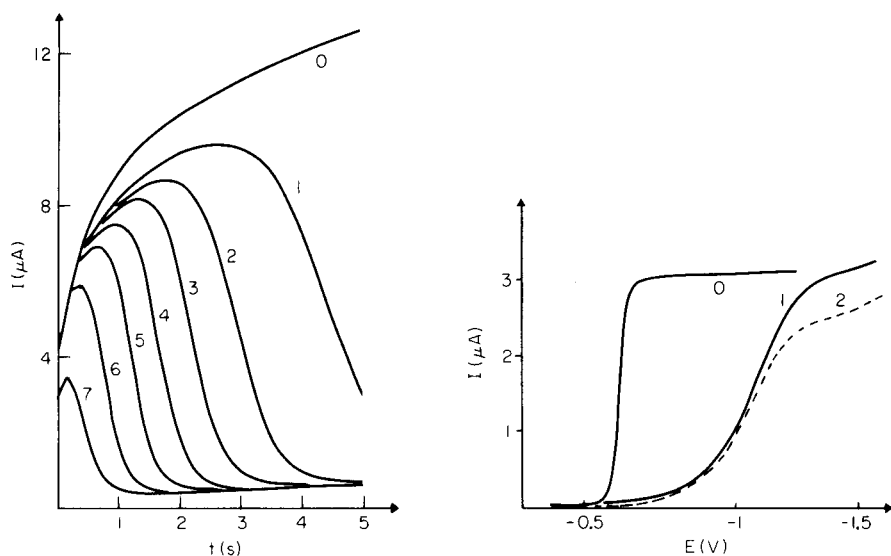


Fig. 5. Current–time curves for a single mercury drop in water + 0.1 M LiClO_4 + $2 \times 10^{-3} \text{ M}$ Cd^{2+} at -0.630 V vs. SCE with increasing amounts of Pluronic F-68: (0) 0; (1) $4.3 \times 10^{-6} \text{ M}$; (2) $5 \times 10^{-6} \text{ M}$; (3) $5.7 \times 10^{-6} \text{ M}$; (4) $6.4 \times 10^{-6} \text{ M}$; (5) $7.2 \times 10^{-6} \text{ M}$; (6) $8.4 \times 10^{-6} \text{ M}$; (7) $9.5 \times 10^{-6} \text{ M}$.

Fig. 6. Current–potential curves in the sampled d.c. mode for reduction of $5 \times 10^{-4} \text{ mol l}^{-1} \text{ Cd}^{2+}$ at pH 3 in (0) water + 0.1 M Na_2SO_4 ; (1) water + 0.1 M Na_2SO_4 + $4 \times 10^{-5} \text{ M}$ Pluronic F-68; (2) Fluosol-43 + 0.1 M Na_2SO_4 .

INHIBITORY EFFECTS OF PLURONIC F-68 IN FLUOSOL-43 EMULSION

The adsorption of a surface-active compound on the mercury drop may cause widely differing modifications at the electrode interface leading to a decrease in the charge-transfer coefficient, a shift of the half-wave potential, a decrease in the limiting current or even complete elimination of the wave [13]. Thallium(I), lead(II) and cadmium(II) ions were selected for examination because their reduction potentials occur close to the e.c.m., which is the potential range in which adsorption of uncharged surfactants is the strongest and where the magnitude of the adsorption is assumed to be steady. In addition, reduction of these cations is well known to present a true reversible character in aqueous media, so that interpretation of the results should be simplified.

Nature of the polarographic waves

In the Fluosol-43 medium containing 0.1 M supporting electrolyte (LiClO_4 or KNO_3), the plots of limiting current versus concentration gave straight lines for all three cations over the range 5×10^{-4} – 5×10^{-3} mol l^{-1} . In a study of the effect of temperature, linear relations were obtained from 20°C to 45°C with a temperature coefficient of about 2% per degree for all three cations at 10^{-3} mol l^{-1} . Plots of $\log I$ vs. $\log h$ gave straight lines with slopes of 0.48 for 10^{-3} mol l^{-1} Tl^+ or Pb^{2+} and 0.8 for 10^{-3} mol l^{-1} Cd^{2+} . These observations indicate that the reduction processes in Fluosol-43 are largely controlled by diffusion.

Polarographic reduction of Tl^+ , Pb^{2+} and Cd^{2+} was studied in Fluosol-43 and in pure water at the same concentration (10^{-3} mol l^{-1}) and under the same conditions of temperature, mercury flow and supporting electrolyte. The results reported in Table 1 show that reduction of thallium(I) is uninhibited in Fluosol-43 whereas inhibition is moderate for lead(II) and very important for cadmium(II) with a large shift of the half-wave potential towards cathodic values.

The diffusion coefficients (Table 2) were determined from Ilkovic's equation [16] from the limiting currents observed in d.c. polarography for each cation at a concentration of 10^{-3} mol l^{-1} . The diffusion coefficients were quite similar for the different supporting electrolytes and the values

TABLE 1

Shift of the half-wave potential (in mV) when passing from water to Fluosol-43

Electrolyte (0.1 M)	LiClO_4	KNO_3	Na_2SO_4
Tl^+	0 r. ^a	0 r.	0 r.
Pb^{2+}	–35 irr.	–55 irr.	—
Cd^{2+}	–260 irr.	–440 irr.	–480 irr.

^ar. = reversible; irr. = irreversible.

TABLE 2

Diffusion coefficients ($\text{cm}^2 \text{ s}^{-1}$) for Ti^+ , Pb^{2+} and Cd^{2+} ($10^{-3} \text{ mol l}^{-1}$) in water and in Fluosol-43 with 0.1 M supporting electrolyte

Medium	Ti^+	Pb^{2+}	Cd^{2+}
Water	2.3×10^{-5}	1.3×10^{-5}	1.1×10^{-5}
Fluosol-43	1.5×10^{-5}	0.84×10^{-5}	0.72×10^{-5}
Ratio	0.65	0.64	0.65

given here represent an average. They were decreased in Fluosol-43 in the same ratio for all the three cations studied.

Determination of $\alpha'n$ and k'_s for lead(II) and cadmium(II) in Fluosol-43

The values of the charge-transfer coefficient (α') and the rate constant (k'_s) at standard potential E° , at the covered electrode surface, were determined from analysis of the I - E curves obtained by d.c. polarography and normal pulse polarography. The equations derived by Oldham and Parry [17] for irreversible systems were used

$$E_{1/2} - E = (0.059/\alpha'n) \log [2x(3-x)/(1-x)] \quad (1)$$

$$\text{with } E_{1/2} = E^\circ + (0.059/\alpha'n) \log 1.35 k'_s (t/D)^{1/2} \quad (2)$$

for d.c. polarography, and for pulse polarography

$$E_{1/2} - E = (0.059/2\alpha'n) \log x^2 [(1.75 + x^2)/(1-x)] \quad (3)$$

$$\text{with } E_{1/2} = E^\circ + (0.059/\alpha'n) \log 2.31 k'_s (t_m/D)^{1/2} \quad (4)$$

In these equations, x is the ratio of the current I for potential E to the limiting current; t is the drop time; t_m is the average time interval between pulse application and current measurement (48 ms for the PAR 174); $E_{1/2}$ is the half-wave potential of the inhibited wave (i.e. in Fluosol-43); E° is the standard potential of the redox couple. As lead(II) and cadmium(II) are reversible systems in water, E° practically coincides with the half-wave potential of the uninhibited wave (i.e., in water). Plots of $\log [2x(3-x)/(1-x)]$ and $\log [x^2(1.75 + x^2)/(1-x)]$ versus potential gave straight lines for Pb^{2+} and Cd^{2+} , which establishes the total irreversibility of the electrode processes. The slopes are $0.059/\alpha'n$ for d.c. waves and $0.059/2\alpha'n$ for n.p. waves, so that $\alpha'n$ can be determined. The intercept through the origin gives $E_{1/2}$, from which k'_s can be determined by application of eqns. (2) and (4). Results are reported in Table 3.

DISCUSSION

The similarity observed between the reactions in Fluosol-43 and the solution of surfactant in water seems to confirm that the adsorption depends

TABLE 3

Half-wave potentials, charge-transfer coefficients and rate constants for reduction of lead(II) and cadmium(II) in Fluosol-43. Comparison of data provided by direct current (d.c.) and normal pulse (n.p.) polarography

Ion ^a	Electrolyte (0.1 M)	$-E_{1/2}$ (V vs. SCE)		$\alpha' n$		k'_s (cm s ⁻¹)	
		d.c.	n.p.	d.c.	n.p.	d.c.	n.p.
Pb ²⁺	LiClO ₄	0.435	0.475	0.84	0.84	0.85×10^{-3}	0.50×10^{-3}
	KNO ₃	0.455	0.505	0.73	0.66	0.57×10^{-3}	0.38×10^{-3}
Cd ²⁺	LiClO ₄	0.850	0.970	0.30	0.30	1.1×10^{-4}	0.64×10^{-4}
	KNO ₃	1.030	1.145	0.31	0.30	1.1×10^{-5}	0.80×10^{-5}
	Na ₂ SO ₄	1.070	1.170	0.32	0.32	0.6×10^{-5}	0.40×10^{-5}

^a 10^{-3} mol l⁻¹.

only on the monomer concentration [18]. Below the CMC the surfactant molecules are present in solution as monomer; beyond the CMC, the monomer concentration undergoes no appreciable change and no further adsorption takes place as the total concentration of surfactant is increased. This supposes that the monomer concentration in Fluosol-43 is at least equal to the CMC of Pluronic F-68 in water. The presence of micelles in the emulsion seems to be responsible only for a decrease in the diffusion coefficients.

As previously stated by Guidelli and Foresti [19], the magnitude of the inhibitory effect on electron-transfer reactions decreases in the order $\text{Cd}^{2+} > \text{Pb}^{2+} > \text{Ti}^+$ although their reduction processes occur in the same potential range. In the reaction involving reduction of metal ion to metal amalgam, it was assumed [19] that formation of the amalgam required the removal of adsorbed molecules from the electrode surface. Thus the difference between Ti^+ , Pb^{2+} and Cd^{2+} would depend mainly on the adsorbed state of the reacting particle.

The results reported in Table 3 show that, for the same cation, the rate constant depends on the nature of the supporting electrolyte and decreases in the same sequence as the adsorbability of the corresponding anions $\text{ClO}_4^- > \text{NO}_3^- > \text{SO}_4^{2-}$ established above from tensammetric curves.

These results indicate that the kinetics of the polarographic reduction of thallium(I), lead(II) and cadmium(II) in Fluosol-43, is not related to Pluronic F-68 adsorption alone. The influence of surfactant is more or less important according to the adsorbability of the other species present near the electrode surface, namely the reacting ions Ti^+ , Pb^{2+} or Cd^{2+} and the anion of the supporting electrolyte.

The author is grateful to S. Desmettre for experimental assistance and to M. Bréant and O. Vittori for helpful criticism of the manuscript.

REFERENCES

- 1 The Green Cross Corporation, Technical Information Ser. no. 3, Sept. 4, 1976, RN/ky/yd, Fluosol-43.
- 2 M. Bréant, J. Georges and M. Mermet, *Anal. Chim. Acta*, 115 (1980) 43.
- 3 M. Bréant and J. Georges, *C. R. Acad. Sci., Ser. C*, 288 (1979) 213.
- 4 I. R. Schmolka, in M. J. Schick (Ed.), *Nonionic Surfactants*, M. Dekker, New York, 1967.
- 5 D. M. Mohilner, in A. J. Bard (Ed.), *Electroanalytical Chemistry*, Vol. 1, M. Dekker, New York, 1966.
- 6 R. G. Barradas and F. M. Kimmerlee, *J. Electroanal. Chem.*, 11 (1966) 128.
- 7 J. Potney and C. C. Addison, *Trans. Faraday Soc.*, 33 (1937) 1243.
- 8 E. L. Colichman, *J. Am. Chem. Soc.*, 72 (1950) 4036.
- 9 W. U. Malik and O. P. Jhamb, *J. Am. Oil Chem. Soc.*, 49 (1971) 170.
- 10 K. Shinoda, T. Nakagawa, B. Tamamushi and T. Isemura, *Colloid Surfactants*, Academic Press, New York, 1963.
- 11 K. N. Prasad, T. T. Luong, A. T. Florence, J. Paris, C. Vaution, M. Seiller and F. Puisieux, *J. Colloid Interface Sci.*, 69 (1979) 225.
- 12 B. Breyer and H. H. Bauer, *Alternating Current Polarography and Tensammetry*, Interscience, New York, 1963.
- 13 R. W. Schmid and C. N. Reilley, *J. Am. Chem. Soc.*, 80 (1958) 2087.
- 14 J. Koryta, *Collect. Czech. Chem. Commun.*, 18 (1953) 206.
- 15 Y. Ayabe, *J. Electroanal. Chem.*, 81 (1977) 215.
- 16 J. Ilkovic, *J. Chim. Phys.*, 35 (1938) 129.
- 17 K. B. Oldham and E. P. Parry, *Anal. Chem.*, 40 (1968) 65; 42 (1970) 229.
- 18 F. J. Trogus, R. S. Schechter and W. H. Wade, *J. Colloid Interface Sci.*, 70 (1979) 293.
- 19 R. Guidelli and M. L. Foresti, *J. Electroanal. Chem.*, 77 (1977) 73.

AN EVALUATION OF DIFFERENTIAL PULSE ANODIC STRIPPING VOLTAMMETRY AT A ROTATING GLASSY CARBON ELECTRODE FOR THE DETERMINATION OF CADMIUM, COPPER, LEAD AND ZINC IN ANTARCTIC SNOW SAMPLES

MICHAEL P. LANDY

British Antarctic Survey, Natural Environment Research Council, Madingley Road, Cambridge, CB3 0ET (Gt. Britain)

(Received 9th July, 1980)

SUMMARY

A procedure is described for the determination without preconcentration of Cd, Cu, Pb and Zn in Antarctic snow, based on differential pulse anodic stripping voltammetry at a rotating glassy carbon electrode with in situ mercury plating. Thirty four surface snow samples from Adelaide Island in the Antarctic Peninsula demonstrate the scope of this method, and allow an assessment of local heavy metal sources such as the rock, the sea, and a manned base. The zinc data are affected by container contamination, but concentrations as low as 0.005, <0.02 and 0.05 ng g⁻¹ were measured for Cd, Cu and Pb, respectively.

Increasing industrial emissions of the heavy metals cadmium, copper, lead and zinc [1] have caused concern that they may be polluting the environment on a global scale. As 90% of anthropogenic emissions take place in the northern hemisphere [2], the remote continent of Antarctica is ideally located for monitoring changes in background aerosol concentrations. Any changes during the industrial period can in principle be measured by comparing heavy metal concentrations in contemporary snow with those in pre-industrial snow deposits from deeper in the ice sheet [3]. Before this can be achieved, geographical variations in trace element distribution must be understood and any influence of local sources of heavy metals on background concentrations must be assessed.

Because concentrations of these metals in polar snow are sub-ppb (<1 ng g⁻¹), previous analytical procedures have mainly involved a preconcentration step, usually non-boiling evaporation [4] or solvent extraction [5]. These operations are difficult to perform without the inherent risks of contamination or loss of analyte by adsorption. A method is presented here based on differential pulse anodic stripping voltammetry (d.p.a.s.v.) at a rotating glassy carbon electrode, whose sensitivity is such that preconcentration is unnecessary, thereby allowing the rapid and direct analysis of snowmelt (melted snow). Accuracy is improved, and much smaller quantities of snow are needed, allowing a more detailed study of seasonal variations down the

snowpack. Analysis of surface snow from a sequence of sites on Adelaide Island (Antarctic Peninsula — 67°S, 69°W) demonstrates the application of this method, and gives an assessment of the relative influence of local sources, namely the sea, rock outcrops, and an operating British base. Results from a more remote location on the Antarctic Peninsula plateau will be presented elsewhere [6]. This technique should lend itself well to the analysis of snow in the field, eliminating the problems of storage and transportation of bulky frozen samples. Although the utmost care must be exercised during the collection and handling of snow samples, the limited sample handling demanded by this technique reduces the need for "clean-room" laboratory conditions. A supply of ultra-pure water is, however, essential.

EXPERIMENTAL

Instruments and reagents

Analyses were done with a PAR 174A polarographic analyser (Princeton Applied Research) in the differential pulse mode, and recorded on a 10-V input potentiometric chart recorder (Watanabe SR651). The voltammetric cell was a Metrohm Universal Titration Vessel EA880-20 (Penton cell top with five electrode apertures). The 30-ml glass cell was treated with 2% dimethyldichlorosilane in 1,1,1-trichloroethane (Repelcote, Hopkin and Williams), in order to reduce metal adsorption [7], then cleaned very thoroughly with 10% nitric acid. The working electrode was a Metrohm E628 rotating glassy carbon electrode (RGCE), rotated at 1500 rpm. This type of electrode is reported to provide the most sensitive system for a.s.v. at present [8]. The active glassy carbon is a disc (5-mm diameter) set in a poly(chlorotrifluoroethylene) shaft with epoxy resin. A very flat carbon surface is required to optimise the electrode properties. This was achieved by mounting the electrode tip vertically in a purpose-made jig, and using a Kent Mark 2A polishing machine (Engis Ltd.) first to lap the surface using a grooved cast iron plate, then to polish it successively, with 6- μ m and 3- μ m Hyprez diamond compounds on woven artificial silk polishing discs. Whilst in use, the electrode was refurbished daily by polishing briefly with a 0.3- μ m alumina paste. It was operated in conjunction with a platinum wire counter electrode (Metrohm EA282/1), and an Ag/AgCl/saturated KCl reference electrode (Metrohm EA437), which was isolated from the sample by a saturated KCl salt bridge and 0.5-mm diameter ceramic diaphragm. A nitrogen purge tube (Metrohm EA1024) was used initially to bubble O₂-free nitrogen (0.22 μ m filtered) through the sample and then to maintain it as a blanket over the sample to prevent oxidation. Purging was aided by a PTFE-covered magnetic stirring bar.

In situ mercury plating was used as it gave more reproducible results than a permanent mercury film. The plating solution was made by dissolving 250 mg of triply-distilled mercury (Ultrar) in 5 ml of nitric acid (Aristar) and finally making the solution up to 100 ml with ultra-pure water. Ultra-

pure water was produced by a four-stage procedure in which tap water was passed through a mixed-bed ion-exchange unit, doubly distilled in glass (Fistreem, Fisons Scientific Apparatus), passed through a Millipore Milli-Q water purification system incorporating a depth filter, an activated charcoal unit, and two mixed-bed ion exchange units in series, and finally filtered through a 0.22- μm membrane [9]. The trace metal content of this water measured by d.p.a.s.v. was typically 0.001 ± 0.001 ppb Cd, $<0.01 \pm 0.01$ ppb Cu, 0.01 ± 0.01 ppb Pb and 0.025 ± 0.025 ppb Zn. A mixed standard of 100 ng g⁻¹ for Cd and Pb and 200 ng g⁻¹ for Cu and Zn in 1% nitric acid was made up by serial dilution of mg g⁻¹ a.a.s. standards (BDH). This and the plating solution were stored in 100-ml glass conical flasks with PTFE-lined screw caps (Corning).

All plastic and glassware used to handle samples in the laboratory was rigorously cleaned before use. Tap water and detergent washes were followed by thorough rinses with distilled water, and lengthy soaking in polypropylene baths containing 10% nitric acid, the mildest conditions which gave consistently low blanks. After rinsing with ultra-pure water, items were left soaking until use in a covered bath containing ultra-pure water. The 500-ml polyethylene snow sample containers were cleaned in the field — rinsed with snowmelt, then washed with two separate portions of 2% perchloric acid /2% nitric acid, followed by extensive rinsing with deionised snowmelt. This procedure may not have been sufficiently rigorous for thorough decontamination (see below).

In the laboratory, all a.s.v. and analytical operations were carried out inside Class-100 horizontal, laminar flow clean-air work stations fitted with HEPA filters (Microflow Ltd.). Volumes under 10 ml were pipetted by using adjustable micropipettes (Finnpipette) with acid-cleaned disposable polypropylene tips. Snowmelt was transferred with a 10-ml glass pipette, stored in 10% nitric acid.

Optimisation of analytical parameters

Because of the very low concentrations of metals in Antarctic snow, it was necessary to optimise the analytical parameters carefully in order to achieve the lowest detection limits compatible with a simple, non-contaminating procedure. In order to detect the major fraction of metal in a snowmelt sample, it is desirable to operate at a low pH for two main reasons. First, at low pH, the metal is found mainly in labile complexes that are "electrochemically available" [10]; only certain organic, colloidal and mineral matter remains strongly bound in complexes at a pH below 3.5 [11]. Only more powerful acid digestion can release these categories of metal [12]. Secondly, the rate of adsorption of metals onto container and electrode surfaces is very pH-dependent, increasing considerably at high pH [13, 14].

Addition of 50 μl of the mercury plating solution to 30 ml of snowmelt produced a sample (5×10^{-5} M Hg²⁺ at pH 2.9) suitable for direct a.s.v. analysis. Further acidification resulted in steeper voltammetric baseline

currents and loss of sensitivity for zinc. This can be corrected by the appropriate use of a buffer (e.g., sodium acetate), but the difficulties of producing a buffer with sufficiently low levels of heavy metal contamination are such that it should be contemplated only when powerful acid digestion is necessary, for example when determining total metal in biological or geological material [11]. In the present work, a lesser degree of acid digestion for comparative purposes was achieved for one aliquot of each snow sample by heating the snowmelt and the plating solution to 110°C for over 4 h in a steel-enclosed PTFE digestion bomb (Scientific Instruments, Loughborough).

The d.p.a.s.v. operating conditions were optimised for each parameter after consultation of earlier work [15–19]. Although Batley and Florence [15] found that d.p.a.s.v. gave little improvement over linear stripping techniques for mercury film electrodes, Valenta et al. [16] achieved a substantial increase in sensitivity by careful optimisation of the square-wave pulse parameters. As recommended by Valenta et al., a 100 Ω resistor was inserted between the RGCE and the voltammeter to eliminate damped oscillations associated with the much larger area of the RGCE compared with the normal hanging mercury drop electrode.

The analytical parameters finally chosen were: plating potential, -1300 mV; electrode rotation, 1500 rpm (during plating only); scan rate, 5 mV s^{-1} (from -1300 to 0 mV); pulse amplitude, 50 mV; pulse repetition time, 0.5 s; pulse length, 57 ms (pre-set); low pass filter, 0.3 s; current ranges, 5 μA to 0.2 mA full-scale.

For a plating time of 10 min, the following sensitivities were recorded at the peak potentials given: Cd, $1.02 \mu\text{A ng}^{-1}$ (-0.66 V); Cu, $0.31 \mu\text{A ng}^{-1}$ (-0.02 V); Pb, $0.58 \mu\text{A ng}^{-1}$ (-0.48 V); Zn, $1.05 \mu\text{A ng}^{-1}$ (-1.11 V). The sensitivities varied linearly with plating time.

Detection limits were dictated by the blank values of the ultra-pure water, but if $<1 \text{ pg g}^{-1}$ metal concentrations in water could be achieved, the voltammetric detection limits would be 0.0005 ppb Cd, 0.005–0.08 ppb Cu (according to electrode response), 0.001 ppb Pb and 0.005 ppb Zn. Sensitivity depended very much on the condition of the RGCE which is especially critical for zinc and copper as their peaks are very close, to the hydrogen reduction and mercury oxidation waves, respectively. The procedural blank values were negligible compared with the metal concentrations in the snow samples under investigation.

Analytical procedure

Snow samples stored at -20°C for over three years since collection were allowed to melt in their containers at room temperature, and 30-ml aliquots were transferred to the voltammetric cell, to which 50 μl of mercury plating solution was added. Before analysis the sample was purged with nitrogen for 10-min, and then plated and stripped three times in quick succession using a rapid scan rate of 100 mV s^{-1} to condition the RGCE [17].

Samples were plated for either 5 or 10 min, and the RGCE rotation was stopped 30 s before stripping. At the end of each scan, the potential was left at 0.0 V for 30 s before recommencing plating. Each sample was run twice to confirm reproducibility, and a third time after a standard addition of 3 ng of Cd and of Pb and 6 ng of Cu and of Zn (30 μ l of mixed standard solution). Some samples were given a second standard addition to check linearity of response, which was found in all cases to be very good. The standard used was regularly checked against freshly prepared standard, and variations in concentration were found to be negligible over several months. After analysis of a sample, the mercury coat was removed by wiping the electrode gently with a medical wipe dampened with ultra-pure water.

Adelaide Island snow samples

Adelaide Island, the second largest island in the Antarctic Peninsula (see Fig. 1), includes a mountain chain down its eastern margin with a large, gently sloping ice piedmont to the west. The geology consists of a thick sequence of altered volcanic and volcanoclastic rocks intruded by olivine gabbro-adamellite plutons [20]. These intrusive rocks appear to have caused hydrothermal alteration and mineralization of the volcanic rocks. The prevailing winds over the island are north-easterly and occasionally very strong, so that a certain amount of dust transport from the mountains to the ice piedmont can be expected. The British base built in 1961 is at the southern

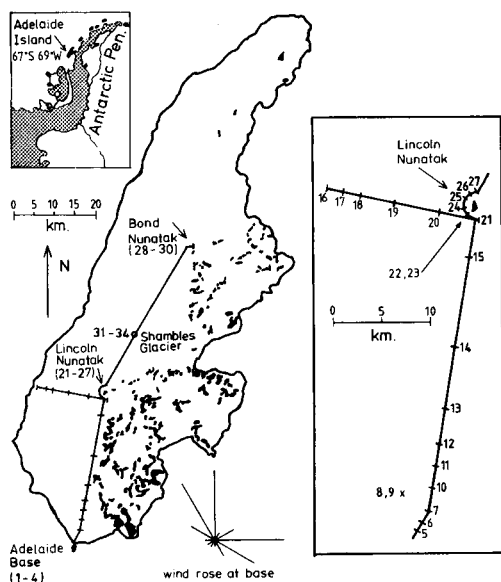


Fig. 1. Map of Adelaide Island showing exposed rock, a wind rose for Adelaide base (1975), and the location of the snow sampling sites (March 1976). The wind rose at the base partly reflects the local topography, but a prevailing north-easterly wind at higher altitudes has been recorded from meteorological balloon flights.

tip of the island, and until its closure in 1977, acted as a local source of trace metal emissions. Although most of this material was carried out to sea by the prevailing winds, the occasional southerly winds were probably sufficient to transport an appreciable amount inland to the ice piedmont. Aircraft fuelled by Jet Al Avtur and based at the station will often have flown over the ice piedmont, primarily near its southern extremity, but a few measurements on surface snow directly exposed to aircraft emissions during take-off at a remote field site indicated that they contribute little to background heavy metal concentrations. Some limited vehicular travel had taken place on the island five months prior to the sampling, involving snowmobiles running on leaded petrol.

Samples were collected in March 1976 during a two week journey (Fig. 1). Transport was provided by dog teams in order to avoid the gaseous emissions of petrol-powered snowmobiles. At the sampling sites soft surface snow upwind of the dog teams was first scraped away using a sample container to expose the harder underlying layer found at a fairly uniform depth over the whole island. Snow samples collected from this layer should be contemporaneous and exposed to similar summer conditions. This underlying snow was carefully scooped into the sample container; occasionally the hardness of the snow necessitated prior loosening by scraping with the container lids.

The snow samples can be subdivided into four groups, each group chosen to reflect changes in the contribution from particular trace element sources on the island:

- (1) sequence from a traverse away from the British base (sample Nos. 1–15, 31–34);
- (2) sequence from a traverse away from the sea (sample Nos. 16–21);
- (3) sequence from a traverse around an isolated rock exposure: Lincoln Nunatak (sample Nos. 21–27);
- (4) samples taken very close to a rock exposure: Bond Nunatak (sample Nos. 28–30).

Samples were sometimes duplicated as a check on the procedure and in order to compare slightly different sampling methods and containers.

RESULTS AND DISCUSSION

Each result presented in Tables 1–4 represents an average of analyses on three aliquots, two of which were carried out after the simple addition of mercury plating solution, and the third following hot digestion. The digested aliquots of many samples had concentrations indistinguishable from the undigested ones. Lead and copper showed increases in some digested aliquots, the largest being for samples taken very near rock. Reproducibility between duplicate analyses of the same snow sample was generally good ($\pm 20\%$), but depended on the particulate content of the snow. Particles were visible to the naked eye in all the melt samples, but were more numerous in samples from the southern half of the island, especially close to the base. The distri-

bution of particles appeared to be heterogeneous and the reproducibility from samples with a high particulate content was often poorer, presumably because metal concentrations depended on the specific nature of the particles in a particular aliquot of snowmelt. This applied similarly to the reproducibility between replicate snow samples, as can be seen in the results (Nos. 8 & 9, 22 & 23, 31 & 32).

Some disparity in concentration is apparent between ostensibly similar sample sites. Although in certain cases this could be accounted for by the heterogeneous nature and distribution of the particulate matter, in others the only reasonable explanation is contamination of the sample at the collection stage. However, the very good reproducibility between duplicated samples suggests that this affected only a few samples, such as Nos. 17 and 20.

The consistently large zinc concentrations (relative to the other metals) and their lack of variability suggest zinc to have a more persistent and serious source of contamination, possibly associated with the sample containers. This was confirmed by analyzing some ultra-pure water stored in a sample container for several days, and shaken before analysis. While the concentrations of the three other metals remained essentially unchanged, that of zinc rose from 0.02 to 1.7 ppb. As a result, little importance can be attached to the zinc data, and for this reason they are not discussed further.

TABLE 1

Samples taken near Adelaide base and during a traverse north from the base, including the pit on Shambles Glacier (samples 31–34)
(Concentration in ng g^{-1})

Sample number	Distance from airstrip (km)	Cd	Cu	Pb	Zn
1–4	<1 ^a	0.39 ± 0.2	0.69 ± 0.69	1.08 ± 0.55	2.95 ± 1.2
5	1.9	0.59	0.18	2.40	2.2
6	3.4	0.08	0.70	0.28	1.9
7	4.6	0.31	<0.08	0.68	2.3
8	6.1 ^b	0.17	0.70	0.65	2.4
9	6.1 ^b	0.31	0.94	0.13	3.5
10	6.6	0.33	<0.05	0.97	1.8
11	8.8	0.06	<0.03	0.18	1.6
12	11.2	0.27	0.28	0.59	2.7
13	14.1	0.91	1.01	1.51	2.0
14	19.4	1.00	0.35	0.28	1.8
15	30.9	0.02	<0.03	0.32	1.4
	Average	0.37 ± 0.30	<0.47 ± 0.47	0.82 ± 0.65	2.27 ± 0.7
31	52 km/20–30 cm depth ^{b, c}	0.13	0.09	0.07	3.2
32	52 km/20–30 cm depth ^{b, d}	0.13	0.09	0.09	2.1
33	52 km/40–50 cm depth ^d	0.05	0.13	0.20	1.1
34	52 km/60–70 cm depth ^c	0.10	0.10	0.15	2.1
	52 km — averages	0.10 ± 0.04	0.10 ± 0.02	0.13 ± 0.06	2.1 ± 0.9

^aAverage of 4 samples. ^bDuplicate samples. ^cCollected near the pit on Shambles Glacier in the usual manner. ^dCollected in the pit on Shambles Glacier with a PTFE scraper.

TABLE 2

Samples taken during traverse from the sea inland
(Concentrations in ng g^{-1})

Sample number	Distance from sea(km)	Cd	Cu	Pb	Zn	Mg ^a
16	1.6	0.005	<0.02	0.06	1.4	70
17	3.2	0.37	0.29	0.34	3.2	24
18	4.8	0.02	<0.02	0.07	2.3	—
19	8.0	0.008	<0.02	0.05	1.5	9
20	11.2	0.42	0.10	0.64	3.0	15
21	14.4	0.02	<0.02	0.06	1.4	9
Average		0.14 ± 0.2	$<0.08 \pm 0.11$	0.20 ± 0.24	2.1 ± 0.8	

^aDetermined by electrothermal atomic absorption spectrometry [22].

Effect of Adelaide base on metal concentrations

The average concentrations in the south of the island (Table 1, 1–15) are systematically greater than those for the rest of the samples (Nos. 16–34) by the following ratios: Cd, 2.6; Pb, 5.5, Cu, 5.2 (excluding samples 29 and 30, obviously affected by nearby mineralization). Copper and lead occur in particularly high concentrations in the immediate base area. These increased heavy metal concentrations reflect the higher concentrations of visible particles in samples from the southern half of the island. Sample 13, which was unusually dirty, also gave larger metal concentrations, but these may well have originated from the nearby exposed rock. However, the general proportion of particulate matter originating from local rock sources compared with that emanating from base activities is thought to be small.

Variations in concentrations with distance from sea

Excluding the two samples which appear to have been contaminated during collection (Table 2, Nos. 17 and 20), the concentrations of cadmium, copper and lead measured on this traverse are very uniform indeed, and possibly represent values close to a regional background for Adelaide Island. These are within the limits of values obtained by other workers in Antarctica [3, 21], especially for their less remote sites. In contrast to the behaviour of metal salts of predominantly marine origin (typified by data for magnesium [22]), there does not appear to be any systematic change in concentration with distance from the sea for any metal, although towards the end of the traverse the sampling sites may have been influenced by wind-blown matter from Lincoln Nunatak.

Variation in concentrations near potential geological sources

With the closer proximity of rock at Lincoln Nunatak, the concentrations of all the metals increased, the most significant increase being that for cadmium (Tables 3 and 4). There was no concurrent increase in visible

TABLE 3

Samples taken during a semi-circular traverse around the exposed western face of Lincoln Nunatak
(Concentrations in ng g^{-1})

Sample number	Bearing and estimated distance to rock(km)	Cd	Cu	Pb	Zn
21	336°, 0.7	0.02	<0.02	0.06	1.4
22	6°, 0.7 ^a	0.27	0.13	0.18	2.8
23	6°, 0.7 ^a	0.30	0.40	0.18	3.1
24	34°, 1.1	0.04	<0.02	0.09	2.9
25	93°, 0.9	0.10	<0.07	0.10	1.9
26	139°, 0.6	0.05	<0.04	0.09	1.4
27	167°, 0.8	0.01	<0.02	0.09	1.9
	Average	0.11 ± 0.12	<0.10 ± 0.14	0.11 ± 0.05	2.2 ± 0.7

^aDuplicate samples.

TABLE 4

Samples taken very close to rock at Bond Nunatak
(Concentrations in ng g^{-1})

Sample number	Distance from rock(m)	Cd	Cu	Pb	Zn
28	50	0.01	<0.02	0.06	1.5
29	5	0.51	3.08	0.18	2.5
30	0 ^a	0.03	1.60	0.17	—
	Average	0.18 ± 0.28	~1.6 ± 1.5	0.14 ± 0.07	2.0 ± 0.7

^aSnow—rock interface.

particulate matter. From a maximum at the duplicated sample (Nos. 22 and 23) taken SSW of the nunatak, concentrations decreased slightly irregularly as the traverse progressed to the north. This pattern is believed to reflect the distribution of wind-blown particles in the prevailing NNE wind, demonstrated by the direction of the snow drift deposits around the outcrop. However the magnitude of the effect may be partly due to the fact that samples 22/23 were collected closer to the exposed rock than samples 24 and 25.

It is interesting to note that at Bond Nunatak, sample 28 taken only 50 m west of the exposed rock was both visibly free of particulate matter, and chemically unenriched in heavy metals (with the exception of lead after digestion), suggesting that even at this short range the winds transport little material west of the source. At much closer range (samples 29 and 30) the metals were measured in greater abundance. Digestion data for three samples deposited close to rock exposures are given in Table 5. For sample 28 the increased concentration in lead with digestion suggests limited mineralization in the nearby rock of Bond Nunatak. However, no increase was obtained for

TABLE 5

Comparison of full data for three samples deposited close to rock exposures
(Concentrations in ng g^{-1})

Sample number	Description	Cd	Cu	Pb	Zn
21	First aliquot	0.018	<0.02	0.056	1.28
	Second aliquot	0.027	<0.02	0.058	1.35
	Digested aliquot	0.023	<0.02	0.062	1.41
	Average	0.02	<0.02	0.06	1.4
22	First aliquot	0.292	0.091	0.150	2.73
	Second aliquot	0.259	0.062	0.148	2.68
	Digested aliquot	0.265	0.233	0.244	2.83
	Average	0.27	0.13	0.18	2.8
28	First aliquot	0.014	<0.02	0.030	1.80
	Second aliquot	0.017	<0.01	0.023	1.32
	Digested aliquot	0.011	<0.02	0.128	1.32
	Average	0.01	<0.02	0.06	1.5

copper, despite the very large copper concentrations in the two samples closer to rock and evidence of copper mineralization — obvious malachite stains on microdiorites found at the snow/rock interface. Increases were found for lead and copper 0.7 km downwind of Lincoln Nunatak (samples 22 and 23), though not for sample 21 only 0.32 km away. At this last site, no rock from the western-exposed face was visible; the results suggest that the snow is effectively shielded from airborne particles. Thus it can be seen that a degree of discrimination between sources can be obtained from the digestion data.

CONCLUSIONS

The results presented must be considered as a preliminary assessment of local heavy metal sources in the Antarctic and the use of d.p.a.s.v. for determining their effect on metal concentrations in snow. This technique seems adequate for the very low concentrations encountered, with the exception of copper, which was often below the detection limit. The increased particle and heavy metal content of snow in the southern half of Adelaide Island suggests an important anthropogenic contribution from the base, though it is difficult to differentiate from local rock sources. Heavy metal contributions from the sea appear to be negligible, but local geology can have a considerable influence on background levels, highly dependent on wind direction and strength. In general, heavy metal concentrations on Adelaide Island are significantly greater than those measured in snow from a more remote site in the Antarctic Peninsula [6].

Refinement of the sampling techniques (including the use of "clean room" clothing), and a careful selection of sampling sites based on these preliminary results should yield improved quantitative data and better information on

the regional distribution of heavy metals in Antarctic snow. The feasibility of heavy metal analysis by a.s.v. in the field was investigated with more basic linear stripping instrumentation (ESA Model 2011) at a remote site on the Antarctic Peninsula plateau. This was possible by adapting the voltammeter to a d.c. battery power source and working inside a laboratory tent. The equipment operated well, but the detection limits were insufficiently low for Antarctic snow. Preconcentration of the heavy metals onto a chelating ion-exchange resin (Chelex-100) [11, 23] followed by elution with 2 M nitric acid, buffering, and analysis by linear a.s.v. was investigated, but the technique failed to give quantitative recovery from spiked samples, and should be used only with caution below the ppb level [24, 25]. With a suitably stable power supply, there seems no reason why the d.p.a.s.v. procedure presented here should not be adapted to the direct field analysis of snow-melt, though the problems of producing ultra-pure water in the field must not be underestimated. This would increase confidence in the measurement and interpretation of such low concentrations.

The author acknowledges the assistance of M. Chantrey, C. Knott and Dr. A. Lipscombe in the collection of the snow samples, and thanks Dr. D. A. Peel, Dr. J. G. Paren and E. W. Wolff for helpful discussions.

REFERENCES

- 1 J. O. Nriagu, *Nature*, 279 (1979) 409.
- 2 E. Robinson and R. C. Robbins, American Petroleum Institute, Washington, DC, Publ. 4070, 1971.
- 3 C. Boutron, Influence des Aerosols Naturels et Anthropogéniques sur la Géochimie des Neiges Polaires, PhD thesis, Université de Grenoble, 1978.
- 4 C. Boutron and S. Martin, *Anal. Chem.*, 51 (1979) 140.
- 5 M. Murozumi, T. J. Chow and C. Patterson, *Geochim. Cosmochim. Acta*, 33 (1969) 1247.
- 6 M. P. Landy and D. A. Peel, *Nature*, submitted.
- 7 R. Salim and B. G. Cooksey, *J. Electroanal. Chem.*, 105 (1979) 127.
- 8 W. Davison and M. Whitfield, *J. Electroanal. Chem.*, 75 (1977) 763.
- 9 M. Oehme and W. Lund, *Talanta*, 27 (1980) 223.
- 10 D. R. Turner and M. Whitfield, *J. Electroanal. Chem.*, 103 (1979) 61.
- 11 M. I. Abdullah, O. A. El-Rayis and J. P. Riley, *Anal. Chim. Acta*, 84 (1976) 363.
- 12 T. M. Florence and G. E. Batley, *Talanta*, 24 (1977) 151.
- 13 L. M. Petrie and R. W. Baier, *Anal. Chim. Acta*, 82 (1976) 255.
- 14 R. Salim and B. Cooksey, *J. Electroanal. Chem.*, 106 (1980) 251.
- 15 G. E. Batley and T. M. Florence, *J. Electroanal. Chem.*, 55 (1974) 23.
- 16 P. Valenta, L. Mart and H. Rützel, *J. Electroanal. Chem.*, 82 (1977) 327.
- 17 W. Lund and D. Onshus, *Anal. Chim. Acta*, 86 (1976) 109.
- 18 H. W. Nürnberg, P. Valenta, L. Mart, B. Raspor and L. Sipos, *Fresenius Z. Anal. Chem.*, 282 (1976) 357.
- 19 H. W. Nürnberg, *Proc. Analyt. Div. Chem. Soc.*, 15 (1978) 275.
- 20 G. J. Dewar, *Brit. Antarct. Surv. Sci. Rep. No. 57*, 1970.
- 21 C. Boutron and C. Lorius, *Nature*, 277 (1979) 551.
- 22 J. Mumford, personal communication, 1980.
- 23 J. P. Riley and D. Taylor, *Anal. Chim. Acta*, 40 (1968) 479.
- 24 M. Zief and J. W. Mitchell, *Contamination Control in Trace Element Analysis*, J. Wiley, New York, 1976, p. 180.
- 25 T. M. Florence and G. E. Batley, *Talanta*, 22 (1975) 201.

VOLTAMMETRIC ON-LINE ANALYSIS FOR SOME SULPHUR-CONTAINING DRUGS

ARI IVASKA*

Department of Analytical Chemistry, Åbo Akademi, 20500 Åbo 50 (Finland)

YUTHSAK VANEESORN

Department of Chemistry, Ching Mai University, Ching Mai (Thailand)

IAN E. DAVIDSON

Wyeth Laboratories, Huntercombe Lane South, Maidenhead, Berks, SL6 0PH (Gt. Britain)

W. FRANKLIN SMYTH

Department of Chemistry, University College Cork, Cork (Eire)

(Received 9th June 1980)

SUMMARY

Some 2-thiobarbituric acid and thioamide drugs are determined voltammetrically in a flow-through cell. Both direct oxidation in the d.c. mode and cathodic stripping on a mercury-coated glassy carbon electrode are examined for the determination of these drugs. The thiobarbituric acids can be determined by both methods; the linear range covers 1–2 orders of magnitude with a detection limit in the range 10^{-8} – 10^{-6} M depending on the method used and the compound. The thioamides do not plate satisfactorily on the mercury film when operated in the on-line mode and can only be determined by the d.c. anodic oxidation method; the linear range covers at least two orders of magnitude with a detection limit of 5×10^{-8} – 5×10^{-7} M depending on the compound.

The electrochemical behaviour of some sulphur-containing drugs has been studied both at dropping and hanging mercury drop electrodes in quiescent and stirred solutions [1–4]. The aim of the present work is to extend these studies by using a voltammetric flow-through cell in on-line analysis for some of those drugs. The applicability of such a technique has already been evaluated [5]. The working electrode employed is a glassy carbon electrode with a mercury film electrolyzed thereon. The most serious disadvantage with solid electrodes compared with a dropping electrode is the non-renewal of their surface but there are several advantages with the use of such a solid electrode rather than a hanging mercury drop in flowing streams. Solid electrodes are easier to handle and thus the construction of the flow-through cell is simpler. In addition, the surface area of a solid electrode is constant while both hanging and dropping mercury electrodes are subject to drop shape distortion; there is no dislodgement problem. High flow-rates can be

used with solid electrodes, increasing the sensitivity of the method because of the increase in mass transport to the electrode surface.

Both d.c. oxidation at a fixed potential and cathodic stripping on a mercury film can be used for determinations of the sulphur-containing drugs. The applicability of these two methods and a comparison with voltammetric methods in quiescent and stirred solutions are described in this paper.

EXPERIMENTAL

Apparatus

The electrochemical flow-through cell used in this work was of the wall-jet type; its performance and usefulness have already been evaluated [5]. The incoming solution impinges on the surface of the working electrode which in this case is a mercury-coated glassy carbon electrode of 3 mm diameter. The platinum auxiliary electrode is placed near the working electrode and when the solution leaves the cell it passes the tip of the saturated calomel reference electrode. The working electrode is therefore not contaminated by the reference electrode, a factor which is particularly important when a mercury coated electrode is used at positive potentials, with calomel being a possible surface contaminant. All potentials in this work are measured against the saturated calomel electrode. The cell volume is adjustable; a volume of about 80 μ l was normally used for this work. A PAR 174A polarograph was used in the voltammetric measurements. The solutions were either pumped to the cell with a 3-roller peristaltic pump with variable rotation speed, or allowed to flow under gravity from elevated electrolyte and sample containers. This resulted in flow-rates of 2–5 ml min⁻¹ being used. The currents were recorded with a strip chart recorder and measurements were done at 22°C.

Reagents

A 0.01 M mercury(II) nitrate solution in 0.05 M nitric acid and Britton—Robinson (BR) buffers of pH 4.0, 8.0 and 11.0 were all prepared from analytical-grade chemicals.

The 2-thiobarbituric acid solutions in the appropriate BR buffers contained 10% (v/v) methanol (analytical grade) to keep them in solution and to aid in the removal of organic contaminants from the electrode surface. The thioamides tested were water-soluble and so methanol was not added.

The four 2-thiobarbituric acid derivatives studied were obtained from J.C.S. Pharmaceuticals (Macclesfield, England) and the three thioamides from Wyeth Laboratories (Maidenhead, England).

Plating of the mercury film

A new mercury film was plated daily on the glassy carbon electrode; this ensured that reproducible results were obtained during the study. The old film was mechanically removed by rubbing the electrode with tissue paper

moistened with methanol. The glassy carbon was then polished by rubbing gently with very fine-textured pumice stone until the electrode surface was mirror-like prior to deposition of new mercury surface layer. If anomalous results were obtained at any time, a new film was immediately deposited. Electrochemical removal of the mercury film by holding the electrode at +1.0 V for 20 min was also tested but this procedure yielded irreproducible results.

Procedure

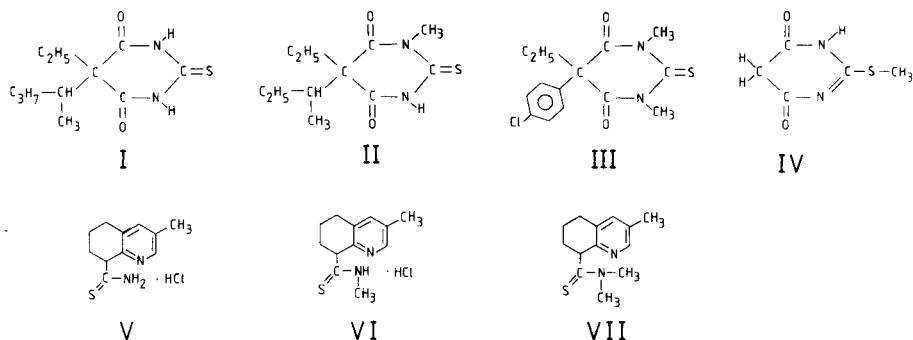
For d.c. anodic oxidation, the supporting electrolyte solution was pumped through the cell. After a steady background current had been obtained, the flow was changed to the analyte solution in the supporting electrolyte and the current change was recorded. The supporting electrolyte was passed through the cell between samples. When high current ranges were used, a steady background current was obtained immediately. A current range setting of $0.1 \mu\text{A}$ was the lowest that was practical; at this setting it took about 2 min to achieve a steady background current for the buffer solution. When the current range was kept constant for a series of different concentrations of the same electroactive compound, the background current reached its steady-state value in about 20 s after the changeover from the analyte to the supporting electrolyte solution.

In the cathodic stripping method, the supporting electrolyte solution was first pumped through the cell with an applied potential of -1.0 V for 1 min; then the pump was stopped and the applied potential switched off. The analyte was then pumped through the cell while the applied potential was still at the "off" position. After 1 min the chosen plating potential ($+0.15$ to $+0.2 \text{ V}$) was applied to the working electrode for 4 min. During the plating period, the flow-rate was kept constant. At the end of the plating time, the applied potential was switched off and the pump was stopped. The solution of the supporting electrolyte was then pumped through the cell while the applied potential to the electrode was still at the "off" position. It was found that no potential should be applied to the electrode (not even the plating potential) when the flow was changed from the analyte to the buffer, otherwise no stripping current was observed. After the buffer had been passed through the cell for 1 min, the pump was stopped. The stripping process was then initiated by scanning the potential from the plating potential to -0.8 V at a scan rate of 10 mV s^{-1} during which the stripping voltammogram was recorded.

RESULTS AND DISCUSSION

The compounds studied in this work were 5-ethyl-5'-(1-methylbutyl)-2-thiobarbituric acid (I), 1-methyl-5-ethyl-5'-(1-methylpropyl)-2-thiobarbituric acid (II), 1,3-dimethyl-5-ethyl-5'-(*p*-chlorophenyl)-2-thiobarbituric acid (III), 2-methyl-thiobarbituric acid (IV), 5,6,7,8-tetrahydro-3-methylquinoline-8-thiocarboxamide hydrochloride (V), 5,6,7,8-tetrahydro-3-methylquinoline-

8-(N-methyl)-thiocarboxamide hydrochloride (VI) and 5,6,7,8-tetrahydro-3-methylquinoline-8-(N-dimethyl)-thiocarboxamide (VII).



D.c. anodic oxidation method

A voltammogram of compound I under hydrodynamic conditions is shown in Fig. 1(a). The voltammogram was recorded at pH 8, which had been shown [6] to be the optimum pH value for analytical application of anodic oxidation of compounds I, II and III in quiescent solutions whereas pH 11 was preferable for compound IV. The voltammograms of compounds II and III under hydrodynamic conditions were quite similar in shape and exhibited the anodic wave at the same potential. Compound IV, however, did not give any anodic wave under the hydrodynamic conditions employed whereas in quiescent solutions it gave a well defined oxidation wave at the hanging

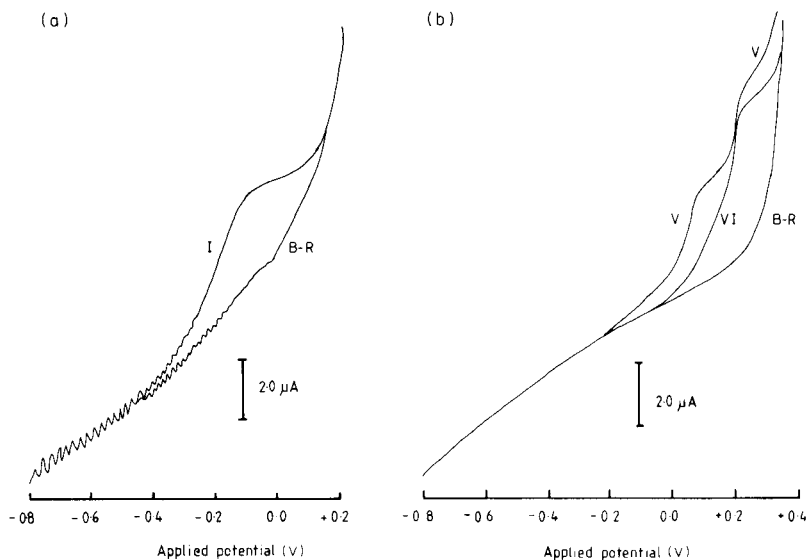


Fig. 1. Hydrodynamic d.c. voltammograms of (a) 1.0×10^{-4} M solution of compound I and pH 8 Britton-Robinson buffer, both solutions containing 10% (v/v) methanol; (b) 1.0×10^{-4} M solution of compounds V and VI and pH 4 Britton-Robinson buffer.

mercury drop electrode [6]. The voltammogram in Fig. 1(a) was obtained while the solution was pumped through the cell. Pressure pulses caused by the peristaltic pump are clearly observable as current fluctuations and are more pronounced at negative potentials. The thioamides (compounds V, VI and VII) were examined by hydrodynamic voltammetry at pH 4; this pH was chosen following studies in quiescent solutions [7]. The voltammograms of compounds V and VI under hydrodynamic conditions are shown in Fig. 1(b). In these studies of thioamides, the flow through the cell was achieved by gravity, and therefore no fluctuations in the current were obtained even at negative potentials. The anodic wave obtained with compound VII under hydrodynamic conditions was so poorly defined that it could not be used for subsequent analytical studies.

The potential applied to the working electrode in the d.c. oxidation method should be chosen to achieve maximum difference between the sample and the supporting electrolyte currents. Application of this principle to the thioamides caused no problems, but with the 2-thiobarbituric acid derivatives, reduction of oxygen interfered at -0.1 V, the potential at which the highest net current would be obtained. Rather than purge the samples with nitrogen to avoid the oxygen interference, a more positive potential was chosen. Thus the 2-thiobarbituric acid derivatives were studied at $+0.1$ V and the thioamides (compounds V and VI) at $+0.25$ V and $+0.20$ V, respectively.

Results of the d.c. oxidation studies are summarized in Table 1, which includes the experimental conditions, the ranges within which linear relationships were obtained between the faradaic current and the concentrations of the different depolarizers, and the detection limits for the compounds studied. The poor responses for compounds IV and VII made it unprofitable to study them further by the on-line system. The relative standard deviations at different concentrations of the studied compounds are given in Table 2.

Compound IV was found not to give any current by the hydrodynamic d.c. voltammetric technique at any concentration level over the pH range 8–11 with Britton–Robinson buffers. This is contrary to the polarographic

TABLE 1

D.c. anodic oxidation at the mercury film electrode

Compound	Applied potential (V)	pH	Linear range (M)	Detection limit (M)
I	+0.1	8	1×10^{-6} – 1×10^{-4}	5×10^{-7}
II	+0.1	8	5×10^{-6} – 1×10^{-4}	1×10^{-6}
III	+0.1	8	5×10^{-6} – 5×10^{-5}	2×10^{-6}
IV	+0.1	11	No reaction	
V	+0.25	4	5×10^{-8} – 1×10^{-5}	5×10^{-8}
VI	+0.2	4	1×10^{-6} – 1×10^{-4}	5×10^{-7}
VII	+0.2	4	No reaction	

TABLE 2

Relative standard deviation (r.s.d.)^a of the measured current in the on-line d.c. anodic oxidation methods for compounds I, II, III, V and VI

Concn. (M)	R.s.d. (%) for					Concn. (M)	R.s.d. (%) for				
	I	II	III	V	VI		I	II	III	V	VI
1×10^{-4}	13	11	—	—	2	1×10^{-6}	7	20	—	4	5
5×10^{-5}	15	3	6	—	1	5×10^{-7}	—	—	—	10	10
1×10^{-5}	32	3	22	12	4	1×10^{-7}	—	—	—	8	—
5×10^{-6}	14	11	39	2	1	5×10^{-8}	—	—	—	37	—

^aFor 8 replicate determinations of each analyte.

investigation of this compound in quiescent solutions [4]. The structure of compound IV is different from that of compounds I, II and III in that the sulphur atom at the 2-position has a substituent methyl group which prevents its reaction with mercury to form an adsorbable compound as for compounds I, II and III. The anodic reaction of compound IV [4] must therefore be different from those of compounds I, II and III with the reactant and/or product adsorption being significantly diminished.

The upper limits of the linear ranges of the 2-thiobarbituric acid derivatives are determined by their solubility in aqueous supporting electrolytes. Thioamides, existing as hydrochlorides, are quite soluble in these electrolytes but at high concentrations the electrode surface became fouled, which caused decreasing signals unsuitable for analytical purposes. The fouling may be due to adsorption of the thioamide on the mercury surface as a result of chemical reaction [8]. Alternatively, the product of the electrochemical reaction may adsorb on the surface and so prevent further thioamide molecules reacting. The upper limits given for the linear ranges of the thioamides are concentrations where an almost constant signal was observed.

The rather high relative standard deviations obtained with the 2-thiobarbituric acid derivatives probably result from uneven rotation of the peristaltic pump; the gravity flow used for the thioamides gave an even flow, resulting in lower relative standard deviations. The thioamide compound V fouled the electrode surface at even lower concentrations than compound VI; this is reflected in the relative standard deviation at the 10^{-5} M level which was the highest concentration suitable for the proposed method.

Calibration plots of $\log i$ vs. $\log C$ for all the studied compounds were linear with a slope of 1, indicating that the electrochemical reaction on the mercury film was diffusion-controlled in the on-line system studied.

Cathodic stripping method

The voltammetric flow-through cell can also be applied to cathodic stripping [5]. In this work, compounds I, II, III, V and VI were studied. From the d.c. voltammograms (Fig. 1), a plating potential of +0.15 V was used for the 2-thiobarbituric acid derivatives and +0.2 V for the thioamides. In cathodic stripping, the cell volume was increased to ca. 100 μ l, so that the flow velocity near the surface was reduced allowing the products of electrolysis to be adsorbed on the mercury film. In the d.c. oxidation method, it was better to have small cell volumes so that the high flow velocity near the surface removed some of the electrochemical reaction products and cleaned the electrode surface mechanically. Results from the cathodic stripping analysis are given in Tables 3 and 4.

The fact that the thioamides do not plate on the mercury film in the flowing stream (Table 3) can be attributed to the inability of the plated compound to adhere satisfactorily to the mercury film. Although some electrolysis must take place, the plated compound is probably swept away from the surface by the stream. Plating was slightly improved by increasing the cell volume, but even with large cell volumes results were not reproducible.

The 2-thiobarbituric acid derivatives plated well on the mercury film except for compound IV; the reason is probably the same as outlined above

TABLE 3

Cathodic stripping from the mercury film electrode

Compound	pH	Plating potential (V)	Stripping potential (V)	Linear range (M)	Detection limit (M)
I	8	+0.15	-0.1	5×10^{-6} — 5×10^{-5}	5×10^{-6}
II	8	+0.15	-0.65	1×10^{-7} — 1×10^{-5}	1×10^{-8}
III	8	+0.15	-0.63	5×10^{-7} — 2×10^{-5}	1×10^{-7}
IV	4-8	+0.2	— ^a	—	—
V	4-8	+0.2	— ^a	—	—

^aDid not plate.

TABLE 4

Relative standard deviation (r.s.d.)^a of the measured current in the on-line cathodic stripping method for compounds I-III

Concn. (M)	5×10^{-5}	1×10^{-5}	5×10^{-6}	1×10^{-6}	5×10^{-7}	1×10^{-7}	5×10^{-8}	1×10^{-8}
R.s.d. (%)								
I	22	19	12	—	—	—	—	—
II	—	3	—	5	6	8	3	8
III	—	12	10	24	22	—	—	—

^aFor 5 replicate determinations of each analyte.

for thioamides. In quiescent solution, compound IV can be plated onto a hanging mercury drop [4]. Compound II was found to plate most satisfactorily, giving the smallest relative standard deviation and lowest detection limit of the compounds studied.

It can be seen from the stripping potentials in Table 3 that the products of electrolysis of compounds II and III are the same; from the potential value HgS would appear to be the most probable product [1]. Compound I behaves differently, and presumably forms a mercury thiobarbiturate as observed in quiescent solutions [4].

The relative standard deviations in the determination of compounds I and III are larger than those for compound II; this may indicate stronger adsorption of compound II and so more reproducible stripping currents. However, when the linear calibration plots for compounds I, II and III were transformed to $\log i$ vs. $\log C$ plots, the slope of the line with compound I was approximately 1 whereas slopes of 0.7 were found for compounds II and III. Thus although plating of compounds II and III is reproducible, it is not quantitative because the stripping current is proportional to the bulk concentration to the power of 0.7 instead of 1 [9]. Clearly, the theoretical explanation of the plating and stripping processes is not simple.

Conclusions

Hydrodynamic d.c. voltammetry is successful for the determination of some 2-thiobarbituric acid derivatives and thioamides. The increased sensitivity for most of the compounds (see Table 5) is mainly due to the hydrodynamic nature of the flowing stream compared to voltammetry in quiescent solution. Several factors influence the improved sensitivity. The diffusion layer adjacent to the electrode becomes very thin, allowing fast diffusion of the electroactive molecules to the electrode surface, i.e., improved mass transport from the solution to the electrode. The greater surface area of a solid electrode compared with a dropping mercury electrode, provides a further increase in sensitivity. With application of a constant potential, no

TABLE 5

Linear concentration ranges for the determination of some sulphur-containing organic compounds by static [6, 7] and on-line voltammetric methods
(Oxidation processes were used except where stated)

Compound	Linear concentration range (M)			
	Refs. [6, 7]		This work	
	D.p.p.	Cathodic stripping	D.c.	Cathodic stripping
I	2×10^{-5} – 1×10^{-4}	1×10^{-6} – 1×10^{-5}	1×10^{-6} – 1×10^{-4}	5×10^{-6} – 5×10^{-5}
II	5×10^{-6} – 4×10^{-5}	2×10^{-6} – 1×10^{-5}	5×10^{-6} – 1×10^{-4}	1×10^{-7} – 1×10^{-5}
III	5×10^{-6} – 4×10^{-5}	1×10^{-6} – 6×10^{-6}	5×10^{-6} – 5×10^{-5}	5×10^{-7} – 2×10^{-5}
V	5×10^{-7} – 5×10^{-6}	5×10^{-8} – 1×10^{-6}	5×10^{-8} – 1×10^{-5}	—

current is needed to charge the double layer, and this decreases the background current, providing a greater net current.

As demonstrated above, sulphur-containing compounds forming a mercury salt can be determined by on-line methods either by direct oxidation on the mercury film or by cathodic stripping. Although a compound may give a well-defined response in quiescent solution, its determination by on-line methods may fail, as demonstrated with compound IV in the d.c. oxidation mode. Compounds I, II and III can be determined by on-line cathodic stripping whereas compounds V and VI give poor results although they have been determined successfully by cathodic stripping in rather complex matrices in quiescent solutions [1].

The compounds studied usually exhibit larger linear concentration ranges and lower detection limits with the proposed on-line methods than for the determinations in quiescent solution. The detection limit of compound V with the on-line d.c. oxidation method is, in fact, similar to that of the cathodic stripping method in quiescent solution [1].

The noise from the peristaltic pump is a serious limitation of the proposed method. It can be overcome by using gravity flow, but further development is required before the method can be fully automated.

REFERENCES

- 1 I. E. Davidson and W. F. Smyth, *Anal. Chem.*, 49 (1977) 1195.
- 2 W. F. Smyth and I. E. Davidson, in W. F. Smyth (Ed.), *Electroanalysis in Hygiene, Environmental, Clinical and Pharmaceutical Chemistry*, Elsevier, Amsterdam, 1979.
- 3 I. E. Davidson, in W. F. Smyth (Ed.), *Polarography of Molecules of Biological Significance*, Academic Press, London, 1979.
- 4 Y. Vaneesorn and W. F. Smyth, *Anal. Chim. Acta*, 117 (1980) 183.
- 5 A. Ivaska and W. F. Smyth, *Anal. Chim. Acta*, 114 (1980) 283.
- 6 Y. Vaneesorn, PhD Thesis, Chelsea College, University of London, 1979.
- 7 I. E. Davidson, PhD Thesis, Chelsea College, University of London, 1979.
- 8 A. J. Hall and D. P. N. Satchell, *J. Chem. Soc. Perkin Trans. 2*, (1975) 778.
- 9 W. J. Blaedel and J. Wang, *Anal. Chem.*, 51 (1979) 1724.

AUTOMATED POTENTIOMETRIC DETERMINATION OF GLUCOSE OXIDASE ACTIVITY WITH A GAS-SENSING SULPHUR DIOXIDE PROBE

P. W. ALEXANDER* and P. SEEGOPPAUL

Department of Analytical Chemistry, University of New South Wales, P.O. Box 1, Kensington, 2033 N.S.W. (Australia)

(Received 23rd April 1980)

SUMMARY

A sulphur dioxide probe is utilised as a sensor in an automated, continuous-flow system for the determination of glucose oxidase. The analytical method is based on a coupled indicator reaction scheme in which the product of the enzymatic reaction (hydrogen peroxide) oxidises hydrogensulphite ions. The change in concentration of hydrogensulphite is then measured with the SO_2 probe. The method is shown to be sufficiently sensitive to detect 0.01 IU ml^{-1} of the enzyme with few interference problems at sampling rates of up to 90 samples per hour.

A variety of electrochemical methods has been developed for the determination of the activity of enzymes in solution. Glucose oxidase in particular has been the subject of a large number of studies using electrodes including the Clark oxygen electrode [1], amperometric [2, 3], potentiometric [4, 5], and ion-selective electrode methods. [6].

The advantages offered by gas-sensing electrode methods [1, 7] or the air-gap electrode system [8] for determination of enzyme activity are mainly associated with better tolerance of interferences. A number of enzyme methods for substrate determinations have been developed by immobilising the enzyme at the surface of the probe. The ammonia gas electrode has been used for the determination of urea in an automated continuous-flow system [9], and also for the determination of urea after immobilising urease on the surface of the ammonia-permeable membrane [10]. A carbon dioxide sensor was used to prepare electrodes sensitive to urea [11], L-tyrosine [11] and uric acid [12], by coupling an immobilised layer of the appropriate enzyme to the surface of the sensor. An air-gap system with a glass electrode as sensor was used to determine urea in whole blood, plasma and serum [13].

The sulphur dioxide probe has not been reported, however, as a sensor for enzyme or substrate determinations. A new coupled-indicator reaction method for monitoring the rate of the glucose oxidase-catalysed reaction utilising the SO_2 probe is reported here. The method is based on the conversion of unreacted hydrogensulphite ions to sulphur dioxide after reaction of

excess of hydrogensulphite with the hydrogen peroxide produced by the enzymatic reaction. In this study, the performance of the probe in a continuous-flow system is reported for fixed-time kinetic determination of glucose oxidase activity. The use of the probe gives high sensitivity and rapid response times for the determination of glucose oxidase activity, with little interference from associated organic molecules.

EXPERIMENTAL

Reagents and solutions

Reagent solutions were prepared from analytical reagent-grade chemicals without further purification. The hydrogensulphite solutions were prepared by serial dilutions of freshly-made 0.1 M sodium metabisulphite in distilled water. The substrate, D(+)-glucose (BDH), was prepared in 0.1 M Na_2HPO_4 — KH_2PO_4 buffer [14] of the appropriate pH to give a final concentration of 0.1 M glucose. The substrate solution was refrigerated overnight for mutarotation equilibrium.

Grade A glucose oxidase (β -D-glucose; oxygen oxidoreductase, GOD, E.C.1.1.3.4) was obtained from Calbiochem, with specific activity given as 123 IU mg^{-1} at 30°C (glucose as substrate). The enzyme solutions were made up in distilled water by dilution of a stock standard of 12.3 IU ml^{-1} . In order to eliminate the catalase impurity present in the enzyme preparation, the stock enzyme solution was allowed to stand at room temperature for at least 36 h.

For interference studies, ascorbic acid and cysteine (Nutritional Biochemical Corporation) and human and bovine albumin (Fract. V; Miles Laboratories Inc.) were used.

Instrumentation

The continuous-flow system for the enzyme analysis is shown in Fig. 1. The system consisted of a Watson—Marlow peristaltic pump, a water-bath for temperature control, an electrode assembly, a pH/mV meter and an mV recorder. The sensing electrode assembly was made up of an E.I.L. Model No. 8010-8 sulphur dioxide probe fitted with a flow-through cap with a dead volume of about 0.1 ml. E.I.L. (Part No. 8010-240) internal filling solution was used to fill the probe after addition of glucose to the solution to give a final concentration of 0.06 M in the probe. This gave a concentration of glucose within the probe approximately equal to its concentration in the substrate stream. The probe potential in mV was continuously monitored with a Radiometer pHM62 pH/mV meter coupled to a National strip chart recorder, Type UP-6511A.

Procedure

The reagent solutions were initially pumped through the flow-cell continuously at a fixed flow rate to establish a base-line potential with a water

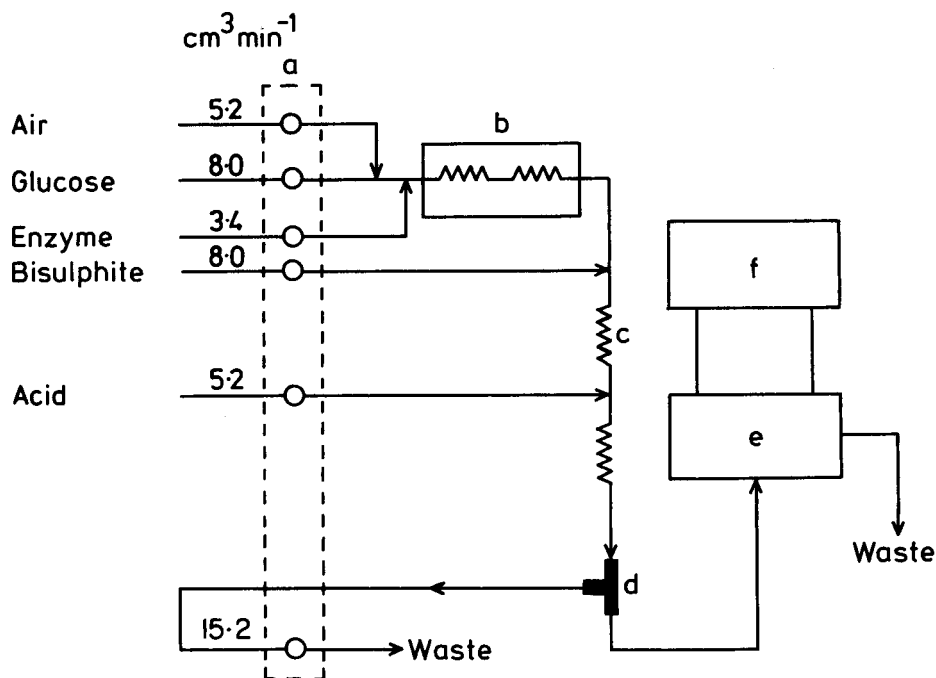


Fig. 1. Schematic diagram of the continuous-flow apparatus. Total flow rate across probe, $15.0 \text{ cm}^3 \text{ min}^{-1}$. (a) Peristaltic pump; (b) water bath; (c) mixing coil; (d) debubbler; (e) electrode assembly; (f) pH/mV recorder.

blank. Unless otherwise mentioned, the reagent concentrations used in the flow system shown in Fig. 1 were: $2.0 \times 10^{-4} \text{ M}$ sodium metabisulphite, 0.1 M glucose solution buffered at pH 5.6 in a solution of $0.1 \text{ M Na}_2\text{HPO}_4$ — $0.1 \text{ M KH}_2\text{PO}_4$, and $1.5 \text{ M H}_2\text{SO}_4$ concentration. The enzyme sample solutions were then manually aspirated into the stream of continuously flowing, air-segmented substrate solution, followed by a water wash after each sample. Sampling times were varied from 30 s to 10 s with a 1:1 sample-to-wash ratio in order to obtain effective sampling rates in the range 60–180 samples per hour.

The solution in which the enzyme-catalysed reaction proceeded was incubated in the mixing coils for 1 min at a fixed temperature and then mixed with hydrogensulphite ions. Sulphuric acid was pumped into the flowing stream to quench the enzyme reaction and to convert the excess of hydrogensulphite to sulphur dioxide. The stream was debubbled by pumping the air and some of the solution to waste, and then fed through the flow cell.

RESULTS

The performance of the SO_2 probe in the continuous-flow analysis system was evaluated first by measuring the response for standard hydrogensulphite solutions at various sampling rates. The response of the probe as a sensor for the enzymatic reaction was then studied using the flow manifold shown in Fig. 1. Optimum reaction conditions for both the enzyme and indicator reactions were determined, and interference effects on the enzyme reaction were studied in the flow system.

Response times

Standard hydrogensulphite solutions were initially pumped directly through the probe for response-time studies. Figure 2 shows the continuous chart readout for sampling of these solutions in the range 5.0×10^{-4} – 1.0×10^{-2} M, at 60 samples per hour. The data from Fig. 2 indicated that the response of the probe was sufficiently rapid to reach 98% of the steady-state potential with a sampling precision of $\pm 0.5\%$ r.s.d. Consecutive samples interacted to some extent, giving a % carry-over of 1.0%, as shown in Fig. 2B. The slope

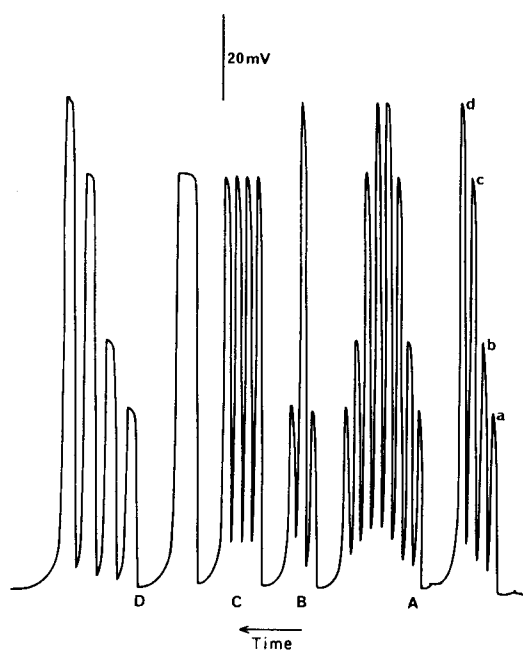


Fig. 2. Continuous-flow recording of hydrogensulphite samples at 60 h^{-1} and a flow rate of $15.0 \text{ cm}^3 \text{ min}^{-1}$ across the probe. (A) Calibration in direction of increasing and decreasing concentrations; (B) illustrates carry-over between consecutive samples; (C) replicate measurements; (D) steady-state potentials. (a) $5.0 \times 10^{-4} \text{ M}$; (b) $1.0 \times 10^{-3} \text{ M}$; (c) $5.0 \times 10^{-3} \text{ M}$; (d) $1.0 \times 10^{-2} \text{ M S}_2\text{O}_3^{2-}$.

for the calibration in Fig. 2A was 57.5 mV per decade at 20°C, as expected for Nernstian response of the probe to sulphur dioxide.

Table 1 shows the results of varying the sampling rate for a flow rate of 15.0 cm³ min⁻¹. At sampling rates in the range 30–180 h⁻¹, greater than 90% of the steady-state potential was recorded and the r.s.d. ranged from ±0.2% to ±2.2%. However, the sample interaction was unacceptable at the high sampling rates, giving 9.0% carry-over at 180 samples per hour.

Table 2 shows the data obtained for response-time studies over a range of solution flow rates at 60 samples per hour. The response decreased at slow flows and only 87.6% of the steady-state potential was obtained at a flow rate of 3.5 cm³ min⁻¹. Increased carry-over and decreased precision were also observed.

Response to enzyme solutions

The flow system shown in Fig. 1. was used to detect the sulphur dioxide produced in the following reaction sequence:

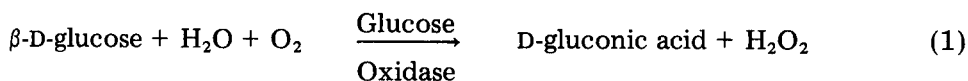


TABLE 1

Performance of the SO₂ probe under continuous-flow conditions at various sampling rates. Total flow rate was 15.0 cm³ min⁻¹

Sampling rate (samples h ⁻¹)	% Steady-state potential	% R.s.d.	% Carry-over
30	99.6	0.2	<1.0
60	98.8	0.5	1.0
90	97.9	0.9	1.8
120	97.1	1.4	4.9
180	93.0	2.2	9.0

TABLE 2

Effect of solution flow rates on response time of the SO₂ probe at 60 samples h⁻¹

Flow rate (cm ³ min ⁻¹)	% Steady-state potential	% R.s.d.	% Carry-over
20.0	>99.0	0.7	1.0
17.0	98.5	0.7	1.1
12.4	98.0	0.8	1.8
8.7	94.2	1.4	2.8
3.5	87.6	2.6	6.6

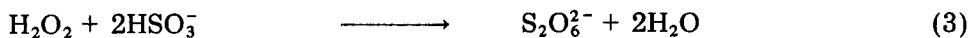


Figure 3 gives the continuous chart readout from the SO_2 probe response to enzyme sample solutions fed into the system with a 1:1 sample-to-wash ratio. It shows that the peak-height response to enzyme activity was linear in the range $0.11\text{--}0.74\text{ IU ml}^{-1}$. Comparisons of Figs. 3C and D show that the sample peaks reached 96% of the steady-state potential with a r.s.d. of $\pm 0.5\%$. Figure 3C shows 1.0% carry-over for a high sample activity preceding a low sample. Figure 4 shows the chart readout for sampling enzyme solutions at 90 h^{-1} , operating at 90% of the steady-state potential, without affecting the precision.

Random sampling of enzyme solutions gave relative errors in activity of $0.2\text{--}6.0\%$, as shown in Fig. 3 and Table 3. The errors were calculated by comparing the peak heights for samples measured randomly as in Fig. 3B, rather than in an ordered manner as in Fig. 3A. The response of the probe to changes in enzyme activity was therefore found to be rapid enough to

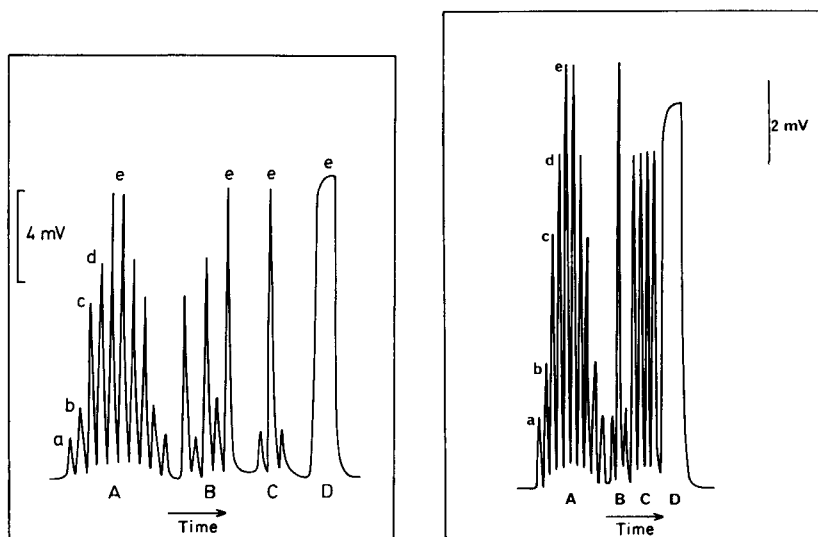


Fig. 3. Continuous-flow recording of glucose oxidase at 60 samples h^{-1} and a base-line concentration of $2.0 \times 10^{-4}\text{ M S}_2\text{O}_6^{2-}$. (A) Calibrations in direction of increasing and decreasing concentrations; (B) random samples; (C) carry-over between consecutive samples; (D) steady-state potential given by $0.74\text{ IU ml}^{-1}\text{ GOD}$. (a) 0.11 ; (b) 0.19 ; (c) 0.48 ; (d) 0.56 ; (e) $0.74\text{ IU ml}^{-1}\text{ GOD}$; $\text{H}_2\text{SO}_4 = 1.5\text{ M}$; glucose = 0.1 M .

Fig. 4. Continuous-flow recording of glucose oxidase at 90 samples h^{-1} with a base-line concentration of $4.0 \times 10^{-4}\text{ M S}_2\text{O}_6^{2-}$. (A) Calibrations in direction of increasing and decreasing concentrations; (B) carry-over between consecutive samples; (C) replicate measurements; (D) steady-state value given by $0.97\text{ IU ml}^{-1}\text{ GOD}$. (a) 0.19 ; (b) 0.36 ; (c) 0.74 ; (d) 0.97 ; (e) $1.2\text{ IU ml}^{-1}\text{ GOD}$; $\text{H}_2\text{SO}_4 = 1.5\text{ M}$; glucose = 0.1 M .

TABLE 3

Relative error in random enzyme samples under continuous-flow conditions at 60 samples h⁻¹

Enzyme activity (IU ml ⁻¹)		Relative error (%)	Enzyme activity (IU ml ⁻¹)		Relative error (%)
Taken	Found		Taken	Found	
0.110	0.116	5.5	0.560	0.561	0.2
0.190	0.201	6.0	0.730	0.747	2.3
0.480	0.487	1.5			

operate at 60 samples per hour without reducing the accuracy or precision of determination of enzyme activity. Operation at 90 samples per hour was also possible with good precision but with carry-over reaching 2%.

Optimization of enzyme reaction conditions

The results shown in Figs. 3 and 4 were obtained using experimental conditions found to give optimum sensitivity of the probe response to changes in enzyme activity. To optimize the enzyme reaction conditions, the effects of incubation temperature, buffer composition and pH were studied.

The rate of the enzyme-catalysed reaction of 0.1 M β -D-glucose was monitored after a fixed 1-min incubation after sampling 0.82 IU ml⁻¹ enzyme under various conditions. Figure 5 shows the effect of incubation temperature on the peak height and indicates maximum reaction rate at 40°C.

The peak height was also recorded at different pH values in 0.1 M phosphate buffer. It was found that pH 5.6 gave greatest sensitivity. Acetate buffer at pH 5.6 gave less sensitivity because of acetic acid interference with the sulphur dioxide probe.

Indicator reaction conditions

As shown in Fig. 1, hydrogensulphite solution and acid were fed into the enzyme reaction stream after the incubation stage. The hydrogen peroxide produced by the enzyme reaction was destroyed by the hydrogensulphite. Figure 6 shows the effect of varying the hydrogensulphite concentration on the peak height. Greatest sensitivity was found with $0.8\text{--}1.0 \times 10^{-4}$ M hydrogensulphite. However, the probe response was found to be slow in this range. Some sensitivity was therefore sacrificed by choosing a higher hydrogensulphite concentration to obtain a more rapid response.

The sulphuric acid concentration fed into the system was varied from 0.2–2.0 M while the other reagent concentrations were kept constant. The peak height for a fixed enzyme activity reached a maximum at 1.5 M acid concentration, which was used for conversion of unreacted hydrogensulphite to sulphur dioxide.

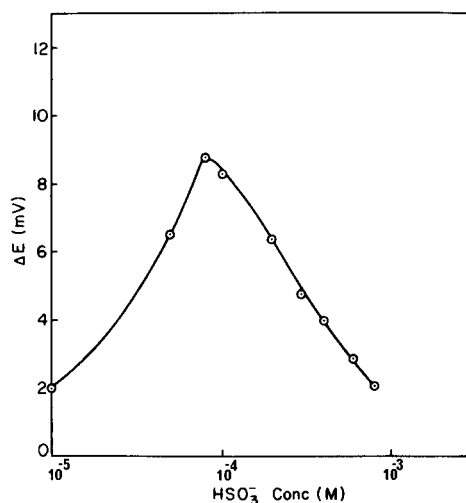
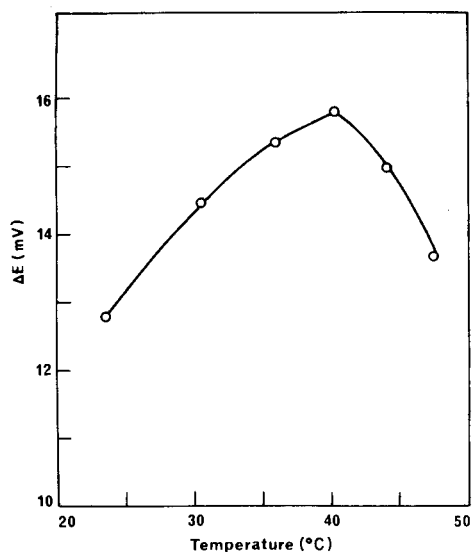


Fig. 5. Temperature dependence of the peak height at pH 5.6 and an incubation time of 1 min with 0.82 IU ml⁻¹ GOD and base-line concentration of 2.0×10^{-4} M $S_2O_5^{2-}$.

Fig. 6. Effect of hydrogensulphite concentration on sensitivity of glucose oxidase measurements at 60 samples h⁻¹ at an enzyme activity of 0.30 IU ml⁻¹.

Interference studies

The effects of various possible interfering species on the peak height of 0.24 IU ml⁻¹ glucose oxidase activity at 60 samples per hour is shown in Table 4. Reducing substances such as ascorbic acid and cysteine interfere in spectrophotometric procedures [15] but a large excess of these substances had no effect on the peak height in the present method. Similarly, for concentrations as high as 1000:1 in excess of the enzyme, urea, sodium chloride, human albumin, and bovine albumin had no effect.

TABLE 4

Effects of other compounds on the enzyme reaction under continuous-flow conditions at 60 samples h⁻¹ and pH 5.6 (Base-line concentration of $S_2O_5^{2-} = 2.0 \times 10^{-4}$ M)

Compound	Concentration (g l ⁻¹)	Peak height (mV) ^a	Compound	Concentration (g l ⁻¹)	Peak height (mV) ^a
—	—	4.0	Sodium chloride	7.0	4.1
Ascorbic acid	0.65	4.0	Human albumin	1.0	3.9
Urea	48	4.0	Bovine albumin	1.0	4.0
Cysteine thiolactone	1.6	3.9			

^aEnzyme activity = 0.24 IU ml⁻¹.

DISCUSSION

The automated continuous-flow system described here has allowed the development of a simple, rapid method for the determination of glucose oxidase activity. The response time was fast enough to allow sampling rates of up to 90 per hour. Bailey and Riley [16] have reported that the more important factors governing the response time of the gas probe are the partition coefficient of the gas between the membrane and the sample, the diffusion coefficient of the gas in the membrane, and the membrane thickness. These parameters are related to the nature of the hydrophobic membrane. The response times of electrode sensors in flowing streams are also dependent on the dead volume of the flow-cell used [17]. It may be possible to decrease the volume of the cell used here and further improve the response time.

In comparison, other electrode methods reported for determination of glucose oxidase activity show similar response times. Llenado and Rechnitz [6] obtained sampling rates of more than 40 h^{-1} in an automated system with an iodide electrode, while Pardue et al. [5] reported measurement times of 10–100 s in an automatic potentiometric method. The oxygen electrode response was also reported to be rapid [18], giving a response time of 20 s. Most spectrophotometric methods used for the assay of glucose oxidase, involving peroxidase and a dye, can be carried out at 60 samples per hour.

An important factor affecting the performance of the sulphur dioxide probe was the effect of the osmotic strength on either side of the membrane. A large difference in osmotic strength resulted in serious drift which was eliminated or substantially reduced by the use of glucose in the internal filling solution to balance the osmotic strength of the test solution. The Nernstian response to sulphur dioxide concentration was not affected.

The most important advantage, however, of the present method is the freedom from interference from reducing substances and proteins. The work of Keilin and Hartree [19] has previously shown that the enzyme is specific for β -D-glucose. It therefore follows that interferences to the sulphur dioxide should be associated solely with the indicator reaction and the sensor used. In this method, interference problems have been shown to be minimal (Table 4). There are two reasons for this. They are the use of hydrogensulphite to reduce the hydrogen peroxide produced by the enzyme-catalysed reaction, and the use of the gas-permeable hydrophobic membrane in the probe assembly. Hydrogensulphite is a much stronger reducing agent than cysteine, ascorbic acid or urea. Hence, these weaker reducing agents do not interfere with the hydrogensulphite–peroxide reaction. In contrast, the effect of such reducing agents is a major source of interference in colorimetric methods for determination of glucose oxidase activity [15]. Reducing agents such as uric acid, ascorbic acid and glutathione interfere either by reducing the coloured oxidation product from the reaction of the dye (e.g. *o*-dianisidine), or by competing with the dye as a hydrogen donor for the enzyme reaction. The use of a gas-permeable hydrophobic membrane eliminates any contact

between the internal glass sensor and the reaction medium. This decreases the possibility of poisoning of the electrode.

The other important feature of the present method is its high sensitivity. The working range reported here as $0.1-0.7 \text{ IU ml}^{-1}$ is about the same as that reported for other ion-selective electrode methods [6] and colorimetric methods [20]. The sulphur dioxide sensor method is therefore selective and sensitive for determination of GOD activity and can be simply automated in a continuous-flow system. Further, it may be possible to apply the method for other enzyme reactions involving hydrogen peroxide formation, and to adapt the method for specific substrate determinations.

REFERENCES

- 1 A. Kadish and D. H. Hall, *Clin. Chem.*, 9 (1965) 869.
- 2 H. Pardue and R. Simon, *Anal. Biochem.*, 9 (1964) 204.
- 3 W. J. Blaedel and C. Olson, *Anal. Chem.*, 36 (1964) 343.
- 4 G. G. Guilbault, B. C. Tyson, D. N. Kramer and P. L. Canon, *Anal. Chem.*, 35 (1963) 582.
- 5 H. Pardue, R. Simon and H. V. Malmstadt, *Anal. Chem.*, 36 (1964) 735.
- 6 R. A. Llenado and G. A. Rechnitz, *Anal. Chem.*, 45 (1973) 826.
- 7 G. J. Moody and J. D. R. Thomas, *Analyst*, 100 (1975) 609.
- 8 J. Růžicka and E. H. Hansen, *Anal. Chim. Acta*, 69 (1974) 129.
- 9 R. A. Llenado and G. A. Rechnitz, *Anal. Chem.*, 46 (1974) 1109.
- 10 T. Anfalt, A. Graneli and D. Jagner, *Anal. Lett.*, 6 (1973) 969.
- 11 G. G. Guilbault and F. R. Shu, *Anal. Chem.*, 44 (1972) 2161.
- 12 G. A. Rechnitz and T. Kwashima, *Anal. Chim. Acta*, 83 (1976) 9.
- 13 E. H. Hansen and J. Růžicka, *Anal. Chim. Acta*, 72 (1974) 353.
- 14 G. Tors and P. G. Ackermann, *Practical Clinical Chemistry*, Little, Brown and Co., Boston, 1975, p. 734.
- 15 J. Okuda and I. Miwa, in D. Glick (Ed.), *Methods of Biochemical Analysis*, Vol. 21, J. Wiley, New York, 1973, p. 171.
- 16 P. L. Bailey and M. Riley, *Analyst*, 100 (1975) 145.
- 17 P. W. Alexander and P. Seegopaul, *Anal. Chem.*, Nov. 1980, in press.
- 18 A. Kadish, R. Little and J. Sternberg, *Clin. Chem.*, 14 (1968) 116.
- 19 D. Keilin and E. F. Hartree, *Biochem. J.*, 50 (1951) 331.
- 20 G. G. Guilbault, in M. K. Schwartz (Ed.), *Clinical and Biochemical Analysis*, Vol. 4, M. Dekker, New York, 1976, p. 106.

REDUCTIVE POTENTIOMETRIC STRIPPING ANALYSIS FOR ELEMENTS FORMING SPARINGLY SOLUBLE MERCURY COMPOUNDS WITH AMALGAMATED METAL AS THE REDUCING AGENT

JOAN KAI CHRISTENSEN, LARS KRYGER*, JOHN MORTENSEN and
JEAN RASMUSSEN

*Department of Chemistry, Aarhus University, Langelandsgade 140, 8000 Aarhus C
(Denmark)*

(Received 20th June 1980)

SUMMARY

The suitability of amalgamated metals as reducing agents in reductive potentiometric stripping analysis is demonstrated. The amalgams are generated in a mercury pool by electrolysis of dissolved metals. During the stripping process, the reducing agent, which is stored inside the working electrode, reacts with sparingly soluble mercury compounds of the analytes preconcentrated on the electrode surface. The importance of the timing of the processes involving amalgam formation and analyte preconcentration is discussed. With amalgamated sodium, the technique is suitable for the determination of selenium and sulphur at the 10^{-7} M level with 1–2 min preconcentration. Halides may be determined at the 10^{-6} M level with a few seconds of preconcentration; a less powerful reducing agent such as amalgamated zinc is then suitable.

Although potentiometric stripping analysis (p.s.a.) is a rather new electro-analytical approach to the determination of trace elements [1, 2], it appears to be as widely applicable as for example differential pulse stripping voltammetry. Most reports on p.s.a. have dealt with the determination of elements which can easily be reduced at and dissolved in a mercury electrode. The stripping, which is monitored potentiometrically, is caused by some oxidizing agent in the sample solution, and the time spent by the electrode at the redissolution potential of the analyte is taken as the analytical signal. Elements such as cadmium can be redissolved easily by an oxidizing agent, e.g., mercury(II), dissolved in the sample solution. Recently, it was shown that even reductive potentiometric stripping analysis is feasible: for example, with a suitable reducing agent, potentiometric stripping analysis for manganese preconcentrated anodically on a platinum electrode as manganese dioxide is possible [3]. Relatively mild reducing agents such as dissolved hydroquinone and pyrogallol are suitable reagents for the dissolution of manganese and lead deposited as the dioxides. For elements like selenium and sulphur, however, it is known that cathodic stripping voltammetry requires the voltammetric scans to be extended to rather (pH-dependent)

cathodic values to dissolve precipitates formed on the surface of a mercury electrode [4]. To carry out a potentiometric stripping analysis for such elements, very strong reducing agents are therefore required.

This paper demonstrates the feasibility of employing one of the most potent reducing agents known — amalgamated sodium — for reductive p.s.a. of analytes such as selenide and sulphide preconcentrated by precipitation on the surface of a mercury electrode. The stripping process involved is different from that described in previous reports on p.s.a.: with amalgamated sodium, the reducing agent is dissolved in the mercury electrode and the stripping of surface-deposited analytes is caused by amalgamated sodium being transported towards the electrode surface from the interior of the electrode. Halide—mercury complexes, which are redissolved at less cathodic potentials, may be determined by using dilute zinc amalgam in a similar fashion.

Potential strong reducing agents in reductive p.s.a. for elements like selenium and sulphur are tin(II), titanium(III) and sodium tetrahydroborate. These reagents are capable of reducing sulphur and selenium from the +4 oxidation state to sulphide and selenide [4]. Moreover, the reduction of mercury(II) to elemental mercury from a precipitate of mercury(II) sulphide is readily accomplished by the addition of sodium tetrahydroborate. The stability in aqueous solution of these reagents is, however, limited, and for lengthy periods of plating of the analyte, their bulk concentrations are likely to diminish significantly. This is unfortunate since for p.s.a. a constant concentration of the reagent causing the redissolution is necessary to obtain quantitative results. It is, therefore, advantageous to generate this agent electrolytically under well defined conditions and during a fixed period of time. Amalgamated sodium is readily generated by electrolysis at a mercury electrode at about -2 V vs. SCE in 1 M sodium hydroxide. In alkaline solution, hydrogen evolution at the mercury electrode takes place only at potentials even more cathodic, and a well defined amount of reducing agent can, therefore, be generated and stored inside the electrode. Moreover, a clean electrode can easily be regenerated simply by resetting the electrode potential to a more anodic value where the amalgamated sodium is oxidized.

Thus, when a suitable concentration of sodium amalgam has been generated, the plating of the analyte (e.g., selenide) is carried out at a more anodic potential. During this step, of course, a fraction of the amalgamated sodium is reoxidized, but with a sufficiently large electrode volume and a proper balancing of the times used for the amalgam generation and for the plating of the analyte, a well defined sodium amalgam concentration will remain even at the end of the plating of the analyte where the stripping begins.

During the stripping step, the amalgamated sodium diffuses from the interior of the mercury electrode towards the surface where redissolution of the analyte deposit takes place. For example, in the stripping of selenium in moderately alkaline medium:



It should be recognized that, during the plating and stripping, the selenium remains in the -2 oxidation state, while mercury(II) is reduced by amalgamated sodium. A similar scheme holds for sulphur.

The halides can be preconcentrated as mercury(I) salts and, since these salts redissolve at less cathodic potentials, electrolytically generated zinc amalgam can be used to dissolve the deposit in a similar fashion. Because of the low solubility of zinc sulphide and zinc selenide, zinc(II) cannot be used for amalgam generation in the determination of selenium and sulphur.

EXPERIMENTAL

Apparatus

The initial potentiometric stripping experiments were done by the simple voltmeter approach [1]. The apparatus comprised a laboratory-built potentiostat, a Radiometer PHM64 research pH meter and a Philips PM8132 X, Y_1, Y_2 recorder. During the later stages of the study, when the necessity of precise timing of the amalgam formation and the plating of the analytes became obvious, a general computerized device for electroanalytical work was employed. During the stripping step, this device, which has previously been reported [5, 6], monitors the potential distribution rather than the potential versus time behaviour of the working electrode, and the resulting potentiograms are equivalent to those obtained by differentiation with respect to potential of the conventional potentiograms.

Electrochemical cell. The electrochemical cell was a Radiometer TTA60 assembly, with a 60-ml beaker. The sample solution could be agitated by a PTFE stirrer bar. The working electrode was a small mercury pool (about 0.15 ml) placed in a conical cavity in the bottom of the beaker. Connection to the mercury pool was established via a platinum wire protruding through the bottom of the cavity. For a few experiments, a Metrohm EA290 hanging mercury drop electrode was used. The reference electrode was a Radiometer K401 saturated calomel electrode. The counter electrode was a platinum wire, 0.5 mm thick and 1 cm long.

To minimize contamination of the sample by the reference electrode, a glass funnel with a porous frit at the tip was filled with the electrolyte and inserted between the electrode and the sample solution. The same precaution was taken with the counter electrode to prevent carryover of anodic deposits formed on the platinum surface. Prior to analysis, solutions were deaerated with argon for 10 min. During the analysis, argon was passed over the sample. The high density of the argon cushion ensures that no oxygen enters the cell, even during standard additions.

Chemicals

All chemicals were of analytical grade, and triply distilled water was used throughout the study. Most stock solutions were prepared from sodium or potassium salts. The stock solutions of selenide were prepared from elemental

selenium dissolved in alkaline solutions containing excess of sodium tetrahydroborate. Zinc(II) solutions were prepared by dissolving elemental zinc in nitric acid. To avoid oxidation of selenide, 0.01 M sodium tetrahydroborate was added to all dilute solutions. (This precaution results in an additional peak in the potentiogram at a potential where it does not interfere with selenium and sulphur.)

RESULTS AND DISCUSSION

Basic stripping experiment

To test the basic idea that sodium amalgam is suitable as the reducing agent in reductive p.s.a., a crude experiment was carried out: a tiny chip (about 1 mm³) of sodium was dissolved in 5 ml of mercury, and 0.15 ml of this dilute amalgam was placed in the electrochemical cell as the working electrode, while the potentiostat was disengaged. The cell contained 40 ml of 1 M sodium hydroxide which had previously been deaerated. The amalgam droplet immediately assumed a potential of about -2000 mV vs. SCE and remained at this potential for several minutes, indicating that the Na(Hg)/Na⁺ couple was the predominant species at the electrode. Now potentiostatic control was established at a potential of -700 mV vs. SCE for 10 s. After this electrolysis, the potentiostat was once more disengaged and the potential versus time behaviour of the working electrode was recorded. The result is shown in Fig. 1, curve a: the potential drops quickly to about -2000 mV vs. SCE.

The experiment was then repeated after the addition of 10⁻⁵ M selenide stabilized with sodium tetrahydroborate. The resulting curve is shown in Fig. 1, curve b. Clearly, a well behaved plateau is associated with the stripping of selenium. The elongated plateau at about -1300 mV vs. SCE can be attributed to the existence of the H₂BO₃/BH₄⁻ couple. Redox couples, where both species are soluble, may be detected in p.s.a. if the bulk concentrations are sufficiently high, and if the rate of conversion of one species to the other is sufficiently low. This is the case for the H₂BO₃/BH₄⁻ couple in alkaline solution [7]. Between pH 5.7 and 13, more than 99% of the selenide exists as the HSe⁻ species [4]. The theoretical variation of the stripping potential with pH is therefore: $\Delta E/\Delta \text{pH} = -29.1$ mV at 20°C. By recording the stripping potential in various phosphate buffers, a value of -29.5 mV was found at ambient laboratory temperature (20°C).

Timing considerations

The reproducibility of the above experiment turned out to be poor: the concentration of amalgamated sodium decreased steadily when several stripping experiments with the same electrode were attempted, and the selenium plateau increased accordingly. Therefore, the amalgam was generated by electrolysis immediately before each experiment. Figure 2 shows the timing scheme used: first, any analyte deposits and any amalgamated sodium

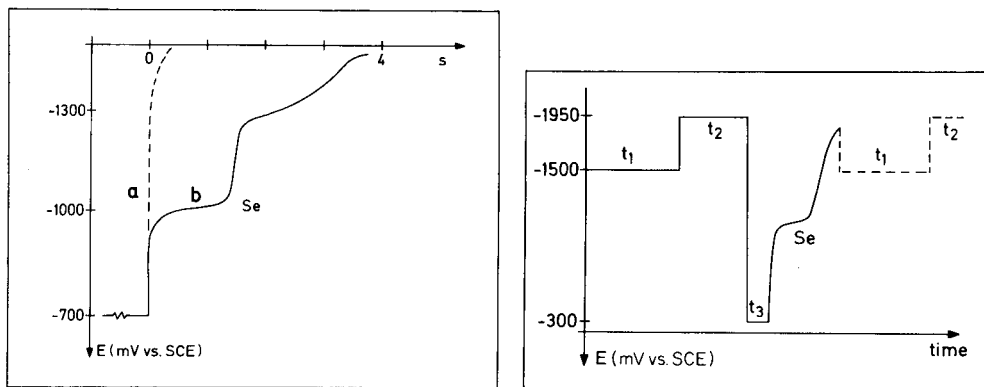


Fig. 1. Basic reductive p.s.a. experiment. Reducing agent: sodium dissolved in mercury droplet. Plating time 10 s. (a) Potentiogram obtained in 1 M sodium hydroxide; (b) potentiogram obtained after the addition of 10^{-5} M selenide in 0.01 M sodium tetrahydroborate.

Fig. 2. Timing scheme for the generation of amalgamated sodium and for the plating of selenium.

remaining in the electrode from a previous experiment are stripped by maintaining the potential at, say, -1500 mV vs. SCE for t_1 seconds. During the next period of t_2 seconds at a potential of -1950 mV vs. SCE, sodium ions are reduced to amalgamated sodium, which diffuses into the electrode. At the end of the amalgam generation, a well defined sodium concentration exists. During the subsequent plating of selenium, for t_3 seconds, at say, -300 mV vs. SCE, some sodium is reoxidized, but the fraction remaining inside the electrode when the stripping begins can be controlled by a proper selection of amalgam formation potential, t_2 , t_3 and the mercury drop size. Experiments where these parameters were varied indicate that $t_2 = 2 \times t_3$, amalgam formation at -1950 mV vs. SCE and a drop volume of about 0.15 ml are a suitable combination, and that with plating for 20 s the analytical signal from 10^{-7} M Se^{2-} can be reproduced with a relative standard deviation of about 3% for a series of 10 experiments. The timing is conveniently controlled by the computerized device [5]. This device also allows for the precise repetition of the experiment and averaging of the results as indicated by the dotted lines in Fig. 2. The computerized device can, of course, be replaced by a simple potentiostat/voltmeter set-up with a number of timer switches.

Effect of amalgam concentration and solution stirring

The sensitivity in stripping analysis mostly increases with the plating time. This is also true for the proposed technique. However, here the sensitivity can be expected to decrease with increasing concentration of amalgamated sodium, i.e. with increasing t_2 . That this is the case is illustrated in Fig. 3 which shows the stripping potentiograms obtained for 4×10^{-7} M Se^{2-} in

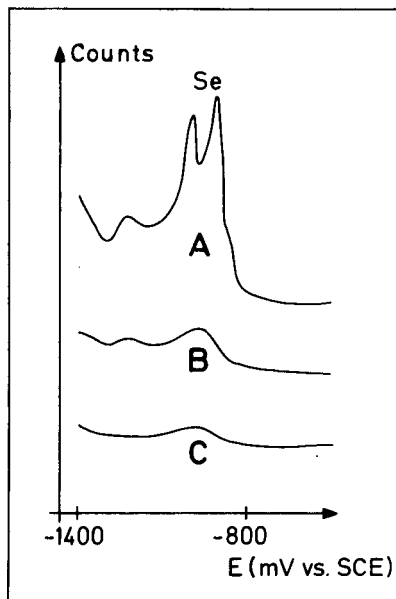


Fig. 3. Dependence of the selenium stripping signal on the time spent at the reduction potential of sodium ions: (A) 30 s; (B) 90 s; (C) 270 s. 4×10^{-7} M selenium in 1 M NaOH—0.01 M NaBH₄; plating for 20 s.

1 M NaOH—0.01 M NaBH₄. Three experiments were carried out with pre-concentration of selenide at -700 mV vs SCE for 20 s. Prior to the pre-concentration, amalgamated sodium was produced at -1950 mV vs. SCE for 30, 90 and 270 s, respectively. For the very high concentration of amalgamated sodium, no stripping signal of selenium was obtained. This suggests that, under these circumstances, the stripping process is controlled by kinetics rather than diffusion or convection, and that no high concentration region of newly stripped material exists at the electrode. Hence, other redox couples govern the electrode potential. A similar behaviour has previously been observed in the determination of manganese [3]. A time t_1 of 10 s was found to be sufficient to ensure complete regeneration of the electrode.

In p.s.a. where the oxidizing or reducing agent is dissolved in the sample solution, stirring of the sample solution has little influence on the magnitude of the analytical signal. This is because the transport rates of the analyte (during the plating step) and of the oxidizing or reducing agent (during the stripping) are increased in much the same manner. When, however, the reducing agent is dissolved in the mercury phase and the analyte in the aqueous phase, agitation of the sample solution increases the rate of plating of the analyte, whereas the transport of reducing agent within the mercury is less affected. Hence, solution stirring can be expected to improve the sensitivity. This was verified experimentally, but the effect was rather small. As in conventional p.s.a., solution stirring improves the reproducibility.

Working electrode

The suitability of various types and sizes of mercury electrodes was tested. The most satisfactory results were obtained with the 0.15-ml mercury pool. Increasing or decreasing the pool size resulted in potentiograms of lower resolution. A hanging mercury drop electrode was tested, but the maximum size of the drop appeared to be too small to hold a sufficiently large amount of amalgam during the plating of the analytes. Moreover, the large potential steps experienced by the electrode caused contractions of the mercury. These contractions were often sufficiently violent to dislodge the drop.

The use of a mercury pool allows all mercury in the cell to be part of the working electrode. This is advantageous since otherwise sulphur compounds, for example, may be lost by reaction with waste mercury from the HMDE [8].

Signal dependence on concentration

The selenium signal increases with concentration, but because of the formation of gradually thicker deposits of varying morphology more than one stripping maximum occurs when the bulk concentration is too high. Figure 4 illustrates the effect of standard additions to a 8×10^{-8} M Se^{2-} in 1 M NaOH–0.01 M NaBH_4 solution. As the selenide concentration increases, the maximum (1) grows, but only up to a certain limit. Then maximum (2) begins to grow, and at even higher concentrations a third maximum (3) appears. For quantitative analysis, the sum of the areas of all peaks appears to be the best measure of concentration since then a linear calibration plot is obtained in the range 4×10^{-8} M– 4×10^{-7} M Se^{2-} with plating for 120 s. If the thickness of the deposit is increased further, a non-linear plot results; this can be attributed to passivation of the electrode. The shoulder visible to the left of the peak (1) increases neither with the selenide concentration nor with the plating time. This shoulder can be attributed to the co-existence of the $\text{H}_2\text{BO}_3/\text{BH}_4^-$ couple.

Figure 5 shows a standard addition experiment with selenide concentrations about 10 times higher than those of Fig. 4. The plating time was restricted here to 10 s to avoid passivation of the electrode. Again, above a certain thickness of deposit, an extra selenium peak develops. The peak corresponding to the $\text{H}_2\text{BO}_3/\text{BH}_4^-$ couple is visible in all 6 potentiograms, (peak 3 at about –1300 mV vs. SCE). The shoulder on the blank potentiogram (Fig. 5A) is not identified definitively. Like the $\text{H}_2\text{BO}_3/\text{BH}_4^-$ peak, this shoulder is independent of the plating time and can possibly be attributed to a trace of dissolved oxygen.

Determination of sulphide

Sulphide can be determined in the manner previously described for selenide. Figure 6 shows the potentiograms resulting from a standard addition experiment where 6×10^{-7} M or 14×10^{-7} M sodium sulphide was added to a solution of 1 M sodium hydroxide–0.1 M sodium tetrahydroborate con-

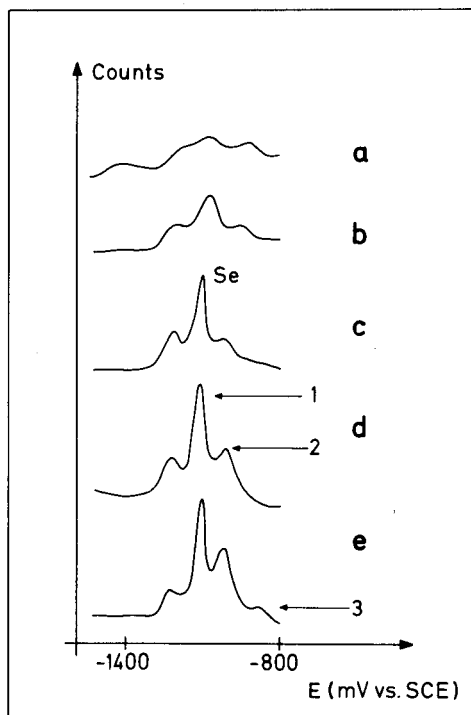


Fig. 4. Standard addition experiment: (a) 0.8×10^{-7} M; (b) 2.4×10^{-7} M; (c) 4.8×10^{-7} M; (d) 7.2×10^{-7} M; (e) 9.5×10^{-7} M selenide in 1 M NaOH–0.01 M NaBH₄. Plating for 120 s at –500 mV vs. SCE.

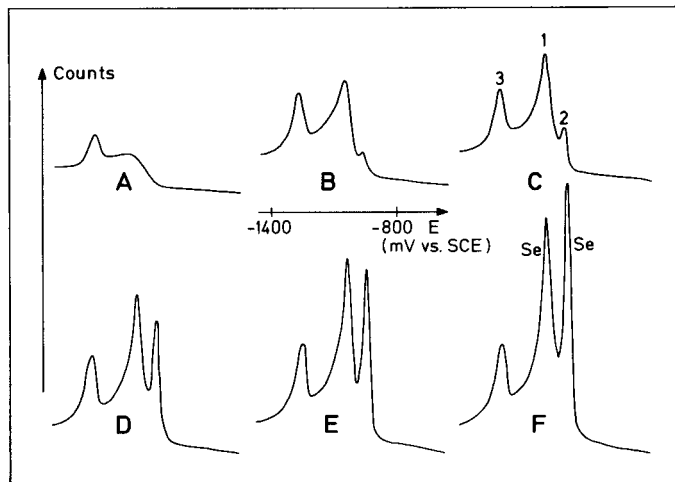


Fig. 5. Standard addition experiment with selenide in 1 M NaOH–0.01 M NaBH₄: (A) blank; (B) 2×10^{-6} M; (C) 3×10^{-6} M; (D) 5×10^{-6} M; (E) 7×10^{-6} M; (F) 9×10^{-6} M. Plating for 10 s at –500 mV vs. SCE.

taining a trace of sulphide. The plating was carried out for 10 s at -400 mV vs. SCE. Although, with such short plating times, the stripping of sulphide lasts only a fraction of a second, it can easily be observed with the computerized instrument which, for this experiment, was operated at a data rate of 5 kHz. With 10 s plating, linear calibration plots for sulphide were obtained in the range 10^{-7} – 1.4×10^{-6} M. Above 1.4×10^{-6} M, the calibration plot became markedly curved, indicating electrode passivation. When standard addition techniques are applied to samples of unknown composition, it is necessary to ensure that such passivation effects do not occur even in the spiked solution. Therefore, before any standard is added to the sample, the signal versus plating time relationship should be recorded. Any non-linearity suggests that a shorter plating time should be selected or the sample be diluted.

At the 10^{-7} M level, a relative standard deviation of about 3% was obtained for 10 consecutive determinations of sulphide as well as selenide.

Detection limits

In stripping analysis, the detection limit depends on the plating time. If 120 s is regarded as a suitable plating time, the detection limits for selenide and sulphide are of the order of 10^{-7} M. Below these concentrations, longer plating times are required, and exhaustive stripping of the amalgamated sodium from the working electrode during the plating of the analyte takes place, so that no reducing agent is left when it is needed. However, preliminary investigations indicate that a dual potentiostat/dual electrochemical cell, the compartments of which are connected with a mercury string acting as a common working electrode, is a suitable system for a continuous production of amalgamated sodium and hence for long preconcentration times. The amalgamated sodium is continuously produced in one compartment at -2000 mV vs. SCE and diffuses through the common mercury working electrode towards the other compartment which contains the sample solution. An ordinary reductive potentiometric stripping analysis can then be carried out in this compartment, by using the second potentiostat. Even after long plating periods, amalgamated sodium is then readily available. The potentiograms obtained with this system are similar to those obtained with the single cell/potentiostat system.

Interferences

In reductive p.s.a., selenide and sulphide interfere mutually when co-precipitated on a mercury electrode. Figure 7 shows the effect on the sulphide peak of adding selenide: the sulphide signal gradually vanishes, and a peak slightly cathodic of the selenium stripping potential appears. Similarly, excess of sulphide may partly suppress the selenium signal. The effect has not been studied in detail but can probably be attributed to exchange reactions in the crystalline deposit. Depending on the concentrations of selenide and sulphide and the plating time, rather complex patterns of

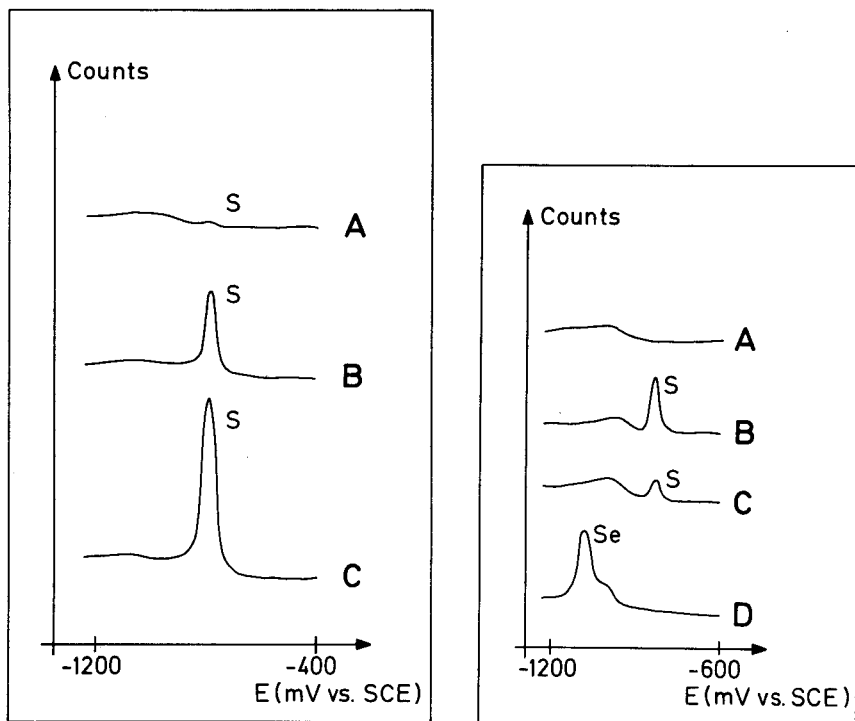


Fig. 6. Standard addition experiment with sulphide in 1 M NaOH–0.01 M NaBH₄: (A) blank; (B) 6×10^{-7} M; (C) 14×10^{-7} M. Plating for 10 s at –400 mV vs. SCE.

Fig. 7. Selenide–sulphide interaction in 1 M NaOH–0.01 M NaBH₄ solutions: (A) blank; (B) 2×10^{-5} M sulphide; (C) 2×10^{-5} M sulphide plus 4×10^{-6} M selenide; (D) 2×10^{-5} M sulphide plus 2×10^{-5} M selenide. Plating for 20 s at –600 mV vs. SCE.

stripping peaks may develop. Only with a careful choice of plating potential can the amount of sulphide deposited during the plating of selenide be minimized and, for selenide determinations, the interference be reduced.

Although metals generally can be expected to be of very low solubility in the reducing, alkaline medium employed, signals indicating the diffusion-controlled reduction of copper(II), lead(II), cadmium(II) and zinc(II) were observed as interferences on the reductive p.s.a. curves at potentials similar to the half-wave potentials in 1 M sodium hydroxide. The reduction of, for example, copper(II) to elemental copper by the excess of sodium tetrahydroborate is obviously not completed instantaneously. Figure 8A shows the reductive p.s.a. of 1.2×10^{-6} M selenide and 5×10^{-5} M copper(II) sulphate, following a plating at –100 mV vs. SCE for 30 s. Although, as pointed out by Dennis et al. [4], sodium tetrahydroborate is incapable of reducing sulphate quantitatively, the maximum at about –800 mV vs. SCE indicates that some sulphide is produced. The copper peak, of course, is not

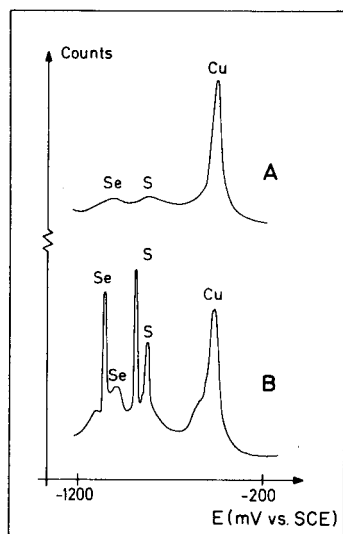


Fig. 8. Reductive p.s.a. of 1.2×10^{-6} M selenide— 5×10^{-5} M copper(II) sulphate in 1 M NaOH—0.01 M NaBH₄. Plating at -100 mV vs. SCE for (A) 30 s; (B) 60 s.

a stripping peak but corresponds to the reduction of copper(II) to amalgamated copper. Because of a limited rate of transport of copper(II) towards the electrode, the innermost region quickly becomes depleted of this species, and the electrode potential drops further. Figure 8B shows the reductive stripping curve obtained with a plating time of 60 s. Since no preconcentration of copper is involved, the corresponding peak remains at its previous value. The magnitudes of the selenide and sulphide signals increase by more than the expected factor of two, and multiple peaks are formed. This behaviour may be attributed partly to sulphide—selenide interaction, and partly to the poor reproducibility of the plating process when heavy deposits are formed as in this experiment; the peak splitting may also be partly due to the formation of copper selenide/-sulphide [9] in the deposit.

For this reason, and because the lead(II) reduction peak overlaps the sulphide stripping peak, it is important in the determination of selenium and sulphur in complex samples to separate the analytes from heavy metals, e.g. by a hydride generation method such as reported by Dennis et al. [4], who used sodium tetrahydroborate to reduce selenite to volatile hydrogen selenide which was trapped in sodium hydroxide in the electrochemical cell. Apart from separating the elements which are volatile in their lowest oxidation state (e.g. sulphur and selenium), this technique can provide a certain degree of preconcentration of the analyte prior to the stripping analysis. Blanks like the one in Fig. 5A can be corrected for, if this technique is employed.

Determination of halides

Since the chloride, bromide and iodide anions can be anodically preconcentrated on the surface of a mercury electrode as sparingly soluble mercury(I) salts, they too can be determined by reductive p.s.a. The stripping determinations of the halides are best carried out in acid or neutral medium [10], and since the stripping potentials are generally less negative than those of selenide and sulphide, amalgamated zinc produced by electrolysis at -1500 mV vs. SCE appears to be a suitable reducing agent. Figure 9 shows the stripping potentiograms obtained after electrolysis a solution 0.5 M in acetate buffer (pH 4.5) and 10^{-3} M in zinc(II) sulphate, containing varying amounts of chloride and iodide at $+300$ mV vs. SCE for 3 s. The chloride potentiograms of Fig. 9(A–C) produce a non-linear calibration plot. This is due to passivation of the electrode. If less material is deposited on the electrode, a linear relationship results; with a plating time of 5 s, calibration plots show linearity within the range 10^{-6} – 10^{-5} M and a blank value of about 2×10^{-6} M.

The effect of adding iodide ions to the sample is demonstrated by Fig. 9 (D–F): as the iodide peak increases, the chloride peak decreases. A similar effect has been observed in cathodic stripping voltammetry [11] and is believed to be caused by exchange reactions. The addition of bromide (not shown) gives rise to an additional peak which is barely resolved from the chloride peak in this medium.

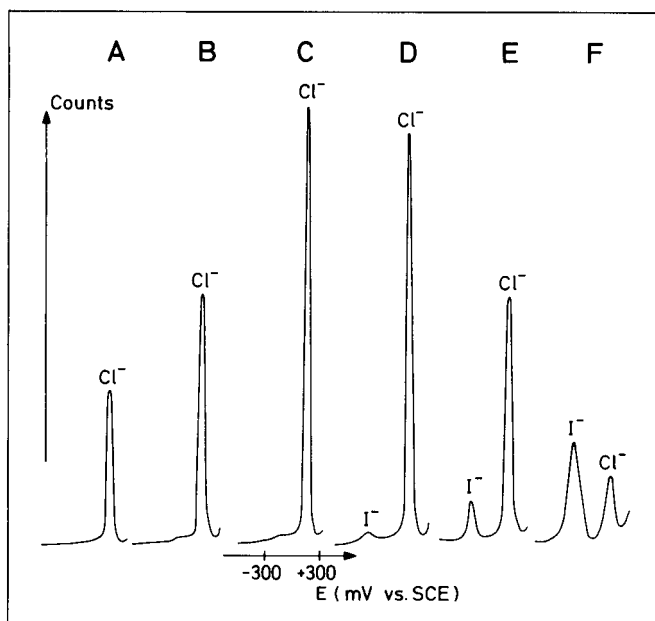


Fig. 9. Reductive p.s.a. of chloride and iodide. Concentrations ($\times 10^{-6}$ M): (A) 2, 0; (B) 20, 0; (C) 100, 0; (D) 100, 10; (E) 100, 40; (F) 100, 140 in 0.5 M acetate buffer (pH 4.5)– 10^{-3} M zinc(II) sulphate. Plating at $+300$ mV vs. SCE for 3 s.

In the determination of the halides, the electrolysis potential must be carefully adjusted to avoid dissolution of the mercury electrode, and hence the formation of a mercury(II) concentration. The rising parts of the potentiograms slightly anodic of the chloride peaks in Fig. 9 indicate mercury(II) reduction. If the electrolysis is carried out at +500 mV vs. SCE for just a few seconds, the mercury(II) concentration thus formed is very large, and the potential never drops below +400 mV when potentiostatic control is abandoned. In the acetate buffer, a plating potential of about +270 mV is suitable for chloride.

Careful control of the plating conditions may provide a means of determining mixtures of halides [12]. We have not yet explored this possibility.

At the 5×10^{-6} M level, 10 consecutive determinations of chloride gave a relative standard deviation of about 5%.

Current research is concentrated on a further development of the dual cell system. In particular, the possibility of employing neutral or acidic medium in the sample compartment is being explored. Preliminary results show that this is possible and that preconcentration of, for example, selenium by reduction from selenite followed by reductive stripping to dissolved selenide is feasible. Hence, the plating/stripping scheme reported by Henze et al. [9] can be employed even in p.s.a.

We acknowledge the support of the Danish Natural Science Research Council (grant no. 511-8032 for the computerized instrument) and of the Danish Technical Science Research Council (Research Fellowship for J.M.).

REFERENCES

- 1 D. Jagner, *Anal. Chem.*, 50 (1978) 1924.
- 2 D. Jagner and A. Graneli, *Anal. Chim. Acta*, 83 (1976) 19.
- 3 J. K. Christensen and L. Kryger, *Anal. Chim. Acta*, 118 (1980) 53.
- 4 B. L. Dennis, J. L. Moyers and G. S. Wilson, *Anal. Chem.*, 48 (1976) 1611.
- 5 H. J. Skov and L. Kryger, *Anal. Chim. Acta*, 122 (1980) 179.
- 6 J. Mortensen, E. Ouziel, H. J. Skov and L. Kryger, *Anal. Chim. Acta*, 112 (1979) 297.
- 7 R. Earl Davis, E. Bromels and C. L. Kibby, *J. Am. Chem. Soc.*, 84 (1962) 885.
- 8 T. M. Florence, *J. Electroanal. Chem.*, 97 (1979) 219.
- 9 G. Henze, P. Monks and G. Tölg, *Fresenius Z. Anal. Chem.*, 295 (1979) 1.
- 10 F. Vydra, K. Štulík and E. Juláková, *Electrochemical Stripping Analysis*, Ellis Horwood, Chichester, 1976, Ch. 5.
- 11 G. Colovos, G. S. Wilson and J. L. Moyers, *Anal. Chem.*, 46 (1974) 1045.
- 12 G. Colovos, G. S. Wilson and J. L. Moyers, *Anal. Chem.*, 46 (1974) 1051.

THE DETERMINATION OF MOLYBDENUM IN HIGH-NICKEL ALLOYS BY POTENTIOMETRIC TITRATION WITH CERIUM(IV) SOLUTIONS

E. L. MONTGOMERY, Jr.

Huntington Alloys, Inc., Huntington, WV 25720 (U.S.A.)

(Received 11th April 1980)

SUMMARY

A combination of ion-exchange separation and potentiometric titration is used in the determination of the molybdenum content of various high-nickel alloys that contain more than 4% molybdenum. The molybdenum(VI) fraction of a sample separated by ion exchange is reduced with tin(II) chloride and titrated with cerium(IV) sulfate. The method facilitates accurate, routine determinations without the extreme care that is required by the standard photometric method or the length and complexity of the gravimetric method. By suitable adjustment of the sample size or the strength of the titration solution, effective titrations can be conducted on samples containing up to 100% molybdenum.

The widely used photometric method for the determination of molybdenum in high-nickel alloys [1] requires extreme care because of the instability of the colored complex and the need to dilute concentrated samples. The gravimetric procedure of Hillebrand et al. [2] is recognized as a standard method, and the gravimetric procedure of ASTM E-30 which relies on α -benzoinoxime is used for "umpire" determinations [3]. These gravimetric methods are considered too lengthy and too technique-dependent to be useful routinely. In addition, the use of ammonia solution to purify the precipitate [3], appears in some instances to lead to negative errors.

Those problems with the photometric and gravimetric methods led to a search for a more suitable routine procedure. Several works cited by Busev [4] indicate that molybdenum can be quantitatively reduced from the hexavalent to the pentavalent state by tin(II) chloride, and Stehlik [5], discusses the potentiometric titration of molybdenum(V) with cerium(IV) sulfate or potassium permanganate after reduction with either titanium(III) or tin(II) chloride, zinc, or lead. A small amount of manganese(II) sulfate was needed as a catalyst during Stehlik's titration.

The proposed method combines ion-exchange separation, which provides molybdenum(VI), with the reduction and titration procedures of Busev and Stehlik to determine molybdenum content in high-nickel alloys. After the amount of tin(II) chloride necessary for complete reduction had been established, titrations of pure molybdenum solutions confirmed the precision of the method.

The molybdenum content of various samples, including proprietary standards of Huntington Alloys, and commercial standards from the United States National Bureau of Standards, was determined by both the gravimetric and the titrimetric procedures after separation of the molybdenum by the ion-exchange chromatography as described below. For the gravimetric method, sulfuric acid was added to the molybdenum fraction and the sample was heated until strong fumes of sulfur trioxide were driven off in order to remove the interfering fluoride ion. The determination was then completed according to the classical procedure of precipitation with α -benzoinoxime [3]. For the titrimetric method, samples of that same series of alloys were dissolved and separated by ion-exchange.

EXPERIMENTAL

Apparatus and reagents

A Fisher Accumet Model 320 pH/mV meter equipped with a calome reference electrode and a platinum electrode was used for all titrations. The ion-exchange columns were made of colorless, transparent, cast acrylic tubing (0.3 m long, 27.5 mm i.d.). The resin used was Bio-Rad AG1-X8 (200–400 mesh).

Molybdenum standard. Dissolve 2.5 g of molybdenum powder (>99.9% pure Alfa standard, Ventron Laboratories) in 30 ml of nitric acid (1 + 1). Add 40 ml of concentrated sulfuric acid, and evaporate to fumes. Cool, and dilute with water to 500 ml. Store in a polypropylene bottle.

Tin(II) chloride. Dissolve 5.0 g of tin(II) chloride dihydrate in 10 ml of 11 M HCl and dilute with water to 100 ml. Prepare this solution just before use. Experiments with molybdenum standard solutions showed that complete reduction of 100 mg of molybdenum(VI) to molybdenum(V) required 4.5 ml of fresh tin(II) solution. The same amount of several-weeks-old SnCl_2 solution failed to reduce 100 mg of molybdenum(VI) completely.

Cerium(IV) sulfate (0.05 M). Dissolve 27 g of reagent-grade $\text{H}_4\text{Ce}(\text{SO}_4)_4$ in 1 l of water containing 25 ml of concentrated sulfuric acid. Filter the solution and store in a polypropylene bottle. Standardize by titrating against a known weight of high-purity iron.

Recommended procedure

Sample preparation. Transfer a 1-g sample to a covered teflon beaker and dissolve it in an appropriate mixture of HCl and HNO_3 . Remove the lid and carefully evaporate the sample to dryness. Add 5 ml of 11 M HCl and 15 ml of 40% hydrofluoric acid and again evaporate to dryness. Repeat the HCl–HF additions and evaporate once again, avoiding any prolonged baking of the sample. Add 5 ml of 11 M HCl, 15 ml of 40% HF, and 280 ml of water, and heat until all of the salts are dissolved. Cool to room temperature.

Ion-exchange separation. The sequence of elution and the reagents used here [6], based on several standard works [7–10], are indicated in Figs. 1

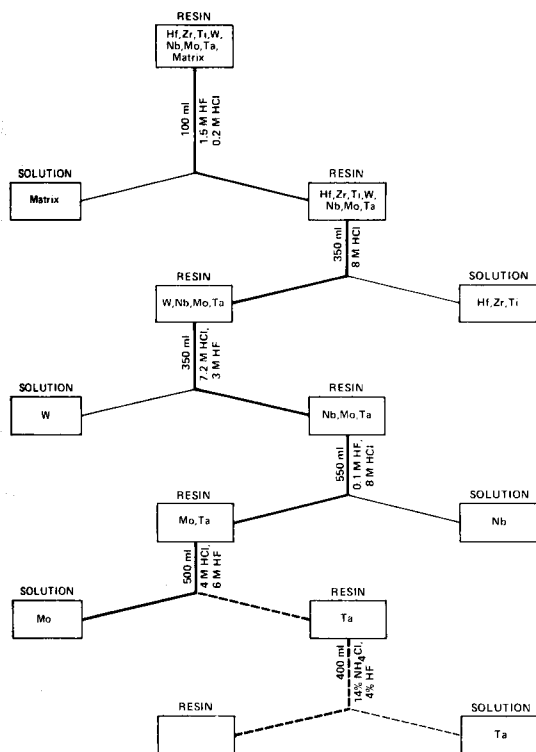


Fig. 1. The sequence of elution showing the types and amounts of reagents used in the ion-exchange separation.

and 2. The uptake of molybdenum on the ion-exchange resin and subsequent elution with a strong hydrofluoric–hydrochloric acid solution completely separated molybdenum from all other elements. The absence of molybdenum from subsequent eluates, as verified by atomic absorption spectrometry, demonstrates the completeness of that separation.

Reduction of molybdenum. To the molybdenum fraction add 80 ml of sulfuric acid (1 + 1) and evaporate the solution to strong fumes. Cool the sample, wash down the sides of the beaker, and evaporate the sample again to strong fumes. Cool to room temperature and dilute the sample to 400 ml with water. Heat the solution to the boiling point and add enough tin(II) chloride (50 g l⁻¹) to reduce the molybdenum. Complete reduction is indicated by a change from colorless to orange, varying in intensity in proportion to the concentration of molybdenum. Continue to boil the sample for 15 min. Cool slightly, and maintain the volume at 400 ml by washing the cover and sides of the beaker with water. Cool the solution in a water bath maintained at 10°C, keeping the beaker covered to minimize oxidation of the molybdenum by air.

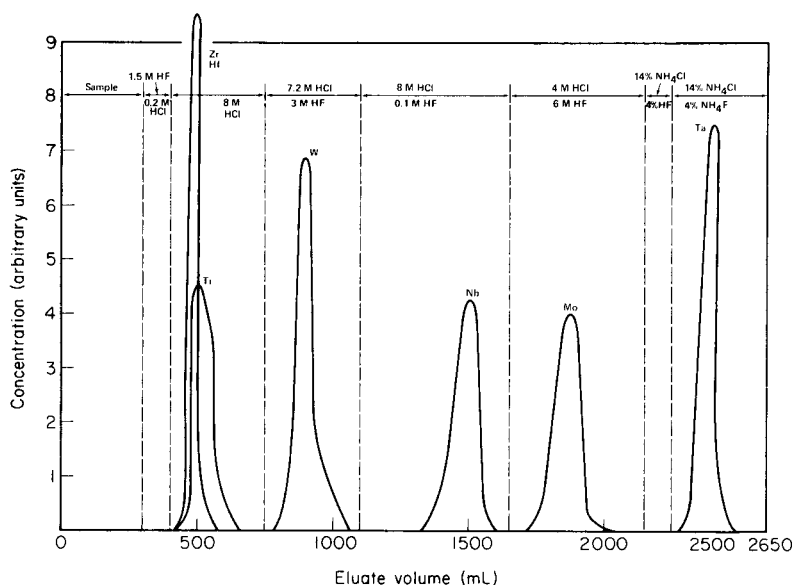


Fig. 2. The scheme of elution used in the ion-exchange separation.

Add 10 ml of a saturated aqueous mercury(II) chloride solution, stir, and let it stand for about 2 min. The appearance of a precipitate of mercury(I) chloride guarantees complete reduction. Subsequent titrations are successful only on samples that produce this characteristic precipitate.

Titration. While stirring the sample, add 0.05 M cerium(IV) sulfate solution fairly rapidly at first then dropwise as the solution gradually loses its orange color, approaching the colorless state which signals the complete oxidation of molybdenum(V) to molybdenum(VI). Estimate the reading of the buret at the end-point to 0.01 ml; the end-point is taken as the maximum change in potential per 0.05 ml of titrant.

RESULTS AND DISCUSSION

The quantitative reduction of molybdenum(VI) to molybdenum(V) takes place in a sulfuric acid medium at approximately 2 M. Higher concentrations of acid do not improve the sharpness of the end-point but may result in a further reduction to molybdenum(III), as reported by Busev [4] for higher concentrations of sulfuric or hydrochloric acid. Lower concentrations of sulfuric acid resulted in partial hydrolysis of the molybdenum upon addition of tin(II) chloride. Because of its reducing potential, tin(II) must be present at the completion of the reduction in greater concentration than that which corresponds to the stoichiometric point of the reaction $2 \text{Mo}^{6+} + \text{Sn}^{2+} \rightleftharpoons 2 \text{Mo}^{5+} + \text{Sn}^{4+}$. From the very early work of Glasmann [11], Kano [12], and Treadwell [13], Stehlik [5] concluded that the point at

which molybdenum had been quantitatively reduced to the trivalent state was not known. Also, elaborate precautions were needed to avoid atmospheric oxidation during titration. Therefore, selective reduction from molybdenum(VI) to molybdenum(V) came to be regarded as a great improvement.

The proposed method allows accurate determinations of the molybdenum content at a precision of ± 0.00043 g (at a confidence limit of 95%) based upon a regression analysis of the titrations of known amounts of pure molybdenum (Table 1). A typical titration curve is illustrated in Fig. 3. The magni-

TABLE 1

Precision of potentiometric titration method

Mo taken (mg)	Mo found (mg)	Coefficient of variation ^a (%)
50.00	50.03	0.32
100.00	100.14	0.30
150.00	150.05	0.13
200.00	200.10	0.09

^aBased on 8 determinations.

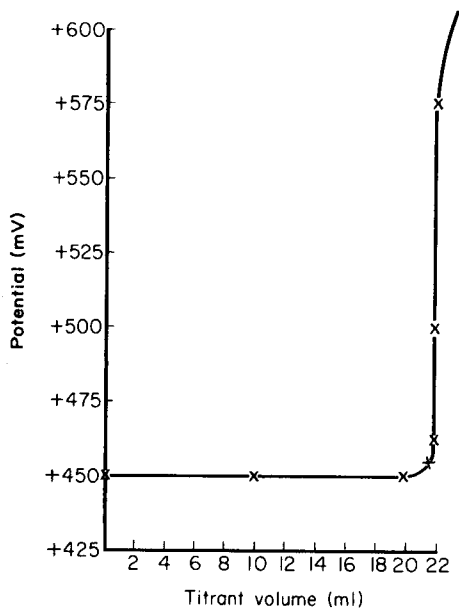


Fig. 3. Potentiometric titration of molybdenum(V) with standard (0.05 M) cerium(IV) solution in 2 M sulfuric acid.

tude of the potential change at the equivalence point is approximately 140 mV per 0.05 ml of cerium(IV) solution.

Table 2 gives a comparison of the titrimetric procedure with the photometric and gravimetric methods for the determination of molybdenum in the alloys. The standard deviation of the titrimetric determinations is less than or equal to that of the photometric or gravimetric procedure in every case except one. The accuracy of the method was evaluated by assuming the results from the NBS to be a true measure of the molybdenum content of the alloy. The mean of the ratio of titrimetric to photometric values was 0.982, indicating that direct photometric measurements of levels of molybdenum above 4% might lead to results with a positive bias. In a further comparison of the titrimetric and photometric methods, where α -benzoinoxime was used to separate the molybdenum, the mean titrimetric/photometric ratio was 1.004, indicating not only the excellent agreement of the widely different methods but also the effectiveness of α -benzoinoxime in isolating molybdenum from the matrix of an alloy.

In the alternative separation, molybdenum was selectively precipitated from the dissolved sample with a solution of α -benzoinoxime. After a thorough washing, the precipitate was transferred back to the beaker and wet-ashed with nitric and sulfuric acids. Residual organic material was destroyed with a few drops of perchloric acid, and the sample was allowed to come to strong fumes in order to remove all traces of nitric acid. After reduction with tin(II) chloride, the sample was titrated with cerium(IV) solution. Separation by α -benzoinoxime could not be expected to serve for alloys which contain niobium or tungsten since the occlusion of niobium and the complete precipitation of tungsten would cause inaccurately high results.

It is significant that for five of the eight different alloys analyzed in this comparison, the potentiometric values were higher than those obtained by

TABLE 2

Comparison of the gravimetric, photometric, and titrimetric methods for the determination of molybdenum in complex nickel alloys

Identification of sample ^a	Certified value (% Mo)	Mean value ^b (% Mo)			Standard deviation		
		Grav.	Phot.	Tit.	Grav.	Phot.	Tit.
NBS-349	4.04	4.03	—	4.04	0.058	—	0.025
NBS-153a	8.85	8.79	8.80	8.85	0.036	0.035	0.028
HAS 1	9.18	9.13	9.25	9.18	0.036	0.056	0.016
HAS 2	8.99	9.01	9.09	9.00	0.021	0.056	0.014
HAS 3	9.58	9.61	9.70	9.65	0.038	0.045	0.025
HAS 4	8.18	8.21	8.30	8.28	0.031	0.025	0.036
HAS 5	2.99	3.02	3.04	3.02	0.027	0.017	0.017

^aNational Bureau of Standards (NBS) and Huntington Alloys standards (HAS). ^bMean value represents the statistical mean of 12 determinations.

the classical gravimetric procedure. One reasonable explanation for that difference lies in the gravimetric procedure itself. Written into the ASTM procedure is a step in which ammonia solution is used to remove impurities from the weighed molybdenum oxide. Apparently, a certain amount of molybdenum is lost from the sample in solution at that step. Measurements by flame atomic absorption spectrometry indicated that 0.1–2.8% of the molybdenum in the impure MoO_3 remained after the leaching of the precipitate with ammonia solution. Incomplete solution of that molybdenum leads to low determinations. No such "correction step" is needed in the gravimetric procedure if the ion-exchange system produces a relatively pure molybdenum fraction.

The author gratefully acknowledges the contribution of F. H. Robinson, who carefully conducted the numerous ion-exchange separations that were essential to this work.

REFERENCES

- 1 N. H. Furman, *Scott's Standard Methods of Chemical Analysis*, D. Van Nostrand, Princeton, NJ, 1962, p. 687.
- 2 W. F. Hillebrand, G. E. F. Lundell, H. A. Bright and J. I. Hoffman, *Applied Inorganic Analysis*, J. Wiley, New York, 1955, p. 310.
- 3 American Society for Testing and Materials, *Annual Book of ASTM Standards*, Part 12, Philadelphia, 1977, p. 20.
- 4 A. I. Busev, *Analytical Chemistry of Molybdenum*, Academy of Sciences of the U.S.S.R., Moscow, 1964 (Translation, IPST, Ann Arbor Publishers, 1970).
- 5 B. Stehlik, *Collect. Czech. Chem. Commun.*, 4 (1932) 418.
- 6 Huntington Alloys' Laboratory Report #740701 (unpublished), Zirconium, Titanium, Hafnium, Tungsten, Niobium, Molybdenum and Tantalum Separation by Ion Exchange, Huntington Alloys Inc., WV 25720, U.S.A.
- 7 J. L. Hague, E. D. Brown and H. A. Bright, *J. Res. Natl. Bur. Stand.*, 53 (1954) 261.
- 8 F. Nelson, R. M. Rush and K. A. Kraus, *J. Am. Chem. Soc.*, 82 (1960) 339.
- 9 J. A. Markinsky, *Ion-Exchange*, M. Dekker, New York, 1966.
- 10 I. M. Kolthoff, P. J. Elving and E. B. Sandell, *Treatise on Analytical Chemistry*, Part II, Vol. 8, J. Wiley, New York, 1963.
- 11 B. Glasmann, *Ber. Dtsch. Chem. Ges.*, 38 (1905) 604.
- 12 N. Kano, *J. Chem. Soc. Jpn.*, 43 (1922) 333.
- 13 W. D. Treadwell, *Helv. Chim. Acta*, 5 (1922) 806.

DETERMINATION OF PHARMACEUTICAL COMPOUNDS CONTAINING COVALENTLY-BOUND HALOGEN BY MEANS OF ION-SELECTIVE ELECTRODES

F. RAKIÁS, K. TÓTH and E. PUNGOR*

Institute for General and Analytical Chemistry, Technical University, Budapest (Hungary)

(Received 21st April 1980)

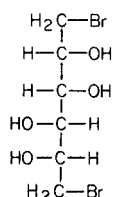
SUMMARY

Organic compounds containing covalently bound halogen can be determined by potentiometric techniques with ion-selective electrodes in different ways. Apart from potentiometric titration of the halide after combustion, direct potentiometric determination of the halide produced at appropriate pH in the solution of the compound in the presence of silver(I) catalyst dissolved from the ion-selective electrode is possible in some cases. In the latter case, the chain length is critical; the chain must have at least three carbon atoms for hydrolysis to take place. Titration with a silver nitrate solution is also possible; prior pH adjustment is then needed for myelobromol but not for the other compounds tested.

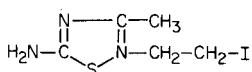
Ion-selective electrodes have found application in widely different fields of chemical analysis since their introduction. Although such electrodes are most widely and advantageously used for determining inorganic components, pharmaceutical analysis which is concerned mainly with organic compounds, may also become an important field of application. The application of ion-selective electrodes is obvious when an inorganic component has to be determined in a basically organic product during a production process. Similarly obvious is the use of ion-selective electrodes for the determination of suitable ions in transfusion solutions [1]. Ion-selective electrodes are readily applied for determinations of predominantly organic substances containing an ionizable inorganic element or group [2]. In such cases, the concentration of the biologically active compound can be determined through the ionizable moiety but this type of method can be accepted only with certain restrictions because the active component is not measured directly. Decreases in the content of the active ingredient by decomposition reactions cannot be detected by such procedures.

If a component for which an ion-selective electrode is available is covalently bound, in a predominantly organic molecule, it can usually be determined potentiometrically after decomposition by, for example, the oxygen-flask combustion method; such methods have been reviewed [3]. In some cases, such components may also be measured after various chemical transformations other than mineralization. For example, cyanocobalamine can be determined via reduction to hydrogen cyanide [4].

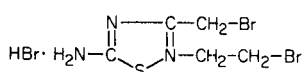
Ion-selective electrodes are also applicable in other ways. For example, organic compounds which complex copper can be determined by using a copper ion-selective electrode [5]. In some cases, organically bound constituents can be determined without preliminary chemical treatment; thus certain sulphur-containing compounds can be determined by potentiometric titration with silver nitrate solution by using a sulphide-selective electrode [6, 7]. In the present paper, a new way of applying ion-selective electrodes will be dealt with in connection with some studies done on myelobromol (I) as a cytostatic agent. The initial problem was to determine the ionic bromide contamination of myelobromol, and this directed attention to the possibility of determining compounds bearing a terminal halogen. The other compounds studied were 2-amino-4-methyl-5-(2-iodoethyl)thiazole (II), 2-amino-4-bromomethyl-5-(2-bromoethyl)thiazole hydrobromide (III) and 2-amino-4-bromomethyl-5-(2-chloroethyl)thiazole hydrochloride (IV).



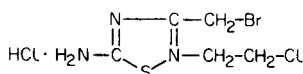
I



II



III



IV

EXPERIMENTAL

Materials and equipment

Myelobromol solution, 10^{-2} M. Dissolve 3.0802 g of myelobromol (1,6-dibromo-1,6-dideoxy-D-mannitol) in distilled water and dilute the solution to 1 l with distilled water in a volumetric flask. The water used for preparing all the solutions was doubly distilled from a silica apparatus.

ITB solution, 10^{-3} M. Dissolve 0.2680 g of ITB (II) in distilled water and dilute the solution to 1 l in a volumetric flask.

DBT solution, 10^{-3} M. Dissolve 0.3693 g of DBT (III) in distilled water and dilute to 1 l in a volumetric flask.

BCT solution, 10^{-3} M. Dissolve 0.2940 g of BCT (IV) in distilled water and dilute to 1 l in a volumetric flask.

Silver nitrate solutions were 10^{-1} M and 10^{-2} M.

The equipment included a precision pH meter (Radelkis, type OP-205), and iodide-selective (Radelkis, type OP-I-7112), bromide-selective (Radelkis, type OP-Br-7112), and chloride-selective (Radelkis, type OP-Cl-7112) elec-

trodes, which were used with a double-junction Ag/AgCl electrode (Radelkis, type OP-8202).

RESULTS AND DISCUSSION

During the determination of the bromide contamination in aqueous solutions of myelobromol (I), it became apparent that the measured value depended on the pH of the solution, whereas the results obtained by another method were independent of pH. This means that the covalently bound bromide underwent hydrolysis to an extent dependent on the solution pH. To establish the optimum pH for the determination of the contaminating bromide, the electrode potential vs. pH curve was measured for a bromide-selective electrode in a 10^{-3} M solution of myelobromol. As shown by Fig. 1, myelobromol is not hydrolysed up to pH 8, but the bromide is completely hydrolysed above pH 11.5. Hydrolysis of the terminal halogen of organic compounds in alkaline medium in the presence of silver(I) catalyst is well known [8]. As shown by the measurements described, the silver(I) dissolved from the surface of the silver halide-based ion-selective electrodes is sufficient to catalyse the hydrolysis.

The hydrolysis constant (K_h) of myelobromol was calculated from the electrode potential–pH function, by using the relationships: $K_h = K_w/K$ and $\text{pH} = 7 - 0.5 \text{ p}K + 0.5 \log c$, where K_w is the ionic product of water (10^{-14}), K is the dissociation constant of the acid formed during hydrolysis, and c is the bromide ion concentration released from myelobromol at a given pH. The K_h calculated from the above relationships was 1×10^{-11} .

Based on these experimental results, the ionic bromide contamination in myelobromol can be determined by direct potentiometry with a bromide-

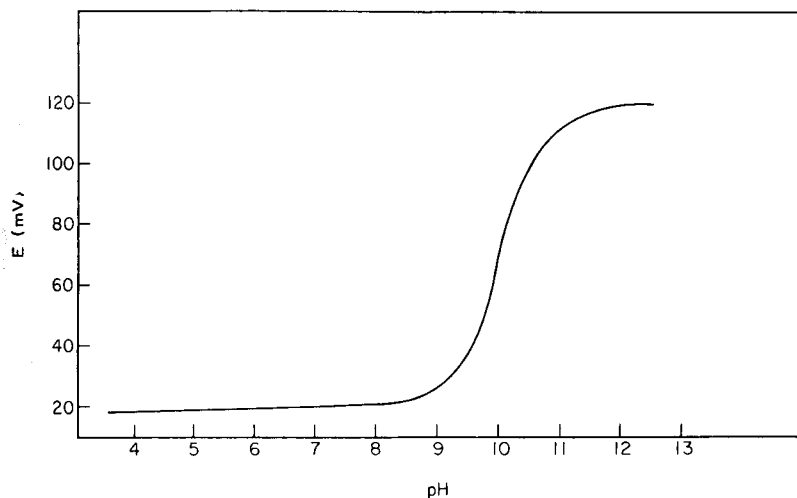


Fig. 1. pH dependence of the potential of a bromide-selective electrode in a 10^{-3} M solution of myelobromol.

selective electrode, if the pH of the solution is between 1 and 8, whereas the bromine covalently bound in the compound can be determined at pH above 11.5, where it is completely hydrolysed to produce bromide ions. In the latter case, obviously, the total bromide content of the solution is measured, and the myelobromol can be determined from the results of measurements at low and high pH.

Some other compounds containing terminal halogen atoms were then investigated. The compounds studied were ITB, DBT and BCT (II–IV). The potential of the corresponding halide-selective electrode was measured as a function of the pH in a 10^{-3} M solution of the compound in question. The E vs. pH curves for ITB, DBT and BCT indicated that hydrolysis takes place in all three cases, which enables the covalently bound halogen to be determined after hydrolysis. The pH ranges below which the halogen in the compound is unhydrolysed and above which it is completely split off are: pH 7–11 for compound II, pH 8–11 for compound III, and pH 8–11 for compound IV. Calculations of the hydrolysis constants showed that iodine is hydrolysed most easily, bromine takes an intermediate position and chlorine is the most difficult to split off (Table 1).

If two halogens are present in a molecule and are attached to chains with different lengths, the question arises whether both or only one of the halogens is hydrolysed. To elucidate this problem, E vs. $\log c_x$ calibration plots were prepared for solutions of the appropriate halides at constant ionic strength. The pH of the solutions of the three compounds investigated was adjusted to a value where hydrolysis was complete. Then, the potential of the appropriate halide-selective electrode was measured in the solution and the concentration of the halide arising from hydrolysis was determined based on the calibration curve. The results showed that the length of the chain to which the halogen is attached has a marked effect on the hydrolysis. The chain must contain at least two carbon atoms for the halogen to be hydrolysable.

The concentrations of the three compounds were determined after hydrolysis both by the direct potentiometric method and by potentiometric titration with 10^{-1} or 10^{-2} M silver nitrate standard solution, using the appropriate halide-selective electrode. The titration curve for myelobromol (Fig. 2A) shows that at the original pH of the solution (pH 3.2) only the bromide contamination is measured, as in direct potentiometric measurements. After the pH of the aqueous solution had been adjusted to above 11.5, both bromine atoms bound covalently are hydrolysed, and can be determined by potentiometric titration with silver nitrate solution by using a bromide-selective electrode (Fig. 2B). The precipitate formed during the titration was filtered, washed and analysed; it consisted solely of silver bromide. No organic constituent could be detected by infrared spectroscopy.

The potentiometric titration curve of a 10^{-3} M solution of ITB monitored with an iodide-selective electrode is shown in Fig. 3A. The hydrolysis takes place at the pH prevailing in pure solutions of ITB in the presence of silver(I)

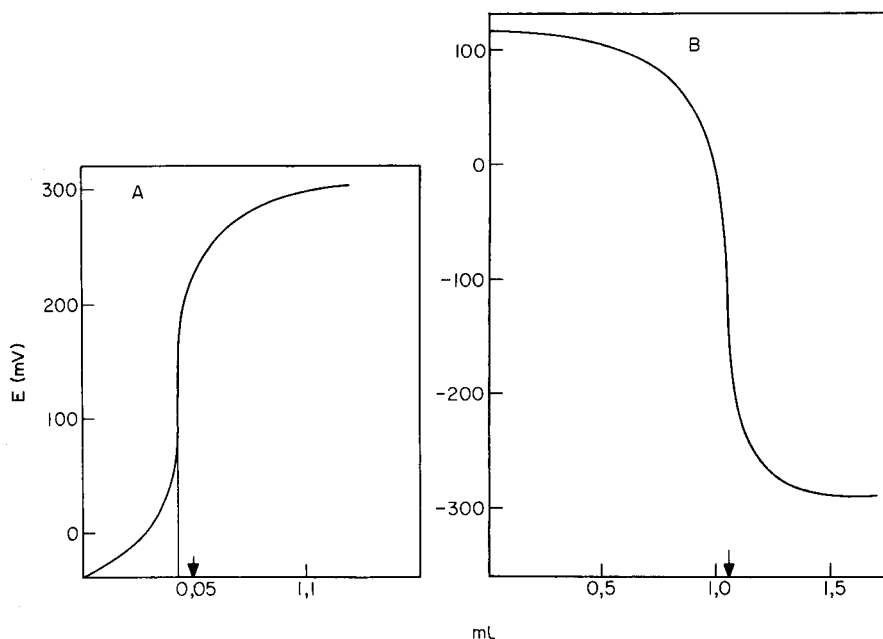


Fig. 2. Determination of (A) ionic bromide contamination in a 10^{-2} M solution of myelobromol by potentiometric titration with 10^{-4} M silver nitrate solution (bromide-selective electrode). (B) covalently bound bromine in a 10^{-2} M solution of myelobromol after pH adjustment by potentiometric titration with silver nitrate solution (bromide-selective electrode).

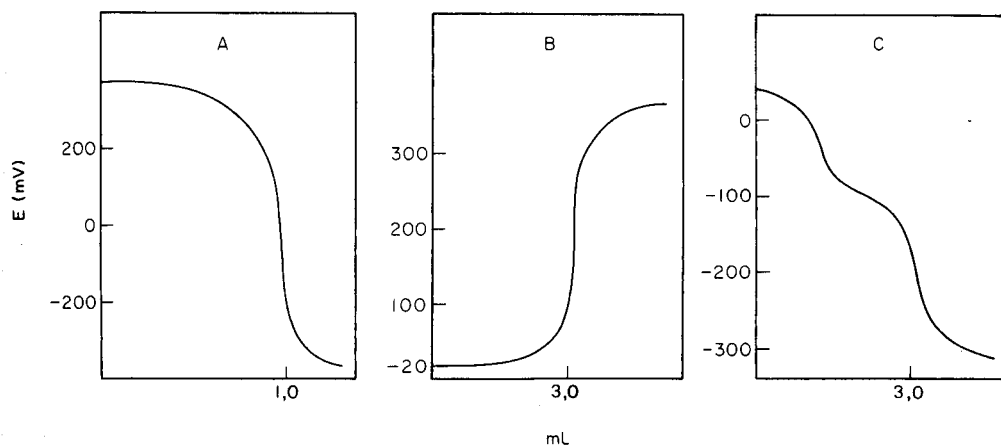


Fig. 3. Potentiometric titrations of 10.0 ml 10^{-3} M sample solution with 10^{-2} M silver nitrate standard solutions (A) ITB with an iodide-selective electrode; (B) DBT with a bromide-selective electrode; (C) BCT with a bromide-selective electrode.

TABLE 1

Hydrolysis constants of various halogen-containing compounds

Compounds	Hydrolysis constant
ITB	10^{-10}
DBT	10^{-11}
BCT	10^{-12}

ions acting as catalyst. The concentration of ITB calculated on the basis of the titration curve agreed with the known original concentration. The precipitate formed during the titration consisted solely of silver iodide.

On titration with silver nitrate, DBT consumed three silver(I) ions per molecule without preliminary pH adjustment (Fig. 3B). Comparison with the results of direct potentiometric measurements shows that whereas the direct measurements detect only one covalently bound bromine atom, titration with silver nitrate measures both covalently bound bromines without adjustment of the pH to the value necessary for hydrolysis. (Obviously, the ionically bound bromine can be measured by both techniques.)

A titration curve of BCT is shown in Fig. 3C; here a bromide-selective electrode was used. The titration curve shows two steps. When the titration was finished at the first equivalence point and the precipitate was filtered and analysed, it was found to consist of silver bromide. The precipitate formed in the second step of the titration was found to be silver chloride.

The compounds investigated were also determined by titration of the halide obtained after Schöniger oxygen-flask combustion. The results agreed well with those of the titrations discussed above (Table 2).

TABLE 2

Comparison of results obtained for halogen content by different techniques

Sample	Actual halogen content (%)	Potentiometric titra- tion after combustion		Direct potentiometry		Potentiometric titration	
		Found (%)	Recovery (%)	Found (%)	Recovery (%)	Found (%)	Recovery (%)
Myelobromol							
Br content	51.87	51.02	98.36	51.09	98.50	51.32	98.94
ITB							
I content	47.35	46.64	98.50	46.87	98.99	46.97	99.20
DBT							
Br content	43.27	42.10	97.30	42.87	99.08	43.03	99.56
BCT							
Br content	27.18	26.87	98.86	—	—	26.97	99.23
Cl content	24.12	23.34	96.77	23.81	98.71	23.81	98.71

The authors thank Dr. E. S. Fehér for valuable discussions.

REFERENCES

- 1 I. Kálmán, K. Tóth and D. Küttel, *Acta Pharm. Hung.*, 42 (1972) 152.
- 2 M. Zádeczky, D. Küttel, J. Havas and L. Kecskés, *Acta Pharm. Hung.*, 48 (1978) 1020.
- 3 S. Dessouky, K. Tóth and E. Pungor, *Analyst*, 95 (1970) 1020.
- 4 S. Dessouky and E. Pungor, *Analyst*, 96 (1971) 443.
- 5 F. M. El-Taras, E. Pungor and G. Nagy, *Anal. Chim. Acta*, 82 (1976) 285.
- 6 M. K. Pápay, K. Tóth and E. Pungor, *Anal. Chim. Acta*, 56 (1971) 291.
- 7 M. K. Pápay, K. Tóth, V. P. Izvekov and E. Pungor, *Anal. Chim. Acta*, 64 (1973) 404; 69 (1974) 173.
- 8 Gy. Bruckner, *Organic Chemistry*, Tankönyvkiadó, Budapest, 1964.

MONOHYDROGENPHOSPHATE-SENSING ELECTRODE FORMULATIONS

GWON-SHIK IHN^a, CHARLES F. NASH and RICHARD P. BUCK*

The William R. Kenan, Jr., Laboratories of Chemistry, The University of North Carolina, Chapel Hill, NC 27514 (U.S.A.)

(Received 3rd March 1980)

SUMMARY

Four-component $\text{Ag}_2\text{S}:\text{PbS}:\text{PbHPO}_4:\text{Ag}_2\text{HPO}_4$ and three-component $\text{Ag}_2\text{S}:\text{PbS}:\text{PbHPO}_4$ formulations have been prepared and evaluated for sensitivity to monohydrogenphosphate. The 3:1:1 composition is superior in terms of ease of preparation, stability, rapidity of response and reproducibility. Testing was done over the range 10^{-1} – 10^{-5} M HPO_4^{2-} in buffer at pH 8.44 with constant ionic strength. Response times to 64% of final values varied between 60 and 300 s depending upon concentration, and potential changes with concentration varied between 25 and 31.5 mV/decade in the 10^{-1} – 10^{-3} M range, depending upon electrode configuration. Many common ions interfere.

Solid electrodes for determination and monitoring of phosphate species have not generally been successful, or commercially available. Liquid ion-exchanger electrodes have been made, and found to function for ideal aqueous solutions containing HPO_4^{2-} and H_2PO_4^- [1–3]. However, common anions such as halides, thiocyanate, nitrate and perchlorate pose serious interference problems. A further problem of liquid electrodes is that they eventually lose solvent and ion exchanger. Some solid-state electrodes are also prone to eventual dissolution, but the Ag_2S - and HgS -based electrodes are very long-lived.

The construction of pressed pellets and heterogeneous electrodes, based on metal phosphate salts, was an early development. Nernstian and non-Nernstian responses were sometimes found [4–6]. Unfortunately, the supporting electrolytes caused large interferences which were not susceptible to removal. Needs for moderate ionic conductivity, selective ion-exchange of phosphate species, and indirectly-selective ion exchange through a common ion effect, have been recognized. Logical approaches to the inclusion of these factors in the design were presented by Rechnitz et al. [7] in construction of a sulfate-sensing electrode, by Shu and Guilbault [8] for monohydrogenphosphate, and by Tacussel [9] for a variety of electrodes. Similar applications of theory for phosphate led Midgley [10] to the $\text{Ag}_2\text{S}-\text{PbS}-\text{PbHPO}_4$ system in which Ag_2S provides good membrane conductivity and

^aOn leave from the Keimyung University, Chemistry Department, Daegu, Korea.

all species are linked by common ions. Thus, if rates of ion exchange are rapid in HPO_4^{2-} -containing electrolytes, the interfacial potential difference should depend upon HPO_4^{2-} activities.

Since Ag_2S is a good electronic conductor, the electrode format is not limited to membrane configurations. All-solid-state versions are possible. Recently, other closely related electrode configurations have been reported [11–13]. A special preparation of silver phosphate in contact with graphite [11] and a Ag_3PO_4 – Ag_2S membrane [12] have been reported.

In this study, a systematic check of responses of solid-state electrodes similar to those described by Midgley [10] to HPO_4^{2-} at pH 8.4 was done. The compositions were 1:1:1, 2:1:1, 3:1:1 and 4:1:1 mole ratios Ag_2S : PbS : PbHPO_4 ; and 1:1:1:1, 2:1:1:1 and 3:1:1:1 mole ratios Ag_2S : PbS : PbHPO_4 : Ag_2HPO_4 . These compositions were chosen on the basis of: (1) a presumed need for an insoluble, ionic, conducting binder such as Ag_2S ; (2) an assumption that an optimum composition relative to Ag_2S will exist; (3) the observation that PbS and PbHPO_4 couple ionically with Ag_2S ; (4) the well-established fact that Ag_2S – PbS compositions can be Pb^{2+} -responsive; and (5) the possibility that Ag_2HPO_4 may be necessary to achieve rapid ion-exchange equilibrium.

Theory

There is some existing theory for deduction of the potential range that would be expected for HPO_4^{2-} responses if the assumption of ionic equilibria were the dominant mechanism for the action of the pressed pellet electrodes. The expected electrode potential of a silver-contact pellet electrode in Pb^{2+} -containing electrolytes has the form

$$\phi = \phi^0 + \frac{1}{2} RTF^{-1} \ln [\text{Pb}^{2+}] - \phi_{\text{ref}} \quad (1)$$

in which ϕ is the measured potential difference. The theory for this case gives two extreme ϕ^0 values [14] depending on the saturation state of the pellet with respect to silver or sulfur. If the pellet is saturated with silver metal, then at 25°C

$$\phi_1^0 = \phi_{\text{Ag}/\text{Ag}^+}^0 + 0.0295 \ln [K_s(\text{Ag}_2\text{S})/K_s(\text{PbS})] \quad (2)$$

or saturated with sulfur

$$\phi_2^0 = \phi_{\text{Pb}/\text{Pb}^{2+}}^0 + 0.0295 \ln K_f(\text{PbS}) \quad (3)$$

In these equations, K_s indicates a solubility product, while K_f is a formation constant from the elements. To develop an expression for the HPO_4^{2-} -response, the solubility product expression for PbHPO_4 is introduced

$$\phi = \phi^0 + 0.0295 \log K_s(\text{PbHPO}_4) - 0.0295 \log [\text{HPO}_4^{2-}] - \phi_{\text{ref}} \quad (4)$$

With the values $\text{p}K_s(\text{Ag}_2\text{S}) = 49.2$; $\text{p}K_s(\text{PbS}) = 26.2$, $\text{p}K_f = -16.24$, and $\text{p}K_s(\text{PbHPO}_4) = 9.89$, the response equation at 25°C will be between

$$\phi = -0.408 - 0.0295 \log [\text{HPO}_4^{2-}] \quad (5)$$

and

$$\phi = -0.185 - 0.0295 \log [\text{HPO}_4^{2-}] \quad (6)$$

for HPO_4^{2-} activities from saturation to about 10^{-5} M.

EXPERIMENTAL

Apparatus and reagents

An Orion Research Model 701 digital pH/mV meter, coupled with a Beckman recorder, was used for all potential measurements. Pellets were prepared using a Carver Press Model C (M-2380) with attached hot plates (M-2381). Experience with preparation of PbS/Ag₂S electrodes for lead ion activities, showed that responses depended strongly on the temperature of the hot press, and depended less strongly on pressure above about 10 tons. Because lead monohydrogenphosphate loses water at about 250°C, pressing temperatures were kept below this value. In seeking an optimum composition and optimum preparation conditions, consideration of pellet stability was important.

A Spex Mixer Mill (Model 5100) was used for sample preparation. A saturated calomel electrode (Fisher Scientific Company, porous plug type) was used as the reference electrode, and a silver/silver chloride electrode (Fisher Scientific Company, porous-plug type) was used as the internal reference electrode. The magnetic stirrer used was a Fisher Model 16. Indicator electrodes (Fig. 1) were made in this laboratory.

AgNO₃, Pb(NO₃)₂, Na₂HPO₄·7H₂O, Na₂HPO₄ (anhydrous) and Na₂S·9H₂O (Fisher Scientific Company) were used without further purification. Silver powder (100 mesh) and silver wire (Alfa Division, Ventron) were used. De-ionized and distilled water was used to prepare all solutions and membrane materials. Ammonium acetate—ammonia (0.1 M) buffer solution was prepared from ammonium acetate dissolved in water and adjusted to pH 8.44 by dropwise additions of ammonia liquor. Standard monohydrogenphosphate solutions were prepared by dissolving Na₂HPO₄ (anhydrous) in the ammoniacal buffer. Other hydrogenphosphate solutions (10^{-2} – 10^{-5} M) were prepared by successive dilution of the 0.1 M solution with buffer. All hydrogenphosphate standards were adjusted to pH 8.44.

Preparation of pellet materials

Silver sulfide—lead sulfide—lead hydrogen phosphate—silver hydrogen phosphate mixtures were prepared as follows. For the equimolar mixture (Ag₂S:PbS:PbHPO₄:Ag₂HPO₄ = 1:1:1:1), lead nitrate (0.1 mol) and silver nitrate (0.1 mol) were dissolved in 100-ml portions of water, and then mixed together. Hydrated sodium sulfide and hydrated disodium hydrogenphosphate (0.1 mol each) were dissolved in 80-ml portions of water, and then mixed and filtered. The filtrate was dripped into the mixed solution of silver nitrate and lead nitrate, while stirring magnetically. The precipitate was first

washed copiously with water by decantation, then filtered, again washed with water several times, and dried at 80°C. Other mixtures were made by adding appropriate amounts of silver sulfide to the equimolar mixture.

Silver sulfide—lead sulfide—lead hydrogenphosphate mixtures were prepared as follows. Silver nitrate (0.2 mol) and lead nitrate (0.1 mol) were dissolved in 100-ml portions of water, and then mixed. Hydrated sodium sulfide (0.1 mol) was dissolved in about 80 ml of water and filtered. The filtrate was dripped into the mixed solution of silver nitrate and lead nitrate. The precipitate obtained (component mole ratio $\text{Ag}_2\text{S}:\text{PbS} = 2:1$) was filtered, washed several times with water, and dried at 80°C. Meanwhile, lead nitrate (0.2 mol) was dissolved in about 150 ml of water. Hydrated disodium hydrogenphosphate and hydrated sodium sulfide (0.1 mol each) were dissolved in 80-ml portions of water, mixed and filtered. The precipitate obtained on mixing, (mole ratio of components $\text{PbHPO}_4:\text{PbS}$, 2:1) was filtered, washed and dried as above. To make equimolar mixtures of three components ($\text{Ag}_2\text{S}:\text{PbS}:\text{PbHPO}_4 = 1:1:1$), the calculated amounts of the two-component mixtures were put into about 500 ml of water again, stirred for 3 h, filtered, washed with water, and dried as above. Mixing these two component precipitates in water gave better-responding electrodes than those obtained after mixing the dry components.

Other mixtures were made by adding appropriate amounts of silver sulfide to the equimolar mixtures.

Preparation of ion-selective electrodes

All active materials were thoroughly mixed with a Spex Mixer Mill for 10 min and ground in a mortar. Three types of membrane pellets made by the hot press method were: (1) laminated active material (0.7–0.8 g)/silver powder (0.4 g), (2) laminated active material (0.7–0.8 g)/silver sulfide (0.4 g)/silver powder (0.4 g), and (3) active material only (0.7–0.8 g). Pellets were pressed under ten tons at various temperatures, then polished in turn with 320, 400, and 500 mesh sandpapers followed by 15, 6, 1, and 0.25- μm diamond pastes. After the pellets had been polished, they were soldered to a silver wire and then mounted at the end of PVC tubes with epoxy resin. The three configurations of phosphate ion-selective electrodes constructed (Fig. 1) were: (A) direct contact of silver metal (powder) with the active phase, (B) contact of silver sulfide/silver metal with the active phase, and (C) contact through an inner solution and silver/silver chloride reference electrode salt bridge (porous plug) with the active phase.

Potential measurements

About 50 ml of the phosphate solutions were placed in 100-ml beakers and stirred magnetically. The electrodes were immersed in the solution, and the potential was recorded when a steady reading was obtained in the stirred solution.

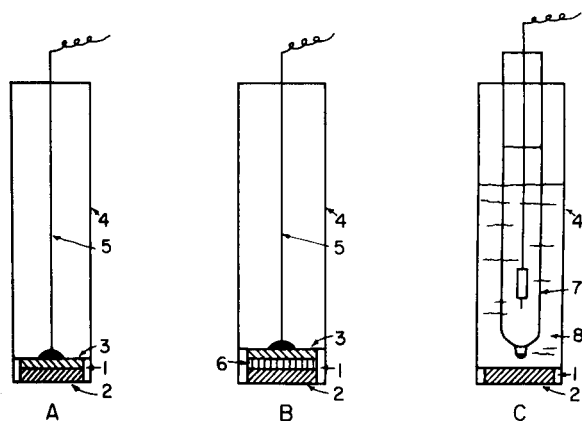


Fig. 1. Designs for phosphate-selective electrodes. (1) Epoxy resin, (2) active materials, (3) silver metal powder, (4) plastic tube, (5) silver wire, (6) silver sulfide powder, (7) AgCl/Ag reference electrode, (8) internal solution (10^{-1} M HPO_4^{2-} in ammonia buffer).

RESULTS AND DISCUSSION

Four-component mixtures ($\text{Ag}_2\text{S}:\text{PbS}:\text{PbHPO}_4:\text{Ag}_2\text{HPO}_4$)

The least attractive of the various combinations was that involving four components. Pellets having the composition mole fraction 1:1:1:1 could be made at temperatures up to 140°C . Above that temperature, the pellets decomposed, and below that temperature, readings were unstable and erratic. Examples of stable pellets made at 140°C in designs A, B and C gave responses which were satisfactory from 10^{-1} to 10^{-3} M with responses of 31

TABLE 1

Responses for systematically varied compositions in type A configurations

Mole ratio ^a	Pressing temperature ^b ($^\circ\text{C}$)	Response to HPO_4^{2-} ($-\text{mV}/\text{decade}$)	Response to Pb^{2+} (mV/decade)
1:1:1:1	140	30 ± 1^c 13–20 ^d	27 ± 1^c
2:1:1:1	160	28 ± 1^c 18–22 ^d	25 ± 1^c
3:1:1:1	180	$19\text{--}25^c$	25 ± 1^c
1:1:1:0	180	$18\text{--}26^c$	28 ± 1^c
2:1:1:0	200	38 ± 1^e 17–23 ^f	28 ± 1^c
3:1:1:0	220	28 ± 1^c 16–20 ^d	28 ± 1^c
4:1:1:0	240	27 ± 1^e 18–25 ^f	26 ± 1^c

^a $\text{Ag}_2\text{S}:\text{PbS}:\text{PbHPO}_4:\text{Ag}_2\text{HPO}_4$. ^b Pressure, 10 tons; time, 15 h. ^c 10^{-1} – 10^{-3} M. ^d 10^{-3} – 10^{-5} M. ^e 10^{-1} – 10^{-2} M. ^f 10^{-2} – 10^{-4} M.

mV/decade, 25 mV/decade, and 28.5 mV/decade for types A, B and C, respectively. Time constants to 64% of final response were 1 min at highest concentrations to 5 min at 10^{-4} M. Responses were sub-Nernstian for activities less than 10^{-3} M. Responses of type-A membranes are given in Table 1. These electrodes are also responsive to lead ion activities.

Pellets with mole ratios 2:1:1:1 could be prepared at 160°C by adding Ag_2S , but were unstable and fragile if heated above that temperature. Responses were marginally better than the 1:1:1:1 case in that slopes were Nernstian (28.5 mV/decade) from 10^{-1} to 10^{-3} M, 22 mV/decade from 10^{-3} to 10^{-4} M and 18 mV/decade from 10^{-4} to 10^{-5} M. The designs were not critical. Electrodes of the C-type exposed to internal electrolyte gave slightly faster responses, but the A-type and B-type were adequate. An example of response is shown in Fig. 2.

Addition of Ag_2S to the previous composition did not improve responses. The composition 3:1:1:1 mole ratio gave only responses of 19–25 mV/decade in the region 10^{-1} – 10^{-3} M, and even less sensitivity as activities were decreased. It was concluded that the 2:1:1:1 composition was best in terms of pellet stability, ease of removal from the press, reproducibility of responses, sensitivity and time constants.

Three-component mixtures ($\text{Ag}_2\text{S}:\text{PbS}:\text{PbHPO}_4$)

Of the four combinations prepared (1:1:1, 2:1:1, 3:1:1 and 4:1:1), the third system listed proved to be best in terms of stability, reproducibility and rapidity of response. The ease of preparation, freedom from cracking, and success rate for removal from the die, improved with additional Ag_2S . The 1:1:1 combination could be prepared only at 180°C or below; the 2:1:1 at 200°C ; the 3:1:1 at 220°C ; and the 4:1:1 at 240°C . Types A, B, and C electrodes were prepared. Responses for the optimum system (3:1:1)

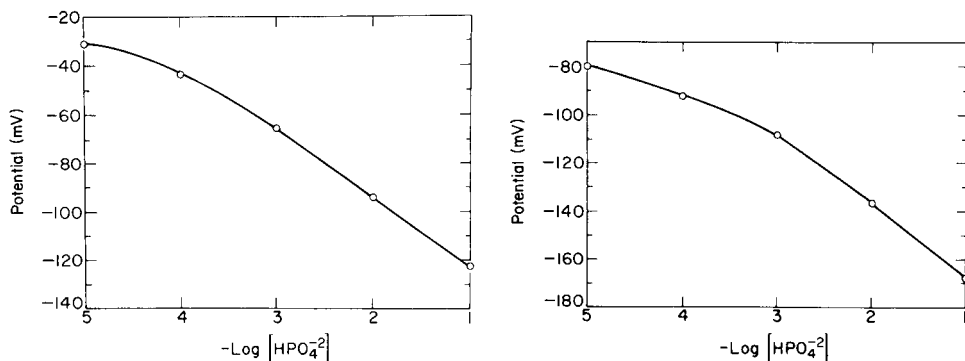


Fig. 2. Response of a four-component formulation $\text{Ag}_2\text{S}:\text{PbS}:\text{PbHPO}_4:\text{Ag}_2\text{HPO}_4$ (2:1:1:1) prepared at 160°C in the C-type form (see text).

Fig. 3. Response of a three-component formulation $\text{Ag}_2\text{S}:\text{PbS}:\text{PbHPO}_4$ (3:1:1) prepared at 220°C in the A-type form (see text).

TABLE 2

Responses of a three-component system^a according to pressing temperature

Pressing temperature ^b (°C)	Response to HPO_4^{2-} (-mV/decade)	Response to Pb^{2+} (mV/decade)
220	28 ± 1^c 16–20 ^d	28 ± 1^c 15–18 ^d
200	28 ± 1^c 16–20 ^d	28 ± 1^c 15–18 ^d
180	28 ± 1^c 13–18 ^d	28 ± 1^e 26 ^f 16–18 ^d
160	27 ± 1^c 10–15 ^d	27 ± 1^e 20 ^f 11–13 ^d
Room temp.	18–25 ^c	20–26 ^c

^a $\text{Ag}_3\text{S}:\text{PbS}:\text{PbHPO}_4 = 3:1:1$, type A. ^bPressure, 10 tons; time, 15 h. ^c 10^{-1} – 10^{-3} M. ^d 10^{-3} – 10^{-5} M. ^e 10^{-2} – 10^{-3} M. ^f 10^{-1} – 10^{-2} M.

were 28 ± 1 mV/decade in the range 10^{-1} – 10^{-3} M; 20 mV/decade for the C-type in this range. 10^{-3} – 10^{-4} M for A and B; but 16 mV/decade for the C-type in this range. An example of response is shown in Fig. 3. Responses for a series of three-component type-A membranes are given in Table 1. Effects of pressing temperatures are given in Table 2. The compositions are responsive to Pb^{2+} ions.

Interferences

A brief test of interferences, using the 3:1:1 composition, was performed for those common ions expected to have minimal effects. Results for 100-fold amounts of F^- , NO_3^- , SO_4^{2-} , HCO_3^- and Cl^- on the response for 10^{-4} M HPO_4^{2-} are shown in Table 3. Hydrogencarbonate and chloride show significant errors. Since this electrode is primarily responsive to lead ion activities, it is not surprising that hydrogencarbonate interferes. Other data in

TABLE 3

Anion interferences at the 10^{-2} M level on the response for monohydrogenphosphate in ammoniacal buffer pH 8.44

Anion	Response (mV) ^a	Δ mV	Anion	Response (mV) ^b	Δ mV
F^-	-92.0	0.0	HAsO_4^{2-}	-150	-13.0
NO_3^-	-92.0	0.0	MoO_4^{2-}	-147	-10.0
SO_4^{2-}	-93.0	-1.0	WO_4^{2-}	-145	-8.0
HCO_3^-	-99.5	-7.5	CrO_4^{2-}	-119	+18.0
Cl^-	-106.0	-14.0	None	-137	0.0
None	-92.0	0.0			

^aFor 10^{-4} M HPO_4^{2-} . ^bFor 10^{-2} M HPO_4^{2-} .

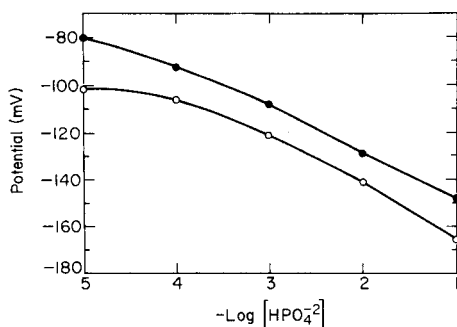


Fig. 4. Response to (●) HPO_4^{2-} and (○) $\text{HPO}_4^{2-}\text{--Cl}^-$ mixtures at 10^{-2} M chloride in ammonium acetate–ammonia buffer.

Table 3 show that arsenate, molybdate, tungstate and chromate are major interferences. The chloride interference is unusual, as shown in Fig. 4. The entire response curve is displaced, although the response to HPO_4^{2-} remains normal. This type of response has not been widely observed. In this case, the effect may arise from the reaction of chloride with Pb^{2+} to form PbCl^+ , and to lower the local activity of Pb^{2+} in the surface region. The chromate interference is interesting because it is consistent with the response potential range for generation of sulfur in the membrane. The experimental data presented in the Figures suggest that all of the electrodes are sulfur-rich, rather than silver-rich. The estimated standard potentials tend to lie nearer to the expected value for eqn. (5). However, the preparations are not uniform at the positive limit. Possibly for the electrode used to study anion interferences, chromate reacted chemically at the surface to form additional sulfur and a shift toward positive potentials.

Lifetimes

After soaking the better electrodes in water for one day, response slopes approached 25 mV/decade from 10^{-3} to 10^{-1} M HPO_4^{2-} . After 1–2 weeks, slopes improved to 28.5 mV/decade. After 1 month, slopes declined to 23 mV/decade, and after 2 months of continued immersion in water, responses virtually disappeared. We have recently found that a new buffer (CHES, Cal Biochem) at pH 9.5 improves response slopes and reproducibility.

This work was supported by the National Science Foundation, Grant No. CHE-77-20491.

REFERENCES

- 1 I. Nagelberg, L. Braddock and G. Barbero, *Science*, 166 (1969) 1403.
- 2 M. Nanjo, T. J. Rohm and G. G. Guilbault, *Anal. Chim. Acta*, 77 (1975) 19.
- 3 G. G. Guilbault and P. J. Brignac, Jr., *Anal. Chim. Acta*, 56 (1971) 139.
- 4 E. Pungor, K. Toth and J. Havas, *Mikrochim. Acta.*, 4 (1966) 689.
- 5 G. Rechnitz, Z. F. Lin and S. B. Zamochnik, *Anal. Lett.*, 1 (1967) 29.

- 6 G. G. Guilbault and P. J. Brignac, Jr., *Anal. Chem.*, 41 (1969) 1136.
- 7 G. A. Rechnitz, G. H. Fricke and M. S. Mohan, *Anal. Chem.*, 44 (1972) 1098.
- 8 F. R. Shu and G. G. Guilbault, *Anal. Lett.*, 5 (1972) 559.
- 9 J. Tacussel, French Patent 2,203,518, May 10 1972, Appl. 36,999 Oct. 13, 1972.
- 10 D. Midgley, *Talanta*, 26 (1979) 261.
- 11 I. Novozamsky and W. H. van Riemsdijk, *Neth. Appl.* 75-15,205 July 4, 1977; *Anal. Chim. Acta*, 85 (1976) 41.
- 12 J. Tacussel and J. J. Fombon, in E. Pungor and I. Buzas (Eds.), *Ion-Selective Electrodes*, Elsevier, Amsterdam, 1978, p. 567.
- 13 T. Tanaka, K. Hiroy and A. Kawahara, *Jpn. Kokai* 78-39,193, April 10, 1978.
- 14 R. P. Buck and V. R. Shepard, Jr., *Anal. Chem.*, 46 (1974) 2097.

ENZYME ELECTRODE SYSTEM FOR OXALATE DETERMINATION UTILIZING OXALATE DECARBOXYLASE IMMOBILIZED ON A CARBON DIOXIDE SENSOR

R. K. KOBOS* and T. A. RAMSEY

Department of Chemistry, Virginia Commonwealth University, Richmond, VA 23284 (U.S.A.)

(Received 2nd June 1980)

SUMMARY

A highly selective enzyme electrode system for oxalate is described in which the enzyme oxalate decarboxylase is immobilized on a carbon dioxide gas-sensing electrode. The response of the system is linear with the logarithm of the oxalate concentration between 2×10^{-4} and 1×10^{-2} M with a slope of 57–60 mV/decade. The oxalate detection limit is 4×10^{-5} M. Electrodes used with chemically immobilized enzyme are not affected by phosphate and sulfate at levels normally found in urine and are very stable showing no decrease in response after one month of operation. The enzyme electrode system functions well in urine, requiring minimal sample pretreatment. The recovery of oxalate added to five aliquots of a human control urine sample averaged 97.7% with an average relative standard deviation of 4.5%.

The determination of oxalate in urine is clinically important for the diagnosis of various forms of hyperoxaluria as well as in urinary stone research. In addition, a simple method for oxalate determination is needed in the analysis of foods and other nonbiological samples [1]. Consequently, many different methods have been reported for the determination of oxalate [1, 2]. Most of these published methodologies are complicated, requiring sample pretreatment as part of the determination.

Enzymatic methods for oxalate have been reported using oxalate decarboxylase (E.C. 4.1.1.2) and more recently oxalate oxidase (E.C. 1.2.3.4). Oxalate decarboxylase is commercially available and has been shown to be highly specific in catalyzing the reaction: oxalate \rightarrow CO₂ + formate. Methods have been developed, using the soluble enzyme, based either on the detection of CO₂ by means of manometric [3, 4], spectrophotometric [5, 6], conductometric [7], and potentiometric techniques [6, 8], or the spectrophotometric detection of formate using NAD requiring formate reductase [9, 10]. The problem with these techniques is that the enzyme is expensive and since the soluble enzyme is used, the methods are very costly. Furthermore, phosphate and sulfate, at levels normally found in urine, have been found to inhibit the enzyme [5, 6], thereby complicating the determination.

Oxalate oxidase catalyzes the reaction: $\text{oxalate} + \text{O}_2 \rightarrow 2\text{CO}_2 + \text{H}_2\text{O}_2$. Methods based on this enzyme have used the detection of a pH change caused by the release of CO_2 into an alkaline buffer using a pH electrode [11], and the spectrophotometric determination of the hydrogen peroxide produced by the immobilized enzyme [12]. Oxalate oxidase is not available commercially and must be isolated from barley seedlings. In addition, several anions and cations, such as calcium, copper, and fluoride [11, 13, 14] in urine, inhibit the enzyme.

Potentiometric enzyme electrode systems have been reported for substances such as urea [15], uric acid [16], and lysine [17] using decarboxylating enzymes immobilized on carbon dioxide gas-sensing electrodes. This configuration has the advantage that the enzyme can be reused for many assays and is therefore very cost-efficient. Furthermore, it has been reported that the effects of enzyme inhibitors can be greatly reduced or eliminated by using chemical immobilization techniques [18, 19]. The use of enzyme activators has also been described to increase enzyme activity and therefore the lifetime of enzyme electrode systems [20].

This paper describes the preparation and evaluation of oxalate enzyme electrode systems based on commercially available oxalate decarboxylase. Chemical immobilization techniques were investigated as a means of reducing phosphate and sulfate inhibition as well as to increase the lifetime of the system. An enzyme activator, hydroquinone, which has been reported to increase the enzyme activity of oxalate decarboxylase by 60–100% [21], was also used to improve the lifetime of the system. The resulting sensor provides a simple method for oxalate determination in complex samples such as urine, with minimal sample pretreatment.

EXPERIMENTAL

Apparatus and reagents

An Orion Model 95-02 carbon dioxide gas-sensor was used in the construction of the sensor systems. Potential measurements were made with a Corning Model 130 digital pH meter in conjunction with a Houston Instruments Omniscrite recorder. All measurements were performed in a thermostated cell.

Oxalate decarboxylase was obtained (Sigma Chemical Company) as a partially purified powder isolated from *Collybia velutipes*. With some lots it was necessary to purify the enzyme further because of low specific activity. An acetone fractionation procedure as described by Shimazono and Hayaishi [21] was used.

Standard sodium oxalate (Thorn Smith), amino acids, bovine serum albumin and glutaraldehyde (Sigma Chemical Company) and ultrapure urea (Schwarz and Mann) were used. All other chemicals were analytical reagent grade. Solutions were prepared with distilled—deionized water. Human control urine samples, Level I (normal), were obtained from Fisher Scientific.

Procedures

Activity determinations were made for each enzyme lot at $37 \pm 0.5^\circ\text{C}$ in pH 3.0 citrate buffer by using the carbon dioxide sensor to monitor the rate of carbon dioxide production. A unit is defined as the amount of enzyme catalyzing the production of $1 \mu\text{mol CO}_2 \text{ min}^{-1}$ at 37°C and pH 3.0.

The enzyme was immobilized either by entrapment within a dialysis membrane (Uni-Pore Polycarbonate Membrane, pore size $0.05 \mu\text{m}$) or by covalent binding to the membrane of the CO_2 electrode using bovine serum albumin (BSA) and glutaraldehyde [17]. In the entrapment method, the desired amount of enzyme was dissolved in $30 \mu\text{l}$ of buffer directly on the gas-permeable membrane. The enzyme solution was covered with the dialysis membrane to hold the enzyme on the electrode surface.

In the covalent-binding procedure, the desired amount of enzyme was dissolved in $30 \mu\text{l}$ of buffer containing 15% BSA on the membrane of the CO_2 sensor. Then, $3 \mu\text{l}$ of 25% glutaraldehyde was added. The solution was mixed thoroughly and allowed to cross-link for 10–15 min until complete solidification was achieved. A dialysis membrane was then placed over the immobilized enzyme.

The enzyme electrode system was conditioned in 0.1 M, pH 3.0 citrate buffer for 1 h before use. All electrode studies were done at $30 \pm 0.5^\circ\text{C}$. Calibration curves were obtained by making additions of 0.1 M sodium oxalate solution to 25 ml of buffer and recording the steady-state potentials.

Recovery studies were performed using Urine Controls, reconstituted with distilled water according to the manufacturer's instructions. The urine sample was then diluted (1 + 1) with double strength buffer. The carbon dioxide level of the diluted urine sample was first determined with the CO_2 sensor and any endogenous carbon dioxide present was removed by passing nitrogen gently through the solution for 15 min. The oxalate sensor was then placed in the sample solution and the stable potential reading obtained. The initial oxalate concentration was determined from a prior calibration curve. Additions of standard oxalate solution were made and the corresponding oxalate levels determined from the calibration curve.

RESULTS AND DISCUSSION

Preliminary studies, with a dialysis-membrane-entrapped enzyme electrode system containing 8 units of oxalate decarboxylase, were done in 0.1 M, pH 3.0 citrate buffer. This pH has been reported to be the optimum for the enzyme [21] and is highly compatible with the gas-sensing electrode, since essentially all of the carbon dioxide in solution is in the CO_2 form. Under these conditions, the enzyme electrode system exhibited a response that was linear with the logarithm of the oxalate concentration between 2×10^{-4} and 1×10^{-2} M with a slope of $57.6 \pm 2.1 \text{ mV/decade}$ and with standard error and correlation coefficient of 1.5 and 0.9994, respectively.

To determine the influence of pH on the enzyme electrode system, it

was placed in a pH 6.0 citric acid buffer containing 1×10^{-3} M oxalate. Additions of concentrated hydrochloric acid were made, and the pH of the solution and the electrode potential were recorded. The results of this study are shown in Fig. 1. The pH maximum response range was found to be 3.2–2.5 for this electrode system with the enzyme entrapped in the dialysis membrane. The chemically immobilized enzyme electrode system had a much broader optimum range, pH 4.5–2.5. All subsequent studies were done at pH 3.0 for purposes of comparison. However, the chemically immobilized enzyme could be used at pH 4.5 with no loss of oxalate response. The response of the carbon dioxide gas-sensor to organic acids is less at this pH [22], therefore the ability to use the enzyme electrode system at pH 4.5 would diminish possible interferences in some samples.

Enzyme electrode systems were prepared by using various amounts of enzyme ranging from 2 to 12 units. It was found that a minimum of 8 units was required to produce maximum response. Therefore, 8–12 units of enzyme were used in all systems studied.

The effect of hydroquinone, a reported activator of oxalate decarboxylase [21], on the response of the enzyme electrode system was also investigated. Figure 2 shows the response of an eight-day old enzyme electrode system, the response of which had begun to deteriorate (slope = 35.5 mV/decade), in the presence of 1×10^{-2} M hydroquinone. The response slope under activated conditions was 49.3 mV/decade, indicating that the hydroquinone has a significant effect on the enzyme activity and therefore can be used to

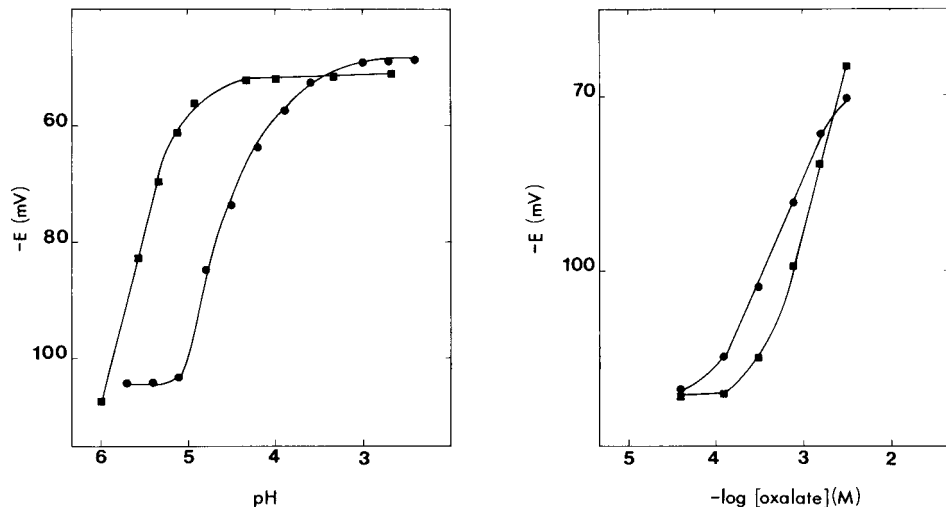


Fig. 1. Effect of pH on the potential of oxalate sensors. Oxalate concentration is 1×10^{-3} M. (●) Dialysis-membrane-entrapped enzyme electrode system; (■) chemically immobilized enzyme electrode system.

Fig. 2. Response of an eight-day old electrode system with enzyme entrapped in dialysis membrane under nonactivated (●) and activated (■) conditions.

increase the lifetime of the system. However, at this concentration level, hydroquinone inhibited the enzyme at low oxalate concentrations, i.e., 1×10^{-4} – 3×10^{-4} M. The optimum amount of hydroquinone to be used was determined by making additions of hydroquinone to a solution containing 1×10^{-4} M oxalate and recording the potential of the enzyme electrode system. Figure 3 indicates that the concentration of the activator for maximum response is between 7×10^{-4} and 1.5×10^{-3} M. Hydroquinone was added to the buffer solution at a concentration of 1×10^{-3} M for all further studies.

Typical calibration curves for the chemically immobilized enzyme electrode system under optimum conditions, i.e., pH 3.0 citrate buffer containing 1×10^{-3} M hydroquinone, are shown in Fig. 4. The response was linear with the logarithm of the oxalate concentration from 2×10^{-4} to 1×10^{-2} M with a slope of 59.5 ± 2.1 mV/decade (standard error 0.66; correlation coefficient 0.9998). Similar response was obtained with the dialysis-membrane-entrapped enzyme electrode system. The lower limit of detection, defined as the concentration at the point of intersection of the extrapolated linear segments of the calibration curve [23], was 4×10^{-5} M. This range is suitable for urinary oxalate determinations, since oxalate is normally present at concentrations of 1.6×10^{-4} – 5.5×10^{-4} M (14 – 50 mg l^{-1}) [1]. If the urine sample is diluted (1 + 1) with double strength buffer, the normal oxalate concentration range would still be above the detection limit of the

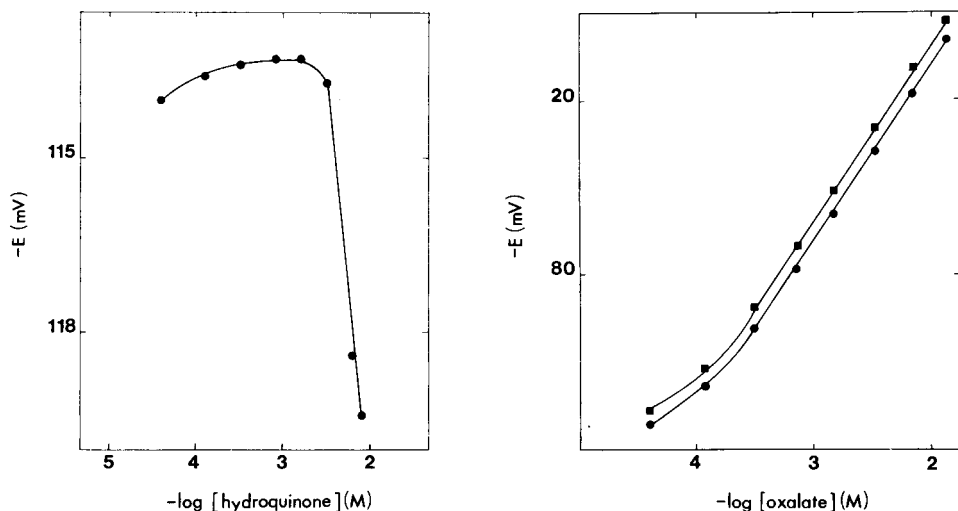


Fig. 3. Effect of hydroquinone on the potential of the enzyme electrode system at an oxalate concentration of 1×10^{-4} M.

Fig. 4. Calibration curves of a chemically immobilized enzyme electrode system. (●) Day 1; (■) day 29.

electrode and could be determined by using the non-linear portion of the calibration curve.

The response times of the enzyme electrode system ranged from 8 to 30 min depending on the thickness of the enzyme layer. Therefore, it is important to use an enzyme preparation with a high specific activity so that the required amount of enzyme results in a thin layer. By purification of the commercially available enzyme, the specific activity could be increased sufficiently to yield a thin enzyme layer, resulting in systems with response times of 8–10 min. A specific activity of 1 unit mg^{-1} of solid was found to be adequate. The slowness of response is probably the most serious limitation of the sensor. However, when compared with other methods which require extensive sample pretreatment, the time of determination is favorable.

The selectivity of the oxalate sensor was studied by testing the response to a number of substances. The L-isomers of the amino acids lysine, glutamic acid, arginine, histidine, phenylalanine, methionine, alanine, asparagine, glutamine, leucine, aspartic acid, and tyrosine as well as urea produced no response at concentrations up to 3×10^{-3} M. Similarly, the enzyme electrode system did not respond to the following organic acids at these levels: acetic, formic, pyruvic, maleic, malonic and succinic acids. Some response was obtained to benzoic and salicylic acids because of the carbon dioxide sensor itself.

The effects of phosphate and sulfate, which are known inhibitors of oxalate decarboxylase [5], were also investigated. The response of the enzyme electrode system based on a dialysis membrane was decreased in the presence of phosphate or sulfate at concentrations of 0.082 M, the highest concentration likely to be encountered in human urine [6]. This effect increased as the activity of the enzyme decreased over a period of one week. Figure 5 shows the result of this level of inhibitors on a seven-day old oxalate sensor.

The chemically immobilized enzyme electrode system was not affected by phosphate and sulfate at this same concentration level. Calibration curves obtained in the presence of phosphate and sulfate, each at a concentration of 0.082 M, had a slope of 59.4 ± 2.8 mV/decade. This response is identical to that obtained in the absence of the inhibitors.

The long-term stability of the two types of enzyme electrode systems differed markedly. The dialysis-membrane-entrapped enzyme electrode system began to show a decrease in response after 4 days when stored refrigerated in pH 4.5 citrate buffer. This pH was chosen for the storage solution because it has been reported that it is optimal for enzyme stability [21]. The response was analytically useful for up to eight days. The lifetime could be extended to two weeks by the use of hydroquinone to activate the enzyme. The chemically immobilized enzyme electrode system, as would be expected, had a much longer lifetime. When stored refrigerated in the storage solution containing 1×10^{-3} M hydroquinone, the system showed no decrease in response after one month of daily use, as shown in Fig. 4.

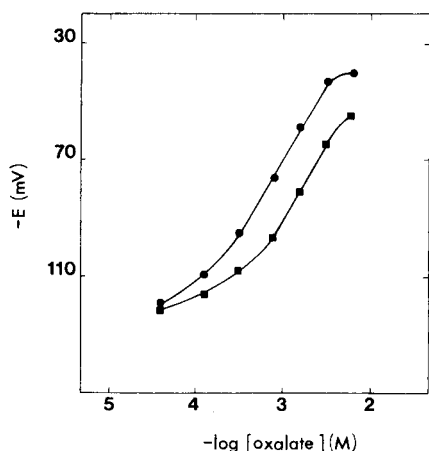


Fig. 5. Effect of phosphate and sulfate on the response of a seven-day old electrode system with enzyme entrapped in dialysis membrane. (●). No inhibitors present; (■) inhibitors present at a concentration of 0.082 M.

TABLE 1

Standard addition studies of oxalate added to human control urine

Oxalate (mg l^{-1})		R.s.d. (%)	Recovery (%)
Added ^a	Found ^b		
0	8.76	0.1	—
18.0	17.9	6.1	99.6
35.9	34.7	4.6	96.6
53.7	53.3	3.4	99.2
89.1	84.9	8.4	95.3

^aAs anhydrous oxalic acid. ^bAverage of three determinations.

In order to demonstrate the possible future application of the oxalate sensor in clinical chemistry, a calibration curve was obtained in a control urine sample. The curve is essentially the same as that obtained in buffer, having a slope of 59.9 ± 1.6 mV/decade with standard error of estimate of 0.76, and a correlation coefficient of 0.9997. Table 1 shows the recovery of oxalate added to control urine samples. The average recovery was 97.7%, indicating the potential usefulness of the enzyme electrode system for urinary oxalate determinations.

We gratefully acknowledge the support of a grant from Research Corporation.

REFERENCES

- 1 A. Hodgkinson, *Oxalic Acid in Biology and Medicine*, Academic Press, New York, 1977.
- 2 A. Hodgkinson, *Clin. Chem.*, 16 (1970) 547.
- 3 G. G. Mayer, D. Markow and F. Karp, *Clin. Chem.*, 9 (1963) 334.
- 4 M. E. Ribeiro and J. S. Elliot, *Invest. Urol.*, 2 (1964) 78.
- 5 C. F. Knowles and A. Hodgkinson, *Analyst*, 97 (1972) 474.
- 6 P. C. Hallson and G. A. Rose, *Clin. Chim. Acta*, 55 (1974) 29.
- 7 J. D. Sallis, M. F. Lumley and J. E. Jordon, *Biochem. Med.*, 18 (1977) 371.
- 8 S. J. Yao, S. K. Wolfson and J. M. Tokarsky, *Bioelectrochem. Bioenerg.*, 2 (1975) 348.
- 9 J. Costello, M. Hatch and E. Bourke, *J. Lab. Clin. Med.*, 87 (1976) 903.
- 10 M. Hatch, E. Bourke and J. Costello, *Clin. Chem.*, 23 (1977) 76.
- 11 G. Kohlbecker, L. Richter and M. Butz, *J. Clin. Chem. Clin. Biochem.*, 17 (1979) 309.
- 12 R. Bais, N. Potezny, J. B. Edwards, A. M. Rofe and R. A. J. Conyers, *Anal. Chem.*, 52 (1980) 508.
- 13 J. Chiriboga, *Biochem. Biophys. Res. Commun.*, 11 (1963) 277.
- 14 J. Chiriboga, *Arch. Biochem. Biophys.*, 116 (1966) 516.
- 15 G. G. Guilbault and F. R. Shu, *Anal. Chem.*, 44 (1972) 2161.
- 16 T. Kawashima and G. A. Rechnitz, *Anal. Chim. Acta*, 83 (1976) 9.
- 17 W. C. White and G. G. Guilbault, *Anal. Chem.*, 50 (1978) 1481.
- 18 G. G. Guilbault, *Handbook of Enzymatic Methods of Analysis*, M. Dekker, New York, 1977, p. 497.
- 19 A. M. Klibanov, *Anal. Biochem.*, 93 (1979) 1.
- 20 M. E. Meyerhoff and G. A. Rechnitz, *Anal. Chim. Acta*, 85 (1976) 277.
- 21 H. Shimazono and O. Hayaishi, *J. Biol. Chem.*, 227 (1957) 151.
- 22 Orion Carbon Dioxide Electrode Instruction Manual, Orion Research Inc., 1977, p. 19.
- 23 IUPAC Analytical Chemistry Division, *Pure Appl. Chem.*, 48 (1976) 127.

ENHANCEMENT OF SELECTIVITY OF A BENZOATE-SENSITIVE LIQUID MEMBRANE ELECTRODE BY ALKYLPHENOL

HIROKAZU HARA, SATOSHI OKAZAKI and TAITIRO FUJINAGA*

Department of Chemistry, Faculty of Science, Kyoto University, Kyoto 606 (Japan)

(Received 26th June 1980)

SUMMARY

The selectivity of the benzoate-sensitive liquid membrane electrode based on tri-*n*-octylmethylammonium benzoate in *o*-dichlorobenzene enhanced is remarkably by the addition of *p*-*t*-octylphenol to the liquid exchanger solution. There is a linear relationship between the change in the logarithmic selectivity coefficient and the pK_a value of the aliphatic monocarboxylic acid interference. Large decreases in the selectivity coefficients are observed for ions having a small proton acceptor ability such as perchlorate and trifluoromethanesulfonate.

The enhancing effect of *p*-*t*-octylphenol on the selectivity of organic sulphonate-sensitive electrodes has already been reported [1]. This effect was attributed to hydrogen bonding between the phenol and sulfonate on the basis of infrared investigations. Electrodes responsive to carboxylate ions have been widely investigated [2]. For example, electrodes sensitive to acetate [3, 4], oxalate [3, 4], salicylate [3–8], trifluoroacetate [9], and benzoate [3–7] have been reported. Improvement of the response characteristics of carboxylate electrodes is important because many materials of biochemical or clinical importance [8, 10] contain carboxylate groups. Little has been done, however, to enhance the selectivity of carboxylate-sensitive electrodes. Materova et al. [11] prepared an acetate electrode with solvents having a trifluoroacetyl group, and Benignetti et al. [12] used decanol as the solvent in a benzoate electrode.

In this paper, the enhancing effect of *p*-*t*-octylphenol on the selectivity of a liquid-membrane benzoate-sensitive electrode is examined. The degree of change in the logarithmic selectivity coefficient is discussed in relation to the proton acceptor ability of each interfering ion.

EXPERIMENTAL

Reagents

The ion-exchanger was a 0.05 mol dm⁻³ solution of tri-*n*-octylmethylammonium benzoate in *o*-dichlorobenzene. The ion-pair was prepared from Capriquat (tri-*n*-octylmethylammonium chloride; Dojin Research Laboratories

Co.) by shaking its chloroform solution with 0.5 mol dm^{-3} sodium benzoate. After evaporation of chloroform under reduced pressure, the ion-pair was used without further purification. To examine the effect of the hydrogen bond donor, 0.5 mol dm^{-3} *p*-*t*-octylphenol (PTOP) was added to the *o*-dichlorobenzene.

Measurements

The body of a Corning probe (No. 476235) with a hydrophobic ceramic junction was used. The membrane potentials were measured at $25 \pm 0.5^\circ\text{C}$ by an Orion Digital Ionalyzer Model 601 equipped with a Matsushita recorder Model VP654A. Leakage of potassium chloride from the calomel electrode was minimized by using an Orion double-junction electrode Model 90-02-00 with 0.1 mol dm^{-3} potassium chloride in its outer chamber. The concentration of potassium chloride leaked into sample solution after 10 min was $1.3\text{--}1.5 \times 10^{-5} \text{ mol dm}^{-3}$ which was a negligible quantity for the determination of selectivity coefficients.

The selectivity coefficients were determined by the separate solutions method, where the membrane potentials for 0.01 mol dm^{-3} sodium benzoate and for a 0.01 mol dm^{-3} solution of the sodium salt of the interfering species were measured separately. The difference between these potentials was divided by the Nernstian slope: 59.1 mV/decade change in activity to obtain the logarithmic selectivity coefficient.

RESULTS AND DISCUSSION

Potential response of the electrodes

In both the presence and absence of PTOp, the electrodes were first tested in standard solutions of sodium benzoate. Linear response from 10^{-1} to $10^{-4} \text{ mol dm}^{-3}$ was obtained with both electrodes after correction for the liquid junction potential between the reference electrode and the sample solution. Response time was within 3 min in the concentration range between 10^{-2} and $10^{-4} \text{ mol dm}^{-3}$. Slower responses were observed at 10^{-1} or $10^{-5} \text{ mol dm}^{-3}$.

Selectivity of the electrodes

The logarithmic selectivity coefficients for 22 possible interferences in the presence and absence of PTOp are listed in Table 1; the differences in the logarithmic selectivity coefficients are also tabulated. With the addition of PTOp almost all the interferences decreased so remarkably that the electrode became quite selective to benzoate ion.

According to the theory of liquid membrane electrodes [13], the selectivity coefficient in the case of strong association, as in the present study, is expressed by

$$K_{\text{Bz},j}^{\text{pot}} = u_{\text{Sj}} K_{\text{SBz}} k_j / u_{\text{SBz}} K_{\text{Sj}} k_{\text{Bz}} \quad (1)$$

TABLE 1

Selectivity coefficients, $\log K^{\text{pot}}$, of benzoate electrode
(Ion-exchanger, (A) 0.05 mol dm⁻³ trioctylmethylammonium benzoate in *o*-dichlorobenzene; (B) (A) + 0.5 mol dm⁻³ *p*-*t*-octylphenol)

Anion tested	$\log K^{\text{pot}}$		$\Delta \log K^{\text{pot}}$	Anion tested	$\log K^{\text{pot}}$		$\Delta \log K^{\text{pot}}$
	A	B			A	B	
ClO ₄ ⁻	3.5	-0.5	-4.0	C ₆ H ₅ SO ₃ ⁻	0.7	-0.4	-1.1
CF ₃ SO ₃ ⁻	2.9	-0.4	-3.3	NO ₃ ⁻	0.6	-1.2	-1.8
SCN ⁻	2.2	-0.2	-2.4	Cl ₂ CHCOO ⁻	0.3	-0.6	-0.9
C ₆ H ₄ (OH)COO ^{-a}	1.8	0.6	-1.2	Br ⁻	-0.1	-1.5	-1.4
C ₆ H ₄ (COOH)COO ^{-b}	1.8	0.1	-1.7	NO ₂ ⁻	-0.5	-1.2	-0.7
I ⁻	1.8	-1.0	-2.8	BrO ₃ ⁻	-0.5	-1.9	-1.4
Cl ₃ CCOO ⁻	1.6	0.1	-1.5	Cl ⁻	-1.0	-1.8	-0.8
CH ₃ C ₆ H ₄ SO ₃ ^{-c}	1.1	0.2	-0.9	ClCH ₂ COO ⁻	-1.0	-1.2	-0.2
C ₇ H ₂ (COOH)COO ^{-d}	0.9	-0.6	-1.5	CH ₃ SO ₃ ⁻	-1.3	-1.9	-0.6
ClO ₃ ⁻	0.9	-1.4	-2.3	HCOO ⁻	-1.6	-1.4	+0.2
CF ₃ COO ⁻	0.7	-0.8	-1.5	CH ₃ COO ⁻	-1.8	-1.1	+0.7

^aSalicylate. ^bHydrogenphthalate. ^c*p*-Toluenesulfonate. ^dHydrogenmaleate.

where u_{Sj} and u_{SBz} are the mobilities of the ion-pairs in the membrane phase, K_{SBz} and K_{Sj} are the ion-pair dissociation constants, k_{j} and k_{Bz} are the single-ion partition coefficients and Bz, j, S are benzoate, interfering ion and trioctylmethylammonium, respectively. As it can be assumed that u and K differ less than k among the various interferences [14], $K_{\text{Bz,j}}^{\text{pot}}$ can be approximated by the ratio $k_{\text{j}}/k_{\text{Bz}}$. The single-ion partition coefficient can be correlated with the free energy of transfer of ion from water to the membrane phase [15]. Then,

$$\log K^{\text{pot}} \approx \log k_{\text{j}} - \log k_{\text{Bz}} = \Delta^{\circ}G_{\text{Bz}}^{\text{tr}}/2.3RT - \Delta^{\circ}G_{\text{j}}^{\text{tr}}/2.3RT$$

$$= [(\Delta G_{\text{Bz org}}^{\circ} - \Delta G_{\text{j org}}^{\circ}) - (\Delta G_{\text{Bz aq}}^{\circ} - \Delta G_{\text{j aq}}^{\circ})]/2.3RT \quad (2)$$

where $\Delta^{\circ}G^{\text{tr}}$ is the free energy change associated with the transfer of ions from water to the membrane phase and ΔG° is the free energy change associated with the transfer of ions from gas phase to the state of solvation.

In the absence of PTOP, the second term in parentheses in eqn. (2) predominates over the first term because the difference of solvation energy in the organic phase is smaller than that in the aqueous phase, the selectivity being determined chiefly by the hydration energy of the interfering ion [16]. The order of decrease in the logarithmic selectivity coefficients for inorganic anions is the same as that of their hydration enthalpy, i.e., ClO₄⁻ > I⁻ > NO₃⁻ > Br⁻ > Cl⁻. This sequence is in accordance with the order of extractability of the anions into organic solvents [17]. A linear relationship between the logarithmic selectivity coefficient and the hydration enthalpy has been reported for these anions [16, 18]. As shown in Fig. 1, there is a clear linear correlation between the hydration enthalpy and the logarithmic selectivity coefficient for several interfering ions.

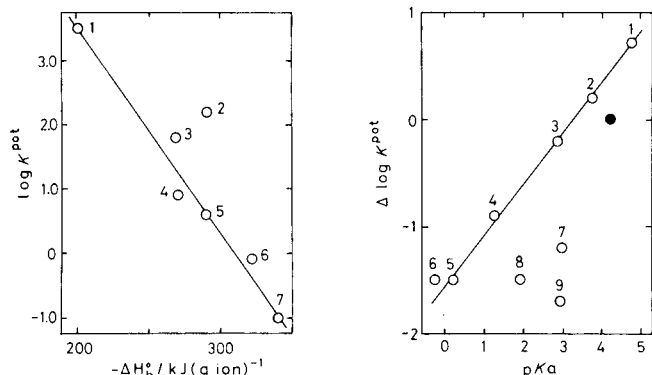


Fig. 1. Relationship between $\log K^{\text{pot}}$ and standard hydration enthalpy $-\Delta H_h^o$ for inorganic anions. (1) ClO_4^- ; (2) SCN^- ; (3) I^- ; (4) ClO_3^- ; (5) NO_3^- ; (6) Br^- ; (7) Cl^- . The $\log K^{\text{pot}}$ values are in the absence of PTOP; the ΔH_h^o values are taken from Ref. [19].

Fig. 2. Relationship between $\Delta \log K^{\text{pot}}$ and pK_a for some carboxylates. (•) benzoate; (1) acetate; (2) formate; (3) monochloroacetate; (4) dichloroacetate; (5) trichloroacetate; (6) trifluoroacetate; (7) salicylate; (8) hydrogenmaleate; (9) hydrogenphthalate; For (7)–(9), the first dissociation constant pK_{a1} is taken.

In the presence of PTOP, the first term of eqn. (2) is not negligible in comparison with the second term; the solvation energy becomes significant for ions having a strong proton affinity because of hydrogen bonding between the ion and PTOP. Thus, the selectivity is influenced not only by the difference in hydration energy but also by the difference in solvation energy in the membrane phase. Because the difference in the free energy change for benzoate ions is constant, the degree of the selectivity change, $\Delta \log K^{\text{pot}}$ depends only on the difference in free energy change of interfering ion j . If ion j is a strong proton acceptor, the difference in the free energy change should be considerable and the interference of ion j will increase much more than that of ions having a small proton affinity. (The pK_a values of weak acids have been used as a measure of the proton acceptor ability of their conjugate anions [20, 21]). Figure 2 shows that there is a good linear relationship between $\Delta \log K^{\text{pot}}$ and the pK_a values for aliphatic monocarboxylates. Anions such as hydrogenmaleate, hydrogenphthalate and salicylate deviate significantly from the line. This can be explained by the fact that the proton acceptor ability of these anions is decreased, compared with that of benzoate, because of the formation of intramolecular hydrogen bonding [21].

For ions such as perchlorate and trifluoromethanesulfonate, which are conjugates of strong acids in water, the order of the increase in $\Delta \log K^{\text{pot}}$ is not consistent with the order of acid strength in non-aqueous media [22–25]. For example, Fujinaga and Sakamoto [22] determined the order of acid strength in acetonitrile and dimethylsulfoxide as $\text{HClO}_4 > \text{HCF}_3\text{SO}_3 > \text{HCH}_3\text{C}_6\text{H}_5\text{SO}_3 > \text{HCH}_3\text{SO}_3$. Hedwig and Parker [23] stated that the proton affinity decreased in the order $\text{Cl}^- > \text{ClO}_3^- > \text{CF}_3\text{SO}_3^- > \text{ClO}_4^-$ in dipolar aprotic solvents such as N, N-dimethylformamide.

In conclusion, the interference of ions with small proton affinity decreases significantly and the $\Delta \log K^{\text{pot}}$ values may be used as a semi-quantitative measure of proton affinity. The importance of the proton acceptor properties of anions in enhancement of the selectivity of anion-sensitive electrodes is clear. The improvement in the selectivity of a liquid membrane benzoate electrode with decanol, reported by Benignetti et al. [12], can be explained analogously. However, the improvement in selectivity was less than that in the present study, because the phenol is a much stronger proton donor than decanol.

REFERENCES

- 1 T. Fujinaga, S. Okazaki and H. Hara, *Chem. Lett.*, (1978) 1201.
- 2 G. E. Baiulescu and V. V. Cosofret, *Applications of Ion-Selective Membrane Electrodes in Organic Analysis*, J. Wiley, New York, 1977, p. 131.
- 3 C. J. Coetzee and H. Freiser, *Anal. Chem.*, 41 (1969) 1128.
- 4 H. James, G. Carmack and H. Freiser, *Anal. Chem.*, 44 (1972) 856.
- 5 T. Sigematsu, A. Ota and M. Matsui, *Bull. Inst. Chem. Res. Kyoto Univ.*, 51 (1973) 268.
- 6 E. Hopirtean and E. Veress, *Rev. Roum. Chim.*, 23 (1978) 273.
- 7 E. A. Materova, S. A. Ovchinnikova and S. A. Smekalova, *Elektrokhimiya*, 14 (1978) 71.
- 8 K. Kina, N. Maekawa and N. Ishibashi, *Bull. Chem. Soc. Jpn.*, 46 (1973) 2772.
- 9 N. Ishibashi and A. Jyo, *Microchem. J.*, 18 (1973) 220.
- 10 M. Matsui and H. Freiser, *Anal. Lett.*, 3 (1970) 161.
- 11 E. A. Materova, S. A. Ovchinnikova, V. S. Karavan and L. O. Ishutkina, *Elektrokhimiya*, 15 (1979) 1185.
- 12 M. T. Benignetti, L. Campanella and T. Ferri, *Fresenius Z. Anal. Chem.*, 296 (1979) 412.
- 13 J. Sandblom, G. Eisenman and J. L. Walker, Jr., *J. Phys. Chem.*, 71 (1967) 3862.
- 14 A. Jyo, H. Mihara and N. Ishibashi, *Denki Kagaku*, 44 (1976) 268.
- 15 J. Rais, *Collect. Czech. Chem. Commun.*, 36 (1971) 3253.
- 16 R. E. Reinsfelder and F. A. Shultz, *Anal. Chim. Acta*, 65 (1973) 425.
- 17 N. A. Gibson and D. C. Weatherburn, *Anal. Chim. Acta*, 58 (1972) 159.
- 18 A. Hulanicki and R. Lewandowski, *Chem. Anal. (Warsaw)* 19 (1974) 53.
- 19 H. Ohtaki, M. Tanaka and S. Funahashi, *Yoeki Hanno no Kagaku (in Japanese)*, Gakkai Shuppan Center, 1977, p. 216.
- 20 J. O. Edwards, *J. Am. Chem. Soc.*, 76 (1954) 1540.
- 21 M. D. Joesten and L. J. Schaad, *Hydrogen Bonding*, M. Dekker, New York, 1974.
- 22 T. Fujinaga and I. Sakamoto, *J. Electroanal. Chem.*, 85 (1977) 185.
- 23 G. R. Hedwig and A. J. Parker, *J. Am. Chem. Soc.*, 96 (1974) 6589.
- 24 R. P. Taylor and I. D. Kuntz, Jr., *J. Am. Chem. Soc.*, 94 (1972) 7963.
- 25 P. L. Huyskens and Y. O. Lambeau, *J. Phys. Chem.*, 82 (1978) 1886.

FIXED-TIME KINETIC ENTHALPIMETRY: IMPROVED SENSITIVITY FOR ENTHALPIMETRIC ENZYME ACTIVITY DETERMINATIONS IN HOMOGENEOUS AND HETEROGENEOUS SYSTEMS

J. KEITH GRIME* and ELIZABETH D. SEXTON

Department of Chemistry, University of Denver, University Park, Denver, CO 80208 (U.S.A.)

(Received 11th April 1980)

SUMMARY

A fixed-time (integral) method is described for the enthalpimetric determination of enzyme activity. The method involves the determination of residual unreacted substrate after a fixed incubation time with the sample. Results are presented for the determination of cholinesterase in aqueous solution and in 0.1-cm³ samples of reference sera using 30-min incubation periods. Results are correlated with a spectrophotometric procedure. A precision of 1.8% relative standard deviation is reported for serum assays. Preliminary data are also presented for the enthalpimetric determination of cholinesterase activity after immobilization onto non-porous glass beads by carbodiimide and glutaraldehyde coupling procedures.

The advantages and limitations of enthalpimetric measurements for the determination of enzyme activity have recently been reviewed [1]. In essence, the prominent feature of the enthalpimetric methodology is that the primary enzymatic event can be monitored without recourse to coupling reactions used with some detectors to produce measurable species. Therefore, the kinetic considerations involved in the incorporation of a secondary reaction can be avoided. Moreover, pretreatment steps are precluded since the enthalpimetric detection system is insensitive to the presence of unreactive, soluble or insoluble matrix constituents.

It has been noted recently that enthalpimetry is not a realistic choice for routine clinical enzyme assay because of limited sample throughput and sensitivity [1]. If sensitivity can be improved however, enthalpimetry does offer a realistic alternative analytical method for fundamental studies or as a universal reference method for clinical determinations. It is possible to increase sensitivity by using microcalorimetric techniques, but this can be achieved only at the expense of sample throughput because of increased thermal equilibration periods. This paper describes an enthalpimetric method, based on the determination of unreacted substrate after a fixed incubation time with the sample, that improves sensitivity without substantially increasing determination time. The method is evaluated for the determination

of cholinesterase in aqueous solution, reference sera, and immobilized onto glass beads. Results are compared with data from a spectrophotometric procedure adapted from a previously published method in which unconsumed butyrylcholine (BuCh) was determined as its iron(III) hydroxamate derivative [2] monitored at 500 nm. The methodological features of fixed-time kinetic enthalpimetry are represented in Fig. 1.

QUANTITATIVE CONSIDERATIONS

Enthalpimetric enzyme assay has hitherto been approached by a direct, derivative rate method, termed "kinetic direct injection enthalpimetry" [3--5]. In this technique, the enzyme is "saturated" (if possible) by an amount of substrate necessary to ensure that pseudo zero-order kinetics prevail. Under these conditions it can easily be shown that the change in temperature with time, dT/dt can be represented

$$dT/dt \approx k_2 [E] V \Delta H / C_p \text{ (} ^\circ\text{C s}^{-1}\text{)} \quad (1)$$

where k_2 is the rate constant for the breakdown of the enzyme-substrate complex (s^{-1}), $[E]$ is the total concentration of enzyme (mol dm^{-3}), V is the volume of the solution in the cell (dm^3), ΔH is the overall molar enthalpy of reaction, including any attendant buffer reactions (J mol^{-1}), and C_p is the heat capacity of the system ($\text{J } ^\circ\text{C}^{-1}$). Equation (1) necessarily involves an approximation because of depletion in substrate concentration as the reaction proceeds. More complex relationships must also be derived in the event of product or substrate inhibition. Under zero-order conditions, $k_2 [E] V$ can be replaced by V_{max} , the maximum velocity of the reaction (mol s^{-1}), which is synonymous with the enzyme activity (EA) expressed in katals. Therefore

$$dT/dt = EA \Delta H / C_p \text{ (} ^\circ\text{C s}^{-1}\text{)} \quad (2)$$

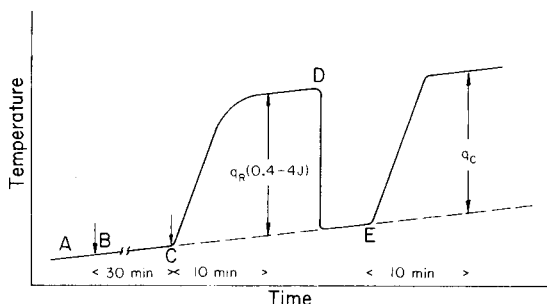


Fig. 1. Sequence of steps in fixed-time kinetic enthalpimetry. AB, isothermal baseline indicates sample and buffer at thermal equilibrium; B, precise amount of substrate injected, stirrer activated for 10 s; BC, incubation period, stirrer activated after 24 min, baseline recorded for 4 min; C, reagent enzyme injected; CD, temperature change recorded as residual butyrylcholine consumed; D, zero offset; E, Joule heating calibration sequence initiated.

Since $dT/dt = dq/dt C_p$, where dq/dt (in $J s^{-1}$) is the rate of heat change, thus

$$dq/dt = EA \Delta H (J s^{-1}) \quad (3)$$

Substitution of a value of 2 nkat (ca. 0.1 IU) and a typical enthalpy change of $40 kJ mol^{-1}$ into eqn. (3) gives a gradient of $8 \times 10^{-5} J s^{-1}$ (ca. 1.2 mcal min^{-1}).

Over a typical 5-min measurement period, a total heat change of 24 mJ (6 mcal) would be generated which is below the detection limit for conventional enthalpimetric equipment with a cell volume greater than $10 cm^3$.

This detection limit can be improved considerably, without a significant decrease in determination time, if the residual unhydrolyzed substrate is determined after a finite incubation period with the sample enzyme. This can be achieved conveniently by the injection of a relatively large concentration of reagent enzyme at the end of the incubation period, and measurement of the heat effect associated with this reaction, q_R (see Fig. 1). The calculation of enzyme activity from this datum can be rationalized as follows. Enzyme activity, EA , can be represented by

$$EA = \Delta S / \Delta t = (S_T - S_R) / \Delta t \quad (4)$$

where S_T and S_R are the total and residual moles of substrate respectively, and Δt is the incubation period. Thus, since $\Delta q_R / \Delta H = S_R$, then

$$EA = [S_T - (\Delta q_R / \Delta H)] / \Delta t \text{ (mol } s^{-1}) \quad (5)$$

where ΔH is the overall enthalpy change associated with the reagent enzyme—substrate reaction. Equation (5) therefore represents the working equation of fixed-time kinetic enthalpimetry.

The increase in sensitivity can be best illustrated by considering the determination of an enzyme activity of 2 nkat (0.1 IU) which, as shown earlier, is not feasible by direct, derivative enthalpimetry. If zero-order kinetics prevail, 3.6×10^{-6} mol of substrate would be consumed in a 30-min incubation period at this level of enzyme activity. Therefore, if a minimum of 20% decrease in the initial amount of substrate is allowed to maintain analytical precision, S_T and S_R would have values of 1.8×10^{-5} mol and 1.4×10^{-5} mol, respectively. Using the same enthalpy change of $40 kJ mol^{-1}$, the reaction of 1.4×10^{-5} mol of residual substrate would generate an enthalpy change of 600 mJ (150 mcal), well within the detection limit of a conventional isoperibol calorimeter. A sensitivity increase of at least 10-fold can therefore be expected (cf. direct derivative kinetic enthalpimetry). The enthalpimetric determination of serum ChE can therefore be achieved using a $0.1\text{-}cm^3$ serum sample, a much more acceptable sample volume for clinical determinations. This report is an examination of the feasibility of this technique, termed "fixed-time kinetic enthalpimetry".

EXPERIMENTAL

Reagents

Deionized water was used throughout. The buffer solution used in all experiments was 0.2 mol dm^{-3} Tris [tris(hydroxymethyl)aminomethane] adjusted to pH 8.0 with hydrochloric acid. Type IV-S horse serum cholinesterase (E.C. 3.1.1.8; nominal activity 15 IU mg^{-1} protein at 37°C), 99% butyrylcholine iodide and reference serum (all from Sigma Chemical Co., St. Louis) were stored, desiccated, below 0°C . Aqueous solutions of all reagents were prepared immediately before use. Reference serum solutions were prepared by dissolution in 0.2 mol dm^{-3} Tris rather than the Sigma diluent.

All reagents used in the spectrophotometric procedure were identical to those recommended earlier [2] except that barbital buffer was replaced by 0.2 mol dm^{-3} Tris and 1.0 mol dm^{-3} hydrochloric acid was used instead of 0.5 mol dm^{-3} acid.

The carbodiimide used in the immobilization procedure, 1-cyclohexyl-3(2-morpholinoethyl)carbodiimide, metho-*p*-toluene sulfonate, was obtained from Calbiochem, San Diego. The silylating reagent, γ -aminopropyltriethoxysilane, was obtained from Pierce Chemical Co., Rockford.

Apparatus

Enthalpimetric measurements were performed on a Tronac 450 titration calorimeter, and recorded on a Hewlett-Packard Model 7100 B strip-chart potentiometer with a Model 17505A plug-in amplification and zero-offset attachment. The recording system should be capable of measuring $200\text{-}\mu\text{V}$ signals. For convenience, a switching device was incorporated into the calorimeter output so that the unbalance potential of the Wheatstone bridge could be monitored either on a Keithley Model 177 microvolt digital voltmeter or on the strip-chart recorder during thermal equilibration periods. The digital voltmeter mentioned was also used to monitor the voltage across the resistance heater and a precision resistor during Joule heating calibration sequences.

The design of the stirrer for the enthalpimetric cell is critical to the success of the method since the heat generated by the stirrer dominates the signal-to-noise ratio in this type of equipment. The original stirrer in the Tronac 450 was replaced by a slotted paddle. The dimensions are represented in Fig. 2. This modification is not trivial; experiments showed that this stirrer design reduces the heat generated in stirring by a factor of 10 compared to the original equipment, while maintaining an adequate homogenization of the solution. This is particularly important with bridge outputs less than 1 mV. Accurate substrate and reagent injections were done with gravimetrically calibrated precision syringes (0.5 cm^3) equipped with Chaney adaptors (Model 1750, Hamilton Co., Reno). Substrate and reagent enzyme solutions were thermostatted in a water-bath maintained at 25.0°C ($\pm 0.002^\circ\text{C}$ short-term stability).

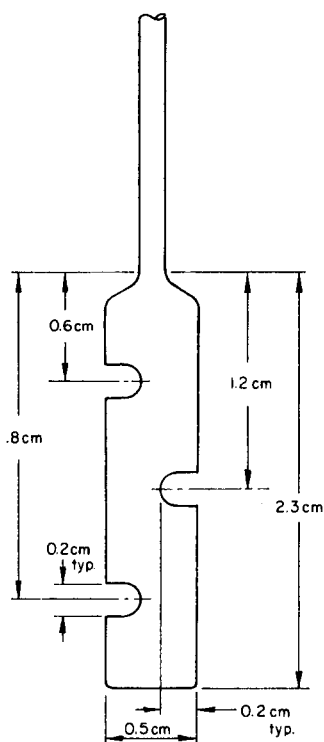
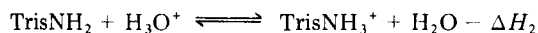
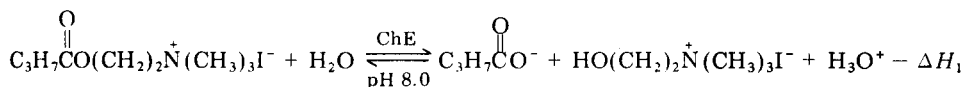


Fig. 2. Slotted paddle stirrer.

A Cary 219 double-beam recording spectrophotometer was used for absorbance measurements.

Preliminary experiments

Assignment of enthalpy change. The enthalpy change associated with the ChE-catalyzed hydrolysis of BuCh was determined in a series of substrate-limiting experiments taken to equilibrium. An amount of ChE sufficient to bring the reaction to completion within 10 min was injected into buffered solutions containing precise amounts of BuCh. The overall enthalpy change, ΔH_R , is that produced by the simultaneous enzymatic hydrolysis of BuCh and the protonation of Tris buffer, $\Delta H_1 + \Delta H_2$.



An operational enthalpy change of $-46.0 \pm 0.4 \text{ kJ mol}^{-1}$ was obtained in these experiments. This figure compares well with a previously reported value [3].

Corrections for non-enzymatic hydrolysis. Butyrylcholine, the optimum substrate for serum ChE, undergoes non-enzymatic hydrolysis. A series of spectrophotometric experiments were carried out to ascertain the pH dependence of this reaction. Predictably, the rate of non-enzymatic hydrolysis increases with increasing pH (Fig. 3). At pH 8.0, the optimum pH for ChE catalyzed hydrolyses, ca. 6% of the butyrylcholine iodide hydrolyzed (non-catalytically) in a 30-min period. It is not realistic however to perform the enzymatic hydrolysis at a pH less than 8.0. Experiments revealed that at pH 7.6, the non-enzymatic hydrolysis decreased to ca. 1.7% while the enzymatic hydrolysis dropped by about 11.5% at the same pH. Clearly, lowering the pH to minimize non-enzymatic hydrolysis would have a deleterious effect on the sensitivity of the method. All experiments were therefore performed at pH 8.0. In order to facilitate computation of enzyme activities determined enthalpimetrically, a calibration graph was constructed to establish the heat change associated with the enzymatic hydrolysis of butyrylcholine iodide incubated for 30 min at 25.0°C. The calibration curve including error bars is shown in Fig. 4. This graph, which incorporates the non-enzymatic hydrolysis correction, was used in all subsequent fixed-time enthalpimetric enzyme activity determinations. In another series of spectrophotometric experiments, it was established that the non-enzymatic hydrolysis of BuCh reaches an equilibrium value after approximately 30 min and is thereafter independent of time within the precision limits of the measurements.

Optimum amount of substrate. The amount of substrate chosen for the determination is governed by three factors. The residual amount of substrate, S_R , must be large enough to determine enthalpimetrically; the decrease in the number of moles of substrate during incubation, ΔS , should be large enough that it does not approach the imprecision of the data; and ΔS must be small enough that pseudo zero-order kinetics are maintained throughout the incubation period.

A compromise must be made in order that the latter two conflicting requirements are met. Pseudo zero-order kinetic behaviour was confirmed by

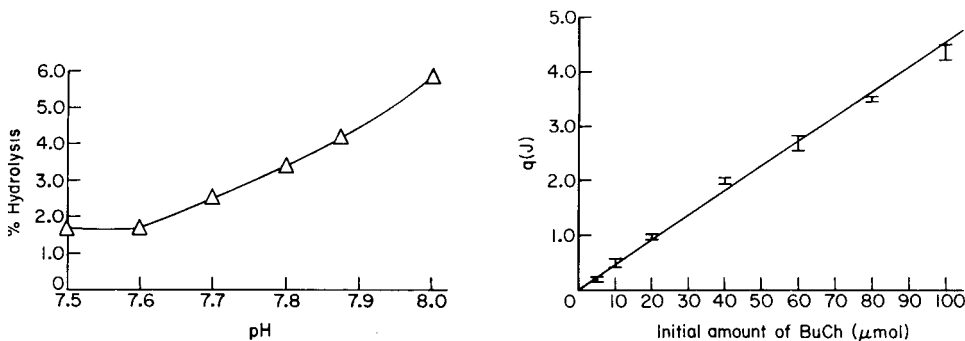


Fig. 3. Dependence of the non-enzymatic hydrolysis of butyrylcholine on pH.

Fig. 4. Calibration plot of heat evolved in the enzymatic hydrolysis of butyrylcholine. Incubation at 25.0°C for 30 min.

constructing a series of plots of determined enzyme activity versus initial substrate concentration at each enzyme concentration. In each case, the classical Michaelis–Menten curve was obtained. At each enzyme activity, the initial substrate concentration was chosen to be consistent with the attainment of pseudo zero-order kinetics as indicated by the plot and to ensure that ΔS during a 30-min incubation period was no less than 20% of the original amount of substrate. In practice, these two requirements proved to be compatible. Typically, an amount of substrate 3–4 times the amount predicted to be consumed (based on V_{\max}) was employed. The amounts used in practice are shown in Table 1.

Recommended procedure

The sequence of events is represented diagrammatically in Fig. 1. The sample enzyme in aqueous solution, reference serum, or immobilized onto glass beads was introduced into the reaction cell and the volume made up to 25.00 cm³ with 0.2 mol dm⁻³ Tris buffer. The substrate and reagent enzyme solutions were loaded into separate 0.5-cm³ syringes. Only the substrate volume must be known precisely. The entire syringe and cell assemblies were then immersed in the thermostatted bath and the cell and its contents brought to the bath temperature (± 0.3 mV of the balance point) by activation of the resistance heater. On attainment of equilibrium, as evidenced by the digital voltmeter, the substrate solution was injected and the stirrer activated for 10 s. After incubation for 24 min at 25.0°C, the stirrer was reactivated to eliminate any local temperature effects in the solution.

The solution was stirred for 2 min and a baseline was recorded for a further 4 min. At bridge outputs less than 500 μ V, this procedure is necessary in order to establish an acceptable baseline. Stirring must be continued throughout the incubation period when determining the activity of immobilized enzymes. Precisely 30 min after the injection of the substrate, a solution containing sufficient ChE to bring the reaction to completion within 10 min

TABLE 1

Determination of cholinesterase activity in aqueous solutions by fixed-time kinetic enthalpimetry

Activity taken (IU)	Activity found (IU)	Specific activity found (IU mg ⁻¹) ^a	R.s.d. % (n = 6)	Initial amount of substrate (μ mol)
0.199	0.199	11.38 \pm 0.15	1.4	25
0.102	0.103	11.41 \pm 0.25	2.2	20
0.082	0.083	11.56 \pm 0.19	1.6	15
0.061	0.061	11.31 \pm 0.56	4.9	10

^a11.35 \pm 0.24 IU mg⁻¹ by derivative kinetic enthalpimetry, and 11.56 \pm 0.21 IU mg⁻¹ by kinetic spectrophotometry (fixed-time approach); each result obtained with 2–3 IU samples.

was injected, and the attendant heat effect, q_R , was monitored. The minimum amount of enzyme required to achieve this goal can be calculated from the integrated Michaelis–Menten equation. The activity of the reagent enzyme is commensurate with the amount of residual substrate. The activities used are shown in Table 1. Joule heating calibration was then performed *in situ*. The amount of residual substrate, S_R , was extrapolated from the calibration curve, which was constructed from identical experiments but in the absence of the sample enzyme. The sample enzyme activity was then calculated from eqn. (5).

Cholinesterase was immobilized onto non-porous glass beads by two different methods; a carbodiimide peptide-binding condensation and an alkylamine coupling approach using glutaraldehyde. Both these procedures have been described in detail elsewhere [6]. In both cases, the functionalization of the glass was achieved with γ -aminopropyltriethoxysilane according to an established procedure [7].

RESULTS AND DISCUSSION

The results of the determination of ChE activity in aqueous solution by the fixed-time kinetic enthalpimetry approach are shown in Table 1. In order that the inherent precision of the technique can be compared with conventional derivative kinetic enthalpimetry, the results have been expressed as an intensive property of the system, the activity of the solid enzyme (activity per unit mass). The data obtained from the spectrophotometric procedure have also been included in the same manner. The precision of the fixed-time enthalpimetry methodology clearly deteriorates badly at an activity of 0.06 IU. At the initial substrate concentration commensurate with zero-order kinetics and a significant fractional substrate depletion at this level of enzyme activity (10 μmol), the signal-to-noise ratio begins to decrease to unacceptable levels. The sensitivity of the method can, of course, be increased by longer incubation periods. Decreased cell volume, e.g. $<5\text{ cm}^3$, would also increase the sensitivity, but this would induce considerable thermal effects, in particular heats of stirring and heat loss, placing the technique firmly in the hands of the specialist.

The enthalpimetric technique also compares favorably with a spectrophotometric method for the determination of ChE activity in a physiological matrix. Activities of 4.28 ± 0.08 and $4.38 \pm 0.09\text{ IU cm}^{-3}$ were determined for identical 0.1-cm^3 samples of reference sera by enthalpimetric and spectrophotometric procedures, respectively. The relative standard deviations (r.s.d.) of the enthalpimetric and spectrophotometric methods are comparable at 1.8% and 2.1% ($n = 6$), respectively.

The technique has a similar precision to a direct (derivative) enthalpimetric approach to the determination of ChE [3], but requires a 10-fold smaller sample. Since thermal equilibration procedures are incorporated into the incubation period, there is effectively no difference in sample throughput

between the derivative and fixed-time enthalpimetric methodologies; both will process two samples per hour. This type of throughput is clearly unacceptable for routine clinical analysis, but the increased sensitivity obtained by this procedure does extend the capabilities of enthalpimetry as a reference method.

Another area of possible application is the enthalpimetric determination of immobilized enzyme activity in systems where low ($<1 \text{ IU g}^{-1}$) enzyme loadings are encountered. Here, enthalpimetry has the distinct advantage that the measurement can be made in the presence of the solid matrix. The need for batch sampling of the supernatant solution or flow-loop devices in order to make a measurement in a transparent solution is obviated. In this regard, the activity of ChE immobilized onto non-porous glass beads has been determined enthalpimetrically and compared with spectrophotometric results on the same systems. Immobilized ChE activities of 0.46 IU g^{-1} and 0.49 IU g^{-1} were determined enthalpimetrically for carbodiimide and glutaraldehyde coupled systems respectively. The enzyme capacity of both systems was determined spectrophotometrically to be 0.49 IU g^{-1} . The latter result was obtained with one extra analytical manipulation, that is the sampling of the supernatant solution after the enzymatic reaction had been quenched. As no information on the stability of this enzyme-carrier conjugate is available to date, no precision data are presented. However, the presence of the glass beads did not significantly affect the shape of the enthalpogram compared to a homogeneous aqueous solution experiment, and acceptable precision can be anticipated. There are several features of a fixed-time kinetic determination which warrant discussion.

The "fixed-time kinetic enthalpimetry" technique has the disadvantages of any two-point kinetic method, in that non-linearity of reaction rate, initial lag phases and non-enzymatic reactions will, if undetected, cause significant errors. Moreover, calculation of enzyme activity by this approach involves the subtraction of two relatively large quantities, S_T and S_R . This operation significantly affects the precision of the data if S_T is not appropriately adjusted at different enzyme activities. A small decrease in enzyme activity, integrated over a 30-min incubation period, will have a deleterious effect on the signal-to-noise ratio if S_T remains constant because S_R approaches S_T under these conditions. These problems are not prohibitive and can easily be avoided with adequate preliminary investigations. At enzyme activities greater than 1 IU , maintenance of zero-order kinetics for a 30-min incubation period becomes difficult and the amounts of substrate necessary to do this become excessive. It is recommended that the direct derivative enthalpimetric procedure [3] should be used for the determination of enzyme activities of this magnitude.

The prerequisite for pseudo zero-order kinetics in this method precludes its application for the determination of Michaelis constants from substrate-dependent rate data. Since such fundamental studies are usually not sample-limited, sensitivity is not problematic; Michaelis constants can therefore be

determined enthalpimetrically by interpolation of rate data from a conventional, substrate-limited, direct injection enthalpogram according to the integrated Michaelis-Menten equation [8].

The reagent enzyme-residual substrate reaction necessarily takes place at the same pH as the same sample enzyme reaction. It should be pointed out that implicit in the use of eqn. (5) is a knowledge of the operational enthalpy of reaction, which may change with pH in the same buffer system [9] and will certainly change with a different buffer system. Such effects must be taken into account when enthalpimetric measurements are used for the determination of the pH dependence of enzyme activity data.

Errors caused by temperature fluctuation during the incubation period are minimized because precise temperature control is an inherent feature of the enthalpimetric method.

Fixed-time kinetic determination is, of course, a well established procedure for many detection systems. Indeed, the spectrophotometric correlation experiments contained in this report are based on the same principle although the conversion of residual substrate in this case is non-enzymatic. This is the first report, however, of a fixed-time kinetic approach to a non-flow calorimetric determination. The most important feature of this technique is that it extends the sensitivity of enthalpimetry without entering into the more specialized area of microenthalpimetry. Although results have been presented for ChE activity determinations only, the technique has general applicability. Indeed, the increased sensitivity opens up many more possibilities for enthalpimetric enzyme assay that previously could not be considered.

This project was supported in part by BRSG Grant 5S077RR07138-08 awarded by the Biomedical Research Grant program, Division of Research Resources, National Institutes of Health.

REFERENCES

- 1 J. K. Grime, *Anal. Chim. Acta*, 118 (1980) 191.
- 2 J. de la Huerga, C. Yesnick and H. Popper, *Am. J. Clin. Pathol.*, 12 (1952) 1126.
- 3 J. K. Grime, B. Tan and J. Jordan, *Anal. Chim. Acta*, 109 (1979) 393.
- 4 J. K. Grime and K. R. Lockhart, *Anal. Chim. Acta*, 106 (1979) 251.
- 5 C. D. McGlothlin and J. Jordan, *Anal. Chem.*, 47 (1975) 786.
- 6 H. H. Weetall, in K. Mosbach (Ed.), *Methods of Enzymology*, Vol. 43, Academic Press, New York, 1976, pp. 140-144.
- 7 D. E. Leyden and G. H. Luttrell, *Anal. Chem.*, 47 (1975) 1612.
- 8 J. K. Grime, K. R. Lockhart and B. Tan, *Anal. Chim. Acta*, 91 (1977) 243.
- 9 N. D. Jespersen, *J. Am. Chem. Soc.*, 97 (1975) 1662.

A CATALIMETRIC THERMOCHEMICAL UNSEGMENTED FLOW SYSTEM BASED ON THE IODIDE-CATALYZED CERIUM(IV)–ARSENIC(III) REACTION

JAMES M. ELVECROG and PETER W. CARR*

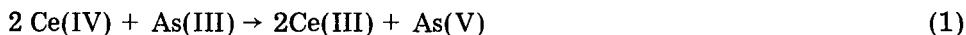
Department of Chemistry, University of Minnesota, Minneapolis, MN 55455 (U.S.A.)

(Received 29th April 1980)

SUMMARY

The theoretical flow system described is able to detect and determine iodide at concentrations in the range 0.01–10 μM in samples as small as 120 μl . This represents the best limit of detection (0.15 ng) thus far reported for a thermochemical methodology. It is shown that sample concentration can alter the relationships between peak height and flow rate, and between peak width and sample volume above certain limits. In chemical engineering, studies of chemical reactions in the presence of mass transport processes have generally been focused on the steady-state (time-independent) behavior. The present work is concerned with transient phenomena and time-dependent properties of the system, i.e., the reactors are used under pulsed conditions.

One of the rapidly expanding fields in analytical chemistry has been the application of catalyzed reactions to quantitative determination [1–3]. A common catalytic method for iodide is based on the redox reaction between cerium(IV) and arsenic(III). The net reaction is



Sandell and Kolthoff [4, 5] were the first to carry out a detailed study of the reaction. Since their work, the reaction has been applied to the determination of iodide in natural waters [6–10], in thyroid hormones [11–13], and to the determination of inhibitors of the reaction, such as mercury and silver [14, 15]. The two other species which strongly catalyze the reaction, osmium [15, 16] and ruthenium [17], have been similarly determined. The reaction has also been used as an indicator reaction in catalimetric titrations [18–22]. Spectrophotometric detection of the decrease in cerium(IV) is generally used to monitor the change in reaction rate; however, potentiometric [3, 19], biamperometric [23], and thermometric [22] methods have been used to detect the onset of the indicator reaction in titrations.

The kinetics of reaction (1) in 0.5 M sulfuric acid have been studied in detail by Rodriguez and Pardue [24]. They concluded that under reaction conditions in which the $[\text{As(III)}]/[\text{Ce(IV)}]$ concentration ratio is greater than about 1.5, the reaction is zero order in arsenic(III) concentration and

first order in both cerium(IV) and iodide. The kinetics of the reaction under these experimental conditions can be written as follows

$$-d[\text{Ce(IV)}]/dt = k'[\text{Ce(IV)}][\text{I}^-] \quad (2)$$

One should note that the integrated rate equation for a product of this reaction, e.g., cerium(III) or heat, will be of the form

$$[\text{Ce(III)}]/[\text{Ce(III)}]_{\infty} = Q/Q_{\infty} = 1 - \exp(-k'[\text{I}^-]t) \quad (3)$$

The significance of this equation will be discussed shortly.

The purposes of the present work were to demonstrate the use of a flow system with thermochemical detection for catalytic determinations and to study the behavior of this reaction when used in a flow system. In principle, thermochemical detection methods can be applied to any reaction which generates or absorbs heat. However, previous work with flow systems using thermometric determination has not dealt with the determination of species via their catalytic characteristics. Since even very low concentrations of catalyst can greatly increase reaction rates, a relatively large amount of heat can be produced by the presence of very low concentrations of a catalyst. If the catalyst concentration is proportional to the heat produced in a fixed time or to the rate of heat production, catalyst determinations should have improved detection limits in comparison to stoichiometrically limited systems.

In this study, a flow enthalpimeter with two fluid streams, as developed by Schifreen et al. [25], is utilized. A cerium(IV) reagent stream is mixed with an arsenic(III) sample stream into which samples of iodide are injected. The resultant heat "pulse" is detected with a differential temperature measurement system. The arsenic(III) and cerium(IV) concentrations are such that the reaction rate is presented by eqn. (2). The cerium concentration is held constant so that the reaction rate, and therefore the heat production, is pseudo-first order in iodide concentration.

EXPERIMENTAL

Reagents and instrumentation

The reagent was 40 mM cerium(IV) ammonium sulfate (G. Frederick Smith Chemical Co., Columbus, OH 43223) in 0.5 M sulfuric acid. Samples were prepared by serial dilution of a reagent-grade potassium iodide (Mallinckrodt Chemical Works) solution. All samples were prepared in 0.5 M sulfuric acid and contained 65 mM sodium arsenite (Mallinckrodt Chemical Works, St. Louis, Missouri 63160). Before use, all solutions were filtered with a 0.45- μm Millipore filter.

The construction of a flow enthalpimeter using an immobilized enzyme reactor was described in detail earlier [26]. The modified flow system used is similar to that used by Schifreen et al. [25].

The "adiabatic" column used (3.3 cm long, 4-mm internal diameter, ca.

0.42-ml volume) was packed with acid-washed 80–120 mesh solid glass beads ($0.1 \text{ m}^2 \text{ g}^{-1}$; A. H. Thomas Co., Philadelphia, PA 19105) to minimize dispersion. A packed bed reactor is used in thermochemical flow injection systems in contrast to the conventional narrow tube in order to minimize heat losses. In general, long thin tubes will have a much higher surface area through which heat can leak than a packed bed of the same volume. The bed is packed with small non-porous beads to minimize axial dispersion. Extremely small columns are not useful because the amount of heat produced is related to the residence time in the reactor.

Procedure

Five minutes before the first sample is injected, the stirring motor and pump are started to ensure thermal equilibration as indicated by a flat baseline. Flow rate is measured at the system outlet as the time required to fill a vessel of known volume. Samples were drawn into the injection valve and injected. Apparent temperature changes were calculated as the product of the measured resistive imbalance of the bridge circuit and the thermistors thermal coefficient of $-400 \Omega \text{ K}^{-1}$. Peak width at half maximum height ($W_{1/2}$) was converted to volume units via the measured flow rate.

RESULTS AND DISCUSSION

Effect of cerium(IV) on peak height

Since the maximum amount of heat which can be produced per unit time is proportional to the concentration of cerium(IV), maximum sensitivity is achieved with the highest possible cerium(IV) concentration. However, the arsenic(III) concentration must be at least 1.5 times the cerium(IV) concentration in order for the reaction to be first order in cerium(IV) and zero order in arsenic(III). The solubility limit for sodium arsenite in 0.5 M sulfuric acid is about 65 mM, so this concentration was used throughout. The effect of the cerium(IV) concentration on peak height can be seen in Fig. 1. The calibration curve for a 40 mM cerium(IV) reagent stream has a much steeper slope ($6.17 \pm 0.08 \text{ mK } \mu\text{M}^{-1}$) than the curve for 10 mM cerium(IV) ($1.64 \pm 0.01 \text{ mK } \mu\text{M}^{-1}$). In both cases, a least-squares line was fitted to the data up to an iodide concentration of $4 \mu\text{M}$, which is the approximate upper limit of linearity. The ratio of slopes is 3.8, in good agreement with the ratio of cerium(IV) concentrations and a first-order dependence of reaction rate on its concentration [24]. The peak height ratio at the two cerium(IV) concentrations drops below 3.8 at high iodide concentrations. This may be due to production of greater amounts of arsenic(V), which has been shown to decrease the reaction rate [24]. It is interesting to note that the non-linearity in the calibration curve develops at about the same iodide concentration, regardless of the cerium(IV) concentration. This is expected for a reaction which is first order in cerium(IV) concentration. The point at which the calibration curve should become non-linear because of depletion

of cerium(IV) can be predicted from eqn. (2) by substituting an appropriate value of the rate coefficient. From the work of Rodriguez and Pardue [24], we estimate that k' will be $1.20 \times 10^4 \text{ M}^{-1} \text{ s}^{-1}$ at $[\text{As(III)}] = 65 \text{ mM}$. When this value is used for the rate coefficient, a constructed calibration curve is apparently linear to approximately 10% up to an iodide concentration of 7–10 μM . The point of non-linearity in the constructed calibration curve approximates that observed in the experimental curves.

It is apparent from Fig. 1 that the system response to iodide will be, at best, linear up to approximately 10 μM . One of our objectives was to study the behavior of the flow system under a variety of chemical and kinetic conditions. At very low iodide concentrations, the amount of heat produced will be limited only by the reaction rate but at very high iodide concentrations the heat produced will be limited by the total available cerium(IV), which is the deficient reagent. The wide-range calibration curve shown in Fig. 2 indicates that at $[\text{I}^-] > 190 \mu\text{M}$, the maximum amount of heat is produced because of depletion of cerium(IV).

To demonstrate the hypothesis that the non-linearity in the calibration curve is due to depletion of cerium(IV), the effluent at various iodide concentrations was collected in individual flasks containing silver nitrate which served to quench the reaction immediately by precipitating iodide. The samples were then appropriately diluted and the absorbance of the unreacted cerium(IV) was measured at 390 nm. Figure 3 (curve A) shows a plot of the normalized change in absorbance versus iodide concentration. The normalized change in absorbance was computed by calculating the difference in absorbance at a given iodide concentration with respect to a blank ($[\text{I}^-] = 0$) and dividing by the maximum change in absorbance which occurred at $[\text{I}^-] = 190 \mu\text{M}$ (see Fig. 2). Figure 3 (curve B) repeats the data of Fig. 2 with the peak height normalized to the value obtained at $[\text{I}^-] = 190 \mu\text{M}$. The two

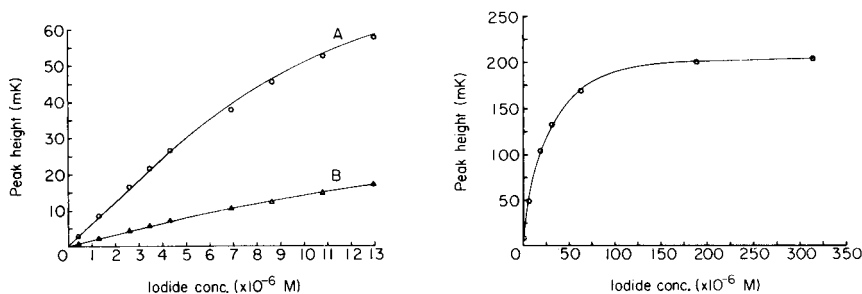


Fig. 1. Effect of ceric concentration on the calibration curve. Total flow rate, 1.5 ml min^{-1} ; sample volume, $120 \mu\text{l}$; $[\text{As(III)}] = 65 \text{ mM}$; $[\text{H}_2\text{SO}_4] = 0.5 \text{ M}$. Curve A $[\text{Ce(IV)}] = 40 \text{ mM}$; curve B $[\text{Ce(IV)}] = 10 \text{ mM}$.

Fig. 2. Effect of very high iodide concentration on signal response. All conditions are as in Fig. 1, curve A.

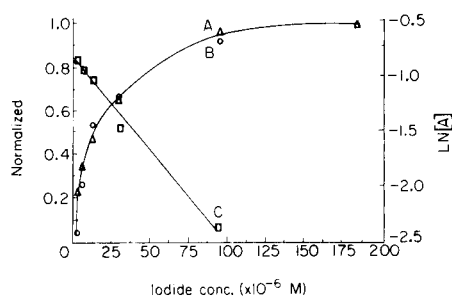


Fig. 3. Correlation of heat production and cerium(IV) consumption. Curve A (Δ): plot of normalized absorbance change vs. iodide concentration. Curve B (\circ): plot of normalized thermal peak height vs. iodide concentration. Curve C (\square): plot of $\ln [A]$ vs. iodide concentration.

curves are very similar, indicating that heat production does in fact follow depletion of cerium(IV). Also shown in Fig. 3 (curve C) is plot of $\ln \Delta A$ versus $[I^-]$. The slope of this line has units of M^{-1} which can be translated into an apparent rate coefficient by dividing by the residence time in the reactor and accounting for dilution of iodide in the T-connector and in the column. An average iodide concentration can be computed via the peak width at half maximum height ($W_{1/2}$) for any given peak. A rate coefficient of $1.63 \pm 0.23 \times 10^4 M^{-1} s^{-1}$ was estimated from the data shown in curve C of Fig. 3 along with the $W_{1/2}$ given in Table 1. Because of the approximations inherent in the measurement, this value may be considered as in reasonable accord with the value of $1.20 \times 10^4 M^{-1}$ obtained from the data of Rodriguez and Pardue [24].

TABLE 1

Effect of low iodide concentrations on peak height, precision, and half-width^{a,b}

Conc. (μM KI)	Peak height (mK)	CV (%) ^c	$W_{1/2}$ (ml) ^d	Conc. (μM KI)	Peak height (mK)	CV (%) ^c	$W_{1/2}$ (ml) ^d
0.04	0.31	2.5	0.53	0.90	8.34	0.4	0.48
0.08	0.60	1.3	0.51	3.28	23.3	1.2	0.48
0.25	1.86	2.6	0.48	5.46	28.6	2.7	0.48
0.41	3.08	0.4	0.48	6.55	34.1	0.5	0.50
0.49	3.80	0.9	0.48	8.74	43.5	0.5	0.49
0.66	5.05	0.6	0.48	10.92	52.2	0.4	0.50
0.82	6.34	0.3	0.48				

^aConditions are the same as in Fig. 1, curve A. ^bLeast-squares data analysis on the range 0.04–1 μM . ^cBased on five replicates at each concentration. ^dPeak width measured at half maximum height.

Effect of chloride on peak height

Several workers [5, 7, 8, 27] have reported the accelerating effect of chloride ions on the iodide-catalyzed reaction, while Rodriguez and Pardue [24] reported that chloride has only an additive effect on the reaction rate, which is most likely due to the addition of contaminating iodide. To test the effect of chloride ions, the cerium and arsenic streams were made up in 0.5 M sulfuric acid and 0.3 M hydrochloric acid. An iodide sample was then injected and the peak height compared to the height seen when the same iodide sample was injected into cerium and arsenic streams made up only in 0.5 M sulfuric acid. The peak heights were the same within experimental error, even though in one case the chloride concentration added was 10^5 -fold higher than the iodide concentration. Clearly, chloride ion has no significant effect on the reaction rate over the range studied here. Although chloride does not interfere in the assay, any species which can kinetically compete with cerium(IV) for the oxidation of iodide may serve as a significant interference. Since the sample is premixed with sodium arsenite in 0.5 M sulfuric acid, it is likely that any strong oxidant in the sample will pre-react and not interfere. Any species which is a stronger reducing agent than arsenic(III) and reacts in the detection cell with cerium(IV) will generate heat and therefore be detected. Possible interfering species include Cu(I), Sn(II) and Cr(II).

Linear dynamic range

After the main chemical conditions for the determination of iodide had been determined, the limit of detection and the analytical reproducibility over the linear range were studied in detail. The results are summarized in Table 1. The limit of detection was determined by the method of Hubaux and Vos [28] using a standard, unweighted linear least-squares data analysis program and shown to be $0.01 \mu\text{M}$ at the 90% confidence interval. The coefficient of variation was better than 3% over the entire range of 0.04 – $11 \mu\text{M}$ iodide. This is the most sensitive thermochemical determination as yet reported for a non-biologically active material. For a detection limit of $0.01 \mu\text{M}$, this corresponds to a total of 0.15 ng of iodide in a $120\text{-}\mu\text{l}$ sample. The methodology reported here should be equally applicable to the determination of many other catalysts, including those which have been employed in titrations with catalimetric–thermometric end-point detection [18].

Effect of flow rate on peak height

All the data presented thus far were obtained at a flow rate of approximately 1.5 ml min^{-1} , which corresponds to a residence time of 7 s. As stated above, part of our interest in this chemical system was to assess the difference in behavior of a flow reactor, in which a material is rapidly and stoichiometrically converted to product, and those systems in which the reaction takes place over the entire length of the reactor. At very high iodide concen-

trations, the sample slug is being rapidly depleted of all cerium(IV). For example, at $[I^-] = 190 \mu\text{M}$, it can be estimated that $t_{1/2} = 0.3 \text{ s}$. In contrast, at very low iodide concentrations ($<1 \mu\text{M}$), the cerium(IV) is less than 5% depleted at a flow rate of 1.5 ml min^{-1} . This difference shows up dramatically in the effect of flow rate on thermometric peak height (Fig. 4). In curve A of Fig. 4, which was obtained at a high iodide concentration, a pronounced maximum in the peak height is observed. It has been shown previously [26] that the roll-off at low flow rates is due to heat loss from the system. This invariably occurs when the reaction is complete. At higher flow rates, the reaction does not go to completion. In contrast, in curve B of Fig. 4, which was obtained at a low iodide concentration, the thermal peak height does not decrease but rather increases at low flow rates. This occurs when more heat is being generated by the chemical reaction than is being lost by poor adiabaticity. The difference in behavior of peak height versus flow rate at high and low iodide concentrations is rationalized in a subsequent section of this paper.

Effect of iodide concentration on peak width

One of the major motivations in undertaking this study was to contrast the behavior of a flow system in which the sample consumption is essentially complete and instantaneous when mixed with reagent, e.g., the reaction of hydrochloric acid with base [25], with the system behavior when the sample is a catalyst and in principle is not consumed. In most of our previous work with unsegmented flow systems and in some work on "flow injection analysis" [29], the peak width, whether it is measured as the variance (σ^2) or half-width, is independent of the sample concentration. This is in accord with the Aris-Taylor [30] equation for the dispersion of a non-reactive species in laminar flow.

The extremely strong dependence of peak width on sample concentration in the present system is shown in Fig. 5. This is not an artifact. To verify

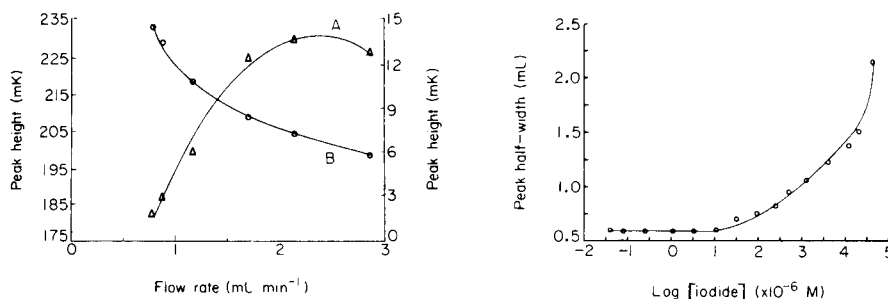


Fig. 4. Effect of flow rate on peak height. All conditions except flow rate are as in Fig. 1, curve A. Curve A, $[I^-] = 190 \mu\text{M}$; curve B, $[I^-] = 0.94 \mu\text{M}$.

Fig. 5. Effect of iodide concentration on peak half-width. All conditions are as in Fig. 1, curve A.

this, the solutions used here were replaced by those used in a previously described system (HCl—THAM [25]). The peak width was essentially independent of the sample concentration. The reaction of iron(II) and cerium(IV) was also tested in this flow system. Again there was no significant effect of sample concentration on peak width.

The extreme dependence of peak width on sample concentration observed for the present reaction is nothing more than a consequence of the non-linear relationship between the measured signal and the sample concentration. As shown by the data of Figs. 1 and 2, the signal is not a linear function of the iodide concentration when it is greater than about 4 μ M. The curve shown in Fig. 2 is approximately describable by a function of the form

$$\phi = \phi_0 [1 - \exp(-\alpha C)] \quad (4)$$

where ϕ represents the instantaneous signal, ϕ_0 is the maximum achievable signal, and C is the instantaneous iodide concentration. It is readily seen that at very high concentrations, ϕ asymptotically approaches ϕ_0 . At very low concentrations, the slope of a plot of ϕ versus C will be $\alpha\phi_0$. Values of both ϕ_0 and α can be obtained from the data of Fig. 2. By comparison to eqn. (3), it is evident that α is merely the product of the rate constant k' and t , the residence time in the reactor.

Since the iodide concentration is a function of time and volume, ϕ will depend upon these independent variables. If a Gaussian peak is assumed at the lowest concentration, i.e.

$$C = C^0 \exp[-(V - V_R)^2/2\sigma^2] \quad (5)$$

where V_R is the volume needed to get to peak maximum, C^0 is the iodide concentration at the peak maximum, and σ^2 is the peak variance, then substitution of eqn. (4) into eqn. (5) leads to

$$\phi/\phi_0 = 1 - \exp[-\alpha C^0 \exp(-(V - V_R)^2/2\sigma^2)] \quad (6)$$

The parameters α and σ were estimated from the slope of the calibration curve (Fig. 1, curve A) and from the peak width at low concentration given in Fig. 5. The results of a series of peak half-width calculations as a function of C^0 are given in Table 2. Since C^0 is the concentration at the peak maxima, whereas the axis of Fig. 5 is the injected concentration, the results are not exactly comparable. Nonetheless, it is clear that most of the observed increase in peak width with concentration is due to the non-linear relationship between the measured response and the iodide concentration.

In the course of this work there was concern that adsorption of even very small amounts of iodide on the packing material could cause the peak broadening shown in Fig. 5. Several non-porous, "inert" solids were tested as packing materials, including silicon carbide and powdered Kel-F, but there was no decrease in peak width. The adsorption hypothesis was also tested by the use of a porous silica (200 $\text{m}^2 \text{g}^{-1}$) packing material. The peak broadening of a 6.26 μ M iodide sample was the same as when a non-porous

TABLE 2

Theoretical estimate of peak half-width^a

C^0 (μM)	$\bar{\phi}^b$	$W_{1/2}$ (ml)	C^0 (μM)	$\bar{\phi}^b$	$W_{1/2}$ (ml)	C^0 (μM)	$\bar{\phi}^b$	$W_{1/2}$ (ml)
1.0	0.0031	0.59	10^2	0.954	0.89	10^4	1.000	1.75
1.0	0.0303	0.59	10^3	1.000	1.38	10^5	1.000	2.05
10	0.265	0.62						

^aEstimated from eqn. (6) with $\alpha = 0.0308$ (μM)⁻¹ and $\sigma = 0.251$ ml. ^bNormalized peak height computed from eqn. (6).

solid packing material was employed. Clearly, adsorption of iodide or iodine does not contribute to peak width under the present experimental conditions. This observation is in accord with radiotracer studies of iodide on glass surfaces [31, 32].

The analytical consequences of the effect observed in Fig. 5 may be quite serious, particularly if a mechanized system is used in which samples are injected at regular intervals. Thus, a very wide signal versus time profile caused by excessively high sample concentration will ruin the determination of a subsequent sample. Those samples in the high iodide concentration range will take considerably longer to achieve a given fractional wash-out and therefore will interfere with the subsequent sample. Obviously, only samples within the linear range of the calibration curve should be analyzed in any case. It should be noted that peak broadening at iodide concentrations in the linear part of the calibration curve is minor (see Table 1).

Effect of sample volume on peak height and width

The effect of sample volume on peak height is shown in Fig. 6 for two iodide concentrations; one concentration is on the linear and the other on the flat portion of the calibration curve. Of course, peak height ultimately becomes independent of sample volume. However, curve A (low iodide) is

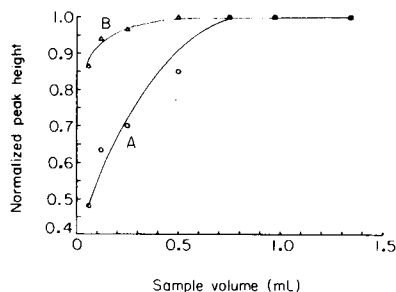


Fig. 6. Effect of sample volume on peak height. All conditions except sample volume are as in Fig. 1, curve A. Peaks are normalized by dividing by the height of the highest volume peak. Curve A, $[\text{I}^-] = 0.94 \mu\text{M}$; curve B, $[\text{I}^-] = 313 \mu\text{M}$.

very similar to those seen in earlier investigations [25, 26], while curve B (high iodide) is distinctly different. This is most likely a consequence of the large dependence of peak half-width on iodide concentrations shown in Fig. 5. This difference in the functional form of the dependence of peak width with sample volume clearly indicated a radical difference in dispersion processes, i.e., factors which establish the peak width, and is consistent with observations in Fig. 5 and the dependence of peak width on sample concentration. Previous work [26] with complete reactions indicated that the increase in peak width with sample volume was in accord with Sternberg's [33] work on the convolution of various sample input distributions with a Gaussian dispersion model. This model is obviously inapplicable to the behavior of the present system at high iodide concentrations.

The difference in system behavior at high and low iodide concentrations is also reflected in the dependence of peak width on sample volume (Fig. 7). The high iodide concentration case (curve B), in addition to having a greater peak half-width, has a greater slope than the low iodide concentration case (curve A). Curve A has a limiting slope of 2.38 ± 0.04 which compares quite favorably to the slope seen in previous work using the same flow system in an acid-base determination [25] and is related to the ideality of the stream mixing process [34]. Curve B, however, has a limiting slope of 3.00 ± 0.09 . The large effect of the sample iodide concentration on the plots of sample volume versus peak height and peak half-width cannot be explained at this time. Until a more exact understanding of the column processes involved in a catalytic reaction system is available, it is not likely that these phenomena will be understood.

Sensitivity of peak shape to column packing

It was found in this study of a catalytic reaction system that peak shape was very dependent on how well the reactor column was packed. Any degradation in column packing generally caused peak shapes to deteriorate significantly, e.g. shoulders developed. It was also found that the column end fitting and its orientation relative to the column outlet had a definite effect on the peak shape at high iodide concentrations (>1 mM). Any constriction of the

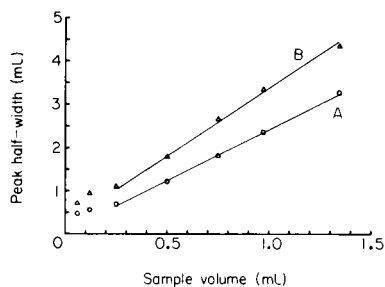


Fig. 7. Effect of sample volume on peak half-width. All conditions except sample volume are as in Fig. 1, curve A. Curve A, $[I^-] = 0.94 \mu\text{M}$; curve B, $[I^-] = 190 \mu\text{M}$.

column outlet caused enormous tailing effects at high iodide concentrations. The constricted outlet probably increased the length of time required to flush out the iodide to a negligible concentration and therefore caused a tailing effect. This rather large dependence of peak shape on column parameters has not been seen in any previous work using the same flow system [25, 26]. Apparently, reaction systems of the type tested here are much more sensitive to column parameters than the stoichiometrically limited systems studied previously.

Knowledge of the effect of slow reactions, particularly those in which the rate term may be non-linear, coupled with dispersion in flow systems, is incomplete, and still requires considerable experimental and theoretical investigation. The above observations that the relationships between peak height and flow rate, and between peak width and sample volume, can be altered by the sample concentration, indicate that present concepts [29, 35–37] of flow injection analysis based on the Aris–Taylor theory [30] are oversimplified.

This work was supported in part by National Science Foundation Grant CHE75-17321.

REFERENCES

- 1 K. B. Yatsimirskii, *Kinetic Methods of Analysis*, Pergamon, Oxford, 1966.
- 2 H. B. Mark, G. A. Rechnitz and R. A. Grienke, *Kinetics in Analytical Chemistry*, Wiley–Interscience, New York, 1968.
- 3 H. Weisz, *Angew. Chem. Int. Ed.*, 15 (1976) 150.
- 4 E. B. Sandell and I. M. Kolthoff, *J. Am. Chem. Soc.*, 56 (1934) 1426.
- 5 E. B. Sandell and I. M. Kolthoff, *Mikrochim. Acta*, (1937) 9.
- 6 R. A. Barkley and T. Thompson, *Anal. Chem.*, 32 (1960) 154.
- 7 H. Malmstadt and T. P. Hadjiioannou, *Anal. Chem.*, 35 (1963) 2157.
- 8 M. Dubravčić, *Analyst*, 80 (1955) 295.
- 9 G. Knapp and H. Spitzzy, *Talanta*, 16 (1969) 1353.
- 10 V. W. Truesdale and P. J. Smith, *Analyst*, 100 (1975) 111.
- 11 R. D. Strickland and C. M. Maloney, *Anal. Chem.*, 29 (1957) 1870.
- 12 G. Knapp and H. Leopold, *Anal. Chem.*, 46 (1974) 719.
- 13 K. Müller, H. Skrube and H. Spitzzy, *Mikrochim. Acta*, (1962) 1081.
- 14 H. Weisz, *Anal. Chim. Acta*, 60 (1972) 385.
- 15 P. A. Rodriguez and H. L. Pardue, *Anal. Chem.*, 41 (1969) 1376.
- 16 R. D. Sauerbrunn and E. B. Sandell, *Mikrochim. Acta*, (1953) 22.
- 17 C. Surasiti and E. B. Sandell, *Anal. Chim. Acta*, 22 (1960) 261.
- 18 E. J. Greenhow, *Chem. Rev.*, 77 (1977) 835.
- 19 T. P. Hadjiioannou, E. A. Piperaki and D. S. Papastathopoulos, *Anal. Chim. Acta*, 68 (1974) 447.
- 20 K. C. Burton and H. M. N. H. Irving, *Anal. Chim. Acta*, 52 (1970) 441.
- 21 T. P. Hadjiioannou and M. M. Timotheou, *Mikrochim. Acta*, (1977) 61.
- 22 H. Weisz, T. Kiss and D. Klockow, *Fresenius Z. Anal. Chem.*, 247 (1969) 248.
- 23 H. Weisz and S. Pantel, *Anal. Chim. Acta*, 62 (1972) 361.
- 24 P. A. Rodriguez and H. L. Pardue, *Anal. Chem.*, 41 (1969) 1369.
- 25 R. S. Schifreen, C. S. Miller and P. W. Carr, *Anal. Chem.*, 51 (1979) 278.
- 26 R. S. Schifreen, D. A. Hanna, L. D. Bowers and P. W. Carr, *Anal. Chem.*, 49 (1977) 1929.

- 27 J. Deman, *Mikrochim. Acta*, (1964) 67.
- 28 A. Hubaux and G. Vos, *Anal. Chem.*, 42 (1970) 849.
- 29 D. Betteridge, *Anal. Chem.*, 50 (1978) 832A.
- 30 R. B. Aris, *Elementary Chemical Reactor Analysis*, Prentice-Hall, Englewood Cliffs, N.J., 1969.
- 31 H. J. Arnikaar, E. A. Daniels and S. V. Kulkarni, *J. Indian Chem. Soc.*, 49 (1972) 649.
- 32 O. P. Mehta, *Indian J. Chem.*, 12 (1974) 315.
- 33 J. C. Sternberg, in J. C. Giddings and R. A. Keller (Eds.), *Advances in Chromatography*, Vol. 2, M. Dekker, New York, 1966.
- 34 J. F. K. Huber, K. M. Jonker and H. Poppe, *Anal. Chem.*, 52 (1980) 2.
- 35 J. Růžicka and E. H. Hansen, *Anal. Chim. Acta*, 99 (1978) 37.
- 36 L. R. Snyder, *Anal. Chim. Acta*, 114 (1980) 3.
- 37 J. M. Reijn, W. E. van der Linden and H. Poppe, *Anal. Chim. Acta*, 114 (1980) 105.

THE DETERMINATION OF BORON IN ZIRCONIUM AND ZIRCALOY BY PROTON ACTIVATION ANALYSIS BASED ON THE $^{10}\text{B}(\text{p}, \alpha)^7\text{Be}$ REACTION

R. MORTIER, C. VANDECASTEELE^a and J. HOSTE*

Institute for Nuclear Sciences, Rijksuniversiteit Gent, Proeftuinstraat 86, B-9000 Gent (Belgium)

(Received 17th July 1980)

SUMMARY

The determination of boron in zirconium and zircaloy based on the $^{10}\text{B}(\text{p}, \alpha)^7\text{Be}$ reaction is described. At the 100 and 20 $\mu\text{g g}^{-1}$ concentration level (doped samples), instrumental analysis is feasible. At lower concentrations, ^7Be is separated from the activities formed from zirconium and its alloying elements or impurities, by anion-exchange in hydrofluoric acid medium followed by precipitation of YF_3 and of BaBeF_4 . The chemical yield of the separation was determined in several ways. The sensitivity of the method was 15 ng g^{-1} . For concentrations ranging from 100 to 0.15 $\mu\text{g g}^{-1}$, the precision ranged from 3.5 to 10.7%. The results are compared with results obtained by other methods.

Zirconium metal and zirconium alloys are often used in the nuclear energy industry as structural materials and as cladding materials for enriched uranium. Zirconium has indeed a very small cross-section for the capture of thermal neutrons, good mechanical properties, and good resistance to corrosion and oxidation. Because of its high cross-section for the capture of thermal neutrons, boron is an important impurity in these materials.

Boron is usually determined in zirconium and its alloys by colorimetry [1], emission spectrometry and spark-source mass spectrometry [2]. However, little is known about the accuracy of these methods. In this context B.C.R., the Reference Bureau of the European Communities, organised a round-robin test for the preparation and analysis of a certified reference material for boron in zirconium. Many laboratories using different techniques participated in the test. B.C.R. delivered six different kinds of samples: zirconium doped with boron (100, 20, 1 and 0.5 $\mu\text{g g}^{-1}$), blank samples and zircaloy samples. The zirconium samples were doped by means of high-frequency levitation melting.

The analyses described in this paper, were carried out by activation analysis with charged particles using the $^{10}\text{B}(\text{p}, \alpha)^7\text{Be}$ reaction. ^7Be has a 53.3-d half-life and emits γ -rays of 477-keV energy. The long half-life allows even a complicated radiochemical separation. The chemical yield can be determined

^a“Bevoegdverklaard navorser” of the N.F.W.O.

for each analysis. The disadvantage is that long irradiation and counting times are required for good sensitivity.

Nuclear reactions

The relative thick target yields of the $^{10}\text{B}(p, \alpha)^7\text{Be}$ reaction and the $^{92}\text{Zr}(p, n)^{92\text{m}}\text{Nb}$ reaction as a function of the energy were determined experimentally (Figs. 1 and 2). $^{92\text{m}}\text{Nb}$ is the principal radionuclide formed from the matrix. The thick target yield for the $^{92}\text{Zr}(p, n)^{92\text{m}}\text{Nb}$ reaction as a function of the energy is a measure of the variation of the matrix activity as a function of the energy. For each curve, all points were normalised to the end of the irradiation for the same irradiation time and intensity. Pellets pressed from boric acid and zirconium disks were irradiated with protons of different energies. The energies of interest were obtained by degrading a 15-MeV proton beam with copper foils of different thickness placed before the targets. The boric acid pellets were irradiated for 10 min at a beam intensity of $0.1 \mu\text{A}$ and the zirconium disks for 1 min at $2 \mu\text{A}$. It is clear from Figs. 1 and 2 that for an instrumental analysis the energy should be below 6 MeV, to avoid activation of the matrix. When the incident energy is decreased from 10 to 4.5 MeV, the $^{92\text{m}}\text{Nb}$ activity decreases by a factor of 30 whereas the ^7Be activity produced from boron decreases only by a factor of 3. For an analysis including chemical separation, a higher energy may be chosen to obtain a higher sensitivity.

The most important nuclear reactions of zirconium and its alloying elements or impurities are given in Table 1. For zircaloy the activity formed from the alloying elements is important. The zircaloy analysed contained $1000 \mu\text{g Cr g}^{-1}$, $2000 \mu\text{g Fe g}^{-1}$, $16000 \mu\text{g Sn g}^{-1}$ and $1200 \mu\text{g O g}^{-1}$.

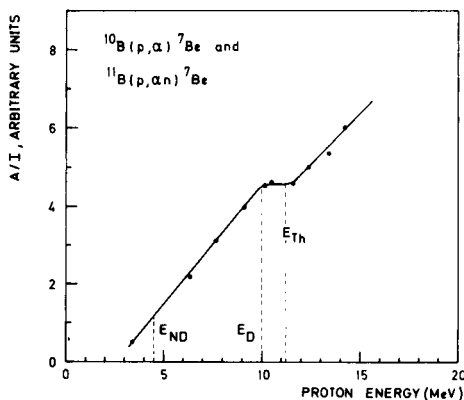


Fig. 1. Thick target yield of the $^{10}\text{B}(p, \alpha)^7\text{Be}$ and $^{11}\text{B}(p, \alpha n)^7\text{Be}$ reactions: A, ^7Be activity at the end of the irradiation; I, beam intensity; E_{ND} , incident energy for instrumental analysis; E_{D} , incident energy for analysis with chemical separation; E_{Th} , threshold energy of the $^{11}\text{B}(p, \alpha n)^7\text{Be}$ reaction.

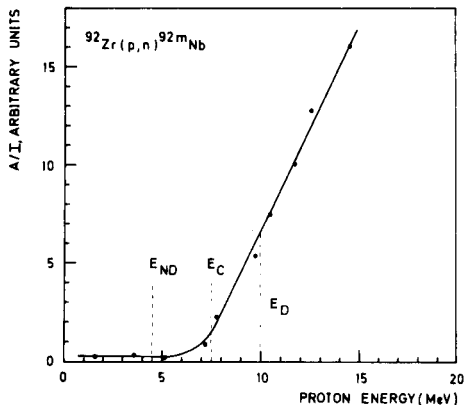


Fig. 2. Thick target yield of the $^{92}\text{Zr}(p, n)^{92\text{m}}\text{Nb}$ reaction: A, $^{92\text{m}}\text{Nb}$ activity at the end of the irradiation; E_{C} , Coulomb barrier. The other symbols have the same meaning as in Fig. 1.

TABLE 1

Nuclear reactions for zirconium and its impurities

Reaction	E_{th} (MeV)	Half-life	Reaction	E_{th} (MeV)	Half-life (d)
$^{92}\text{Zr}(p, n)^{92m}\text{Nb}$	2.8	10.16 d	$^{122}\text{Sn}(p, n)^{122}\text{Sb}$	2.4	2.72
$^{91}\text{Zr}(p, n)^{91m}\text{Nb}$	2.5	64.00 d	$^{120}\text{Sn}(p, n)^{120m}\text{Sb}$	3.5	5.8
$^{96}\text{Zr}(p, 2n)^{95}\text{Nb}$	7.6	35.00 d	$^{124}\text{Sn}(p, n)^{124}\text{Sb}$	1.4	60.2
$^{90}\text{Zr}(p, d)^{89}\text{Zr}$	9.9	78.4 h	$^{52}\text{Cr}(p, n)^{52}\text{Mn}$	5.6	5.6
$^{96}\text{Zr}(p, d)^{95}\text{Zr}$	5.8	65.5 d	$^{56}\text{Fe}(p, n)^{56}\text{Co}$	5.5	77.3
$^{90}\text{Zr}(p, \alpha)^{87}\text{Y}$	1.1	80.0 h	$^{48}\text{Ti}(p, n)^{48}\text{V}$	4.9	16.2
$^{91}\text{Zr}(p, \alpha)^{88}\text{Y}$	$Q > 0$	106.6 d			
$^{94}\text{Zr}(p, \alpha)^{91}\text{Y}$	$Q > 0$	58.5 d			

EXPERIMENTAL

Samples and standards

The samples were cylindrical disks, 15 mm in diameter and 1 mm thick. The standards were pellets pressed from boric acid (p.a.) with 20 mm diameter and about 1 mm thickness.

Irradiation and chemical etching

The samples and the standards were irradiated in vacuum with a 6- or 12-MeV proton beam extracted from the CGR-MeV 520 isochronous cyclotron of Gent University. The beam was collimated with a 12-mm diameter collimator. A metal foil was placed before the sample and the standard to serve as a beam intensity monitor. Table 2 summarizes the irradiation conditions.

After irradiation the samples were etched for 1 or 2 min in a mixture (1 + 40) of hydrofluoric acid (50%) and water at room temperature to remove a surface layer of 7–13 mg cm⁻². After etching, the sample was rinsed by dipping in water and in acetone and dried. In the case of the zircaloy samples, the surface was cleaned after etching by dipping the sample for a few seconds in 6 M HNO₃. The thickness removed was determined by weighing and checked by means of a micrometer.

Chemical separation of ⁷Be

For the samples doped with boron (100 and 20 µg g⁻¹), an instrumental analysis is feasible. For the other samples, ⁷Be must be separated from the radionuclides formed from zirconium and its alloying elements or impurities.

Chemical separation from zirconium. ⁷Be must be separated from Nb, Zr and Y radionuclides produced from the zirconium matrix and from ⁴⁸V and ⁵⁶Co produced from Ti and Fe by the reactions shown in Table 1. Anion exchange on Dowex 1-X8 in 6 M hydrofluoric acid [3], followed by precipitation of YF₃ and BaBeF₄ was used.

TABLE 2

Irradiation conditions

	Zirconium doped with 100 and 20 $\mu\text{g B g}^{-1}$		Zirconium doped with 1 and 0.5 $\mu\text{g B g}^{-1}$. Blank zirconium and zircaloy	
	Sample	Standard	Sample	Standard
Beam energy (MeV)	6	6	12	12
Beam energy corresponding to etching depth (MeV)	4.2–4.5		9.8–10.0	
Beam intensity (μA)	2	0.1	4	0.1
Irradiation time (min)	120	10	180	10
Beam intensity monitor	Cu-foil (30 μm)	Cu-foil (30 μm)	Zr-foil (100 μm)	Zr-foil (100 μm)
Beam intensity normali- sation	$^{65}\text{Cu}(\text{p}, \text{n})^{65}\text{Zn}$		$^{92}\text{Zr}(\text{p}, \text{n})^{92\text{m}}\text{Nb}$	
$T_{1/2}$ (d)		243.6		10.16
E_γ (keV)		1115		935

The optimum conditions for the chemical separation by anion exchange were studied. An irradiated zirconium sample was dissolved in 10 ml of 6 M hydrofluoric acid, placed on a column filled with Dowex 1-X8 (see below) and eluted with 6 M hydrofluoric acid. Successive 10-ml fractions of the eluate were collected and the activity measured. No $^{92\text{m}}\text{Nb}$ and ^{95}Zr activity was observed in the eluate. These elements are thus quantitatively retained on the column. The elution curves for ^7Be , ^{48}V , ^{56}Co and ^{87}Y are shown in Fig. 3. The elution curve for ^7Be was determined by treating similarly some irradiated boric acid dissolved in 6 M HF together with an inactive zirconium sample. From these curves, it is clear that discarding the first 80 ml of eluate and collecting the next 200 ml allows ^7Be to be separated quantitatively from Nb and Zr activities and also from the main part of the ^{48}V , ^{56}Co and ^{87}Y activities. The remaining ^{48}V and ^{56}Co do not affect the detection of ^7Be . A further separation from ^{87}Y which emits 484-keV γ -rays is necessary. This is achieved by precipitation of YF_3 . Eventually ^7Be is precipitated as BaBeF_4 to allow the detection of ^7Be in the same geometrical conditions as the standard and with high efficiency.

Procedure for the separation of ^7Be from zirconium. Dissolve the sample and 10 mg of beryllium metal in 10 ml of 6 M hydrofluoric acid in a plastic bottle. Add 2 ml of concentrated hydrofluoric acid. Add the solution to the top of a teflon column (i.d. 1.8 cm; height 40 cm) filled with 30 g of Dowex 1-X8 resin kept at constant temperature (25°C). The resin was previously converted to the fluoride form by washing with 250 ml of 6 M HF. Elute with 6 M HF at a flow rate of 2.5 ml min^{-1} . After discarding the first 80 ml of eluate, collect the next 200 ml. Add dropwise 50 mg of $\text{Y}(\text{NO}_3)_3 \cdot 6\text{H}_2\text{O}$ dissolved in 10 ml of water while stirring with a magnetic stirrer. Continue

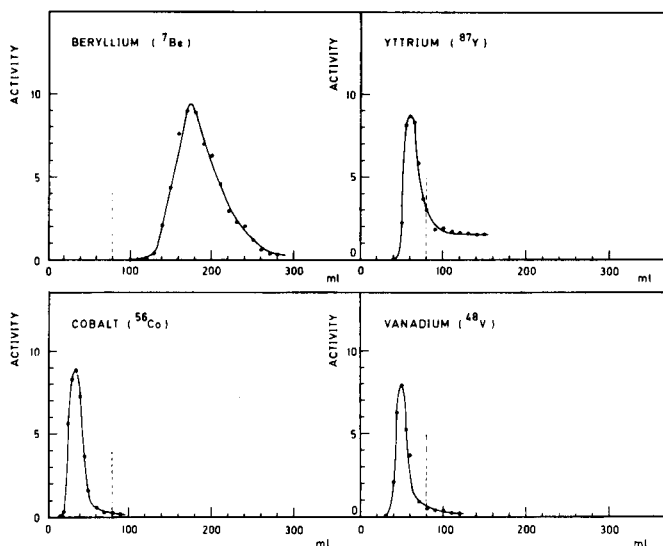


Fig. 3. Elution curves.

stirring for 15 min. Filter off the YF_3 precipitate on a membrane filter. Add while stirring 6 ml of 0.5 M barium nitrate. After 15 min, filter off the BaBeF_4 precipitate, wash with ethanol and dry at 80°C .

The effectiveness of the chemical separation is illustrated by the $\text{Ge}(\text{Li})$ spectra shown in Figs. 4 and 5.

Chemical separation from zircaloy. After chemical separation by anion exchange as described above, the eluate of an irradiated zircaloy sample contains important activities mainly of $^{120\text{m}}\text{Sb}$, ^{122}Sb and ^{124}Sb (formed from Sn), ^{87}Y , ^{88}Y , ^{91}Y (from Zr) and ^{52}Mn , ^{48}V and ^{56}Co (from Cr, Ti and Fe). If Sb^{3+} is oxidised to Sb^{5+} with hydrogen peroxide before the elution, the ^{122}Sb is completely retained by the resin. The fraction of the eluate between 80 ml and 280 ml still contains considerable amounts of ^{48}V , ^{56}Co and ^{52}Mn because the zircaloy contains more Cr, Fe and Ti than zirconium. To avoid significant coprecipitation of these radionuclides with the BaBeF_4 precipitate some V, Co and Mn carrier is added before precipitation.

Procedure for the separation of ^7Be from zircaloy. Dissolve the sample as for zirconium. Add 2 ml of hydrogen peroxide (30%) and 2 ml of hydrofluoric acid (50%). Add the solution onto the column and elute as for zirconium, collecting the fraction of the eluate between 80 and 280 ml. Precipitate YF_3 at $70\text{--}80^\circ\text{C}$ and stir for 1 h. Filter off on a membrane filter. Dissolve 50 mg of V_2O_3 , 50 mg of $\text{MnCl}_2 \cdot 4\text{H}_2\text{O}$ and 50 mg of $\text{CoCl}_2 \cdot 6\text{H}_2\text{O}$ in the filtrate and add dropwise 6 ml of 0.5 M barium nitrate while stirring. Filter off the precipitate, wash with ethanol and dry at 80°C .

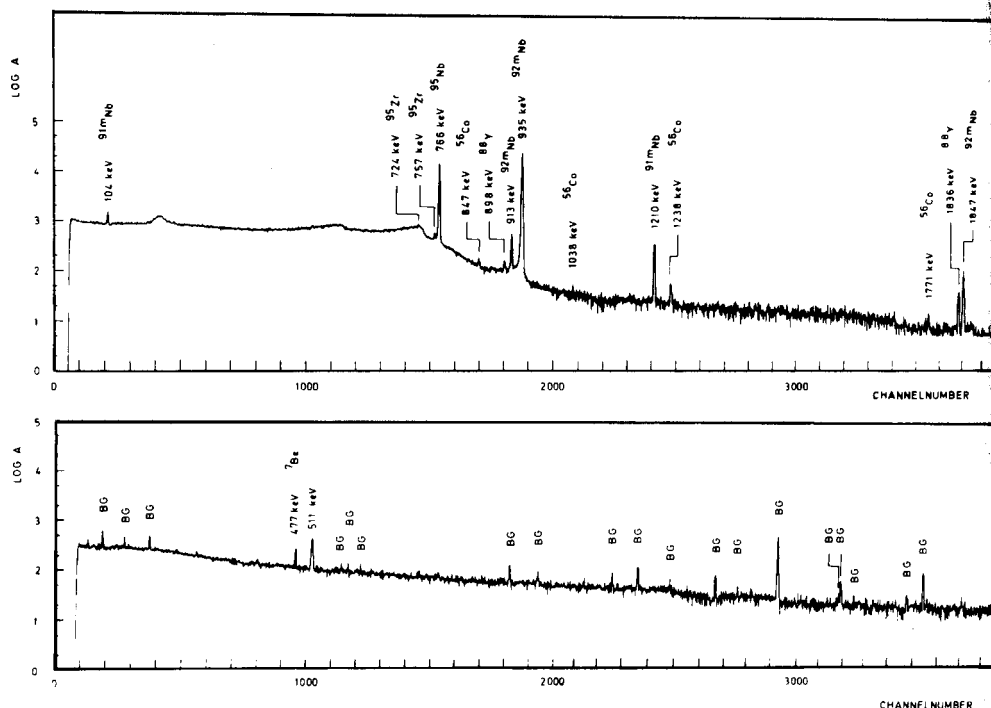


Fig. 4. Spectrum of a dissolved sample measured for 5 min at low detection efficiency.

Fig. 5. Spectrum for a BaBeF_4 precipitate measured for 60 h at high detection efficiency. BG means background activity.

Chemical yield

Calculation of the chemical yield from the weight of the precipitate was inaccurate because some barium fluoride also precipitated. Attempts were made to avoid this coprecipitation but this resulted in low yields for BaBeF_4 . Therefore the chemical yield was checked with different methods.

Tracer experiments with ^7Be indicated a yield of 93–97%. A boric acid pellet was irradiated and the ^7Be activity measured. The pellet was dissolved together with 1 g of zirconium and 10 mg of beryllium in 15 ml of 6 M hydrofluoric acid. The separation scheme was then carried out. The BaBeF_4 precipitate contained 93–97% of the original ^7Be activity.

Atomic absorption and i.c.p.e.s. (inductively coupled plasma emission spectrometry) were also applied. A known quantity of beryllium (10 mg) was added during dissolution of the sample and the amount of beryllium in the precipitate was determined. In both cases the standard addition method gave accurate results. The 234.86-nm line of beryllium was measured. The yields determined by these methods ranged also from 93 to 97%.

Measurements

The measurements were done with a Ge(Li) detector (relative detection

efficiency, 20%; resolution, 2.1 keV at 1333 keV) coupled to a multichannel analyser. For an instrumental analysis, the samples were measured for 10 h after a cooling time of 70–80 days. The samples analysed by chemical separation were generally separated one day after irradiation and measured for 60 h. Standards were measured for 1 h, one day after irradiation.

Standardisation

The boron concentration is obtained from the equation

$$c_x = c_s A_x I_s S_s R_s / A_s I_x S_x R_x$$

where c is the concentration ($\mu\text{g g}^{-1}$); A the ${}^7\text{Be}$ activity at the end of the irradiation; I the beam intensity obtained from the ${}^{65}\text{Zn}$ or the ${}^{92\text{m}}\text{Nb}$ activity of the beam intensity monitor; S the saturation factor for ${}^7\text{Be}$ production; and R the range of the charged particles in the material (g cm^{-2}) [4, 5]. The subscripts x and s refer respectively to the sample and the standard.

After irradiation, a surface layer is removed from the sample. Because of energy degradation within this layer, the effective incident energy differs from the energy incident on the standards. Therefore several standards are irradiated behind a different thickness of metal foils. This is illustrated in Fig. 6 for a 6-MeV proton beam.

Calculations were carried out by the method of Ricci and Hahn [6]. It was verified that calculation of the results by the "numerical integration method" yielded the same results within the experimental error [7].

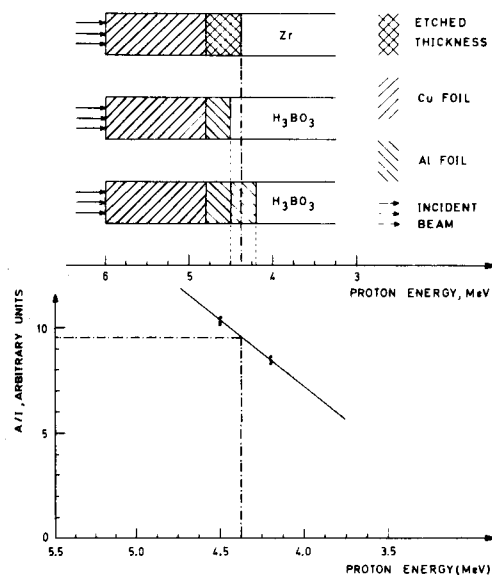


Fig. 6. Standardisation with 6-MeV protons. A , ${}^7\text{Be}$ yield in the standard at the end of the irradiation; I , beam intensity.

RESULTS AND DISCUSSION

Some results are given in Table 3. Detection limits were calculated by the Currie criterion [8]. For an irradiation with a 2- μ A beam of 6-MeV protons, the detection limit is 8.9 $\mu\text{g B g}^{-1}$ for an instrumental analysis. The detection limit for an analysis with chemical separation of ^7Be ($<0.033 \mu\text{g g}^{-1}$) mentioned in Table 3 for the blank sample could be lowered by carrying out the measurements with an anti-Compton spectrometer; background activity from Compton scattering is strongly reduced with this equipment. The natural background is also reduced because the detector is better shielded. A detection limit of 0.015 $\mu\text{g B g}^{-1}$ was obtained in this way.

Table 4 compares the present results with those obtained in the B.C.R. round-robin. At the 100 and 20 $\mu\text{g g}^{-1}$ concentration levels, practically all methods yield acceptable results. For the 1 and 0.5 $\mu\text{g g}^{-1}$ samples, the average results lie in the ranges 0.97–3.5 $\mu\text{g g}^{-1}$ and 0.36–1.5 $\mu\text{g g}^{-1}$, respectively. At the 0.5 $\mu\text{g g}^{-1}$ level, which is the most important one from a technological point of view, the present results have a better precision than those of other methods. They agree for all concentrations with those expected from the preparation method, which seems to prove the accuracy. Moreover, as appears from the upper limits for the "blank" samples, the sensitivity of the present method exceeds that of the other methods.

Interferences

The $^{10}\text{B}(\text{p}, \alpha)^7\text{Be}$ reaction is interfered with by the $^7\text{Li}(\text{p}, \text{n})^7\text{Be}$ reaction [9]. From the blank samples, i.e. samples of the starting material used for the preparation of the doped zirconium by high-frequency levitation melting, a detection limit of 15 ng B g^{-1} was obtained. This is, of course, also an upper limit for the lithium interference in the blank samples. Assuming that no lithium contamination occurred during the sample preparation, this is also an upper limit for the lithium interference for the doped samples.

TABLE 3

Results ($\mu\text{g g}^{-1}$)

Sample nr.	1	2	3	4	5	Mean $\pm s$ (%)
Zr doped with:						
100 $\mu\text{g g}^{-1\text{a}}$	106.6	98.0	103.6	101.8		102.5 \pm 3.6 (3.5)
20 $\mu\text{g g}^{-1\text{a}}$	21.1	20.9	21.6	19.1	20.6	20.7 \pm 1.0 (4.8)
1 $\mu\text{g g}^{-1\text{b}}$	1.16	0.97	1.03	1.00		1.04 \pm 0.08 (7.7)
0.5 $\mu\text{g g}^{-1\text{b}}$	0.489	0.476	0.493	0.458		0.479 \pm 0.016 (3.3)
Blank zirconium ^b	<0.033					
Zircaloy ^b	0.155	0.180	0.140			0.158 \pm 0.017 (10.1)

^aInstrumental analysis. ^bWith chemical separation of ^7Be .

TABLE 4

Comparison of the results obtained in the B.C.R. round-robin [10]

	Zr "O"	Boron content spiked ($\mu\text{g g}^{-1}$)			
		0.5	1	20	100
S.s.m.s. ^a	—	0.47 ± 0.06	1.44 ± 0.12	21.5 ± 1.9	98 ± 11
	—	0.52 ± 0.12	1.10 ± 0.22	heterogen.	heterogen.
	—	0.55 ± 0.16	1.19 ± 0.10	—	—
E.s. ^b	—	0.76 ± 0.12	1.32 ± 0.05	>5	>5
	—	1.5	3.5	—	—
	—	1.4	2.5	24	135
	—	1.0 ± 0.3	2.0 ± 0.5	17 ± 4	91 ± 17
I.c.p.e.s.	<0.04	0.68 ± 0.11	1.02 ± 0.18	22.7 ± 2.7	—
		0.58 ± 0.06	1.11 ± 0.14		
Photometry	—	0.62 ± 0.03	0.97 ± 0.06	—	—
	0.05	0.51 ± 0.04	1.02 ± 0.06	19.4 ± 1.0	97.5 ± 4.2
	—	0.53 ± 0.06	1.03 ± 0.13	—	—
	—	0.36 ± 0.04	1.03 ± 0.17	—	—
Prompt α	—	1.2 ± 0.5	1.9 ± 0.6	18.3 ± 2.2	98 ± 4
Prompt γ	—	0.60 ± 0.18	1.12 ± 0.17	19.6 ± 1.2	99.1 ± 2.6
(p, α) activation	—	0.70 ± 0.26	1.05 ± 0.45	19.7 ± 0.4	102.2 ± 1.0
Instrumental					
This work	<0.015	0.48 ± 0.02	1.04 ± 0.08	20.7 ± 1.0	102.5 ± 3.6

^aSpark-source mass spectrometry. ^bEmission spectrometry.

The interference of the $^{14}\text{N}(\text{p}, 2\alpha)^7\text{Be}$ reaction is avoided by reducing the incident energy to below 11.26 MeV.

In conclusion, the method described allows the determination of boron in zirconium and zircaloy with good sensitivity (15 ng g^{-1}), precision and accuracy. An advantage is that the yield of the chemical separation can be determined for each analysis. Disadvantages are the possible interference of lithium and the long irradiation and counting times.

Grateful acknowledgement is made to J. Pauwels (B.C.M.N., Geel) for providing the samples, to B.C.R. for organising the round-robin test, to P. Schutyser and E. Janssens for the measurements with the i.c.p. spectrometer, to B. Desmet for the measurements with the a.a.s. spectrometer and to the I.I.K.W. and N.F.W.O. for financial support.

REFERENCES

- 1 M. Freegarde and J. Cartwright, *Analyst*, 87 (1962) 214.
- 2 H. E. Beske, G. Fierichs, M. D. Jahn and F. G. Melchers, *Mikrochim. Acta* (Wien), Suppl. 8, (1979) 493.
- 3 J. P. Faris, *Anal. Chem.*, 32 (1960) 521.
- 4 C. Williamson, J. Boujot and J. Picard, *Tables of Range and Stopping Power of Chemical Elements for Charged Particles of Energy 0.05 to 500 MeV*, Rapport C.E.A. -R 3042, 1966.

- 5 H. H. Andersen and J. F. Ziegler, *The Stopping and Ranges of Ions in Matter*, Vols. 3 and 4, Pergamon, Oxford, 1977.
- 6 E. Ricci and R. L. Hahn, *Anal. Chem.*, 39 (1967) 794.
- 7 C. Vandecasteele and K. Strijckmans, *J. Radioanal. Chem.*, 57 (1980) 121.
- 8 L. A. Currie, *Anal. Chem.*, 40 (1968) 587.
- 9 B. Vialatte, *J. Radioanal. Chem.*, 8 (1971) 269.
- 10 Minutes of the B.C.R. Meeting, Brussels, 18 September, 1979.

MULTI-ELEMENT DETERMINATIONS OF TRACE ELEMENTS IN GLASS BY INSTRUMENTAL PHOTON ACTIVATION ANALYSIS

YUKIO KANDA*, TOMOMASA OIKAWA and TETSUKICHI NIWAGUCHI

National Research Institute of Police Science, Sanban-cho, Chiyoda-ku, Tokyo 102 (Japan)

(Received 2nd June 1980)

SUMMARY

An instrumental photon activation method is reported for multi-element determinations in glass. The concentrations of 17 elements in NBS standard glass can be determined by irradiation with 30-MeV bremsstrahlung and measurement of the resulting γ -rays with a Ge(Li) detector. The average of all relative standard deviations is 2.7%; the relative deviations from the NBS certified values range from 1.4 to 3.4%.

The characterization of materials by their elemental profiles is particularly useful in forensic examinations. Instrumental neutron activation analysis has been successfully applied for discrimination of various types of forensic samples because of its high sensitivity and capability of simultaneous multi-element determinations. However, instrumental neutron activation analysis of glass samples, one of the most important materials for evidence in traffic accidents, is limited in the number of elements that can be determined, because of interference from the very high ^{24}Na activity induced from the sodium oxide component of the glass matrix. Coleman and Goode [1] have described a destructive neutron activation method for the determination of 25 elements in glass by using solvent extraction for radiochemical group separation.

The present paper is concerned with an alternative nuclear method, photon activation analysis, which permits the non-destructive analysis of glass without serious matrix interferences. The photonuclear (γ , n) and (γ , p) reactions often produce radioactive nuclides with suitable half-lives and γ -ray energies for analysis. In photon activation analysis, moreover, interferences from the activities of nuclides produced from elements such as Na, K, Cl and Mn, which frequently give problems in neutron activation analysis of biological and geological materials, are not serious for multi-element determinations. Applications of instrumental photon activation to biological [2, 3], geological [3–5] and environmental [3, 6, 7] materials have proved that this method is useful as a complement to instrumental neutron activation. Several compilations of photonuclear reactions and nuclear characteristics of nuclides are now available [3, 8–11].

It is shown below that the concentrations of 17 elements in NBS standard glass can be determined non-destructively by activation with 30-MeV bremsstrahlung with good precision.

EXPERIMENTAL

Sample and comparative standard

The NBS SRM 613 glass is supplied in the form of wafers with a thickness of 1 mm. The surfaces of samples were wiped with a gauze soaked with ethanol, washed gently with dilute (1 + 10) nitric acid as recommended by the supplier, and then powdered in an agate mortar. A portion (0.3 g) of the powdered sample was wrapped in a small piece of aluminium foil and made into a disc with a diameter of 10 mm.

The comparative standard was prepared by adding appropriate amounts of As_2O_3 , CeO_2 , Co, CsCl, MgO, Mn, Nb_2O_5 , Ni, RbCl, Sb_2O_3 , Sc_2O_3 , SrCl_2 , Ti, Y_2O_3 and ZrO_2 to a synthetic glass matrix, which was prepared by mixing SiO_2 (79.5%), CaO (12.7%) and Na_2O (7.8%). The chemical reagents used were of 99.9% purity or better, and anhydrous silica, SiO_2 , was obtained by igniting extra-pure silica gel (Merck) for 6 h in a crucible. The concentration levels of the elements added to the comparative standard were in the range 250–500 $\mu\text{g g}^{-1}$. Portions (0.3 g) of the comparative standard were wrapped in small pieces of aluminium foil and made into discs with a diameter of 10 mm.

Irradiation and counting

Each glass sample was sandwiched between the comparative standards and sealed in a silica tube. The tube was placed in a water-cooled sample holder aligned on the bremsstrahlung axis just behind a photon-producing converter made of platinum. Irradiation was carried out for 2 h with bremsstrahlung from 30-MeV electrons at the linear accelerator of Tohoku University. The electron beam current was typically 100 μ , and the photon flux in the 10–25 MeV region was about 10^{12} quanta/ cm^2 s.

After irradiation, the aluminium wrapper was removed from each sample and the contents were repacked in fresh aluminium foils. The γ -ray spectra were measured with a 68- cm^3 (Ortec) or a 30- cm^3 (Harshow) Ge(Li) detector coupled to a 4096-channel pulse-height analyzer. During counting, a 10-mm thick lucite plate was placed between the sample and the detector in order to absorb positrons from a number of positron-emitting nuclides. Counting times of 500 s, 3000 s and 20000 s were used for short-, medium- and long-lived products, respectively. The photopeaks in the observed spectra were assigned to the radioactive nuclides by comparing their energies and half-lives with those in the lists of nuclear data [12].

RESULTS AND DISCUSSION

After cooling for 2 h for the decay of strong 511-keV annihilation radiation from positron emitters (mainly 2-min ^{15}O), and the activities of 2.3-min

^{28}Al and 6.6-min ^{29}Al produced from silicon by the $^{29}\text{Si}(\gamma, p)^{28}\text{Al}$ and $^{30}\text{Si}(\gamma, p)^{29}\text{Al}$ reactions, the γ -ray spectrum of each sample was measured. Measurements were repeated three times over a period of one month.

Figure 1 shows typical γ -ray spectra of the NBS SRM 613 glass irradiated with 30-MeV bremsstrahlung. In the spectrum of Fig. 1A, taken 2 h after irradiation, the photopeaks of 22.4-h ^{43}K , 15.0-h ^{24}Na , 4.0-h ^{44}Sc and 2.83-h $^{87\text{m}}\text{Sr}$ are distinctly seen. After cooling for 5 d, a rather complicated spectrum with photopeaks of the nuclides produced from 18 elements is obtained (Fig. 1B). Table 1 gives the γ -rays and half-lives of the nuclides used for the determination of the 17 elements in the NBS SRM 613 glass. The practical detection limits are listed also in Table 1. These limits were calculated as the concentration which gives a photopeak intensity corresponding to three times the standard deviation of background activity.

Calcium could be determined either by the 619-keV peak of ^{43}K from the $^{44}\text{Ca}(\gamma, p)^{43}\text{K}$ reaction, or by the 1298-keV peak of ^{47}Ca from the $^{48}\text{Ca}(\gamma, n)^{47}\text{Ca}$ reaction. Agreement between the values obtained from these two peaks was within $\pm 1.4\%$.

In the determination of arsenic and cobalt by the $^{75}\text{As}(\gamma, n)^{74}\text{As}$ and the $^{59}\text{Co}(\gamma, n)^{58}\text{Co}$ reactions, the 596-keV peaks of ^{74}As and the 811-keV peak of ^{58}Co were subject to spectral interferences from the ^{43}K 591-keV and ^{47}Ca 808-keV γ -rays, respectively. Only the 811-keV γ -ray was observed for ^{58}Co . The 634-keV peak of ^{74}As was also observed, but could not be used for the concentration determination because of its low peak-to-background ratio. Since the half-lives of ^{74}As and ^{58}Co are sufficiently longer than those of ^{43}K and ^{47}Ca , respectively, the 596-keV and 811-keV peaks were completely free from these spectral interferences after decay periods of about 9 d and 30 d, respectively.

Serious interferences from the matrix by competing reactions were observed for the determination of magnesium and titanium. The determination of magnesium by the $^{25}\text{Mg}(\gamma, p)^{24}\text{Na}$ reaction is subject to interference from aluminium through the $^{27}\text{Al}(n, \alpha)^{24}\text{Na}$ reaction. The ratio of ^{24}Na activities produced from the same weights of magnesium and aluminium has been reported to be 210 in irradiation with 30-MeV bremsstrahlung [3]. From this value and from the aluminium content in the sample (2% as oxide, nominal value), the contribution of the $^{27}\text{Al}(n, \alpha)^{24}\text{Na}$ reaction to the total ^{24}Na activity was estimated to be 13.5%, corresponding to 53 ppm Mg. The concentration of magnesium listed in Table 2 was corrected for aluminium in this way.

The $^{48}\text{Ti}(\gamma, p)^{47}\text{Sc}$ reaction can be conveniently used for the determination of titanium. In this case, the $^{51}\text{V}(\gamma, \alpha)^{47}\text{Sc}$ and $^{48}\text{Ca}(\gamma, n)^{47}\text{Ca} \xrightarrow{\beta^-} ^{47}\text{Sc}$ reactions are possible sources of interference. The ratios of ^{47}Sc activities produced from the same weights of titanium, vanadium and calcium have been reported to be about 68/2.8/1 at 136 h after 30-MeV bremsstrahlung irradiation [3]. From these data and the nominal vanadium concentration of 50 ppm in this sample, the effect of interference from vanadium was estimated to be only

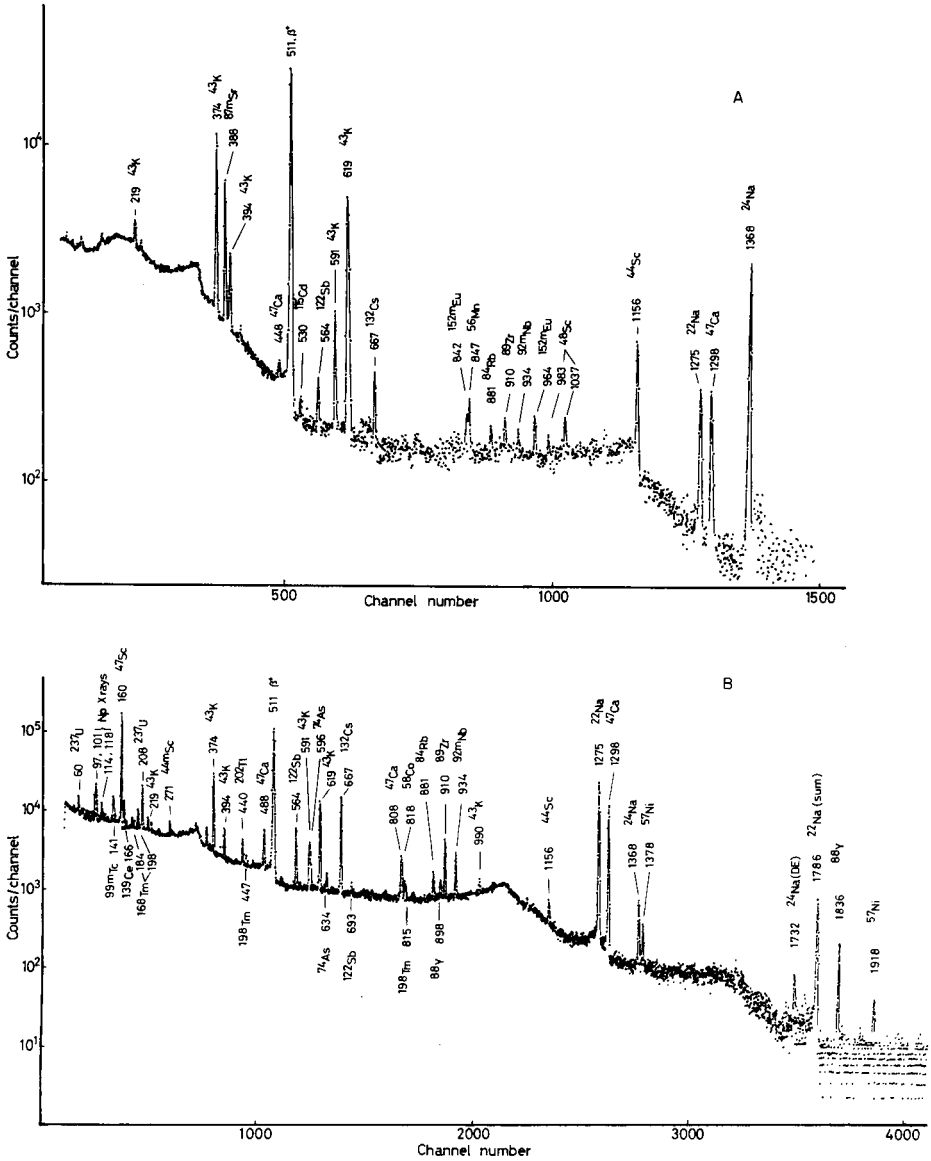


Fig. 1. γ -ray spectrum of NBS SRM 613 measured (A) 2 h after irradiation, and (B) 5 d after irradiation. For (A), each channel corresponds to 1.0 keV, and for (B) 0.5 keV.

about 3%. As the sample contains a large amount of calcium, however, the effect of interference from calcium by the $^{48}\text{Ca}(\gamma, n)^{47}\text{Ca} \xrightarrow{\beta^-} ^{47}\text{Sc}$ becomes very serious for the determination of titanium. The longer decay period increases the contribution of calcium to the total ^{47}Sc activity. Thus it is desirable to measure the ^{47}Sc activity soon after irradiation. In this glass

TABLE 1

Nuclear data of the photon activation products used for determination

Element	Process	Nuclide	Half-life	γ -ray used (keV)	Practical limit of detection ($\mu\text{g g}^{-1}$)
As	(γ , n)	^{74}As	17.9 d	596	0.9
Ca	(γ , p)	^{43}K	22.4 h	619	350
	(γ , n)	^{47}Ca	4.53 d	1298	450
Ce	(γ , n)	^{139}Ce	140 d	166	1.3
Co	(γ , n)	^{58}Co	71.3 d	811	2.3
Cs	(γ , n)	^{132}Cs	6.5 d	667	0.4
Mg	(γ , p)	^{24}Na	15.0 h	1368	20
Mn	(γ , n)	^{54}Mn	303 d	835	18
Na	(γ , n)	^{22}Na	2.60 y	1275	110
Nb	(γ , n)	$^{92\text{m}}\text{Nb}$	10.16 d	934	2.1
Ni	(γ , n)	^{57}Ni	36.0 h	1378	1.5
Rb	(γ , n)	^{84}Rb	33.0 h	881	1.5
Sb	(γ , n)	^{122}Sb	2.80 d	564	0.8
Sc	(γ , n)	^{44}Sc	4.0 h	1156	0.5
Sr	(γ , p)	$^{87\text{m}}\text{Sr}$	2.83	388	1.3
Ti	(γ , p)	^{47}Sc	3.43 d	160	10
Y	(γ , n)	^{88}Y	108 d	1836	0.4
Zr	(γ , n)	^{89}Zr	78.4 h	910	0.9

sample, however, the strong Compton backgrounds from 511-keV annihilation radiation and the ^{43}K activity obscured the 166-keV peak of ^{47}Sc at decay periods less than one day. The ratio of ^{47}Sc activities produced from the same weights of titanium and calcium was found to be about 340 at 2 d after irradiation. From this result and the calcium content, the calcium contribution to the total ^{47}Sc activity was estimated to be 83% in this sample. The titanium concentration listed in Table 2 was corrected for calcium. Although an alternative $^{47}\text{Ti}(\gamma, p)^{48}\text{Sc}$ reaction does not suffer serious interference, this reaction could not be used for the determination because the sensitivity obtained was about 100 times worse than that achieved with the $^{48}\text{Ti}(\gamma, p)^{47}\text{Sc}$ reaction. There were no other interference problems in this work.

For the correction of the flux gradient along the beam axis, the sample was sandwiched between two comparative standards, and the concentration of each element was calculated by comparing the peak area for each nuclide produced in the sample with the mean value of the corresponding peak areas in the two comparative standards.

The amounts of impurities in silica, which was used as the major component of the synthetic glass matrix of the comparative standard, were also determined by the instrumental photon activation method. The concentrations of Ca, Mg, Na, Sr, Ti and Zr were found to be 290, 47, 200, 12, 90 and 38 $\mu\text{g g}^{-1}$ of silica, respectively. The concentrations of these elements in the comparative standard were corrected for these blanks.

TABLE 2

Elemental abundances of NBS SRM 613 glass

Element	Amount present ($\mu\text{g g}^{-1}$)			Element	Amount present ($\mu\text{g g}^{-1}$)		
	This work	NBS certificate ^a	Haney [13]		This work	NBS certificate ^a	Ha [1]
As	35.6 \pm 0.3			Ni	40.1 \pm 1.1	38.8 \pm 0.2	
CaO (%)	12.1 \pm 0.2			Rb	32.0 \pm 1.4	31.4 \pm 0.4	31
Ce	40.6 \pm 0.2	(39)	41.2	Sb	39.4 \pm 0.3		
Co	33.3 \pm 1.0	(35.5 \pm 1.2)		Sc	38.2 \pm 1.2		
Cs	44.8 \pm 1.2			Sr	77.3 \pm 1.3	78.4 \pm 0.2	76
Mg	341 \pm 16			Ti	55.2 \pm 8.3	(50.1 \pm 0.8)	
Mn	39.0 \pm 2.6	(39.6 \pm 0.8)		Y	37.9 \pm 1.4		
NaO (%)	14.2 \pm 0.2			Zr	41.8 \pm 1.1		
Nb	38.1 \pm 1.0						

^aCertified (and uncertified) values for SRM 613, National Bureau of Standards, August 1972.

The concentrations of 17 elements in the NBS SRM 613 glass were determined; the results obtained from triplicate samples are shown in Table 2. Satisfactory reproducibilities were obtained for all these elements except titanium, and the average relative standard deviation was within $\pm 2.7\%$. The poor reproducibility for titanium was due to the strong interference from the matrix as outlined above.

Although the data for the SRM 613 glass from NBS were not complete, comparison of the results obtained for Ce, Ni, Rb, and Sr with the certified values and some literature values [13] given in Table 2, indicates good agreement within 1.4–3.4%. In addition to these 17 elements, the peaks of the nuclides produced from Mo, Tl, Tm and U were also observed clearly, but were not utilized in this study.

From these results, instrumental photon activation analysis appears to be very useful for multi-element determinations in glass. This method has distinct advantages over neutron activation analysis in forensic applications, because key elements such as Rb, Sr and Zr for characterizing glass samples [13] can be determined more easily.

The authors express their gratitude to Professors N. Suzuki and T. Kato for their continuous encouragement, and to members of the LINAC machine and radioisotope groups at the Institute of Nuclear Science, Tohoku University, for their cooperation with the irradiations.

REFERENCES

- 1 R. F. Coleman and G. C. Goode, *J. Radioanal. Chem.*, 15 (1973) 367.
- 2 T. Kato, N. Sato and N. Suzuki, *Anal. Chim. Acta*, 81 (1976) 337.
- 3 T. Kato, K. Masumoto, N. Sato and N. Suzuki, *J. Radioanal. Chem.*, 32 (1976) 51.

- 4 T. Kato, I. Morita and N. Sato, *J. Radioanal. Chem.*, 18 (1973) 97.
- 5 A. Chattopadhyay and R. E. Jervis, *Anal. Chem.*, 46 (1974) 1630.
- 6 T. Kato, N. Sato and N. Suzuki, *Talanta*, 23 (1976) 517.
- 7 N. K. Aras, W. H. Zoller, G. E. Gordon and G. J. Lutz, *Anal. Chem.*, 45 (1973) 1481.
- 8 G. J. Lutz, *Anal. Chem.*, 41 (1969) 424.
- 9 V. Galatanu and M. Grecescu, *J. Radioanal. Chem.*, 10 (1972) 315.
- 10 T. Kato, *Res. Rep. Lab. Nucl. Sci. Tohoku Univ.*, 5 (1972) 315; *J. Radioanal. Chem.*, 16 (1973) 307.
- 11 M. E. Toms, *J. Radioanal. Chem.*, 20 (1974) 177.
- 12 C. M. Lederer, J. M. Hollander and I. Perlman, *Table of Isotopes*, 6th edn., J. Wiley, New York, 1967.
- 13 M. A. Haney, *J. Forensic Sci.*, 22 (1977) 534.

REDUCTION OF SPECTRAL INTERFERENCES IN FLAME EMISSION SPECTROMETRY BY SELECTIVE SPECTRAL-LINE MODULATION

S. W. DOWNEY, J. G. SHABUSHNIG and G. M. HIEFTJE*

Department of Chemistry, Indiana University, Bloomington, Indiana 47405 (U.S.A.)

(Received 11th July 1980)

SUMMARY

Spectral interferences in flame emission spectrometry can be significantly reduced through the use of selective spectral-line modulation (s.l.m.). In this method, a mirrored, rotating chopper is used to direct the emission from a sample flame alternately through and around a second (modulating) flame; selective modulation is achieved when the modulating flame contains absorbing atoms identical to emitting analyte atoms in the sample flame. The effects of optical configuration and modulating conditions on working curve slope, linearity, and signal-to-noise ratio are examined. Also, the ability of s.l.m. to minimize broad-band and narrow-line spectral interferences is demonstrated. In particular, it has been shown that the interference of the 554-nm CaOH band on barium determinations can be largely overcome. Also, interference of several palladium lines on nickel in the 350-nm region can be reduced. Finally, it is shown how the interference of flame background itself can be restricted in s.l.m. procedures.

Atomic emission spectrometry (a.e.s.) is becoming the technique of choice for rapid simultaneous or sequential multi-element determinations. Unfortunately, a.e.s. is often plagued with spectral interference problems, unless scanning high-resolution spectral dispersing systems are employed. These interferences can take several forms and arise from various sources. Overlapping spectral lines from the source background or matrix concomitants and scattered light are commonly encountered spectral interferences. Even in recent a.e.s. instruments [1–3], spectral interferences can be troublesome, subtle, and difficult to overcome [4].

The most straightforward approach to minimize spectral interferences is to use a high-resolution spectrometer. Unfortunately, this solution is costly and often accompanied by a loss in optical speed, and it is sometimes difficult to identify and lock onto the correct spectral line, especially if the source or matrix produces complex background spectra. Selective modulation can serve to minimize spectral interferences and to avoid many of the limitations of the high-resolution approach. In this scheme, analyte radiation alone is modulated while all other spectral components remain unaffected. Synchronized detection of the modulated signal then rejects interfering radiation.

Some forms of selective modulation have included a periodically interrupted sample introduction system [5, 6], wavelength modulation, and

derivative spectrometry [7]. Unfortunately, these forms of modulation discriminate only against source background and broad-band spectral interference. Alkemade and Milatz [8] used a flame as a selective wavelength absorber, and other types of atom reservoirs have also been used to modulate selected spectral lines that can then be detected preferentially in the presence of spectral interferences [9, 10]. Selective spectral-line modulation (s.l.m.) has been studied further and used in this laboratory to increase the slope and linearity of working curves in continuum-source atomic absorption flame spectrometry [11, 12]. Modulation of the analytical absorption line provided added effective resolution for the 0.35-m monochromator used, thus increasing the working curve slope and linearity.

In the present work, an a.e.s.—s.l.m. system similar to that of Alkemade and Milatz [8] was constructed (cf. Fig. 1) and tested with updated flames and modern detection equipment. Two flames were used, one acting as the emission source, the other serving as the selective spectral line modulator. Radiation emitted from the source flame is alternately directed through and around the modulating flame by a dual-beam optical system; a net difference in intensities between the two beams is then caused by the selective absorption that occurs in the modulating flame. Signals derived from radiation in this selected spectral region are therefore alternating current (a.c.) in nature and can be detected in the presence of the direct current (d.c.) radiation by frequency-selective detection.

The analytical working graphs produced by the a.e.s.—s.l.m. process were found to be linear, and the sensitivity and signal-to-noise ratio are dependent on modulating solution concentration. At least three types of spectral interferences can be reduced by using s.l.m.; broad-band and narrow-line con-

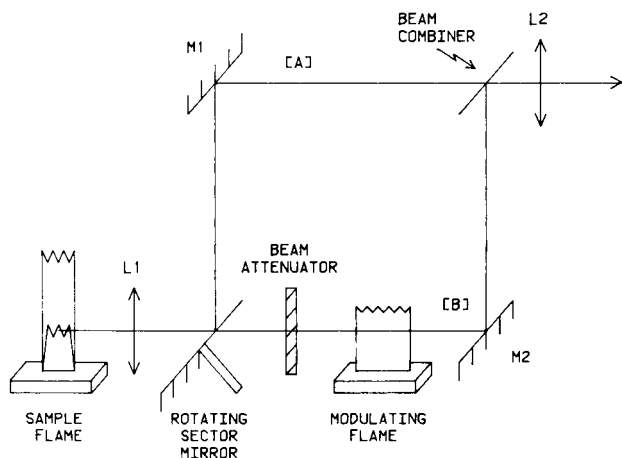


Fig. 1. Schematic diagram of the double-beam a.e.s.—s.l.m. system. The rotating sector mirror also produces the reference signal for the lock-in amplifier. See Table 1 for details of components. Radiation leaving this system falls on the entrance slit of the monochromator. The overall length of the system is about 40 cm. The distance between beam paths is about 10 cm. See Experimental section for further details.

comitants and source background. The interferences studied in this work are the CaOH band overlap with the 553-nm line of barium, closely spaced palladium and nickel lines near 350 nm, and the nitrous oxide/acetylene flame background.

EXPERIMENTAL

A schematic diagram of the a.e.s.—s.l.m. system used is shown in Fig. 1. Details concerning the individual components are summarized in Table 1. In the system, the sample flame is imaged by L_1 into the center of the modulating flame, just above the primary combustion region, and again by L_2 at the monochromator entrance slit. The rotating sector mirror and beam combiner produce the double-beam operation necessary for s.l.m. use. A variable beam attenuator is used to compensate differences in optical throughput between the two beam paths (path B was brighter throughout this work). A basic improvement in design of the system over that described earlier [12] is the position of the chopper. Here, any emission from the modulating flame will be at a constant level and suppressed by a.c. detection.

The two beams in the a.e.s.—s.l.m. system must be completely balanced to avoid false s.l.m. signals. Imbalances can arise from either path throughput differences or spatial inhomogeneities in either beam; the first source of imbalance can be corrected using the variable beam attenuator, while the second can only be overcome through careful optical design.

The importance of this second, more insidious, problem was especially evident when a non-homogeneous (Swiss cheese) beam combiner was used. In such an optical element, the substrate is coated with a 50% matrix of small reflective dots, such that half the incident light is reflected. The resulting discrete regions of reflective and transparent surface are highly sensitive to beam wander and inhomogeneity and produced drastically changing relative beam intensities as wavelength was scanned. Of course, for fixed wavelength work, any kind of beam recombination optics can be used, but for multi-wavelength applications, a homogeneous combiner is superior. Even with spatially homogeneous optics, small differences in spectral transmission and reflection can create artificial beam imbalances over broad wavelength ranges, and must be overcome through proper calibration.

Optimal modulating solution concentrations were determined from detected signal-to-noise ratios (S/N) at various sample solution concentrations. The S/N was determined in the manner suggested by St. John et al. [13].

Three spectral interferences were studied using the a.e.s.—s.l.m. system. The barium resonance line at 553.5 nm suffers interference from the band emission of CaOH with a maximum at 554.0 nm. Wavelength modulation has been shown to be effective in reducing this interference [7] and enables a useful comparison between the methods to be made. A palladium—nickel mixture will produce two sets of lines that fall within the spectral bandpass of a medium-resolution monochromator. The Pd 351.69-nm and the Ni 351.50-nm lines will overlap, as will the Pd 346.077-nm and Ni 346.165-nm

TABLE 1

System components and operating conditions for a.e.s.—s.l.m.

<i>Burner and flames</i>	
Sample burner	5 cm N_2O/C_2H_2 slot burner with counterflow jet spray nebulizer (Instrumentation Laboratory, Inc., Wilmington, MA)
Modulating burner	10.5 cm air/ C_2H_2 slot burner with impinging bead nebulizer (Varian Techtron, Palo Alto, CA)
Gas flow rates	Sample flame: 3 l N_2O min^{-1} , 2 l C_2H_2 min^{-1} Modulating flame: 15 l air min^{-1} , 3 l C_2H_2 min^{-1} .
Gas handling	Purified flame gases (Matheson Co., Joliet, IL) controlled by needle valves (Series M, Nupro Co., Cleveland, OH) monitored by calibrated rotameters (No. VFB, Dwyer Instruments, Inc., Michigan City, IN)
Solution uptake	Sample solution: 4 ml min^{-1} Modulating solution: 3 ml min^{-1}
Observation height	Approximately 1 cm above burner tops
<i>Optics</i>	
Monochromator	EU 700 GCA/McPherson Instrument (Acton, MA), 0.35-m Czerny—Turner mount, slit width dependent upon experiment (50, 100, 300 μm)
Chopper	Half-and-half configuration, front-surface aluminum, 11.5-cm diameter, rotated at 30 Hz by synchronous motor
Plane mirrors	Front-surface aluminum; M_1 diameter 2.5 cm, M_2 diameter 5.1 cm (Melles Griot, Irvine, CA)
Lenses	L_1 diameter 4.5 cm, F.L. 30 cm; L_2 diameter 2.5 cm, F.L. 7.5 cm; lens material Suprasil I (Melles Griot, Irvine, CA)
Beam attenuator	NRC (Fountain Valley, CA) 50600 AV.1 variable circular attenuator, optical density 0.5–1.0 \pm 0.5 at 633 nm, with evaporated aluminum, diameter 5 in.
Beam combiner	Diameter 2.5 cm (No. 6–1325u, Special Optics, Little Falls, NJ) approximately 30% T , 30% R for 200–400 nm
<i>Detection</i>	
Photomultiplier	RCA 1P28, operated at 500–900 V, supplied by a Fluke model 415B high-voltage power supply
Reference detector	2N577 photodarlington transistor wired in a common-collector configuration, triggered by chopped light from a 12-V tungsten flashlight bulb
Signal processing	Photocurrent converted to a proportional voltage by a model 215 operational amplifier and sent to a model 220 lock-in amplifier via a model 210A frequency-selective amplifier. Reference signal sent to the model 220 amplifier via another model 210A amplifier. All of the above powered by model 200 N1M BIN supply (Princeton Applied Research Corp., Princeton, NY). Typical time constant, 1–3 s
Recorder	Heath/Schlumberger strip chart type, operated at 10 V full scale

lines. Finally, the N_2O/C_2H_2 flame background can also be a major spectral interference, especially around 380 nm where the CN bands are located.

Conventional emission spectra of these three interference systems were obtained with the lock-in detection system by blocking entirely the path

through the modulating flame. This approach provides the desired detection mode and enables the same optical system to be used, so that an appropriate comparison can be made.

All stock solutions were prepared as described by Dean and Rains [14] using reagent grade metals, salts, and acids. For the Ca/Ba interference study, all solutions contained potassium (1 mg ml^{-1}) as an ionization suppressant.

RESULTS AND DISCUSSION

Effect of modulating solution concentration

Figure 2 reveals the influence of modulating solution concentration on working curve slope and linearity. Understandably, all curves show good linearity over the concentration range studied and the slopes of the curves are greater at higher modulating solution concentrations.

The practical upper limit to modulating solution concentration will vary from element to element and will be dictated by the amount of noise generated by emission from the modulating element and by concentration-related line broadening effects. In continuum-source atomic absorption, such line broadening limits s.l.m. sensitivity and linearity [11, 12]. Here, however, the analyte emission line is about the same width as the modulating absorption line, so modulation of background continuum is not a severe performance-reducing problem.

Although not evident over the concentration ranges shown in Fig. 2, a.e.s.-s.l.m. working curves exhibit self-absorption-caused non-linearity at high sample concentrations, just as do other flame emission methods.

A far more important criterion than linearity for selecting optimal modulating conditions is the signal-to-noise ratio. Although the present s.l.m. system does not respond directly to emission from the modulating flame, the shot noise such emission generates can still be a problem and, for some

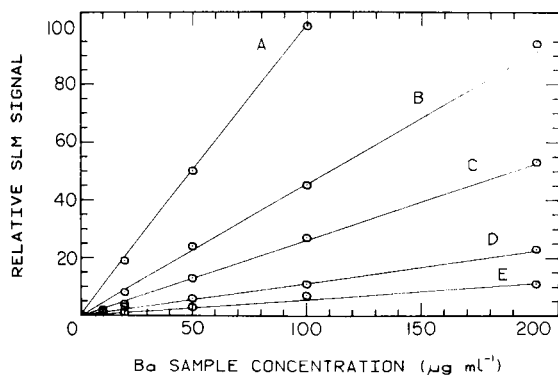


Fig. 2. The effect of modulating solution concentration on barium (553.5 nm) analytical curves. Concentration of barium ($\mu\text{g ml}^{-1}$) in modulating solution: (A) 10,000; (B) 1000; (C) 500; (D) 200; (E) 100. Monochromator spectral slit width, 0.6 nm.

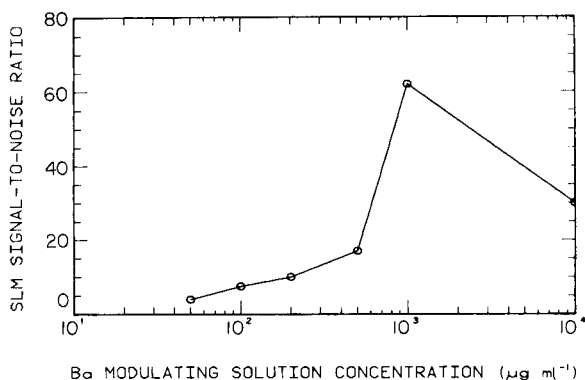


Fig. 3. Determination of optimal modulating concentrations for barium (553.5 nm). The sample solution contains $50 \mu\text{g Ba ml}^{-1}$. Spectral slit width, 0.6 nm.

elements, can dominate at high modulating solution concentrations. Moreover, flicker noise from the modulating flame will further degrade S/N for any element.

In Fig. 3, the decrease in S/N at high modulating solution concentrations is due to both a substantial noise increase and small signal increase. Obviously, compromises must be made to achieve optimal modulating conditions and optimal conditions will vary. Understandably, strongly emitting elements will have lower optimal modulating concentrations while weaker emitters can have higher modulating concentrations.

A further complication of the use of high-modulation solution concentrations is salt buildup in the modulating nebulizer and burner.

Other noise sources

Noise generated by the chopper is especially troublesome, for the chopper defines the modulating frequency [12]. Any roughness or other inhomogeneity present over a small portion of the mirrored surface of the chopper can add a significant amount of noise to the s.l.m. signal. The rotation of the heavy chopper can upset the system through mechanical vibration and the generation of air currents which cause the flames to flutter at the chopper frequency.

The chopper frequency (30 Hz) increased the system noise in the present device. For example, the mercury 546.0-nm line from room illumination was found to produce a false signal with just the detection electronics in operation. Later work with a modulation frequency of 13.7 Hz alleviated this problem.

Flicker noise sources are minimized in this s.l.m. system but are still present. The position of the modulating flame prevents the modulation of any background flicker noise originating there. However, any flicker of the absorption analyte line is multiplicative and would appear as a detected fluctuation in the selective attenuation. Conveniently, source-flame-based

flicker noise is modulated only over the bandwidth of the modulating atoms and not over the entire spectral bandpass of the spectrometer, thereby reducing its effect. This situation is in contrast to previous s.l.m. work [12] where the chopper position produced modulation of the emission from the modulating flame.

Reduction of spectral interferences

Figure 4 (curve A) shows a portion of the conventional emission spectrum of a solution containing $10 \mu\text{g Ca ml}^{-1}$ and $20 \mu\text{g Ba ml}^{-1}$; curve B shows the barium-selective a.e.s.—s.l.m. scan of the same sample. Clearly, the s.l.m. procedure has essentially overcome interference from the CaOH band. Significantly, in the s.l.m. technique, the resolution is not determined by the monochromator, so high optical throughput need not be sacrificed to obtain high effective resolution.

The results seen in Fig. 4 compare favorably with those produced by wavelength modulation [7]. Both techniques are able to reject unwanted contributions to the analytical signal from broad background sources. In s.l.m., however, a small portion of the background is modulated and detected, specifically that portion of background within the modulator bandpass. Here, the bandpass is approximately 0.005 nm , resulting in a small but finite background contribution.

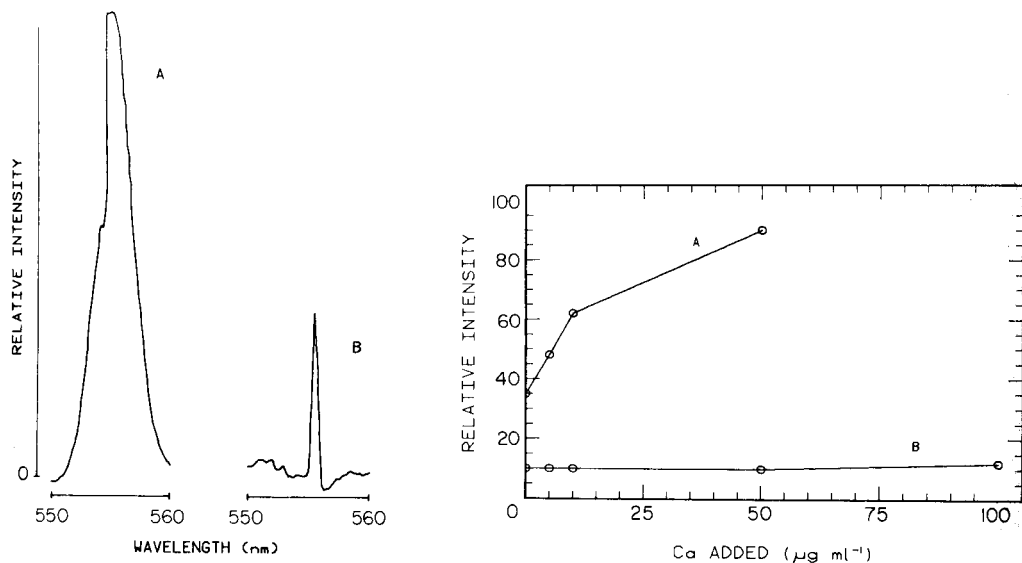


Fig. 4. Reduction of CaOH spectral interference on barium resonance line (553.5 nm). (A) Emission scan of $10 \mu\text{g Ca ml}^{-1}$ and $20 \mu\text{g Ba ml}^{-1}$; (B) s.l.m. scan of the same sample, with a $1000 \mu\text{g Ba ml}^{-1}$ modulating solution.

Fig. 5. The effect of added calcium on the s.l.m. detection of the barium resonance line (553.5 nm). Barium concentration is a constant $10 \mu\text{g ml}^{-1}$. (A) Without s.l.m.; (B) with s.l.m., using $1000 \mu\text{g Ba ml}^{-1}$ modulating solution. See text for details.

The ability of s.l.m. to reject increasing amounts of interfering radiation is illustrated by Fig. 5. The s.l.m. signal at 553.5 nm from a fixed barium concentration ($10 \mu\text{g ml}^{-1}$) is shown to be nearly immune to large amounts of interfering radiation. The practical limit on the amount of excess radiation that can be tolerated by s.l.m. is governed by both the residual background modulation discussed above and by the shot noise that the background generates. The first of these limitations is manifested in Fig. 5 (B) as the slight upward curvature of the plot. The second limitation is similar to that which restricts modulating solution concentrations (cf. Fig. 3).

Also evident in Fig. 5 is a difference in intensity between the a.e.s. and a.e.s.—s.l.m. signals of a $10 \mu\text{g Ba ml}^{-1}$ solution alone. This difference arises because the s.l.m. method does not result in total modulation of the analyte line; that would require an infinite atom concentration in the modulating flame. As a consequence of this reduced signal and the higher noise level in s.l.m. discussed earlier, the s.l.m. approach is somewhat less sensitive than conventional emission measurements.

As a further illustration of the ability of s.l.m. to overcome spectral interferences, the Pd 351.69-nm and Ni 351.50-nm lines are considered. As shown in the spectral scan of Fig. 6B, these lines appear as an unresolved doublet in a conventional a.e.s. measurement using the moderate-resolution monochromator employed here. In contrast, a nickel-selective s.l.m. scan (Fig. 6A) results in a significant reduction of all palladium features. Specifically, the Pd 348.1- and 351.69-nm lines have been greatly reduced and the nickel lines at 351.50 and 346.16 nm are better resolved. Significantly, the nickel features of Fig. 6 cannot be reduced by using palladium as the modulating solution. All of the palladium lines that appear in Fig. 6 are the more energetic nonresonance lines whose lower levels are not sufficiently populated in the air/acetylene modulating flame used here to produce significant selective modulation. With palladium alone in the modulating solution, the spectral region of Fig. 6 appears to be featureless.

In the reduction of line interferences (cf. Fig. 6), s.l.m. should prove superior to wavelength modulation. In the latter method, the resolution of the a.e.s. system is still determined by the monochromator whereas in s.l.m. the effective resolution is that of an atomic absorption linewidth.

Figure 7 illustrates the ability of s.l.m. to overcome spectral interference from source background. Curve A shows a conventional scan of the $\text{N}_2\text{O}/\text{C}_2\text{H}_2$ flame background between 320 and 490 nm. The intense CN band at 390 nm is the major feature. The CN band is greatly reduced in the a.e.s.—s.l.m. spectrum (curve B). Of course, not all background features will be removed by s.l.m. The two flames used here (air/ C_2H_2 and $\text{N}_2\text{O}/\text{C}_2\text{H}_2$) have some species in common, e.g. OH, and these will experience some modulation. In the spectral region shown in Fig. 7, however, it is seen that these common species have little effect.

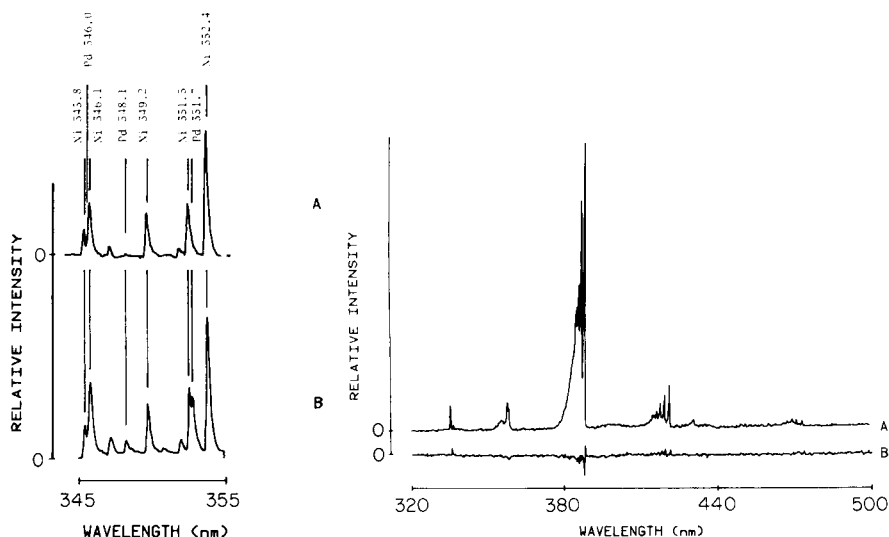


Fig. 6. Reduction of palladium line interference on various nickel lines. Pd concentration, 250 $\mu\text{g ml}^{-1}$; Ni concentration, 200 $\mu\text{g ml}^{-1}$. (A) S.l.m. scan using 1000 $\mu\text{g Ni ml}^{-1}$ modulating solution; (B) conventional emission scan. Monochromator spectral slit width, 0.1 nm.

Fig. 7. Reduction of flame background by s.l.m. (A) Conventional emission scan of $\text{N}_2\text{O}/\text{C}_2\text{H}_2$ flame background; (B) s.l.m. scan of the same flame with only solvent sprayed into the modulating flame.

CONCLUSION

It is important in s.l.m. that the excitation atom reservoir is at a higher temperature than the modulating atom reservoir. If the temperatures were equal, no net absorption or emission would occur, and no s.l.m. signal would be seen. This factor limits the choice of modulating flame or other atom reservoirs to those which are relatively cool and therefore exhibit poor atomization efficiency for some elements. This situation might restrict s.l.m. to the determination of only selected elements or combinations of elements. Moreover, because ions are not in high concentrations in most flames, the s.l.m. measurement of ion lines will be difficult or will require alternative selective absorption cells. This factor might preclude the useful application of s.l.m. to plasma emission.

The s.l.m. concept should also be applicable to nondispersive detection. Although such an application would suffer an increase in noise level, spectral interference should be minimized since effective isolation of the analytical line occurs prior to detection.

Work is currently underway in our laboratories to apply s.l.m. to other analyte and matrix combinations and to other sources (e.g. i.c.p.) where source background, overlapping lines, stray light, and other spectral interferences limit analytical attractiveness.

This work was supported in part by the Office of Naval Research and by the National Science Foundation through grant CHE 79-18073.

REFERENCES

- 1 G. W. Johnson, H. E. Taylor and R. K. Skogerboe, *Appl. Spectrosc.*, 33 (1979) 451.
- 2 G. F. Larson, V. A. Fassel, R. K. Winge and R. N. Kniseley, *Appl. Spectrosc.*, 30 (1976) 384.
- 3 R. K. Winge, V. J. Peterson and V. A. Fassel, *Appl. Spectrosc.*, 33 (1979) 206.
- 4 P. W. J. M. Boumans, *Spectrochim. Acta, Part B*, 31 (1976) 147.
- 5 V. Bojovic and A. Antic-Javanovic, *Spectrochim. Acta, Part B*, 27 (1972) 385.
- 6 V. G. Mossotti, F. N. Abercrombie and J. A. Eakin, *Appl. Spectrosc.*, 25 (1971) 331.
- 7 W. Snelleman, T. C. Rains, D. W. Yee, H. D. Cook and O. Menis, *Anal. Chem.*, 42 (1970) 394.
- 8 C. T. J. Alkemade and J. M. W. Milatz, *Appl. Sci. Res.*, 4B (1955) 289.
- 9 J. A. Bowman, J. V. Sullivan and A. Walsh, *Spectrochim. Acta, Part B*, 22 (1966) 205.
- 10 O. I. Matveev, N. A. Tolstikova and E. P. Cheremukhin, *Zavod. Lab.*, 45 (1979) 724.
- 11 R. L. Cochran and G. M. Hieftje, *Anal. Chem.*, 49 (1977) 98.
- 12 R. L. Cochran and G. M. Hieftje, *Anal. Chem.*, 50 (1978) 791.
- 13 P. A. St. John, W. J. McCarthy and J. D. Winefordner, *Anal. Chem.*, 39 (1969) 1495.
- 14 J. A. Dean and T. C. Rains, *Flame Emission and Atomic Absorption Spectrometry*, Vol. II, M. Dekker, New York, 1969, Ch. 13.

OPTIMISATION OF SULPHUR EMISSION IN MOLECULAR EMISSION CAVITY ANALYSIS

Effects of Variation in Cavity Position and Phosphate Addition

T. J. CARDWELL, P. J. MARRIOTT

Department of Chemistry, La Trobe University, Bundoora, Victoria, 3083 (Australia)

D. J. KNOWLES*

Department of Chemistry, Preston Institute of Technology, Plenty Road, Bundoora, Victoria, 3083 (Australia)

(Received 30th July 1980)

SUMMARY

Temperature profiles are measured for hydrogen flames used for m.e.c.a. and discussed in terms of the emission intensities produced by some sulphur compounds in different regions of the flame. The effect of addition of phosphoric acid or phosphate buffers on sulphates and ammonium thiocyanate is re-examined and the enhancing effect of "residual phosphate" discussed.

Molecular emission cavity analysis (m.e.c.a.) has been applied to the determination of a wide range of elements, with the most extensive investigations being carried out on inorganic sulphur-containing species [1–5]. The need to optimise the emission response is fundamental to the sensitivity of the technique. For sulphur compounds, factors which have received greatest attention during optimisation include variation of the flame gas composition, the nature of the cavity material and holder, and the enhancement of S_2 emission or elimination of cationic interferences by addition of phosphoric acid or phosphate buffers to the sample.

The importance of the position of the cavity in the flame has been alluded to in several reports; Belcher et al. [1] measured the variation in S_2 emission intensity from iron(II) sulphate with vertical and horizontal displacement of the cavity in a pre-mixed air–hydrogen flame. Flame gas composition affects the temperatures in various regions of the flame, which in turn may have a marked effect on the emission responses from different sulphur compounds because of differences in their volatilities and/or thermal decomposition. Some correlations between flame temperature measurements and S_2 emission responses from selected sulphur compounds are reported in this paper.

Addition of phosphoric acid to samples of sulphur-containing anions has been shown to eliminate the interference from metal ions and produce an enhancement of S_2 emission [2]; optimal response was obtained with 0.07 M

phosphoric acid for sulphate samples, and solutions 0.1 M in phosphoric acid have generally been used in subsequent reports for other sulphur anions [3–5]. In contrast, a later report recommends that the optimal concentrations of a phosphate buffer for enhancement of emission response from a variety of sulphur species is around 10^{-2} M [4]. This variation in the concentrations of “phosphate” from different sources appeared to be inconsistent and worthy of further investigation. In addition, during the course of this work, other unusual phosphate effects were encountered and are reported below.

EXPERIMENTAL

Equipment

An Anacon Model 22 m.e.c.a. Analyser coupled to a Rikadenki recorder were used throughout. The analyser was modified so that the burner, normally in a fixed position, could be moved horizontally to a reproducible position under the cavity after the latter had been rotated into line with the optical system. The cavity was pitched 8° below the horizontal and S_2 emission was monitored at 384 nm using a slit width of 0.5 mm (bandwidth 8.5 nm). A silica-lined stainless steel cavity was used, unless otherwise specified. Sample solutions were delivered to the cavity using a SGE 5- μ l syringe. Peak areas were measured by triangulation or electronic integration.

Cavity and flame temperatures were measured by using a chromel-alumel thermocouple with an ice-bath reference. To obtain cavity temperatures, a side inlet hole was drilled in the stainless steel cavity so that the thermocouple could be positioned at the base of the silica insert. The flame temperatures measured may not be strictly accurate because of possible catalytic effects of the probe in the flame, but they are adequate for comparative purposes.

Vertical displacement studies were performed by maintaining the cavity in a fixed position directly in line with the detector and the burner assembly was adjusted vertically.

Solutions

Analytical reagent-grade chemicals were used in all cases. Phosphate buffer stock solutions, all 0.1 M total phosphate, had the compositions 0.05 M H_3PO_4 /0.05 M $(NH_4)H_2PO_4$, 0.05 M $(NH_4)H_2PO_4$ /0.05 M $(NH_4)_2HPO_4$ and 0.05 M $(NH_4)_2HPO_4$ /0.05 M $(NH_4)_3PO_4$; 20 cm³ of buffer was added to 80 cm³ of sample solution and the resulting solutions had pH values of 2.9, 7.2 and 8.9, respectively.

Ammonium diethyldithiocarbamate was prepared by passing a solution of sodium diethyldithiocarbamate in aqueous ethanol through a cation-exchange resin in the NH_4^+ form.

RESULTS AND DISCUSSION

Cavity heating rate

Although it is generally agreed that the rate of heating of a m.e.c.a. cavity and the maximum temperature achieved depend on factors such as the position of the cavity in the flame and flame composition, only one report presents a heating rate curve and this is a very general one [1]. Heating rate curves for a stainless steel cavity were measured in the present work in an attempt to highlight the effects of both the horizontal and vertical position of the cavity in the flame and variation of gas flows.

Typical heating rate curves are presented in Fig. 1. Comparison of curves II, III and V shows clearly that the horizontal position of the cavity in the flame has a marked effect on the heating rate; in particular, a cavity placed in the edge of the flame farther from the spectrometer slit shows slower heating and a lower maximum temperature than positions close to the centre of the flame. One would normally expect to observe faster heating rates and higher temperatures in the edge of the flame because of oxygen diffusion, but greater heat loss through thermal conductivity may contribute to the experimental observations in this region of the flame as the cavity and holder are less exposed to the flame than in the centre of the flame. In contrast, the vertical position of the cavity centre in the flame has little effect between 17 and 40 mm above the burner head. Decreasing the hydrogen flow or increasing the nitrogen flow at a fixed position in the flame results in slower heating rates as expected for cooler flames (compare curves II, IV and VI). Introduction of air into the flame produces a hotter flame as expected and faster heating is observed (curve I).

Temperature profiles within the flame

S_2 emission is best developed in low-temperature flames, but such temperatures may be insufficient to decompose and volatilize every type of sulphur compound. Therefore, it seemed of interest to measure the temperatures in various positions of the flame for the type of burner used in the Anacon

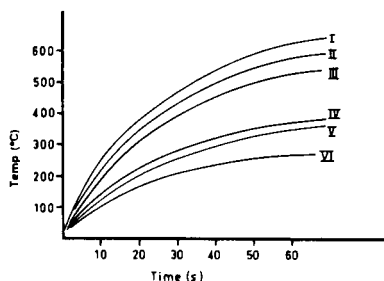


Fig. 1. Heating rate curves for a silica-lined cavity in various positions of flames of various flame compositions (all in $l\ min^{-1}$) (I) 4.0 H_2 , 4.0 N_2 , 2.5 air, flame centre; (II) 4.0 H_2 , 4.0 N_2 , no air, flame centre; (III) as II, 3 mm off-centre; (IV) 2.0 H_2 , 4.0 N_2 , no air, flame centre; (V) as II, flame edge; (VI) 2.0 H_2 , 6.0 N_2 , no air, flame centre.

Analysed so that the data might be correlated with emission responses for various cavity positions. The burner head on the above instrument was circular with a hexagonal pattern of six holes and an additional hole in the centre.

As shown in Fig. 2, for an entrained air flame and a pre-mixed flame, the temperature of the flame centre increases with distance from the burner head. Both curves reach a plateau, which the pre-mixed flame achieves close to the burner head because of greater completion of the combustion process in this region of the flame.

Horizontal variation in temperatures (Fig. 3) shows that temperatures at the centre of the flame are lower than those in the outer regions, consistent with the general observations for similar flames where the central region is surrounded by a hotter reaction zone. The central region is shielded from the effects of oxygen diffusion into the flame because the entrained air is completely consumed in the flame front and the oxygen content decreases rapidly inside the flame front [6].

Emission intensities as a function of cavity position in the flame

Variations in S_2 m.e.c.a. emission intensity and time to maximal emission (t_m) with both vertical and horizontal displacement for an iron(II) sulphate sample have previously been described [1]. Because of the considerable variation in temperatures in different regions of the flame outlined above and the differences in thermal stability of compounds in the flame, the optimised cavity position in the flame leading to the most efficient breakdown of the sample and formation of the emitting species may vary from one compound to another. Therefore, compounds other than iron sulphate were investigated as described below.

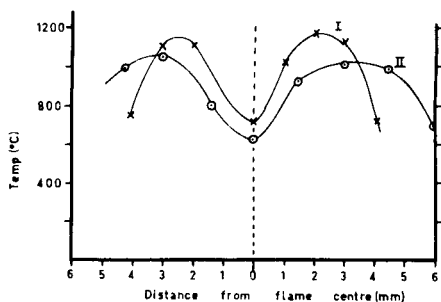
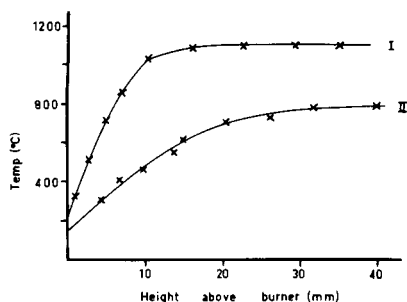


Fig. 2. Variation in flame temperature with height above burner, measured at the flame centre. (I) 4.0 l H_2 min^{-1} , 2.0 l N_2 min^{-1} , 2.0 l air min^{-1} ; (II) 4.0 l H_2 min^{-1} , 4.0 l N_2 min^{-1} , no air.

Fig. 3. Horizontal variation of flame temperature. (I) 4.0 l H_2 min^{-1} , 2.0 l N_2 min^{-1} , 2.0 l air min^{-1} , 5 mm above burner; (II) 4.0 l H_2 min^{-1} , 4.0 l N_2 min^{-1} , no air, height 15 mm above burner.

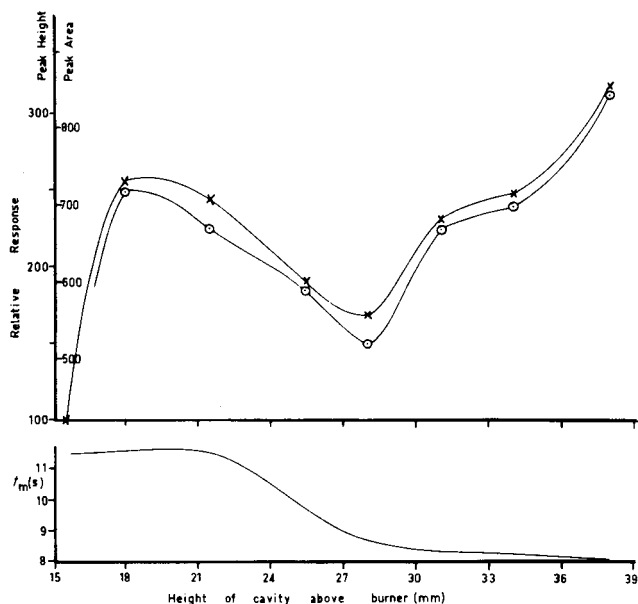


Fig. 4. Effect of vertical displacement of cavity at flame centre on emission response and time to maximal emission (t_m) for $(\text{NH}_4)_2\text{SO}_4$ ($100 \mu\text{g S cm}^{-3}$). Flame composition, $4.0 \text{ l H}_2 \text{ min}^{-1}$, $4.0 \text{ l N}_2 \text{ min}^{-1}$, no air. (x) Peak height; (o) peak area data.

Ammonium sulphate. Figure 4 shows the effect of height of cavity above the burner head on S_2 emission intensity and t_m for ammonium sulphate; the cavity aperture must be positioned precisely in the centre of the flame as it has been observed that emission intensity and t_m measurements lack reproducibility when the cavity is 2–3 mm off-centre. At cavity heights less than 28 mm, the relative emission intensity curves for peak height and integrated peak area are similar to the results reported previously for iron(II) sulphate [1]; there is a sudden decrease in emission intensity close to the burner (<18 mm) and a gradual, almost linear, decrease in intensity with increasing cavity height over the region 18–28 mm. At cavity heights greater than 28 mm, a region not investigated in the previous work on iron sulphate, there is a gradual increase in emission intensity. The t_m values are also dependent on distance of the cavity from the burner head; at heights less than 26 mm, t_m approaches 11 s and for heights greater than 26 mm, t_m approaches 8 s. Comparing these results with the temperature profile in Fig. 2 (curve I), it is clear that cavity heights below 26 mm correspond to cooler zones in the flame resulting in longer t_m values whereas heights above 26 mm represent hotter regions of the flame, decreasing t_m to 8 s, a value consistent with earlier observations [2].

Figure 5 shows the effect of horizontal displacement of the cavity on emission intensity and t_m values. In the edge of the flame farther from the spectrometer slit, where temperatures are higher than at the centre (Fig. 3),

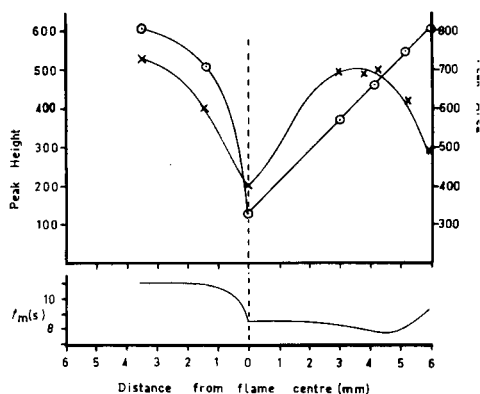


Fig. 5. Effect of horizontal displacement of cavity on emission response and time to maximal emission (t_m) for $(\text{NH}_4)_2\text{SO}_4$ ($100 \mu\text{g S cm}^{-3}$). Flame composition as for Fig. 4. (X) Peak height and (o) peak area data.

the emission intensity is greater (possibly as a result of higher radical concentration) and the t_m value slightly less than that measured at the flame centre. Peak broadening accompanies the shortening of t_m at this edge of the flame. When the cavity is placed through the flame centre to the edge of the flame nearest to the spectrometer slit, there is a marked increase in both emission intensity and t_m . The emission intensities for ammonium sulphate and sulphuric acid show similar trends with horizontal displacement of the cavity in the flame to those of iron(II) sulphate [1]. However, t_m values display marked differences, with the emission from iron sulphate occurring more quickly as the cavity moves further into the flame, and remaining constant beyond the flame centre (cf. Fig. 5).

The observations for both horizontal and vertical positioning of the cavity are in accord with previous work [1] in that hotter flames or regions of the flame tend to enhance emissions from sulphates. What must be remembered is that the regions of maximum intensity may not necessarily be those of greatest precision and care must be taken to ensure that the correct balance is achieved. Moreover, it would appear that the optimum flame position for analysis may vary from instrument to instrument.

Ammonium thiocyanate. Thiocyanates are generally classified as reasonably fast emitters, with t_m values dependent on gas flow-rates and the associated cation [5]. The ammonium salt was selected for the present study in order to avoid the interference usually encountered in the presence of alkali and transition metal ions [2]. Vertical displacement of the cavity gives an emission response curve similar to that observed for ammonium sulphate, but for heights above 32 mm there is a decrease in emission intensity for ammonium thiocyanate. The variation in peak height for ammonium thiocyanate is not as pronounced as it is for the sulphate. This may be illustrated by comparing the peak heights for both samples at the maximum (~ 20 mm) and the minimum (28 mm) on the intensity-height curves; for the sulphate, the minimum

corresponds to about 30% decrease in peak height from the maximum, whereas for the thiocyanate the decrease is only 15%. In addition, t_m values for the latter decrease marginally from 8.5 s to 7.5 s on increasing the height of the cavity above the burner.

Horizontal displacement of the cavity also leads to only minor variations in the emission response and t_m values for ammonium thiocyanate in marked contrast to the sulphate. It is clear that the sulphate is more dependent on flame conditions than ammonium thiocyanate for efficient production of the emitting species, S_2 . The differences in the behaviour of the two compounds may be related to the different reduction steps necessary in each case to produce the emitting species.

Ammonium diethyldithiocarbamate. Preliminary studies with a silica-lined cavity established that the optimum gas flows for ammonium diethyldithiocarbamate are either $H_2 = 3.75$ and $N_2 = 5.0$ l min⁻¹ for an entrained-air flame, or $H_2 = 3.75$, $N_2 = 6.0$ and air 2.5 l min⁻¹ for a pre-mixed flame. Under all conditions, two emission peaks are observed. The first is sharp, almost instantaneous and somewhat similar to that for a simple sulphide [5], whereas the second peak is broader with $t_m = 7.5$ –9.0 s in the entrained-air flame and $t_m = 4.0$ –5.5 s in the hotter pre-mixed flame.

Vertical displacement of the cavity produces emission response curves which are quite different for the two peaks, as shown in Fig. 6. The predominating peak depends on the height of the cavity above the burner head; the second peak predominates only at 18–25 mm with a maximum response being observed around 22 mm above the burner. These observations may be explained by the different environment of each sulphur in the dithiocarbamate anion [7]. One sulphur, weakly bound so that it is readily released, behaves like a simple sulphide, thus acting as a fast emitter. Therefore, one would expect fairly constant emission responses in all regions of the flame. The second sulphur, being more strongly bound, displays behaviour similar to sulphates or thiocyanates and is therefore more dependent on flame conditions.

Horizontal displacement of the cavity suggests that the sulphur atom giving rise to the second peak acts more like a thiocyanate than a sulphate; the emission response and t_m value of the second peak show little variation with changing cavity position. These observations are not unexpected as the removal of a sulphur atom from the dithiocarbamate anion during the thermal breakdown process in the cavity would lead to the formation of thiocyanate-type species [8].

Effect of added phosphoric acid

Orthophosphoric acid has been used most effectively to enhance the S_2 emission response from certain metal salts [2–4]. However, it was of interest to investigate the effect of added phosphoric acid on salts which readily give an S_2 emission in the absence of the acid, in particular sulphur acids themselves and their ammonium salts.

Figure 7 shows the effect of added phosphoric acid on the emission response from ammonium thiocyanate. Previous studies have generally

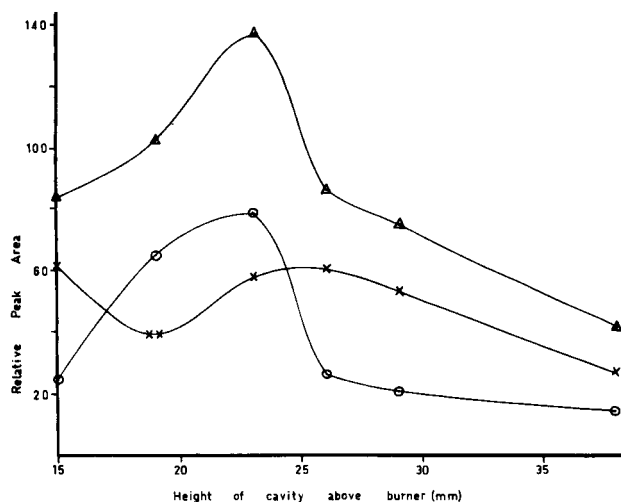


Fig. 6. Effect of vertical displacement of cavity on emission responses from ammonium diethyldithiocarbamate. Flame composition, 3.75 l H_2 min^{-1} , 5.0 l N_2 min^{-1} . (X) First peak area; (O) second peak area; (Δ) total area.

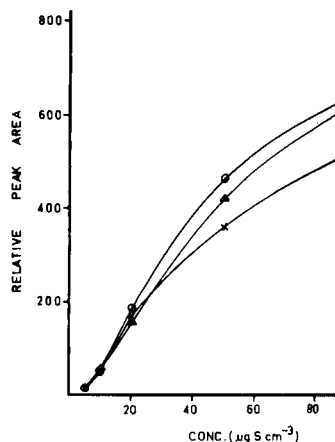


Fig. 7. Effect of addition of phosphoric acid on the emission response from ammonium thiocyanate: (X) no H_3PO_4 added; (O) samples contain $100 \mu\text{g P cm}^{-3}$; (Δ) samples are 0.1 M in H_3PO_4 .

used 0.1 M phosphoric acid (3.1 mg P cm^{-3}) to enhance emissions, but for this salt, this concentration appears to give only a marginal increase in response based upon either peak height or peak area; $100 \mu\text{g cm}^{-3}$ of added phosphorus gives a greater but still insignificant enhancement. The higher concentration of phosphoric acid (0.1 M) produces a decrease in t_m to 4–5, in agreement with a previous investigation [5], whereas the other solutions in Fig. 7 had t_m values of 8.0–8.5 s. The log–log calibration plot in the presence of $100 \mu\text{g P cm}^{-3}$ has a slope of ca. 2.0, identical to that obtained in the absence of the acid. A similar plot for 0.1 M phosphoric acid displays a departure from linearity at high concentrations of thiocyanate ($>10 \mu\text{g S cm}^{-3}$); the slope varies from <1.7 at high concentrations to about 2.0 at low concentrations. Therefore, there appears to be no overall advantage to be gained by adding phosphoric acid to ammonium thiocyanate samples in m.e.c.a.

For sulphuric acid solutions, there is a clear enhancement of the S_2 emission in the presence of phosphoric acid (Fig. 8), when the emission response is measured by peak area. Greater enhancement is achieved by adding 100 or $500 \mu\text{g P cm}^{-3}$ rather than 0.1 M phosphoric acid. It has been common practice to use peak heights to represent emission responses, but it was found here that sulphuric acid peak heights tend to show little or no enhancement in 0.1 M phosphoric acid. As for ammonium thiocyanate, addition of 0.1 M phosphoric acid to sulphuric acid samples also leads to non-linear log–log calibration plots based on peak areas.

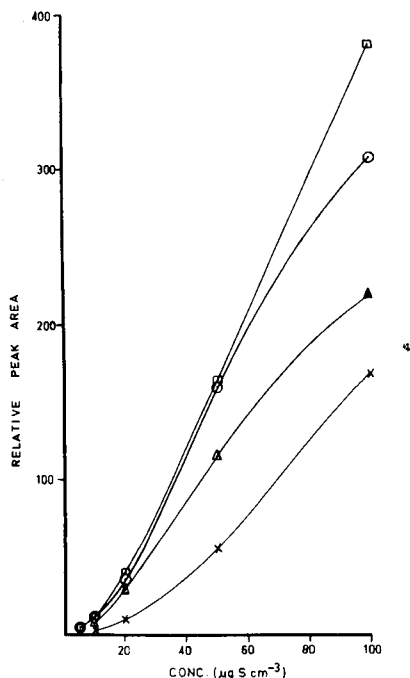


Fig. 8. Effect of addition of phosphoric acid on the emission response from sulphuric acid: (x) no H_3PO_4 added; (o) samples contain $100 \mu\text{g P cm}^{-3}$; (\square) samples contain $500 \mu\text{g P cm}^{-3}$; (Δ) samples contain $3100 \mu\text{g P cm}^{-3}$.

In order to determine if the above effects are general, a wide variety of phosphoric acid concentrations was added to a fixed concentration of sulphuric acid ($50 \mu\text{g S cm}^{-3}$). The results are presented in Fig. 9. Peak heights do not vary greatly as the phosphoric acid concentration is increased up to $500 \mu\text{g P cm}^{-3}$, but there is a marked decrease in $3100 \mu\text{g P cm}^{-3}$, accompanied by an increase in t_m ; peak area data do not exhibit this marked decrease at the higher concentration of phosphoric acid, mainly because of peak broadening. In contrast to these observations, Belcher et al. [2] reported that phosphoric acid concentrations exceeding 0.07 M had no further effect on the emission from sulphates and peaks were recorded at $t_m = 8 \text{ s}$. The results in Fig. 9 clearly point to a possible interference effect upon S_2 emission in 0.1 M phosphoric acid. The increase in t_m indicates either a decrease in the accessibility of the sulphur species or less efficient flame radical interaction with the sample in the presence of this concentration of phosphoric acid.

One significant observation, not previously reported, is the effect of "residual phosphate", probably a pyrophosphate, in the cavity. In successive trials, it was found that the green HPO emission intensifies and persists in the cavity. This emission is attributed to a phosphorus compound which lines the inner surface of the silica cavity; extensive heating of the cavity

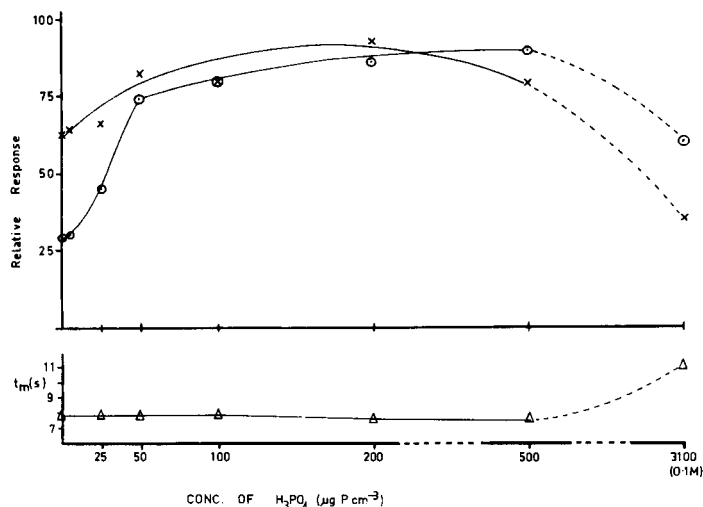


Fig. 9. Effect of H_3PO_4 concentration on emission response and t_m for H_2SO_4 ($50 \mu\text{g S cm}^{-3}$); (x) peak height, (o) peak area data.

with a much hotter pre-mixed flame is required to remove this deposit. If a solution containing only sulphuric acid is added to a cavity which displayed the HPO emission on the previous run, the resultant S_2 emission far exceeds the emission intensity obtained for the same concentration of sulphuric acid with phosphoric acid added. Typical emission-time profiles showing this effect are presented in Fig. 10. Subsequent trials with samples containing only sulphuric acid regenerate the profile normally obtained for that acid in a cavity which has not been used previously for phosphate trials. The above phenomenon supports the suggestion that the phosphate effect could include a contribution from a "pyrophosphate" lining in the cavity which may increase the radical concentration within the cavity by prevention of radical recombination at the walls [9]. Such coatings are commonly used in gas radical kinetic studies where the reaction vessel walls are pretreated with phosphoric acid and then "fired" to give a stable coating.

One serious problem encountered in these investigations with samples containing phosphate was the limited lifetime of the silica cavities. After extended use of a cavity, lack of reproducibility of the S_2 emission response becomes the main feature in the deterioration of cavity performances. Furthermore, after replacement with a new cavity, it was found necessary to "recondition" it with phosphate before obtaining results of the same precision as those obtained with the previous cavity. Therefore, in carrying out routine analysis with samples containing phosphate, serious consideration should be given to ageing and previous usage of the cavity and, if it is necessary to change the cavity during a series of analyses, matching and reconditioning is of utmost importance.

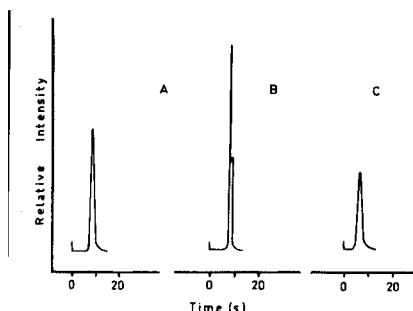


Fig. 10. Emission-time profiles illustrating the "residual phosphate" enhancement of the S_2 emission from H_2SO_4 ($20 \mu g S cm^{-3}$); (A) H_2SO_4 containing H_3PO_4 ; (B) H_2SO_4 in a cavity conditioned with "residual phosphate"; (C) H_2SO_4 alone in a new cavity or a previously used cavity which has been strongly heated.

Effect of addition of phosphate buffers

The effect of phosphate buffers upon S_2 emission may be two-fold; there may be a pH effect as well as the phosphate effects described above. Addition of any of the phosphate buffers described to ammonium sulphate or sulphuric acid samples, gives results that are remarkably similar. In contrast to the addition of phosphoric acid to these samples, phosphate buffers approximately double both peak height and area for concentrations of sulphur up to $100 \mu g cm^{-3}$. The reason for this better enhancement is unknown, because in every other respect the effects of the different source of phosphorus are identical. For example, the "residual phosphate" effect still operates for phosphate buffers, with emission-time profiles being comparable to those shown in Fig. 10. In addition, the log-log calibration plots display the same degree of curvature towards the concentration axis and t_m values for sulphate are around 12 s in all cases. There is no evidence for a pH effect on the S_2 emission from sulphate samples.

The above results indicate that the addition of phosphate, either as phosphoric acid or as a phosphate buffer, to ammonium sulphate or sulphuric acid samples produces two apparently opposing (or competing) effects. On the one hand, there is a marked enhancement resulting from "residual phosphate" in the cavity from a previous trial, even though phosphate has not been added to the sample being analysed. On the other hand, there is an interference effect when phosphate is present in the analyte solution which results in non-linear calibration plots and much less enhancement of S_2 emission compared to that achieved from "residual phosphate". Both these effects suggest that the phosphate-sulphate interaction in the cavity is rather complex and cannot simply be reconciled with the production of the acid form of the sulphate as previously suggested [2].

Conclusions

Emission intensities measured in different regions of the m.e.c.a. flame and correlated with temperature profiles clearly show that hotter regions of the flame give the maximum sensitivities for different sulphur compounds, but the precision in these regions is not as good as that obtained at the flame centre. In addition, there is some variation in behaviour from one compound to another, and it is recommended that the cavity position should be optimised for each compound.

Addition of phosphoric acid in concentrations greater than $500 \mu\text{g P cm}^{-3}$ was found to depress the emission from sulphuric acid samples, whereas "residual phosphate" from a previous run resulted in greater enhancement of S_2 emission than that observed when phosphate was deliberately added to the sample. Furthermore, use of phosphate to enhance emission intensities tended to shorten the lifetime of silica cavities.

P. J. Marriott thanks the Australian Government for the award of a Commonwealth Scholarship.

REFERENCES

- 1 R. Belcher, S. L. Bogdanski and A. Townshend, *Anal. Chim. Acta*, 67 (1973) 1.
- 2 R. Belcher, S. L. Bogdanski, D. J. Knowles and A. Townshend, *Anal. Chim. Acta*, 77 (1975) 53.
- 3 R. Belcher, S. L. Bogdanski, D. J. Knowles and A. Townshend, *Anal. Chim. Acta*, 79 (1975) 292.
- 4 M. Q. Al-Abachi, R. Belcher, S. L. Bogdanski and A. Townshend, *Anal. Chim. Acta*, 86 (1976) 139.
- 5 D. J. Knowles, *Proc. Anal. Div. Chem. Soc.*, 15 (1975) 209.
- 6 A. G. Gaydon and H. G. Wolfhard, *Flames*, 4th edn., Chapman and Hall, London, 1979, Ch. 6.
- 7 D. Coucouvanis, *Prog. Inorg. Chem.*, 11 (1970) 233.
- 8 J. Krupcik, P. A. Leclercq, J. Garaj and J. Masaryk, *J. Chromatogr.*, 171 (1979) 285.
- 9 H. W. Melville and B. G. Gowenlock, *Experimental Methods in Gas Reactions*, 2nd edn., Macmillan, London, 1964.

DETERMINATION OF SOLUBLE/INSOLUBLE TUNGSTEN COMPOUNDS AS DISCRETE ENTITIES IN INDUSTRIAL HYGIENE SAMPLES

R. D. HULL* and J. C. HAARTZ

National Institute for Occupational Safety and Health, Division of Physical Sciences and Engineering, Cincinnati, Ohio 45226 (U.S.A.)

(Received 17th December 1979)

SUMMARY

A method was developed for the determination of soluble and insoluble tungsten compounds collected simultaneously in industrial hygiene air samples. Soluble tungsten compounds are leached from the collection filter using deionized water. The residual tungsten material is dissolved by a HNO_3/HF digestion, after the removal of potential interfering metal ions by a hydrochloric acid extraction. Atomic absorption spectrometric determination of tungsten in a nitrous oxide–acetylene flame is feasible over the range 10–500 $\mu\text{g ml}^{-1}$ at the 255.1-nm line; the working range may be extended to 1000 $\mu\text{g ml}^{-1}$ without dilution of the sample by using the 400.8-nm line.

Numerous industrial uses have been found for tungsten and its compounds as a result of the intrinsic physical properties of these substances that include high melting point and tensile strength, good electrical and thermal conductivity, low coefficient of expansion and, in the case of tungsten carbide, a hardness approaching that of diamond. Data have been compiled [1] which indicate that tungsten and its compounds may cause transient or permanent lung damage and skin irritation to exposed workers. Therefore, the American Conference of Government Industrial Hygienists (ACGIH) [2] recommended that worker's exposure be limited to time-weighted-average (t.w.a.) air concentrations of 1 mg m^{-3} and 5 mg m^{-3} for soluble and insoluble tungsten compounds, respectively [1]. Samples collected to determine exposure should be collected near the worker's breathing zone, when possible. For particulate hazards, the sampling apparatus (a filter cassette with filter) is pinned to the worker's lapel and connected to a battery-operated pump which is attached to the worker's belt and operated at a nominal flow rate of 2 l min^{-1} for 8 h. Thus, the expected sample for analysis would contain 0.48–9.6 mg W.

The terms "soluble" and "insoluble" have not been defined by ACGIH. The NIOSH Criteria Document [1] defines "soluble" as those compounds of tungsten which are listed in a chemical handbook as soluble in water and "insoluble" as those compounds which are listed as "water insoluble" or as having a solubility of less than 0.1 mg ml^{-1} of water. These definitions have been used in the present work. Although several methods for the deter-

mination of tungsten in alloys and ores have been reported [3–8], only two methods for the determination of tungsten in industrial hygiene samples have been described [9, 10] and neither differentiates between soluble and insoluble tungsten compounds nor utilizes atomic absorption spectrometry (a.a.s.). In addition, neither of these methods deals with the potential interference problems posed by metal ions such as Fe(III) and Co(II) which are expected concomitants in industrial hygiene samples. The purpose of the present work was to (a) evaluate the feasibility of flame a.a.s. for determining tungsten and its compounds in industrial hygiene samples, and (b) evaluate the feasibility of quantifying as discrete species, water-soluble and water-insoluble tungsten compounds collected simultaneously in workplace atmospheres.

EXPERIMENTAL

Apparatus and operating parameters

Atomic absorption measurements were made with a Perkin-Elmer Model 306 spectrometer equipped with a tungsten hollow-cathode lamp, simultaneous deuterium-arc background correction and a nitrous oxide–acetylene burner with a 5-cm slot. A hollow-cathode lamp operated at 40 mA and a monochromator slit width of 0.2 nm were used for all determinations. Burner position and flame stoichiometry were optimized for maximum absorbance prior to each series of determinations after a warm-up period greater than 15 min. Maximum absorbance was obtained when the nitrous oxide–acetylene ratio was adjusted to give an interconal zone height of approximately 3.5 cm. Operation of the nitrous oxide–acetylene flame in the fuel-rich (reducing) manner, necessary for maximum sensitivity, produced a build-up of carbon deposits on the burner head. These deposits caused a depression in sensitivity and were removed as they occurred, with a spatula. White deposits in the spray chamber (most likely from the basicity of the solution) caused erratic absorption values. These deposits were removed by scrubbing the spray chamber and the inside of the burner with a brush after every ten hours of operation.

Reagents

Reagents were ACS reagent grade or better and were used as received except for the nitric acid which was redistilled.

Emission spectrographic analysis of the tungsten metal (Matheson, Coleman and Bell, Norwood, OH) and tungsten carbide (Alpha/Ventron, Danvers, MA) indicated that the tungsten carbide contained traces of Ca and Cr; there was no evidence of other metals (Cu, Fe, Hg, Zn, Ni, Mg, Mo, Al, V, Pb, Mn, P, B, Ti, Si, Ba, Sn, or Au). Although no metallic contaminants were observed in the emission spectrographic analysis of the tungsten metal, an X-ray diffraction scan contained extraneous peaks, indicating the presence of an impurity (1–2%). Replicate a.a.s. determinations of the metal after

acid digestion (2:1 HNO_3/HF) and standards prepared by dissolving sodium tungstate (Mallinckrodt, St. Louis, MO) in deionized water indicated that the metal was $98.4 \pm 2.4\%$ tungsten. Analogous assay of the WC and WO_3 (Fisher Scientific Co.) yielded average ($N = 3$) values of $89.7 \pm 2.3\%$ (calculated = 93.9%) and $77.5 \pm 1.0\%$ (calculated = 79.3%), respectively. All ensuing experiments were based on these determinations. All solutions (standards and samples) used for a.a.s. determinations were adjusted to contain 2% (w/v) sodium sulfate at pH 12.7.

To simulate samples collected in industrial environments, filters (Millipore HA, 37 mm) were "spiked" with soluble tungsten compounds with aliquots (3.5–70 μl) of a tungsten stock solution (10 mg ml^{-1}) and were then air-dried under a dust cover for a minimum of 24 h. A similar procedure was followed when Fe(III) and Co(II) were tested as potential interferences. Filters were spiked with known quantities of insoluble tungsten compounds (W, WC, WO_3) by weighing 5–30 mg of the compound into beakers and washing with water onto filters held in Buchner funnels by vacuum. Powdered cobalt (A. O. MacKay, New York) and iron (Fisher Scientific) were added to the filters in an identical manner. Separate sets of spiked filter samples were used for the determination of soluble tungsten and insoluble tungsten compounds since erratic particulate loss was noted for those filters which were subjected to the additional handling involved in a second step. The particle size of the powder used was considerably larger than that (0.5–10 μm) which would be expected for industrial hygiene samples and consequently would not adhere well to the dry filters.

Development of analytical procedure

The characteristic concentration [11], working concentration range, and an estimate of precision were determined at each of the two analytical wavelengths for tungsten (255.1 and 400.8 nm) by the analysis of replicates over a concentration range of 5–1000 $\mu\text{g W ml}^{-1}$. Since sodium sulfate has been reported to increase sensitivity and mask interferences [12], the dependence of absorbance on the concentration of sodium sulfate and pH was investigated by using a two-level factorial design [13] for solutions over the concentration range 1–4% (w/v) sodium sulfate and a pH range of 7–13 (adjusted with NaOH).

The effect of background correction was investigated by comparing absorbances of filter blanks (ashed in HF/HNO_3 , evaporated to dryness and dissolved in sodium hydroxide solution) and reagent blanks obtained both with and without background correction. Comparisons were also made between standards and samples analyzed with and without background correction applied.

Three different procedures for the separation of soluble tungsten from insoluble tungsten were investigated. In the first, the spiked filter was placed in a teflon beaker, agitated with deionized water and after standing at room temperature for 10 min, the filter and solids were separated from the extract

by vacuum filtration on a Buchner funnel. A second extraction procedure involved adding deionized water (about 3 ml) to the spiked filter in a Buchner funnel, followed by vacuum filtration after a wait of 1, 3 or 5 min. The third procedure, a variation of the second, used hot (50°C) water. Recoveries of soluble tungsten from filters spiked with potential interferences (W, WC, WO₃, Fe, and Co) were included in these studies.

Since acidic solutions are more amenable to a.a.s. than are basic solutions, experiments were conducted to determine if there was a limiting pH at which no tungstic acid would precipitate, and if the presence of potential interferences (Fe, Co and/or Na₂SO₄) enhanced or depressed precipitation in tungsten solutions. The concentrations used were based on those expected for samples collected in atmospheres in compliance with the Occupational Safety and Health Permissible Exposure Limit [14].

A method similar to that of Quin and Brooks [15] for the dissolution of insoluble tungsten compounds was adopted. Tungsten compounds digested in a mixture of nitric and hydrofluoric acids are converted to WO₃ which is dissolved in sodium hydroxide solution and diluted to volume, after addition of sodium sulfate. The effect of digestion conditions on the recovery of the tungsten compounds from spiked filters was investigated by varying the quantities and relative amounts of the two acids used. The effect of sodium hydroxide concentration used for dissolving the trioxide was investigated by comparing the recoveries obtained using 0.5 M with those obtained from 5.0 M NaOH solutions, after the acid digestion. Concomitants such as Fe(III) and Co(II), which will precipitate in alkaline solutions, can be eliminated from filters containing insoluble tungsten compounds by using an extraction with hot (120°C) hydrochloric acid. After the extraction, the procedure described previously is followed. The effects of varying hydrochloric acid concentration, extraction/digestion order and the concomitant metal (Fe/Co) were investigated.

Recommended procedure

The filter containing the sample is placed in a Buchner funnel which is attached to a side-arm test tube, moistened and seated firmly by briefly applying a vacuum. The soluble tungsten compounds are dissolved and removed from the filter by using two successive 3-ml aliquots of water and vacuum filtration. The solution is transferred to a volumetric flask and the test tube is washed successively with sodium sulfate solution (20% w/v) and water and combined with the extract. The solution should be 2% (w/v) in sodium sulfate, and "water-soluble" tungsten is determined by a.a.s. at 255.1 nm.

Acid-soluble metal compounds are extracted from the filter by heating (ca. 120°C) in a teflon beaker for 30 min with 10 M HCl. After cooling, the filter residue and insoluble tungsten are removed by filtration (see above) through a second cellulose ester filter followed by successive 1 M HCl and water washes.

The filters and residue are digested (200°C) for about 12 h with concentrated nitric acid, and then slowly evaporated (110°C) to dryness. If charring occurs (black residue), concentrated nitric acid is added and the evaporation is repeated as necessary until the organic matter has been removed. The "insoluble tungsten" is digested with 1:1 HNO₃/HF for about 2.5 h at 110°C, taken to dryness and subsequently dissolved in 0.5 M NaOH by gentle heating for about 15 min at 110°C. The solution is transferred to a volumetric flask and the beaker rinsed with sodium sulfate solution (20% w/v) and water. After diluting to volume (2% w/v Na₂SO₄), "insoluble" tungsten is determined by a.a.s. at 255.1 nm.

RESULTS AND DISCUSSION

Characteristic concentration, precision, and working range

The characteristic concentration and precision for tungsten determination found in this study (Table 1) were comparable to values reported previously [16] for the 255.1-nm line. However, the characteristic concentration for the 400.8-nm line was greater relative to the 255.1-nm line than the previously reported values (3:1 vs. 2:1). The linear measurement range extended to concentrations of 500 µg W ml⁻¹ for the 255.1-nm line and to 1000 µg W ml⁻¹ for the 400.8-nm line (Fig. 1). The lower limit of the working range is defined here as that concentration where the relative standard deviation (s_r) of replicate measurements is about 10%. At concentrations of 25 and 10 µg W ml⁻¹, s_r = 8.3% and 11.8%, respectively, for the 400.8-nm line and s_r = 2.9% and 14.0%, respectively, for the 255.1-nm line. Similarly, with the addition of sodium sulfate to the solutions, at concentrations of 10 and 5 µg W ml⁻¹, s_r = 5.3% and 20.0%, respectively, for the 400.8-nm line and s_r = 6.7% and 15.4%, respectively, for the 255.1-nm line (Fig. 1, Table 1). Thus, with the addition of sodium sulfate, the working range can be extended to a lower concentration limit.

The enhancement of absorbance (40%) for standards containing sodium sulfate was relatively insensitive to changes in sodium sulfate concentration or pH. Measurement over a pH range of 7–13 and 1–4% sodium sulfate

TABLE 1

Effect of sodium sulfate on analytical parameters for tungsten determination

Wavelength (nm)	Na ₂ SO ₄ added	Working range (µg ml ⁻¹)	Characteristic concentration (µg ml ⁻¹)	\bar{s}_r^a
255.1	No	25–700	10.6	0.022
255.1	Yes	10–500	7.9	0.029
400.8	No	25–1000	31.7	0.038
400.8	Yes	10–1000	23.1	0.031

^a \bar{s}_r = pooled relative standard deviation.

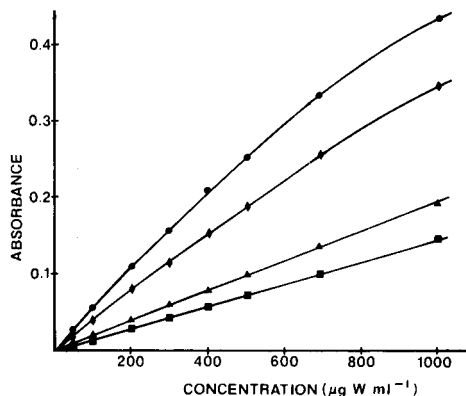


Fig. 1. Calibration curves for tungsten solutions. (●) 255.1 nm with solutions 2% (w/v) in Na_2SO_4 ; (♦) 255.1 nm (Na_2SO_4 not added); (▲) 400.8 nm with solutions 2% (w/v) in Na_2SO_4 ; (■) 400.8 nm (Na_2SO_4 not added).

indicated no change in the mean absorbance value (Table 2) for solutions with $200 \mu\text{g W ml}^{-1}$. The absorbance enhancement, which is in agreement with an earlier study [12], not only allows increased sensitivity for the measurements but also masks interferences. Although metal cations cause varying degrees of enhancement for tungsten determinations [12], the addition of sodium sulfate to standards and samples makes the enhancement constant and effectively eliminates this variable bias.

Absorbances for filter and reagent blanks were minimal regardless of whether or not background correction was used, however, with background correction applied, the baseline drift was so severe that repetitive accurate determinations could not be made. Extensive warm-up (3–4 h) of the deuterium and hollow-cathode lamps minimized, but did not overcome, this problem. Also, the pooled s_r (\bar{s}_r) for the measurement of 10 standard solutions (4 replicates per solution) covering the range of $50\text{--}500 \mu\text{g W ml}^{-1}$ was greater when background correction was used ($\bar{s}_r = 0.036$ with correction and 0.025 without background correction). Consequently, background correction was not used in subsequent experiments.

TABLE 2

Absorbance stability as functions of pH and sodium sulfate concentrations

Trial no.	pH	Na_2SO_4 conc. (%)	Mean absorbance ^a
1	7.0	1.0	0.112 ± 0.001
2	13.0	1.0	0.111 ± 0.001
3	7.0	4.0	0.113 ± 0.001
4	13.0	4.0	0.113 ± 0.001
5 (median)	10.0	2.5	0.113 ± 0.001

^aMean of 4 determinations.

Results of the different extraction procedures for the separation of soluble tungsten from insoluble tungsten are summarized in Table 3 and indicated that the 10-min water extraction of soluble tungsten from filters in beakers yielded less than optimum recoveries. However, analysis of the solutions from filters extracted in the Buchner funnels gave recoveries of essentially 100% for each of the three extraction times. The use of hot (50°C) water, which also yielded 100% recovery, is apparently unnecessary.

Good recoveries were also obtained for the determination of soluble tungsten extracted (1.0 min) from spiked filters containing tungsten and tungsten carbide ($97.1 \pm 1.6\%$ and $98.5 \pm 1.2\%$, respectively, $N = 3$). However, filters spiked with sodium tungstate and tungsten trioxide yielded a precipitate in the filtrate almost immediately after vacuum was applied. The precipitate formed, which is probably a paratungstate or similar compound [17], can be redissolved by the addition of sodium hydroxide followed by heating. Reaction of these two species should not cause a sampling and determination problem in the event of their simultaneous occurrence in contaminated environments, since the reaction would most likely occur before sampling and the resulting compound would be treated as an "insoluble" tungsten species. Likewise, the addition of metal ions (e.g., Fe(III), Co(II)) to tungstate in solution causes the metal tungstate to precipitate. This reaction, analogous to the preceding example, would most likely occur before sampling and result in "insoluble" tungsten species.

Tungsten compounds, after conversion to the anhydride by treatment with HF/HNO₃, are soluble and stable in basic solution but precipitate as

TABLE 3

Recovery of "soluble" tungsten (Na₂WO₄) from spiked filters

Filter extraction technique	Time (min)	mg W/filter	Concomitant	Average recovery ^a (% \pm s _r)
Funnel	1.0	0.513	None	101 \pm 1.5
		0.513	W	98.5 \pm 1.2
		0.513	WC	97.1 \pm 1.6
		0.513	WO ₃	— ^b
Funnel	1.5	0.513	Co	103 \pm 2.9
		0.513	Fe	103 \pm 1.9
Funnel	2.0	0.360	W	99.6 \pm 4.5
		0.720	W	102.0 \pm 2.0
		1.440	W	100.0 \pm 1.2
Funnel	3.0	0.513	None	102 \pm 1.4
Funnel	3.0	0.513	None	101 \pm 1.3
hot H ₂ O (50°C)				
Funnel	5.0	0.513	None	101 \pm 1.0
Beaker	10	0.204	None	93.8 \pm 3.2
		0.306	None	90.8 \pm 3.4

^a Average of at least 3 determinations. ^b Precipitate formed.

tungstic acid at low pH. However, other metal ions present will precipitate as hydroxides in slightly acid or basic solutions with resulting nebulization problems and/or low recoveries for tungsten because of entrainment in the precipitates, or formation of metal tungstate species. Experiments designed to determine a limiting pH at which no tungstic acid would precipitate covered the pH range of 1.2–3.0 (Fig. 2) and indicated that solutions containing only sodium tungstate could be analyzed without a decrease in response at a pH as low as 1.8 and, in the presence of 2% sodium sulfate, the linear response could be extended to pH 1.4. However, the addition of Fe(III) and/or Co(II) decreases the absorbance dramatically, even at low concomitant concentrations and low pH values. This decrease is probably due to the formation of cobalt tungstate or iron(III) tungstate; a precipitate was noted in these solutions even at low pH. Since Fe(III) or Co(II) will most likely be present in industrial atmospheres containing tungsten and the use of an acidic sample solution does not alleviate the interference, additional steps had to be taken to remove these contaminants in the development of the analytical procedure. The remaining work was conducted in a basic environment, after an acid extraction of acid-soluble metals.

Recoveries of tungsten metal and tungsten carbide from spiked filter samples were similar for all acid combinations used (Table 4). Likewise, recoveries from filters spiked with W, WC, or WO_3 were not dependent on the concentration of sodium hydroxide (0.5 or 5.0 M) used for dissolution of the tungsten trioxide resulting from the acid digestion (Table 4). As an additional check on the digestion procedure, comparisons were made of the recoveries of tungsten trioxide obtained from samples carried through the acid (1:1 HF/ HNO_3) digestion procedure and those obtained from straightforward dissolution in sodium hydroxide solution without acid digestion. Sample sizes (8–25 mg) were comparable to those used in the filter recovery studies (Table 4) and the mean recovery obtained for tungsten trioxide samples which were acid-ashed was $102 \pm 5.0\%$ while the mean recovery for aliquots treated only with base was $102 \pm 2.0\%$. These recoveries further confirm the ruggedness of the digestion and dissolution parameters and the relative insensitivity of absorbance to pH.

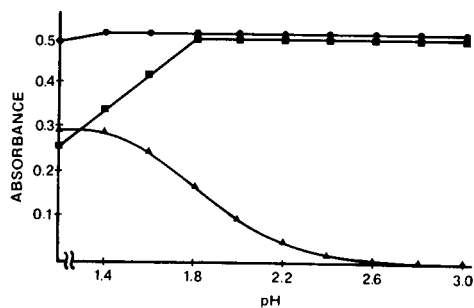


Fig. 2. Absorbance of tungsten solutions ($500 \mu\text{g ml}^{-1}$) as a function of pH. (●) Na_2WO_4 with Na_2SO_4 (2% w/v); (■) Na_2WO_4 only; (▲) Na_2WO_4 with Na_2SO_4 (2% w/v), CoCl_2 ($2.5 \mu\text{g Co ml}^{-1}$), and FeCl_3 ($500 \mu\text{g Fe ml}^{-1}$).

TABLE 4

Recovery of "insoluble" tungsten from spiked filters

Digestion technique		Tungsten species	Range mg W/filter	Average recovery % $\pm s_r$	N
Acid ratio (HF/HNO ₃)	NaOH (M)				
1:3	0.5	W	8-30	99.1 \pm 1.6	4
		WC		104 \pm 4.1	3
4:3	0.5	W	8-33	99.4 \pm 1.9	4
		WC		104 \pm 2.4	3
1:1	0.5	W	9-11	93.2 \pm 1.3	2
		WC		97.5	1
		WO ₃		96.2 \pm 0.1	2
1:1	5.0	W	9-14	96.4	1
		WC		99.5 \pm 0.7	2
		WO ₃		96.5 \pm 0.2	2

The effects of hydrochloric acid extraction of concomitant metals on tungsten recovery are shown in Table 5. Reversing the order of the extraction/digestion procedure for one set of filters spiked with tungsten and Co or Fe metals proved to be more difficult to handle experimentally and resulted in somewhat decreased recoveries. Although the use of 5 M HCl for extraction was sufficient to eliminate Fe(III) and Co(II) interferences in the subsequent procedures, the use of a more concentrated (10 M) HCl solution increased

TABLE 5

Recovery of "insoluble" tungsten from spiked filters using the HCl extraction procedure

Procedure	HCl (M)	Tungsten species	Range mg W/filter	Concomitant	Average recovery % $\pm s_r^a$
Extraction/ digestion	5	W	10-31	Fe	101 \pm 1.4
		W		Co	99.9 \pm 2.3
Digestion/ extraction	5	W	17-29	Fe	93.3 \pm 5.1
		W		Co	86.1 \pm 2.8
Extraction/ digestion	10	WO ₃	9-26	Fe	98.9 \pm 3.7
		WO ₃		Co	99.6 \pm 2.8
Extraction/ digestion	10	WC	10-25	Fe	95.4 \pm 1.4
		WC		Co	90.0 \pm 3.4
Extraction/ digestion	10	WC	9-26	Fe	98.0 \pm 3.0
		WC		Co	90.8 \pm 7.4
Extraction/ digestion	5	WC	16-22	—	105 \pm 2.8
Extraction/ digestion	5	WC	7-20	Co	104 \pm 2.1
Digestion only	—	WC	18-24	—	105 \pm 3.3

^aAverage of 3 determinations.

the dissociation of the original filter matrix and facilitated the filtering procedure. The recoveries of tungsten carbide, although within an acceptable range (Tables 4, 5), are somewhat more variable than those obtained for tungsten or tungsten trioxide. The source of this variation is not clear at this point; elimination of the hydrochloric acid extraction or the presence of cobalt metal (Table 5) did not change significantly the percentage recoveries in a single set of experiments. If a degree of accuracy greater than $\pm 10\%$ is required for a given set of samples, the analysis of control samples would be obligatory.

REFERENCES

- 1 Criteria for Recommended Standard: Occupational Exposure to Tungsten and Cemented Tungsten Carbide, U.S. Government Printing Office, Washington, DC, 1977.
- 2 ACGIH, Threshold Limit Values for the Workroom Environment with Intended Changes for 1978, Cincinnati, OH, 1978, p. 30.
- 3 G. G. Welcher and O. H. Kriege, *At. Absorpt. Newsl.*, 9 (1970) 61.
- 4 R. C. Rooney and C. G. Pratt, *Analyst*, 97 (1972) 400.
- 5 J. Husler, *At. Absorpt. Newsl.*, 10 (1971) 60.
- 6 D. R. Thomerson and W. J. Price, *Analyst*, 96 (1971) 825.
- 7 P. D. Rao, *At. Absorpt. Newsl.*, 9 (1970) 131.
- 8 E. Keller and M. L. Parsons, *At. Absorpt. Newsl.*, 9 (1970) 92.
- 9 G. S. Salyamon and L. A. Krashenitsyna, *Gig. Sanit.*, 37 (1972) 78.
- 10 A. Pergud and V. Gernet, *Chemical Analysis of Air in Industrial Enterprises*, 3rd edn., Khimiya, Leningrad, 1973, p. 638.
- 11 H. M. N. H. Irving, H. Freiser and T. W. West, *Compendium of Analytical Nomenclature*, Pergamon, Oxford, 1978, p. 131.
- 12 R. M. Edgar, *Anal. Chem.*, 48 (1976) 1653.
- 13 E. I. duPont de Nemours and Co., Applied Technology Div., *Strategy of Experimentation*, Wilmington, DE, 1974.
- 14 U.S. Department of Labor, Occupational Safety and Health Administration, *Occupational Safety and Health Standards*, Fed. Reg. 29 CFR 1910.1001, 1975.
- 15 B. F. Quin and R. R. Brooks, *Anal. Chim. Acta*, 65 (1973) 206.
- 16 Perkin-Elmer Corp., *Analytical Methods for Atomic Absorption Spectrophotometry*, Norwalk, CT, 1976.
- 17 F. A. Cotton and G. Wilkinson, *Advanced Inorganic Chemistry: A Comprehensive Text*, 3rd edn., Interscience, New York, 1972, p. 952.

DETERMINATION OF PHOSPHORUS IN WASTE-WATERS BY INDUCTIVELY-COUPLED PLASMA ATOMIC EMISSION SPECTROMETRY

T. ISHIZUKA* and K. NAKAJIMA

Government Industrial Research Institute Nagoya, Hirate-machi, Kita-ku, Nagoya 462 (Japan)

H. SUNAHARA

Department of Industrial Chemistry, Faculty of Engineering, Hiroshima University, Senda-machi, Hiroshima 730 (Japan)

(Received 27th May 1980)

SUMMARY

Inductively coupled plasma—atomic emission spectrometry offers a simple and rapid method for the determination of total phosphorus in waste-waters: the optimum operating conditions are described. The detection limits are 0.02, 0.04, and 0.11 $\mu\text{g ml}^{-1}$ at the 213.618, 214.914, and 253.565-nm lines, respectively. Interferences by other elements are negligible at the concentration levels of these elements in environmental and waste-waters, except for the spectral interference of copper on the lines at 213.618 and 214.914 nm. Differences in emission response for various inorganic and organic phosphorus compounds are small. Analytical results for phosphorus in municipal and industrial waste-waters agree well with those obtained by standard methods.

Recently, eutrophication in lakes and reservoirs has become an important problem. Phosphorus is a critical nutrient aiding the eutrophication process. The principal sources of phosphorus in environmental waters are agricultural effluents, municipal waste-waters, industrial waste-waters, etc. The determination of phosphorus in these waters has thus become increasingly important. Phosphorus in such waters is present in various inorganic and organic forms, which, in general, have been converted to orthophosphate for colorimetric determination [1]. Digestion methods for the conversion of all the phosphorus to orthophosphate are time-consuming. The colorimetric methods are sensitive, but suffer from several chemical interferences. There is also an indirect atomic absorption method for the determination of phosphorus [2]; orthophosphate is determined by this method, but the other types of phosphorus compounds are not. To determine the phosphorus content of various waters, a simple, rapid, sensitive, and accurate method is desirable.

Inductively coupled plasma—atomic emission spectrometry (i.c.p.—a.e.s.) is an excellent method for the determination of major and trace levels of metals and metalloids in environmental materials. Analyses of such materials

by i.c.p.—a.e.s. have been described in many reports [3–10], several of which have dealt with the determination of phosphorus in soils and biological tissues [3, 5, 8, 9]. In these studies, phosphorus has been introduced into an i.c.p. as orthophosphate. To determine total phosphorus, the emission intensity in the i.c.p. should not depend on the type of phosphorus compounds present. In addition, the influence of other elements present in the samples on the phosphorus emission intensity must be examined. The present paper investigates those effects and describes the determination of phosphorus in several waste-waters.

EXPERIMENTAL

Apparatus

The i.c.p.—a.e.s. system used in this study was a Nippon Jarrell-Ash Model ICAP-1000S spectrometer with an i.c.p. source. Sample solution was introduced into a cross-flow nebulizer with a peristaltic pump. Table 1 shows the specification of the system, and Table 2 shows the operating conditions and the analytical lines used for phosphorus measurements. The optimum operating conditions for carrier gas flow rate, observation height, and r.f. power to the plasma are discussed below.

Reagents

A standard solution of phosphorus ($1000 \mu\text{g ml}^{-1}$) was prepared by dissolving potassium dihydrogenphosphate (reagent grade) in distilled water. Other inorganic and organic phosphorus compounds used were reagent grade, and the solutions of the compounds were prepared freshly for every experiment, to minimize the hydrolysis of the compounds to orthophosphate. All other chemicals used were reagent grade.

TABLE 1

Instrumentation

R.f. generator	Crystal-controlled type; frequency, 27 MHz; automatic power control; maximum power output, 2 kW
Plasma torch	All quartz
Plasma gas	Argon
Nebulizer	Pneumatic cross-flow type
Sample uptake	Tokyo Rikakikai MP-1011 peristaltic pump
Spectrometer	Czerny-Turner 1-m mounting; 2400 lines/mm grating blazed at 240 nm; reciprocal dispersion, 0.4 nm mm^{-1}
Optics	Plasma source focussed as 1:1 image onto entrance slit with a 6-cm focal length quartz lens
Detector	HTV R-456
Signal measurement	D.c. amplification/10-s integration; digital voltmeter readout

TABLE 2

Operating conditions

R.f. power	1.2 kW
Coolant gas flow	14 l min ⁻¹
Plasma gas flow	0.5 l min ⁻¹
Carrier gas flow	0.55 l min ⁻¹
Sample uptake rate	1.7 ml min ⁻¹
Observation height	12.5 mm above the load coil
Slit width	Entrance, 50 μ m; exit, 75 μ m
Slit height	3 mm
Analytical lines	213.618, 214.914, and 253.565 nm

RESULTS AND DISCUSSION

Optimization of operating parameters

In i.c.p.—a.e.s., carrier gas flow rate, observation height, and r.f. power to the plasma are important parameters affecting the emission intensities of elements [11]. Optimum operating conditions were thus established for the determination of phosphorus.

Figure 1 shows the effect of carrier gas flow rate on the emission intensity of phosphorus at a concentration of 10 μ g ml⁻¹. The carrier gas flow rate was varied over the range 0.3–0.65 l min⁻¹. The signal intensity was highest at a flow rate of 0.5 l min⁻¹. The background intensity near the emission line decreased with increasing flow rate. The signal-to-background ratio was highest at a flow rate of 0.55 l min⁻¹. The dependence of signal intensity on coolant and plasma gas flow rates was slight, and the values shown in Table 2 were used throughout.

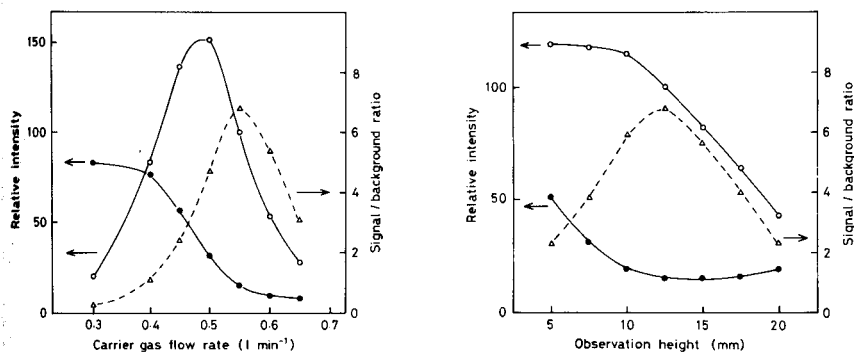


Fig. 1. (left). Effect of carrier gas flow rate on the emission intensity of phosphate (10 μ g P ml⁻¹). (○) P signal; (●) background; (△) signal-to-background ratio; wavelength, 213.618 nm.

Fig. 2. (right). Effect of observation height on the emission intensity of phosphate (10 μ g P ml⁻¹). (○) P signal; (●) background; (△) signal-to-background ratio; wavelength, 213.618 nm.

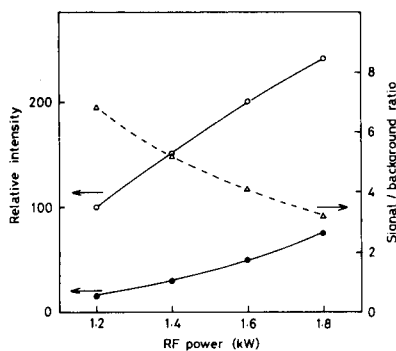


Fig. 3. Effect of r.f. power on the emission intensity of phosphate ($10 \mu\text{g P ml}^{-1}$). (\circ) P signal; (\bullet) background; (\triangle) signal-to-background ratio; wavelength, 213.618 nm.

Figure 2 shows the effect of observation height on the emission intensity of phosphorus at a concentration of $10 \mu\text{g ml}^{-1}$. The observation height above the load coil was varied over the range 5–20 mm. The phosphorus signal intensity was almost constant at heights of 5–10 mm, but decreased at greater observation heights. In contrast, the background intensity decreased as the observation height increased to 10 mm, and remained approximately constant at greater heights. The signal-to-background ratio was highest at a height of 12.5 mm: this value was used as the optimum observation height.

Figure 3 shows the effect of r.f. power to the plasma on the emission intensity of a solution containing $10 \mu\text{g P ml}^{-1}$. The power was varied in the range 1.2–1.8 kW; the apparatus could not be operated at a power below 1.2 kW. Both the signal and background intensities increased with increasing power: however, the signal-to-background ratio decreased with increasing power, and a power of 1.2 kW was used throughout. The optimum conditions are summarized in Table 2.

Interferences

Waste-waters contain various inorganic and organic materials: the effects of other elements on the phosphorus emission intensity were therefore studied.

The effect of anions was examined using the corresponding inorganic acids. Chloride at concentrations up to 10 mg ml^{-1} (as in sea water), and nitrate and sulfate at the same concentration had a negligible effect on the emission intensity of a phosphate solution ($10 \mu\text{g P ml}^{-1}$). Kawaguchi et al. [5] reported that phosphorus emission intensity decreased appreciably in the presence of sulfuric acid at the 10 mg ml^{-1} level because the increased viscosity reduced the rate of sample uptake into the nebulizer. In this work, since the sample uptake rate was kept constant with the peristaltic pump, this effect was not observed.

Sodium, potassium, calcium and magnesium ions occur at major levels in environmental and waste-waters. The emission intensity of phosphate

($10 \mu\text{g P ml}^{-1}$) was hardly affected by sodium concentrations up to $3000 \mu\text{g ml}^{-1}$ and by K, Mg, and Ca concentrations up to $1000 \mu\text{g ml}^{-1}$. However, sodium concentrations over $10000 \mu\text{g ml}^{-1}$, and K, Mg, and Ca concentrations of $3000 \mu\text{g ml}^{-1}$ produced slight decreases (4–7%) in the emission intensity.

Environmental and waste-waters also contain various elements at minor levels. The effect of these elements on the emission intensity of phosphate ($10 \mu\text{g P ml}^{-1}$) was studied using the phosphorus line at 213.618 nm, except for the study of the effect of copper. The lines at 213.618 and 214.914 nm were subject to significant spectral interference from neighbouring copper lines, so the effect of copper was examined using the phosphorus line at 253.565 nm. (The emission intensity of $10 \mu\text{g Cu ml}^{-1}$ equalled the phosphorus intensity for $11.4 \mu\text{g ml}^{-1}$ at 213.618 nm, and for $5.2 \mu\text{g ml}^{-1}$ at 214.914 nm.) The phosphorus emission intensity was almost unaffected by NH_4^+ , Al, Cu, Mn, Si, and Ti at concentrations up to $300 \mu\text{g ml}^{-1}$. Because of spectral interferences from iron and zinc lines near the 213.618-nm line, the phosphorus emission intensity increased slightly with increasing concentrations of these two metals. Iron and zinc concentrations of $300 \mu\text{g ml}^{-1}$ produced increases of 4 and 9% in the emission intensity, respectively. However, as the concentrations of iron and zinc in waste-waters are generally below a few tens of $\mu\text{g ml}^{-1}$, these spectral interferences can normally be neglected.

Organic materials are frequently found in waste-waters. The effect of organic materials on the emission intensity of phosphate ($10 \mu\text{g P ml}^{-1}$) was examined using dextrose and tartaric acid. Dextrose and tartaric acid at concentrations of 10– $3000 \mu\text{g ml}^{-1}$ did not affect the emission. A concentration of $3000 \mu\text{g ml}^{-1}$ corresponds to a TOC (total organic carbon) level of 1000– $1200 \mu\text{g ml}^{-1}$.

Analytical curves and precision

One of the major advantages of an i.c.p. source is its ability to produce linear analytical graphs over 4 or 5 orders of magnitude. Calibration graphs for phosphorus were constructed in the concentration range 0.1 – $100 \mu\text{g ml}^{-1}$ for the lines at 213.618, 214.914, and 253.565 nm. The net intensity plots obtained had a slope of unity, indicating a linear relationship between background-corrected intensity and concentration. In the construction of these analytical plots, the solutions at each concentration were measured five times: the precision (relative standard deviation) ranged from 0.2 to 1.6%.

Detection limits

The detection limits of phosphorus at the three lines were determined by using solutions containing 0.1 or $0.3 \mu\text{g P ml}^{-1}$. The detection limit is defined as the concentration which gives a net signal equal to twice the standard deviation of the background level. The background levels were measured with distilled water at each line. The detection limits obtained were 0.02,

0.04, and $0.11 \mu\text{g ml}^{-1}$ at 213.618, 214.914, and 253.565 nm, respectively. These values are lower than those obtained by other investigators [3–5, 12], possibly for the following reasons. First, because i.c.p. sources have been used for simultaneous multi-element analysis, the operating conditions used for the determination of phosphorus have been a compromise [4, 12]; secondly, direct reading methods have been used instead of the signal integration method [3, 5].

Emission response per unit phosphorus for various phosphorus compounds

Phosphorus in waste-waters is present as various inorganic and organic compounds. From the viewpoint of total phosphorus determination, the same response per unit phosphorus should be obtained for all phosphorus compounds. Table 3 shows the relative emission responses at the $10 \mu\text{g ml}^{-1}$ level for the various phosphorus compounds. Nearly equal emission responses were obtained for all the compounds except hexametaphosphate, for which a somewhat lower response was obtained. Cyclic hexametaphosphate introduced into the i.c.p. decomposes first to straight-chain polyphosphate or orthophosphate, and then excited phosphorus atoms are formed from the phosphate. Therefore, the number of phosphorus atoms formed in the i.c.p. from hexametaphosphate is somewhat less than for the orthophosphate. With this single exception, the i.c.p.—a.e.s. method is an excellent analytical method for the determination of total phosphorus in waste-waters.

Analysis of practical waste-water samples

Phosphorus in several practical wastewater samples were determined by the i.c.p.—a.e.s. method. Each sample was filtered through a $0.45\text{-}\mu\text{m}$ membrane filter paper in a Swinny holder, and the filtrates were put on the nebulizer. Table 4 shows analytical results for phosphorus in the samples. The values of phosphorus content obtained by the persulfate digestion—

TABLE 3

Emission response per unit phosphorus ($10 \mu\text{g ml}^{-1}$) for various phosphorus compounds

Compound	Emission response
Potassium dihydrogenphosphate, KH_2PO_4	100
Sodium pyrophosphate, $\text{Na}_4\text{P}_2\text{O}_7 \cdot 10\text{H}_2\text{O}$	100
Sodium triphosphate, $\text{Na}_5\text{P}_3\text{O}_{10}$	98
Sodium hexametaphosphate, $\text{Na}_6\text{P}_6\text{O}_{18}$	94
Sodium hypophosphite, $\text{NaH}_2\text{PO}_2 \cdot \text{H}_2\text{O}$	103
Sodium phosphite, $\text{NaH}_2\text{PO}_3 \cdot 5\text{H}_2\text{O}$	102
Adenosine-5'-triphosphate disodium salt, $\text{C}_{10}\text{H}_{14}\text{N}_5\text{O}_{13}\text{P}_3\text{Na}_2 \cdot 3\text{H}_2\text{O}$	98
Flavin mononucleotide sodium salt, $\text{C}_{17}\text{H}_{20}\text{N}_4\text{O}_9\text{PNa} \cdot 2\text{H}_2\text{O}$	99
α -D-glucose-1-phosphate dipotassium salt, $\text{C}_6\text{H}_{11}\text{K}_2\text{O}_5\text{P} \cdot 2\text{H}_2\text{O}$	101
Disodium phenylphosphate, $\text{C}_6\text{H}_5\text{Na}_2\text{PO}_4 \cdot 2\text{H}_2\text{O}$	99
Sodium β -glycerophosphate, $\text{C}_3\text{H}_7\text{Na}_2\text{O}_6\text{P} \cdot 5\text{H}_2\text{O}$	98

TABLE 4

Analytical results (in $\mu\text{g ml}^{-1}$) of phosphorus in several waste-waters

Sample	I.c.p. method		Standard method Concn.
	Concn.	r.s.d.	
Raw municipal water	1.75	0.8	1.91
Treated municipal water	1.42	1.0	1.46
Treated water in coagulating sedimentation process (1) ^a	0.35	3.9	0.37
Treated water in coagulating sedimentation process (2) ^a	0.38	4.5	0.39
Treated water in coagulating sedimentation process (3) ^a	0.21	8.8	0.22

^aEach sample (effluent) was from a pilot plant for a coagulating sedimentation process for industrial waste-waters containing phosphate; samples (1–3) were withdrawn at different times.

colorimetric method (molybdenum blue with ascorbic acid) given in Standard Methods [1] are also shown. The values obtained by the i.c.p.—a.e.s. method agree well with those obtained by the Standard Method.

REFERENCES

- 1 American Public Health Association, American Water Works Association and Water Pollution Control Federation, Standard Methods for the Examination of Water and Waste-water, APHA, Washington, DC, 14th edn., 1975, p. 466.
- 2 C. I. Lin and C. O. Huber, *Anal. Chem.*, 44 (1972) 2200.
- 3 G. F. Kirkbright, A. F. Ward and T. S. West, *Anal. Chim. Acta*, 62 (1972) 241.
- 4 R. K. Winge, V. A. Fassel, R. N. Kniseley, E. DeKalb and W. J. Haas, Jr., *Spectrochim. Acta*, 32B (1977) 327.
- 5 H. Kawaguchi, T. Ito and A. Mizuike, *Bunseki Kagaku*, 27 (1978) 53.
- 6 J. A. C. Broekaert and F. Leis, *Anal. Chim. Acta*, 109 (1979) 73.
- 7 J. R. Garbarino and H. E. Taylor, *Appl. Spectrosc.*, 33 (1979) 220.
- 8 N. R. McQuarker, P. D. Kluckner and G. N. Chang, *Anal. Chem.*, 51 (1979) 888.
- 9 N. R. McQuarker, D. F. Brown and P. D. Kluckner, *Anal. Chem.*, 51 (1979) 1082.
- 10 F. E. Lichte, S. Hopper and T. W. Osborn, *Anal. Chem.*, 52 (1980) 1020.
- 11 V. A. Fassel, *Anal. Chem.*, 51 (1979) 1290A.
- 12 R. K. Winge, V. J. Peterson and V. A. Fassel, *Appl. Spectrosc.*, 33 (1979) 206.

MOLEKÜLABSORPTIONSSPEKTROMETRIE BEI ELEKTRO-THERMISCHER VERDAMPFUNG IN EINER GRAPHITROHRKÜVETTE

Teil 6. Bestimmung von Chloridspuren durch die Molekülabsorption von AlCl_3 , GaCl_3 und InCl_3 -Molekülen

KLAUS DITTRICH* und PETRA MEISTER

Sektion Chemie der Karl-Marx-Universität Leipzig, Analytisches Zentrum, 7010 Leipzig (G.D.R.)

(Eingegangen den 3. Juli 1980)

SUMMARY

(Molecular absorption spectrometry with electrothermal volatilization in a graphite tube. Part 6. Determination of traces of chloride by molecular absorption of AlCl_3 , GaCl_3 and InCl_3 molecules)

The use of molecular absorption spectrometry of thermally stable molecules such as AlCl_3 , GaCl_3 , InCl_3 and TlCl_3 , generated in a normal graphite tube, is assessed for determination of chloride. Optimal experimental conditions are discussed. The presence of Na^+ , Sr^{2+} and Ba^{2+} ions increases the signals. These influences and also those of other ions are discussed. The sensitivities (0.01 absorbance) for chloride are 1.5 ng for AlCl_3 , 9 ng for GaCl_3 and 3 ng for InCl_3 .

ZUSAMMENFASSUNG

Es wurde die Anwendbarkeit der Molekülabsorption thermisch stabiler Moleküle, wie AlCl_3 , GaCl_3 , InCl_3 und TlCl_3 , die in einer normalen Graphitrohrküvette erzeugt wurden, für die Bestimmung des Chlorids untersucht. Die experimentellen Bedingungen wurden optimiert. Die Gegenwart von Na^+ , Sr^{2+} - und Ba^{2+} -Ionen bewirkt eine Signalerhöhung. Diese Einflüsse und auch die Einflüsse anderer Ionen werden ausführlich diskutiert. Die reziproken Empfindlichkeiten für Chlorid bezogen auf 0,01 Extinktion sind: 1,5 ng für AlCl_3 , 9 ng für GaCl_3 und 3 ng für InCl_3 .

Die Bestimmung von Chlorid durch Atomabsorptionsspektrometrie (AAS) und Atomemissionsspektrometrie (AES) ist wegen der ungünstigen Lage der empfindlichen Spektrallinien nicht möglich im Spurenbereich. Indirekte AAS-Bestimmungsmethoden sind für Chlorid nach der Abtrennung als AgCl bzw. CrO_2Cl_2 entwickelt worden [1]. Sowohl hinsichtlich des Nachweisvermögens als auch der Selektivität sind solche Methoden jedoch nicht besonders gut.

Ionenselektive Elektroden auf $\text{AgX}/\text{Ag}_2\text{S}$ -Basis können ebenfalls zur Chloridbestimmung eingesetzt werden. Diese Methoden sind sehr nach-

treten jedoch viele Störungen auf. Versuche zur Bestimmung von Chloridionen unter Benutzung zweiatomiger Moleküle wurden ebenfalls gemacht. Zuerst wurden CuCl -Moleküle benutzt. Der Beilstein-Test [2] und der Smissen-Brenner [3] waren Ergebnisse dieser Arbeit. Gilbert [4] modifizierte den Smissen-Brenner, indem er das Kupfer durch Indium ersetzte und die InCl -ME (Molekülemission) bei 359,9 nm in einer kühlen H_2 -Luft-Flamme zum Chlornachweis benutzte. Für den spezifischen Nachweis Chlor-haltiger, organischer Materialien wurde von Gutsche, Herrmann und Rüdiger [5–7] ebenfalls die InCl -ME benutzt. Die erzielten Nachweisgrenzen liegen im Nanogramm-Bereich. In laminaren H_2 - N_2 -Diffusionsflammen konnte ebenfalls die InCl -ME nachgewiesen werden [8]. Auch die MECA-Technik wurde für die Chlorid-Bestimmung durch InCl -ME genutzt [9]. All diese Untersuchungen zeigen, daß die Molekülemission zur Bestimmung von Chlorid eingesetzt werden kann. Probleme hinsichtlich des Nachweisvermögens, der Reproduzierbarkeit und Richtigkeit treten auf.

Im Zusammenhang mit der Entwicklung der AAS beschäftigte man sich in zunehmendem Maße ebenfalls mit der Molekülbildung in Plasmen, da diese sowohl zur Erhöhung des Untergrundes [10–12] als auch zu Signaldepressionen führen kann. Entsprechende MeCl -Molekülbildungen wurden bei der Indium-AA [13–15], Kupfer-AA [16, 17] Zink-, Cadmium- und Mangan-AA [18, 19], Blei-AA [18, 20] festgestellt. Eine Übersicht über diese Probleme wird gegeben [21].

In der 1. Mitteilung dieser Serie berichteten wir über die intensiven Molekülabsorptionen (MA) der GaCl - und InCl -Moleküle [22] und wiesen auf die Möglichkeit der analytischen Nutzung hin. Unabhängig von diesen Arbeiten berichten Yoshimura et al. [23] über die Ausnutzung der InCl -MA und Tsunoda et al. [24] über die Ausnutzung der AlCl -MA zur Bestimmung von Chlorid. Die Nachweisgrenzen lagen bei 8,7 bzw. 0,12 ng Cl^- . Die vorliegende Arbeit hat das Ziel, die analytischen Möglichkeiten, die sich aus der Ausnutzung der MAS der zweiatomigen Moleküle AlCl , GaCl , InCl und TlCl ergeben, zu ermitteln und zu vergleichen. Dies soll unter dem Gesichtspunkt gleicher experimenteller Bedingungen erfolgen. Weiterhin soll der Einfluß der Matrices, besonders der schweren Halogenide und der Kationen die zu Signalerhöhungen führen, betrachtet werden.

EXPERIMENTELLES

Apparatur und Reagenzien

Zweikanal-Zweistrahle-AA-Spektrometer Typ 811 (Jarrell-Ash) H_2 -Hohlkathodenlampe, 30 mA; Spektrale Spaltbreite, 0,4 nm; Wellenlänge, vgl. Tab. 1 und 2; Untergrundkompensation nach der Zweilinienmethode (vgl. Tab. 2); Graphitrohrküvette, Typ 1268 (Beckman).

Die Stammlösungen der Metalle wurden durch Auflösen der reinen Metalle bzw. reinen TlNO_3 in Salpetersäure hergestellt (100 mg Me ml^{-1} M HNO_3). Außerdem wurden folgende Lösungen eingesetzt: 0,1 M Ba(OH)_2 ; 0,1 M

TABELLE 1

Charakteristika der untersuchten Molekülbanden

Molekül	Intensivster Übergang	MA-Bande Wellenlänge (nm)	Energieaufnahme (eV)	Dissoziationsenergie (eV)	Siedepunkt Metall (°C)
AlCl	$A^1\Pi \leftarrow X^1\Sigma^+$	261,4; 262,0	4,7	5,1	2450
GaCl	$C^1\Pi \leftarrow X^1\Sigma^+$	249,1; 248,1	4,9	4,9	2237
InCl	$C^1\Pi \leftarrow X^1\Sigma^+$	267,2; 266,1	4,5	4,5	2000
TlCl	$C,D \leftarrow X^1\Sigma^+$	251,9	4,9	3,8	1457

TABELLE 2

Optische und thermische Bedingungen für die analytische Anwendung der AlCl-, GaCl- und InCl-Molekülabsorptionen

	AlCl	GaCl	InCl
Wellenlänge zur Messung der Gesamtabsorption (nm)	261,4	248,1	267,2
Wellenlänge zur Messung des Untergrundes (nm)	260,0	254,0	263,0
Veraschung	20s; 1050°C	10s; 1500°C	10s; 1500°C
Verdampfung	20s; 3300°C	15s; 3300°C	10s; 3050°C

weisstark. In Gegenwart anderer Ionen, besonders der schweren Halogenide $Sr(OH)_2$; 0,1 M $Ca(OH)_2$; 2 M NaOH, NaF, NaBr, NaJ, $LiNO_3$, KNO_3 , $RbNO_3$, $Be(NO_3)_2$, $Mg(NO_3)_2$, $Ca(NO_3)_2$, $Zn(NO_3)_2$, $Fe(NO_3)_2$, $Co(NO_3)_2$, $Ni(NO_3)_2$, $Cr(NO_3)_3$, jeweils in Wasser.

Verfahrensweise

Mikrovolumina von 5–100 μl der entsprechend zusammengesetzten Lösungen werden in die Graphitrohrküvette gegeben (Dosierung), getrocknet (Trocknung), thermisch überarbeitet (Veraschung) und verdampft (Verdampfung und Molekülbildung) (vgl. Tab. 2). Die Aufnahme der Spektren erfolgte durch punktweises Messen bei ausgewählten Wellenlängen.

UNTERSUCHUNG UND OPTIMIERUNG DER EXPERIMENTELLEN BEDINGUNGEN

Aufnahme und Auswertung der Spektren

In der Abb. 1 sind die Spektren, die bei der Verdampfung von AlCl-, GaCl-, InCl- und TlCl-Molekülen erhalten wurden, dargestellt. In allen Fällen wurden Molekülabsorptionsbanden gefunden, die mit Hilfe von Tabellen [25] identifiziert wurden (vgl. Tab. 1). Intensive MA-Banden treten vor allem beim AlCl, GaCl und InCl auf. Die TlCl-MA-Bande ist relativ breit

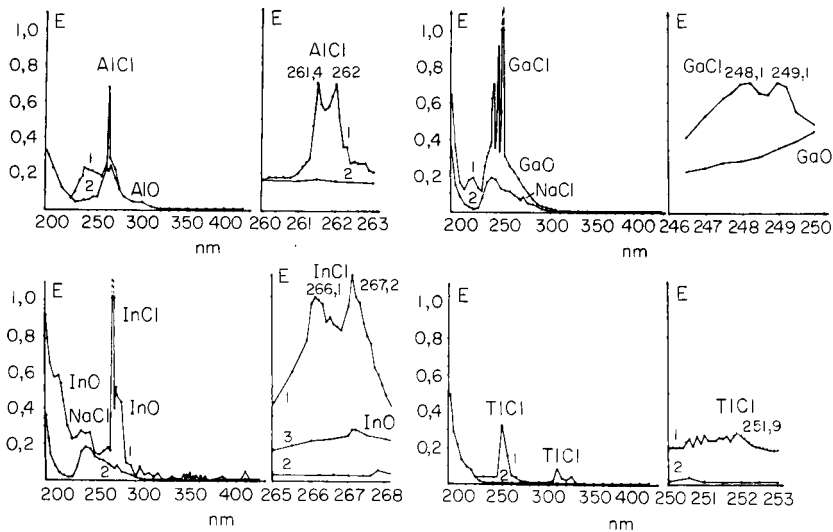


Abb. 1. Molekülabsorptionsspektren von AlCl-, GaCl-, InCl- und TiCl-Molekülen bei Verdampfung in einer Graphitrohrküvette. Kurven 1: $2 \mu\text{g Al}^{3+}/10 \mu\text{l}$; $10 \mu\text{g Ga}^{3+}$ bzw. In^{3+} bzw. $\text{Ti}^{4+}/10 \mu\text{l}$ (als NO_3^-); $10 \mu\text{g Cl}^-/10 \mu\text{l}$ (als NaCl). Kurven 2: Wie 1 ohne Cl^- .

und schwach. Einesteils ist das auf die niedrige Dissoziationsenergie dieses Moleküls (Tab. 1) und andererseits auf die relativ hohe, bei der Absorption aufgenommene Energiemenge zurückzuführen. Bei der Absorption geht dieses Molekül demzufolge in einen instabilen Zustand über. Durch Prädissoziation oder andere Effekte ergibt sich somit die große Bandenbreite. Detaillierte analytische Untersuchungen erfolgten nicht.

Gegenüber den bisher beschriebenen MeX-MA-Banden (mit $\text{X} = \text{F}$ [26], Br [27], J [28]) ergibt sich ein Unterschied: alle drei Moleküle verfügen über zwei ähnlich intensive Bandenmaxima (Tab. 1). Zum Zweck der analytischen Anwendung mußten Wellenlängen für die Untergrundkompensation gefunden werden, denn alle MeCl-Banden überlappen mit breiten MeO-Banden. Die optimalen Wellenlängen wurden in Tab. 2 zusammengestellt.

Untersuchung der thermischen Bedingungen der Verdampfung und Molekülbildung

In der Abb. 2 wurde die Abhängigkeit der Intensität der AlCl-, GaCl- und InCl-MA von den thermischen Bedingungen dargestellt. Die Abhängigkeit von der Veraschungstemperatur verläuft bei allen Molekülen ähnlich, d.h. mit zunehmender Veraschungstemperatur nimmt die Extinktion ab. Das ist auf die vorzeitige Verdampfung von Cl-Apezies zurückzuführen. Da die AlCl-MA bereits bei relativ niedrigen Temperaturen zurückgeht (Abb. 2A, Kurve 1), ist die Ursache der Signaldepression nicht in der Verdampfung der metallischen Komponente zu sehen, denn das Al siedet höher

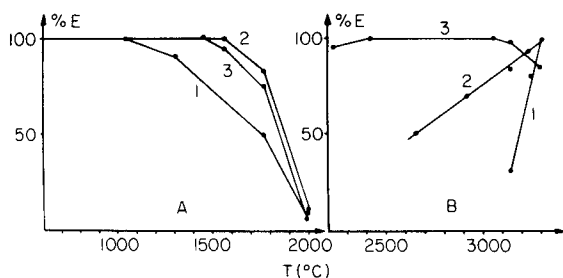


Abb. 2. Abhängigkeit der relativen Extinktion der MA von AlCl (1), GaCl (2) und InCl (3) Molekülen von den thermischen Bedingungen der Graphitrohrküvette. (A) Temperatur der Veraschungsphase variiert; Messung der Extinktion in der Verdampfungsphase. (B) Temperatur der Verdampfungsphase variiert.

als die anderen Metalle. Wahrscheinlicher ist es, daß sich die thermische Hydrolyse bei dem relativ schwach basischen Aluminium bereits bei relativ niedrigen Temperaturen durch HCl-Abspaltung auswirkt. Die in Abb. 2B dargestellte Abhängigkeit der Extinktion von der Atomisierungstemperatur unterstreicht diese Aussage. Die maximale Extinktion wird bei der AlCl- und GaCl-MA bei den thermischen Maximalparametern der Apparatur erzielt. Bei diesen Bedingungen ergibt sich eine optimale Übereinstimmung der Verdampfungszeiten der Me- und Cl-Spezies, so daß folglich hohe MeCl-Konzentrationen zu erwarten sind. Infolge des höheren Siedepunktes des Aluminiums ergibt sich die stärkere Temperaturabhängigkeit (Abb. 2B, Kurve 1). In Gegenwart von Indium, welches einen niedrigeren Siedepunkt hat, wird bereits bei relativ niedrigen Temperaturen der Verdampfung dieses optimale Me/Cl-Verhältnis erzielt. Steigert man die Temperatur weiter, so setzt die Dissoziation des InCl-Moleküls ein, denn dieses ist weniger stabil als GaCl und AlCl (vgl. Tab. 1). Dies führt zu einer Abnahme der Extinktion bei hohen Temperaturen (Abb. 2B, Kurve 3). Aus diesen Untersuchungen wurden die in Tab. 2 zusammengefaßten optimalen thermischen Bedingungen abgeleitet.

Einfluß der Metallkonzentration

In der Abb. 3 wird der Einfluß der Metallkonzentration auf die Intensität der MA dargestellt. Entsprechend der durch die Me-Erhöhung nach $\text{Me} + \text{Cl} \rightleftharpoons \text{MeCl}$ günstigen Beeinflussung des Gleichgewichts ergibt sich auch in jedem Fall eine Erhöhung der MeCl-MA. Für die AlCl-MA wird schnell ein konstanter Endwert erreicht. Der Grund dafür ist die hohe Stabilität des AlCl-Moleküls (Tab. 1). Andererseits sind hohe Al-Mengen wegen der schlechten Verdampfbarkeit des Al nicht einsetzbar (Memory-Effekte). Entsprechend den abnehmenden Molekülstabilitäten werden für optimale GaCl-MA- und InCl-MA-Werte größere Überschüsse an Gallium (4 μg) bzw. Indium (10 μg) benötigt. Die deutliche Abnahme der GaCl-MA bei noch höheren Ga-Mengen kann nicht über das Gleichgewicht erklärt werden. Wahrscheinlich spielen Verdampfungseffekte eine Rolle. Außerdem

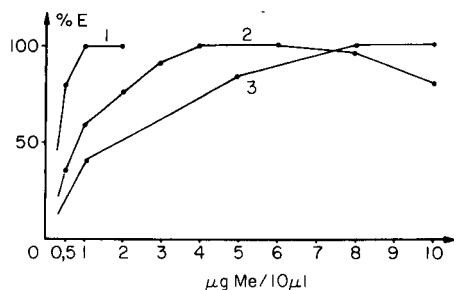


Abb. 3. Abhängigkeit der relativen Extinktion der MA von AlCl (1), GaCl (2) und InCl (3) Molekülen von der jeweiligen Me-Konzentration.

ist es möglich, daß die Absolutmenge des vorhandenen Chlorids einen Einfluß ausübt. Für hohe Chloridmengen ergeben sich somit immer kleinere Extinktionszunahmen. Gekrümmte Eichkurven sind das Resultat.

Unter Berücksichtigung dieser Gesichtspunkte wurden folgende optimale Me-Konzentrationen gewählt: Al^{3+} 1 $\mu\text{g}/10 \mu\text{l}$; Ga^{3+} 4 $\mu\text{g}/10 \mu\text{l}$; In^{3+} 10 $\mu\text{g}/10 \mu\text{l}$.

Einfluß von Na^+ -, Sr^{2+} - und Ba^{2+} -ionen

Bereits bei der Untersuchung anderer Molekülabsorptionen, z.B. der MeF-MA [26], hatten wir sowohl depressive als auch signalerhöhende Einflüsse gefunden. Auch Tsunoda et al. [24] berichten über den positiven Einfluß von Sr^{2+} -ionen und depressive Wirkungen durch Alkaliionen bei der AlCl-MA. Aus diesen Gründen wurden von uns systematische Untersuchungen des Einflusses der Alkali- und Erdalkaliionen auf die AlCl-, GaCl- und InCl-MA durchgeführt.

Im Fall der AlCl-MA wurde festgestellt, daß die Gegenwart von Na^+ -, K^+ -, Sr^{2+} - und Ba^{2+} -ionen einen positiven, signalerhöhenden Einfluß ausübt. Da die Zugabe der Kationen in Form der Hydroxide erfolgte, ergab sich gleichzeitig eine Erhöhung des pH-Wertes. Die Ergebnisse der Untersuchungen sind in der Abb. 4 dargestellt worden. Die Kurven 1'—3' stellen den unspezifischen Untergrund dar. Gegenüber der Gesamtextinktionserhöhung ist die Untergrunderhöhung unwesentlich. Der Abzissenmaßstab wurde so gewählt, daß die Zugaben hinsichtlich der OH^- -Konzentration gleich sind. Daraus folgt, daß die Ionenkonzentrationen für Ba^{2+} und Sr^{2+} gleich, die der Na^+ -ionen jedoch doppelt so groß sind. Deutlich ist aus den Kurven die starke Zunahme der Extinktion der AlCl-MA in Gegenwart der ausgewählten Ionen zu erkennen. Auffällig ist der starke Unterschied zwischen Alkalien und Erdalkalien. Zur Aufklärung dieser Einflüsse wurden zunächst die Auswirkungen der Kationen auf die GaCl- und InCl-MA untersucht. Diese Ergebnisse wurden ebenfalls in der Abb. 4 dargestellt. Wegen der Schwerlöslichkeit von $\text{Ga}(\text{OH})_3$ und $\text{In}(\text{OH})_3$ konnte die Zugabe von NaOH , $\text{Sr}(\text{OH})_2$ und $\text{Ba}(\text{OH})_2$ nur bis zu den angegebenen Grenzen erfolgen. Deutlich ist zu erkennen, daß

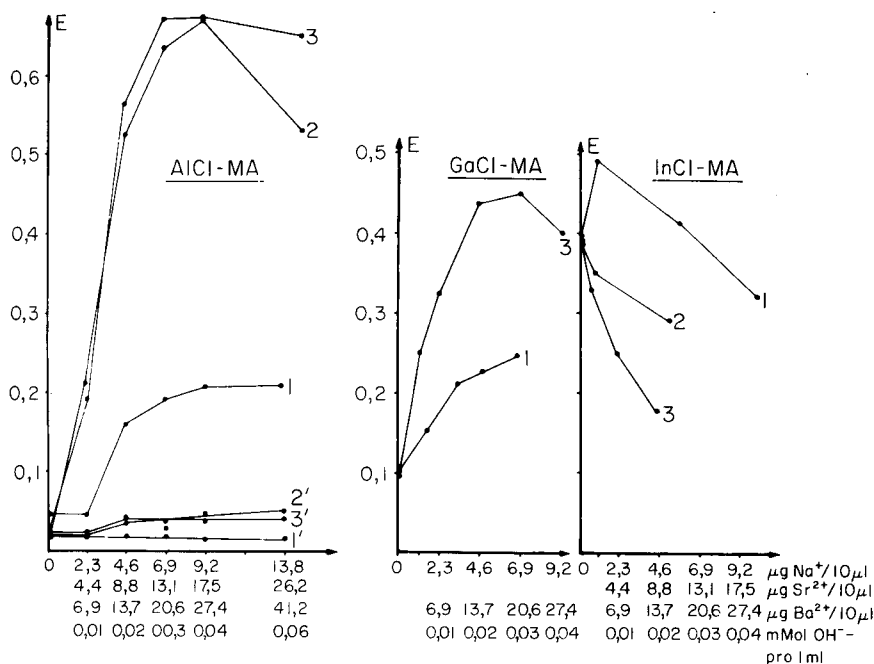


Abb. 4. Abhängigkeit der MA der AlCl-, GaCl- und InCl-Moleküle von der Gegenwart von Zusatzstoffen (Erdalkalien). Kurven 1', 2', 3' stellen den unspezifischen Untergrund dar.

der Einfluß gegenüber dem bei der AlCl-MA kleiner ist. Stellen wir für die GaCl-MA noch eine Steigerung fest, so ist bereits deutlich die depressive Wirkung der Kationen auf die InCl-MA zu erkennen. Zu berücksichtigen ist dabei allerdings, daß die zusatzfreie Lösung bei der InCl-MA die höchsten Werte liefert.

Folgende Gründe sind u.E. für diese Einflüsse verantwortlich. Der Anstieg der Extinktionswerte der zusatzfreien Lösungen nach AlCl, GaCl und InCl ist auf die zunehmende Basizität der Kationen zurückzuführen. Infolge dieser Basizität wird die thermische Hydrolyse in der Trocknung und Veraschung zurückgedrängt. Das bedeutet, daß in der Verdampfungsphase in Gegenwart von In^{3+} -ionen die größte Cl-Menge zur MeCl-Bildung zur Verfügung steht. Ein Hauptfaktor für die Extinktionssteigerung durch die Zusätze liegt ebenfalls in der Zurückdrängung der thermischen Hydrolyse. In Gegenwart der Zusätze bilden sich während der Trocknung NaCl, SrCl_2 (SrOHCl), BaCl_2 (BaOHCl). Diese Salze sind thermisch stabil und erleiden keine thermische Hydrolyse. Somit steht während der Verdampfung eine hohe Cl-Menge für die MeCl-Bildung zur Verfügung. Diesem positiven Einfluß wirkt ein anderer Effekt entgegen. Dieser besteht darin, daß auch die zugefügten Zusätze mit dem Chlor zwei -atomige Moleküle bilden können. Die Dissoziations-

energien sind: NaCl 4,3 eV; SrCl 4,3 eV; BaCl 4,6 eV. Vergleicht man diese Werte mit denen der Tab. 1 (AlCl, GaCl, InCl), so findet man beim InCl nahezu den gleichen Wert. Das bedeutet, daß die InCl-Konzentration mit zunehmender Konzentration der anderen Metalle am stärksten zurückgedrängt wird.

Eine Klärung des stärkeren, signalerhöhenden Einflusses der Ba^{2+} - und Sr^{2+} -ionen gegenüber den Na^{+} -ionen auf die AlCl- und GaCl-MA ist auf der bisherigen Basis nicht möglich. Es ist zu vermuten, daß es sich um einen Verdampfungseffekt handelt. Aus diesem Grund wurden bei der AlCl-MA Extinktions—Zeit-Kurven für verschiedene Substanzen aufgenommen. In der Abb. 5 sind die Resultate dargestellt worden: die AlCl-MA (Kurve 1) stark mit der Al-AA (Kurve 2) überlappt, d.h. erst wenn genügend Al-Atome verdampft sind, bildet sich eine ausreichende AlCl-Menge im Plasma. Die Extinktions—Zeit-Kurve (Kurve 3) für die NaCl-MA zeigt, daß der größte Teil des NaCl weit vor dem Al verdampft, somit ist der größte Teil des Chlorids schon entfernt, wenn die Al-Atome verdampfen. Somit müßte eine Verzögerung der Cl-Verdampfung zu einer Verbesserung der AlCl-Molekülbildung führen. Nach den Siedepunkten von NaCl, SrCl_2 und BaCl_2 ist eine solche Verzögerung nicht zu erwarten. Geht man jedoch davon aus, daß diese Salze bei den Erdalkalien wegen des Unterschusses des Chlorids als $\text{SrCl}(\text{OH})$ bzw. $\text{BaCl}(\text{OH})$ vorliegen, so kann man die eigentliche Verdampfung besser durch die Verfolgung der Verdampfung der Ba- bzw. Sr-Atome über die Ba-AA bzw. Sr-AA (Kurven 4 und 5) ermitteln. Es ist in der Abb. 5 zu erkennen, daß das Maximum der Ba- bzw. Sr-AA nach dem der Al-AA bzw. AlCl-MA liegt. Ursache dafür ist die starke Carbidbildungstendenz des Ba bzw. Sr. Es ist denkbar, daß durch diese Verhältnisse auch Chlor-Spezies, die an Ba bzw. Sr gebunden sind, relativ spät verdampfen. Damit ergibt sich eine

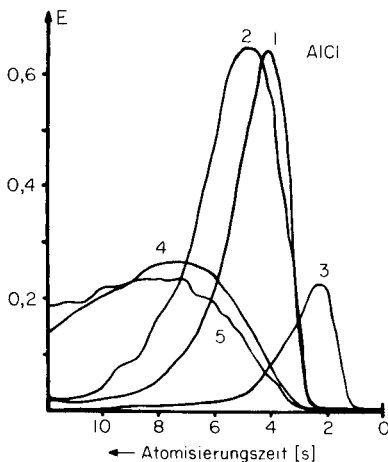


Abb. 5. Extinktions—Zeit-Kurven der Verdampfungsphase in der Graphitrohrküvette: (1) AlCl-MA; (2) Al-AA; (3) NaCl-MA; (4) Ba-AA; (5) Sr-AA.

bessere Überlappung mit der Al-Verdampfung und somit eine optimale AlCl-Konzentration im Plasma. In Gegenwart von Gallium wurden die gleichen Untersuchungen durchgeführt, die zu ähnlichen Ergebnissen führten.

Aus diesen Untersuchungen ergeben sich folgende optimale Bedingungen: AlCl-MA, 20,6 $\mu\text{g Ba}^{2+}/10 \mu\text{l}$; GaCl-MA, 13,6 $\mu\text{g Ba}^{2+}/10 \mu\text{l}$; InCl-MA, ohne Zusatz. Zur weiteren Bestätigung der gegebenen Erklärungen wurden in Ergänzung unserer Mitteilungen über die AlF-MA [26] auch für dieses System ähnliche Untersuchungen durchgeführt. Zusatz von Ca^{2+} -, Sr^{2+} - oder Ba^{2+} -ionen führten auch hier gegenüber NaOH zu weiteren Extinktionssteigerungen. Die Extinktions-Zeit-Kurven beweisen einen ähnlichen Verdampfungsverlauf. Die optimalen Werte lagen für die Fluorbestimmung bei 1 $\mu\text{g Al}^{3+}$, 17,5 $\mu\text{g Sr}^{2+}$ oder 27,5 $\mu\text{g Ba}^{2+}/10 \mu\text{l}$.

Einfluß anderer Kationen auf die MeCl-Molekülabsorption

Werden in Gegenwart der optimalen Mengen des molekülbildenden Metallkations und des Zusatzkationes weitere Kationen hinzugefügt, so ergeben sich in jedem Fall Signaldepressionen. Die Resultate sind in Abb. 6 zusammengefaßt. In vielen Fällen besteht die Ursache der Depressionen darin, daß die zugefügten Kationen ebenfalls mit Chlor MeCl-Moleküle im Plasma bilden. Die von Tsunoda et al. [24] beschriebenen zusätzlichen Signal-

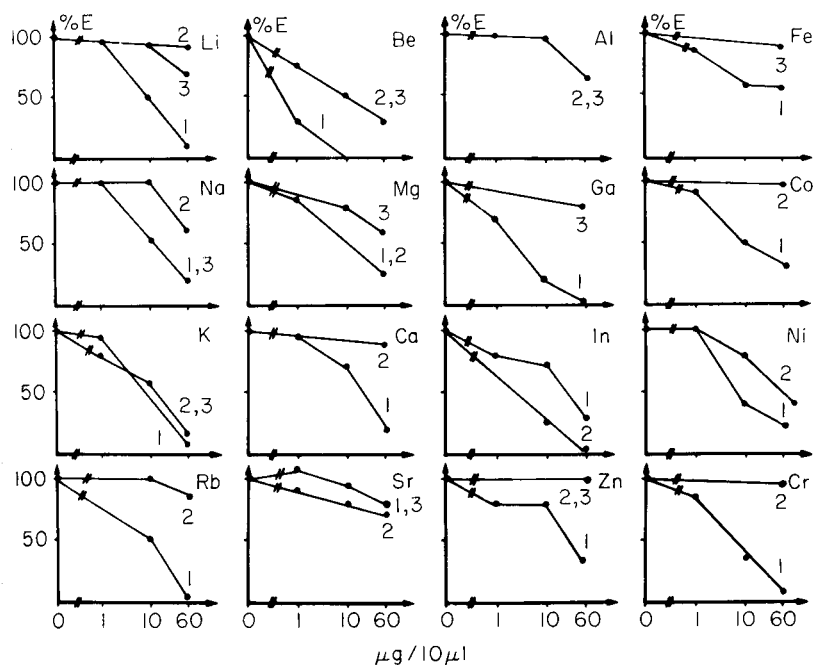


Abb. 6. Abhängigkeit der relativen Extinktion der MA der AlCl (1), GaCl (2) und InCl (3) Moleküle von der Konzentration anderer Kationen (in Gegenwart optimaler Konzentrationen von Zusatzstoffen, vgl. Text).

erhöhungen bei Gegenwart von zwei Zusatzkationen, wie z.B. Ba^{2+} und Co^{2+} konnten nicht bestätigt werden. Auch die angegebene Untergrunderniedrigung durch Zusätze wurde von uns nicht gefunden, da wir insgesamt nur einen geringen Untergrund feststellten. Auf Grund dieser Feststellungen ist die Additionstechnik für unbekannte Proben zu empfehlen.

RESULTATE UND DISKUSSION

Analytische Ergebnisse

Unter Verwendung der optimalen Bedingungen wurden für die Bestimmung des Chlorids die in der Abb. 7 und Tab. 3 dargestellten Resultate erhalten. Es ist ersichtlich, daß die AlCl-MA am besten für die Chloridbestimmung geeignet ist. Danach folgt die InCl- und die GaCl-MA . Die von uns erhaltenen Werte sind schlechter als die von Tsunoda et al. [24] für die AlCl-MA , jedoch besser als die von Yoshimura et al. [23] für die InCl-MA erzielten. Weiterhin ist festzustellen, daß über einen Bereich von 1,5–2 Zehnerpotenzen eine lineare Beziehung zwischen Extinktion und Konzentration vorliegt. Durch Einsatz des Ba^{2+} konnten auch die Werte für die Fluoridbestimmung [26] etwas verbessert werden.

Die Angabe des Nachweisvermögens als reziproke Empfindlichkeit pro 0,01 Extinktion entspricht der Nachweisgrenze und ermöglicht einen besseren Vergleich. Eine Verbesserung des relativen Nachweisvermögens ist durch Einsatz von größeren Probevolumina im begrenzten Umfang möglich. Bezogen auf andere Kationen sind nach der Additionstechnik Bestimmungen des Chlorids für Konzentrationsverhältnisse $\text{Cl}^-:\text{M}$ wie 1:1 bis 10^5 möglich (vgl. Abb. 6).

Einfluß anderer Halogenide auf die MeCl-MA

In der Abb. 8 ist der Einfluß der anderen Halogenide auf die Chloridbestimmung dargestellt. Bei Anwendung der AlCl- und GaCl-MA ist der Einfluß des Fluorids am stärksten. Dies ist auf die hohe Stabilität von AlF und GaF zurückzuführen. Durch die Bildung dieser Moleküle wird die Me-Konz.

TABELLE 3

Ergebnisse der Bestimmung des Chlorids und des Fluorid

Molekül	Reziproke Empfindlichkeit pro 0,01 Extinktion	
	ng X^-	(M) ^a
AlCl	1,5	4×10^{-6}
GaCl	9	$2,5 \times 10^{-5}$
InCl	3	8×10^{-6}
AlF	0,3	$1,6 \times 10^{-6}$

^aProbeinsatz 0,01 ml.

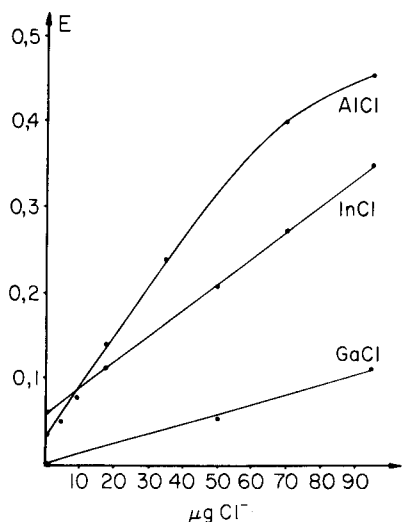


Abb. 7. Eichkurven für die Cl^- -Spurenbestimmung durch AlCl_3 , GaCl_3 und InCl_3 -MA.

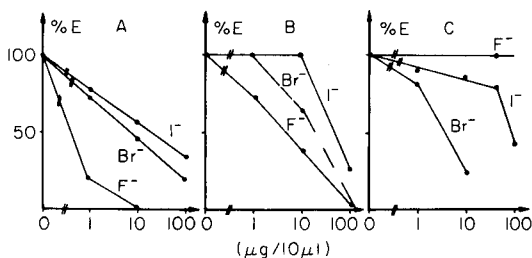


Abb. 8. Abhängigkeit der relativen Extinktion der (A) AlCl_3 -, (B) GaCl_3 - und (C) InCl_3 -MA in Gegenwart anderer Halogenide.

tration und damit die MeCl -Konzentration im Plasma erniedrigt. Bei Einsatz der InCl_3 -MA tritt diese Depression nicht auf. Das Fluorid wird in der Trocknung und Veraschung durch thermische Hydrolyse als HF abgetrennt, da in diesem Fall ohne Zusätze gearbeitet wird, welche das Fluorid stabilisieren würden, wie dies als BaF_2 bzw. SrF_2 bei der AlCl_3 -MA der Fall ist. Somit ist in Gegenwart von Fluorid die InCl_3 -MA am besten geeignet für die Chloridbestimmung (mögliches Konzentrationsverhältnis: $\text{Cl}^-:\text{F}^-$ wie $1:10^5$). Hinsichtlich der schweren Halogenide Bromid und Jodid gibt es die erwarteten depressiven Effekte. Jodid ist von geringerem Einfluß. In beiden Fällen sind jedoch Chloridbestimmungen bei Konzentrationsverhältnissen von $\text{Cl}^-:\text{Br}^-/\text{J}^-$ wie $1:10^3/10^4$ möglich. In dieser Hinsicht ist diese Methode den ionensensitiven Elektroden überlegen.

Allgemeine Diskussion der analytischen Anwendung der MAS

Aus den bisherigen Untersuchungen zur analytischen Anwendung der MAS mit elektrothermischer Verdampfung lassen sich einige allgemeine Gesichtspunkte ableiten. Zur Erzielung einer optimalen Linie—Untergrund-Verhältnisses benötigt man ein hohes Signal und einen möglichst niedrigen Untergrund. Ein hohes Signal läßt sich erzielen, wenn eine hohe Molekkonzentration des Analyten im Plasma vorliegt, und wenn diese Moleküle einen hohen Absorptionskoeffizienten besitzen. Eine hohe Molekkonzentration kann durch Anwendung von Molekülen mit hohen Dissoziationsenergien, durch niedrige Plasmatemperaturen und durch gleichzeitige Ver-

dampfung der beiden molekülbildenden Spezies hervorgerufen werden. Der niedrige Untergrund ist hingegen erzielbar bei hohen Plasmatemperaturen, da dann geringes Streulicht und geringe Fremd-MA auftritt. Da diese Bedingung der obigen entgegengerichtet ist, muß in jedem Fall ein Optimum ermittelt werden. Durch thermische Matrix-Spur-Trennungen in der Graphitrohrküvette sind ebenfalls Erniedrigungen des Untergrundes möglich. Trotzdem sind praktisch in jedem Fall apparative Komensationen des Untergrundes notwendig.

Um diese Zielstellung erreichen zu können, müssen bei der Probeherstellung bzw. bei ihrer thermischen Behandlung folgende Gesichtspunkte berücksichtigt werden:

Lösungsherstellung. Man wählt einen möglichst großen Me-Überschuß, um die Lage des Gleichgewichts $\text{Me} + \text{X} \rightleftharpoons \text{MeX}$ entsprechend zu beeinflussen. Durch weitere Zusatzstoffe wie z.B. Alkaliionen verhindert man oftmals eine Verflüchtigung leicht flüchtiger Anionen. Man verwendet gegebenenfalls, auch Laugen um den pH-Wert zu erhöhen.

Trocknung. Das Ziel dieser Phase besteht darin, aus der Lösung einen Feststoff zu erhalten. Das Problem dieses Schrittes kann in einer Verflüchtigung leicht flüchtiger Säuren durch schwache, aber schwerer flüchtiger Säuren bestehen. Man kann auch diesem Effekt durch vorherigen Alkalizusatz entgegenwirken.

Veraschung. Das Ziel dieser Phase besteht in der Gewinnung eines definierten Feststoffes in der Graphitrohrküvette. Dabei ist es günstig, wenn es gelingt, während der thermischen Behandlung einen Teil der Matrix abzutrennen. Das Problem dieser Phase ist die thermische Hydrolyse, die zur Verflüchtigung von HX führt. Diesem Effekt kann man durch Zugabe von Alkalien oder Erdalkalien oder auch durch Verwendung schwer löslicher, thermisch stabiler Salze (wie TlBr oder TlI) entgegenwirken. Selbstverständlich sind die thermischen Parameter wie Maximaltemperatur und Aufheizgeschwindigkeit dieses Schrittes zu optimieren.

Molekülbildung und Verdampfung. Das Ziel dieser Phase ist die Erzeugung einer hohen Molekülkonzentration (MeX) im Plasma durch gleichzeitige Verdampfung des Me-Überschusses mit der zu bestimmenden X-Spur. Das Problem dieser Phase besteht meist darin, daß die X-Komponente oft leichter flüchtig als die Me-Komponente ist. Es gibt verschiedene Möglichkeiten, diesem Problem entgegenzuwirken. Einmal kann man leicht flüchtige Me-Komponenten verwendet (z.B. Tl, Mg Ag u.a.), zum anderen kann man durch Zusatzstoffe eine Verlangsamung der Verdampfung der X-Komponente erreichen, wie dies durch die BaCl_2 -Bindung bei der AlCl-MA der Fall ist.

LITERATUR

- 1 M. M. Goldstein und I. G. Judelewitsch, Zh. Anal. Khim., 31 (1976) 870.
- 2 F. Beilstein, Ber. Dtsch. Chem. Ges., 5 (1872) 620.
- 3 C. E. van der Smissen, U.S. Patent, 3025 141, März 1962.
- 4 P. T. Gilbert, Anal. Chem., 38 (1966) 1920.

- 5 B. Gutsche, R. Herrmann und K. Rüdiger, *Fresenius Z. Anal. Chem.*, 241 (1968) 54.
- 6 B. Gutsche und R. Herrmann, *Fresenius Z. Anal. Chem.*, 242 (1968) 13; 245 (1969) 274.
- 7 R. Herrmann und B. Gutsche, *Analyst*, 94 (1969) 1033.
- 8 G. Henrion und D. Marquardt, *Z. Chem.*, 17 (1977) 28.
- 9 R. Belcher, S. L. Bogdanski, Z. M. Kassir, D. A. Stiles und A. Townshend, *Anal. Lett.*, 7 (1974) 751.
- 10 N. Furuta, E. Yoshimura, H. Haraguchi und K. Fuwa, *Spectrochim. Acta*, 33B (1978) 715.
- 11 B. R. Culver und T. Surles, *Anal. Chem.*, 47 (1975) 920.
- 12 M. W. Pritchard und R. D. Reeves, *Anal. Chim. Acta*, 82 (1976) 103.
- 13 H. Haraguchi, M. Shiraishi und K. Fuwa, *Chem. Lett.*, (1973) 251.
- 14 H. Haraguchi und K. Fuwa, *Bull. Chem. Soc. Jpn.*, 48 (1975) 3056.
- 15 K. Dittrich, S. Schneider, B. Ja. Spiwakow, L. W. Suchowejewa und Ju. A. Zolotow, *Spectrochim. Acta*, 34B (1979) 257.
- 16 K. Fujiwara, H. Haraguchi und K. Fuwa, *Anal. Chem.*, 47 (1975) 1670.
- 17 T. Nakahara und S. Musha, *Anal. Chim. Acta*, 80 (1975) 47.
- 18 S. Yasuda und H. Kakiyama, *Anal. Chim. Acta*, 89 (1977) 369.
- 19 K. Dittrich, W. Mothes und P. Weber, *Spectrochim. Acta*, 33B (1978) 325.
- 20 W. Frech und A. Cedergren, *Anal. Chim. Acta*, 82 (1976) 93.
- 21 K. Dittrich, *Progr. Anal. Atom. Spectrosc.*, im Druck.
- 22 K. Dittrich, *Anal. Chim. Acta*, 97 (1978) 59.
- 23 E. Yoshimura, Y. Tanaka, K. Tsunoda, S. Toda und K. Fuwa, *Bunseki Kagaku*, 26 (1977) 643.
- 24 K. Tsunoda, K. Fujiwara und K. Fuwa, *Anal. Chem.*, 50 (1978) 861.
- 25 B. Rosen (Ed.), *International Tables of Selected Constants*, 17, *Spectroscopic Data Relative to Diatomic Molecules*, Pergamon, Oxford, 1970.
- 26 K. Dittrich, *Anal. Chim. Acta*, 97 (1978) 69; 111 (1979) 123.
- 27 K. Dittrich und S. Schneider, *Anal. Chim. Acta*, 115 (1980) 189.
- 28 K. Dittrich und S. Schneider, *Anal. Chim. Acta*, 115 (1980) 201.

BREAKDOWN OF ORGANIC MERCURY COMPOUNDS BY HYDROCHLORIC ACID—PERMANGANATE OR BROMINE MONOCHLORIDE SOLUTION FOR THE DETERMINATION OF MERCURY BY COLD-VAPOUR ATOMIC ABSORPTION SPECTROMETRY

O. SZAKÁCS, A. LÁSZTITY and ZS. HORVÁTH*

Institute of Inorganic and Analytical Chemistry, L. Eötvös University, PO Box 123, 1443 Budapest (Hungary)

(Received 21st April 1980)

SUMMARY

Hydrochloric acid—potassium permanganate and bromine monochloride are examined for the decomposition of methylmercury(II) chloride, Ceresan, phenylmercury(II) borate and thiomersal added to waters. Both procedures give quantitative recovery of mercury. Bromine monochloride has many advantages: blanks are low, the limit of detection (3σ) is $0.06 \mu\text{g Hg l}^{-1}$, routine work is simplified because only two reagents are needed and the reaction time is 5–10 min. The reagent also acts as a preservative. Common contaminants (chloride, bromide, sulphide, alcohols, benzene) do not interfere.

The cold-vapour atomic absorption technique for the determination of mercury in water is very widely applied [1]. The determination requires that all mercury compounds present be converted to elemental mercury. For the degradation of organomercurials, numerous oxidizing agents such as potassium permanganate, hydrogen peroxide, potassium persulphate or potassium dichromate in acidic media have been examined. An automatic method with ultraviolet irradiation for the determination of total mercury in fresh and saline waters was reported by Agemian and Chau [2] who found this method (in the presence of potassium dichromate and sulphuric acid as preservatives) to be the best of the oxidation procedures investigated. Recovery of organic mercury was poor when a potassium permanganate—potassium persulphate—sulphuric acid digestion was used. A collaborative study to establish a standard method for the determination of total mercury in water samples has been reported [3]. It was found that ultraviolet irradiation in the presence of potassium dichromate and nitric acid or sulphuric acid gave low blanks but total recovery of mercury failed in the presence of organic solvents like methanol, ethanol and isopropanol.

Organomercurials can be degraded with halogens according to the following equations [4]: $\text{HgR}_2 + \text{X}_2 \rightleftharpoons \text{RHgX} + \text{RX}$; $\text{RHgX} + \text{X}_2 \rightleftharpoons \text{HgX}_2 + \text{RX}$ ($\text{X} = \text{Br}, \text{Cl}$). For the decomposition of organomercurials in various waters, Becknell et al. [5] used chlorine gas, Farey et al. [6, 7] and Nelson [8] a

bromate—bromide reagent in hydrochloric acid, and Olafsson [9] bromine vapour.

The purpose of the work reported here was to unify the oxidizing and destructive effects of potassium permanganate and chlorine by using a hydrochloric acid—potassium permanganate treatment to break down organomercurials in water. A rapid and simple procedure based on bromine monochloride was also developed. Conversion to bromine monochloride increases the reactivity of bromine [10]. The bromine monochloride reagent was prepared by mixing bromate and bromide in a mole ratio of 1:2 in hydrochloric acid, as described by Schulek and Burger [10]. The total mercury content of tap water and various waters was determined by the two procedures. Experiments were done on the time and concentration dependence of the breakdown of organomercurials like phenylmercury(II) borate, Ceresan, thiomersal and methylmercury(II) chloride. The limit of detection and the coefficient of variation were determined, and the effects of possible interfering ions and organic solvents were investigated.

EXPERIMENTAL

Reagents

All reagents were of analytical-reagent grade. High-purity water (mercury-free), prepared by passing distilled water through a column of cellulose ion-exchangers [11], was used for all solutions. For working out the procedures, tap water was spiked with organomercurials; Budapest tap water did not contain detectable mercury. The hydrochloric acid used (12 M; Carlo Erba or Reanal) was tested and found to be free of mercury.

Tin(II) chloride (10% w/v) solution. Dissolve 10 g of tin(II) chloride dihydrate in 110 ml of 2 M hydrochloric acid. Add 2 or 3 pieces of tin metal to the solution. Mercury traces usually present in the salt are removed by boiling the solution. Cool to room temperature and dilute to 100 ml if necessary.

Stock organomercurial solutions. Phenylmercury(II) borate ($C_6H_5HgOH \cdot C_6H_5HgBO_2$), thiomersal ($C_2H_5Hg \cdot S \cdot C_6H_4COONa$; Takeda Chemical Industries, Japan), and Ceresan ($CH_3OC_2H_4HgCl$; caustic mercury content, 25 mg g^{-1} ; Bayer FRG) were each dissolved in water to give 0.1–1 mg $Hg\ l^{-1}$ solutions. Methylmercury(II) chloride (CH_3HgCl ; Merck—Schuchardt) was dissolved in acetone [12]; this stock solution was diluted with water as required.

Bromine monochloride standard solution (0.05 M). Dissolve 2.784 g of potassium bromate and 3.967 g of potassium bromide in a 1-l standard flask in 400–600 ml of water. Add 200 ml of 12 M hydrochloric acid, mix and cool to room temperature. Dilute to volume. Small changes in the titre of this solution do not influence the procedure.

Cleaning of glassware. Before use, the glassware was soaked in 0.05 M bromine monochloride solution for at least 30 min and then rinsed with high-purity water. Bromine monochloride solution proved to be highly effective in removing mercury contamination from glassware.

Apparatus

A Perkin-Elmer Model 303 atomic absorption spectrometer was used with a Perkin-Elmer mercury hollow-cathode lamp (253.6 nm, slit width 0.7 nm, lamp current 6 mA) and a Hitachi-Perkin-Elmer recorder. For the cold-vapour technique, a MOM mercury detection unit (MOM, Hungary) was used.

Procedures

Procedure 1. Hydrochloric acid—potassium permanganate method. Transfer 8.3 ml of 12 M hydrochloric acid to a 100-ml standard flask and make up to volume with the water sample. Mix by shaking. Add 0.6 ml of potassium permanganate solution (6% w/v, from the recrystallized salt), swirl to mix and allow to stand for at least 30 min at room temperature. Just prior to mercury cold-vapour determination, add 1 or 2 drops of concentrated hydrogen peroxide (30% w/v) solution and mix carefully. The oxidation can also be terminated with 0.2 ml of hydroxylammonium chloride solution (20% w/v).

Procedure 2. Bromine monochloride method. Transfer about 80 ml of the water sample to a 100-ml standard flask, add 10 ml of the 0.05 M bromine monochloride solution and dilute to volume with the rest of the water sample immediately. Mix thoroughly. Allow to stand for at least 10 min at room temperature. Just prior to the cold-vapour determination of mercury, add 0.1 ml of hydroxylammonium chloride solution (20% w/v) to reduce the excess of bromine monochloride. When the solution is completely decolourized, which takes only seconds, mercury can be determined by the cold-vapour atomic absorption method.

Determination of mercury content by cold-vapour atomic absorption spectrometry. Transfer a 10.0-ml aliquot of the water sample treated as above to the sample cell of the mercury detection unit. Add 1 ml of the tin(II) chloride solution to the sample, stir magnetically and allow to stand for 1 min. Open the stopcocks and let air blow through the sample. Measure the absorbance at 253.7 nm. The calibration curves of absorbance versus mercury content are linear up to $10 \mu\text{g Hg l}^{-1}$. The magnesium perchlorate used as desiccant in the drying tube of the unit should be changed after every thirty determinations.

RESULTS AND DISCUSSION

Table 1 shows the time dependence of the recovery of inorganic mercury from tap water spiked with methylmercury(II) chloride, Ceresan, or phenylmercury(II) borate following hydrochloric acid—potassium permanganate breakdown. It should be noted that the decomposition of methylmercury(II) chloride is slow and is still incomplete after reaction for 30 min when the excess of oxidant is destroyed with hydroxylammonium chloride. When the reaction is terminated with hydrogen peroxide, the recoveries are much better, which means that hydrogen peroxide takes part in the decomposition

TABLE 1

Recoveries of inorganic mercury from organomercurials^a added to tap water after the hydrochloric acid—potassium permanganate treatment

Time (min)	Recovery (%)		Ceresan	Phenylmercury(II) borate
	CH ₃ HgCl			
	I ^b	II ^c		
1	—	—	71	29
2	—	—	91	58
5	48	90	95	96
10	79	95	96	98
15	84	95	—	—
20	90	—	—	—
30	95	100	100	100
180	100	100	101	—

^aFor CH₃HgCl, 5 µg Hg l⁻¹; for other compounds, 10 µg Hg l⁻¹. ^bAddition of hydroxyl-ammonium chloride. ^cAddition of hydrogen peroxide.

of methylmercury(II). The limit of detection (3σ) of the method is 0.12 µg Hg l⁻¹.

The decomposition of methylmercury(II) with bromine monochloride is rapid. Table 2 shows the dependence of the decomposition of the organomercurials investigated on the reaction time and on the concentration of the bromine monochloride. While Ceresan, phenylmercury(II) borate and thiomersal can be destroyed very easily, the full recovery of mercury from methylmercury(II) chloride in tap water requires 0.005 M bromine monochloride and a 5-min reaction time. In environmental pollution, methylmercury(II) is the most frequent and the main toxic form of mercury in natural waters [13]. Bromine monochloride is a good reagent for decomposing this compound prior to the determination of mercury. Its advantages are similar to those of the brominating reagent used by Farey et al. [6, 7], i.e. it can be used on site as a preservative, and it destroys organomercurials rapidly. The bromine monochloride procedure is good for routine work, because it needs only two reagents (bromine monochloride and hydroxyl-ammonium chloride). Bromine monochloride has a low blank value, and the limit of detection (3σ) is 0.06 µg Hg l⁻¹, which is less than the value found for the chemical methods [3]. The coefficients of variation of the hydrochloric acid—potassium permanganate and of the bromine monochloride methods are shown in Table 3.

Finally, the possible interferences of different ions (chloride, bromide, sulphide) and organic solvents (methanol, ethanol, isopropanol, benzene) in the bromine monochloride procedure were investigated. Sodium chloride (3% w/v), potassium bromide (0.5% w/v), and methanol, ethanol or isopropanol (10–100 µl l⁻¹) had no interfering effect on the determination of mercury in organomercurials. Bromine monochloride eliminated the inter-

TABLE 2

Recoveries of inorganic mercury from organomercurials^a added to tap water after the bromine monochloride treatment

Bromine monochloride (M)	Time (min)	Recovery (%)			
		CH ₃ HgCl	Phenylmercury(II) borate	Thiomersal	Ceresan
0.005	1	79	100	98	100
	5	100			
	10	100			
	30	100	99	100	100
	90	100			
0.0025	1	52	100	98	100
	5	69			
	10	95			
	15	99			
	30	100	102	100	98
0.00125	1	22	100	101	99
	5	55			
	10	82			
	15	95			
	30	100	102	100	100

^aFor CH₃HgCl, 5 µg Hg l⁻¹; for other compounds, 10 µg Hg l⁻¹.

ference of benzene (which absorbs at 254 nm); the recovery of mercury (5 µg l⁻¹) from the organomercurials was quantitative when benzene was present at levels up to 40 mg l⁻¹, and up to 400 mg l⁻¹ can be tolerated if deuterium compensation is used. A mineral water of high sulphide content (Parádi water; 6.4 mg S²⁻ l⁻¹) spiked with methylmercury(II) chloride (2 µg Hg l⁻¹) was analyzed for mercury after the bromine monochloride procedure with excellent recoveries.

TABLE 3

Coefficient of variation for the determination of mercury after the decomposition of phenylmercury(II) borate

Mercury (ng)	Coefficient of variation (%) ^a	
	HCl—KMnO ₄	BrCl
50	2.1	1.03
25	2.1	1.15
5	11.1	5.6
2.5		9.2

^aFrom 11 determinations.

The results of this investigation show that organomercurials in tap water can be converted quantitatively to inorganic mercury at room temperature with either hydrochloric acid—permanganate or bromine monochloride as the reagent. The bromine monochloride reagent has many advantages as the breakdown of methylmercury(II) chloride is rapid, common contaminants do not interfere, and the reagent blank is low. The reagent is also good for cleaning glassware before sampling, and can be used for the preservation of the water samples without loss of mercury after several days standing.

REFERENCES

- 1 A. M. Ure, *Anal. Chim. Acta*, 76 (1975) 1.
- 2 H. Agemian and A. S. Y. Chau, *Anal. Chem.*, 50 (1978) 13.
- 3 Working Party of the Bureau International Technique du Chlore (Bruxelles, Belgium), *Anal. Chim. Acta*, 109 (1979) 209.
- 4 A. N. Nesmeyanov, K. A. Kocheskova and A. G. Makarova, *Metodi elementorganicheskoy khimii Rtuty*, Nauka, Moskva, 1965, p. 275.
- 5 D. E. Becknell, R. H. Marsh and W. Allie, *Anal. Chem.*, 43 (1971) 1230.
- 6 B. J. Farey, L. A. Nelson and M. G. Rolph, *Analyst*, 103 (1978) 656.
- 7 B. J. Farey and A. Nelson, *Anal. Chem.*, 50 (1978) 2147.
- 8 L. A. Nelson, *Anal. Chem.*, 51 (1979) 2289.
- 9 J. Olafsson, *Mar. Chem.*, 6 (1978) 87.
- 10 E. Schulek and K. Burger, *Talanta*, 1—2 (1958) 219.
- 11 Zs. Horváth, *J. Chromatogr.*, 102 (1974) 409.
- 12 N. Velghe, A. Campe and A. Clacys, *At. Absorpt. Newsl.*, 17 (1978) 139.
- 13 Mercury and the environment, Organization for Economic Cooperation and Development, Paris, 1974.

SYNTHESIS AND ANALYTICAL PROPERTIES OF AN N-PHENYL-HYDROXAMIC ACID RESIN

RICHARD J. PHILLIPS and JAMES S. FRITZ*

Ames Laboratory and Department of Chemistry, Iowa State University, Ames IA 50011 (U.S.A.)

(Received 7th April 1980)

SUMMARY

A procedure for attaching N-phenylhydroxamic acid groups to Amberlite XAD-4 is described. The extraction of 20 metal ions from 2 M hydrochloric acid by this resin is discussed. Conditions for the quantitative extraction and back-extraction of 9 ions are reported. The results are compared with work on solvent extraction with N-phenylbenzohydroxamic acid.

The study of polymeric hydroxamic acids was pioneered by Deuel and co-workers, who prepared hydroxamic acid derivatives of Amberlite IRC-50 and other poly(methacrylic acid) resins [1-3]. The products showed a greater affinity for iron(III) than their poly(methacrylic acid) precursors, but little change was seen for copper(II) and zinc(II). Kern and Schulz [4] prepared a linear poly(hydroxamic acid) by hydroxylaminolysis of poly(methyl acrylate); the product gave precipitates with several metal ions.

Schouteden [5] described the conversion of poly(amidoximes) to poly(hydroxamic acids) in about 50% yield by mild hydrolysis. Poly(amidoximes) had been prepared previously by the reaction of poly(acrylonitrile) and hydroxylamine in dimethylformamide [6]. Fetscher [7] obtained a patent for the invention of a radioactive source consisting of a poly(amidoxime) or poly(hydroxamic acid) complexed with a radioactive metal. Conditions were described for the immobilization of Pu, U, Co, and Th with these resins.

Petrie et al. [8] described the preparation of a hydroxamic acid derivative of Amberlite IRC-50 via the sequence acid chloride, methyl ester, hydroxamic acid. The product showed increased retention of V(V), Fe(II, III), Mo(VI), Ti(IV), Hg(II), Cu(II), U(VI), and Ce(IV). Inoue et al. [9] obtained a patent for a hydroxamic acid resin with 8% cross-linking, produced by hydroxylaminolysis of a copolymer of divinylbenzene and butyl acrylate.

Vernon and Eccles published four papers dealing with the synthesis, properties, and applications of poly(hydroxamic acids) [10, 11]. The preferred synthetic route was partial hydrolysis of a macroporous acrylonitrile-divinylbenzene copolymer to a poly(acrylamide), followed by hydroxylaminolysis. They obtained several successful analytical separations. Uranium

was concentrated from 1-l samples of synthetic sea water and eluted by 2 M hydrochloric acid with 95% recovery.

Ramirez and Andrade [12] reacted poly(acrolein) with desferroxamine B, a naturally occurring hydroxamic acid. Iron sorption was demonstrated qualitatively for this product, which was proposed for the treatment of severe iron poisoning. Winston and co-workers [13, 14] studied the effect of the spacing of hydroxamic acid units in a polymer on its affinity for iron. The most stable complexes were formed by a polymer in which N-methylhydroxamic acid groups were linked to a poly(methacrylamide) matrix by ethylene groups.

A major disadvantage of most chelating ion-exchange resins has been the length of time required for equilibration [15, 16]. Kinetic aspects of chelating ion exchangers have been studied by Schmuckler et al. [17] who demonstrated that sorption takes place by a shell-progressive mechanism. The reaction zone moves inward from the surface of the resin particle as the chelating sites are occupied. The rate-limiting step is diffusion of the ions through the reacted layer. As a result, the reaction kinetics are controlled by the physical properties of the resin matrix.

Chelating resins may be prepared either by polymerization of a chelating monomer or by the preparation of a chelating derivative of an existing polymer. An advantage of the latter approach is that it is possible to choose a starting polymer with known chemical and physical properties. One such substrate which has been used successfully [18] is Amberlite XAD-4, a macroreticular polymer of divinylbenzene. This resin is chemically and mechanically stable and has good mass-transfer characteristics.

This paper describes the synthesis and characterization of N-hydroxy-N-phenylcarbamoyl XAD-4. This is one of the first aromatic poly(hydroxamic acids) to be reported. Since it contains an N-phenyl group, it is chemically similar to N-phenylbenzohydroxamic acid, the most popular hydroxamic acid for analytical applications [19]. The extraction of twenty metal ions from 2 M hydrochloric acid by this resin is discussed, and conditions for the quantitative extraction and back-extraction of nine of these are described. These results are compared with the work of Forster and Schwabe on solvent extraction with N-phenylbenzohydroxamic acid [20].

EXPERIMENTAL

Reagents

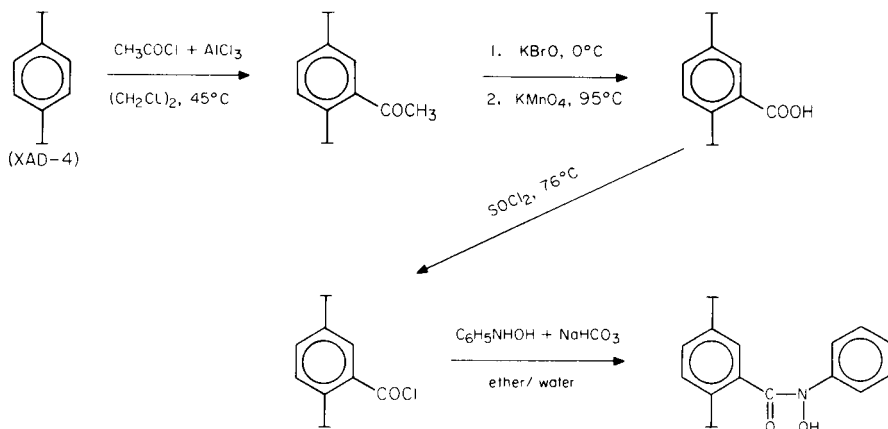
Amberlite XAD-4 resin (Rohm and Hass Co.) was rinsed with methanol and dried by suction filtration. It was ground immediately and sieved into 100–150, 150–200 and 200–325 mesh fractions. Fines were removed by slurring the resin with methanol, allowing it to settle, and decanting the solvent. This process was repeated several times until all the particles with settling times greater than 5 min had been removed. The fractionated resin was stored under methanol until needed. Phenylhydroxylamine was prepared

immediately before use by the reduction of nitrobenzene with zinc dust, as described by Vogel [21]. All other chemicals used in the resin synthesis, including solvents, were commercially available, reagent-grade materials.

Solutions of most metal ions were prepared by dissolving the metals or their salts in dilute acid or base. Solutions of titanium(IV), arsenic(III), and antimony(III) were prepared from the oxides. Solutions of uranium(IV) were prepared by passing solutions of uranium(VI) in 3 M hydrochloric acid through a column (5 mm i.d., 10 cm) containing granular lead [22]. A 0.001 M solution of niobium(V) was prepared by dissolving niobium metal in a mixture of nitric acid and hydrofluoric acid; concentrated sulfuric acid was added, and the solution was heated to heavy fumes to eliminate fluoride, allowed to cool and diluted with aqueous 5% (w/v) sodium tartrate solution.

Synthesis

The N-phenylhydroxamic acid resin was prepared by the sequence of reactions shown below



A mixture of 1.78 g of anhydrous aluminium chloride and 4 ml of 1,2-dichloroethane was prepared in a 50-ml flask and stirred until it appeared homogeneous. The flask was cooled in an ice-water bath, and 1.55 g of 100–150 mesh XAD-4 which had been dried at 110°C for 2 h was slowly added with stirring. The sides of the flask were washed down with an additional 2 ml of 1,2-dichloroethane. A drying tube was attached, and the reaction mixture was heated at 40°C without stirring for 8 h. The reaction was quenched by pouring it onto a mixture of cracked ice and concentrated hydrochloric acid. After several hours, the resin was collected by suction filtration and rinsed with methanol, water, and concentrated hydrochloric acid. It was rinsed again with water and methanol, and dried overnight at 60°C .

A solution of 4.2 g of sodium hydroxide in 35 ml of water was cooled to 0°C in an ice-salt bath. The solution was stirred magnetically while 2 ml of

bromine was added slowly. When all the bromine had dissolved, the acetyl XAD-4 was added with stirring. The mixture was allowed to stand at room temperature for 3 h and then boiled for 10 min. The product was isolated by suction filtration and further oxidized by adding it to a solution of 2 g of sodium hydroxide and 1.6 g of potassium permanganate in 100 ml of water. This was heated at 90–100°C for about 2 h. The product and the precipitated manganese dioxide were collected by suction filtration. The latter was removed by rinsing with concentrated hydrochloric acid. The product, which was light yellow, was rinsed with water and methanol, and dried at 60°C.

The carboxy XAD-4 was treated with thionyl chloride at 76°C for 2.5 h with intermittent stirring. The chloroformyl XAD-4 was isolated by suction filtration, washed with diethyl ether, and dried by continued suction. It was added to a 100-ml beaker containing 0.5 g of sodium hydrogencarbonate, 1 ml of water, and 10 ml of a solution in diethyl ether of phenylhydroxylamine, freshly prepared from 5 ml of nitrobenzene. This mixture was allowed to stand at room temperature for 90 min. The product was collected by suction filtration, washed with water and methanol and stored under methanol. Additional details of the synthesis, including an improved procedure for the oxidation step, have been reported [23].

Characterization

The hydrogen ion capacity of the carboxy XAD-4 was determined by back-titration of a mixture of 200 mg of the resin and 10 ml of 0.1 M sodium hydroxide. The infrared spectra of the starting material, the carboxy intermediate, and the final product were obtained with potassium bromide pellets. A dried sample of the final product was analyzed for nitrogen with a Perkin-Elmer Model 240 Elemental Analyzer. The presence of hydroxamic groups in the final product was confirmed by qualitative tests with iron(III) and vanadium(V). A column (5 mm i.d.) packed to a depth of 5 cm with about 250 mg of resin, was used for these tests. Characteristic colored bands were obtained when solutions of the above ions were passed through the column.

Kinetics

The rate of copper(II) uptake was estimated by the following experiment. A solution of 0.518 mmol of $\text{CuSO}_4 \cdot 5 \text{H}_2\text{O}$ in 50 ml of 1 M sodium sulfate was adjusted to pH 4.0 with dilute sulfuric acid. A 0.5-ml aliquot was taken to determine the initial copper concentration. About 1 ml of resin, which had been stored under methanol, was dried by suction filtration and added to the copper(II) solution with stirring. The pH was kept at 4.0 by additions of 0.1 M sodium hydroxide. Additional 0.5-ml aliquots were taken at intervals of 5, 15, 20, 40, and 80 min. The stirring was stopped for 90 s prior to sampling to allow the resin to settle. The aliquots were analyzed for copper colorimetrically using bis(2-hydroxyethyl)dithiocarbamate. After the experiment, the resin was collected by suction filtration and washed with

1 M hydrochloric acid to remove sorbed copper. The weight after drying at 60°C was 0.244 g.

Column extraction and recovery of metal ions

A gravity column (5 mm i.d., 5 cm) packed with about 250 mg of resin was used to determine the extent of extraction of various ions from 2 M hydrochloric acid. The column was conditioned by passing 5 ml of 2 M HCl through it. A 5-ml aliquot of a 0.001 M solution of the test ion in 2 M HCl was passed through the column at about 1 ml min⁻¹, followed by 5 ml of 2 M HCl. The amount of test ion in the effluent was determined by colorimetry or atomic absorption spectrometry. Similar experiments were performed to test the extraction of selected elements at pH 1–4.

The general procedure for column extraction was also used in the recovery studies. This was followed by elution with 5 ml of back-extracting solution. The overall recovery of the test ion was determined by colorimetric determination in the effluent from the back-extraction.

RESULTS AND DISCUSSION

The hydrogen ion capacity of the carboxylic acid intermediate was 2.81 mmol g⁻¹. The nitrogen content of the final resin was 1.08 mmol g⁻¹. At best, this represents a 40% conversion from carboxylic acid to hydroxamic acid. The actual yield may be still lower because of the possibility of some O-acylation. The infrared spectrum of the carboxy intermediate showed distinct bands at 1720 and 1290 cm⁻¹ similar to those found in the spectrum of benzoic acid [24]. The spectrum of the final product is consistent with the assumption that at least two types of carbonyl groups are present.

The rate of copper(II) uptake by the resin at pH 4.0 was studied. The results (Table 1) indicate a rapid equilibration rate with a $t_{1/2}$ of less than 5 min. The copper(II) capacity under the conditions of this experiment was 0.4 mmol g⁻¹. The most successful of the hydroxamic acid resins, prepared by Vernon and Eccles [11], had a $t_{1/2}$ value of approximately 22 min and a maximum capacity of 3.2 mmol g⁻¹ for copper(II) at pH 6.0. Although direct comparison of these data with ours is not possible because of experimental differences, the results indicate that the present resin exhibits faster

TABLE 1

Kinetics of copper(II) extraction at pH 4 by N-hydroxy-N-phenylcarbamoyl-XAD 4 resin

Time (min)	5	15	20	40	80
Cu extracted (mmol g ⁻¹)	0.29	0.36	0.36	0.39	0.39
Cu extracted (%) ^a	73	91	91	100	100

^aPercentage of final amount extracted.

kinetics at the price of decreased capacity. Chelating resins of various types previously prepared from XAD-4 resin have shown excellent kinetic characteristics [25].

Several qualitative experiments were carried out to ascertain the general behaviour of columns filled with the hydroxamic acid resin. Iron(III) was retained from pH 3 tartrate solution with the formation of a rust-colored band which could be removed by elution with 3 M hydrochloric or 5 M phosphoric acid. Bismuth(III) was retained from pH 6 tartrate solution and eluted by 1 M hydrochloric acid. Zirconium(IV) was retained in 0.5 M HCl, and remained on the column despite attempted elution with 2.4 and 10 M HCl. Vanadium(V) was retained from 0.2 M sulfuric acid with the formation of a dark band. Successful elution with 0.5, 2.4 and 10 M HCl changed the color of the band to deep purple without moving it. Similar colors have been observed in the solvent extraction of vanadium(V) by N-phenylbenzohydroxamic acid from sulfuric acid and hydrochloric acids [19]. The colored band was removed slowly by continued elution with 6% hydrogen peroxide in dilute sulfuric acid. Elution with 1 M sodium hydroxide removed the colored band quickly, but also caused a permanent change in the color of the resin and, after repeated use, a loss in complexation ability.

Quantitative studies of the retention of various metal ions on columns of hydroxamic acid resin were performed. The results of column extraction of various ions from 2 M hydrochloric acid are given in Table 2. Extraction of antimony(III), uranium(IV), zirconium(IV), tin(IV), molybdenum(VI), and tungsten(VI) is virtually complete, as predicted by the data of Forster and Schwabe on solvent extraction with N-phenylbenzohydroxamic acid [20]. Less satisfactory results were obtained with niobium(V) and titanium(IV). The incomplete extraction of niobium may have been caused by slow kinetics. Solvent extraction of niobium and tantalum is reported to proceed relatively slowly [26]. Vanadium(V) was not included in this study, because it is relatively unstable in hydrochloric acid solution.

The difference in extraction of uranium(IV) and uranium(VI) is consistent with the published formation constants for uranium(IV) and uranium(VI) benzohydroxamates [27]. The hydroxamic acid resin offers a convenient method for the separation of these species.

Quantitative data for retention of metal ions from less acidic aqueous

TABLE 2

Extraction of various ions from 2 M HCl by N-hydroxy-N-phenylcarbamoyl XAD-4

Ion	% Extraction	Ion	% Extraction
Mg(II), Ca(II), Cu(II), Pb(II), Hg(II), Al(III), Bi(III), V(IV)	0	Nb(V) Mo(VI)	94 98
As(III), Th(IV), U(VI)	1	Sn(IV), U(IV)	99
Ti(IV)	57	Sb(III), Zr(IV), W(VI)	100
Fe(III)	70		

solutions are shown in Table 3. Thorium(IV) and titanium(IV) are completely taken up by the resin column from 0.1 M hydrochloric acid, copper(II) is quantitatively retained from pH 3 tartrate solution, and aluminium(III), iron(III) and uranium(VI) are completely taken up from pH 4 acetate solution. It will be noted that most of the iron(III) is taken up from the more acidic solutions, but either slow kinetics or partial reduction to iron(II) causes some iron to pass through except at pH 4.

Several metal ions are so strongly complexed by the hydroxamic resin that it becomes a challenge to find suitable ways of eluting the metal ions from the resin column. However, effective eluents were found for elution of most metal ions, as shown in Table 4. In each case, retention and subsequent elution gave quantitative recovery of the metal ions ($100 \pm 1\%$). Copper(II), thorium(IV) and uranium(VI) could be eluted with acidic eluents. The remaining ions required the use of complexing agents for fast, quantitative elution. Forster and Schwabe [20] used 5 M sulfuric acid for the back-extraction of titanium, zirconium, and hafnium N-phenylbenzohydroxamates. However, this was ineffective for the elution of zirconium from the chelating resin. The use of oxalic acid as an eluent for zirconium was suggested by the

TABLE 3

Column extraction of selected metal ions by N-hydroxy-N-phenylcarbamoyl XAD-4

Metal ion	Percentage extraction			
	pH 1 (0.1 M HCl)	pH 2 (0.1 M NH_4Cl)	pH 3 (0.01 M tartrate)	pH 4 (0.1 M acetate)
Ca(II)	—	—	—	0
Cu(II)	1	16	100	100
Al(III)	3	57	—	100
Fe(III)	88	94	82	100
Th(IV)	100	—	—	—
Ti(IV)	100	—	—	—
U(VI)	0	94	97	100

TABLE 4

Conditions for quantitative recovery of metal ions by N-hydroxy-N-phenylcarbamoyl XAD-4

Ion	Extraction	Back-extraction	Ion	Extraction	Back-extraction
Cu(II)	pH 4 acetate	0.1 M HCl	Ti(IV)	pH 2 lactic acid	0.3 M HF
Al(III)	pH 4 acetate	0.1 M oxalic acid	U(VI)	pH 4 acetate	0.1 M HCl
Fe(III)	pH 4 acetate	0.1 M oxalic acid	Mo(VI)	2 M HCl^a	1 M NH_3^a
Th(IV)	0.1 M HCl	1 M HCl	W(VI)	2 M HCl^a	0.1 M sodium tartrate
Zr(IV)	2 M HCl	0.1 M oxalic acid			

^aPlus 0.1 M tartrate.

work of Mazzucotelli et al. [28]. It proved to be effective for the rapid and quantitative elution of iron(III) and aluminium(III) as well as zirconium(IV) from the hydroxamic acid resin. The use of hydrofluoric acid as an eluent for titanium(IV) was suggested by the high formation constants for the fluoro complexes of this element [29]. The use of neutral and basic tartrate solutions for the back-extraction of tungsten(VI) and molybdenum(VI), respectively, was suggested by the work of Pyatnitskii and Kravtsova [30] on solvent extraction of these elements from tartrate and citrate media by N-phenylbenzohydroxamic acid.

This research was supported by the Director of Energy Research, Office of Basic Energy Sciences, U.S. Dept. of Energy, WPAS-KC-03-02-03.

REFERENCES

- 1 J. P. Cornaz and H. Deuel, *Experientia*, 10 (1954) 137.
- 2 J. P. Cornaz, K. Hutschneker and H. Deuel, *Helv. Chim. Acta*, 40 (1957) 2015.
- 3 H. Deuel and K. Hutschneker, *Chimia*, 9 (1955) 49.
- 4 W. Kern and R. C. Schulz, *Angew. Chem.*, 69 (1957) 153.
- 5 F. L. M. Schouteden, *Makromol. Chem.*, 27 (1958) 246.
- 6 F. L. M. Schouteden, *Makromol. Chem.*, 24 (1957) 25.
- 7 C. A. Fetscher, U.S. Patend 3 154 499, 1964, *Chem. Abstr.*, 62 (1965) 4882d.
- 8 G. Petrie, D. Locke and C. E. Meloan, *Anal. Chem.*, 37 (1965) 919.
- 9 H. Inoue, K. Mizutani, T. Morishita and H. Ito, *Jpn. Kokai*, 74 72, (1974) 382, *Chem. Abstr.*, 82 (1975) 58883z.
- 10 F. Vernon and H. Eccles, *Anal. Chim. Acta*, 77 (1975) 145; 79 (1975) 229.
- 11 F. Vernon and H. Eccles, *Anal. Chim. Acta*, 82 (1976) 369; 83 (1976) 187.
- 12 P. S. Ramirez and J. P. J. Andrade, *Macromol. Sci. Chem.*, 7 (1973) 1035.
- 13 A. Winston and E. T. Mazza, *J. Polym. Sci., Polym. Chem. Ed.*, 13 (1975) 2019.
- 14 A. Winston and G. R. McLaughlin, *J. Polym. Sci., Polym. Chem. Ed.*, 14 (1976) 2155.
- 15 D. K. Hale, *Res. (London)*, 12 (1956) 104.
- 16 G. Schmuckler, *Talanta*, 12 (1965) 281.
- 17 M. Nativ, S. Goldstein and G. Schmuckler, *J. Inorg. Nucl. Chem.*, 37 (1975) 1951.
- 18 J. S. Fritz and E. M. Moyers, *Talanta*, 23 (1976) 590.
- 19 A. K. Majumdar, *N-Benzoylphenylhydroxylamine and its Analogues*, Pergamon, Oxford, 1972.
- 20 H. Forster and K. Schwabe, *Anal. Chim. Acta*, 45 (1969) 511.
- 21 A. L. Vogel, *Practical Organic Chemistry*, 3rd edn., Longmans, Green and Co., London, 1957, pp. 629-630.
- 22 Rodden, C. J., in *Analysis of Essential Nuclear Reactor Materials*, U.S. Atomic Energy Commission, 1964, Ch. 1.
- 23 R. J. Phillips, Ph.D. Dissertation, Iowa State University, Ames, IA, 1980.
- 24 R. T. Conley, *Infrared Spectroscopy*, 2nd edn., Allyn and Bacon, Boston, 1972, p. 163.
- 25 G. M. Orf, Ph.D. Dissertation, Iowa State University, Ames, IA, 1977.
- 26 O. A. Vita, W. A. Levier and E. Litteral, *Anal. Chim. Acta*, 42 (1968) 87.
- 27 A. Barocas, F. Baroncelli, G. B. Biondi and G. Grossi, *J. Inorg. Nucl. Chem.*, 28 (1966) 2961.
- 28 A. Mazzucotelli, R. Franche, A. Dadone and F. Baffi, *Talanta*, 24 (1977) 690.
- 29 A. Ringbom, *Complexation in Analytical Chemistry*, Interscience, New York, 1963.
- 30 I. V. Pyatnitskii and L. F. Kravtsova, *Sov. Prog. Chem. (Eng. Transl.)*, 35(1) (1969) 73; *Ikr. Khim. Zh.*, 35 (1969) 77.

DETERMINATION OF TOTAL SULPHUR IN FUEL OILS BY ION CHROMATOGRAPHY

M. J. McCORMICK

*Laboratory Services Branch, Environment Protection Authority, 240 Victoria Parade,
East Melbourne, 3002 Victoria (Australia)*

(Received 13th June 1980)

SUMMARY

A method is described for the determination of total sulphur in fuel oils. The oils are burnt in an oxygen flask and the resulting sulphur dioxide is oxidised with hydrogen peroxide to sulphate which is subsequently determined by ion chromatography. With a 50-mg oil sample the limit of detection is 0.007% sulphur. The procedure is simple and has a r.s.d. of 2.7%. Blanks are negligible and the only interferences can be from metal ions that form insoluble sulphates. The method is compared with m.e.c.a, x.r.f. and titrimetric procedures.

The determination of the sulphur content of fuel oils is one which is commonly carried out in order to monitor and control the amount of sulphur dioxide produced during combustion. Direct determination by x-ray fluorescence requires specialised and costly equipment which is not available to most laboratories. The search for a satisfactory indirect method has been going on for over twenty years [1] and many methods have been proposed. Almost all of these involve combustion of the oil in an oxygen flask, the sulphur dioxide produced being oxidised to sulphate with dilute hydrogen peroxide, and subsequently determined.

Many ways have been proposed to analyse solutions of sulphate in the range 1–50 mg ml⁻¹. These have involved direct titration against barium chloride with thorin [2] and other indicators [3], gravimetric [4], nephelometric [5] and molecular emission cavity analysis [6]. Some procedures utilise the precipitation of metal sulphates and subsequent determination of excess metal ions by ion-selective electrode potentiometry [7] or atomic absorption spectrometry [8, 9]. Visible spectrophotometry has also been used [10], and can be improved if solvent extraction is performed first [11]. These methods are affected by interfering ions, and often require pretreatment of the sample before the final measurement [12].

The simplest and most commonly used method is direct titration against barium perchlorate with thorin indicator. It does, however, have several drawbacks: thorin and the possible alternatives, arsenazo-III or sulphonazo-III, have subtle colour changes at the end-point [3] so that operator error may

be large, and there are many interferences [2, 13] even with the more recent indicators such as nitrososulphonazo-III [14].

This paper describes a procedure which employs ion chromatography for direct determination of the sulphate produced by the combustion of sulphur in oils in an oxygen flask. The technique involves the separation of sulphate ions from other anions in solution on an ion-exchange column, followed by removal of the background cations in the eluant stream with a stripper column which exchanges them for hydrogen ions. The resultant acid is detected using a conductivity meter [15]. The principal difficulties with this method arise from the fact that it cannot handle turbid samples or a large excess of another anion with a retention time close to that of the anion being determined. Neither of these situations should arise when determining sulphur in oils.

EXPERIMENTAL

Equipment

The following items were used: Dionex Model 10 ion chromatograph, with 0.0030 M NaHCO_3 —0.0024 M Na_2CO_3 as eluant unless otherwise specified; Telsec Model Lab-X 350 x-ray fluorescence spectrophotometer; Anacon Inc. m.e.c.a. spectrophotometer; Perkin-Elmer Model 3920 gas chromatograph equipped with a flame ionisation detector. A 300-ml oxygen flask of the Schöniger type was also used.

Reagents and materials

All reagents were analytical grade; the water was deionized and distilled. The reagents used were hydrogen peroxide, 30% (w/v), sulphur-free oxygen and sulphate solutions prepared as follows. For the stock standard ($1000 \text{ mg SO}_4^{2-} \text{ l}^{-1}$) 1.4796 g of anhydrous sodium sulphate was dissolved in 1 l of water. Working standards containing 40, 10, 4.0 and 1.6 $\text{mg SO}_4^{2-} \text{ l}^{-1}$ were prepared by suitable dilution with water.

Absorbent pellets were prepared from Whatman No. 541 ashless filter papers. Approximately 100 ml of water and 15 filter papers were placed in a liquidiser and shredded until the paper was completely pulped. The slurry obtained was filtered under vacuum and pressed into a disc about 5 mm thick at the pump. After filtration the paper was sliced into small squares (0.1 g) with a blade and dried in an oven at 110°C for 2 h. They were allowed to cool in a desiccator and stored in an open bottle protected from dust, near the balance. Strips of the same paper were used as wicks.

Procedure

The oil sample (0.05 g) was weighed to the nearest 0.1 mg onto a pre-weighed pellet, from a Pasteur pipette. Solid samples were liquefied by heating in a water bath at 55°C . Water (15 ml) and hydrogen peroxide (5 drops) were added to the combustion flask and the air in the flask was

displaced with oxygen. An oil-covered pellet was placed in the platinum cage along with a wick, which was ignited using a sulphur-free flame. The cage was immediately placed in the flask, which was quickly inverted so that the liquid formed a seal at the neck. After combustion was complete, the flask was shaken for 2 min and allowed to stand for 25 min to ensure that all of the sulphur dioxide had been absorbed and converted to sulphate. While standing, the flared top of the flask was sealed with 2–3 ml of water. The solutions were diluted to 50 ml and analyzed by ion chromatography and the concentration of sulphate determined from a calibration curve which was prepared daily.

The percentage of sulphur was calculated from $\%S (w/w) = [SO_4^{2-}] / 600 W$, where $[SO_4^{2-}]$ is the sulphate concentration found in $mg\ l^{-1}$ and W is the weight of oil used in g.

RESULTS AND DISCUSSION

A five-point calibration curve was prepared with sulphate concentrations of 0, 1.6, 4.0, 10 and 40 $mg\ l^{-1}$ which were injected into the chromatograph prior to each sample run. The calibration curve obtained by plotting peak height against sulphate concentration was linear. The range chosen covers sulphur concentrations of 0–2.5% in oil. The NBS Standard 1621 was analysed six times. The mean sulphur content found was 0.99% with a relative standard deviation of 2.7%. This compares favourably with the precision of the standard titrimetric method [13] which is 5% for an oil with the same sulphur content.

In initial experiments high sulphate blanks were encountered. Each reagent was tested to discover the source of the sulphate contamination. A hydrogen peroxide blank of 0.8 $mg\ SO_4^{2-}\ l^{-1}$ was obtained on an opened bottle. This blank probably arises from the oxidation of atmospheric sulphur dioxide. A new batch gave a negligible blank. Provided the hydrogen peroxide solution is exposed to the atmosphere for only short periods of time, the sulphate blank from this source can be reduced to negligible levels. However, a blank determination must be included to ensure that the hydrogen peroxide has not been contaminated with sulphate. A blank on the ashless filter paper used showed a sulphate content of $1.78 \pm 0.16\ mg\ g^{-1}$. In the experimental design used only 0.1 g of paper is burnt and the final solution is made up to 50 ml. Thus, the sulphate blank contribution from the filter paper in the final solution is $3\ \mu g\ l^{-1}$ which is well below the detection limit, and can thus be ignored. The only other possible source that could yield a blank sulphate value is the water used to make up the solutions. However, this contained no detectable sulphate.

The eluant recommended by the manufacturer is 0.0030 M $NaHCO_3$ –0.0024 M Na_2CO_3 , which gives the best separation of anions that can be determined directly by ion chromatography. In the solutions produced from the oxygen flask, the sulphate peak eluted at 21 min and was the last

peak to emerge. It is this step that is rate-determining in the instrumental part of the analysis. To increase sample throughput another eluant was used, 0.005 M Na_2CO_3 ; this decreased the sulphate elution time to 11 min. However, under these conditions there was significant overlap with the nitrate peak, which arises in part from the filter paper used and in part from nitrogen compounds in the oil which are oxidised in the combustion step. Since it is not possible to eliminate all the nitrate, the alternative eluant cannot be used without reducing the precision and accuracy of the determination.

Delays between weighing the oil sample and the oxidation step may cause errors because of volatilisation of lighter fractions of some oils. This was tested by weighing a filter paper immediately on applying the oil and again after 1 h. For NBS Standard 1621 the losses were small and fairly constant at $0.3 \pm 0.1\%$. However, weight losses from Sample 3 (see Table 1) were large and variable, being $7.6 \pm 1.5\%$. This experiment shows that it is essential not to delay between weighing the oil onto the filter paper and burning it.

Eight samples, including NBS Standards, were analyzed by using ion chromatography, molecular emission cavity analysis (m.e.c.a.), titration with barium ions to a thorin end-point after conversion to sulphate in the oxygen flask, and directly by x-ray fluorescence (x.r.f.). The oils were burnt in triplicate and the ion chromatography and m.e.c.a. analyses were carried out on the same solutions. Titration data were obtained from separate combustions. A gas chromatogram of each oil was recorded to identify its nature.

The ion chromatography method was compared with the other methods

TABLE 1

Results for the determination of the sulphur content (%) of oils using different methods

Sample	Ion chromatography ^a	M.e.c.a. ^a	Titration ^a	X.r.f. ^b	Description of oil
NBS Standard 1621 % S = 1.05 ± 0.02	0.99 ± 0.03^c	0.9 ± 0.1^c	1.05 ± 0.03	1.06	Heavy residual fuel oil
NBS Standard 1623 % S = 0.268 ± 0.004	0.265 ± 0.004	0.26 ± 0.02	0.29 ± 0.05	0.27	Light distillate fuel oil
NBS Standard 1634 % S = 2.14 ± 0.02	2.154 ± 0.009	2.0 ± 0.2	2.0 ± 0.1	2.17	Heavy fuel oil with small amount of residue
1	2.60 ± 0.03	2.13 ± 0.02	2.845 ± 0.006	2.67	Heavy fuel oil with no residual stock
2	0.08 ± 0.01	0.087 ± 0.004^d	0.19 ± 0.02	0.10	Diesel oil C10—C25
3	0.24 ± 0.01	0.18 ± 0.09^d	0.16 ± 0.01	0.26	Industrial diesel oil C11—C30
4	2.78 ± 0.02	2.5 ± 0.2	2.50 ± 0.04	2.86	Blended oil containing kerosene to lower viscosity
5	0.101 ± 0.009	0.096 ± 0.001^d	0.16 ± 0.01	0.10	Diesel oil C10—C25
Student's <i>t</i> -test	—	2.255	0.125	3.274	

^aBased on triplicate analyses unless otherwise stated; mean \pm standard deviation. ^bBased on single analyses. ^cBased on six replicate analyses. ^dBased on duplicate analyses.

cited using a paired population comparison test [16] to discover whether or not they gave equivalent results. Table 1 contains the results of each determination while Table 2 shows the statistical data. All comparisons were with respect to the ion chromatographic results. The results are equivalent if $t \leq -t_{(1-\alpha/2)(1-n)}$ or $\geq t_{(1-\alpha/2)(1-n)}$, where $\alpha = 0.05$ and $t(0.975(7)) = 2.365$. The m.e.c.a. and ion chromatographic methods are statistically equivalent at the $\alpha = 0.05$ level, but the m.e.c.a. precision at high concentrations was worse. The accuracy of the m.e.c.a. method can be determined by evaluating its performance on the three NBS standards. Except for NBS Standard 1621, the m.e.c.a. method produced satisfactory results within the large standard deviations obtained. The composition of the fuel mixture, the position of the cavity and the flame relative to the optics are all critical factors that affect the reproducibility of the m.e.c.a. method and make this approach highly dependent on operator skill.

Although Student's t -test indicates that the chromatography and titration methods are equivalent at the $\alpha = 0.05$ level, a careful study of the differences between these two methods for individual samples shows a wide spread. The titration method is particularly suspect at low concentrations, giving concentrations for samples 2 and 5 significantly larger than the values obtained using the other three methods and significantly lower for Sample 3. Those variations reflect the difficulty in identifying the end-point at low concentrations. The x.r.f. method does not give results equivalent to the ion chromatography method at the $\alpha = 0.05$ level; in all but one sample the concentrations determined by x.r.f. are higher. A single x.r.f. determination of the sulphur content of the oils sampled made it impossible to determine the precision of the method. However, on the data available, x.r.f. gave consistently slightly high values for the NBS standards. The source of this inaccuracy is unclear.

The accuracy of the values obtained by ion chromatography for the NBS standard oils, is satisfactory except for Standard 1621 which was consistently lower than the certified concentration. This oil includes residual stock, which often contains heavy metals. These may form insoluble sulphates thus lowering the amount of dissolved sulphate. Metals that form insoluble sulphates present the only interferences in the ion chromatographic method. This problem is common to all methods based on conversion of sulphur in

TABLE 2

Statistical data for comparison of methods

Method compared with ion chromatography	Mean difference	Variance of differences	t	Equivalent
M.e.c.a.	0.1321	0.0279	2.2381	Yes
Titration	0.00075	0.0237	0.0128	Yes
X.r.f.	-0.0338	0.00098	-3.0472	No

the oil to sulphate for the final determination. Only the x.r.f. method will be unaffected by the presence of metals.

No measurable blank was found in routine chromatographic determinations. However, the limit of detection can be measured from the noise, which is equivalent to a sulphate concentration of 0.1 mg l^{-1} . Accordingly the detection limit can be estimated as twice the noise, which is equivalent to a sulphur content of 0.007%, in an oil sample weighing 0.05 g.

Although it takes 25 min for the chromatogram to be produced, the instrument can be left unattended after the sample has been injected. The next combustion can be carried out during this interval, thus increasing the number of possible determinations per day for one analyst to eight to ten.

The author is grateful to Mr. M. Tuminello of the BHP Oil and Gas Laboratory, Clayton, for his x.r.f. and gas chromatographic data and to Mr. P. Marriott of the Department of Inorganic and Analytical Chemistry, Latrobe University, Bundoora, Victoria, for the m.e.c.a. results. The author also thanks Mr. B. J. Townsend and Mr. I. R. Gray for carrying out the titrations and Mr. A. Tawfik for his useful suggestions.

REFERENCES

- 1 J. F. Alicino, *Microchem. J.*, 3 (1958) 83.
- 2 J. S. Fritz and S. S. Yamamura, *Anal. Chem.*, 27 (1955) 1461.
- 3 K. Hozumi and K. Umemoto, *Microchem. J.*, 12 (1967) 46.
- 4 American Society for Testing and Materials, D119-64 and IP 61/65.
- 5 E. W. Bauman, Report DP 1437, National Technical Information Service, U.S. Dept. of Commerce, Springfield, VA, 1976.
- 6 J. D. Flanagan and R. A. Downie, *Anal. Chem.*, 48 (1976) 2047.
- 7 E. P. Schiede and R. A. Durst, *Anal. Lett.*, 10 (1977) 55.
- 8 D. D. Siemer, R. Woodriff and J. Robinson, *Appl. Spectrosc.*, 31 (1977) 168.
- 9 R. W. Looyenga and C. O. Huber, *Anal. Chim. Acta*, 55 (1971) 179.
- 10 K. Tōei, H. Miyata and Y. Yamawaki, *Anal. Chim. Acta*, 94 (1977) 485.
- 11 W. W. Flynn, *Anal. Chim. Acta*, 90 (1977) 343.
- 12 M. J. Fishman and D. E. Erdmann, *Anal. Chem.*, 51 (1977) 317R.
- 13 Institute of Petroleum, Standards for Petroleum and its Products, Vol. 2, 38th edn., no. IP 242/69, p. 242, 1979.
- 14 G. K. Pagenkopf, W. Brady, J. Clampet and M. A. Purcell, *Anal. Chim. Acta*, 98 (1978) 177.
- 15 H. Small, T. S. Stevens and W. C. Bauman, *Anal. Chem.*, 47 (1975) 1801.
- 16 B. Ostle and R. W. Mensing, *Statistics in Research*, Iowa State University Press, Ames, 3rd edn., 1975, p. 120.

THE SEPARATION OF RHODIUM AND IRIIDIUM BY ION FLOTATION

EUGENE W. BERG* and DANIEL M. DOWNEY

Department of Chemistry, Louisiana State University, Baton Rouge, LA 70803 (U.S.A.)

(Received 2nd June 1980)

SUMMARY

Mixtures of iridium(IV) and rhodium(III) as IrCl_6^{2-} and RhCl_6^{3-} are separated by ion flotation. The iridium(IV) is selectively floated from aqueous solutions of pH 2 and 0.05% Ce(IV) with either hexadecyltripropylammonium bromide (HTPAB) or hexadecyltributylammonium bromide (HTBAB). The rhodium(III) does not float under the same conditions. The floated iridium sublimate is collected in *n*-butyl acetate without contamination by the unfloated rhodium. Data are presented also for the separation and recovery of the Ir(IV) and Rh(III) with the above surfactants, hexadecyltrimethylammonium bromide (HTMAB) and hexadecyltriethylammonium bromide (HTEAB) from solutions of various sodium chloride and hydrochloric acid concentrations. The use of solvent sublation for recovering the floated iridium is examined. The separation is fast, practical, simple and does not require expensive reagents or apparatus. For these reasons, the separation of iridium and rhodium by ion flotation offers advantages over previous methods.

In an earlier ion-flotation study of chloro complexes of various platinum group metals, Berg and Downey [1] noted significant differences in the amount of RhCl_6^{3-} and IrCl_6^{2-} which could be floated from aqueous hydrochloric acid and saline solutions under identical experimental conditions with various quaternary ammonium bromide surfactants. This paper describes a simple, practical, quantitative, and rapid ion-flotation separation of rhodium and iridium which evolved from the earlier study.

The separation is based on a charge factor and a steric factor. The divalent IrCl_6^{2-} forms readily floatable products (sublates) of empirical formula MS_2 , where M is the metal complex anion and S is the surfactant cation. The trivalent RhCl_6^{3-} , however, requires three surfactant molecules per ion for flotation and forms floatable products only under certain conditions. The addition of three surfactant molecules to the RhCl_6^{3-} is sterically unfavorable and results in little or no flotation of the rhodium.

An earlier study by Berman and McBryde [2] indicated that quaternary ammonium functional groups partially reduce Ir(IV) to Ir(III). Since the iridium(III) exhibits flotation behavior similar to rhodium(III) [1], it was necessary to use an oxidant, cerium(IV), to oxidize any reduced iridium.

In addition, solvent sublation [3] was examined as a means of quantitatively recovering the floated iridium free of rhodium. Solvent sublation is

an auxiliary method to ion flotation in which a water-immiscible organic solvent is added to the top of the aqueous flotation sample and the rising gas bubbles carry the sublate directly into the organic layer without foam formation. Thus the foam interstitial liquid, which contains unfloated contaminants, is excluded and the sublate can be recovered relatively pure.

Even though many separation methods have been described for the chloro complexes of Rh(III) and Ir(IV) [4–6] which are readily obtained by reacting the metals with chlorine and dissolving in hydrochloric acid, all are either time-consuming or inefficient, or require expensive reagents and equipment. The ion flotation described here offers an alternative approach to a difficult separation and may be useful for both laboratory and industrial separations of iridium and rhodium.

EXPERIMENTAL

Reagents

High-purity sodium hexachloroiridate(IV) (Alfa Ventron Chemical Co.) was activated for one month with thermal neutrons from ^{252}Cf to produce the radioactive ^{192}Ir ($t_{1/2}$ 74.2 d). The radioactive salt was dissolved in 6 M HCl, and chlorine was passed through the solution to ensure complete oxidation of all the iridium to Ir(IV). After boiling to dryness, the solution was made up in 2 M HCl. The radioactive iridium solutions were allowed to decay for four days before use to eliminate the activity of ^{24}Na ($t_{1/2}$ 15 h).

High-purity sodium hexachlororhodate(III) (Alfa Ventron Chemical Co.) was dissolved in concentrated hydrochloric acid. After refluxing the solution for several hours to ensure that all the rhodium was present as RhCl_6^{3-} , the final solution was made up in 2 M HCl.

Surfactants of the type $\text{RNR}_3'\text{Br}$ were prepared for these studies [1]. The surfactants were hexadecyltrimethylammonium bromide (HTMAB), hexadecyltriethylammonium bromide (HTEAB), hexadecyltripropylammonium bromide (HTPAB) and hexadecyltributylammonium bromide (HTBAB). All surfactant stock solutions were prepared as 0.10 M and 0.02 M in absolute ethanol.

A 1% (w/v) cerium(IV) solution was prepared by dissolving 10 g of cerium(IV) hydrogensulfate in a mixture of 100 ml of sulfuric acid and 500 ml of water, the mixture being diluted to 1 l.

All other chemicals used were analytical-reagent grade.

Apparatus

The flotation cell was made by lengthening an ordinary 60-ml glass Buchner funnel to 30 cm. The Buchner funnel contained a fine sintered (4–5.5 μm) glass frit. A port was drilled 1 cm above the frit and fitted with a rubber septum for sample removal. The entire flotation system was of the same design as that of Rubin and Johnson [7].

General flotation procedure

Sample solutions generally were prepared for flotation in the following manner. Aliquots of the Rh(III) and radioactive Ir(IV) stock solutions were heated with 0.25 ml of the cerium(IV) solution at 140°C for 3–5 min. The total acidity of these solutions did not exceed 1.5 M. After cooling, the mixture was transferred to a 200-ml volumetric flask that contained a known amount of surfactant, 2 ml of ethanol, and an additional 0.25 ml of the cerium(IV) solution. The mixture was diluted and mixed for 10 min. Exactly 100 ml of the mixture was then pipetted into the flotation cell for flotation.

In addition to the above procedure, certain sample solutions were prepared with aliquots of stock solutions of hydrochloric acid and sodium chloride to give final solutions ranging from 0.01 to 3.0 M HCl or NaCl.

After the sample solutions had been transferred to the flotation cell, nitrogen that had been previously filtered and saturated with water vapor was passed through the solution with a controlled flow rate of 10 ml min⁻¹.

After the flotation reached steady state, the floated metal was recovered by adding *n*-butyl acetate to the flotation cell. The addition of the solvent causes some of the sublate to be redispersed in the bulk solution, thus flotation was continued for an additional 10 min in order to float all the redispersed sublate into the organic layer.

The organic and aqueous layers were then separated and both were analyzed for rhodium and iridium. The sublate salt was recovered from the organic layer after rotary evaporation of the solvent. The metal–chloro complex was recovered by wet ashing the sublate with sulfuric or nitric acid or hydrogen peroxide and fuming to dryness with hydrochloric acid.

Analytical technique

The course of the flotation was monitored by measurements on small aliquots (1–5 ml) of sample solution removed from the flotation column at appropriate intervals. The concentration of iridium remaining in the solution was determined by counting the activity of the aliquot with a 2 × 2-in. NaI(Tl) well crystal detector coupled with a TMC 401D multichannel analyzer. The concentration of rhodium was determined spectrophotometrically [8]. Rate of removal curves were obtained by dividing the concentration of solute remaining in solution at any time, C_t , by the original concentration, C_0 , and plotting vs. flotation time. In addition, the percentage of metal floated at any time may be calculated as $\%F_t = (1 - C_t/C_0)(100)$.

RESULTS AND DISCUSSION

The initial solutions for flotation were 5×10^{-5} M in both Rh(III) and Ir(IV) and 2×10^{-4} M in either HTMAB, HTEAB, HTPAB, or HTBAB. These concentration levels were chosen so that the sample solutions contained less than 10 ppm of each metal and more than a stoichiometric excess of surfactant. The rate of removal curves for the flotation of Ir(IV) and

Rh(III) mixtures with these surfactants are shown in Fig. 1. The percentage of Ir(IV) floated increases and the percentage of Rh(III) floated decreases as the quaternary ammonium functional group substituents increase in chain length from methyl to n-butyl. The surfactants HTPAB and HTBAB completely float the Ir(IV) but do not float Rh(III). Apparently the crowding of three bulky quaternary ammonium groups around the RhCl_6^{3-} , which is required for flotation, is sterically unfavorable. Thus, the rate of removal curves provided in Fig. 1 suggest that a single-stage, batch flotation separation is feasible by selective flotation of the Ir(IV) with HTPAB or HTBAB.

Studies by Berman and McBryde [2] indicated that anion-exchange resins of the type $\text{RN}(\text{CH}_3)_3^+$ partially reduce Ir(IV) to Ir(III). Since the surfactants used in these studies were also of the quaternary ammonium type, it was necessary to utilize an oxidizing reagent to prevent the formation of Ir(III). Cerium(IV) was chosen as the oxidant because it readily oxidizes Ir(III) to Ir(IV), it exists in cationic complexes which were not floated by the cationic surfactants used in these studies, and it can be removed from the flotation samples by passing the solutions through a bed of strong cation-exchange resin.

It was found that treatment of both the iridium solutions and surfactants with equimolar or greater amounts of cerium(IV) before mixing was necessary for the maximum flotation of iridium. The percentages of Ir(IV) floated with and without cerium(IV) added are given in Table 1. The data indicate the importance of the oxidant for the quantitative flotation of iridium. The percentage of Ir(III) floated under the same conditions is also provided for comparison.

In some cases, the floated iridium was recovered mechanically from the foam, but its separation from unfloated rhodium was incomplete as the foam interstitial liquid contained rhodium. Thus, solvent sublation was used to exclude the foam liquid from the iridium sublimate so that a complete separation was obtained.

Data are presented in Table 2 for the recovery of Ir(IV) floated with HTPAB by solvent sublation into several common solvents. Even though the

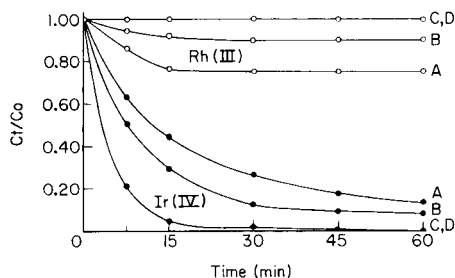


Fig. 1. Flotation of mixtures of Rh(III) and Ir(IV) with various surfactants. Initial conditions: $[\text{Rh(III)}] = [\text{Ir(IV)}] = 5 \times 10^{-5} \text{ M}$, $[\text{surfactant}] = 2 \times 10^{-4} \text{ M}$, pH 2.0, N_2 flow rate 10 ml min^{-1} . (○) Rh(III); (●) Ir(IV); (A) HTBAB; (B) HTEAB; (C) HTPAB; (D) HTBAB.

TABLE 1

Flotation of iridium from solutions with and without added cerium(IV)

Surfactant	Ir(IV) floated (%)		Ir(III) floated (%)
	With Ce(IV)	Without Ce(IV)	
HTMAB	87 ± 2	64 ± 2	57 ± 3
HTEAB	92 ± 2	69 ± 2	40 ± 3
HTPAB	99 ± 2	71 ± 2	16 ± 2
HTBAB	99 ± 2	73 ± 2	7 ± 2

TABLE 2

Solvent sublation and solvent extraction studies of iridium(IV) with HTPAB

(Initial conditions were $[\text{Ir(IV)}] = 5 \times 10^{-5} \text{ M}$; $[\text{HTPAB}] = 2 \times 10^{-4} \text{ M}$, pH 2.0, 100 ml of aqueous sample solutions, 25 ml of organic solvent; solvent sublation—flotation time, 1 h; extraction, 10 min shaking)

Solvent	Ir(IV) recovered (%)		Solvent	Ir(IV) recovered (%)	
	Solvent sublation	Solvent extraction		Solvent sublation	Solvent extraction
Benzene	86 ± 3	— ^a	n-Propyl acetate	95 ± 2	85 ± 4
2-Octanol	50 ± 10	— ^a	n-Butyl acetate	91 ± 2	77 ± 6 ^a
Ethyl acetate	98 ± 2	96 ± 3	n-Pentyl acetate	78 ± 5	64 ± 10 ^a

^aForms emulsion.

solvent sublation method was useful for recovering the iridium free of rhodium, the iridium was not quantitatively recovered with any of the solvents. Furthermore, the efficiency of solvent sublation was found to be dependent on the solution chloride concentration. The recovery data for the solvent sublation of Ir(V) with HTPAB into ethyl acetate from solutions of various sodium chloride concentrations plotted in Fig. 2 indicate that the recovery significantly decreases as the chloride concentration increases. This is in contrast to the rate of removal curves of Fig. 3 for the ion-flotation separation of Ir(IV) and Rh(III) with HTPAB from 0.5 M and 3.0 M NaCl solutions which indicate only a slight decrease in the percentage of Ir(IV) floated from 3.0 M NaCl solutions. The reduction in recovery by solvent sublation is the result of increasing amounts of surfactant cations being carried into the organic layer with chloride ion, rather than IrCl_6^{2-} , as counter ions with increasing chloride ion concentration. The chloride competition is not as significant in the ion-flotation process because much of the surfactant paired with chloride in the interstitial liquid is returned by reflux action to the bulk solution where the equilibrium is shifted and more metal complex anions are floated.

Because of the inefficiency of solvent sublation for quantitatively recovering the floated iridium, a modified solvent sublation method was used.

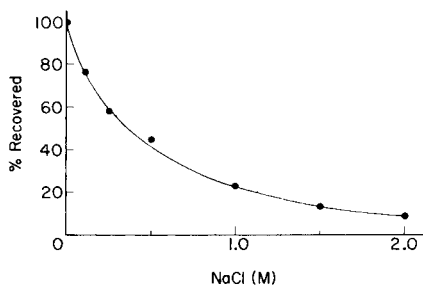


Fig. 2. Solvent sublation of Ir(IV) with HTPAB into ethyl acetate from solutions of various NaCl concentrations. Initial conditions: $[\text{Ir(IV)}] = 5 \times 10^{-5} \text{ M}$, $[\text{HTPAB}] = 2 \times 10^{-4} \text{ M}$, pH 2.0, N_2 flow rate 10 ml min^{-1} . Flotation time 1 h. Volumes: 100-ml sample solutions, 25 ml of ethyl acetate.

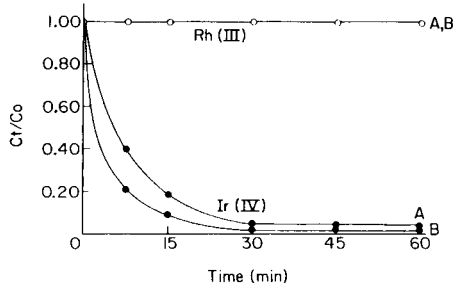


Fig. 3. Flotation of mixtures of Rh(III) and Ir(IV) with HTPAB from solutions of various NaCl concentrations. Initial conditions: $[\text{Rh(III)}] = [\text{Ir(IV)}] = 5 \times 10^{-5} \text{ M}$, $[\text{HTPAB}] = 2 \times 10^{-4} \text{ M}$, N_2 flow rate 10 ml min^{-1} . (○) Rh(III); (●) Ir(IV); (A) 3.0 M NaCl; (B) 0.5 M NaCl.

In the adapted procedure, the organic solvent was not added until the flotation steady state was attained. Then the solvent was added which, in turn, caused the foam to collapse and its interstitial liquid to return to the bulk aqueous solution. Most of the sublimate dissolved in the solvent as it was added, but that which was redispersed by turbulence into the bulk aqueous solution was quickly and efficiently floated into the organic layer by purging additional gas through the solution.

The data for the modified solvent sublation of Ir(IV) and Rh(III) with each surfactant from solutions of various sodium chloride concentrations are given in Table 3. By using the modified solvent sublation procedure with *n*-butyl acetate as the solvent, a quantitative separation is obtained from several solutions. Butyl acetate was chosen as the solvent because the iridium sublimate is very soluble in it, it has a low miscibility level for water and it has a low boiling point which facilitates solvent removal by flash evaporation.

It should be noted that the amount of Ir(IV) floated from 0.1 M NaCl solutions is much less than the amount floated from other solutions. This reduction in flotation was noted in a previous study [1] and similar behavior for the flotation of palladium(II) was discussed by Walkowiak and Bartecki [9].

It is of interest to separate iridium and rhodium in acidic (HCl) solutions. Therefore the selective flotation of Ir(IV) from Rh(III) in various concentrations of hydrochloric acid was studied. The rate of removal curves for the flotation of IrCl_6^{2-} and RhCl_6^{3-} with HTPAB from solutions of various hydrochloric acid concentration are shown in Fig. 4 and the data for the modified solvent sublation of the metals with each surfactant from various concentrations of hydrochloric acid are given in Table 4. The floated iridium was again recovered by the modified solvent sublation method with *n*-butyl acetate.

TABLE 3

Recovery data for the separation of iridium(IV) and rhodium(III) from solutions of various sodium chloride concentrations
(Initial separation conditions were $[\text{Ir(IV)}] = [\text{Rh(III)}] = 5 \times 10^{-5} \text{ M}$, $[\text{surfactant}] = 2 \times 10^{-4} \text{ M}$, pH 2.0, 100-ml sample solutions; flotation time 1 h; recovery of Ir(IV) in *n*-butyl acetate, and Rh(III) from residual aqueous solution; 0.5 ml of 1% Ce(IV) solution added to prevent Ir(IV) reduction)

Surfactant	NaCl (M)	Rh (mg) recovered ^a	Rh (%) recovered	Ir (mg) recovered ^b	Ir (%) recovered
HTMAB	— ^c	0.361	70	0.806	84
	0.10	0.438	85	0.705	68
	0.50	0.515	100	0.778	81
	1.00	0.515	100	0.750	78
	2.00	0.516	101	0.759	79
	3.00	0.514	99	0.721	75
HTEAB	— ^c	0.458	89	0.875	91
HTPAB	— ^c	0.510	99	0.951	99
	0.10	0.505	98	0.700	73
	0.50	0.510	99	0.942	98
	1.00	0.520	101	0.932	97
	2.00	0.506	98	0.914	95
	3.00	0.514	100	0.922	96
HTBAB	— ^c	0.519	101	0.971	101
	0.10	0.505	98	0.814	85
	1.00	0.501	97	0.951	99
	3.00	0.525	102	0.932	97

^aRh added, 0.515 mg. ^bIr added, 0.961 mg. ^cNo NaCl added.

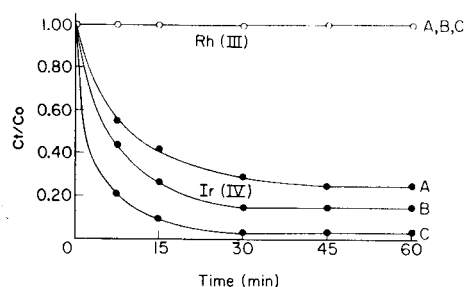


Fig. 4. Flotation of mixtures of Rh(III) and Ir(IV) with HTPAB from solutions of various HCl concentrations. Initial conditions: $[\text{Rh(III)}] = [\text{Ir(IV)}] = 5 \times 10^{-5} \text{ M}$, $[\text{HTPAB}] = 2 \times 10^{-4} \text{ M}$, N_2 flow rate 10 ml min^{-1} . (○) Rh(III); (●) Ir(IV); (A) 3.0 M HCl; (B) 1.0 M HCl; (C) 0.5 M HCl.

TABLE 4

Recovery data for the separation of iridium(IV) and rhodium(III) from solutions of various hydrochloric acid concentrations
(Initial separation conditions were $[\text{Ir(IV)}] = [\text{Rh(III)}] = 5 \times 10^{-5} \text{ M}$, $[\text{surfactant}] = 2 \times 10^{-4} \text{ M}$, 100-ml sample solutions; flotation time 1 h; recovery of Ir(IV) in n-butyl acetate, and Rh(III) from residual aqueous solution; 0.5 ml of 1% Ce(IV) solution added)

Surfactant	HCl (M)	Rh (mg) recovered ^a	Rh (%) recovered	Ir (mg) recovered ^b	Ir (%) recovered
HTMAB	0.01	0.361	70	0.806	84
	0.10	0.421	82	0.797	83
	0.50	0.520	101	0.780	81
	1.00	0.516	100	0.760	79
	2.00	0.524	102	0.693	72
	3.00	0.505	98	0.595	62
HTEAB	0.01	0.458	89	0.875	91
HTPAB	0.01	0.510	99	0.951	99
	0.10	0.511	99	0.935	97
	0.50	0.515	100	0.910	95
	1.00	0.526	102	0.894	93
	2.00	0.514	100	0.788	82
	3.00	0.509	99	0.692	72
HTBAB	0.01	0.519	101	0.971	101
	0.10	0.510	99	0.940	98
	1.00	0.520	101	0.837	87
	3.00	0.514	100	0.750	78

^aRh added, 0.515 mg. ^bIr added, 0.961 mg.

The amount of Ir(IV) floated decreases significantly as the acid concentration increases. It is thought that the decrease in flotation is due in part to the loss of cerium(IV). Cerium(IV) oxidizes chloride to chlorine in hydrochloric acid. In solutions of greater than 2.0 M HCl, the reaction proceeds very rapidly, but does not proceed rapidly in concentrated sodium chloride solutions. Since the added cerium(IV) is lost by an alternative reaction, it is no longer available to prevent Ir(IV) reduction by the quaternary ammonium surfactants. Thus for a quantitative flotation and recovery of iridium it is necessary to keep the acid concentration less than 0.1 M.

The mole ratios of Ir(IV) and Rh(III) in the initial solutions were varied in order to determine the influence of metal concentration on the efficiency of flotation separation. The data given in Table 5 indicate that the initial concentrations of Ir(IV) and Rh(III) are not significant for achieving quantitative separations as long as there is an excess of the stoichiometric amount of surfactant in the initial solutions.

It seemed reasonable that simple solvent extraction could be substituted for the flotation-solvent sublation procedure, but in fact, when flotation sample solutions were shaken with 25-ml portions of the solvents used for

TABLE 5

Recovery data for the separation of iridium(IV) and rhodium(III) with HTPAB (Initial separation conditions were solution pH 2.0, 100-ml sample solutions; flotation time 1 h; recovery of Ir(IV) in n-butyl acetate, and Rh(III) from residual aqueous solution; Ce(IV) added)

Rh(III) ($\times 10^{-5}$ M)	Ir(IV) ($\times 10^{-5}$ M)	HTPAB ($\times 10^{-5}$ M)	Rh recovered (%)	Ir recovered (%)
5.0	5.0	20.0	100	99
5.0	0.5	5.0	100	98
5.0	40.0	100.0	100	99
0.5	5.0	20.0	98	101
40.0	5.0	100.0	100	99

solvent sublation (Table 2), Ir(IV) was not recovered as efficiently as it was by solvent sublation methods. Karger et al. [3, 10] has established that solvent sublation has advantages over solvent extraction in that it is volume-independent, liquid-liquid equilibrium is not attained, and emulsions are avoided.

REFERENCES

- 1 E. W. Berg and D. M. Downey, *Anal. Chim. Acta*, 120 (1980) 237.
- 2 S. S. Berman and W. A. E. McBryde, *Can. J. Chem.*, 36 (1958) 845.
- 3 B. L. Karger, in R. Lemlich (Ed.), *Adsorptive Bubble Separation Techniques*, Academic Press, New York, 1972, p. 145.
- 4 F. E. Beamish and J. C. van Loon, *Analysis of Noble Metals: Overview and Selected Methods*, Academic Press, New York, 1977, p. 226.
- 5 S. I. Ginzburg, *Analytical Chemistry of the Platinum Metals*, Halsted, New York, 1975, p. 413.
- 6 R. Gilchrist and W. A. E. McBryde, *Can. J. Chem.*, 35 (1958) 845.
- 7 A. J. Rubin and J. D. Johnson, *Anal. Chem.*, 39 (1967) 298.
- 8 E. B. Sandell, *Colorimetric Determination of Traces of Metals*, 3rd edn., Interscience, New York, 1959, p. 769.
- 9 W. Walkowiak and A. Bartecki, *Nucleonika*, 18 (1973) 133.
- 10 B. L. Karger, T. A. Pinfold and S. E. Palmer, *Separ. Sci.*, 5 (1970) 603.

DESCRIPTION OF LIQUID—LIQUID EXTRACTION EQUILIBRIA IN EXCHANGE EXTRACTIONS OF CHELATES

Part 1. Exchange Equilibria of Diethyldithiocarbamates in Chloroform—Water and Carbon Tetrachloride—Water Systems

D. VANČO*

Institute of Preventive Medicine, 80958 Bratislava (Czechoslovakia)

F. MACÁŠEK

Department of Nuclear Chemistry, Comenius University, Bratislava (Czechoslovakia)

(Received 1st October, 1979)

SUMMARY

The concepts of total complexation and total ligand numbers in descriptions of chelate equilibria in two-phase systems containing stoichiometrically comparable amounts of metal ion and chelating agent, are applied to zinc diethyldithiocarbamate as extractant. Experimental verification of this concept on cobalt(II), zinc(II) and iron(II) exchange extraction enables the distribution ratio and optimal conditions for separation of metals in exchange extractions to be calculated.

An extraction agent can be used as a metal chelate (or in stoichiometrically comparable amounts with a metal ion) for increasing the stability of the extraction agent and the selectivity of the extractive separation. The separation of metals into two groups or the selective separation of one metal can be achieved by a suitable choice of such systems.

In general, calculation of a free ligand concentration $[A]$ can be used in describing the distribution of other metals present. The simplest method of predicting the extraction behaviour of two elements rests in comparing their extraction constants, i.e. neglecting all equilibria apart from the formation of complexes (MA_n , NA_p) extracted into the organic phase [1, 2]. The separation factor (D_N/D_M) of the two elements should be proportional to $(n - p)\log[A]$ in this case and a constant when $n = p$, regardless of the composition of aqueous phase.

Bajo [3] presented a mathematical model of metal extraction with excess of diethyldithiocarbamic acid (HDDC) based on the formation of one chelate and Ringbom coefficients for side complexation, which was in agreement with experimental results. Simple calculations have also been proposed for determining a free ligand concentration in systems with equivalent amounts, or an excess of metal [4, 5].

The use of total ligand numbers is convenient for treating mass balance in

two-phase systems, as was demonstrated in the application of Job's method [6] and extraction titrations [7]. In such a case, the completeness of material balance acquires great importance especially when the extraction agent is in stoichiometric ratio or substoichiometric ratio to the metal [8]. Accordingly, this paper treats exchange extraction systems in which one metal (N), usually present in microconcentrations, is extracted when a second metal (M) is present as a chelate (MA_n) or in a concentration similar to that of the chelating agent. Particularly, such an approach facilitates the calculations of free ligand concentrations considering both chelating and side reactions (metal hydrolysis and/or masking, chelating agent dissociation, etc.). For experimental verification diethyldithiocarbamate and oximate systems were studied; the results for the former are presented below.

THEORY

(For convenience, the symbols used in this paper are listed in Table 1.)

The mass balance of a chelating agent with a metal ion in a two-phase system involving mononuclear complex formation, can be formulated [8] as:

TABLE 1

Symbols used

n, p	= charges on metal ions M and N, respectively
A	= anionic ligand (anion of an extraction agent HA)
B	= competing ligand (OH^- etc.)
[]	= equilibrium concentrations (with subscript "o" in organic phase)
$C_A, C_{M(N)}$	= initial (total) concentrations of extraction agent (in organic phase) and metals (in aqueous phase), respectively
V, V_o	= equilibrium volumes of aqueous and organic phases
V', V'_o	= initial volumes of aqueous and organic phases
v	= V/V' , volume change of aqueous phase during extraction
r'	= V'_o/V' , initial phase volume ratio
r	= V_o/V , equilibrium phase volume ratio
D	= distribution ratio
$(K_D)_{MA_n}$	= $[MA_n]_o/[MA_n]$, distribution constant for MA_n (likewise $(K_D)_{NA_p}$ for NA_p)
β_n	= $[MA_n]/[M][A]^n$, the stability constant (likewise β_p for NA_p);
α	= $1 + r(K_D)_A + \{1 + r(K_D)_{HA}\} K_{HA}^{-1} [H] + \{1 + r(K_D)_{H_2A}\} K_{HA}^{-1} K_{H_2A}^{-1} [H]^2$, the ratio of the amount of all forms of the free extraction agent, generally A^- , HA and H_2A^+ , in the two-phase system to the amount of A^- in the aqueous phase
$(K_D)_{HA}$	= $[HA]_o/[HA]$, distribution constant of HA
$(K_D)_A, (K_D)_{H_2A}$	= distribution constants of ion pairs with the anions or cations formed from HA
K_{HA}	= $[H][A]/[HA]$, dissociation constant of HA
K_{H_2A}	= $[H][HA]/[H_2A]$, dissociation constant of H_2A^+
K_{ex}	= $[MA_n]_o[H]^n/[M][HA]^n$, extraction constant
X_{MB}	= $\sum_{i=0}^n [MB_i]/[M^{n+}]$, the complexation function of the central atom M with competing ligand B (likewise X_{NB} for N)

$c_A r' = \alpha [A] v + \bar{n}_t c_M$, where \bar{n}_t is the mean total ligand number for a system containing complexes MA_n and MB (and neither mixed complexes nor lower complexes with ligand A) can be expressed as:

$$\bar{n}_t = (n\beta_n \{r(K_D)_{MA_n} + 1\} [A]^n) / (\beta_n \{r(K_D)_{MA_n} + 1\} [A]^n + X_{MB})$$

where X_{MB} is the complexation function (Fronaeus function) [9] for side ligands (especially for hydroxide ions in this instance). If $r(K_D)_{MA} \gg 1$, then:

$$\bar{n}_t = (nr\beta_n (K_D)_{MA_n} [A]^n) / (r\beta_n (K_D)_{MA_n} [A]^n + X_{MB})$$

From these equations, the mass balance of the extraction agent is:

$$c_A r' = \alpha [A] v + c_M (nr\beta_n (K_D)_{MA_n} [A]^n) / (r\beta_n (K_D)_{MA_n} [A]^n + X_{MB})$$

The form of this equation suitable for calculation of $[A]$, if volume changes are negligible ($v = 1$, $r' = r$), is:

$$\alpha r\beta_n (K_D)_{MA_n} [A]^{n+1} + r\beta_n (K_D)_{MA_n} (nc_M - rc_A) [A]^n + \alpha [A] X_{MB} - rc_A X_{MB} = 0 \quad (1)$$

From this equation it can be observed that $[A]$ is affected not only by the c_M/c_A ratio and the dissociation of the extraction agent (given by α) but also by the hydrolysis (or masking) of M. Therefore, the effect of pH is included in the α and X_{MB} values. As there is a large change of $[A]$ in the stoichiometric region ($nc_M = c_A r'$), systems of ligand buffers ($nc_M > c_A r'$) have been used; these can also be treated by eqn. (1).

It can easily be demonstrated that if the metal N, present at low concentration ($c_N \ll c_M$, so that the mass balance is not affected), is extracted as NA_p , its distribution ratio is determined by

$$D_N = \beta_p (K_D)_{NA_p} [A]^p / (\beta_p [A]^p + X_{NB}) \quad (2)$$

and $[A]$ is determined from the equilibrium of the macro components included in eqn. (1). Then D_N can be treated according to eqn. (2) as a function of pA and pH and $\beta_p (K_D)_{NA_p}$ can be obtained. A special case occurs when the metals M and N are identical; then D_N describes the distribution during isotope exchange extraction, and the two-phase stability constants $\beta_p (K_D)_{NA_p}$ and $\beta_n (K_D)_{MA_n}$ are identical if there are no deviations from thermodynamic ideality in systems with and without excess of chelating agent.

The reference data on $\beta_n (K_D)_{MA_n}$ values, obtained under conditions of $c_A r' \gg c_M$, are of great importance, because the $\beta_p (K_D)_{NA_p}$ values obtained for zinc, iron and cobalt are to be considered with respect to a reference value for zinc diethyldithiocarbamate, $Zn(DDC)_2$.

It should be noted that $[A]$ can also be calculated semi-empirically from an expression of the type of eqn. (2) so that

$$[A]^n = D_M X_{MB} / \beta_n \{(K_D)_{MA_n} - D_M\} \quad (3)$$

However, though the same species are included in the mass balance as in eqn. (1), the calculation may become sensitive to the difference $(K_D)_{MA_n} -$

D_M , unless $\beta_n[A]^n \gg X_{MB}$. When an overstated $(K_D)_{MA_n}$ value is used in the calculation, the value of $[A]$ is underestimated in a region of low distribution ratio and overestimated at high D_M values. Hence, the advantage of eqn. (1) lies in the fact that the product $\beta_n(K_D)_{MA_n}$ can be obtained (like K_{ex}) in systems where $\beta_n[A]^n + X_{MB} \approx 1$, whereas the value $(K_D)_{MA_n}$ should be precise at high pH values.

EXPERIMENTAL

The chemicals used were all of analytical-reagent grade. Solutions of $Zn(DDC)_2$ in chloroform or carbon tetrachloride were prepared as described by Wyttenbach and Bajo [1]. The radionuclides used were of commercial radioactive purity.

Extractions were done with 10 ml of aqueous phase which was 5.0×10^{-6} M in the labelled metal N (Fe, Zn, Co) chloride and contained 0.1 M $NaClO_4$, 0.05 M acetate buffer and 1.0×10^{-5} M $ZnCl_2$. The same volume of organic phase was used; this phase was 2.5×10^{-3} or 5.0×10^{-4} M $Zn(DDC)_2$ in chloroform or carbon tetrachloride. Both phases were shaken mechanically at 20°C. After equilibration, 1-ml aliquots of each phase were measured by a NaI(Tl) scintillation detector connected to a single-channel analyzer.

RESULTS AND DISCUSSION

The various values of dissociation, distribution and two-phase stability constants used in the various calculations are given in Table 2. The stability constants of the hydroxo complexes used to calculate the complexation functions in eqns. (1) and (2) are given in Table 3.

Calculations were done under the reasonable suppositions for the extraction systems used that there are no volume changes ($r = r' = 1$, $v = 1$), or anion (DDC^-) or cation (H_2DDC^+) extractions [$(K_D)_A = (K_D)_{H_2A} = 0$]. As an example, pA values calculated from eqns. (1) and (3) under different conditions for the $Zn(DDC)_2$ -chloroform system are given in Table 4. The results confirm the validity of the formulae used. The pA values calculated by means of eqn. (1) were used to describe the cobalt(II) and iron(II) extractions.

TABLE 2

Equilibrium constants for diethylthiocarbamic acid and $Zn(DDC)_2$ used in the calculations.

pK_{HA}	System	$\log(K_D)_{HA}$	$\log K_{ex}$	$\log \beta_n(K_D)_{MA}$
3.4 [11]	CCl_4/H_2O	2.39 [11]	2.96 [12]	14.38
3.6 [10]	CCl_4/H_2O	2.60 [10]	2.96 [12]	15.38 [12]
3.4 [11]	$CHCl_3/H_2O$	3.37 [11]	—	16.30 [10]
3.4 [11]	$CHCl_3/H_2O$	3.37 [11]	2.30 [13]	15.80
3.4 [11]	$CHCl_3/H_2O$	3.37 [11]	2.39 [2]	15.93

TABLE 3

Stability constants of hydroxo complexes [14]

Ion	Log β_1	Log β_2	Log β_3	Log β_4
Co(II)	5.1	9.2	10.5	—
Fe(II)	5.7	9.0	—	—
Zn(II)	4.4	12.9	14.2	15.5

TABLE 4

Calculated free ligand concentration in the system 0.0025 M $\text{Zn}(\text{DDC})_2$ in $\text{CHCl}_3/0.1$ M NaClO_4 —0.05 M $\text{CH}_3\text{COO}(\text{Na},\text{H})$ — 10^{-5} M Zn^{2+} ($r = 1$, $c_M = 2.51 \times 10^{-3}$ M, $c_A = 5.00 \times 10^{-3}$ M)

pH	Log D	pA ^a			pA ^b		
		Eqn. (3)		Eqn. (1)	Eqn. (3)		Eqn. (1)
		I ^c	II ^d		I	II	
3.10	0.93	7.68	7.68	7.44	7.43	7.43	7.27
3.28	1.12	7.59	7.59	7.38	7.34	7.34	7.21
3.34	1.18	7.56	7.56	7.36	7.31	7.31	7.19
3.35	1.15	7.57	7.57	7.35	7.32	7.32	7.18
3.54	1.27	7.52	7.51	7.29	7.27	7.26	7.13
3.78	1.47	7.42	7.41	7.22	7.17	7.16	7.05
3.92	1.63	7.34	7.33	7.18	7.09	7.08	7.00
4.05	1.64	7.33	7.32	7.14	7.08	7.07	6.96
4.06	1.70	7.30	7.29	7.14	7.05	7.04	6.96
4.08	1.66	7.32	7.31	7.13	7.07	7.06	6.95
4.14	1.68	7.31	7.30	7.12	7.06	7.05	6.94
4.18	1.74	7.28	7.27	7.11	7.03	7.02	6.92
4.28	1.76	7.27	7.25	7.08	7.02	7.00	6.90
4.36	1.87	7.21	7.20	7.06	6.96	6.95	6.87
4.38	1.77	7.26	7.25	7.05	7.01	7.00	6.87
4.89	2.09	7.10	7.08	6.94	6.85	6.83	6.74
5.03	2.09	7.10	7.07	6.91	6.85	6.82	6.71
5.27	2.19	7.06	7.02	6.88	6.81	6.77	6.67
5.53	2.37	6.96	6.91	6.85	6.71	6.66	6.63
5.61	2.44	6.93	6.86	6.84	6.68	6.61	6.62
6.06	2.40	6.95	6.89	6.82	6.70	6.64	6.58
6.54	2.42	6.94	6.87	6.80	6.69	6.55	6.56

^aLog $\beta_n(K_D)_{MA_n} = 16.3$ for $\text{Zn}(\text{DDC})_2$. ^bLog $\beta_n(K_D)_{MA_n} = 15.80$ for $\text{Zn}(\text{DDC})_2$. ^cI, $(K_D)_{MA_n} > D_M$. ^dII, $(K_D)_{MA_n} = 10^3$.

Values of the two-phase stability constants for $\text{Zn}(\text{DDC})_2$, $\text{Fe}(\text{DDC})_2$, $\text{Co}(\text{DDC})_2$ and $\text{Co}(\text{DDC})_3$ in chloroform—water and carbon tetrachloride—water were calculated from eqn. (2) for systems of various compositions and at pH values where the formation of hydroxo complexes was not significant

(1.63–4.68 for Co(II) and 3.30–7.30 for Fe(II)). The data obtained (Tables 5 and 6) are consistent with values obtained previously. Regardless of the conditions, no shift occurs at higher values of pH and c_M . The calculated values of $\beta_p(K_D)_{NA_p}$ had a normal distribution with a reasonably small skewness and kurtosis [15], considering the set of 20 calculated points. The

TABLE 5

Comparison of values of two-phase stability constants obtained for some metal diethyldithiocarbamates in the system $\text{CCl}_4/0.1 \text{ M NaClO}_4\text{--}0.05 \text{ M CH}_3\text{COO}(\text{Na,H})\text{--}10^{-5} \text{ M Zn}^{2+}$ with published data

Chelate	Calculated complex composition A:M	Log $\beta_p(K_D)_{NA_p}$			Published values
		Present work			
		Mean	Skewness	Kurtosis	
Co(DDC) ₂	1.83 ± 0.17	16.15 ± 0.06 ^a	−0.10	−1.40	18.53 [16]
		15.20 ± 0.07 ^b			14.75 [12]
Fe(DDC) ₂	2.12 ± 0.13	14.12 ± 0.07 ^a 13.16 ± 0.07 ^b	0.04	−1.52	13.42 [12]
Zn(DDC) ₂	—	15.18 ± 0.03 ^a	−0.29	−1.57	15.40 [16]
		14.23 ± 0.03 ^b			15.38 [12]

^aLog $\beta_n(K_D)_{MA_n}$ for Zn(DDC)₂ = 15.38 ^bLog $\beta_n(K_D)_{MA_n}$ for Zn(DDC)₂ = 14.38.

TABLE 6

Comparison of values of two-phase stability constants obtained for some metal diethyldithiocarbamates in the system $\text{CHCl}_3/0.1 \text{ M NaClO}_4\text{--}0.05 \text{ M CH}_3\text{COO}(\text{Na,H})\text{--}10^{-5} \text{ M Zn}^{2+}$ with published data

Chelate	Calculated complex composition A:M	Log $\beta_p(K_D)_{NA_p}$			Published values
		Present work			
		Mean	Skewness	Kurtosis	
Co(DDC) ₃	2.94 ± 0.07	22.43 ± 0.06 ^a 21.92 ± 0.07 ^b	0.04	−1.41	19.76 [16]
Co(DDC) ₂	—				
Fe(DDC) ₂	2.02 ± 0.18	14.56 ± 0.12 ^a 14.16 ± 0.10 ^b	0.69	−1.60	—
Zn(DCC) ₂	—	15.94 ± 0.05 ^a	0.11	−1.44	16.30 [10]
		15.56 ± 0.05 ^b			15.93 [2]
					15.88 [16]
					15.80 [13]

^aLog $\beta_n(K_D)_{MA_n}$ for Zn(DDC)₂ = 16.30. ^bLog $\beta_n(K_D)_{MA_n}$ for Zn(DDC)₂ = 15.80.

average values may contain a systematic error, being based on the reference constants in Table 1.

The correctness of results depends also on the exact estimation of the extracted complex composition. The analysis of the extraction curves $\log D = f(pA)$ for zinc(II) proved the composition as $Zn(DDC)_2$ in both carbon tetrachloride and chloroform, as was expected [2, 12]. Likewise, the iron(II) chelate was shown to be $Fe(DDC)_2$ in both organic solvents (Tables 5 and 6) and was confirmed by extraction in the presence of metallic zinc.

Analysis of the extraction curves for cobalt shows the chelate to be $Co(DDC)_2$ in carbon tetrachloride, but $Co(DDC)_3$ in chloroform. Any influence of chloride anions in the organic solvents was excluded and the explanation that cobalt(II) is oxidized to cobalt(III) during chloroform extraction is preferred. This was confirmed by extractions from systems containing metallic zinc. The extraction into carbon tetrachloride was practically the same as before, but extraction into chloroform had considerably lower distribution ratios. This effect has caused a discrepancy in literature data [1, 16], and requires further investigation.

Thus, eqns. (1) and (2) are convenient for describing extraction equilibria in exchange extractions, particularly of diethyldithiocarbamates, even under conditions where dissociation of free reagent and metal hydrolysis occur.

REFERENCES

- 1 A. Wytténbach and S. Bajo, *Anal. Chem.*, **47** (1975) 1813.
- 2 S. Bajo and A. Wytténbach, *Anal. Chem.*, **51** (1979) 376.
- 3 S. Bajo, *Anal. Chim. Acta*, **105** (1979) 281.
- 4 B. Ya. Spivakov and Yu. A. Zolotov, *Zh. Anal. Khim.*, **23** (1968) 1124.
- 5 F. Macásek, *Zh. Anal. Khim.*, **24** (1969) 1443.
- 6 H. Irving and T. B. Pierce, *J. Chem. Soc.*, (1959) 2365.
- 7 B. S. Jensen, *Acta Chem. Scand.*, **13** (1959) 1347.
- 8 F. Macásek, *Chem. Zvesti*, **28** (1974) 3.
- 9 F. J. C. Rossotti and H. Rossotti, *The Determination of Stability Constants and Other Equilibrium Constants in Solution*, McGraw-Hill, London, 1961.
- 10 E. Still, *Fin. Kemisteamfundets Medd.*, **73** (1964) 90.
- 11 J. Starý, M. Kyrš and M. Marhol, *Separation Methods in Radiochemistry* (in Czech), Academia, Prague 1975, p. 34.
- 12 J. Starý and K. Kratzer, *Anal. Chim. Acta*, **40** (1968) 93.
- 13 P. C. A. Ooms, V. A. Brinkman and H. A. Das, *Radiochem. Radioanal. Lett.*, **31** (1977) 317.
- 14 L. G. Sillén and A. E. Martell, *Stability Constants of Metal-Ion Complexes*, The Chemical Society, London, 1964.
- 15 L. Sachs, *Statistische Auswertungsmethoden*, Springer-Verlag, Berlin/New York, 1972.
- 16 Yu. I. Usatenko, V. S. Barkalov and F. M. Tulyupa, *Zh. Anal. Khim.*, **25** (1970) 1458.

GASEOUS CATALYSTS FOR END-POINT INDICATION IN TITRIMETRIC ANALYSIS IN THE MICROGRAM RANGE

HERBERT WEISZ* and JOACHIM SCHLIPF

*Lehrstuhl für Analytische Chemie, Chemisches Laboratorium der Universität,
Freiburg i.Br. (F.R.G.)*

(Received 14th July 1980)

SUMMARY

The method of end-point detection described is very sensitive. In titrations with sodium sulphide, the first drop of titrant in excess cause evolution of hydrogen sulphide which acts as a catalyst for the indicating iodine—azide reaction. The gas formed at the end-point is transferred by a nitrogen stream to the indicator vessel. Microgram amounts of metal ions (Sb, Ni, Fe, Hg + Cd, Pb + Cu, Ag + Cu) and permanganate can be titrated in acidic solution with standard sulphide solution. In a variation of this method, acid—base titrations are possible.

The application of catalyzed reactions for end-point indication in titrimetric analysis has led to the development of numerous methods in recent years [1, 2]. The basic principle of this kind of titrimetric analysis can be generally described as follows. The catalyst itself serves as the titrant. Substances (inhibitors) can be titrated which diminish the activity of the catalyst by precipitation, complex formation or oxidation [3]. After all the inhibitor has reacted, i.e., at the end-point of the titration, the first drop of the titrant in excess immediately accelerates the indicator reaction. The course of the indicator reaction can be observed either visually or instrumentally (e.g. potentiometry [4], photometry [5], thermometry [6], biamperometry [7]). The advantage of catalytic titration end-points is that the excess of titrant is used only as a catalyst; accordingly, a very small excess will catalyze rather large amounts of the indicating reaction mixture. That means that such end-points are remarkably sensitive.

In the new method described in this paper, a gas is evolved at the end-point and acts as a catalyst for the indicating reaction; this reaction takes place in a separate indicator vessel. To illustrate the method, titrations with sodium sulphide standard solutions using the well known iodine—azide reaction [8] as indicator system are discussed. Some other possibilities for gaseous catalysts in titrimetric analysis are also outlined.

Sodium sulphide can be used as standard solution for the determination of a number of metal ions (precipitation) and permanganate (redox reaction), both in acidic solution. At the end-point, hydrogen sulphide is liberated and

transferred by a stream of nitrogen into a separate vessel containing the iodine—azide mixture; immediately, the iodine—azide reaction is catalyzed and the colour of the solution disappears.

EXPERIMENTAL

Apparatus

Figure 1 shows the simple arrangement necessary. A test tube (1) of suitable size (volume 0.5 ml) serves as the titration vessel. Through the stopper lead three capillary tubes: one for the titrant, one for nitrogen, and one to connect the titration vessel with the indicator reaction vessel (2) which has a volume of 2 ml. The titrant solution is delivered at a constant speed by using an automatic syringe burette (3) with a capacity of 50 ml. This large volume means that the sodium sulphide solution is protected against air and consequently stable for at least 2 weeks. The flow of nitrogen is regulated by using a flowmeter (Rota, Wehr, Tube L0.025/1,9).

General procedure

For all the titrations described here, the following indicator reagent solution (iodine—azide) was placed in the indicator reaction vessel: 100 μl of 2×10^{-3} M iodine, 50 μl of 0.5% starch solution, and 1000 μl of 0.5 M sodium azide solution. For the determination of metal ions (precipitation) and of permanganate (oxidation), a 3×10^{-3} M sodium sulphide solution was delivered at a constant speed of 25 $\mu\text{l min}^{-1}$. To determine sodium hydroxide with acid (2×10^{-3} M H_2SO_4), sodium sulphide is used only as the indicator (see below).

The flow of nitrogen was always 4.5 ml min^{-1} . In all determinations, the time for the delivery of titrant (Na_2S) was exactly measured (stopwatch) between the start of the titration and the complete decolorization of the iodine—azide—starch solution. In all examples a blank had to be determined by graphic extrapolation. This blank is due to the time difference between the liberation of the hydrogen sulphide in the titration vessel and the complete reaction in the indicator vessel. Evaluation of the measurements is described below.

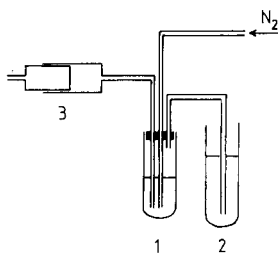


Fig. 1. Schematic representation of the titration arrangement: (1) titration vessel; (2) indication vessel; (3) automatic syringe burette.

RESULTS AND DISCUSSION

Determination of antimony(III)

The antimony(III) solution (100 μ l containing 2.5–25 μ g Sb(III)) in 2 M HCl and 100 μ l of water is titrated with the sodium sulphide standard solution (3×10^{-3} M). The time required for complete decolorization is observed, and the blank (time) is deducted. This blank value is found and the titrant solution is standardized by measuring two titration times for two known standard amounts of antimony. These standard times are plotted against the known amounts of the metal. The intersection of the line with the time axis gives the blank value (cf. Fig. 2). Unknown solutions are evaluated as follows: unknown mass = standard mass $\times (t_x - t_b)/(t_s - t_b)$, where t is time and the subscripts x, b and s correspond to the unknown, blank and standard, respectively. As an example of a calculation (cf. Table 1), for $t_x = 157$ s, $t_b = 29$ s, and $t_s = 265$ s (for 25 μ g), the unknown mass is $25(157 - 29)/(265 - 29) = 13.6 \mu$ g Sb.

Some results for single determinations are given in Table 1.

Determination of nickel by back-titration

Because nickel cannot be precipitated as sulphide in acidic medium whereas an acidic medium is necessary for indication of the end-point, a known excess of sodium sulphide is added to the ammoniacal sample solution followed by a defined excess of a copper standard solution and then the solution is acidified. This procedure is possible because nickel sulphide once precipitated in ammoniacal medium is acid-resistant (by ageing). The unconsumed copper is back-titrated with sodium sulphide standard solution. The more nickel is present, the more copper has to be back-titrated.

In the procedure, to 100 μ l of the sample solution (1.5–15 μ g Ni) and 20 μ l of 2 M ammonia, 70 μ l of standard sulphide solution are added to the titration vessel whilst nitrogen is flowing. After about 30 s, 100 μ l of copper

TABLE 1

Titration of single species with sodium sulphide

<i>Titration of antimony (μg/0.2 ml)</i>										
Time(s)	60	84	84	103	131	157	179	186	203	234
Sb found	3.4	5.8	5.8	7.8	11.7	13.6	16.2	16.6	18.4	22.1
Sb taken	3.2	5.8	6.5	8.5	11.7	13.7	16.5	17.7	21.2	23.5
<i>Titration of nickel (μg/0.34 ml)</i>										
Ni found	2.9	3.1	4.0	4.3	6.0	7.7	8.1	9.6	12.4	12.9
Ni taken	2.3	2.9	4.7	5.0	5.3	6.9	8.1	9.9	12.6	13.9
<i>Titration of iron (μg/0.2 ml)</i>										
Fe found	1.5	1.6	2.6	2.6	3.2	5.2	8.0	9.0	13.0	12.4
Fe taken	1.6	2.0	1.8	3.4	4.2	6.8	7.6	9.6	13.2	13.6

standard solution (containing $12\text{ }\mu\text{g Cu}^{2+}$) and $50\text{ }\mu\text{l}$ of 2 M acetic acid are added and the excess of copper is titrated as described for the determination of antimony. Evaluation of the results is also done similarly. Table 1 shows some results. Obviously, cobalt(II) could be determined in the same way.

Determination of iron(III) by displacement titration

As an example of a metal ion which does not form a sulphide stable in acidic solution, the determination of iron(III) is described. Iron(III) can be determined by a displacement titration. An equivalent amount of copper is demasked from its EDTA complex by the ion to be determined and titrated with sodium sulphide standard solution.

In a typical procedure, $100\text{ }\mu\text{l}$ of Cu-EDTA solution ($0.315\text{ }\mu\text{mol}$) is added to $100\text{ }\mu\text{l}$ of the sample solution ($1.5\text{--}15\text{ }\mu\text{g Fe}^{3+}$) in 0.2 M glycine buffer (pH 2.6) and the demasked copper is titrated as described for the determination of antimony.

In this particular case, the results have to be evaluated by extrapolation from a standard graph (Fig. 3) because the relationship between the amount of iron and the volume of titrant is not linear. Table 1 gives some results.

Determination of mercury and cadmium

Mercury is precipitated from 1 M HCl solution. Under these conditions cadmium is not precipitated. After mercury has been titrated with sodium sulphide, the solution is adjusted to pH 4.6 and then cadmium can be titrated.

In a typical procedure, $200\text{ }\mu\text{l}$ of the sample solution ($4.5\text{--}45.0\text{ }\mu\text{g Hg}$ and $2.5\text{--}25.0\text{ }\mu\text{g Cd}$) in 1 M HCl is first titrated with sodium sulphide (for the determination of mercury). Then $100\text{ }\mu\text{l}$ of a buffer solution (4 M NaOH and 0.4 M acetate buffer pH 4.6, $1 + 1$) is added and cadmium is titrated. The results for the two ions are evaluated as described above for antimony. It was found that the results for cadmium were not independent of the amount of

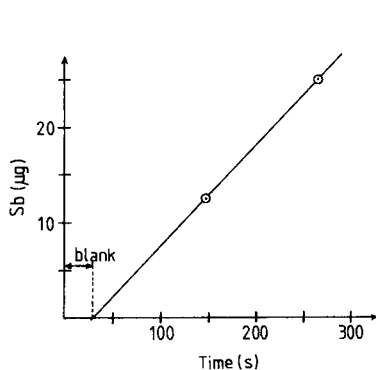


Fig. 2. Determination of the blank value for the titration of antimony.

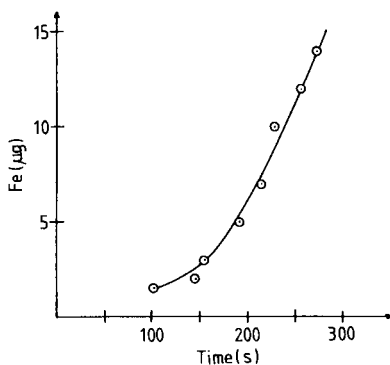


Fig. 3. Standard graph for the determination of iron(III).

TABLE 2

Titrations of binary mixtures with sodium sulphide

<i>Titration of mercury and cadmium ($\mu\text{g}/0.2\text{ ml}$)</i>										
Hg found	6.3	5.5	13.5	22.0	29.0	36.0	36.0	38.0	42.5	40.0
Hg taken	5.2	7.8	12.8	21.1	29.0	35.9	36.7	40.2	41.4	41.7
Cd found	2.9	19.2	22.9	8.6	2.8	18.0	10.9	23.4	12.0	5.6
Cd taken	2.6	18.7	22.4	9.4	3.9	17.9	11.6	23.0	11.5	4.7
<i>Titration of copper and lead ($\mu\text{g}/0.2\text{ ml}$)</i>										
Cu found	3.1	4.0	4.9	5.7	6.7	9.0	10.6	10.2	11.9	14.7
Cu taken	2.0	3.9	4.5	5.9	6.6	8.3	10.8	11.0	12.8	14.7
Pb found	12.3	44.8	44.5	27.8	9.5	17.8	26.0	4.9	5.5	15.6
Pb taken	12.0	44.0	47.5	25.5	10.0	16.0	26.8	5.5	5.2	17.5
<i>Titration of silver and copper ($\mu\text{g}/0.2\text{ ml}$)</i>										
Ag found	14.0	12.8	21.0	27.2	40.5	43.2	46.9	58.9	61.9	68.5
Ag taken	10.0	11.7	21.0	24.8	36.0	40.5	46.5	57.0	61.5	69.0
Cu found	14.1	7.2	2.3	2.5	9.3	12.4	9.0	10.1	3.2	2.7
Cu taken	14.2	7.2	2.4	1.8	9.6	13.8	9.3	10.2	3.3	3.3

mercury present, and so a correction was determined empirically to overcome this systematic error: $\text{Cd (found)} - 0.083 \text{ Hg (found)} = \text{Cd (corrected)}$.

Some results of single determinations of binary mixtures are given in Table 2.

Determination of copper and lead

Copper and lead can be determined similarly to mercury and cadmium.

Typically, 100 μl of the sample solution (1.5–15 μg Cu and 5–50 μg Pb) and 100 μl of 1 M HNO_3 are titrated with sodium sulphide (for the determination of copper). Then 100 μl of buffer solution (2 M NaOH and 0.4 M acetate buffer pH 4.6, 1 + 1) is added and the lead is titrated.

Some results of the determinations are given in Table 2.

Determination of silver and copper

Copper can be masked with EDTA against sulphide precipitation. After the silver has been titrated, the copper is demasked with iron(III) and then titrated likewise.

In a typical procedure, 200 μl of the sample (7.5–75 μg Ag and 1.5–15 μg Cu) in 0.5 M acetic acid containing 2×10^{-3} M EDTA solution is titrated with sodium sulphide (for the determination of silver). Then 50 μl of 8.2×10^{-3} M iron(III) is added and the copper is titrated. Some results are given in Table 2.

Determination of permanganate by redox titration

An aliquot (100 μl) of the permanganate solution (0.21–2.1 μmol) and 100 μl of 1 M H_2SO_4 are titrated with sodium sulphide standard solution

TABLE 3

Titration of permanganate ($\mu\text{mol}/0.2\text{ ml}$) with sodium sulphide

Found	0.33	0.40	0.60	0.66	1.08	1.28	1.26	1.37	1.71	1.80
Taken	0.29	0.38	0.55	0.67	0.92	1.16	1.32	1.43	1.81	1.98

($3 \times 10^{-3}\text{ M}$). The titration data are evaluated as described for the determination of antimony.

Some results for single determinations are given in Table 3.

Determination of sodium hydroxide

Not only precipitation and redox titrations but also acid–base titrations are possible. In this case, the sodium sulphide serves only as the indicating substance. The general procedure is explained for the determination of sodium hydroxide.

In order to achieve adequate precision with sodium sulphide as indicator, so that it can be compared with a common acid–base indicator such as methyl red, it is necessary to use a large sample volume (5 ml) and a high flow rate of nitrogen (35 ml min^{-1}).

In the general procedure, 0.1 ml of $3 \times 10^{-3}\text{ M}$ sodium sulphide is added to 0.5 ml of the sample solution ($0.3\text{--}3\text{ }\mu\text{mol}$) and the mixture is diluted to 5 ml with water. It is then titrated with $2 \times 10^{-3}\text{ M H}_2\text{SO}_4$ at a constant speed of 0.112 ml min^{-1} . At the end-point, hydrogen sulphide is formed. The titration data are evaluated in the way described for the other examples.

The results were compared with results obtained for the same samples with methyl red as indicator. The agreement is reasonably good (Table 4).

Other gaseous catalysts

Hydrogen sulphide is certainly not the only gaseous catalyst that can be used for end-point indication. Another possibility is the application of the well-known iodide-catalyzed cerium(IV)–arsenic(III) reaction described by Sandell and Kolthoff [9]. Thus in titrations with bromate solutions, free bromine is formed at the end-point and this reacts with iodide to form volatile iodine, which can be transferred by nitrogen to the indicator vessel. Preliminary experiments with a number of ions, e.g., antimony(III) seem very promising; these methods will be described at a later date.

TABLE 4

Titration of sodium hydroxide ($\mu\text{mol}/5\text{ ml}$) with sulfuric acid using methyl red (MR) or sodium sulphide (Na_2S) as indicator

Found MR	0.26	0.46	0.47	0.99	1.08	1.10	1.53	1.58	2.30	3.06
Na_2S	0.28	0.37	0.49	1.01	1.11	1.13	1.51	1.56	2.28	2.98
Taken	0.30	0.40	0.50	1.00	1.10	1.10	1.51	1.60	2.24	3.00

REFERENCES

- 1 H. Weisz and U. Muschelknautz, *Fresenius Z. Anal. Chem.*, 215 (1966) 17.
- 2 T. P. Hadjiioannou, *Rev. Anal. Chem. Isr.*, 3 (1976) 82.
- 3 S. Pantel and H. Weisz, *Anal. Chim. Acta*, 116 (1980) 421.
- 4 H. Weisz and D. Klockow, *Fresenius Z. Anal. Chem.*, 232 (1967) 321.
- 5 H. Weisz and S. Pantel, *Anal. Chim. Acta*, 62 (1972) 361.
- 6 H. Weisz, T. Kiss and D. Klockow, *Fresenius Z. Anal. Chem.*, 247 (1969) 248.
- 7 S. Pantel and H. Weisz, *Fresenius Z. Anal. Chem.*, 281 (1976) 211.
- 8 F. Feigl, *Fresenius Z. Anal. Chem.*, 74 (1928) 369.
- 9 E. B. Sandell and I. M. Kolthoff, *J. Am. Chem. Soc.*, 56 (1934) 1426.

NEW METALLOCHROMIC INDICATORS FOR COMPLEXIMETRIC TITRATION OF CALCIUM

H. WADA* and G. NAKAGAWA

Laboratory of Analytical Chemistry, Nagoya Institute of Technology, Showa-ku, Nagoya (Japan)

(Received 17th June 1980)

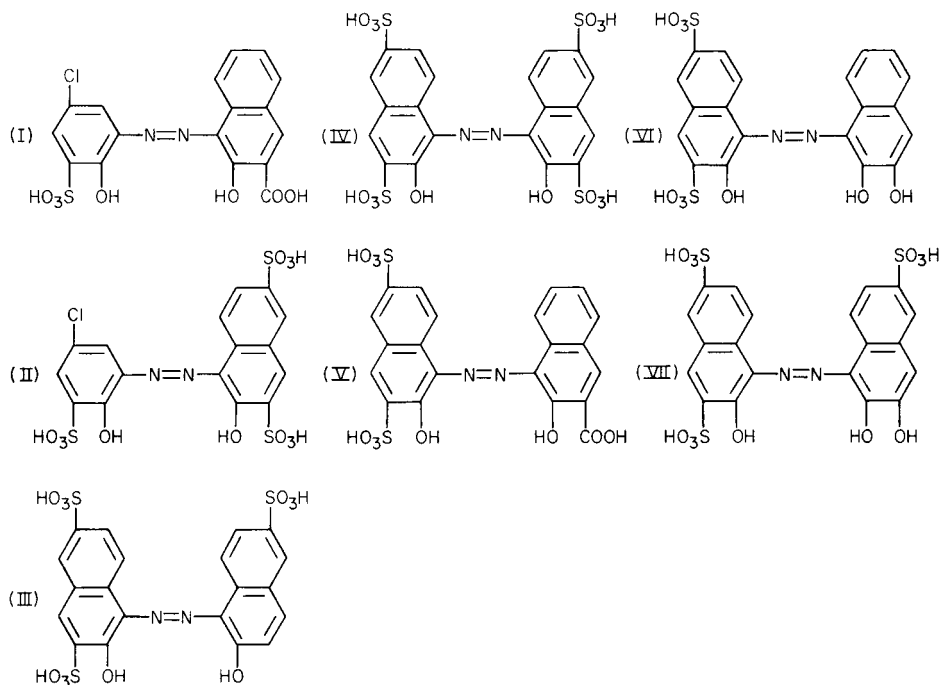
SUMMARY

Seven *o,o'*-dihydroxyazo dyes were synthesized and tested as metallochromic indicators for calcium: 1-(2-hydroxy-3-sulfo-5-chloro-1-phenylazo)-2-hydroxy-3-naphthoic acid (I), 1-(2-hydroxy-3-sulfo-5-chloro-1-phenylazo)-2-naphthol-3,6-disulfonic acid (II), 1-(2-hydroxy-6-sulfo-1-naphthylazo)-2-naphthol-3,6-disulfonic acid (III), 2,2'-dihydroxy-1, 1'-azonaphthalene-3,3', 6,6'-tetrasulfonic acid (IV), 1-(2-hydroxy-3-carboxy-1-naphthylazo)-2-naphthol-3,6-disulfonic acid (V), 1-(2,3-dihydroxy-1-naphthylazo)-2-naphthol-3,6-disulfonic acid (VI), 1-(2,3-dihydroxy-6-sulfo-1-naphthylazo)-2-naphthol-3,6-disulfonic acid (VII). The acid dissociation constants and the formation constants of the calcium and magnesium chelates of these dyes were determined. The rate of the decomposition of these dyes and their calcium chelates in alkaline solutions was also examined. From the results of photometric and visual titrations of calcium in the presence of magnesium, indicators III and IV provide the sharpest end-points and the best stability in alkaline solutions.

Determination of calcium and magnesium is one of the oldest problems in compleximetric titrations. Eriochrome black T or calmagite gives a reasonably satisfactory end-point for the titration of the sum of calcium and magnesium at pH 10, but none of the many indicators that have been proposed for the titration of the calcium in the presence of magnesium hydroxide at pH 12–13 is fully satisfactory with respect of the sharpness or contrast of the end-point color change and/or stability in solution. For example, Patton and Reeder's dye (abbreviated as NN or HSN) is unstable in alkaline solution, and calcon can be used only in a narrow pH range. With calcein and methyl thymol blue, the recovery of calcium falls off as the ratio of magnesium to calcium is increased [1]. Hydroxynaphthol blue (HNB) was recommended by Itoh and Ueno [2] because of the stability of its solutions and the slightly better end-point compared with that of NN.

In the present work, seven *o,o'*-dihydroxy dyes were synthesized, and the stabilities of these dyes and their calcium chelates in alkaline solutions were examined. Their acid dissociation constants and the formation constants of their calcium and magnesium chelates were determined. From the results of the photometric and visual titrations it was found that 1-(2-hydroxy-6-

sulfo-1-naphthylazo)-2-naphthol-3,6-disulfonic acid (III) and 2,2'-dihydroxy-1,1'-azonaphthalene-3,3',6,6'-tetrasulfonic acid (IV) are much better indicators than NN and HNB. Moreover, the solutions of these dyes are more stable.



- [I] 1-(2-Hydroxy-3-sulfo-5-chloro-1-phenylazo)-2-hydroxy-3-naphthoic acid.
 [II] 1-(2-Hydroxy-3-sulfo-5-chloro-1-phenylazo)-2-naphthol-3,6-disulfonic acid.
 [III] 1-(2-Hydroxy-6-sulfo-1-naphthylazo)-2-naphthol-3,6-disulfonic acid.
 [IV] 2,2'-Dihydroxy-1,1'-azonaphthalene-3,3',6,6'-tetrasulfonic acid.
 [V] 1-(2-Hydroxy-3-carboxy-1-naphthylazo)-2-naphthol-3,6-disulfonic acid.
 [VI] 1-(2,3-Dihydroxy-1-naphthylazo)-2-naphthol-3,6-disulfonic acid.
 [VII] 1-(2,3-Dihydroxy-6-sulfo-1-naphthylazo)-2-naphthol-3,6-disulfonic acid.

EXPERIMENTAL

Synthesis of dyes

[I] and [II]. 2-Amino-4-chlorophenol-6-sulfonic acid was dissolved in 5% sodium carbonate solution and the solution was acidified with 11 M HCl; then 20% sodium nitrite solution was added at 0°C. The diazo compound produced was coupled with 2-hydroxy-3-naphthoic acid in 2.5 M NaOH or with 2-naphthol-3,6-disulfonic acid in 1 M NaOH. The solution was allowed to stand for 1 h and then acidified with 11 M HCl: the crude dye precipitated.

[III], [IV], [V], [VI] and [VII]. Disodium 1-nitroso-2-naphthol-3,6-disulfonate was reduced with tin(II) chloride in 11 M HCl solution. The amino compound obtained was dissolved in water and a small amount of

copper(II) sulfate was added. Then the solution was adjusted to pH 5–6 with sodium carbonate and diazotized with 20% sodium nitrite solution. The diazo compound was obtained by salting out. 2-Naphthol-6-sulfonic acid or 2-naphthol-3,6-disulfonic acid in 1 M NaOH solution was added to the diazo compound in 0.1 M Na_2CO_3 . The mixture was heated at 60°C for 2–3 h, and allowed to stand overnight at room temperature. In the cases of V, VI and VII, the coupling reaction was carried out at room temperature.

Purification of dyes

Every crude dye was dissolved in a small amount of water and concentrated hydrochloric acid was added gradually. After one or two days the precipitate was filtered. This recrystallization was repeated several times. The crystalline powder obtained was dried for at least a week in a desiccator over phosphorus pentoxide and sodium hydroxide pellets separately. According to Diehl and Ellingboe [3], *o*-hydroxyazo dyes do not react with calcium and magnesium. Since all these dyes react with calcium and magnesium to form purple chelates and their molar absorptivities are higher than $10^4 \text{ dm}^3 \text{ mol}^{-1} \text{ cm}^{-1}$, none of them can be *o*-hydroxyazo dyes. The dark violet crystalline powder of each compound is almost pure with respect to active dye: only one spot for each dye appeared on a paper chromatogram developed with a propanol–ethyl acetate–water mixture (5 + 5 + 4) or with *n*-butanol saturated with 2 M HCl, and the absorption spectra of the dyes and calcium or magnesium chelates at different pH show clear isosbestic points. These dyes may contain some amounts of water and sodium. Elemental analyses of the dyes were not carried out because of the hygroscopic properties of the dyes.

NN and HNB were obtained from Dojin Chemical Laboratory, Kumamoto, Japan. HNB was purified by recrystallization from 11 M HCl solution.

Reagents and apparatus

The stock solutions were prepared from analytical-grade calcium oxide and magnesium chloride hexahydrate. Dye solutions were prepared by dissolving weighed amount of dyes in water and stored in a refrigerator. An EDTA solution was standardized against a standard zinc(II) solution with xylenol orange as indicator. Buffers comprising $\text{ClCH}_2\text{COOH}-\text{ClCH}_2\text{COONa}$ (pH 2–4), $\text{CH}_3\text{COOH}-\text{CH}_3\text{COONa}$ (pH 4–6), $\text{KH}_2\text{PO}_4-\text{Na}_2\text{HPO}_4$ (6.5–8.5), $\text{Na}_2\text{B}_4\text{O}_7-\text{HCl}$ (pH 8.5–9) and $\text{Na}_2\text{B}_4\text{O}_7-\text{KOH}$ (pH 9–11) were used. For pH in the range above 11, the pH was adjusted by addition of standard potassium hydroxide solution standardized with sodium hydrogen-phthalate and stored free from CO_2 .

A Hitachi Model 124 double-beam spectrophotometer, a Hirma automatic titrator, and a Yanagimoto pH meter calibrated with standard buffer solutions of pH 6.86 and pH 9.18 (25°C) were used.

RESULTS AND DISCUSSION

Stability of the dyes and their calcium chelates in solution

The dyes and their calcium chelates gradually decompose in alkaline solutions. The decreases in absorbances of the dye solutions and their calcium chelate solutions were measured over 20 min at pH 12 and 13. The results are shown in Table 1. In the cases of I, II, III, and IV, the solutions of both the indicator and the calcium chelate are much more stable than those of NN or HNB.

Acid dissociation constants and formation constants

Generally, sulfonic and carboxylic acids dissociate at low pH; the dissociations of *o,o'*-dihydroxy groups are shown as:



with $k_1 = [\text{HL}][\text{H}]/[\text{H}_2\text{L}]$, $k_2 = [\text{L}][\text{H}]/[\text{HL}]$

TABLE 1

Percentage decrease in the absorbances of the indicators and their calcium chelates with time

Dye	Dye solution					Ca chelate solution				
	λ (nm)	pH	% Decrease			λ (nm)	pH	% Decrease		
			Time (min)					Time (min)		
			2	5	20			2	5	20
NN	650	12	0	0	3.5	560	12	41.1	98.1	98.3
		13	0.5	0.8	41.8		13	0.8	5.5	36.8
HNB	645	12	0.3	1.0	14.3	560	12	1.0	3.2	25.5
		13	0.8	6.8	55.1		13	0	0	1.3
I	600	13	0	1.7	5.8	535	13	0	0	0
II	595	12	0	0	0	535	12	0	0	0
		13	0	0	0		13	0	0	0
III	640	12	0	0	0	555	12	0	0	6.4
		13	0.4	0.9	1.6		13	0	0	0
IV	643	12	0.4	0.6	0.6	560	12	0	0	7.3
		13	0.6	0.8	2.6		13	0	0	0
V	642	12	0.3	0.5	2.3	560	12	17.1	34.7	93.5
		13	0.9	1.9	7.6		13	0.8	2.5	17.2
VI	625	12	0.3	0.5	2.3	560	12	2.1	5.5	17.6
		13	0.9	1.9	7.6		13	0.7	2.1	11.0
VII	628	12	0	0	0.3	540	12	22.5	63.8	87.5
		13	0	0.3	1.7		13	0.2	0.6	13.8

(Charges are omitted for simplicity.) As an example, absorption spectra of III at various pH values are shown in Fig. 1. The absorption maxima of the H_2L , HL and L forms of the indicator dyes are summarized in Table 2. Dissociation constants k_1 and k_2 were determined by Hildebrand and Reilley's method [4]. In each case the plot of $\log[HL]/[H_2L]$ or $\log[L]/[HL]$ vs. pH yielded a straight line with a slope of unity. All first dissociation constants k_1 are mixed constants involving activity of hydrogen ion measured with glass electrode, while all second dissociation constants k_2 are concentration constants involving the concentration of hydrogen ion calculated from the KOH concentration. The values of k_1 and k_2 obtained are shown in Table 3.

The dyes react with calcium and magnesium to give purple chelates in the pH range above 8, and above 7, respectively. The absorption spectra of the calcium and magnesium chelates of I, II, III, and IV are shown in Fig. 2. The absorption maxima of the calcium chelates are listed in Table 2. In the pH range 8–10, since the free indicators are present as HL, the equilibrium for the calcium or magnesium chelate is given by $M + HL \rightleftharpoons ML + H$, where M represents Ca^{2+} or Mg^{2+} . The equilibrium constant is given by $K_{ML}^{HL} = [ML][H]/[M][HL]$, and so $\log K_{ML}^{HL} = \log[ML]/[HL] - pH - \log[M]$.

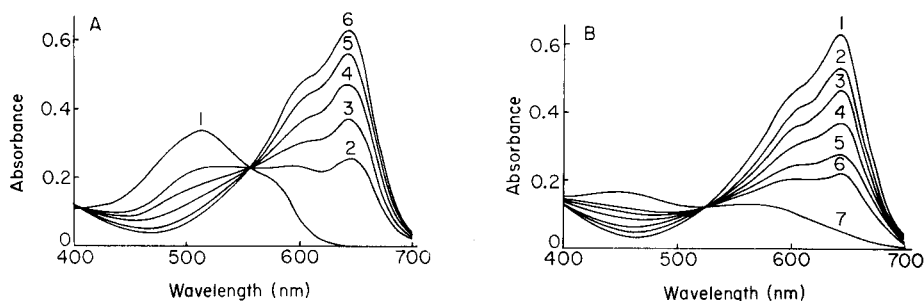


Fig. 1. Absorption spectra of indicator III (3×10^{-5} M). (A) At pH (1) 3.19–3.66; (2) 5.46; (3) 5.84; (4) 6.23; (5) 6.71; (6) 7.94–8.37. (B) At pH (1) 9.96–10.73; (2) 12.73; (3) 13.03; (4) 13.33; (5) 13.57; (6) 13.73; (7) >14.

TABLE 2

Absorption maxima of the dyes and their calcium chelates

Dye	H_2L (nm)	HL (nm)	L (nm)	CaL (nm)
I	490	580	500	540
II	505	600	535	537
III	515	643	550	558
IV	515	648	565	562
V	550	642	560	558
VI	520	637	—	550
VII	494	630	540	535

TABLE 3

Acid dissociation constants of the dyes and the formation constants of their calcium and magnesium chelates (Ionic strength 1.0, $25 \pm 1^\circ\text{C}$)

Reagent	pK_1	pK_2	$-\log K_{\text{CaL}}^{\text{HL}}$	$-\log K_{\text{MgL}}^{\text{HL}}$
I	7.34	13.5	6.81	6.13
II	5.96	12.5	6.37	5.33
III	5.69	13.4	7.94	6.51
IV	5.73 ^a	13.5	7.94	6.64
V	9.25 ^a	14.0	8.46	—
VI	5.99	—	—	—
VII	5.80	—	—	—
NN ^b	9.26 ^a	13.7 ^a	7.82 ^a	—
HNB	6.05	12.9	7.79	6.83
HNB ^{b,c}	6.44 ^a	12.9 ^a	6.82 ^a	6.83 ^a

^a $\mu = 0.1$. ^bReference [2]. ^cReference [5].

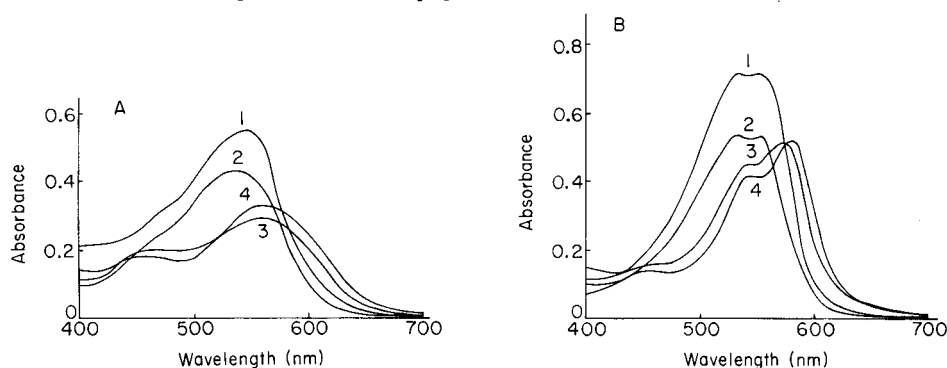


Fig. 2. Absorption spectra of (A) calcium and (B) magnesium chelates. 4×10^{-3} M metal ion; 2.5×10^{-5} M reagent. Dye: (1) I, (2) II, (3) III, (4) IV.

If a large excess of metal ion is present, $[M]$ is nearly equal to the total concentration of metal. $\log[ML]/[HL]$ can be calculated from the measured absorbance. Absorbance of the solution containing an indicator dye and a 100-fold excess of calcium or magnesium was measured at various pH values. The plots of $\log[ML]/[HL]$ vs. pH for I, II, III, IV or V yielded straight lines with a slope of unity. The equilibrium constants obtained are shown in Table 3. These are mixed constants involving hydrogen ion activity measured with a pH meter.

Photometric titration of calcium

The sharpness of the indicator color change at the equivalence point was examined by photometric titration. A 10^{-3} M calcium solution was titrated with 0.01 M EDTA solution by using these dyes as indicators. The results at pH 12.5–13 are shown in Fig. 3. In the cases of I, II, III, IV, V and HNB, satisfactorily sharp end-points were obtained, while in the cases of VI, VII and NN the color change appeared before the equivalence point.

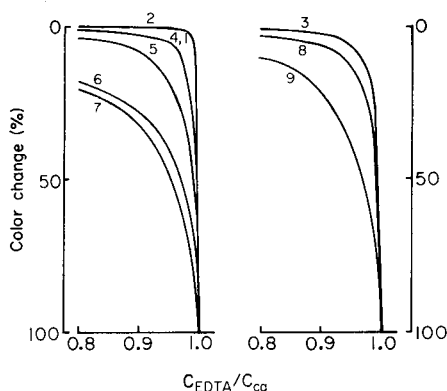


Fig. 3. Photometric titration curves of calcium at pH 12.5–13. Indicator: (1) I; (2) II; (3) III; (4) IV; (5) V; (6) VI; (7) VII; (8) HNB; (9) NN.

Visual titration of calcium

The sharpness of color change depends not only on the formation constant of the calcium chelate but also on the color contrast between the chelate and the free indicator and on the rate of the decomposition of the calcium chelate during the titration. Therefore the results of photometric titrations sometimes may not agree with those of visual titrations. The procedure used for testing was as follows: an aliquot of 10^{-2} M calcium solution was diluted to about 50 ml with water and 1, 2 or 4 ml of 8 M KOH solution was added. The solution was titrated with 10^{-2} M EDTA solution after adding 0.5–1 ml of 10^{-4} M indicator solution.

In the cases of indicators I and III, an excellent color change was observed at the equivalence point. Indicators IV and V gave sharp end-points, while with VI and VII premature end-points appeared as in the case of NN. With indicator II, because of the large k_2 value, the color contrast between the indicator and its calcium chelate was too small for visual titration when more than 2 ml of KOH was added. HNB also did not give a distinct color change when 4 ml of KOH was used.

Titration of calcium in the presence of magnesium

Titration of calcium in the presence of magnesium were usually done by using the procedure outlined above. When the molar ratio of $\text{Mg}^{2+}/\text{Ca}^{2+}$ exceeded 1, the method recommended by Patton and Reeder [6] was used. When the molar ratio of $\text{Mg}^{2+}/\text{Ca}^{2+}$ exceeded 10, the method recommended by Kodama et al. [7] was also employed. For this procedure, an aliquot of sample solution was diluted to 50 ml, 2 ml of 8 M KOH was added and the solution was allowed to stand for 3 min; after addition of indicator, the solution was titrated until the blue end-point appeared, hydrochloric acid (1 + 1) was added until the precipitate of $\text{Mg}(\text{OH})_2$ disappeared, then 3 ml of 8 M KOH was added, and the purple solution was titrated further to the blue end-point color.

TABLE 4

Titration of calcium (4.00 mg) in the presence of magnesium

Indicator	8 M KOH (ml)	Mg taken (mg)	Ca found ^a (mg)	Indicator	8 M KOH (ml)	Mg taken (mg)	Ca found ^a (mg)
I	4	2.46	4.10 ^b	V	2	2.46	3.98
III	2	2.46	4.00		4	2.46	3.98
	2	8.59	4.00	VI	2	2.46	3.98
	2	24.56	4.00 ^c		4	2.46	3.96
	4	8.59	4.00	VII	2	2.46	3.98
	4	24.56	3.98 ^d		4	2.46	3.98
IV	2	2.46	4.00	NN	2	8.59	3.97
	2	8.59	3.97		2	24.56	3.99 ^c
	2	24.56	3.95 ^c	HNB	2	8.95	3.99
	4	8.59	3.98		2	24.56	3.98 ^c
	4	24.56	3.96 ^d		4	24.56	3.97 ^d

^aAverage of 5 titrations. ^bIndistinct end-point. ^cKodama's method. ^dPatton and Reeder's method.

The results of these titrations are given in Table 4.

In the titration of calcium in the presence of magnesium at pH higher than 12, adsorption of the indicator on magnesium hydroxide precipitate sometimes disturbs the end-point color change. In the cases of the indicators I and II, sharp end-points could not be obtained. Because the stabilities of the magnesium complexes of these dyes are high, they react with magnesium hydroxide and the red precipitate may undergo slow reaction with EDTA. With indicators VI and VII the color change occurred considerably before the equivalence point even in the absence of magnesium. Indicator V gave a sharp color change when the molar ratio Mg^{2+}/Ca^{2+} was less than 2, but the contrast decreased with increasing amounts of magnesium. In the presence of a large amount of magnesium, indicators III and IV were excellent; the color changes at the equivalence points were much sharper than in the absence of magnesium, as was observed with NN. In these cases, probably some magnesium-indicator complex may participate in the end-point color change. The larger stability of the indicator-magnesium chelate than that of calcium improves the sharpness of the end-point. Among the seven indicators synthesized, indicator III is the best for the titration of calcium in the presence of magnesium, and IV is still much better than NN and HNB. Indicator I is excellent when calcium is titrated in the absence of magnesium.

We thank Professor Kyoji Tōei of Okayama University for his valuable advice on the synthesis and purification of the indicator dyes.

REFERENCES

- 1 R. Belcher, R. A. Close and T. S. West, *Talanta*, 1 (1958) 238.
- 2 A. Itoh and K. Ueno, *Analyst*, 95 (1970) 583.
- 3 H. Diehl and J. Ellingboe, *Anal. Chem.*, 32 (1960) 1120.
- 4 G. P. Hildebrand and C. N. Reilley, *Anal. Chem.*, 29 (1957) 258.
- 5 A. Itoh and K. Ueno, *Bunseki Kagaku*, 19 (1970) 393.
- 6 J. Patton and W. Reeder, *Anal. Chem.*, 28 (1956) 1026.
- 7 K. Kodama, M. Mizuno, T. Oga and M. Katsuda, *Bunseki Kagaku*, 14 (1965) 474.

ASYMMETRICALLY SUBSTITUTED DIPHENYLCARBAZONES AS CHELATE FORMERS

N. CZECH, B. FRIESE and F. UMLAND*

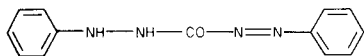
Anorganisch-Chemisches Institut, Lehrstuhl für Anorganisch-Analytische Chemie der Westfälischen Wilhelms-Universität Münster, Gievenbecker Weg 9-11, D-4400 Münster/Westf. (Federal Republic of Germany)

(Received 3rd March 1980)

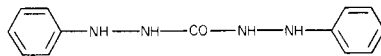
SUMMARY

Two isomeric asymmetrically substituted diphenylcarbazones, 1-(4-nitrophenyl)-5-phenylcarbazone and 1-phenyl-5-(4-nitrophenyl)carbazone, were synthesized by introducing one nitro group selectively. Their chelate complexes with several cations show increased molar absorptivities compared to those of the unsubstituted reagents, thus giving improved analytical sensitivity. The structure of the chelates is discussed; a five-membered ring structure is very plausible.

1,5-Diphenylcarbazone (I) has long been used in analytical chemistry [1]. It is particularly valuable for the spectrophotometric determination of mercury and diorganoboric acids, the most important of which is diphenylboric acid (Ph_2BOH) [2]. The determination of chromate with 1,5-diphenylcarbazide (II) is also based on the reaction of the carbazone with chromium (III) [1].



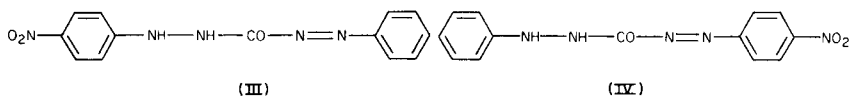
(I)



(II)

There are different opinions on the structure of these chelates [3, 4]. Asymmetrically substituted diphenylcarbazones, which are of interest not only in elucidation of the structure of the diphenylcarbazone chelates, but also for analytical applications in spectrophotometry and polarography, have not previously been described. Given suitable substituents, such compounds could be expected to form chelates with increased analytical sensitivity.

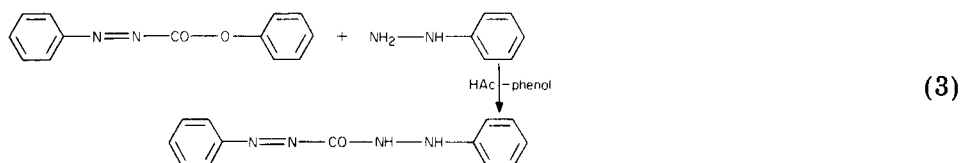
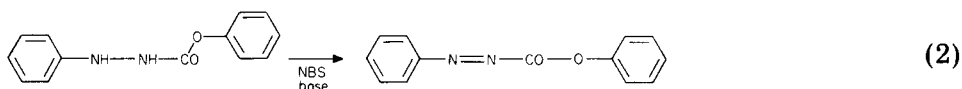
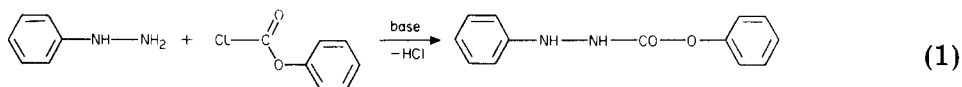
In the work described here, a new synthesis for 1,5-diphenylcarbazone, suggested by Friese [5], was utilized for the synthesis of two isomeric asymmetrically substituted diphenylcarbazones: 1-(4-nitrophenyl)-5-phenylcarbazone (III) and 1-phenyl-5-(4-nitrophenyl)carbazone (IV). The nitro group was chosen for substitution because of its auxochromic effect, and because the initial substances were easily accessible.



EXPERIMENTAL

Preparation of the chelate formers with reference to Fries [5]

Fries's synthesis consists of three steps



The following modifications were needed for the synthesis. For compound III, in step (3), 4-nitrophenylhydrazine (75% of the stoichiometric amount) was used with chloroform as solvent and refluxing was continued for 30 min (yield 43%).

For compound IV, in step (1), 4-nitrophenylhydrazine was used, the reflux time was 1 h, and the product was recrystallized from benzene/ethanol (1:2.5); the yield of pale yellow, large crystals (m.p. 160°C) was 44%. In step (2), after recrystallization from benzene, the yield of orange crystals (m.p. 59°C) was 63%. In step (3), twice the stated amount of acetic acid was used and recrystallization was from ethanol (yield 32%).

Characterization of the compounds

Compound III. The dark red crystals (m.p. 137°C) had a distinctive i.r. (KBr) band at 1690 cm^{-1} indicating C=O. The elemental results were: found 54.7% C, 3.8% H, 24.5% N; calculated 54.7% C, 3.9% H, 24.6% N.

Compound IV. The brown crystals (m.p. 153°C) had a distinctive i.r. (KBr) band at 1700 cm^{-1} indicating C=O. The elemental results found were 54.5% C, 4.0% H, 24.6% N.

The structures of the two compounds were examined by spectroscopic means. The mass spectra were particularly valuable for differentiating the two isomers. The main fragments obtained are listed in Table 1. Fragments 4 and 5 can be regarded as the most characteristic for compound III, and 9 and 11 for compound IV.

COMPARISON OF SOME CHELATES OF THE ISOMERIC CARBAZONES III AND IV WITH THOSE OF COMPOUND I

The chelates of compounds III and IV with diphenylboric acid, Cu(II), Cd(II), Hg(II), Mn(II), Co(II) and Ni(II) were studied by means of their u.v.—visible spectra. All chelates were measured in aqueous acetate-buffered

TABLE 1

Mass spectral data

Compound III			Compound IV		
Fragment	<i>m/z</i>	Relative intensity	Fragment	<i>m/z</i>	Relative intensity
1 C ₆ H ₅ —	77	100	7 C ₆ H ₅ —	77	100
2 O ₂ N—C ₆ H ₄ —NH	137	73	8 C ₆ H ₅ —NH—	92	84
3 O ₂ N—C ₆ H ₄ —	122	61	9 C ₆ H ₅ —NH—NH—	107	73
4 O ₂ N—C ₆ H ₄ —NH—NH—	152	56	10 O ₂ N—C ₆ H ₄ —	122	54
5 C ₆ H ₅ —N=N—	105	26	11 O ₂ N—C ₆ H ₄ —N=N—	150	19
6 Molecule	285	1	12 Molecule	285	1

solution at pH 4.8 and ionic strength 0.1 mol l⁻¹ (25°C.). The concentration of the metal ions was 5 mmol l⁻¹, and the concentration of the chelate formers added was 14 mmol l⁻¹. The absorbances were measured against an appropriate reagent blank within 30 min, as the solutions were not very stable. The wavelengths of maximum absorption and the molar absorptivities are specified in Table 2. For comparison, the appropriate data for the unsubstituted carbazone are also listed.

As expected, the molar absorptivities of the chelates are higher for the new isomers than for the unsubstituted 1,5-diphenylcarbazone, except in the case of the chelate of compound IV with diphenylboric acid. Simultaneously, a bathochromic shift of the absorption maxima can be observed, again with the exception of the diphenylboric acid chelates. The spectra showed just one maximum. The spectra of the copper chelates had a weak shoulder shifted about 25 nm to higher wavelengths; this indicates the existence of two differently composed chelates under the above-mentioned conditions. The Lambert-Beer law was followed over wide ranges. The upper limits of the linear ranges of the absorbance vs. concentration curves are listed in Table 3.

TABLE 2

Absorption maxima, λ_{\max} (nm), and molar absorptivities, ϵ (l mol⁻¹ cm⁻¹)

	Compound I		Compound III		Compound IV	
	λ_{\max}	ϵ	λ_{\max}	ϵ	λ_{\max}	ϵ
Ph ₂ BOH	540	7000	518	11000	521	6800
Cu(II)	451	16000	462	28000	490	38000
Zn(II)	522	630	571	3100	537	1000
Cd(II)	527	100	549	1300	543	800
Hg(II)	569	8600	600	16000	596	12000
Mn(II)	531	580	595	1700	572	1500
Co(II)	527	1000	579	4500	541	1800
Ni(II)	530	4800	591	6500	550	5500

TABLE 3

Upper limits of the linear ranges of the absorbances vs. concentration curves for chelates of compounds I, II, and IV.

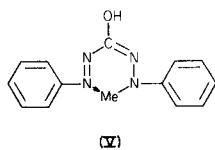
(The concentrations of the chelated species are given in mmol l^{-1} . Experimental conditions as mentioned above)

Chelated species	I	III	IV	Chelated species	I	III	IV
Ph_3BOH	5	22	14	Hg(II)	90	85	80
Cu(II)	10	10	10	Mn(II)	75	79	79
Zn(II)	60	75	83	Co(II)	55	70	63
Cd(II)	105	97	90	Ni(II)	34	49	53

The composition of the complexes and the complex dissociation constants were determined in solution according to the straight line method of Asmus et al. [6].

The ratio of the components in the complexes MeX_n is 1:2 for Cd(II) and Hg(II) ; all other chelates studied can be regarded as 1:1 complexes. The three chelating reagents do not differ in these respects. The dissociation constants determined by the method of Asmus et al. were corrected to equal ligand concentration as described by Schwarzenbach and Flaschka [7]; this was necessary, as the acidity constants of the particular diphenylcarbazones have different values (I, $\text{p}K_s = 8.0$; III, $\text{p}K_s = 6.4$; IV, $\text{p}K_s = 6.2$; these values were determined by titration with 0.1 M sodium hydroxide). The results listed in Table 4 show that the chelates of the substituted diphenylcarbazones are a little weaker than those of 1,5-diphenylcarbazone itself. Evidently, the electron density in the chelate-forming centre is decreased by the electron-attracting effect of the nitro group.

Some conclusions became possible about the structure of the diphenylcarbazone chelates. Marchart [4] proposed a six-membered ring structure (V) for these chelates.



If this formazan structure were correct, the chelates of compounds III and IV should just be mesomeric structures (VI and VII) and thus behave identically. However, this can be excluded confidently on account of their different spectra and stability constants.

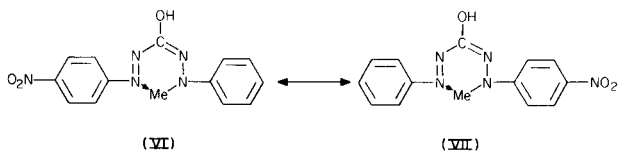
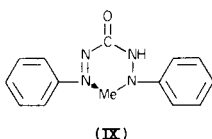
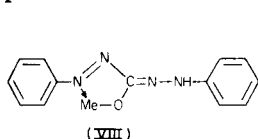


TABLE 4

pK_D values for the chelates of compounds I, III and IV (pH 4.8; ionic strength 0.1 mol l^{-1} ; 25°C)

Chelated species	I	III	IV	Chelated species	I	III	IV
Ph_2BOH	4.97	4.65	4.40	Hg(II)	16.30	14.98	14.86
Cu(II)	5.42	5.05	4.94	Mn(II)	4.12	3.61	3.50
Zn(II)	4.50	3.85	3.73	Co(II)	4.92	4.65	4.45
Cd(II)	7.01	6.21	6.30	Ni(II)	5.00	4.37	4.19

Here, preference is given to a five-membered ring structure (VIII) with coordination on the azo side of the molecule; this structure was proposed by Thierig and Umland [2] and was demonstrated by Friese and Umland for the diphenylboric acid chelate [8, 9]. A six-membered ring structure deriving from the keto form of the diphenylcarbazone cannot be excluded utterly. But for electronic reasons, this structure does not seem to be very plausible.



Conclusion

The very high molar absorptivity of the copper(II) chelate of compound III, and the very high stability of the mercury(II) chelates combined with increased absorptivities, are particularly interesting for spectrophotometric determinations, especially in conjunction with high-performance liquid chromatography. Generally, the new diphenylcarbazones should be suitable for all applications in which the unsubstituted compound has been used previously; in nearly all cases increased sensitivity can be counted upon.

We thank the Verband der Chemischen Industrie for material support.

REFERENCES

- 1 E. B. Sandell, *Colorimetric Determination of Traces of Metals*, Interscience, New York, 1959.
- 2 D. Thierig and F. Umland, *Fresenius Z. Anal. Chem.*, 221 (1966) 229.
- 3 R. T. Pflamm and L. C. Howick, *J. Am. Chem. Soc.*, 78 (1956) 4862.
- 4 H. Marchart, *Anal. Chim. Acta*, 30 (1964) 11.
- 5 B. Friese, *Liebigs Ann. Chem.*, (1977) 2110.
- 6 E. Asmus, U. Hinz, K. Ohls and W. Richly, *Fresenius Z. Anal. Chem.*, 178 (1960/61) 104.
- 7 See F. Umland, A. Janssen, D. Thierig and G. Wünsch, *Theorie und praktische Anwendung von Komplexbildnern in der Analytik*, Verlag Chemie, Weinheim, 1971, p. 276.
- 8 B. Friese and F. Umland, *Monatsh. Chem.*, 109 (1978) 711.
- 9 B. Friese and F. Umland, *Anal. Chim. Acta*, 96 (1978) 303.

FLOW INJECTION DETERMINATIONS OF POLYPHOSPHATES BASED ON COLORED METAL COMPLEXES OF XYLENOL ORANGE AND METHYLTHYMOL BLUE

NORIMASA YOZA*, YOUICHI KUROKAWA, YUKIO HIRAI and SHIGERU OHASHI

Department of Chemistry, Faculty of Science, Kyushu University, Hakozaki, Higashiku, Fukuoka 812 (Japan)

(Received 28th July 1980)

SUMMARY

Substitution reactions between samples and colored metal complexes, such as magnesium–methylthymol blue and cerium(III)–xylenol orange, are applied to flow injection determinations of orthophosphate, diphosphate, triphosphate and EDTA. Various types of manifold with a stopped-flow device are used; the importance of addition of reagents in a logical sequence is stressed. Kinetic and thermodynamic factors associated with the substitution reactions were found to be significantly reflected in the f.i.a. profiles and stopped-flow signals. The working ranges of the methods are 10^{-5} – 10^{-4} M.

Flow injection analysis (f.i.a.), a new type of continuous flow analysis [1, 2], has been successfully applied to the determinations of not only orthophosphate [1], but also polyphosphates such as diphosphate (pyrophosphate) and triphosphate (tripolyphosphate) [3, 4]. In f.i.a. for these phosphorus compounds, the sample solution is usually injected into a carrier stream of a molybdenum reagent to produce a heteropoly blue complex that can be automatically detected in a flow-through cell. Orthophosphate can be determined with a relatively simple manifold [1], because it reacts rapidly with the reagent to form the colored complex. For the determination of polyphosphates, the recommended flow injection system is held at higher pressure, and the hydrolysis of polyphosphates and the color reaction of the resultant orthophosphate with the molybdenum reagent are achieved simultaneously in a reaction coil maintained at 140°C [3, 4].

An alternative approach is to determine polyphosphates at room temperature without their chemical decomposition to orthophosphate. A cerium(III) solution as a carrier solution showed some promise for the determination of polyphosphates by measurement of the u.v.-absorption of the cerium(III) polyphosphate complexes [5]. Unfortunately, there are no appropriate reagents that react directly with polyphosphates to form colored complexes. Therefore, the indirect methods proposed in this paper were based on substitution reactions between colored metal complexes, $M-R$, and polyphosphates, P_n : $M-R + P_n \rightarrow M-P_n + R$. Cerium(III) and magnesium were examined for M and xylenol orange (XO) and methylthymol blue (MTB) for R . XO

and MTB have been widely used as reagents in batchwise colorimetric methods [6–8]. P_n represents orthophosphate (P_1), diphosphate (P_2) and triphosphate (P_3). EDTA was also tested as a reference sample.

When P_n is injected into a carrier stream of $M-R$, P_n reacts with M to form a colorless $M-P_n$ complex, which results in a decrease of the absorption in the sample zone. Two types of manifold were employed, with a valve for stopped-flow experiments, and the effects of kinetic and thermodynamic factors on the concentration profiles were studied. The advantages and limitations of this indirect method are discussed from the analytical and physicochemical viewpoints.

EXPERIMENTAL

Unless otherwise stated, all chemicals (Wako, Osaka) were used without further purification. Colorimetric reagents were methylthymol blue (MTB), xlenol orange (XO) and cerium(III) chloride. Orthophosphate, KH_2PO_4 , diphosphate, $Na_4P_2O_7 \cdot 10H_2O$ and triphosphate, $Na_2P_3O_{10} \cdot 6H_2O$, were used as samples. Only triphosphate was purified by the repeated recrystallization.

An ammonia–ammonium chloride buffer (pH 10.1) was used for the MTB complex, and a hexamine–nitric acid buffer (pH 6.2) for the XO complex.

The apparatus for f.i.a. consisted of a reciprocating pump (Kyowa KWU-90H), a spectrophotometer (Hitachi 200-10) with a flow-through cell (8- μ l volume, 8 mm path), a loop valve sample injector (Kyowa KMM-4V2) and a switching valve for the stopped-flow (Kyowa KMM-4V).

The sample (80- μ l) was introduced via a loop valve sample injector, combined with a bypass coil (PTFE, 0.3 mm i.d., 1 m length). The bypass coil helps to eliminate the injection shock. An elastic precoil (polyvinyl chloride, 2 mm i.d., 1 m length) before the injector was effective for damping the pumping pulse [3, 4]. The switching valve was located just before the detector to observe the variation in absorbance of the sample zone stopped in the flow cell. When the sample zone reached the flow cell, the valve was switched to lead the carrier solution to waste W_2 and to stop the sample zone in the flow cell. (The same effect would have been achieved by stopping the pump, with some types of pump.) The extent of the reaction was estimated by recording the variation in absorbance for about 2 min. The valve was then switched again on line to the detector.

The flow rate through each pumping channel was 1.1 ml min^{-1} . The residence times of sample zones in the manifolds (b) and (c) were 35 and 65 s, respectively.

RESULTS AND DISCUSSION

Manifolds

In f.i.a. the chemical reactions in the reaction coil should be as fast as possible for rapid sample throughput. Therefore, the manifolds must be

designed so as to achieve effective mixing of sample solutions with appropriate reagents in a reasonable sequence.

Figure 1(a) shows a manifold in which the sample solution (S) is injected into a carrier stream of colored M-R complex with a constant absorbance level. This one-channel system is commercially inexpensive, but has the significant drawback that a marked blank signal or solvent signal appears when solvent (water) is injected. This blank signal becomes very troublesome if one wants to determine samples at very low concentrations [4, 9].

To eliminate this blank signal, the two-channel system in Fig. 1(b) is recommended. The sample is injected into a carrier stream of water that is allowed to mix with the M-R reagent from another channel. This confluence method has been widely recognized as effective in eliminating the signals that arise from "schlieren" effects. It should be noted that the total concentrations of both M and R can be kept constant even in the sample zone.

The sequence of mixing the reagents with the sample in the analytical line becomes very important when competitive reactions are involved, e.g., when P_n and R compete with each other to react with M. The manifold (b) in Fig. 1 is recommended for use when the substitution reaction between M-R and P_n to form M- P_n is fast. If this forward reaction is slow, manifold (c) must be employed to permit the reaction of P_n with M in reaction coil C_2 prior to the reaction of R with M. The reverse substitution reaction then proceeds in reaction coil C_1 : $M-P_n + R \rightarrow M-R + P_n$. A drawback of manifold (c) is that the total concentration of M is diluted by the sample injection to produce a background signal, though the total concentration of R is kept constant.

Magnesium—MTB reagent system

Magnesium ions are well known to react rapidly with diphosphate, triphosphate and EDTA at about pH 10 to form 1:1 complexes with stability

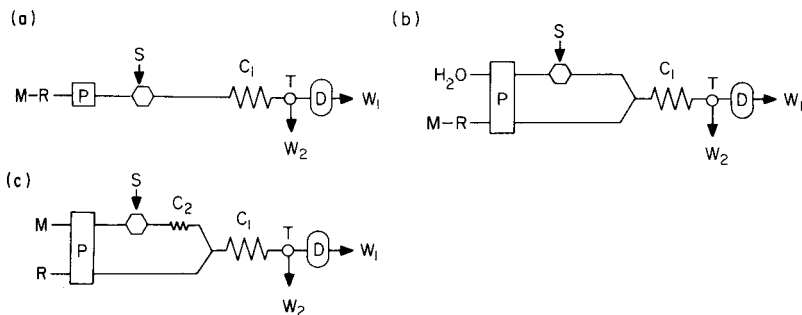


Fig. 1. Three types of manifold for f.i.a. P, pump; S, sample injector; T, stopped-flow valve; D, detector; C_1 , reaction coil (0.5-mm i.d., 4-m long); C_2 , reaction coil (0.5-mm i.d., 1.5-m long); W_1 and W_2 , waste; H_2O , water; M, magnesium(II) or cerium(III) solution; R, MTB or XO solution; M-R, Mg-MTB or Ce(III)-XO solution.

constants in the order $\text{Mg-P}_2 < \text{Mg-P}_3 < \text{Mg-EDTA}$ [10]. It is also known that MTB reacts with magnesium ions to form a colored 1:1 complex, Mg-MTB , with an absorption maximum at 610 nm. Experiments were done to examine whether or not the difference between the stability constants of these metal complexes is reflected in the f.i.a. profiles of orthophosphate, diphosphate, triphosphate and EDTA when the Mg-MTB reagent is used as a carrier solution. Both MTB and Mg-MTB show absorption in the visible region (400–700 nm), while the Mg-P_2 , Mg-P_3 and Mg-EDTA complexes are colorless. The measurements were done at 610 nm where the difference between the absorptivities of the free MTB and the Mg-MTB complex at pH 10.1 was maximum. The baseline level in f.i.a. experiments was about 0.45 absorbance unit (a.u.).

The f.i.a. profiles for orthophosphate, diphosphate, triphosphate and EDTA obtained by employing manifold (b) in Fig. 1 are shown in Fig. 2. As the samples were injected into a carrier stream of water, a blank signal was not observed on injecting water. Orthophosphate did not respond even when the sample concentration was as high as 10^{-4} M, which can be attributed to the low complexing ability of orthophosphate, though the exact stability constant of magnesium orthophosphate complex is not known [10]. The detection sensitivities of diphosphate, triphosphate and EDTA increased expectedly in the order $\text{P}_2 < \text{P}_3 < \text{EDTA}$. The difference in complexing ability between orthophosphate, diphosphate, triphosphate and EDTA seems to be significantly reflected in the f.i.a. profiles.

The stopped-flow patterns for diphosphate, triphosphate and EDTA are shown in Fig. 3. For each component, the same sample was injected successively in duplicate to obtain a normal f.i.a. signal and a broad stopped-flow signal. The stopped-flow signal was recorded by stopping the sample zone in the detector to observe the time dependence of absorbance or the further progress of the reaction. The absorbance was expected to vary with time if the reaction had not been completed. The stopped-flow signals with plateaux in Fig. 3 lead to the conclusion that the equilibria of all the substitution

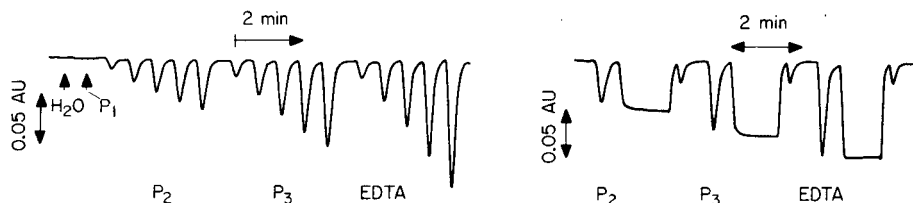


Fig. 2. F.i.a. profiles for orthophosphate (P_1), diphosphate (P_2), triphosphate (P_3) and EDTA. Manifold (b); reagent, 5×10^{-5} M Mg-MTB ; sample concentrations, increasing from left to right, $2, 4, 6, 8, 10 \times 10^{-5}$ M for P_2 , P_3 and EDTA and 10^{-4} M for P_1 ; H_2O , injection of water.

Fig. 3. Stopped-flow signals for diphosphate (P_2), triphosphate (P_3) and EDTA. Manifold (b); reagent, 5×10^{-5} M Mg-MTB ; sample concentrations, each 8×10^{-5} M.

reactions are almost reached and hence kinetic factors are not likely to affect the f.i.a. profiles in Fig. 2. The ghost peaks that appeared regularly after each stopped-flow signal in Fig. 3 have not yet been clarified, though the valve switching for stopping the flow seems to be associated with it.

The overall features of the dependence of peaks heights on sample concentration are shown in Fig. 4. As would be seen from conventional photometric titration curves, the shapes of these calibration curves could be discussed theoretically on the basis of the respective stability constants of the metal complexes of MTB and samples. However, they are not discussed in detail here, because there is uncertainty about the stability constant of the Mg-MTB complex and the purity of MTB reagent used.

The f.i.a. profiles (Fig. 5) were also obtained in the same way by employing manifold (c). As expected, a marked blank signal appeared when water was injected into the stream of magnesium ions. Therefore, this manifold was concluded to be less favorable than manifold (b) for determinations at low concentrations.

Stopped-flow profiles obtained with manifold (c) were similar to those in Fig. 3. This confirms that the $M-R + P_n \rightarrow M-P_n + R$ reaction proceeds so quickly that equilibrium is achieved in the detector.

Cerium(III)-XO reagent system

The Mg-MTB reagent is unstable, and the reagent solution must be prepared daily. Another disadvantage is that the reagent is unable to detect orthophosphate. To overcome these problems a cerium(III)-XO reagent was examined for the determination of orthophosphate, diphosphate, triphosphate and EDTA. Both XO and the Ce(III)-XO complex absorb in the region 400–650 nm. The measurement was done at 580 nm, which corresponds to the absorption maximum of Ce(III)-XO at pH 6.2. The baseline in f.i.a. experiments was about 0.76 a.u.

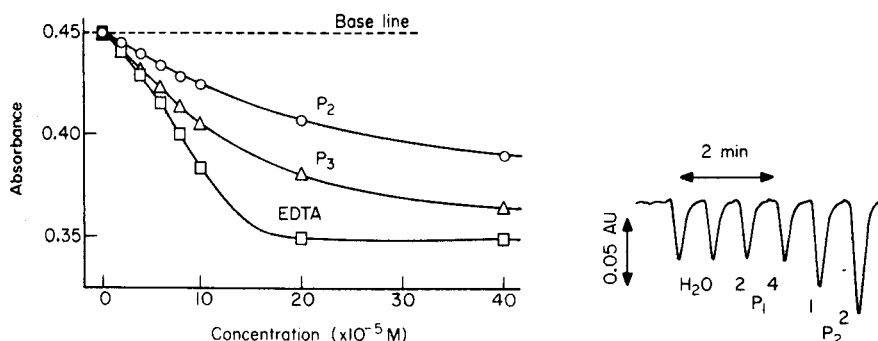


Fig. 4. Calibration curves for diphosphate (P_2), triphosphate (P_3) and EDTA. Manifold (b); reagent, 5×10^{-5} M Mg-MTB.

Fig. 5. F.i.a. profiles for orthophosphate (P_1) and diphosphate (P_2). Manifold (c); reagents, 5×10^{-5} M Mg and 5×10^{-5} M MTB; sample concentrations, 2 and 4×10^{-4} M for P_1 and 1 and 2×10^{-4} M for P_2 ; H_2O , injection of water.

Manifold (b) was employed, with injection of the samples into a stream of water. Blank signals were not observed, as expected. Diphosphate, triphosphate and EDTA, except orthophosphate, were detected with almost equal sensitivities in the concentration range below 2×10^{-4} M. A f.i.a. profile for triphosphate is shown as an example in Fig. 6. The establishment of the equilibria of the reactions of diphosphate, triphosphate and EDTA was confirmed from their stopped-flow signals with horizontal plateaux.

Figure 7. shows the f.i.a. profile for orthophosphate. A stopped-flow signal is also shown for the strongest sample of orthophosphate; this signal with its steep slope is quite different from the horizontal stopped-flow signals of diphosphate, triphosphate and EDTA. The slope indicates that the substitution reaction, $\text{Ce(III)-XO} + \text{P}_1 \rightarrow \text{Ce(III)-P}_1 + \text{XO}$, proceeds slowly in the detector so that the absorbance changes with time. The poor sensitivity for orthophosphate with this manifold may be ascribed, not to the low complexing ability of orthophosphate for cerium(III), but to the slow substitution reaction.

The f.i.a. profiles obtained with manifold (c) are shown in Fig. 8. Orthophosphate, as well as diphosphate and triphosphate, were then detected sensitively. Orthophosphate gave a stopped-flow signal with a plateau, similar to those for diphosphate and triphosphate; this suggests that the substitution reaction, $\text{Ce(III)-P}_1 + \text{XO} \rightarrow \text{Ce(III)-XO} + \text{P}_1$, is fast enough for equilibrium to be attained in the reaction coil.

The peak widths (4σ) in the f.i.a. profiles shown above were calculated to be 25–30 s, indicating a sampling rate of 120 samples per hour defined in terms of $1/4\sigma$ [11]. The relative standard deviations were 0.5–1.5% when measurements were done in the working range 10^{-5} – 10^{-4} M. From the analytical viewpoint, the indirect methods with the Mg–MTB and Ce(III)–XO complexes are less favorable as a whole than the heteropoly blue method [3, 4]. A great disadvantage is that only a very limited working range is

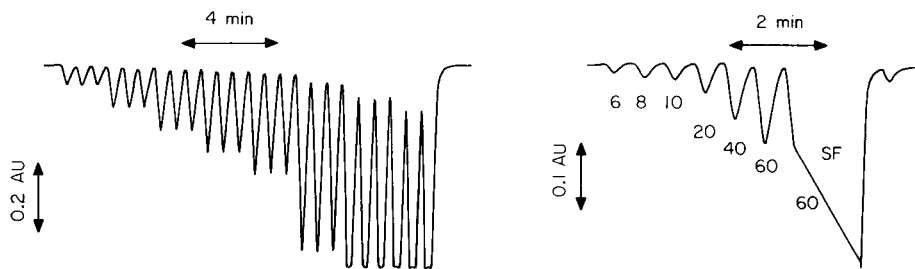


Fig. 6. F.i.a. profile for triphosphate. Manifold (b); reagent, 5×10^{-5} M Ce(III)–XO; sample concentrations, increasing from left to right, $2, 4, 6, 8, 10, 20, 40, 60 \times 10^{-5}$ M. Each sample was injected in triplicate.

Fig. 7. F.i.a. profile and stopped-flow signal for orthophosphate. Manifold (b); reagent, 5×10^{-5} M Ce(III)–XO; sample concentrations, increasing from left to right, $6, 8, 10, 20, 40, 60 \times 10^{-5}$ M. SF is the stopped-flow signal for 60×10^{-5} M orthophosphate.

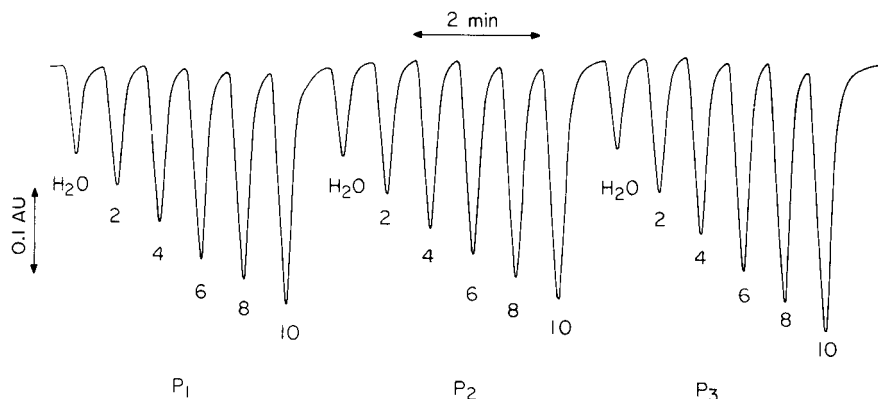


Fig. 8. F.i.a. profiles for orthophosphate (P_1), diphosphate (P_2) and triphosphate (P_3). Manifold (c); reagents, 5×10^{-5} M Ce(III) and 5×10^{-5} M XO; sample concentrations, increasing from left to right 0(H_2O), 2,4,6,8,10 $\times 10^{-5}$ M.

available and that quantitative work at low concentrations is difficult, mainly because of the strong absorption by the free ligands, MTB and XO. Improved results would be obtained with a reagent system comprising a ligand with no or very weak absorption and a metal complex with strong absorption.

The principle of f.i.a. shown in this paper should be useful in characterizing complexation reactions, because thermodynamic and kinetic factors associated with the substitution reactions are directly reflected on the f.i.a. profiles and stopped-flow signals. For example, Fig. 2 gives valuable thermodynamic information on the relative values of the stability constants. The stopped-flow experiment in Fig. 7 also indicates the kinetic conclusion that the reaction between Ce(III)—XO and orthophosphate proceeds more slowly than that between Ce(III)—XO and triphosphate.

REFERENCES

- 1 J. Růžička and E. H. Hansen, *Anal. Chim. Acta*, 114 (1980) 19.
- 2 D. Betteridge, *Anal. Chem.*, 50 (1978) 832A.
- 3 Y. Hirai, N. Yoza and S. Ohashi, *Anal. Chim. Acta*, 115 (1980) 269.
- 4 Y. Hirai, N. Yoza and S. Ohashi, *Chem. Lett.*, (1980) 499.
- 5 N. Yoza, Y. Hirai and S. Ohashi, presented at 38th Symposium of the Japan Society for Analytical Chemistry, Nara, 1977.
- 6 M. Otomo, *Bunseki Kagaku*, 21 (1972) 436.
- 7 E. Mitropolska and R. Borissova, *Fresenius Z. Anal. Chem.*, 294 (1979) 285.
- 8 K. Veno, *Kireto Tekiteiho*, Nankodo, Tokyo, 1976.
- 9 H. Bergamin F^2 , B. F. Reis and E. A. G. Zagatto, *Anal. Chim. Acta*, 97 (1978) 427.
- 10 L. G. Sillen and A. E. Martell, *Stability Constants of Metal Ion Complexes*, Special Publication, 17 and 25, The Chemical Society, London, 1964 and 1971.
- 11 J. H. M. van den Berg, R. S. Deelder and H. G. M. Egberink, *Anal. Chim. Acta*, 114 (1980) 91.

PHOSPHORIMETRIC ASSAY FOR β -GLUCURONIDASE IN BIOLOGICAL MATERIALS

MASATOSHI YAMAGUCHI, SHIRYU MIYAMOTO, KAZUYA KOHASHI and YOSUKE OHKURA*

Faculty of Pharmaceutical Sciences, Kyushu University 62, Maidashi, Higashi-ku, Fukuoka 812 (Japan)

(Received 9th June 1980)

SUMMARY

A highly sensitive phosphorimetric method for the assay of β -glucuronidase in biological samples is described. *p*-Nitrophenol, formed enzymatically from *p*-nitrophenyl β -D-glucuronide, is extracted with ether and determined phosphorimetrically in a mixture of ether and ethanolic potassium hydroxide. The method is rapid, precise, and very sensitive, requiring as little as 0.5–5 μ l of human serum or urine, or 0.3–3.0 μ g of protein of rat tissue. The limit of detection for the *p*-nitrophenol formed is 20 pmol.

β -Glucuronidase (β -D-glucuronide glucuronohydrolase, EC 3.2.1.31) catalyses the hydrolysis of the β -D-glucuronides of a variety of phenolic, alcoholic and carboxylic compounds. Abnormal activities of β -glucuronidase in human body fluids (serum, cerebrospinal fluid, gastric juice, vaginal discharge, sputum, urine and others) and various tissues have been observed in patients with atherosclerosis, diabetes, cancer or thyroid diseases. Many colorimetric and fluorimetric methods have been reported for the assay of β -glucuronidase in biological samples. Presently available colorimetric methods use chromogenic substrates, the β -D-glucuronides of *p*-nitrophenol [1, 2] and phenolphthalein [3–5]: fluorimetric methods, based on β -D-glucuronides of 4-methylumbelliferone [6], umbelliferone [7], 1- and 2-naphthol [8, 9] and harmalol [10] as substrates, are more sensitive. These methods require long incubation times (2–24 h).

Recently, it was found that *p*-nitrophenol could be detected phosphorimetrically at a concentration of 0.1 pmol ml⁻¹ in an alkaline solution at 77 K [11]. A highly sensitive and rapid method for the assay of β -glucuronidase in biological samples has therefore been developed, based on the phosphorimetric determination of the *p*-nitrophenol formed from *p*-nitrophenyl β -D-glucuronide. Human serum, urine, and rat tissue homogenates were employed to establish assay procedures.

EXPERIMENTAL

Reagents and apparatus

All chemicals and solvents were of reagent grade, unless otherwise stated. Double-distilled water was used. *p*-Nitrophenol (Sigma) was purified by recrystallization. *p*-Nitrophenyl β -D-glucuronide (Sigma) was exhaustively washed with ether to remove contaminating *p*-nitrophenol.

The uncorrected phosphorescence spectra and intensities were measured with the samples in the form of clear solids at liquid nitrogen temperature (77 K), using a Hitachi MPF-3 spectrofluorimeter equipped with a Hitachi phosphoroscope attachment and quartz sample tubes (4.0 mm i.d., 5.0 mm o.d., 200 mm long; sample volume, 150 μ l). The spectral bandwidths of the excitation and emission monochromators were both 10 nm. Phosphorescence lifetimes were measured on a Hitachi V-051 synchroscope. pH was measured with a Hitachi-Horiba M-7 pH meter at 25°C.

Biological sample solutions

Normal sera were obtained from healthy volunteers in this laboratory. Pathological sera were supplied from Noguchi Hospital (Beppu, Oita, Japan). Urine samples (24 h) from the healthy volunteers were stored at 4°C without preservative and used within 2 days. Rat tissue homogenates were prepared as follows. Male Donryu rats were killed by decapitation, and portions (30–50 mg) of liver, spleen, lung, adrenal and kidney were rapidly removed, blotted and placed in 4.0–5.0 ml of ice-cold 0.25 M sucrose. The tissue was homogenized in a Potter-Elvehjem homogenizer and centrifuged at 1000 *g* for 20 min. The supernatant liquid was diluted with 0.25 M sucrose to contain 0.3–3.0 μ g of tissue in 5 μ l. Protein concentration was determined by the method of Lowry et al. [12].

Procedure

The substrate solution consisted of 25 μ l each of 0.2 M phosphate buffer and 20.0 mM *p*-nitrophenyl β -D-glucuronide. The pH of the buffer was 4.3 for human serum and rat tissue homogenate, and 5.0 for human urine. 5 μ l of sample solution was added to the solution, and the mixture was incubated at 37°C for 15 min. The reaction was stopped by cooling in ice-water for ca. 2 min, and the *p*-nitrophenol produced was extracted into 1.0 ml of ether by shaking for ca. 5 min. After a brief centrifugation, 0.7 ml of the ether layer was diluted with 0.2 ml of ethanolic 0.1 M potassium hydroxide.

For the blank, the same procedure was carried out, except that the substrate solution was cooled in ice-water and then added to the sample solution; incubation was omitted. To obtain a standard curve the substrate solution was replaced with *p*-nitrophenol (0.02–50 nmol): the curve was linear up to at least 50 nmol of *p*-nitrophenol and passed through the origin. The phosphorescence intensities were measured at 520 nm with an excitation wavelength of 375 nm.

RESULTS AND DISCUSSION

Optimal pH values were 4.0 for the reactions of β -glucuronidase in human serum and rat liver, lung and kidney homogenates, and 4.5 for those in rat spleen and adrenal homogenates; pH 4.3 was used in the procedure because the activities at this pH were virtually identical to those at the individual optimum pH values. The enzyme in human urine was apparently most active at pH 5.0. A maximum and constant activity was obtained in the presence of 7.0–40.0 mM *p*-nitrophenyl β -D-glucuronide, with K_m values of 3.1–3.2 mM for β -glucuronidase in human serum and urine, and rat liver homogenate. Thus, 9.0 mM *p*-nitrophenyl β -D-glucuronide was used as a saturating concentration for the enzyme reaction.

The reaction rate was linear with time up to at least 60 min at 37°C (Fig. 1). When strong acids such as trichloroacetic acid or perchloric acid were added to the incubation mixture in order to stop the reaction, the substrate was hydrolyzed non-enzymatically. The β -glucuronidase-inhibitor sodium azide did not completely stop the enzyme reaction even when added at concentrations of 0.1–0.5% (w/v). The reaction proceeded very slowly at 0°C and the amount of *p*-nitrophenol formed in 10 min was negligible (Fig. 1). The reaction was thus stopped by cooling the mixture in ice-water, and a blank was prepared without incubation. The amount of *p*-nitrophenol formed in 15 min was proportional to human serum or urine sample-size up to at least 50 μ l, and to the amount of protein in rat tissue homogenate up to at least 30 μ g.

The *p*-nitrophenol was effectively extracted from the incubation mixture with ether. The extract (0.7 ml) readily formed a clear solid at 77 K after mixing with 0.1–0.3 ml of ethanol; 0.2 ml of ethanol was routinely used. Potassium hydroxide in the ethanol increased the *p*-nitrophenol phosphorescence: ≥ 0.07 M potassium hydroxide was required for maximum phosphorescence and 0.1 M solutions were routinely employed.

The phosphorescence excitation (maximum, 375 nm) and emission (maximum, 520 nm) spectra and lifetime (0.2 s) for the final solution were identical with those of *p*-nitrophenol dissolved in the same solvent (Fig. 2).

The limit of detection for *p*-nitrophenol was 20 pmol, which gave a phosphorescence intensity of twice the blank. This limit of detection is much better than those of the fluorimetric methods [6–10], and may permit the assay of β -glucuronidase in only 0.5 μ l of serum or 0.3 μ g of protein in rat tissue homogenate.

Comparison with a popular colorimetric method [1], also based on *p*-nitrophenol formation (but requiring larger samples and a 10-h incubation), was made for normal and pathological sera. The correlation coefficient was 0.99 ($n = 20$), and the regression equation for the present method (x) against the colorimetric method (y) was $y = 1.0x - 0.1$. The within-day precision of the phosphorimetric method was examined using sera with mean β -glucuronidase activities of 3.52 and 1.05 $\mu\text{mol min}^{-1} \text{ l}^{-1}$. The coefficients of variation were 3.9 and 4.7% ($n = 15$), respectively.

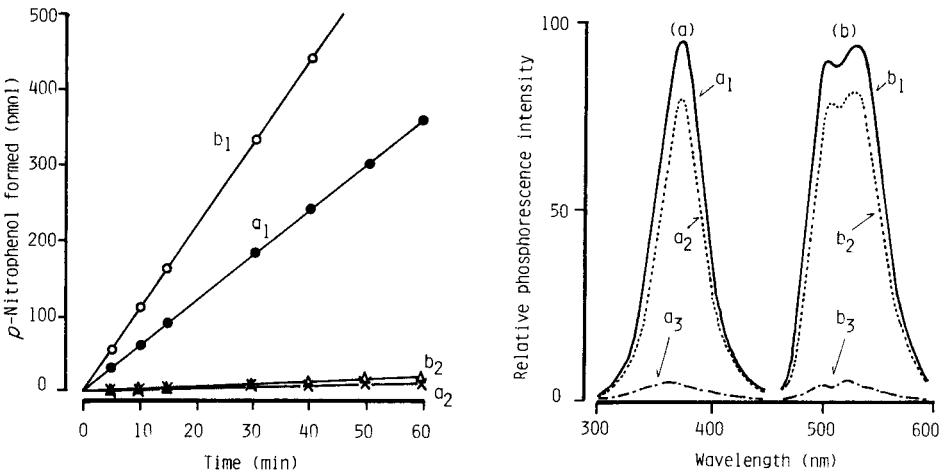


Fig. 1. Effect of incubation time and temperature on the enzyme activity. Portions (5 μ l) of (a_1 , a_2) human serum (β -glucuronidase activity, 1.20 μ mol $\text{min}^{-1} \text{l}^{-1}$) and of (b_1 , b_2) rat lung homogenate containing 4.2 μ g of protein (β -glucuronidase activity, 2.67 $\text{pmol min}^{-1} \mu\text{g protein}^{-1}$) were incubated at (a_1 , b_1) 37°C and (a_2 , b_2) 0°C.

Fig. 2. Phosphorescence excitation (375 nm) and emission (520 nm) spectra of the final assay solutions and of *p*-nitrophenol: (a_1 , b_1) 5- μ l portions of human serum (β -glucuronidase activity of 1.20 μ mol $\text{min}^{-1} \text{l}^{-1}$) were assayed; (a_2 , b_2) *p*-nitrophenol (70 pmol ml^{-1}) was dissolved in ether-ethanolic 0.1 M potassium hydroxide (7/2, v/v); (a_3 , b_3) blank corresponding to a_1 and b_1 .

β -Glucuronidase activity in normal serum assayed by the present method was $1.22 \pm 0.70 \mu\text{mol min}^{-1} \text{l}^{-1}$ (mean \pm s.d., $n = 20$) (Fig. 3). The activities in sera of the patients with hyperthyroidism and hypothyroidism were $2.47 \pm 1.04 \mu\text{mol min}^{-1} \text{l}^{-1}$ ($n = 30$) and $0.81 \pm 0.64 \mu\text{mol min}^{-1} \text{l}^{-1}$ ($n = 9$), respectively (Fig. 3). These data are in agreement with some previously published results [13] obtained by the colorimetric method. The values of β -glucuronidase activity in 24-h urine of 18 healthy persons assayed by the present method (Table 1) also agreed with earlier results [14]. β -Glucuronidase activities in rat tissue homogenates were 2.83 (liver), 6.17 (spleen), 2.67 (lung), 0.50

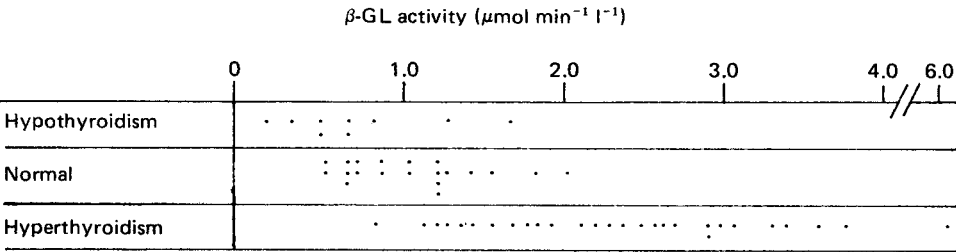


Fig. 3. Serum β -glucuronidase activities in healthy volunteers and in patients with thyroid diseases.

TABLE 1

Urinary excretion (24 h) of β -glucuronidase from healthy persons

Age ^a	Volume of 24-h urine (ml)	β -GL activity ^b	Age ^c	Volume of 24-h urine (ml)	β -GL activity ^b
49	1740	24.0	40	1120	33.1
42	1320	68.1	35	1200	23.2
33	1520	27.7	32	1050	50.6
31	1380	58.8	28	1250	48.3
29	1870	92.0	27	1300	48.1
27	1640	23.6	22	810	28.8
24	1980	45.9	22	1100	53.7
23	855	17.4	22	710	47.0
22	1240	34.9	22	1300	36.7
22	1190	42.1	22	900	81.5

^aAll male subjects. ^b*p*-Nitrophenol formed, $\mu\text{mol min}^{-1} \text{I}^{-1}$. ^cAll female subjects.

(adrenal) and 1.33 (kidney) $\text{pmol min}^{-1} \mu\text{g protein}^{-1}$. These results are similar to those obtained by a fluorimetric method based on 1-naphthyl β -D-glucuronide as substrate [14].

This study provides the first phosphorimetric method for the assay of β -glucuronidase. The method is very rapid and precise, and should be useful for biomedical investigations where only minute samples are obtainable.

A Grant-in-Aid for Scientific Research from the Ministry of Education, Science and Culture of Japan and the supply of sera from Noguchi Hospital are gratefully acknowledged.

REFERENCES

- 1 K. Kato, K. Yoshida, H. Tsukamoto, M. Nobunaga, T. Masuya and T. Sawada, *Chem. Pharm. Bull.*, 8 (1960) 239.
- 2 R. H. Nimmo-Smith, *Biochim. Biophys. Acta*, 50 (1961) 166.
- 3 C. Plaice, *J. Clin. Pathol.*, 14 (1961) 661.
- 4 G. Goldstein, *Clin. Chem.*, 7 (1961) 136.
- 5 H. Schön and M. Leipold, *Klin. Wochenschr.*, 40 (1962) 292.
- 6 J. A. R. Meads, J. N. Smith and R. T. Williams, *Biochem. J.*, 61 (1955) 569.
- 7 J. H. Woolen and P. G. Walker, *Clin. Chim. Acta*, 12 (1965) 659.
- 8 M. A. Verity, R. Caper and W. J. Brown, *Arch. Biochem. Biophys.*, 106 (1964) 386.
- 9 L. J. Greenberg, *Anal. Biochem.*, 14 (1965) 265.
- 10 K. P. Wong, *Anal. Biochem.*, 35 (1970) 35.
- 11 Y. Ohkura, M. Yamaguchi and S. Miyamoto, *Chem. Pharm. Bull.*, 28 (1980); E. A. Martin, *Can. J. Pharm. Sci.*, 5 (1970) 13.
- 12 O. H. Lowry, N. J. Rosenbrough, A. L. Farr and R. J. Randall, *J. Biol. Chem.*, 193 (1951) 265.
- 13 T. Shimada and A. Kihara, *Sapporo Igaku Zasshi*, 43 (1974) 155.
- 14 M. Nobunaga, T. Sawada and T. Masuya, *Fukuoka Igaku Zasshi*, 51 (1960) 205.

A FLUORIMETRIC METHOD FOR THE DETERMINATION OF TRACES OF GALLIUM

J. J. LASERNA, A. NAVAS and F. GARCIA-SANCHEZ*

Department of Analytical Chemistry, Faculty of Sciences, University of Malaga (Spain)

(Received 8th February 1980)

SUMMARY

A fluorimetric method for the determination of gallium, based on the formation of a fluorescent 1:1 chelate with benzyl-2-pyridylketone-2-pyridylhydrazone, is described. In 90% ethanol, the fluorescent species has excitation and emission maxima at 469 and 545 nm, respectively, and the calibration graph is linear over the range 1.4–350 ppb Ga at pH 5. Methods of removing interferences are discussed.

Although the fluorescent characteristics of many gallium chelates have been established, only one pyridylhydrazone, 2-hydroxy-1-naphthaldehyde-2-pyridylhydrazone, has been reported to be suitable for the determination of gallium. This reagent was used to detect gallium, indium or scandium in 70% ethanol at an apparent pH of 3.9–4.5, with detection limits of ≤ 0.04 ppb [1]. Other sensitive fluorimetric methods for the determination of traces of gallium are not common; the most sensitive is that reported by Pilipenko et al. [2] who used the azomethine derivatives obtained by condensation of 4-aminoantipyrine and 2-hydroxy-5-methylbenzaldehyde. Such methods are summarized in Table 1.

In the present paper, the synthesis of benzyl-2-pyridylketone-2-pyridylhydrazone (BPKPH) and its application in a rapid, simple and sensitive fluorimetric determination of gallium are described. The reagent also gives fluorescent chelates with indium, zinc, cadmium and scandium [3]. The method is applied in 90% ethanol at an apparent pH of 5; a five-fold excess of aluminium and double quantities of thallium(III) and indium do not interfere. The detection limit is 1.4 ppb and the range of applicability is 1.4 to 350 ppb.

EXPERIMENTAL

Reagents

BPKPH was synthesized by refluxing equimolar quantities of benzyl-2-pyridylketone and 2-hydrazinopyridine at 50–60°C for 6 h. After cooling to room temperature, the reaction mixture was put in a refrigerator and, after a short time, brown crystals separated. These were filtered, washed, and re-

TABLE 1

Methods for the fluorimetric determination of gallium(III)

Reagent	Sensitivity (ppb) ^c	Ref.
4-Aminoantipyrine azomethine	0.2	2
5-Chloro-2,2',4'-trihydroxyazobenzene-3-sulphonic acid	1	4
Sulphonaphtholazoresorcinol ^{a, b}	2	5
Salicylidene-4-aminoantipyrine ^a	1	6
Resorcyldene-4-aminoantipyrine ^a		
4-(5-Chloro-2-hydroxyphenylazo)-resorcinol ^{a, b}	4.6	7
Quercetin-3'-glucoside	5.6	8
Kaempferol ^b	2	9
Lumogallion ^b	8	10
2-Hydroxy-5-sulphoaniline-N-salicylidene	2	11
2-(Salicylideneamino)-3-hydroxyfluorene ^b	8	12
Resorcyal-cysteine Schiff base	7	13
BPKPH	1.4	This paper

^aExtraction procedure. ^bStanding time. ^cMinimum concentration used for calibration.

dissolved in ethanol, from which brown crystals (m.p. 114–115°C) separated again on cooling. The reagent was characterized by its infrared spectrum, purity being confirmed by elemental analysis (required for C₁₈H₁₆N₄, 75.0% C, 5.55% H, 19.4% N; found, 75.05% C, 5.7% H, 19.4% N). Solutions of the reagent (5×10^{-4} M) were prepared daily in absolute ethanol (Merck p.a.).

A stock solution of gallium was prepared by dissolving 0.5026 g of Ga(NO₃)₃·8H₂O in 250 ml of 2 M hydrochloric acid. The exact gallium content was determined by titration with EDTA and xylenol orange indicator. Solutions of lower concentration were made by dilution with deionized water.

Buffer solutions of pH 3.5 were prepared from 50 ml of 0.1 M potassium hydrogenphthalate and 8.2 ml of 0.1 M hydrochloric acid, diluted to 100 ml with deionized water.

Apparatus

All fluorimetric measurements were performed on a Perkin-Elmer fluorescence spectrophotometer, model MPF-43A, equipped with an Osram XBO 150-W xenon lamp, excitation and emission grating monochromators, 1 × 1-cm quartz cells, R-508 photomultiplier and a Perkin-Elmer 023 recorder. A standard bar of rhodamine B (10^{-7} M) gave 60 units with the following parameters: λ_{ex} = 480 nm, λ_{em} = 570 nm, excitation and emission slits 5 nm, sensitivity 10 coarse and 7 fine, temperature 25°C.

Procedure

Place exactly 1 ml of sample solution (pH 3–5) containing 0.07–17.5 µg of gallium(III), in a 50-ml volumetric flask. Add BPKPH to make the final solution 10^{-6} – 10^{-5} M in BPKPH, and 4 ml of pH 3.5 buffer solution, and

make up to volume with ethanol. Measure the fluorescence intensity at 545 nm with excitation at 469 nm.

RESULTS AND DISCUSSION

The excitation and emission spectra of the gallium—BPKPH complex in 90% ethanol at an apparent pH of 5 are shown in Fig. 1. Under the conditions used, the reagent gave no fluorescence.

Effect of experimental conditions

In order to evaluate the effect of pH, 1×10^{-5} M solutions of the reagent and gallium(III) were prepared in 90% ethanol. The pH was changed by addition of 4 ml of several buffer solutions. Constant maximum intensity was obtained in the apparent pH range 4.8–5.2; the intensity decreased at lower and higher pH values, being 55 at pH 4.5, 69 at pH 5.0 and 35 at pH 5.7.

Similar experiments were carried out at apparent pH 5 to determine the optimum percentage of ethanol. The results (Fig. 2) show that the ethanol concentration is critical and must be precisely controlled. They also show that a high percentage of ethanol is necessary for high sensitivity. A 90% ethanol solution is recommended, because higher concentrations limit the amount of aqueous solutions (buffer and cation) that can be added.

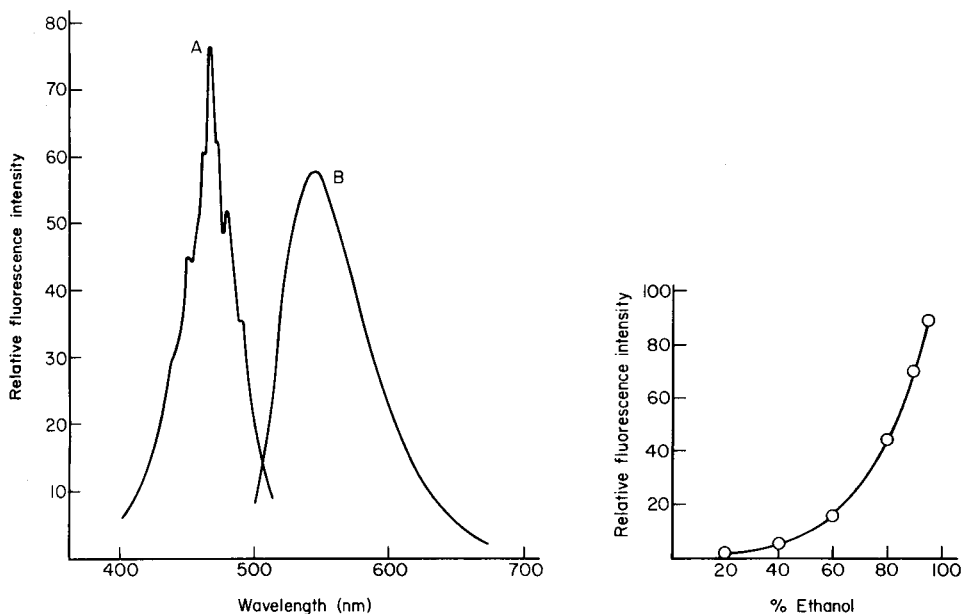


Fig. 1. Uncorrected (A) excitation and (B) emission spectra of the gallium—BPKPH chelate at apparent pH 5. $[Ga] = [BPKPH] = 1 \times 10^{-5}$ M. Sensitivity 0.1 coarse, 7 fine.

Fig. 2. Influence of ethanol concentration on the fluorescent emission of the gallium—BPKPH chelate at apparent pH 5. $[Ga] = [BPKPH] = 1 \times 10^{-5}$ M. Sensitivity 0.1 coarse, 4 fine.

In order to understand this behaviour, excitation and emission spectra of the complex (1×10^{-5} M) in 2, 10, 50, 90 and 95% ethanol were recorded. No shifts in excitation and fluorescence maxima were observed when changing from a highly polar solvent (2% ethanol, $\epsilon = 77$) to a less polar solvent (95% ethanol, $\epsilon = 26.5$). This suggests that substantial changes in polarity of the complex do not take place upon excitation [14] and that the solvation energy of the molecule will not differ to a large extent on changing the solvent [15]. Thus, the fluorescence intensity enhancement in ethanolic media cannot be ascribed to these effects, and may be explained by the low solubility of the complex in water. The appearance of turbidity in weakly ethanolic solutions 0.5 h after the mixtures had been prepared and the lack of stability of the 2 and 10% ethanolic solutions lend some support to this conclusion. In 90% ethanol, the fluorescence intensity is constant for at least 2 h.

The effect of BPKPH concentration on the intensity from 1×10^{-6} M gallium under conditions similar to those of the recommended method, is shown in Fig. 3. Reagent concentrations below 4×10^{-5} M must be used so as to avoid fluorescence inversion phenomena. Figure 3 shows that 1×10^{-5} M BPKPH is adequate.

The fluorescence intensity diminishes by 5% on raising the temperature from 10 to 30°C. Further increase to 50°C causes a further decrease of 20%. The work reported here was done at $25 \pm 0.5^\circ\text{C}$.

Calibration

Linear calibration graphs were established for three ranges of gallium(III) concentration, covering a total range of 1.4–350 ppb gallium with three con-

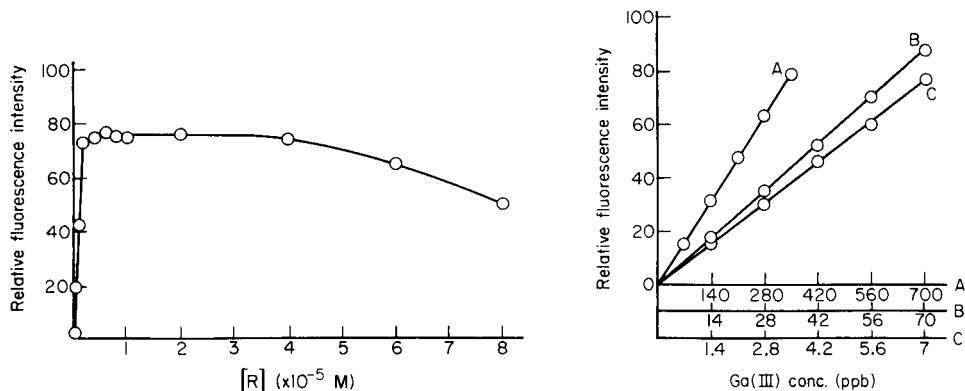


Fig. 3. Influence of BPKPH concentration on the fluorescent emission of the gallium—BPKPH chelate at apparent pH 5 $[\text{Ga}] = 1 \times 10^{-6}$ M. Sensitivity 1 coarse, 3 fine.

Fig. 4. Calibration curves at apparent pH 5. (A) $[\text{BPKPH}] = 1 \times 10^{-5}$ M, sensitivity 0.1 coarse, 10 fine; (B) $[\text{BPKPH}] = 2 \times 10^{-6}$ M, sensitivity 1 coarse, 4 fine; (C) $[\text{BPKPH}] = 1 \times 10^{-6}$ M, sensitivity 10 coarse, 8 fine, corrected for reagent blank.

centrations of BPKPH (Fig. 4). For three series of 11 measurements on 280, 42 and 5.6 ppb gallium(III), relative errors of 0.9, 1.8, 2.8% and relative standard deviations of 1.3, 2.7 and 4.1% were obtained, respectively.

Interference studies

The effect of diverse ions on the determination of 42 ppb gallium was studied. Ten-fold amounts of Tl(I), Be, Mg and Ca, five-fold amounts of Mn, Cd, Al, Fe(III), Y and Sn(IV), twice the amount of In, As(III), Tl(III), Sc, Ti(IV) and V(V), equal weights of Ni, and half the amount of Zn, Fe(II), Cu(II) and Cr(III) did not interfere; 15 ppb Co also did not interfere. Only 1 ppb Sn(II), however, can be tolerated. A 100-fold weight excess of SO_4^{2-} and BrO_3^- , a 50-fold amount of NO_3^- , Cl^- and CN^- , a ten-fold amount of SCN^- and half the amount of EDTA and oxalate did not interfere; 15 ppb phosphate could be tolerated. Figure 5 shows the effects produced by some of these ions.

Zinc, cadmium, indium and scandium cause negative interferences. Although these ions form fluorescent chelates with BPKPH, the relevant pH range at which they exist is different so that at apparent pH 5 the only fluorescent species is the gallium chelate. The interference of nickel, zinc, iron(II), copper(II), chromium(III) and cobalt can be attributed to the fact that these elements form strong coloured BPKPH complexes thus decreasing the concentration of reagent. In addition, these complexes cause decreased fluorescence through scattering or absorption of incident and fluorescence radiation. The strong quenching caused by tin(II) is not so readily explained. It does not form a complex with the reagent, and, as it is present at such low levels that only a physical process, probably complex-to-metal energy transfer, can explain its effect.

The removal of iron(II), copper(II) and zinc(II) interferences was effectively accomplished by masking with cyanide, and that of chromium(III) with thiocyanate. Tin(II) was oxidized with iron(III), the iron(II) formed being masked with cyanide. The most troublesome interference was that caused

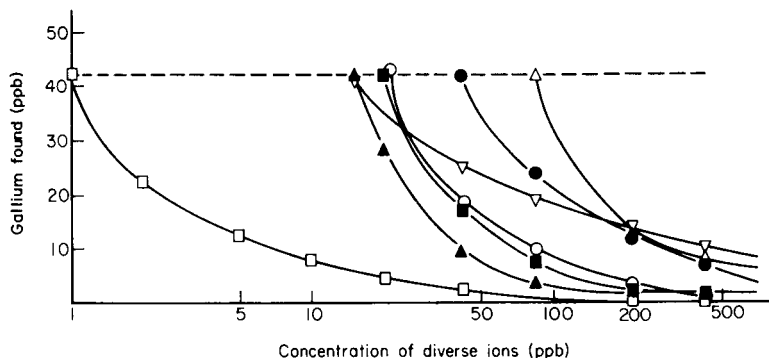


Fig. 5. Effect of diverse ions on the determination of (42 ppb) (Δ) Sc, Ti, V; (●) Ni; (○) EDTA; (■) Zn; (▲) Co; (▽) H_2PO_4^- (□) Sn(II).

by cobalt ions; this could be removed by adding a drop of dilute hydrogen peroxide to the sample in ammoniacal medium, then adjusting to pH 3–5, and finally adding reagent, buffer and ethanol, as recommended. The fluorescence intensity remained constant for 30 min after such treatment.

Stoichiometry, stability constant, and sensitivity

The stoichiometry was established by the traditional methods of Job, Yoe and Jones, and Harvey and Manning. All three showed that at the apparent pH 5, only a 1:1 metal–ligand complex was formed. The stability constant of the complex, deduced from the Job method, was $10^{6.58}$.

The detection limit, defined arbitrarily as the amount of gallium that gave a signal-to-noise ratio of 2:1, was 1.4 ppb or 70 ng of gallium in 50 ml of measured solution.

Comparison with other reagents

The present method compares favourably in sensitivity, simplicity and ease of application with other fluorimetric methods for gallium. This is shown in Table 1, where reagents with "sensitivities" better than 10 ppb are compared. Since not all the papers consulted gave information about detection limits, "sensitivities" have been taken as the minimum concentration of gallium in the calibration solutions.

REFERENCES

- 1 L. Sommer, W. P. Maung-Gyee and D. E. Ryan, *Scr. Fac. Sci. Nat. Univ. Purkynianae Brun.*, 2 (1972) 115.
- 2 A. T. Pilipenko, S. L. Lisichenok, A. I. Volkova and V. Ya. Demchenko, *Ukr. Khim. Zh.*, 43 (1977) 536.
- 3 J. J. Laserna, Doctoral Thesis, University of Malaga, in preparation.
- 4 A. M. Lukin and E. A. Bozhevol'nov, *Zh. Anal. Khim.*, 15 (1960) 43.
- 5 E. A. Bozhevol'nov, A. M. Lukin and M. N. Gradinarskaya, *Anal. Abstr.*, 7 (1960) 3164.
- 6 A. T. Tashkhodzhaev, L. E. Zel'tser, Sh. T. Talipov and Kh. Khikmatov, *Zavod. Lab.*, 41 (1975) 281.
- 7 L. N. Thu, *Zh. Anal. Khim.*, 22 (1967) 636.
- 8 Sh. T. Talipov, Z. T. Maksimycheva, Z. P. Pakudina and A. S. Sadykov, *Izv. Vyssh. Uchebn. Zaved. Khim. Khim. Tekhnol.*, 16 (1973) 1154.
- 9 Sh. T. Talipov, Z. T. Maksimycheva, Z. P. Pakudina and A. S. Sadykov, *Izv. Vyssh. Uchebn. Zaved. Khim. Khim. Tekhnol.*, 17 (1974) 348.
- 10 K. Kina and N. Ishibashi, *Microchem. J.*, 19 (1974) 26.
- 11 K. Morishige, *Anal. Chim. Acta*, 72 (1974) 295.
- 12 K. P. Stolyarov, N. N. Grigor'ev and P. Kh. Ioannu, *Tr. Khim. Khim. Tekhnol.*, 3 (1974) 55.
- 13 A. T. Tashkhodzhaev, L. E. Zel'tser, T. Sh. Sabirova and Sh. T. Talipov, *Uzb. Khim. Zh.*, 19 (1975) 9.
- 14 S. G. Schulman, *Fluorescence and Phosphorescence Spectroscopy: Physicochemical Principles and Practice*, Pergamon, Oxford, 1977.
- 15 M. Goldman and E. L. Wehry, *Anal. Chem.*, 42 (1970) 1178.

THE FLUORESCENCE PROPERTIES OF METAL COMPLEXES OF ALKYL DERIVATIVES OF AROMATIC SCHIFF BASES

KIYOTOSHI MORISHIGE

Department of Fundamental Education, Faculty of Science and Technology, Kinki University, Kowakae, Higashi-Osaka (Japan)

(Received 2nd June 1980)

SUMMARY

Seventeen alkylated salicylidene-*o*-aminophenol derivatives were tested as fluorimetric reagents for aluminium, gallium, indium, scandium and beryllium. The aluminium, gallium and beryllium complexes are intensely fluorescent, and the scandium and indium complexes weakly fluorescent. The fluorescence properties of the aluminium, gallium and beryllium complexes were studied and conditions for the fluorimetric determination of these metals were established. 2-Hydroxy-4-methylaniline-*N*-2-hydroxy-4-methylbenzylidene is a good reagent because of the reproducibility and sensitivity of the fluorescence. The optimal ranges for determination are 0.005–3 $\mu\text{g Al}/25\text{ ml}$, 0.1–7 $\mu\text{g Ga}/25\text{ ml}$ and 0.02–7 $\mu\text{g Be}/25\text{ ml}$. In all cases, 1:1 metal–ligand complexes are formed. Optimal reaction conditions and interference studies are reported.

Aromatic Schiff bases such as 2-hydroxyaniline-*N*-salicylidene (salicylidene-*o*-aminophenol) react with aluminium, gallium, beryllium and other metal ions to form complexes, whose fluorescence emission can be utilized for the determination of these ions [1–7]. In this paper, aromatic Schiff base derivatives with alkyl groups at the position *m*- or *p*- to the $-\text{CH}=\text{N}-$ group of salicylidene-*o*-aminophenol are described, and the effects of the substituent groups on the fluorescence properties of their metal complexes are reported.

EXPERIMENTAL

Apparatus and materials

Uncorrected fluorescence spectra were measured with a Hitachi Model 204 fluorescence spectrophotometer fitted with a 150-W xenon lamp. A Hitachi-Horiba pH Meter, Model M-5, was used for pH measurements.

Schiff bases. These were synthesized as previously described [3, 4] and identified by elemental analysis, melting point, i.r. and n.m.r. spectra. Samples (0.1g) were dissolved in *N,N*-dimethylformamide (DMF) and diluted to 100 ml with DMF.

Standard solutions of aluminium, gallium and beryllium. Solutions of Al, Ga and Be (1 mg ml⁻¹) were prepared by dissolving 0.1 g of Al (99.999%), 0.1344 g of Ga₂O₃ (99.99%), or 0.2774 g of BeO (99.9%) in 20 ml of 6 M

HCl, 10 ml of 6 M HCl or 10 ml of concentrated sulfuric acid, respectively, and diluting to 100 ml with water. Working solutions were prepared by dilution with 0.1 M hydrochloric acid.

Uranine and quinine standard solutions. Uranine (0.1 g; Nakarai Chemicals) was dissolved in 100 ml of water, and the solution was diluted to give solutions containing 0.125–0.5 $\mu\text{g ml}^{-1}$. Quinine (0.1 g; Nakarai Chemicals) was dissolved in 100 ml of 0.1 M sulfuric acid, and the solution was diluted to give solutions containing 0.125–0.25 $\mu\text{g ml}^{-1}$. These solutions were employed as reference fluorescence standards in adjusting the sensitivity of the instrument.

General procedure

To a solution containing an appropriate amount of metal ion, 1–2 ml of a 0.1% Schiff base–DMF solution and 2 ml of 20% ammonium acetate or 5 ml of 20% ammonium chloride solution were added. The pH was adjusted to the required value with dilute hydrochloric acid or ammonia solution, and the solution diluted to 25 ml with water. The fluorescence intensity was measured at the optimal excitation and emission wavelengths, using uranine or quinine as an intensity standard.

RESULTS AND DISCUSSION

The stability of Schiff bases in solution was exemplified by examining salicylidene-*o*-aminophenol: the variation of its absorption spectrum in DMF with time was studied. Very dilute (10^{-4} M) solutions were unstable: the spectrum changed and the absorbance decreased to about 50% of its initial value after a few days. More concentrated solution (5×10^{-3} M) were stable for at least one month. Other Schiff bases behaved similarly. When the Schiff bases were used as fluorimetric reagents, solutions were made up as freshly as possible.

Fluorescence properties of metal–Schiff base complexes

The fluorescence properties of the metal complexes formed with aromatic Schiff bases were investigated. The Schiff bases reacted with aluminium, gallium, indium and scandium to form the fluorescent complexes in weakly acidic solution, whereas beryllium formed fluorescent complexes in alkaline solution. The aluminium, gallium and beryllium complexes were intensely fluorescent, and the indium and scandium complexes weakly fluorescent. Aluminium, gallium and beryllium complexes with salicylidene-*o*-aminophenol and sixteen alkyl derivatives were thus studied; their fluorescence characteristics are summarized in Table 1.

The fluorescence intensities of the aluminium complexes decreased in the following order: compound XVI > XVII > IV > VIII > V \approx III > VII > I \approx VI > XI > X \approx XII \approx XIII > XIV > II \approx XV \approx IX. For compounds with a methyl group at the *m*-position (II, IV) or the *p*-position (III) to the

TABLE 1

Optimal conditions for fluorimetry of aluminium, gallium and beryllium complexes with Schiff bases^a

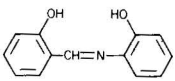
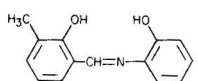
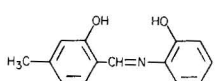
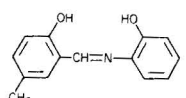
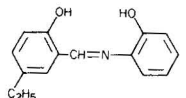
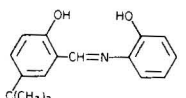
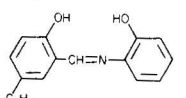
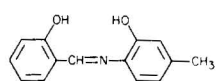
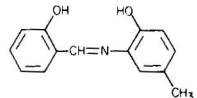
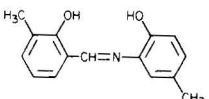
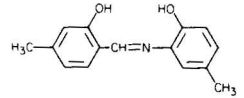
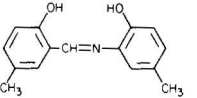
Compd. no.	Schiff base	Ion	λ_{ex} (nm)	λ_{em} (nm)	pH	RFI ^b Net intensity per 1 μg metal	Determinable range ($\mu\text{g}/25\text{ ml}$)
		Al	405	505	5.8	51.9	0.01–5
		Ga	410	515	4.0	6.6	0.2–10
		Be	337	440	10.5	59.4	0.1–15
II		Al	415	510	6.0	7.7	0.1–20
		Ga	417	515	4.5	1.3	1.0–20
		Be	360	480	9.5	5.4	0.5–25
III		Al	405	498	6.0	69.5	0.008–4
		Ga	410	510	4.5	9.7	0.15–10
		Be	345	435	9.5	41.5	0.1–15
IV		Al	415	500	6.0	79.3	0.008–4
		Ga	415	510	4.5	8.1	0.2–10
		Be	350	455	9.5	78.5	0.05–10
V		Al	415	500	5.8	70.9	0.008–4
		Ga	415	510	4.0	9.6	0.15–10
		Be	355	450	8.7	97.0	0.01–5
VI		Al	415	500	5.8	51.7	0.01–5
		Ga	415	510	4.0	9.0	0.15–10
		Be	350	450	8.7	91.0	0.01–5
VII		Al	415	503	5.0	64.0	0.01–5
		Ga	420	512	3.5	10.2	0.15–10
		Be	360	465	10.5	28.4	0.2–20
VIII		Al	405	503	5.5	77.5	0.01–5
		Ga	410	510	3.5	8.6	0.15–10
		Be	340	435	9.5	73.3	0.03–10
IX		Al	415	525	6.0	5.6	0.1–20
		Ga	417	535	4.5	0.8	1.5–30
		Be	345	435	9.5	76.4	0.03–10
X		Al	420	520	6.0	15.4	0.04–10
		Ga	425	530	4.5	1.3	1.0–20
		Be	350	455	10.0	34.6	0.2–20
XI		Al	415	520	6.0	22.8	0.02–7
		Ga	420	530	4.5	2.3	0.6–15
		Be	345	430	9.5	52.3	0.1–15
XII		Al	420	525	6.0	14.3	0.04–10
		Ga	425	535	4.5	1.2	1.0–20
		Be	350	450	9.5	90.0	0.01–5

TABLE 1 (continued)

Compd. no.	Schiff base	Ion	λ_{ex} (nm)	λ_{em} (nm)	pH	RFI ^b Net intensity per 1 μg metal	Determinational range ($\mu\text{g}/25\text{ ml}$)
XIII		Al	420	525	6.0	13.9	0.04–10
		Ga	420	535	4.1	1.3	1.0–20
		Be	355	450	8.5	94.6	0.01–5
XIV		Al	415	523	6.0	10.6	0.05–10
		Ga	420	533	4.0	1.0	1.0–20
		Be	355	450	8.5	68.0	0.05–10
XV		Al	420	525	5.5	6.7	0.1–20
		Ga	425	535	3.0	0.9	1.0–20
		Be	360	460	10.5	28.0	0.2–20
XVI		Al	405	500	5.5	99.4	0.005–3
		Ga	420	510	4.0	12.8	0.1–7
		Be	340	437	9.5	78.5	0.02–7
XVII		Al	412	500	5.0	94.0	0.005–3
		Ga	415	510	3.8	12.0	0.1–7
		Be	353	450	10.0	104.0	0.01–5

^aFor all reagents, complex formation was immediate with beryllium, but needed 5 min at room temperature with gallium and 10 min at 50°C with aluminium. ^bRelative fluorescence intensities (RFI) were measured at maximal fluorescence wavelength.

—CH=N— group in the α -ring, the order of intensities is thus IV > III > II. Of the different substituents at the 5-position in the α -ring, $\text{CH}_3 \approx \text{C}_2\text{H}_5 > \text{C}_6\text{H}_5 > \text{H} \approx \text{C}(\text{CH}_3)_3$, i.e. IV \approx V > VII > I \approx VI. The position of a methyl in the N-ring had a marked effect (VIII > IX). In most cases, the fluorescence intensities of aluminium complexes of dialkyl derivatives were less than those of monoalkyl derivatives.

For gallium complexes, the order is XVI > XVII > VII > III \approx V > VI > VIII > IV > I > XI > II \approx X \approx XIII > XII > XIV > XV > IX. The fluorescence intensities of the beryllium complexes decreased in the following order: compound XVII > V > XIII > VI \approx XII > IV \approx XVI > IX > VIII > XIV > I > XI > III > X > VII \approx XV > II. The fluorescence of the beryllium complexes was usually unstable: 2-hydroxy-4-methylaniline-N-2-hydroxy-5-methylbenzylidene (compound XVII) is the recommended reagent, the complexes having high sensitivity and reasonable stability.

The excitation and emission spectra of some aluminium and beryllium complexes are shown in Figs. 1 and 2; the optimal wavelengths of excitation and emission are listed in Table 1. Excitation at 405–420 nm is effective for aluminium complexes, and at 337–360 nm for beryllium complexes.

The fluorescence maxima of the aluminium complexes occur at 498–525 nm, and those of the beryllium complexes at 430–480 nm. For the alu-

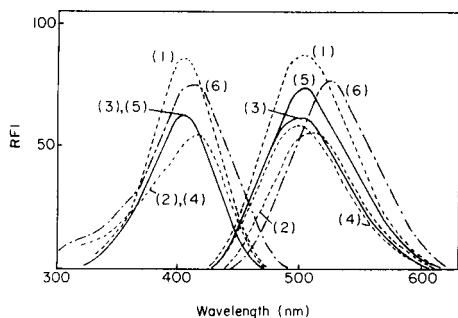


Fig. 1. Excitation and emission spectra of aluminium complexes with Schiff bases. (1) Compound I; (2) Compound II; (3) Compound III; (4) Compound IV; (5) Compound VIII; (6) Compound IX.

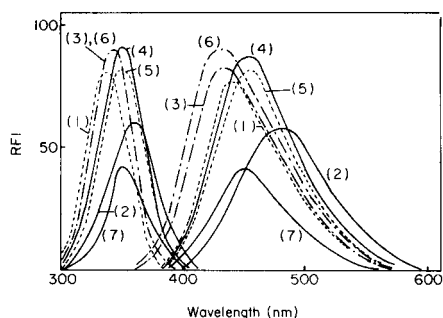


Fig. 2. Excitation and emission spectra of beryllium complexes with Schiff bases. (1) Compound I; (2) Compound II; (3) Compound III; (4) Compound IV; (5) Compound X; (6) Compound XI; (7) Compound XII.

minimum complexes, alkyl groups at the *m*- or *p*-position to the $-\text{CH}=\text{N}-$ group in the α -ring cause a blue shift of the fluorescence compared with salicylidene-*o*-aminophenol complexes. The fluorescence of beryllium complexes with salicylidene-*o*-aminophenol derivatives substituted in the α -ring shows a red shift, while those substituted in the N-ring show a blue shift, compared with the beryllium-salicylidene-*o*-aminophenol complexes. Complexes having substituents in both rings also show the red shift.

It was found that 2-hydroxy-4-methylaniline-N-2-hydroxy-4-methylbenzylidene (compound XVI) was the best reagent for the determination of aluminium, gallium and beryllium, yielding highly reproducible results. The analytical conditions were therefore investigated further.

Analytical characteristics of compound XVI

The excitation and emission spectra of the aluminium, gallium and beryllium complexes of 2-hydroxy-4-methylaniline-N-2-hydroxy-4-methylbenzylidene are shown in Fig. 3. The optimum excitation and emission wavelengths are listed in Table 1.

Because the reactions of all the Schiff bases with aluminium were very slow, the solutions were warmed at 50°C for 10 min after the pH adjustment (Fig. 4). Gallium complexes showed full fluorescence immediately after the pH adjustment. The fluorescence of the aluminium and gallium complexes was stable for at least 3 h, but that of the beryllium complex fell to ca. 50% of its initial value after 1 h.

The effect of pH on the fluorescence intensity of the metal complexes is indicated in Fig. 5. The aluminium complex showed maximal fluorescence at $\text{pH } 5.5 \pm 0.2$, the gallium complex at $\text{pH } 4.0 \pm 0.2$, and the beryllium complex at $\text{pH } 9.5 \pm 0.2$.

Various amounts of 0.1% Schiff base solution were added to solutions

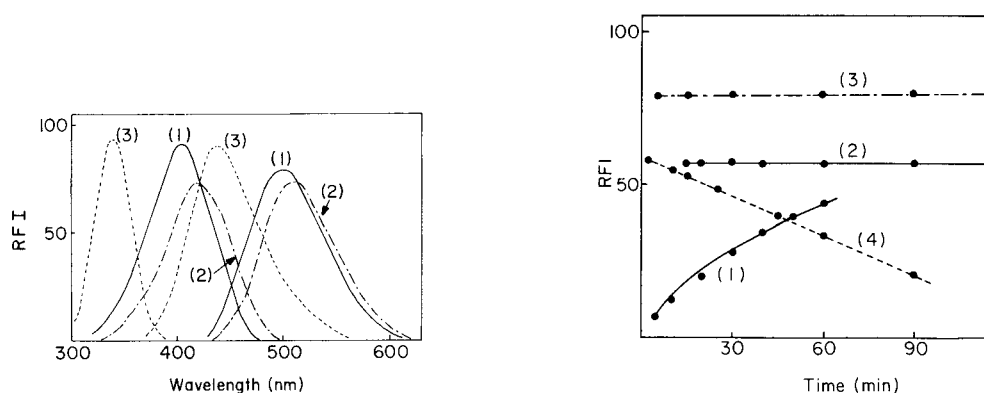


Fig. 3. Excitation and emission spectra of aluminium (1), gallium (2) and beryllium (3) complexes with 2-hydroxy-4-methylaniline-N-2-hydroxy-4-methylbenzylidene (compound XVI).

Fig. 4. Development of fluorescence intensity of metal-Schiff base complexes. (1) Al, 2 μg , at room temperature, 405 nm/500 nm, fluorimeter set at 10 units with 0.5 μg uranine ml^{-1} solution; (2) Al, 2 μg , at 50°C for 10 min., 405 nm/500 nm, 10 units; (3) Ga, 5 μg , at room temperature, 420 nm/510 nm, 50 units (0.5 μg uranine ml^{-1}); (4) Be, 5 μg , at room temperature, 340 nm/437 nm, fluorimeter set at 20 units with 0.25 μg quinine ml^{-1} solution.

containing 2 μg of aluminium or 5 μg of gallium or beryllium, and the fluorescence intensities were measured at the optimal pH. Figure 6 shows that 2 ml of 0.1% Schiff base in 25 ml solution was required for the determination of aluminium and gallium, and 1 ml for beryllium.

Calibration curves. Figure 7 shows the calibration curves for the determination of aluminium, gallium and beryllium. The fluorescence intensity was measured using 0.25–0.5 $\mu\text{g ml}^{-1}$ uranine solution (for aluminium and gallium) or 0.125–0.25 $\mu\text{g ml}^{-1}$ quinine solution (for beryllium) as intensity standards. Aluminium, gallium and beryllium can be determined with a relative error of 3% in the following concentration ranges: aluminium, 0.005–3 $\mu\text{g}/25\text{ ml}$; gallium, 0.1–7 $\mu\text{g}/25\text{ ml}$; beryllium, 0.02–7 $\mu\text{g}/25\text{ ml}$.

Effect of diverse ions. The interference of foreign cations in 100-fold amounts on the determinations of aluminium, gallium and beryllium were studied.

In the determination of aluminium, no interference was caused by Sb(III), As(III), Ba(II), Be(II), B(III), Bi(III), Cd(II), Ca(II), Ce(IV), Eu(III), Ge(IV), La(III), Mg(II), Mn(II), Hg(II), Se(IV), Sr(II), Tl(I), W(VI), Y(III), or Zn(II). Negative errors were caused by Cr(VI), Co(II), Cu(II), Ga(III), In(III), Fe(III), Mo(VI), Ni(II), and Sc(III).

For the determination of gallium, negative errors were caused by Co(II), Cu(II), Cr(VI), Mo(VI), Ni(II), and Fe(III). Indium and scandium did not interfere. Aluminium(III) caused positive errors, as expected.

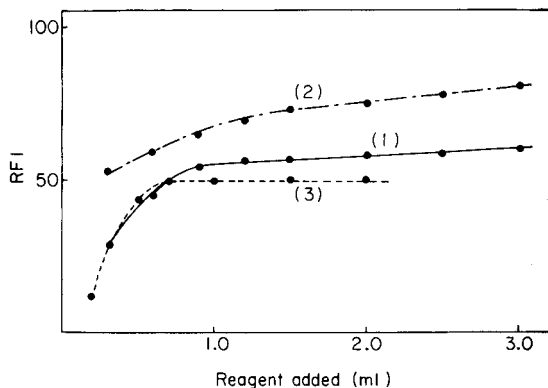
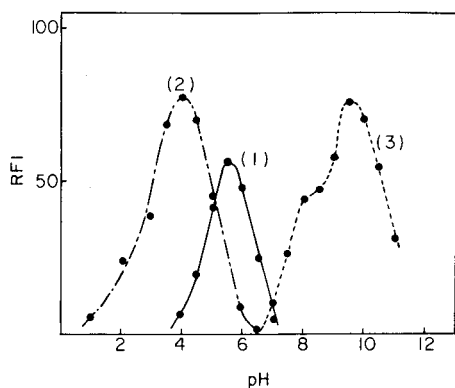


Fig. 5. Effect of pH solution on fluorescence intensity for compound XVI. (1) Al, 2 μg , 405 nm/500 nm, 10 units. 0.5 μg uranine ml^{-1} ; (2) Ga, 5 μg , 420 nm/510 nm, 50 units. 0.5 μg uranine ml^{-1} ; (3) Be, 5 μg , 340 nm/437 nm, 30 units. 0.25 μg quinine ml^{-1} .

Fig. 6. Effect of reagent concentration. (1) Al, 2 μg , 405 nm/500 nm, 10 units (0.5 μg uranine ml^{-1}); (2) Ga, 5 μg , 420 nm/510 nm, 50 units (0.5 μg uranine ml^{-1}); (3) Be, 5 μg , 340 nm/437 nm, 20 units (0.25 μg quinine ml^{-1}).

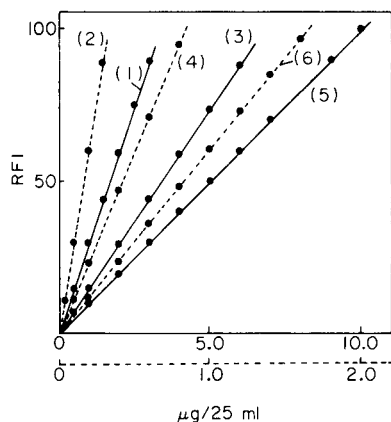


Fig. 7. Calibration curves for aluminium, gallium and beryllium. (1) Al, 405 nm/500 nm, 10 units (0.5 μg uranine ml^{-1}); (2) Al, 50 units 0.5 μg uranine ml^{-1} ; (3) Ga, 420 nm/510 nm, 50 units (0.5 μg uranine ml^{-1}); (4) Ga, 40 units (0.25 μg uranine ml^{-1}); (5) Be, 340 nm/437 nm, 20 units (0.25 μg quinine ml^{-1}); (6) Be, 60 units (0.125 μg quinine ml^{-1}).

For the determination of beryllium, Sb(III), As(III), B(III), Bi(III), Cd(II), Ca(II), Mg(II), Hg(II), Tl(I), W(VI), U(VI), and Zn(II) did not interfere. Aluminium(III), Cr(VI), Cu(II), Co(II), Ga(III), In(III), Fe(III), Mn(II), Ni(II), Sc(III), Sn(IV), V(V), and Y(III) caused negative errors.

Determination of metal-ligand ratio. The metal-ligand ratios in the aluminium, gallium and beryllium complexes with compound XVI were

TABLE 2

Analysis of the metal—Schiff base complexes of compound XVI

Chemical formula	N calc. (%)	N found (%)	Me calc. (%)	Me found (%)
$C_{15}H_{13}NO_2Al \cdot 3H_2O$	4.4	4.3	8.4	8.3
$C_{15}H_{13}NO_2Ga \cdot 3H_2O$	3.9	3.8	19.2	19.2
$C_{15}H_{13}NO_2Be \cdot H_2O$	5.3	5.1	3.4	3.3

determined fluorimetrically by the continuous variation or kinetic methods [3, 4]. The results for each metal complex indicated a metal—ligand ratio of 1:1. Table 2 summarizes the results of elemental analysis of the metal—Schiff base complexes which confirm that the metal—ligand ratios are 1:1.

REFERENCES

- 1 R. M. Dagnall, R. Smith and T. S. West, *Chem. Ind.*, (1965) 1499; *Talanta*, 13 (1966) 609.
- 2 A. K. Babko and S. L. Lisichenko, *Ukr. Khim. Zh.*, 35 (1969) 98.
- 3 K. Morishige and N. Aomi, *J. Fac. Sci. Technol., Kinki Univ.*, 8 (1973) 309.
- 4 K. Morishige, *Anal. Chim. Acta*, 72 (1974) 295; 73 (1974) 245; *J. Inorg. Nucl. Chem.*, 40 (1978) 843.
- 5 K. Morishige, S. Sasaki, K. Hiraki and Y. Nishikawa, *Bunseki Kagaku*, 24 (1975) 321.
- 6 K. Morishige, K. Hiraki, Y. Nishikawa and T. Shigematsu, *Bunseki Kagaku*, 27 (1978) 109.
- 7 M. Deguchi, T. Masumoto, K. Morishige and I. Okumura, *Bunseki Kagaku*, 28 (1979) 127.

Short Communication

SPURENANALYSE VON HUMINSTOFFEN IM TRINKWASSER

H. SOHR* und K. WIENHOLD

Forschungsstelle für chemische Toxikologie der Akademie der Wissenschaften der DDR, Permoserstraße 15, 705 Leipzig (G.D.R.)

(Eingegangen den 1. April 1980)

Summary. (*The d.c. polarographic determination of traces of humic substances in potable waters*) The inhibiting effect of a tri-n-butylphosphate layer adsorbed at the mercury drop on the polarographic wave of copper(II) is reduced by humic substances. This effect can be utilized to determine humic substances in the range 0.05–1 mg l⁻¹. The standard substance used was isolated from peaty water. Humic and fulvic acids are not differentiated but amino acids, peptides and polyhydroxy compounds do not interfere.

Zusammenfassung. Es wird eine polarographische Methode zur direkten Bestimmung von Huminstoffen im Trinkwasser vorgeschlagen, wobei als Bezugseinheit ein aus Moorwasser isolierter Huminstoffstandard verwendet wird. Obgleich die Differenzierung der Huminstoffe in Humin- und Fulvosäuren nicht möglich ist, besitzt diese Methode eine hohe Selektivität bezüglich anderer im Trinkwasser gelöster organischer und anorganischer Substanzen. Die Erfassungsgrenze für in Wasser gelöste Huminstoffe liegt etwa bei 50 µg l⁻¹.

Bekanntlich sind Huminstoffe in der Natur weit verbreitet. Sie kommen u.a. als organische Inhaltsstoffe natürlicher Gewässer vor und sind auch normalerweise im Trinkwasser in sehr unterschiedlichen Konzentrationen enthalten, wobei Konzentration und molekulare Verteilung nach Herkunft und Aufbereitungsort des Wassers stark differieren können. Chemisch stellen diese Substanzen im allgemeinen Phenolkörperpolymerisate mit polyanionischem Charakter dar, deren Molekulargewichte in weit gesteckten Grenzen etwa zwischen 200 und 10⁵ liegen [1]. Die niedermolekularen Huminstoffe sind auf Grund ihrer Carboxylgruppen und phenolischen Hydroxylgruppen gut wasserlöslich. Bis etwa zum Molekulargewicht 10⁴ bezeichnet man diese Substanzen gewöhnlich als Fulvosäuren.

Bisher wurden die Huminstoffe zusammen mit anderen löslichen oxidierbaren Inhaltsstoffen im Trinkwasser oxidimetrisch durch Titration mit KMnO₄-Lösungen bestimmt, ohne daß eine Spezifizierung möglich war [2]. Für die Analytik der Huminstoffe allgemein werden auch andere Methoden eingesetzt, wie z.B. die UV-Spektroskopie, die jedoch für die Bestimmung von Huminstoffen im Trinkwasser zu unempfindlich ist [3]. Ebenso wie die UV-Spektroskopie erreicht auch eine andere Methode, die auf der differentiell-pulspolarographischen Bestimmung nitrosierter Huminstoffe bzw. Lignin-

sulfonsäuren beruht, nur eine Empfindlichkeit von etwa 1 mg l^{-1} Wasser. Allerdings ist im letzteren Fall die Nebeneinanderbestimmung von Huminstoffen und Ligninsulfonsäuren möglich [4].

Wir können Huminstoffe sowie Ligninsulfonsäuren mit Hilfe einer indirekten polarographischen Methode bestimmen, indem wir die durch diese Substanzen katalysierte Abscheidung von Cu(II) -Ionen ausnutzen. Obgleich Humin-, Fulvo- und Ligninsulfonsäuren nicht nebeneinander bestimmt werden können, ist die Selektivität bezüglich anderer organischer Inhaltsstoffe des Wassers gut. Im Vergleich zu dem von uns verwendeten Standard sind Huminstoffe im Trinkwasser bis zu einer Konzentration von $5 \mu\text{g l}^{-1}$ erfaßbar.

Experimentelles

Die polarographischen und tensammetrischen Messungen wurden mit einem Polarographen vom Typ GWP 563 (Akademiewerkstätten, Berlin) durchgeführt. Die gleichstrompolarographischen Messungen sind in einer auf pH 5,0 eingestellten Grundlösung folgender Zusammensetzung durchgeführt worden: $0,25 \text{ M Na}_2\text{SO}_4$; $3 \times 10^{-3} \text{ M CuSO}_4$; 10^{-3} M KCl und $4 \times 10^{-4} \text{ M}$ Tri-*n*-butylphosphat (TBP). Zwecks Einstellung des Lösungsgleichgewichts des in Wasser schwerlöslichen TBP wurde diese Grundlösung vor den Messungen 2 Std. mechanisch geschüttelt. Für die tensammetrischen Messungen diente eine $0,25 \text{ M Na}_2\text{SO}_4$ Lösung, die ebenfalls auf pH 5,0 eingestellt war. Die Amplitude der Wechsellspannung betrug 14 mV und die Frequenz 78 Hz . Die verwendete Tropfenelektrode hatte folgende Charakteristik: $h = 98 \text{ cm}$; $t = 5,6 \text{ s}$; $m = 1,03 \text{ mg s}^{-1}$. Als Spülgas diente Reinstickstoff. Sämtliche Potentiale wurden gegen die gesättigte Kalomelektrode (SCE) gemessen. Die Temperatur bei allen Messungen betrug 25°C .

Das als Grundlektrolyt verwendete Na_2SO_4 war eine mehrfach umkristallisierte pA-Substanz, die 5 Std. bei 500°C geglüht wurde. Das destillatir gereinigte TBP hatte einen Brechungsindex $n_D^{20} = 1,4220$. Die übrigen Substanzen besaßen pA-Reinheit. Das verwendete Wasser war viermal destilliert.

Als Fulvosäurestandard verwendeten wir ein Na-Fulvat, das wir aus Pb-Fulvat herstellten (aus Moorwasser extrahiert), das uns in dankenswerter Weise von Frau Prof. Klöcking (Medizinische Akademie Erfurt) zur Verfügung gestellt wurde (Molekulargewicht bei pH 7,0: 3000–5000 [5]). Die Zugabe des Huminsäurestandards zur Grundlösung erfolgte mit Hilfe einer graduierten $50 \mu\text{l}$ -Pipette aus Stammlösungen mit einem Huminsäuregehalt von $10 \mu\text{g ml}^{-1}$ bis 10 mg ml^{-1} . Bei den Trinkwasseruntersuchungen wurden die Grund- bzw. Meßlösungen im allgemeinen mit 20% Trinkwasser angesetzt. Dieser Anteil läßt sich je nach Huminstoffgehalt des Trinkwassers beliebig verändern.

Ergebnisse und Diskussion

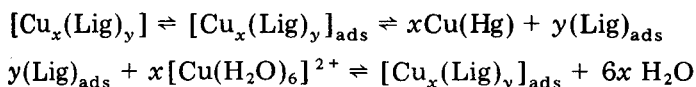
Huminstoffe sind normalerweise untoxisch. Im Trinkwasser können sie in Form von chelatartigen Metallkomplexen vorliegen. Infolge dieser Komplexbildung sinkt die orale Toxizität der Metalle ab. Im Gegensatz dazu steigt die Toxizität dieser Komplexe bei intravenöser und intraperitonealer Appli-

kation an [6]. Davon ausgehend, erscheint die Kenntnis des Gehaltes an Huminstoffen, besonders im Hinblick auf den Einsatz von künstlichen Nieren, von besonderer Bedeutung.

Die benutzte indirekte polarographische Methode der Bestimmung von Huminstoffen im Trinkwasser ist dann vorteilhaft, wenn sich die zu bestimmenden Substanzen durch hohe Oberflächenaktivität und gute Komplexbildungstendenzen auszeichnen. Außerdem müssen die zu bestimmenden Substanzen einen stark polaren und multifunktionellen Charakter haben. Zur Darstellung des oberflächenaktiven Charakters dieser Substanzen wurden einige tensammetrische Kurven aufgenommen (Abb. 1). Diesen Anforderungen entsprechen z.B. auch die Nukleotide, die mit dieser Methode mit hoher Empfindlichkeit quantitativ erfaßt werden können [7]. Auch die Huminstoffe, besonders die Fulvosäuren, entsprechen diesen Forderungen in optimaler Weise.

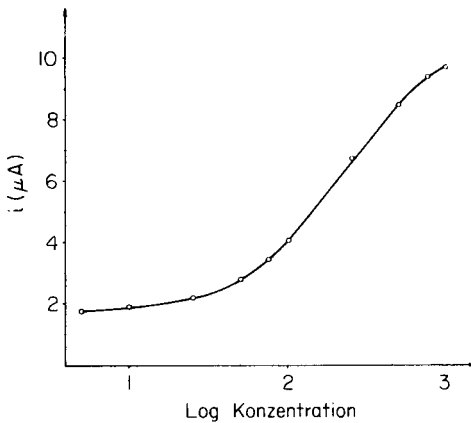
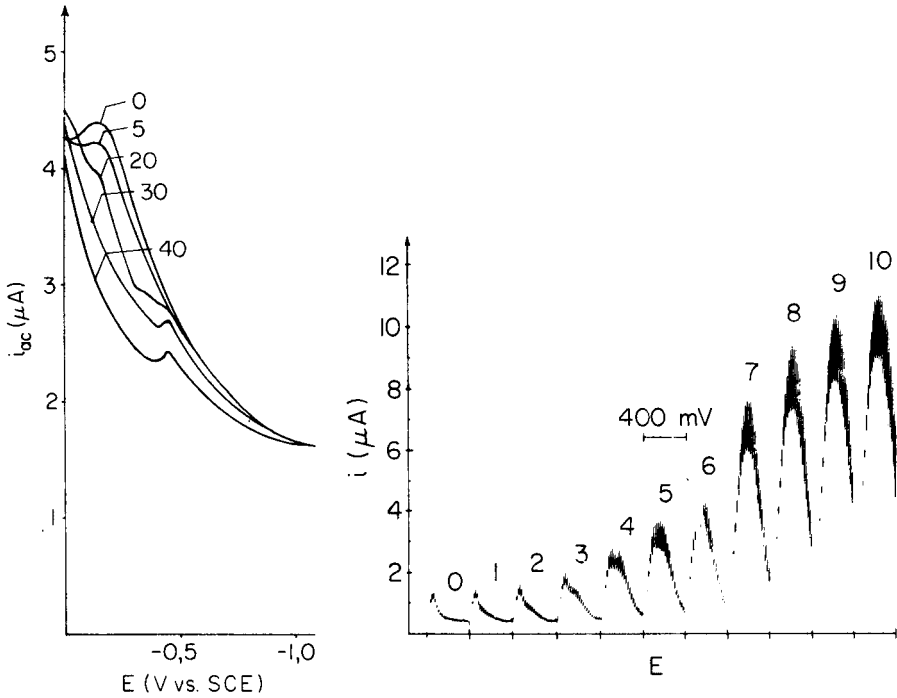
Das Prinzip dieser Methode beruht darauf, daß die Inhibitionswirkung einer geschlossenen Adsorptionsschicht von TBP-Molekülen an der Hg-Tropfелеktrode auf die gleichstrompolarographische Abscheidung von Cu(II)-Ionen durch Substanzen, wie sie oben beschrieben wurden, in einem bestimmten Potentialbereich zum Teil oder ganz aufgehoben wird. Bei den Huminstoffen liegt dieser Potentialbereich zwischen 0 und $-0,4$ V. Die durch die Huminstoffe verursachten katalytischen Strompeaks sind konzentrationsabhängig und sehr gut auswertbar (Abb. 2). In Abb. 3 ist die entsprechende Eichkurve des Huminsäurestandards in halblogarithmischer Form dargestellt. Vor allem der nahezu lineare Teil des sigmoiden Kurvenverlaufes ist für die quantitative Analyse gut geeignet. Die Höhe der Strompeaks (i_p) nähert sich asymptotisch dem Wert von i_D (Diffusionsstromstärke der Cu(II)-Abscheidung).

In Anbetracht der ungenügenden Kenntnis der Struktur der Komplexe und deren Bildung läßt sich nur ein ganz allgemeiner Mechanismus formulieren, der lediglich prinzipielle Aspekte dieser Cu(II)-Abscheidung wiedergibt:

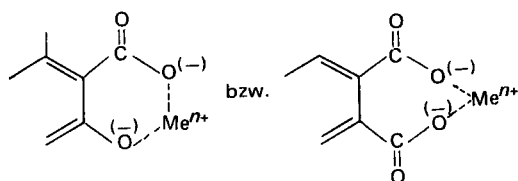


(Lig = $\sum_i (\text{HS})^{Z_s}$; HS = Huminstoff; Z_s = Summe der negativen Ladungen der einzelnen HS mit verschiedenen Molekulargewichten; x = Zahl der Cu(II)-Ionen in den HS-Komplexen; y = Zahl der funktionellen Gruppen, die an der Komplexbildung beteiligt sind.)

Danach bilden sich zunächst die entsprechenden Cu(II)-Komplexe in der Lösung aus, die dann in die geschlossene Adsorptionsschicht, bestehend aus TBP-Molekülen, eingelagert werden. Diese eingelagerten, adsorbierten Moleküle wirken dann als Katalysatoren für die gehemmte Cu(II)-Abscheidung [8]. Obgleich die in der Lösung bzw. an der Hg-Oberfläche gebildeten Komplexe nicht genau bekannt sind, muß man vor allem davon ausgehen, daß phenolische Hydroxyl- bzw. Carboxylgruppen als Liganden fungieren.



Nach Martell [9] ist bei Huminstoffen vom Fulvosäuretyp mit folgenden Strukturen zu rechnen



Um modellmäßige Vergleiche zu ziehen, wurden Salizyl- und *o*-Phthalsäure in die Untersuchungen einbezogen. Dabei zeigte sich, daß *o*-Phthalsäure ebenfalls eine starke katalytische Aktivität zeigt. Schon bei einer Konzentration von $2,5 \times 10^{-8}$ M erhält man eine signifikante Erhöhung des Grundpeaks. Die Peaks sind allerdings wesentlich schmaler als jene, die durch Huminstoffe verursacht werden. Salizylsäure ist wesentlich inaktiver als *o*-Phthalsäure, da erst bei einer Konzentration von 5×10^{-6} M ein leichter Anstieg des Grundstromes erfolgt.

Ausgehend von diesen Ergebnissen haben wir Wasserproben aus verschiedenen Teilen der DDR untersucht und festgestellt, daß die Konzentration der Huminstoffe in verschiedenen Trinkwasserproben in den Grenzen zwischen $100 \mu\text{g l}^{-1}$ und $2,6 \text{ mg l}^{-1}$ lagen. Die Form der erhaltenen Peaks war in allen Fällen mit jenen des Standards in Abb. 2 identisch.

Die Bestimmung der Huminstoffe im Trinkwasser wurde von anderen organischen und anorganischen Inhaltsstoffen des Wassers nicht gestört. Weder die anorganischen Anionen noch die ebenfalls im Trinkwasser vorkommenden Aminosäuren bzw. Peptide und Polyhydroxyverbindungen haben in den möglicherweise vorhandenen Konzentrationen einen störenden Einfluß. Auch eventuell vorhandene Silikate haben keinen Einfluß auf die Meßergebnisse. Zur weiteren Charakterisierung der Stromstärkepeaks wurden die zu untersuchenden Wasserproben sowohl im sauren wie im alkalischen pH-Bereich mit Chloroform extrahiert. Die Peakhöhen nahmen dabei nicht ab. Erst die Behandlung der Wasserproben mit Al_2O_3 führte zur Verringerung bzw. zur Beseitigung dieser Stromstärkepeaks. Bedingt durch die hohe Oberflächenaktivität der Huminstoffe ist es wichtig, daß die Wasserproben entweder sofort nach der Entnahme gemessen oder im gefrorenen Zustand aufbewahrt und dann gemessen werden. Ausgehend von der auf pH 5,0 eingestellten Grundlösung sind alle Messungen bei pH 5,0 durchgeführt worden. Eine Verringerung des pH-Wertes führt zur Reduzierung des katalytischen Effektes und somit zur Empfindlichkeitsverminderung. Bei hohen pH-Werten ist die Gefahr der Ausfällung von $\text{Cu}(\text{OH})_2$ gegeben.

LITERATUR

- 1M. Schnitzer und S. U. Kahn, *Humic Substances in the Environment*, M. Dekker, New York, 1972.

- 2 D. Eichelsdörfer, in Handbuch der Lebensmittelchemie, Bd. 8/1, Wasser und Luft, Springer-Verlag, Berlin, 1969, S. 610, 624.
- 3 M. Schnitzer, in Soil Biochemistry, Vol. 2, M. Dekker, New York, 1971, S. 60.
- 4 S. H. Eberle, C. Hoesle und Chr. Krückeberg, Bericht KFK 1969 UF, Kernforschungszentrum, Karlsruhe, Juni 1974, S. 44.
- 5 R. Klöcking, Diss., Universität Rostock (1967).
- 6 R. Klöcking, Proc. Europ. Soc. Toxicol., 16 (1975) 258.
- 7 H. Sohr und K. Wienhold, Anal. Chim. Acta, 60 (1972) 413.
- 8 H. Sohr und K. Wienhold, J. Electroanal. Chem., 35 (1972) 219.
- 9 A. E. Martell, Pure Appl. Chem., 44 (1975) 81.

Short Communication

POLAROGRAPHIC STUDY OF ADSORBED TELLURIUM AT THE HANGING AND DROPPING MERCURY ELECTRODES IN 1 M HYDROCHLORIC OR PERCHLORIC ACID SOLUTIONS

O. VITTORI

Laboratoire de Chimie Analytique III, ERA 474, Université Claude Bernard Lyon I, 43 Boulevard du 11 novembre 1918, 69622 Villeurbanne Cedex (France)

(Received 28th April 1980)

Summary. Studies of tellurium(IV) reduction at a mercury drop electrode are difficult because the two-step electrochemical scheme is complicated by adsorption of elemental tellurium at the mercury surface. Anomalous $i-t$ curves at the HMDE are presented in order to confirm the important rôle of the primary adsorbed monolayer and the unusual behaviour of elemental tellurium when the deposit is increased by more than this monolayer.

Since the first investigations by Schwaer and Suchy [1] and Lingane and Niedrach [2] on the polarographic reduction of tellurium, it has become obvious that elemental tellurium, $\text{Te}(0)$, is adsorbed at the mercury surface and that the maximum which appears on the plateau of the wave corresponds to a second step, the reduction to telluride, $\text{Te}(\text{II})$. A previous study [3] has shown the anomalous polarographic curves recorded when a.c. and linear sweep polarography are used. Shinagawa et al. [4, 5] have pointed out the influence of u.v. irradiation on the reduction scheme of the first step. Other studies have shown that the adsorbed tellurium leads to anomalies even for dilute solutions [6–9]. The present communication deals essentially with the $i-t$ curves at HMDE observed for relatively concentrated tellurium(IV) solutions in 1 M hydrochloric or perchloric acid solutions.

Experimental

Instrumental. Two Tacussel Solea PRG 3 and PRG 4 polarographs were used. For fast recording of $i-t$ curves, a Tektronix 5115 oscilloscope was used, as well as an x-y Sefram recorder. The HMDE was an E410 Metrohm micrometer; the ease of reproduction of the drops is better than 1%. A sodium sulfate salt bridge was used to avoid precipitation of potassium perchlorate in the reference electrode junction when experiments were done in 1 M HClO_4 .

Reagents. Tellurium oxide and perchloric and hydrochloric acids were of analytical grade (Merck). Dissolution of tellurium oxide is easy in a few milliliters of sodium hydroxide and then a 10^{-2} M stock solution was obtained by adjusting with appropriate acid. For electrochemical studies, an exact amount

of stock solution was diluted with the acid at the desired concentration, so that the sodium concentration was negligible.

Results and discussion

Because pH has a strong influence, 1 M HCl and 1 M HClO₄ were used exclusively and the tellurium(IV) concentration was fixed at 10⁻³ M in most experiments. For such a concentration, a prewave appears, its shape being different for each acid (Fig. 1). A well developed wave is observed about 0.1 or 0.2 V towards more negative potentials than the prewave, and the typical intense and narrow maximum is 0.4 V more cathodic again, but its study is beyond the scope of this communication.

I-t curves at DME. As shown in Table 1, the maximum time observed in 1 M HCl in the prewave range, seems to be influenced mainly by the concentration change and only slightly by the potential. This suggests an adsorption prewave very similar to a Brdicka prewave [10, 11] but it is impossible to confirm this suggestion here because of the anodic limitation caused by the mercury wave in the presence of chloride. In spite of this difficulty, evaluation of Γ_m by means of Koryta's equation [12] leads to a value only slightly lower than the expected theoretical value computed by assuming that tellurium atoms are in a compact monolayer (2.24×10^{-9} mol cm⁻² if the atomic radius is 1.37×10^{-8} cm [13]). Adsorption of a chlorocomplex before reduction is a possible explanation [14].

In 1 M HClO₄ a maximum time appears on *i-t* curves for 10⁻³ M Te(IV); its value decreases as the potential is made more cathodic, which suggests a simple inhibition by the reduction product adsorbed strongly at the surface drop, i.e. tellurium atoms in the present case. When the tellurium concentration is less than 10⁻³ M, different maxima are observed (Table 2). It is difficult to interpret such a result unless it is assumed that adsorption of

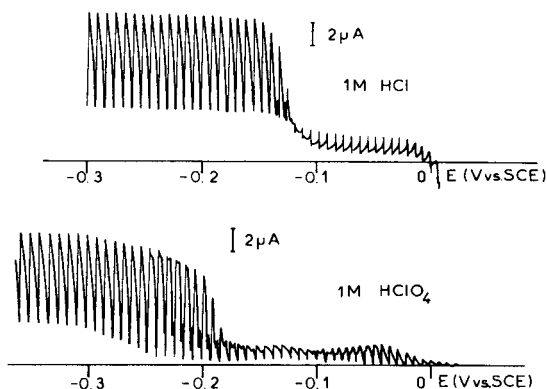


Fig. 1. D.c. polarograms of 10⁻³ M Te(IV) in 1 M HCl and 1 M HClO₄. Natural drop time (about 7 s).

TABLE 1

Surface concentration Γ_m and maximum time t_m at DME in 1 M HCl for different Te(IV) concentrations

E (V vs. SCE)	Te(IV) conc. ($\times 10^{-3}$ mol l $^{-1}$)							
	1.00		0.625		0.50		0.357	
	t_m (s)	Γ_m^a	t_m (s)	Γ_m^a	t_m (s)	Γ_m^a	t_m (s)	Γ_m^a
-0.02	0.65	2.01	0.90	1.48	1.35	1.45	2.10	1.29
-0.04	0.55	1.85	0.95	1.52	1.30	1.42	2.20	1.32
-0.06	0.55	1.85	0.95	1.52	1.40	1.48	2.20	1.32
-0.08	0.50	1.77	0.95	1.52	1.35	1.45	2.40	1.38
-0.09	0.50	1.77	1.00	1.56	1.35	1.45	2.60	1.44

^aExpressed in 10^{-9} mol cm $^{-2}$.

TABLE 2

Evolution of maximum time t_m (s) at DME with variable concentration of Te(IV) in 1 M HClO $_4$

E (V vs. SCE)	Te(IV) conc. ($\times 10^{-3}$ mol l $^{-1}$)				E (V vs. SCE)	Te(IV) conc. ($\times 10^{-3}$ mol l $^{-1}$)			
	1.00	0.65	0.49	0.33		1.00	0.65	0.49	0.33
-0.035	6.30	—	—	—	-0.160	4.00	7.05	d	d
-0.040	5.50	n.o. ^a	—	—	-0.180	2.55	4.50	6.80	d
-0.050	4.20	5.85	n.o.	—	-0.200	1.25	2.65	3.80	6.80
-0.060	3.25	4.30	6.30	—	-0.220	1.25	1.85	2.45	3.85
-0.080	2.05	2.60	3.45	n.o.	-0.240	d	1.25	1.70	2.40
-0.090	1.70	2.20	2.75	5.55	-0.260	—	0.90	1.30	1.90
-0.100	1.55	2.00	2.50	4.55	-0.280	—	d	d	1.70
-0.120	1.90	2.90	4.00	7.30	-0.300	—	—	—	d
-0.140	3.65	6.25	d ^b	d					

^an.o., not observable. ^bd, disappears.

tellurium atoms is not regular, and that some redistribution is possible depending on the potential.

I-t curves at HMDE. For 10^{-3} M tellurium(IV) solution, the *i-t* curves are very similar in both acids, indicating that the adsorbed reduction product is the determining factor for the shape. Because drop area does not vary, the current is essentially dependent on the rate of growth of the deposit on mercury. The potential range where investigations were made is at the end of the prewave and the foot of the wave (Fig. 2). In both acids, the decrease in the current is faster than a $t^{-1/2}$ law would allow when the potential step is applied, with the less cathodic values. After a delay, up to 1–2 min, an increase of the current can be observed, followed by a final decrease. The more

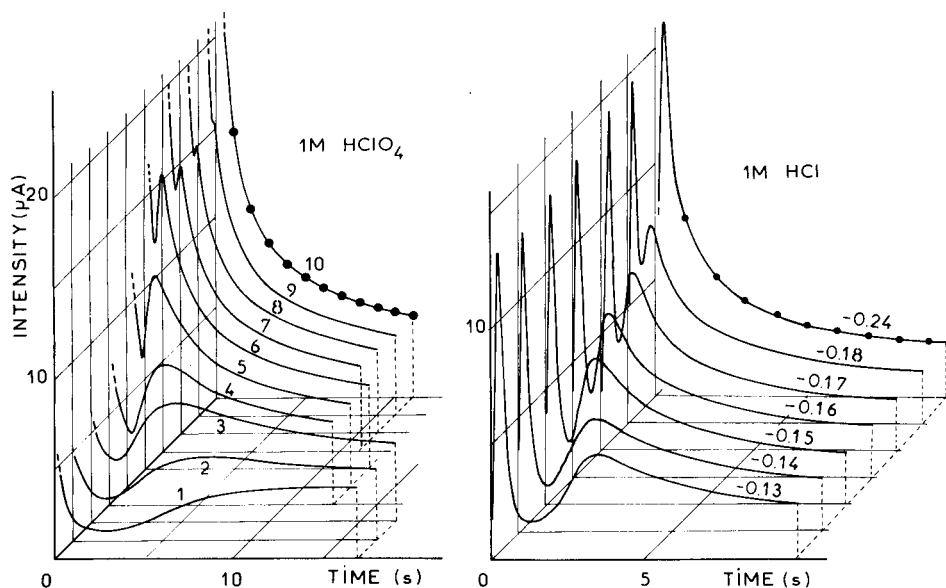


Fig. 2. $I-t$ curves at HMDE for 10^{-3} M Te(IV) in 1 M HClO_4 and in 1 M HCl . (•) Calculated current value. For 1 M HClO_4 the potentials are: (1) -0.16 ; (2) -0.18 ; (3) -0.19 ; (4) -0.20 ; (5) -0.22 ; (6) -0.24 ; (7) -0.26 ; (8) -0.28 ; (9) -0.30 ; (10) -0.40 (V vs. SCE). For 1 M HCl , the potentials are shown on the curves.

negative the applied potential, the shorter the delay, until at last the $i-t$ curve adopts the classical shape for very negative potentials.

Evaluation of the electrochemical charge which has flowed through the electrode from the application of the potential step to the time when the current is at a minimum (after subtraction of the blank to avoid any capacitive effect) indicates clearly that a compact monolayer of adsorbed tellurium atoms covers the electrode (Table 3). Results were very similar for 1 M HCl and 1 M HClO_4 . Calculation of currents for the most cathodic potentials, when the full wave had developed, showed that the $t^{-1/2}$ law is exactly

TABLE 3

Surface concentration Γ_m deduced from the electrical charge that flowed through the HMDE before the current jump for 10^{-3} M Te(IV) in 1 M HCl

Drop area ($\times 10^{-2} \text{ cm}^2$)	Electrical charge ($\times 10^{-6} \text{ C}$)	Γ_m ($\times 10^{-9} \text{ mol cm}^{-2}$)
4.11	25.43	1.60
3.51	20.35	1.50
2.91	19.32	1.72
2.21	12.80	1.50

verified. Diffusion coefficients were determined by application of the Ilkovič equation.

In order to explain, at least partly, such departures from the usual $i-t$ curves at the HMDE, two aspects should be considered. First, at the less negative potentials, there seems to be progressive adsorption as Te(IV) reaches the electrode by diffusion; this leads to a monolayer. Because reduction is easier on any part of the drop where tellurium has not been adsorbed, the current decreases very rapidly. After the monolayer has been attained, the Te(IV) concentration in the vicinity of the drop is greater than the concentration that would be present if reduction were uncomplicated. The electrode then again plays an indicative rôle and the current increases; the tellurium deposit is sufficiently compact to allow the current to flow, like a metallic electrode. Secondly, at the more negative potentials, the results suggest that the deposit grows more and more rapidly and that its metallic character is enhanced by the applied potential; thus the delay decreases and the initial current finally obeys the $t^{-1/2}$ law.

In conclusion, these observations seem to support the concept of a conducting effect of elemental tellurium when adsorbed on mercury, for cathodic potentials at the end of the prewave, tellurium becoming conductive if the necessary energy is provided. These results are consistent with the results of Shinagawa et al. [4, 5] who reported the semiconductor effect of u.v. irradiation.

REFERENCES

- 1 L. Schwaer and K. Suchy, Collect. Czech. Chem. Commun., 7 (1935) 135.
- 2 J. J. Lingane and L. W. Niedrach, J. Am. Chem. Soc., 70 (1948) 4115; 71 (1949) 196.
- 3 M. Volaire, O. Vittori and M. Porthault, Bull. Soc. Chim. Fr., (1974) 823.
- 4 M. Shinagawa, N. Yano and T. Kurosu, Talanta, 19 (1972) 439.
- 5 M. Shinagawa, N. Soramasu, Y. Mori and T. Okuma, J. Electroanal. Chem., 75 (1977) 809.
- 6 M. Duflo-Plissonier, R. Carlier and J. Lemaire, J. Electroanal. Chem., 71 (1976) 279.
- 7 M. Kopanica and V. Stara, J. Electroanal. Chem., 91 (1978) 351; 98 (1979) 213.
- 8 M. Volaire, O. Vittori and M. Porthault, Anal. Chim. Acta, 71 (1974) 185.
- 9 S. K. Nuor and O. Vittori, Anal. Chim. Acta, 91 (1977) 143.
- 10 R. Brdicka, Z. Elektrochem., 48 (1942) 278.
- 11 E. Laviron, J. Electroanal. Chem., 63 (1975) 245; 52 (1974) 355.
- 12 J. Koryta, Collect. Czech. Chem. Commun., 18 (1956) 206.
- 13 R. T. Sanderson, Inorganic Chemistry, Reinhold, New York, 1967.
- 14 M. W. Hanson, W. C. Bradbury and J. K. Carlton, Anal. Chem., 29 (1957) 490.

Short Communication

DOSAGE MERCURIMETRIQUE DES THIOETHERS EN MILIEU ACETIQUE ANHYDRE

M. HAMON et P. EPIFANOFF

*Faculté des Sciences Pharmaceutiques et Biologiques, Université de Paris-Sud,
Rue J. B. Clément, 92290 Chatenay-Malabry (France)*

(Reçu le 29 avril 1980)

Summary. (Titrimetric determination of thioethers with mercury(II) perchlorate in anhydrous acetic acid media). Thioethers form mercury(II) complexes which are less stable than the thiol complexes. Potentiometric titrations at the millimolar level are possible with a silver amalgam indicating electrode if mercury(II) perchlorate is used as titrant and the medium is anhydrous acetic acid.

Résumé. Les thioethers sont susceptibles de former des complexes avec le mercure(II); mais ceux-ci sont beaucoup moins stables que les dérivés des thiols. Cependant, il est possible de réaliser grâce à une indication potentiométrique un dosage simple et précis des thioethers aliphatiques à deux conditions. La première est d'utiliser comme réactif le perchlorate de mercure(II). La seconde est d'opérer en milieu acétique anhydre. En effet, le caractère peu dissociant de ce solvant renforce la stabilité des complexes qui y sont dissous.

Le dosage des thiols ou des composés susceptibles de donner une forme tautomère thiolique (thiourées ou thiosemicarbazides) est facilement réalisé en utilisant la réaction bien connue de ces composés avec les sels de mercure(II) [1]. Tant en milieu aqueux, qu'en solution acétique anhydre, ces composés réagissent stoechiométriquement avec l'acétate de mercure(II). Une indication potentiométrique permet de déterminer le point d'équivalence [2, 3]. Il existe cependant une différence entre ces deux milieux au niveau des mécanismes réactionnels. Dans l'eau, on observe exclusivement la formation de liaisons ioniques entre soufre et mercure alors que dans l'acide acétique, on constate à côté de ce premier type de liaison l'apparition de liaisons de coordinance [3, 4].

Cette dernière observation, jointe au fait que la stabilité des complexes est largement favorisée par la faible constante diélectrique du solvant [5] nous a conduit à envisager la possibilité de dosage des thioethers dans les mêmes conditions. En effet, ceux-ci sont également susceptibles de mettre en jeu un doublet libre de l'atome de soufre et de former ainsi des complexes. L'addition d'une solution d'ions mercure(II) dans l'acide acétique à une solution de thioether dans le même solvant devrait donc permettre par l'étude de la variation de pHg la détermination d'un point d'équivalence caractéristique.

Partie expérimentale

Réactifs, électrodes et étalonnage. Les réactifs sont: acide acétique pur pour analyse, une solution de perchlorate de mercure(II) 0,05 M, et méthionine pure conformant à la Pharmacopée Française (8^e édition).

L'électrode de référence est une électrode au sulfate de mercure(I) comportant la chaîne suivante: mercure—sulfate de mercure(I)—solution aqueuse saturée de sulfate de potassium. Il est utile lors de l'utilisation de protéger cette électrode à l'aide d'un système en verre poreux rempli de solution aqueuse saturée de sulfate de potassium (Tacussel Solea PDK2). L'électrode de mesure est une électrode d'argent amalgamé, obtenue par immersion pendant environ 30 min d'un fil d'argent de 1 à 2 mm de diamètre dans le mercure métallique.

Pour l'étalonnage, une prise d'essai de l'ordre de 0,30 mmol (environ 45 mg) est pesée exactement puis dissoute dans un volume suffisant d'acide acétique pour permettre l'immersion des électrodes. Le dosage est alors réalisé par la solution de perchlorate de mercure(II), en ajoutant le réactif à vitesse constante et en enregistrant la variation du potentiel (ou sa dérivée) en fonction du volume utilisé: 1 mmol de méthionine (soit 149 mg) correspond à 0,5 mmol de perchlorate de mercure(II). Il est souhaitable de déterminer le titre de la solution toutes les semaines en cas de longue conservation.

Mode opératoire. Une prise d'essai exactement pesée et contenant une quantité de thioéther allant de 0,20 à 0,40 mmol est dissoute dans un volume suffisant d'acide acétique. Le titrage est réalisé par la solution de perchlorate de mercure(II), en ajoutant le réactif à une vitesse voisine de celle utilisée pour l'étalonnage, à l'aide du système d'électrodes indiqué ci-dessus, et en utilisant soit la courbe classique, soit la courbe dérivée.

Détermination des conditions optimales

Le choix de l'acide acétique a été guidé par deux considérations principales. La première qui a déjà été mentionnée précédemment est sa faible constante diélectrique ($\epsilon = 6,2$) qui permet une stabilité des complexes beaucoup plus grande que dans un solvant dissociant tel que l'eau. La Figure 1 montre nettement cette différence. Une seconde raison du choix de ce milieu est son grand pouvoir dissolvant vis à vis de nombreuses molécules soufrées.

L'électrode de référence au sulfate de mercure(I) a été préférée à la classique électrode au calomel, en raison de l'absence de pouvoir complexant des ions sulfate vis à vis du mercure(II). L'emploi d'un pont salin constitué d'une solution saturée de sulfate de potassium permet d'éviter toute difficulté provenant de l'action des dérivés sulfurés sur l'électrode. Quant à l'électrode de mesure, elle doit être constituée de mercure métallique. Pour des raisons de commodité, nous avons choisi l'électrode d'argent amalgamé, obtenu par immersion dans du mercure d'un fil d'argent.

Dans le cas du dosage des thiols, c'est l'acétate de mercure(II) qui a été choisi en raison de sa bonne solubilité dans l'acide acétique. En effet, la

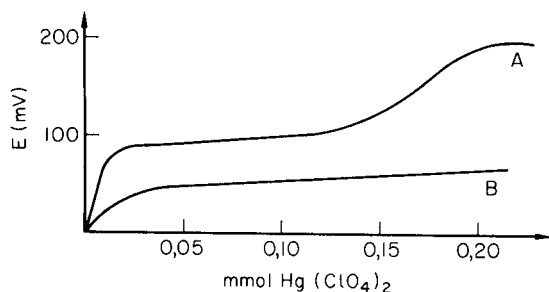


Fig. 1. Variation du potentiel d'une électrode de mercure plongeant dans une solution de méthionine (0,35 mmol dans 60 ml d'acide acétique) lors de l'addition d'une solution de perchlorate de mercure(II). (A) En milieu acétique anhydre; (B) en milieu aqueux.

différence de stabilité des complexes formés est telle que le faible caractère complexant de l'ion acétate n'est pas une entrave au dosage. En revanche, avec les thioéthers il n'est pas possible d'observer de variation de potentiel en utilisant une solution de ce sel. Aussi avons-nous choisi le perchlorate qui ne permet aucune liaison de coordinance entre l'anion et le cation. Sa solubilité dans l'acide acétique est suffisante pour réaliser sans difficultés des solutions titrées.

L'inconvénient pour la préparation d'une solution anhydre, est que ce sel n'existe qu'à l'état de trihydrate. On peut cependant en préparer une solution strictement anhydre en faisant réagir une solution titrée d'acide perchlorique dans l'acide acétique, sur une quantité exactement calculée d'oxyde de mercure(II). Il convient de noter toutefois que tout excès local d'oxyde entraîne alors le risque de réaction avec le solvant et donc la formation d'acétate de mercure(II) qui n'est pas susceptible de réagir avec les thioéthers.

Les risques d'évaporation du solvant, et à un moindre degré de fixation du mercure sur le verre entraîne une diminution du titre au cours du temps. Il est donc souhaitable de vérifier le titre de la solution mercurique en cas d'utilisation intermittente.

Influence de la vitesse de réaction et choix de l'étalon. Nous avons initialement envisagé d'utiliser l'acétate de sodium pour étalonner la solution de perchlorate de mercure(II). Ce sel, bien défini et obtenu très pur, présente en outre l'avantage que son anion est la base conjuguée du solvant [6]. Cependant, les essais de dosage de la méthionine que nous avons réalisés en utilisant une solution titrée dans ces conditions ont donné les résultats correspondant à un rapport mercure(II)/méthionine supérieur à celui que l'on pouvait attendre, puisqu'il est de 0,55. Or, par analogie avec les résultats obtenus lors du dosage des thiols [3] il était normal d'attendre un rapport de 0,50.

Pour tenter d'expliquer cette consommation anormalement élevée de sel mercurique, nous avons envisagé que, dans ce milieu peu dissociant, l'équilibre de la réaction peut être assez lent à se réaliser, et ceci d'autant plus que la stabilité des complexes est moins grande. Déjà, lors du dosage des acétates [6] l'un de nous avait observé un phénomène similaire. Pour vérifier cette

hypothèse nous avons déterminé le volume de solution de mercure(II) consommé par une même quantité de méthionine en fonction de la durée du dosage. Les résultats confirment notre hypothèse, puisqu'en augmentant la durée de l'addition de réactif le rapport diminue de 0,55 pour 4 min, à 0,52 pour 16 min et tend ainsi vers la valeur théorique de 0,50.

En raison de ces observations et pour diminuer au maximum une telle interférence du temps de réaction, il nous paraît souhaitable de préconiser un étalonnage de la solution à l'aide d'un échantillon de thioéther pur. La méthionine peut très généralement servir d'étalon, car les différences de titre observées pour différents dérivés analogues, thioéther (tétrahydrothiophène ou thioester (spironolactone), sont négligeables.

Résultats

Bien que le groupement fonctionnel thioéther de méthionine ne soit pas le seul susceptible de donner des liaisons semipolaires, nous avons pu constater qu'il réagit selon un mécanisme mettant en jeu deux molécules de produit soufré pour une molécule de perchlorate de mercure(II). Les résultats de deux séries de dosages réalisés chacune sur 10 essais, ont donné pour l'une, une teneur de $99,2 \pm 1,4\%$ pour l'autre $101,7 \pm 2,1\%$. Ces valeurs montrent une reproductibilité satisfaisante.

Nous avons choisi le tétrahydrothiophène en raison de la simplicité de sa formule qui permet d'exclure toute possibilité de réaction secondaire due à la présence d'autres groupements fonctionnels dans la molécule. La Figure 2 montre que le tétrahydrothiophène réagit d'une façon satisfaisante vis à vis du perchlorate mercurique. Ici encore la stoechiométrie est de 2 molécules de produit soufré pour une molécule de perchlorate de mercure(II). Il est à remarquer qu'un premier maximum apparaît sur la courbe; il correspond à

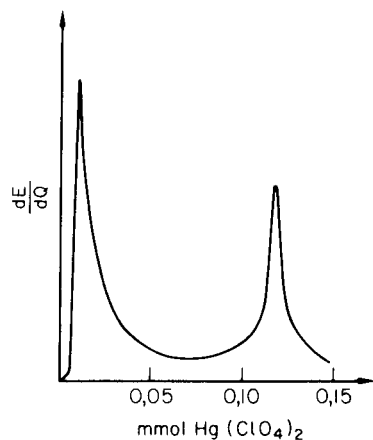


Fig. 2. Dosage du tétrahydrothiophène (0,23 mmol) par le perchlorate de mercure(II) en milieu acétique anhydre (courbe dérivée).

l'existence d'un point d'inflexion sur la partie initiale qui n'a aucune signification analytique.

Parallèlement au cas précédent, nous avons essayé de faire réagir le thio-phène lui-même. Dans cette molécule, les doublets électroniques libres de l'hétéroatome sont conjugués à des doubles liaisons. Ceci provoque une aromatisation de l'ensemble et affaiblit par là même le caractère de base de Lewis de la molécule. Dans ce cas, il n'est plus possible de réaliser un dosage. Il en est de même pour le nitrate de thiamine ou l'atome de soufre entre également dans une structure conjuguée.

Dans le cas de la phénothiazine enfin, le mercure(II) réagit comme oxydant. Aussi, bien que l'on observe un point d'inflexion très prononcé lors du dosage, n'avons nous pas actuellement poursuivi nos recherches sur cette molécule. En revanche, un thioester comme la spironolactone dans laquelle existe un groupement thioacétate peut aisément être dosé par cette méthode.

Conclusion

Les quelques exemples de réaction de thioéthers aliphatiques ou alicycliques qui sont donnés dans ce travail montrent qu'il est possible de réaliser leur dosage par une méthode mercurimétrique en milieu acide acétique anhydre. Cette méthode est susceptible d'être étendue à des dérivés thioesters. En revanche, lorsque l'atome de soufre se trouve engagé dans une structure aromatique la méthode n'est plus applicable.

BIBLIOGRAPHIE

- 1 J. H. Karchmer, *The Analytical Chemistry of Sulfur and its Compounds*, Wiley—Interscience, New York, part 1, 1970; part 2, 1972.
- 2 A. Billabert, M. Callanquin et M. Hamon, *Analisis*, 3 (1975) 258.
- 3 A. Billabert et M. Hamon, *Analisis*, 5 (1977) 29.
- 4 F. Pellerin, Communication au premier congrès de Chimie analytique, Budapest, 1961.
- 5 G. Charlot et B. Tremillon, *les réactions chimiques dans les solvants et les sels fondus*, Gauthier Villars, Paris, 1963.
- 6 B. Larouci, A. Billabert et M. Hamon, *Analisis*, 7 (1979) 150.

Short Communication

MEASUREMENT OF CALCIUM AND TITANIUM FROM ^{47}Sc BY INSTRUMENTAL NEUTRON ACTIVATION ANALYSIS

J. YELLIN*, I. PERLMAN and S. TANDY

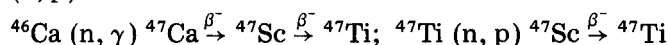
The Hebrew University of Jerusalem (Israel)

(Received 25th June 1980)

Summary. A procedure is outlined for measuring calcium and titanium from ^{47}Sc by instrumental neutron activation analysis. Precise calcium measurements obtained from ^{47}Sc are compared with measurements based on ^{47}Ca and ^{49}Ca . The method is particularly suitable for low levels (ca. 1%) of calcium.

Calcium is an important element to measure in archaeological provenance studies based on chemical analysis. Two direct measurements are possible when instrumental neutron activation analysis (i.n.a.a.) is used: (1) ^{49}Ca produced by the (n, γ) reaction on ^{48}Ca [1], and (2) ^{47}Ca produced by the (n, γ) reaction on ^{46}Ca . Both methods have problems and yield poor results for low levels of calcium ($\leq 10\%$) because of the low abundance of the stable isotopes (^{46}Ca 0.0033%, ^{48}Ca 0.185%) and the neutron capture cross-sections (^{46}Ca 0.3 barn, ^{48}Ca 1.1 barn). An additional complicating factor for ^{49}Ca is the short half-life (8.8 min) which requires that the analyzing facility be on or near the reactor site. Most facilities dedicated to archaeological investigations are located far from reactor sites. The ^{47}Ca measurement is complicated by an ^{59}Fe γ -peak at 1292 keV which interferes strongly with the much smaller ^{47}Ca γ -peak at 1297 keV.

An alternative and more precise though more complicated measurement can be based on ^{47}Sc . The latter is produced by the decay of ^{47}Ca and by an (n, p) reaction on ^{47}Ti



Owing to the low terrestrial concentration of vanadium and the low isotopic abundance of vanadium-50 (0.2%), production of ^{47}Sc from ^{50}V by the (n, α) reaction can be ignored. The complex growth-decay curve of ^{47}Sc is shown in Fig. 1. Clearly, a measurement of ^{47}Sc at two points in time can yield the respective contributions of calcium and titanium to the ^{47}Sc signal if there are no interferences. ^{47}Sc is detected with good precision on the 159-keV γ -ray. The only known interference is the 158-keV γ -ray of $^{117\text{m}}\text{Sn}$ ($t_{1/2} = 14$ d). Fortunately, the abundance of tin in the earth's crust is low so that tin does not usually interfere.

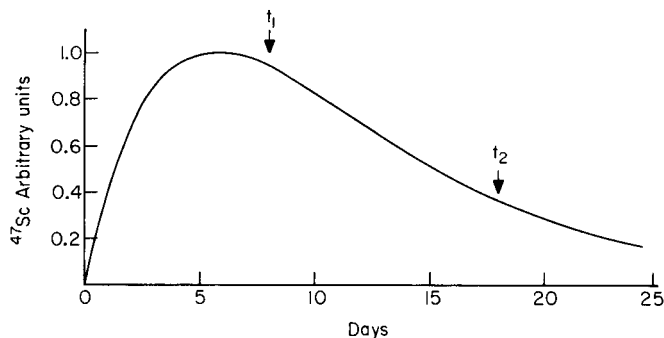


Fig. 1. Growth-decay curve for ^{47}Sc produced from ^{47}Ca . For simplicity only eqn. (2) below, is plopped.

Procedure

If $N(t)$ is the ^{47}Sc count at time t , then

$$N(t) = N^T(t) + N^C(t) \quad (1)$$

where $N^T(t) = N^T(0) \exp(-\lambda_{\text{Sc}} t)$

$$N^C(t) = N_{\text{Ca}}(0) \{ k \exp(-\lambda_{\text{Sc}} t) + [\lambda_{\text{Ca}} / (\lambda_{\text{Ca}} - \lambda_{\text{Sc}})] [\exp(-\lambda_{\text{Sc}} t) - \exp(-\lambda_{\text{Ca}} t)] \} \quad (2)$$

$N^T(t)$ is the contribution to the ^{47}Sc count due to titanium and $N^C(t)$ is the contribution to the ^{47}Sc count due to calcium. λ_{Sc} is the decay constant for ^{47}Sc and λ_{Ca} for ^{47}Ca . $k \cdot N_{\text{Ca}}(0)$ is the count from ^{47}Sc produced from calcium during the neutron bombardment. k can be estimated and is generally very small ($k \ll 1$).

Writing $f(t)$ for $\exp(-\lambda_{\text{Sc}} t)$, and $g(t)$ for the whole term in curly brackets in eqn. (2), we have $N(t) = N^T(0) f(t) + N_{\text{Ca}}(0) g(t)$. If $N(t)$ is measured at t_1 and t_2 (Fig. 1), then

$$N^T(0) = (N(t_2) g(t_1) - N(t_1) g(t_2)) / D$$

$$N_{\text{Ca}}(0) = (N(t_1) f(t_2) - N(t_2) f(t_1)) / D$$

where $D = g(t_1) f(t_2) - g(t_2) f(t_1)$. The calcium and titanium fractions can then be calculated. Denoting a sample by X and the standard by S and writing for brevity $f_i = f(t_i)$, $g_i = g(t_i)$, $i = 1, 2$ then

$$[\text{Ca fraction}]_X = [(N_{X1} f_{X2} - N_{X2} f_{X1}) / (N_{S1} f_{S2} - N_{S2} f_{S1})] [D_S / D_X] \times$$

$$[\text{Ca fraction}]_S$$

$$[\text{Ti fraction}]_X = [(N_{X2} g_{X1} - N_{X1} g_{X2}) / (N_{S2} g_{S1} - N_{S1} g_{S2})] [D_S / D_X] \times$$

$$[\text{Ti fraction}]_S.$$

If a pure calcium standard is employed for the calcium determination then $N_{\text{Si}}^T = 0$ and $N_{\text{Si}} = N_{\text{Si}}^C = N_{\text{Ca}}(0) g_i$, $i = 1, 2$. In that case

$$[\text{Ca fraction}]_X = [(N_{X1} f_{X2} - N_{X2} f_{X1}) / N_{\text{Si}}] [g_{\text{Si}} / D_X] [\text{Ca fraction}]_S$$

($i = 1$ or 2). A single measurement of the calcium standard then suffices and since the counting statistics are better at t_1 than at t_2 , t_1 is the preferred time. A similar simplification is obtained for titanium if a pure (calcium-free) titanium standard is employed. The errors associated with the calcium and titanium fractions are obtained by the usual rules for compounding the counting errors. Thus, if e is the relative error in the measurements, then $e^2(\text{Ca}) = e_X^2(\text{Ca}^0) + e_S^2(\text{Ca}^0)$, where Ca^0 stands for $N_{\text{Ca}}(0)$, $e_A(\text{Ca}^0) = \sigma(\text{Ca}^0)_A / N_{\text{Ca}}(0)_A$, $A = X$ or S and $\sigma^2(\text{Ca}^0)_A = (f_{X2}^2 \sigma_{A1}^2 + f_{X1}^2 \sigma_{A2}^2) / D_X^2$. The counting error σ_{Ai} ($i = 1, 2$) relates to the count of ^{47}Sc at t_1 and t_2 , respectively. Similar relationships apply for the error in the titanium measurement.

The ^{47}Sc measurements were made at approximately $t_1 = 8$ d and $t_2 = 18$ d, and the counts were normalized to constant weight and live time.

Results

Table 1 compares calcium measurements obtained from ^{47}Ca and from ^{47}Sc . A pure calcium carbonate standard was employed in these measurements. In measuring calcium from ^{47}Ca the relative intensity of the 1297-keV γ -ray was evaluated by integrating half of the γ -peak, the half away from the ^{59}Fe peak. This way of integrating the calcium peak results in a slight loss of precision, but minimizes the iron interference and is thought to be more reliable. The half peak that is integrated is corrected for iron. Agreement between the ^{47}Ca and ^{47}Sc measurements is as good as can be expected from counting statistics across the range of calcium values shown (2–11%). The counting error of the ^{47}Sc measurements is very much lower than that of the ^{47}Ca measurements. The ^{47}Ca measurements were made with a large volume coaxial geometry Ge(Li) detector. The ^{47}Sc measurements were made with a small planar geometry pure Ge detector. A 10-min count was taken for ^{47}Ca , and a 20-min count for each of the two measurements of ^{47}Sc .

Table 2 compares calcium measurements for five specimens based on ^{49}Ca with ^{47}Sc measurements. The ^{49}Ca measurements were done at the Lawrence Berkeley Laboratory (LBL) as part of an interlaboratory study of i.n.a.a. measurements between LBL and Hebrew University (HU) [2]. Also shown in Table 2 are titanium measurements for the same specimens. The LBL titanium values were obtained from ^{47}Sc corrected for calcium from the ^{49}Ca measurements. The HU measurements were obtained simultaneously with the calcium values by the procedure outlined above. The agreement

TABLE 1

Calcium determinations (in %) from ^{47}Ca and ^{47}Sc

Sample	193I	206I	197U	199N	204W
From ^{47}Ca	1.9 ± 0.6	3.0 ± 0.9	6.6 ± 0.8	9.9 ± 0.9	10.7 ± 0.7
From ^{47}Sc	0.68 ± 0.24	2.04 ± 0.44	5.80 ± 0.24	10.90 ± 0.33	10.57 ± 0.39

TABLE 2

Calcium and titanium determinations obtained at Hebrew University (HU) from ^{47}Sc and analogous values for the same specimens obtained at Lawrence Berkeley Laboratory (LBL). (The LBL measurements are based on ^{49}Ca and ^{47}Sc)

Sample	CIN5	CIN8	KERM1	BISH26	BISH27
Ca(%) HU (^{47}Sc)	6.71 ± 0.24	7.51 ± 0.25	2.15 ± 0.24	0.79 ± 0.11	0.55 ± 0.10
Ca(%) LBL(^{49}Ca)	7.63 ± 0.51	7.99 ± 0.13	2.05 ± 0.47	1.26 ± 0.58	0.55 ± 0.36
Ti(%) HU (^{47}Sc)	0.500 ± 0.026	0.529 ± 0.026	1.049 ± 0.051	0.066 ± 0.018	0.046 ± 0.016
Ti(%) LBL(^{47}Sc , ^{49}Ca)	0.512 ± 0.016	0.488 ± 0.019	1.108 ± 0.017	0.079 ± 0.021	0.064 ± 0.014

between the paired Ca and Ti values are as good as can be expected from counting statistics. The results shown in Tables 1 and 2 show that the calcium measurements obtained by the above procedure are consistent with both ^{47}Ca and ^{49}Ca direct measurements but that better precision may be expected from ^{47}Sc . In both the HU and LBL measurements, Standard Pottery [1] was employed as the titanium standard; a correction was applied for its calcium content.

Discussion

The measurement of calcium from ^{47}Sc is very sensitive to what is chosen for the ^{47}Sc half-life. The recommended half-life of 3.422 d which is based on β -spectroscopic measurements [3] was used here; this value was also used for the titanium measurements shown in Table 2. When the recommended ^{47}Sc half-life is used and the net ^{47}Sc count in a pure calcium standard measured at t_2 is decay-corrected to t_1 , and the results compared, a discrepancy of about 1% is observed. This discrepancy disappears if instead of the recommended ^{47}Sc half-life, the value of 3.345 d obtained from γ -spectroscopic measurements [3] is used, although this value then leads to an analogous discrepancy in the titanium measurements. From the preceding, the ^{47}Sc count at t_1 , N_{S1} , is related to the count at t_2 by $N_{S2} = N_{S1} g_2/g_1$ or $N_{S1} g_2/N_{S2} g_1 = 1$ but experimentally the ratio differs from 1 by about 1% when the ^{47}Sc half-life based on β -spectroscopic measurements is used. Whether the observed discrepancy is in fact due to inaccuracies in the ^{47}Sc half-life or to some as yet undiscovered systematic error is not clear at this point.

The method outlined above is most useful for measuring low levels of calcium and for the measurement of titanium. For high (>10%) levels of calcium, good results for calcium can be obtained from ^{47}Ca .

REFERENCES

- 1 I. Perlman and F. Asaro, *Archaeometry*, 11 (1969) 21.
- 2 J. Yellin, I. Perlman, F. Asaro, H. Michel and D. Mosier, *Archaeometry*, 20 (1978) 95.
- 3 C. M. Lederer and V. S. Shirley (Eds.), *Table of Isotopes*, 7th edn., J. Wiley, New York, 1978.

Short Communication

DETERMINATION OF TRACE ELEMENTS IN SEA WATER BY INDUCTIVELY-COUPLED PLASMA EMISSION SPECTROMETRY

AKIYOSHI SUGIMAE

Environmental Pollution Control Center of Takaishi City, 1-26, 4-chome, Takashinohama, Takaishi, Osaka (Japan)

(Received 19th March 1980)

Summary. Pb, Zn, Cd, Ni, Mn, Fe, V and Cu in sea water are determined by extraction of their complexes with sodium diethyldithiocarbamate into chloroform, decomposition of the chelates and inductively-coupled plasma emission spectrometry. When 1-l water samples are used, the lowest determinable concentrations are: 0.063 $\mu\text{g Mn l}^{-1}$, 0.13 $\mu\text{g Zn l}^{-1}$, 0.25 $\mu\text{g Cd l}^{-1}$, 0.25 $\mu\text{g Fe l}^{-1}$, 0.38 $\mu\text{g V l}^{-1}$, 0.5 $\mu\text{g Ni l}^{-1}$, 0.5 $\mu\text{g Cu l}^{-1}$, and 2.5 $\mu\text{g Pb l}^{-1}$. Above these levels, the relative standard deviations are better than 12% for the complete procedure.

Interest in inductively-coupled plasmas (i.c.p.) as the excitation source for optical emission spectrometry (e.s.) has accelerated dramatically since the i.c.p. was first applied to the determination of trace elements [1, 2]. Several authors have subsequently investigated the feasibility of i.c.p.e.s. for the simultaneous determination of many elements in materials such as steel [3, 4], plants [5], geological materials [6–8], biological fluids [9, 10], and environmental samples [11–14]. The advantages of the technique are its high sensitivity, minimum sample preparation and relative freedom from chemical interferences. Its use in sea-water analysis, however, has been strangely restricted.

The importance of trace elements in natural water systems is well established. Optical spectrometric techniques are generally not sensitive enough for direct application to unpolluted sea waters, so that preliminary concentration of trace elements is essential, and this is also true for i.c.p.e.s. Moreover, direct aspiration of sea waters into the plasma usually results in clogging of the nebulizer within 20–30 min, and further difficulties are caused by the high concentrations of some other constituents such as sodium, calcium and magnesium, all of which can affect the spectral background levels. These difficulties can be overcome by close matching of sample and standard composition, but the accuracy and sensitivity at high salt levels are generally poorer than those obtained for pure aqueous solutions.

Quantitative concentration and separation of trace elements from the bulk of the salts were therefore necessary. Very high concentration factors are not necessary because of the high sensitivity of i.c.p.e.s. The commonest pre-concentration treatments that have been employed are co-precipitation,

solvent extraction and ion exchange. Of the various possibilities considered, chelation and solvent extraction with diethyldithiocarbamate and/or pyroldinecarbodithioate have been most frequently used in recent publications to bring the trace element abundances of sea water to within the required sensitivity ranges and to separate the trace elements from the major constituents of sea water. This communication describes the development of an i.c.p.e.s. method which permits the determination of eight important trace elements (Pb, Zn, Cd, Ni, Mn, Fe, V and Cu) in sea water. The chelation of trace elements with diethyldithiocarbamic acid (DDTC) and extraction with chloroform is followed by decomposition of the extract and i.c.p.e.s. This combination proved to be very useful for routine sea-water analysis.

Experimental

Instrumentation. An Applied Research Laboratories (ARL) ICPQ system (based on a QA 137 polychromator) was used. The system consists of a high-frequency generator, a plasma torch, a sample nebulizer and the direct-reading polychromator. The experimental facilities and the pertinent plasma operating conditions [14] are summarized in Table 1.

Reagents. For the stock standards for each of the elements ($100 \mu\text{g ml}^{-1}$), dissolve a weighed portion of the high-purity metal or salt in 10 ml of nitric acid and dilute to volume in a volumetric flask. For the acetate buffer, pH 6.2, dissolve 60 g of sodium acetate in 1 l of distilled water and adjust the pH of solution to 6.2 by adding 1 M acetic acid.

Optimum conditions for the simultaneous extraction of the eight trace elements. The effect of pH on the extraction of Pb, Zn, Cd, Ni, Mn, Fe, V

TABLE 1

Experimental facilities and plasma operating conditions

Spectrometer	ARL QA 137. 1-m Pachen-Runge mounting, grating ruled 1920 lines/mm, 0.52 nm mm^{-1} reciprocal linear dispersion (1st order), primary slit width $20 \mu\text{m}$, secondary slits $50 \mu\text{m}$, Hamamatsu R-300 photomultipliers.		
Programmed wavelengths	Pb(II) 220.35 nm, Zn(II) 202.55 nm, Cd(II) 226.50 nm, Ni(II) 231.60 nm, Mn(II) 257.61 nm, Fe(II) 259.94 nm, V(II) 311.07 nm, Cu(I) 324.75 nm		
Readout	Digital readout of integrated signal.		
R.f. generator	Henry Radio 3000 PGC/27. Frequency 27.12 MHz, crystal controlled.		
Plasma torch assembly	Fused quartz with capillary injector.		
Nebulizer and spray chamber	Glass pneumatic nebulizer into dual-tube spray chamber.		

Plasma operating conditions

Frequency	27.12 MHz	Argon plasma gas flow rate	1.3 l min^{-1}
Forward power	1600 W	Argon carrier gas flow rate	1.0 l min^{-1}
Reflected power	$<10 \text{ W}$	Observation height in plasma	16 mm above load coil
Argon coolant gas flow rate	11.0 l min^{-1}		

and Cu with DDTC in chloroform was investigated. Known amounts of the eight elements were added both to a composite sea-water sample and to a synthetic sea water sample, containing 2.72% NaCl, 0.381% MgCl_2 , 0.166% MgSO_4 , 0.126% CaSO_4 , 0.0863% K_2SO_4 , 0.0123% CaCO_3 and 0.0076% MgBr_2 (all w/w). The pH values of six 500-ml aliquots of each solution were adjusted by addition of an appropriate buffer to values varying from 2.0 to 8.6; the upper limit is set by the precipitation of calcium and magnesium which commences at ca. pH 9.1. The trace elements mentioned above were separated from the 500-ml aliquot by extraction of their DDTC complexes into chloroform and subsequently determined by i.c.p.e.s. The original samples were analysed in conjunction with the spiked samples.

Except for manganese, all the elements examined were easily and effectively extracted at pH 3.8. The manganese extraction was very poor at this pH and was severely affected by the shaking time. When the shaking time was increased, the manganese extraction was gradually increased, reaching a maximum at 30 min and then falling off rapidly. This is probably because the manganese chelate is not stable in the chloroform phase and is stripped back into the acidic aqueous phase during very long shaking times. Rigid control of extraction conditions and timing, both unsuitable for routine work, was required to obtain consistent recoveries of manganese. Manganese could only be easily and effectively extracted from solutions of pH higher than 6.0. However, the extraction of iron, which is hydrolysed readily in solutions of pH higher than ca. 4.0, was then reduced. The precipitation of hydrated iron(III) oxide also caused problems because of co-precipitation of other trace elements when moderately high concentrations of iron were present. This problem was readily overcome by addition of citrate which forms a water-soluble complex with iron(III). The extraction from 0.5% ammonium citrate solution at pH 6.2 gave quantitative extraction of Pb, Zn, Cd, Ni, Mn, Fe and Cu, and 83% extraction of vanadium.

Sampling and preservation of samples. Collect 2 l of sea water and filter it through a 0.45- μm membrane filter. Immediately acidify the filtered sea water with hydrochloric acid to pH 1 in order to lessen the danger of adsorption or precipitation of colloidal materials on the walls of the container.

Procedure for extraction. Transfer a 1-l aliquot of the acidified water sample to a 1-l beaker and evaporate to about 400 ml on a hot plate. Transfer to a 1-l separatory funnel, rinsing with distilled water, dilute to 500 ml with distilled water and mix. (These steps are precautionary measures to prevent emulsification during solvent extraction and are only necessary for the analysis of polluted coastal sea and estuarine waters which may contain emulsifying agents. Clear phase separation is aided by increasing the concentrations of electrolytes like NaCl, i.e., salting-out. A 500-ml aliquot of the acidified water sample is usually measured into the separatory funnel.) Add a few drops of bromocresol green indicator, 25 ml of aqueous 10% (w/v) ammonium citrate solution and sufficient sodium hydroxide solution to give a light-blue color, indicating pH 5.5–6.0. Add 30 ml of acetate buffer pH 6.2,

which should adjust the pH to about 6.2. Add 20 ml of aqueous 2% (w/v) sodium diethyldithiocarbamate solution and mix. Add 100 ml of chloroform and shake vigorously for 10 min on a mechanical shaker. Allow the chloroform layer to separate and filter this layer through an 11-cm Toyo No. 5C filter-paper into a 200-ml conical flask. Again add 20 ml of chloroform to the aqueous layer, shake for 1 min and allow the chloroform layer to separate. Combine the two chloroform layers.

Preparation of final solution for i.c.p.e.s. Direct nebulization of the chloroform extract into the plasma affects the resistive impedance of the plasma to a large extent and makes it difficult to couple the radio-frequency energy into the plasma [15]. This leads to complicated changes in signal intensity and considerably reduced sensitivity [16]. Accordingly, the trace elements were dissolved in appropriate acids for i.c.p.e.s. The final solution is prepared as follows; ultra-pure acids were used. Evaporate the combined extract almost to dryness by gentle heating. Add 12 ml of nitric acid and 4 ml of hydrochloric acid. Evaporate to dryness, add 5 ml of (1 + 9) nitric acid and quantitatively transfer to a 25-ml volumetric flask with distilled water for nebulization.

Results and discussion

Analytical calibration. The i.c.p.e.s. system could be calibrated with just one aqueous composite standard solution for all the determinations, because the responses of the system were confirmed to be linear over the concentration ranges usually encountered in actual water samples. The composite standard solution containing $1 \mu\text{g ml}^{-1}$ of each of Pb, Zn, Cd, Ni, Mn, Fe, V and Cu was prepared by mixing the requisite amounts of stock standards, adding sufficient nitric acid and diluting with distilled water. The concentration of nitric acid in the standard solution should be equivalent to that present in the sample solution. The standard solution is made up to be (1 + 49) nitric acid solution. Irregularities in sample nebulization caused by variation in acid concentration are thus avoided.

Recovery tests indicated that all the trace elements examined with the exception of vanadium were completely extracted; the recoveries ranged from 97% to 99%, so that no compensating correction was needed. A correction is however, necessary for the incomplete ($83 \pm 5\%$) extraction of vanadium.

The reagents used may contain significant amounts of metal-salt impurities. A blank should be carried out with each set of samples and its signal intensities subtracted from those obtained for the samples.

Detection limits. Detection limits (defined as the concentration necessary to produce a signal equivalent to twice the standard deviation of the background signal) obtained for the eight elements in the 500-ml aliquot of the original water sample were as follows: $0.025 \mu\text{g l}^{-1}$ for Mn; $0.05 \mu\text{g l}^{-1}$ for Zn; $0.10 \mu\text{g l}^{-1}$ for Cd and Fe; $0.15 \mu\text{g l}^{-1}$ for V; $0.20 \mu\text{g l}^{-1}$ for Ni and Cu; and $1 \mu\text{g l}^{-1}$ for Pb. These values could be halved by using 1-l samples.

Precision. The overall precision of the method was estimated by carrying

out replicate analysis for all eight elements in six identical samples of sea water from Osaka Bay. The short-term precision was also evaluated by analysing a combined sample of the 6 solutions 12 times at regular intervals of 3 min without any instrumental adjustment after the initial standardization. The precision data are presented in Table 2. The lowest determinable concentrations (defined as the concentration needed to produce a signal equivalent to 10 times the standard deviation of the background signal) are also shown in Table 2.

The lowest determinable concentrations for all elements except Pb and Cd lay below the trace element concentrations in actual sea water. Above the limits set, determinations could be carried out with satisfactory precision. The overall precision and the short-term precision were better than $\pm 12\%$ and better than $\pm 3\%$, respectively.

Analysis of sea water. Table 3 shows the results obtained for sea-water

TABLE 2

Precision data obtained for 1-l samples of sea water from Osaka Bay, Japan

Element	Mean concentration ($\mu\text{g l}^{-1}$)	R.s.d. (%)		Limit of determination ($\mu\text{g l}^{-1}$)
		Overall	Short-term	
Pb	1.2	25	18	2.5
Zn	17.0	4.1	0.58	0.13
Cd	0.05	44	29	0.25
Ni	2.83	6.0	1.8	0.5
Mn	14.6	1.3	0.56	0.06
Fe	18.4	5.9	0.42	0.25
V ^a	0.71	12	2.8	0.38
Cu	1.38	8.8	1.4	0.5

^aIncludes correction for incomplete extraction.

TABLE 3

Trace elements in sea-water samples from Osaka Bay, Japan

Sample	Concentration ($\mu\text{g l}^{-1}$)						Volume of water used (ml)
	Zn	Ni	Mn	Fe	V	Cu	
1	15.0	3.86	17.5	15.4	0.76	1.73	1000
	(16.1)	(3.99)	(17.6)	(12.8)	(0.65)	(1.70)	500
2	5.34	2.41	25.5	21.6	0.88	0.89	500
	(7.39)	(2.58)	(25.8)	(23.4)	(0.75)	(0.96)	500
3	9.61	2.98	7.38	22.1	0.44	2.11	500
4	14.3	3.03	11.1	10.3	0.36	1.69	1000
5	29.1	5.33	30.6	65.5	0.23	2.66	1000
	(28.6)	(4.63)	(29.3)	(63.0)	(0.24)	(2.48)	1000
6	13.3	2.98	13.9	24.2	0.76	1.87	500
7	15.0	3.37	5.64	25.0	0.85	1.72	500

samples taken from Osaka Bay. Data are given only for those elements which were at concentrations exceeding the limit of determination; in general, lead and cadmium were at the concentrations almost equivalent to their detection limits. Three of the samples were analysed in duplicate at a later date and gave good agreement with earlier values; these are shown in parentheses in Table 3.

The author thanks T. Shikita and S. Imada for their contributions to this work.

REFERENCES

- 1 S. Greenfield, L. W. Jones and C. T. Berry, *Analyst*, 89 (1964) 713.
- 2 R. H. Wendt and V. A. Fassel, *Anal. Chem.*, 37 (1965) 920.
- 3 C. C. Butler, R. N. Kniseley and V. A. Fassel, *Anal. Chem.*, 47 (1975) 825.
- 4 I. Tanaka, S. Tahara, T. Ohtsuki, K. Sato and R. Matsumoto, *Bunseki Kagaku*, 28 (1979) 371.
- 5 R. H. Scott and A. Strasheim, *Anal. Chim. Acta*, 76 (1975) 71.
- 6 R. H. Scott and M. L. Kokot, *Anal. Chim. Acta*, 75 (1975) 257.
- 7 J. O. Burman, C. Ponter and K. Boström, *Anal. Chem.*, 50 (1978) 679.
- 8 H. Uchida, T. Uchida and C. Iida, *Anal. Chim. Acta*, 108 (1979) 87.
- 9 R. N. Kniseley, V. A. Fassel and C. C. Butler, *Clin. Chem.*, 19 (1973) 801.
- 10 R. M. Barman and J. S. Genna, *Anal. Chem.*, 51 (1979) 1065.
- 11 R. K. Winge, V. A. Fassel, R. N. Kniseley, E. Dekalb and W. J. Haas, *Spectrochim. Acta, Part B*, 32 (1977) 327.
- 12 N. R. McQuaker, P. D. Kluckner and G. N. Chang, *Anal. Chem.*, 51 (1979) 888.
- 13 J. R. Garbarino and H. E. Taylor, *Appl. Spectrosc.*, 33 (1979) 1220.
- 14 A. Sugimae, *Bunseki Kagaku*, 28 (1979) 555; *J. Jpn. Soc. Air Pollut.* 14 (1979) 389.
- 15 T. Ito, H. Kawaguchi and A. Mizuike, *Bunseki Kagaku*, 28 (1979) 648.
- 16 S. Greenfield, H. McD. McGeachin and P. B. Smith, *Anal. Chim. Acta*, 84 (1976) 67.

Short Communication

DOSAGE SIMULTANE PAR CHROMATOGRAPHIE LIQUIDE A HAUTE PERFORMANCE DE L'ACIDE BENZOIQUE ET DE L'ACIDE SORBIQUE

A. COLLINGE et A. NOIRFALISE*

Laboratoire d'analyse des denrées alimentaires, Université de Liège, 151 Boulevard de la Constitution, B-4020 Liège (Belgique)

(Reçu le 28 juillet 1980)

Summary. *High-performance liquid chromatographic determination of benzoic and sorbic acids.* Quantitative h.p.l.c. for benzoic and sorbic acids in foodstuffs, especially soft drinks, is described. Recoveries were $101.49\% \pm 1.39$ for sorbic acid and $99.52\% \pm 1.05$ for benzoic acid in the concentration ranges normally used (50–100 mg l⁻¹).

Résumé. Les auteurs proposent une technique h.p.l.c. pour le dosage simultané de l'acide benzoïque et de l'acide sorbique dans les denrées alimentaires liquides du genre limonade. La récupération est pour des concentrations de 50–100 mg l⁻¹ de $101,49\% \pm 1,39$ pour l'acide sorbique et $99,52\% \pm 1,05$ pour l'acide benzoïque.

Le contrôle de la présence d'agents conservateurs dans les denrées alimentaires représentait jusqu'il y a peu un travail souvent long et relativement peu précis. L'avènement de la chromatographie liquide à haute performance (h.p.l.c.) a bouleversé les données du problème [1–6] en permettant le plus souvent de limiter à une seule manipulation les quatre ou cinq étapes antérieures (l'extraction, la purification, la concentration, l'identification et le dosage). Dans la présente note, nous proposons une technique simple et rapide de dosage simultané de l'acide benzoïque et de l'acide sorbique applicable dès à présent aux aliments liquides, les limonades en particulier.

Partie expérimentale

Matériel et équipement. Le chromatographe liquide à haute performance (h.p.l.c.) utilisé est un Pye-Unicam type LC-XPD, pompe haute pression à double piston réciproque type XPD 700 BAR, vanne Rhéodyne Model 7120 de 20 µl, détecteur Pye-Unicam u.v. à longueur d'onde variable (190–380 nm) couplé à un enregistreur Philips PM 8251/02. La colonne est une colonne métallique Chrompack 27811 (25 cm de long et 0,46 cm de diamètre intérieur) remplie de LiChrosorb 10 RP18 (Merck).

Les conditions instrumentales sont les suivantes: colonne débit 2,0 ml min⁻¹; température (ambiante) 22–26°C; longueur d'onde, 225 nm; déroulement du papier, 5 mm min⁻¹.

Solutions standards. Simultanément à l'acide benzoïque et à l'acide sorbique, nous avons testé l'acide salicylique, l'acide *p*-hydroxybenzoïque

et ses esters propylique et méthylique (Formenti). Les solutions "stock" étaient à 1000 mg l^{-1} , et les solutions de travail à des concentrations comprises entre 20 et 200 mg l^{-1} . L'eau utilisée était demineralisée sur résine échangeuse d'ions puis distillée dans un appareil en verre.

Phases mobiles. Nous avons successivement testé une phase aqueuse renfermant 1% d'acide perchlorique et 20, 30 et 50% de méthanol (point d'ébullition $64-65^{\circ}\text{C}$), et une phase aqueuse renfermant 1% d'acide perchlorique et 20, 30 et 50% d'isopropanol. Devant les résultats obtenus, nous avons finalement choisi de travailler avec une phase aqueuse renfermant 1% d'acide perchlorique et 18% d'isopropanol.

Préparation des échantillons. Les limonades et jus de fruits examinés sont préalablement filtrés sur membranes Millipore ($0,45 \mu\text{m}$).

Quantification (dosage). Nous n'avons pas cru devoir recourir au service d'un étalon interne et ceci compte tenu de la bonne précision et de l'excellente reproductibilité des résultats obtenus. Les dosages ont été effectués par mesure soit de la hauteur du pic, soit de la surface du pic et comparaison avec une droite d'étalonnage.

Resultats et discussion

Suivant les conditions opératoires mises au point (1% d'acide perchlorique, 18% d'isopropanol, colonne de LiChrosorb 10 RP18) les temps de rétention sont de 8,50 min pour l'acide sorbique et 9,95 min pour l'acide benzoïque. L'acide *p*-hydroxybenzoïque, les esters méthylique et propylique de l'acide *p*-hydroxybenzoïque et l'acide salicylique n'interfèrent en rien sur ces déterminations, les deux premiers ayant des temps de rétention inférieurs et les deux autres, des temps de rétention supérieurs. Aucune interférence n'est à redouter par ailleurs de la part de la caféine et de la saccharine qui ont des temps de rétention nettement inférieurs.

Le Tableau 1 donne les pourcentages de récupération obtenues après addition d'acide benzoïque et/ou d'acide sorbique à des concentrations de 50 et 100 mg l^{-1} dans de l'eau et dans une limonade au citron dans laquelle l'absence d'acide benzoïque et/ou acide sorbique avait préalablement été vérifiée.

Il n'existe aucune différence significative entre les résultats obtenus pour l'un comme pour l'autre agent conservateur tant dans l'eau que dans la limonade au citron. Le bonne qualité des pics obtenus peut expliquer les reproductibilités et sensibilités meilleures observées par le mode de calcul utilisant la seule hauteur de pic de préférence à celui utilisant la surface.

Conclusion

Les conditions opératoires que nous proposons permettent de réaliser dans un temps court un dosage simultané précis de l'acide benzoïque et de l'acide sorbique dans des liquides aqueux du genre limonade. Les dosages réalisés sont à l'abri de toute interférence de la part d'autres agents conservateurs tels que l'acide salicylique, l'acide *p*-hydroxybenzoïque et ses esters méthylique

TABLEAU 1

Pourcentages de récupération de l'acide benzoïque et de l'acide sorbique en solution dans l'eau et en solution dans une limonade au citron

Ajoutés mg l ⁻¹	Eau				Limonade au citron			
	Acide benzoïque		Acide sorbique		Acide Benzoïque		Acide sorbique	
	(1) ^a	(2) ^b	(1) ^a	(2) ^b	(1) ^a	(2) ^b	(1) ^a	(2) ^b
100	100,35	106,85	100,38	98,99	99,59	97,84	102,43	101,01
	100,82	101,12	100,38	94,28	100,41	94,54	101,41	95,24
	102,45	102,76	101,41	97,62	100,82	105,23	102,94	96,68
50	99,58	96,96	99,50	102,58	97,96	96,24	99,36	102,64
	100,82	102,26	101,52	104,68	98,97	93,00	102,44	101,00
	101,24	102,70	101,92	105,14	99,59	97,84	100,38	101,35
Moyennes	100,88 ± 0,95	102,11 ± 3,19	100,85 ± 0,91	100,55 ± 4,30	99,52 ± 1,05	97,45 ± 4,26	101,49 ± 1,39	99,65 ± 2,96

^aCalcul à l'aide de la seule hauteur du pic. ^bCalcul à l'aide de la surface du pic.

et propylique, ou de la part d'autres ingrédients occasionnels des limonades tels que la caféine et la saccharine. Dès à présent, nous étudions la possibilité d'améliorer cette technique en introduisant l'emploi d'un étalon interne, encore que cette nécessité ne soit pas évidente dans le cas présent. Nous nous proposons par ailleurs de réaliser grâce à cette technique l'étude d'un échantillonnage du marché belge des limonades.

BIBLIOGRAPHIE

- 1 D. S. Smyly, B. B. Woodward et E. C. Conrad, J. Assoc. Off. Anal. Chem., 59(1) (1976) 14.
- 2 M. C. Bennett et D. R. Petrus, J. Food Sci., 42(5) (1977) 1220.
- 3 F. Eisenbeiss, M. Weber et S. Ehlerding, Chromatographia, 10(5) (1977) 262.
- 4 M. A. McCalla, F. G. Mark et W. H. Kipp, J. Assoc. Off. Anal. Chem., 60(1) (1977) 71.
- 5 J. G. Faugère, Ann. Falsif. Expert. Chim., 72 (1979) 774, 227.
- 6 U. Leuenberger, R. Gauch et E. Baumgartner, J. Chromatogr., 173 (1979) 343.

Short Communication

AN AUTOMATIC SPECTROPHOTOMETRIC METHOD FOR THE DETERMINATION OF URANIUM(VI) EXTRACTED INTO A LIQUID ION-EXCHANGER MEDIUM

SAMUEL J. LYLE* and MASSOUD TAMIZI

The Chemical Laboratories, The University of Kent at Canterbury, Kent CT2 7NH (Gt. Britain)

(Received 30th April 1980)

Summary. An earlier procedure based on 2-(5-bromo-2-pyridylazo)-5-diethylaminophenol is adapted for use with a Technicon AutoAnalyzer; 60 samples per hour can be analyzed. The range is 0.2–3 g of uranium per litre of extract. The method is readily modified for the determination of uranium ($\geq 200 \mu\text{g l}^{-1}$) in ground waters.

Recently, a spectrophotometric method was described [1] for the determination of uranium(VI) in trialkylamine sulphate/kerosene extracts from sulphuric acid leach liquors. The colour-forming reagent used was 2-(5-bromo-2-pyridylazo)-5-diethylaminophenol (Br-PADAP). In order to optimize partition of the uranium between the liquid phases in a uranium recovery plant, it is desirable to be able to determine the uranium concentration in the amine phase frequently and rapidly. Because of the nature of the aforementioned method, it lends itself to automation; in this communication, an automatic version is described. The segmented continuous-flow technique originated by Skeggs [2] was made the basis of the method with Technicon AutoAnalyzer modules and components.

The layout and performance of the manifold is described and its adaptation for the determination of uranium in surface waters (e.g. in mineral prospecting) is discussed.

Experimental

Reagents and apparatus. The reagents were those described previously [1] except that $\text{UO}_2\text{SO}_4 \cdot 3.5\text{H}_2\text{O}$ replaced $\text{UO}_2(\text{NO}_3)_2 \cdot 6\text{H}_2\text{O}$.

The AutoAnalyzer modules consisted of a Sampler II, Pump I, colorimeter and dual-pen recorder. Solvaflex tubing was used in manifold construction, along with fittings (tube connectors and pulse suppressors), the mixing coil and 2-ml disposable polystyrene sample cups (Technicon Corporation, Tarrytown, NY). The colorimeter was fitted with a tubular flow-cell (optical path length 4 mm) and a set of optical filters transmitting at 570 nm having a transmission bandwidth at half-height of 18 nm.

The pump manifold and general lay-out of the automatic system are presented in Fig. 1.

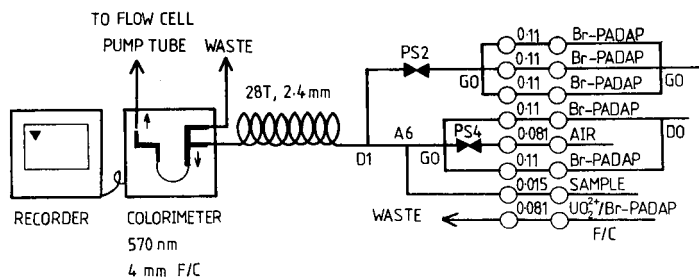


Fig. 1. The pump manifold and general layout of the system. The numbers on the manifold refer to the internal diameters of the pumping lines (in inches). Tube connectors and pulse suppressors are labelled as in the Technicon catalogue.

Br-PADAP. The dye (0.150 g) is dissolved in about 700 ml of industrial methylated spirit (IMS). Tri-*n*-octylamine (TOA; 20 ml) is mixed in and followed by distilled water (40 ml). The total volume is made up to 1 l with IMS.

Uranium-free solvent (UFS). TOA (50 ml) and octan-2-ol (20 ml) are diluted to 1 l with kerosene. The amine is converted to its sulphate form by shaking with 1 M sulphuric acid (100 ml).

Uranium-containing solvent (UCS). Sufficient solid $\text{UO}_2\text{SO}_4 \cdot 3.5\text{H}_2\text{O}$ is dissolved in UFS to give a stock solution containing an accurately known amount of uranium(VI) around 5 g l^{-1} . A small addition of octanol may be necessary to prevent formation of a second organic phase. This solution appropriately diluted with UFS is used for calibration purposes.

Results and Discussion

The concentration of Br-PADAP solution is set at 0.15 g l^{-1} to ensure a minimum molar ratio of Br-PADAP to uranium of 10. The manifold is designed to process samples at the rate of 60 per hour (sampler with CAM60). Data relating to cross-contamination or carryover from a sample with high concentration (2.36 g U l^{-1}) to one of low concentration (0.37 g U l^{-1}) at this sampling rate are presented in Fig. 2. Although the resolution improves significantly as the sample-to-wash ratio decreases from 2:1 to 1:2, the effects of sample carryover for each of the three operating ratios is negligible (≤ 0.01 units of absorbance). However, operation at ratios 1:1 or 1:2 is preferable because of the better resolution attainable at extremes of the concentration range. Replicate determinations (Fig. 3) using CAM60 and a sample-to-wash ratio of 1:2 indicate that reproducibility is good and the liquid/air stream is stable. The overall performance of the manifold is illustrated by the results shown in Fig. 4. In all the measurements described here, IMS was used as the wash solution between samples.

Calibration graphs of absorbance against uranium concentration for CAM60 with a sample-to-wash ratio of 1:2 are presented in Fig. 5. The Beer-Lambert law is obeyed to quite high absorbances. However, the effective uranium(VI) concentration range is from about 0.2 to 3 g l^{-1} . To investigate

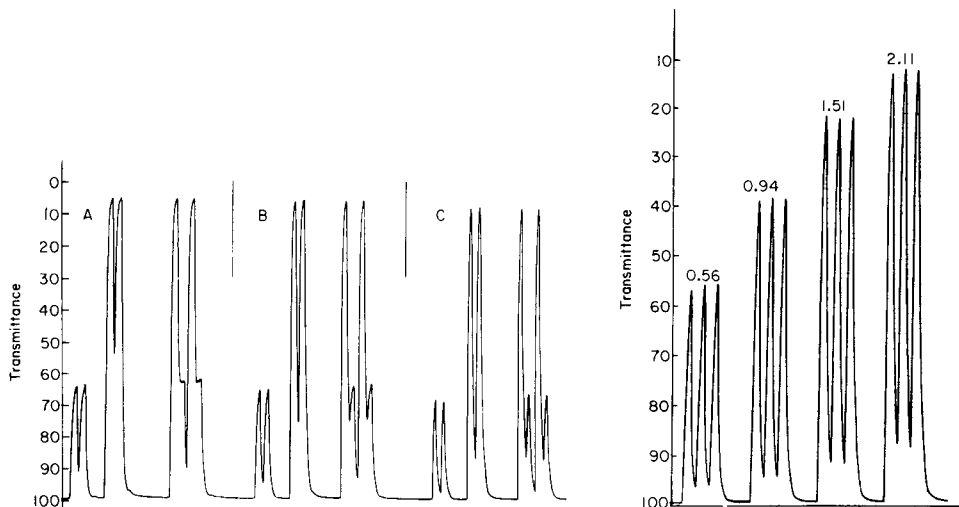


Fig. 2. Cross-contamination and resolution tests at different sample-to-wash ratios (A, 2:1; B, 1:1; C, 1:2) for a sampling rate of 60 samples per hour (CAM60). Uranium concentrations are 0.37 g l^{-1} for each of the smaller peaks and 2.36 g l^{-1} for the larger peaks.

Fig. 3. Reproducibility tests using a sample-to-wash ratio of 1:2 and CAM60. The numbers on the peaks are uranium concentrations in g l^{-1} .

the effect of time and temperature on the calibration plots, a thermostatted delay coil (20 ft. long, 1.6 mm i.d.) was placed before the colorimeter. It was found that temperature changes from 26 to at least 36°C did not affect the signal. Colour intensity was affected, however, by the overall residence time between mixing at A6 (Fig. 1) and the colorimeter cell. This would make desirable the preparation of a new calibration graph whenever the manifold tubes need to be replaced. The flow rate of amine extract through a sample line with an internal diameter less than 0.015 in. was unstable. This would suggest that uranium concentrations greater than 3 g l^{-1} can be analysed only if a sample dilution greater than that allowed by the manifold in Fig. 1 is made or a 2 mm flow-cell is used.

It has been shown [3] that dibenzoylmethane (DBM) can be used in place of Br-PADAP for the determination of uranium in amine sulphate extracts. The lower apparent molar absorptivity of the uranium-DBM complex makes it possible in the automated method [4] to cover the range up to 5 g U l^{-1} in the extract without resorting to the high dilution needed with Br-PADAP. Thus, there is a saving in solvents when the former is used in the automated system. Tolerances of both reagents to other ions including sulphate is good with respect to uranium recovery from leach liquors [1, 3]. However, a major advantage of Br-PADAP is the relatively high sensitivity in dealing with low uranium concentrations. TOA will recover small amounts of uranium from sulphate solutions with improved efficiency if benzene is used as diluent instead of kerosene. (Partition ratios of 150 for equal phase volumes

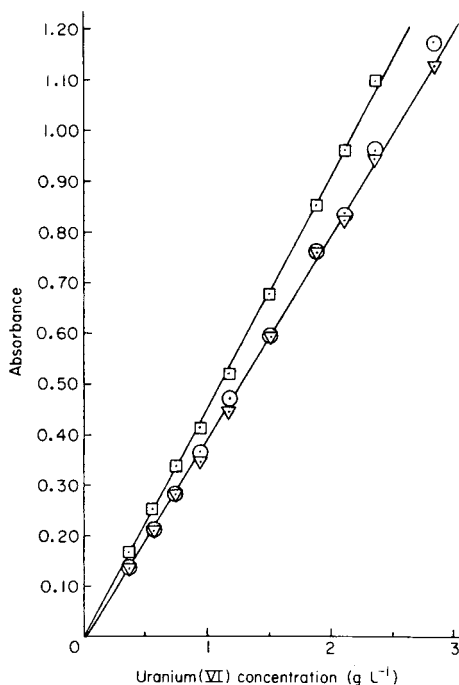
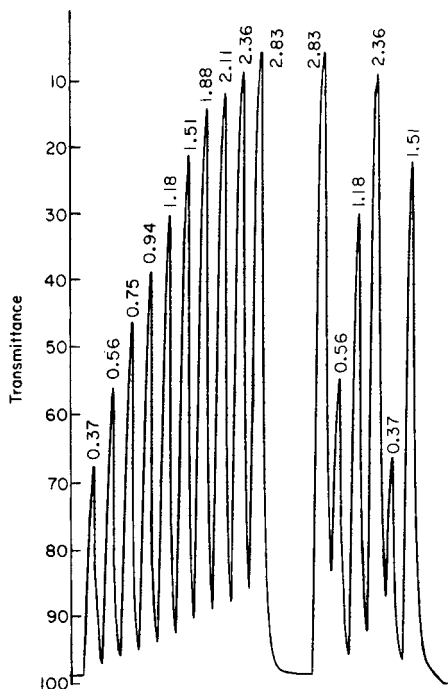


Fig. 4. Manifold performance in the continuous analysis of a systematically increasing and a random selection of uranium concentrations. The flow time between A6 (Fig. 1) and the colorimeter cell was 22 s. The sample-to-wash ratio is 1:2.

Fig. 5. Standard curves of absorbance against uranium concentration in the amine extract. (□) Data with delay coil absent (i.e. 20°C, time 22 s); (▽, ●) thermostatted delay coil inserted to give a residence time of 65 s and a temperature of 26°C (▽) or 36°C (●).

have been reported [5, 6].) Thus by using an amine-to-aqueous phase ratio of 1:10 for the extraction, reducing the flow-rate of Br-PADAP solution by a factor of 2, increasing the sample (amine extract) flow-rate by a factor of 4 and using an optical cell of path-length 50 mm, it would be possible to determine uranium concentrations of $\geq 200 \mu\text{g l}^{-1}$ in water. Such an adaptation of the method proposed here would find application in the analysis of mine waters and in exploration for uranium deposits by analysis of ground waters. Single-stage liquid-liquid extraction is readily automated [7] and a suitable module could be incorporated into the system described here.

REFERENCES

- 1 S. J. Lyle and M. Tamizi, *Anal. Chim. Acta*, 108 (1979) 267.
- 2 L. T. Skeggs, *Am. J. Clin. Pathol.*, 28 (1957) 311.
- 3 S. J. Lyle and M. Tamizi, *Anal. Chim. Acta*, 108 (1979) 437.
- 4 S. J. Lyle and M. Tamizi, *Trans. Inst. Min. Metall. (London), Sect. C*, 89 (1980) 83.
- 5 C. F. Coleman, K. B. Brown, J. G. Moore and D. J. Crouse, *Ind. Eng. Chem.*, 50 (1958) 1756.
- 6 C. Deptula and S. Minc, *J. Inorg. Nucl. Chem.*, 29 (1967) 221.
- 7 J. K. Foreman and P. B. Stockwell, *Automatic Chemical Analysis*, Ellis Horwood, Chichester, 1975, Ch. 10.

Short Communication

PURGE VESSEL DESIGN IN DETERMINATIONS OF VOLATILE ORGANIC COMPOUNDS

TORRE RAMSTAD* and TERRY J. NESTRICK

Analytical Laboratories, 574 Building, Dow Chemical U.S.A., Midland, MI 48640 (U.S.A.)

(Received 23rd April 1980)

Summary. Five purge vessels are described for use in determinations of volatile organics. Less conventional designs permit extension of the technique to untraditional samples, including soil and viscous glues.

Volatile organics determination (v.o.d.) has proved to be a useful technique for the determination of neutral/nonpolar volatile organics in aqueous systems. Most reported applications of v.o.d. utilize a Bellar and Lichtenberg (B and L) type stripping vessel [1]. The original B and L design consists of an undulated glass tube with a medium porosity frit at the bottom. Finely divided gas bubbles contact an aqueous 5–10 cm³ sample along a length of several cm. The purged compounds are swept out the top, through an optional foam trap for use with excessively foaming samples. While the B and L purge vessel is well suited for stripping organics out of 5–10 cm³ of “well-behaved” aqueous systems, it may be totally unsuitable for certain less traditional samples. In this laboratory several samples have necessitated the design of specialized purge devices. This report compares (1) a slightly-modified B and L stripping vessel, (2) a miniaturized B and L apparatus, (3) a miniaturized B and L with foam trap, (4) a vessel packed with glass wool for severely foaming samples, and (5) a particulate sampler/stripper which has been used for soil samples. These five vessels are shown in Fig. 1.

Experimental

All experiments were performed on a v.o.d. apparatus constructed in this laboratory. The system was coupled to a Hewlett–Packard 5710A gas chromatograph with subambient capability used with flame ionization, photoionization, electrolytic conductivity, or mass spectrometric detection. The mass spectrometer was a LKB 9000. Purging was ordinarily carried out for 10 min and desorption was conducted at 200°C.

Results and discussion

Bellar and Lichtenberg purge vessel (B and L). This is the workhorse device of v.o.d. The vessel shown in Fig. 1a is a slightly modified, water-jacketed version. The Vigreux elements are included to alleviate some

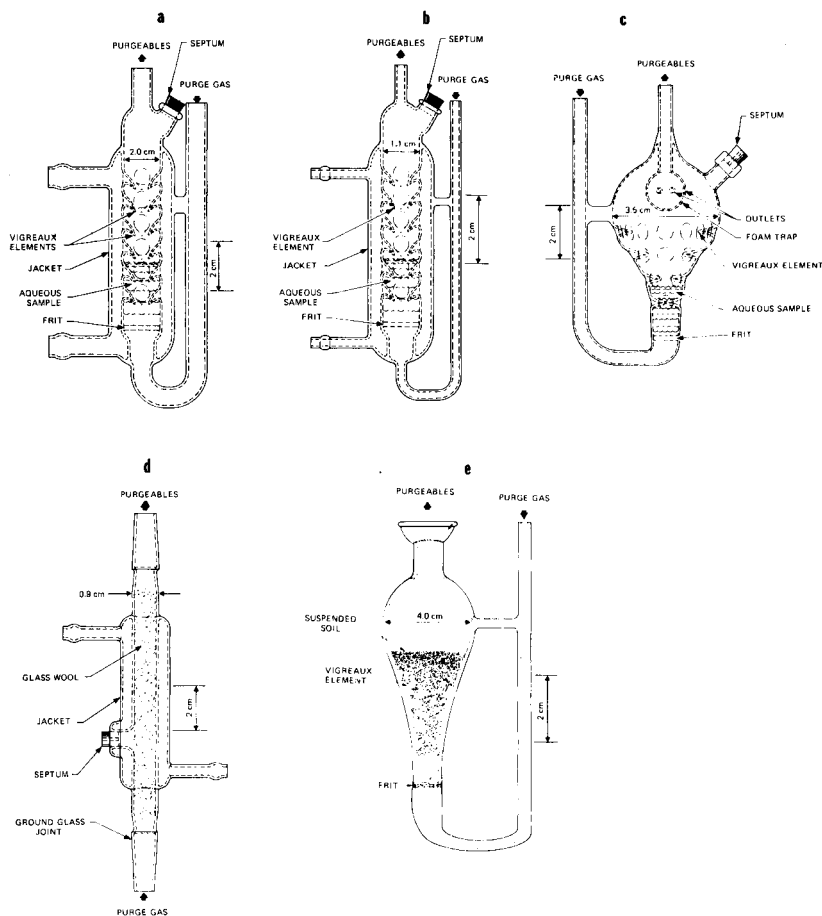


Fig. 1. Selected purging vessels. (a) Bellar and Lichtenberg purge vessel; (b) miniaturized Bellar and Lichtenberg stripping vessel; (c) miniaturized Bellar and Lichtenberg apparatus with foam trap; (d) packed purge vessel; (e) particulate sampler/purger.

foaming. Sample capacity is 10 cm^3 ; a minimum of 1 cm^3 is required to cover the frit. For favorable compounds, detection limits are sub part-per-billion. Sample introduction is through the septum by a syringe with hypodermic needle.

Mini B and L. In an effort to extend detection limits downward, a number of investigators have constructed larger purge vessels [2, 3]. Many applications do not require the low detection limits afforded by large volume samples, e.g., some industrial wastestreams. For these samples the capacity offered by the B and L device of Fig. 1a is not required. When solute concentration is high, a sample may be diluted and then run in a standard B and L purge vessel. However, this procedure has two drawbacks: specially-purified water (freed from volatile organics) is necessary to avoid purging volatiles

from the water diluent, and the efficiency of purging is lower in a large stripping vessel so that a comparatively large volume of purge gas is required (and a correspondingly longer time) to effect quantitative stripping. To accommodate 0.2–1 cm³ of sample, the Mini B and L device shown in Fig. 1b was constructed. When many samples are to be run, a shortened purge time is helpful. A small device such as this one should be particularly useful where sample size is limited, as, for example, with some physiological fluids. The Mini B and L has proven to be an efficient purger for various industrial wastestreams investigated here. The jacketed device has been particularly useful for the determination of polar/water-soluble volatiles by v.o.d., where the highest attainable efficiency is desired.

Mini B and L with foam trap. In situations where less than 1.5 cm³ of sample is required, where an efficient purge is desired, but where foaming may be severe, the device of Fig. 1c is useful. The narrow diameter above the frit allows intimate contact between finely dispersed bubbles and a column of aqueous sample. Both the Vigreux projections and the large surface area provided by the pear shape help to disperse foaming. However, if foaming is severe, the foam trap, which is a glass bulb punctuated by small holes, should, in most cases, break the last bubbles.

Packed purge vessel. For samples which foam excessively and/or for samples for which high purging efficiency is desired, the device shown in Fig. 1d was constructed. The center tube is packed with a material, usually glass wool, that presents a large surface area to the applied sample. With the aqueous sample spread out in a thin film, intimate contact is established between the purge gas and volatile compounds present in the sample. It is important that the tube be loosely packed; otherwise channeling may occur. The capacity of this device is 1–1.5 cm³. The same high purging efficiency may not be retained upon scale-up. With the packed purge vessel it was possible to analyze the solvents composition of two commercially-available water-soluble glues. Foaming was so severe than even the Mini B and L with foam trap could not entirely break the foam. However, with the packed purger, foaming was completely suppressed.

Particulate purge vessel. Although v.o.d. is ordinarily used to determine volatiles in water containing minimal particulate matter, the technique can be extended to sediment or soil with a suitably designed vessel. Use of the device depicted in Fig. 1e permitted benzene to be determined down to 1 ppb in soil by v.o.d. This device contains a fine-porosity frit, as do the other fritted stripping devices. A fine-porosity frit yields finely-dispersed bubbles, and lessens the chance of plugging of the frit with soil. Use of a high-velocity purge rate (40 cm³ min⁻¹) combined with the pear shape results in vigorous agitation of a soil slurry (2 g soil/20 cm³ water). Volatile organics determination is effective in this application because by constantly removing benzene (purging), diffusion out of the soil into the water is promoted. A 9-mm opening at the top of the vessel allows for convenient introduction of a sample. A jacketed version (not shown) permits purging at elevated tempera-

tures which may aid considerably the recovery of volatiles from soils. This is presently being investigated. While the device shown was designed expressly to handle soil, it should have general utility for particulate samples, including sediment and sludges.

REFERENCES

- 1 T. A. Bellar and J. J. Lichtenberg, *J. Am. Water Works Assoc.*, (1974) 739.
- 2 P. P. K. Kuo, E. S. K. Chain, F. B. DeWalle and J. H. Kim, *Anal. Chem.*, 49 (1977) 1023.
- 3 F. C. Kopfler, R. G. Melton, R. D. Lingg and W. E. Coleman, in L. H. Keith (Ed.), *Identification and Analysis of Organic Pollutants in Water*, Ann Arbor Science, Ann Arbor, Michigan, 1976, Ch. 6.

AUTHOR INDEX

- Alexander, P. W.
— and Seegopaul, P.
Automated potentiometric determination of glucose oxidase activity with a gas-sensing sulphur dioxide probe 61
- Berg, E. W.
— and Downey, D. M.
The separation of rhodium and iridium by ion flotation 239
- Bond, A. M.
— and Jones, R. D.
The analytical performance of direct current, normal pulse and differential pulse polarography with static mercury drop electrodes 1
- Buck, R. P., see Ihn, G.-S. 101
- Cardwell, T. J.
—, Marriott, P. J. and Knowles, D. J.
Optimisation of sulphur emission in molecular emission cavity analysis. Effects of variation in cavity position and phosphate addition 175
- Carr, P. W., see Elvecrog, J. M. 135
- Christensen, J. K.
—, Kryger, L., Mortensen, J. and Rasmussen, J.
Reductive potentiometric stripping analysis for elements forming sparingly soluble mercury compounds with amalgamated metal as the reducing agent 71
- Collinge, A.
— et Noirfalise, A.
Dosage simultané par chromatographie liquide à haute performance de l'acide benzoïque et de l'acide sorbique 337
- Czech, N.
—, Friese, B. and Umland, F.
Asymmetrically substituted diphenyl-carbazones as chelate formers 275
- Davidson, I. E., see Ivaska, A. 51
- Dittrich, K.
— und Meister, P.
MolekülabSORPTIONSSPEKTROMETRIE bei elektrothermischer Verdampfung in einer Graphitrohrküvette. Teil 6. Bestimmung von Chlorids Spuren durch die MolekülabSORPTION von $AlCl_3$, $GaCl_3$ und $InCl_3$ -Molekülen 205
- Downey, D. M., see Berg, E. W. 239
- Downey, S. W.
—, Shabushnig, J. G. and Hieftje, G. M.
Reduction of spectral interferences in flame emission spectrometry by selective spectral-line modulation 165
- Elvecrog, J. M.
— and Carr, P. W.
A catalimetric thermochemical unsegmented flow system based on the iodide-catalyzed cerium(IV)—arsenic(III) reaction 135
- Epifanoff, P., see Hamon, M. 321
- Franklin Smyth, W., see Ivaska, A. 51
- Friese, B., see Czech, N. 275
- Fritz, J. S., see Phillips, R. J. 255
- Fujinaga, T., see Hara, H. 119
- Garcia-Sanchez, F., see Laserna, J. J. 295
- Georges, J.
— Electrochemistry in fluosol-43, a perfluorinated blood substitute. The influence of pluronic F-68 surfactant on some polarographic electrode processes 29
- Grime, J. K.
— and Sexton, E. D.
Fixed-time kinetic enthalpimetry: improved sensitivity for enthalpimetric enzyme activity determinations in homogeneous and heterogeneous systems 125
- Haartz, J. C., see Hull, R. D. 187
- Hamon, M.
— et Epifanoff, P.
Dosage mercurimétrique des thioethers en milieu acétique anhydre 321
- Hanekamp, H. B.
— and van Nieuwkerk, H. J.

- Theoretical considerations on the performance of electrochemical flow-through detectors 13
- Hara, H.
—, Okazaki, S. and Fujinaga, T.
Enhancement of selectivity of a benzoate-sensitive liquid membrane electrode by alkylphenol 119
- Hieftje, G. M., see Downey, S. W. 165
- Hirai, Y., see Yoza, N. 281
- Holub, K., see Trojánek, A. 23
- Horváth, Zs., see Szakács, O. 219
- Hoste, J., see Mortier, R. 147
- Hull, R. D.
— and Haartz, J. C.
Determination of soluble/insoluble tungsten compounds as discrete entities in industrial hygiene samples 187
- Ihn, G.-S.
—, Nash, C. F. and Buck, R. P.
Monohydrogenphosphate-sensing electrode formulations 101
- Ishizuka, T.
—, Nakajima, K. and Sunahara, H.
Determination of phosphorus in wastewaters by inductively-coupled plasma atomic emission spectrometry 197
- Ivaska, A.
—, Vaneesorn, Y., Davidson, I. E. and Franklin Smyth, W.
Voltammetric on-line analysis for some sulphur-containing drugs 51
- Jones, R. D., see Bond, A. M. 1
- Kanda, Y.
—, Oikawa, T. and Niwaguchi, T.
Multi-element determinations of trace elements in glass by instrumental photon activation analysis 157
- Knowles, D. J., see Cardwell, T. J. 175
- Kobos, R. K.
— and Ramsey, T. A.
Enzyme electrode system from oxalate determination utilizing oxalate decarboxylase immobilized on a carbon dioxide sensor 111
- Kohashi, K., see Yamaguchi, M. 289
- Kryger, L., see Christensen, J. K. 71
- Kurokawa, Y., see Yoza, N. 281
- Landy, M. P.
— An evaluation of differential pulse anodic stripping voltammetry at a rotating glassy carbon electrode for the determination of cadmium, copper, lead and zinc in Antarctic snow samples 39
- Laserna, J. J.
—, Navas, A. and Garcia-Sanchez, F.
A fluorimetric method for the determination of traces of gallium 295
- Lásztity, A., see Szakács, O. 219
- Lyle, S. J.
— and Tamizi, M.
An automatic spectrophotometric method for the determination of uranium(VI) extracted into a liquid ion-exchanger medium 341
- Macáček, F., see Vančo, D. 249
- Marriott, P. J., see Cardwell, T. J. 175
- McCormick, M. J.
— Determination of total sulphur in fuel oils by ion chromatography 233
- Meister, P., see Dittrich, K. 205
- Miyamoto, S., see Yamaguchi, M. 289
- Montgomery, Jr., E. L.
— The determination of molybdenum in high-nickel alloys by potentiometric titration with cerium(IV) solutions 85
- Morishige, K.
— The fluorescence properties of metal complexes of alkyl derivatives of aromatic Schiff bases 301
- Mortensen, J., see Christensen, J. K. 71
- Mortier, R.
—, Vandecasteele, C. and Hoste, J.
The determination of boron in zirconium and zircaloy by proton activation analysis based on the $^{10}\text{B}(p, \alpha)^7\text{Be}$ reaction 147
- Nakagawa, G., see Wada, H. 265
- Nakajima, K., see Ishizuka, T. 197
- Nash, C. F., see Ihn, G.-S. 101
- Navas, A., see Laserna, J. J. 295
- Nestrick, T. J., see Ramstad, T. 345
- Nieuwkerk, H. J. van, see Hanekamp, H. B. 13
- Niwaguchi, T., see Kanda, Y. 157
- Noirfalise, A., see Collinge, A. 337
- Ohashi, S., see Yoza, N. 281
- Ohkura, Y., see Yamaguchi, M. 289
- Oikawa, T., see Kanda, Y. 157
- Okazaki, S., see Hara, H. 119

- Perlman, I., see Yellin, J. 327
- Phillips, R. J.
— and Fritz, J. S.
Synthesis and analytical properties of an N-phenylhydroxamic acid resin 225
- Pungor, E., see Rakiás, F. 93
- Rakiás, F.
—, Toth, K. and Pungor, E.
Determination of pharmaceutical compounds containing covalently-bound halogen by means of ion-selective electrodes 93
- Ramsey, T. A., see Kobos, R. K. 111
- Ramstad, T.
— and Nestrick, T. J.
Purge vessel design in determinations of volatile organic compounds 345
- Rasmussen, J., see Christensen, J. K. 71
- Schlipf, J., see Weisz, H. 257
- Seegopaul, P., see Alexander, P. W. 61
- Sexton, E. D., see Grime, J. K. 125
- Shabushnig, J. G., see Downey, S. W. 165
- Sohr, H.
— und Wienhold, K.
Spurenanalyse von Huminstoffen im Trinkwasser 309
- Sugimae, A.
— Determination of trace elements in sea water by inductively-coupled plasma emission spectrometry 331
- Sunahara, H., see Ishizuka, T. 197
- Szakács, O.
—, Lásztity, A. and Horváth, Zs.
Breakdown of organic mercury compounds by hydrochloric acid — permanganate or bromine monochloride solution for the determination of mercury by cold-vapour atomic absorption spectrometry 219
- Tamizi, M., see Lyle, S. J. 341
- Tandy, S., see Yellin, J. 327
- Toth, K., see Rakiás, F. 93
- Trojánek, A.
— and Holub, K.
The continuous removal of oxygen from flowing solutions 23
- Umland, F., see Czech, N. 275
- Vančo, D.
— and Macáček, F.
Description of liquid-liquid extraction equilibria in exchange extractions of chelates. Part 1. Exchange equilibria of diethyldithiocarbamates in chloroform-water and carbon tetrachloride-water systems 249
- Vandecasteele, C., see Mortier, R. 147
- Vaneesorn, Y., see Ivaska, A. 51
- van Nieuwkerk, H. J., see Hanekamp, H. B. 13
- Vittori, O.
— Polarographic study of adsorbed tellurium at the hanging and dropping mercury electrodes in 1 M hydrochloric or perchloric acid solutions 315
- Wada, H.
— and Nakagawa, G.
New metalochromic indicators for compleximetric titration of calcium 265
- Weisz, H.
— and Schlipf, J.
Gaseous catalysts for end-point indication in titrimetric analysis in the microgram range 257
- Wienhold, K., see Sohr, H. 309
- Yamaguchi, M.
—, Miyamoto, S., Kohashi, K. and Ohkura, Y.
Phosphorimetric assay for β -glucuronidase in biological materials 289
- Yellin, J.
—, Perlman, I. and Tandy, S.
Measurement of calcium and titanium from ^{47}Sc by instrumental neutron activation analysis 327
- Yoza, N.
—, Kurokawa, Y., Hirai, Y. and Ohashi, S.
Flow injection determinations of polyphosphates based on colored metal complexes of xylene orange and methylthymol blue 281

ANALYTICA CHIMICA ACTA
(including COMPUTER TECHNIQUES AND OPTIMIZATION)

INFORMATION FOR AUTHORS

Analytica Chimica Acta publishes original papers, short communications, preliminary communications, and reviews dealing with every aspect of modern chemical analysis, both fundamental and applied. The section on *Computer Techniques and Optimization* is devoted to new developments in chemical analysis by the application of computer techniques and by interdisciplinary approaches, including statistics, systems theory and operation research.

Reviews are written by invitation of the editors, who welcome suggestions for subjects. Short communications are usually complete descriptions of limited investigations, and should generally not exceed four printed pages. Preliminary communications of important urgent work can be printed within 4 months of submission, if the authors are prepared to forego proofs.

Submission of papers

Authors should submit three copies of the manuscript in double-spaced typing on one side of the paper only, with a margin of 4 cm, on pages of uniform size. If any variety of machine copying is used (e.g. xerox), authors should ensure that all copies are easily legible and that the paper used can be written on with both ink and pencil. Authors are advised to retain at least one copy of the manuscript. Manuscripts should be preceded by a sheet of paper carrying (a) the title of the paper, (b) the name and full postal address of the person to whom proofs are to be sent, (c) the number of pages, tables and figures.

Manuscripts should be sent to the editorial addresses given on the covers of current issues; submission to the publisher leads to delays. Submission of a manuscript implies that the work described has not been, and will not be, published elsewhere (except as an abstract, or as part of a lecture, review or academic thesis). Upon acceptance of the manuscript, the author(s) resident in the U.S.A. will be asked to transfer the copyright of the article to the publisher. This transfer will ensure the widest possible dissemination of information under the U.S. Copyright Law. For articles by authors not resident in the U.S.A., the copyright passes to the publisher upon acceptance of the manuscript, if it has not been previously reserved by a government institution or company.

The preferred language of the journal is English, but French and German manuscripts are also acceptable. For authors whose first language is not English, French or German, linguistic improvement is provided as part of the normal editorial processing.

Notes on the preparation of manuscripts

Authors are given every latitude, consistent with clarity and brevity, in the style and form of their papers. Very useful advice is provided in the Handbook for Authors issued by the Chemical Society and American Chemical Society.

Title and initial layout. All manuscripts should be headed by a concise but informative title. This is followed by the names of the authors, and the address of the laboratory where the work was carried out. The author to whom correspondence should be addressed must be indicated by an asterisk (without a footnote). If the present address of an author is different from that mentioned, it should be given in a footnote. Acknowledgements of financial support should not be made in footnotes but at the end of the paper.

Summary. Research papers and reviews begin with a Summary (50–250 words) which should comprise a brief factual account of the contents of the paper, with emphasis on new information. Uncommon abbreviations, jargon and reference numbers must not be used. The Summary should be suitable for use by abstracting services without rewriting. Papers in French or German require a *Résumé* or *Zusammenfassung* followed by a Title and Summary in English; authors are encouraged to provide translations where necessary. Short communications and preliminary communications require summaries, which should not exceed 50 words.

Introduction. The first paragraphs of the paper should contain accounts of the reasons for the work, any essential historical background (as briefly as possible and with key references only) and preliminary experimental work.

Experimental. The experimental methods may be described after the introductory material, or after the discussion of results, depending on the nature of the paper. Detailed experimental descriptions should, however, be restricted to one section of the paper, and not scattered throughout the text. Working procedures should be given in the imperative mood; sufficient detail should be given to allow any reasonably experienced worker to carry out the procedure. Detailed descriptions of well-known techniques and equipment are unnecessary, as are simple preparations of reagents or solutions, and lists of common chemicals. Manufacturers should be named only if the product differs essentially from that of other manufacturers. Local suppliers for multi-national concerns should not be named. In writing, complete sentences should be used, and procedural steps should not be numbered.

Results and Discussion. These may be treated together or separately. In discussing results, unnecessary repetition of experimental detail, unsupported elaboration of hypotheses, and verbose exposition of ideas should be avoided. Chemical formulae should not be used in the text unless confusion is likely to arise from the use of names. Formulae should, however, be used for brevity in Tables and Figures. Calculations well known to specialists are unnecessary. Conclusions should be added only if needed for interpretation; they should not be used as extended summaries.

Acknowledgements. These should be kept as short as possible, and placed, without a heading, at the conclusion of the text.

References

The references should be collected at the end of the paper, numbered in the order of their appearance in the text (*not* arranged alphabetically), and typed on a separate sheet. If the paper forms part of a series, the reference to the previous part should appear as the first reference, the number being cited at the title of the paper. References given in Tables should be numbered according to the position of the Table in the text. Every reference listed must be cited in the text. Reference numbers in the text are set in square brackets on the line. Numerals referring to equations are placed in parentheses.

In the list of references, the following forms should be adopted.

Journals

- 1 W. Lund and M. Salberg, *Anal. Chim. Acta*, 76 (1975) 131.
- 2 M. McDaniel, A. D. Shendrikar, K. D. Reizneir and P. W. West, *Anal. Chem.*, 48 (1976) 2240.

The title of the journal must be abbreviated as in the Bibliographic Guide for Editors and Authors.

Books

- 1 D. D. Perrin, *Masking and Demasking of Chemical Reactions*, Interscience-Wiley, New York, 1970, p. 188.
- 2 S. Hofmann, in G. Svehla (Ed.), *Wilson and Wilson's Comprehensive Analytical Chemistry*, Vol. 9, Elsevier, Amsterdam, 1979, p. 89.

Titles of papers are unnecessary. Citations of reports which are not widely available (e.g. reports from government research centres) should be avoided if possible. Authors' initials should not be used in the text, unless real confusion could be caused by their omission. If the reference cited contains three or more names, only the first author's name followed by *et al.* (e.g. McDaniel *et al.*) should be used in the text; but the reference list must contain the initials and names of *all* authors.

Tables, Computer Programs and Figures

Tables and Figures must be essential for the clear and concise presentation of the material. The same information should not be given in Tables and Figures, and material from the published literature should not be reproduced.

Tables. All Tables should be numbered with Arabic numerals, and have brief descriptive headings; they should be typed on separate pages. The layout should be given serious thought, so that the significance of the results can be grasped quickly. Column headings should be brief.

Tables with only two or three headings are best printed horizontally, e.g.

Hg ²⁺ added (μg)	1.0	2.0	3.0	5.0
Extraction (%)	95.0	99.8	99.5	89.0

Experimental information which is relevant to all the results in the Table is best given in parentheses immediately after the heading. No column should contain the same number or unit throughout its length. Footnotes to Tables are denoted by superscript a, b, c . . . The units used should be clearly stated. Confusion can arise from the use of powers in column headings. The following usage is recommended: e.g., if molar absorptivities are listed, the heading should be $\epsilon \times 10^{-4} \text{ l mol}^{-1} \text{ cm}^{-1}$) so that a number 2.32 in the column signifies 23 200.

Alphanumeric computer output is usually unsuitable for reproduction and should therefore be retyped and presented as Tables; capitals can be used to simulate computer output if such simulation is essential for illustration.

Computer programs. Computer algorithms should be described clearly; a standard high-level programming language or a suitable algorithmic notation should be used as necessary. Complete program listings, however, are not normally admissible. Extensive flow charts should be avoided if the material can equally well be given in descriptive or tabular form. Statements on the portability of the software described to other computer systems, as well as on its availability to interested readers, should be given.

Figures. Figures should be prepared in black waterproof drawing ink on drawing or tracing paper of the same size as that on which the manuscript is typed. One original (or sharp glossy print) and two photostat (or other) copies are required. Attention should be given to line thickness, lettering (which should be kept to a minimum) and spacing on axes of graphs, to ensure suitability for reduction during printing. Axes of a graph should be clearly labelled, along the axes, and outside the graph itself.

The following standard symbols should be used in graphs:

▼ ▽ ■ □ + × ● ○ ▲ △

Simple straight-line graphs are not acceptable, because they can readily be described in the text by means of an equation or a sentence. Explanatory information should be placed not in the figure, but in the legend, which should be typed on a separate sheet of paper. All Figures should be numbered with Arabic numerals, and require descriptive legends.

Photographs should be glossy prints and be as rich in contrast as possible; colour photographs cannot be accepted. In general, line diagrams are more informative and less liable to dating than photographs of equipment, which are therefore not usually acceptable.

Computer outputs for reproduction as Figures must be of good quality on blank paper, and should preferably be submitted as glossy prints.

Nomenclature, abbreviations and symbols

In general, the recommendations of the International Union of Pure and Applied Chemistry (IUPAC) should be followed, and attention should be given to the recommendations of the Analytical Chemistry Division in the journal *Pure and Applied Chemistry*. (see also *IUPAC Compendium of Analytical Nomenclature*, 1978).

Basic SI and other accepted metric nomenclature are given in the Appendix. In accordance with IUPAC rules, the mass number, atomic number, number of atoms and ionic charge should be designated by a left upper index, a left lower index, a right lower index and a right upper index, respectively, placed round the atomic symbol. For example, the phosphate ion should be designated as PO_4^{3-} (not PO_4^{-3} or PO_4^{--}), and phosphorus-32 as ^{32}P (not P^{32} or P-32).

The Stock notation for the indication of stoichiometric valency states (and indirectly the proportion of the constituents) should be used. Examples are iron(III) chloride rather than ferric chloride, and potassium hexacyanoferrate(II) rather than potassium ferrocyanide. These rules are valid for French and German as well as English usage.

The use of nanometre (nm) and micrometre (μm), for the expression of analytical wavelengths has long superseded $m\mu$ or \AA or μ , all of which should be avoided, although \AA is sensibly retained in crystallographic work.

Natural or Napierian logarithms should be denoted by \ln and decadic logarithms by \log .

In analytical chemistry, the term normality (N) serves many useful purposes and will be retained. It should not, however, be used if no ambiguity is introduced by the use of molarity (M). The term formality (F) should be avoided.

Unusual abbreviations require definition when first used. Abbreviations for long chemical names (e.g. EDTA, HEDTA, TBAH, en, pn, Tris) are useful, especially in equations, Tables or Figures. For ease of distinction, well-known techniques should be abbreviated by using lower-case letters and full stops, such as, g.c.-m.s., u.v., i.r., a.a.s., n.m.r., a.s.v., d.p.p., etc.

Ambiguity in expressing dilution can be avoided by the use of e.g. (1 + 2) rather than 1:2 which could mean either one part diluted with two parts or one part diluted to twice its volume.

Symbols, formulae and equations should be written with great care, capitals and lower-case letters being distinguished where necessary. Greek letters and unusual symbols should be defined by name in the left-hand margin beside their first appearance in the paper. Wherever possible, mathematical expressions should be typed on one line, by using brackets, e.g., $\{[()]\}$, and the solidus, e.g., $A/b = x^{1/2}/(u + v)^{5/6}$, which is valuable in conserving vertical space. Particular attention should be given to the correct sequence of brackets and to the correct placing of superscripts and subscripts in complicated equations; careful proof-reading of such equations is essential. Short equations should not be numbered unless required for subsequent reference.

Decimal points should be indicated by full stops in papers written in English and by commas in French and German papers.

Appendix

Basic SI units

metre	m	candela	cd
kilogram	kg	mole	mol
second	s	(an Avogadro number of any	
ampere	A	particle: atoms, molecules,	
degree Kelvin	K	ions, electrons, etc.)	

Derived SI units

joule	J	$\text{kg m}^2 \text{s}^{-2}$	farad	F	A s V^{-1}
newton	N	J m^{-1}	weber	Wb	V s
watt	W	J s^{-1}	henry	H	V s A^{-1}
coulomb	C	A s	tesla	T	V s m^{-2}
volt	V	$\text{J A}^{-1} \text{s}^{-1}$	hertz	Hz	s^{-1}
ohm	Ω	V A^{-1}	degree Celsius	$^{\circ}\text{C}$	$\text{K} - 273.15$

Other units

litre	l	10^{-3} m^3	hour	h	$3.6 \times 10^3 \text{ s}$
gram	g	10^{-3} kg	dyne	dyn	10^{-5} N
poise	P	$10^{-3} \text{ m}^{-1} \text{s}^{-1}$	atmosphere	atm	$101.325 \text{ kN m}^{-2}$
electron volt	eV	$1.6021 \times 10^{-19} \text{ J}$	molar	M	mol l^{-1}
calorie	cal	4.184 J	molal	m	mol kg^{-1}
minute	min	60 s	curie	Ci	$3.7 \times 10^{10} \text{ s}^{-1}$

Prefixes to abbreviations for the names of units indicating

Multiples

tera ($\times 10^{12}$)	T
giga ($\times 10^9$)	G
mega ($\times 10^6$)	M
kilo ($\times 10^3$)	k

Sub-multiples

milli ($\times 10^{-3}$)	m
micro ($\times 10^{-6}$)	μ
nano ($\times 10^{-9}$)	n

pico ($\times 10^{-12}$)	p
femto ($\times 10^{-15}$)	f
atto ($\times 10^{-18}$)	a

JOURNAL OF ORGANOMETALLIC CHEMISTRY LIBRARY

A series of books presenting reviews of recent developments and techniques in the expanding field of organometallic chemistry.

Coordinating Editor: D. SEYFERTH, *Massachusetts Institute of Technology, Cambridge, Mass., U.S.A.*

Volume 7: Organometallic Chemistry Reviews

CONTENTS: Non-catalytic hydrogenation via organoboranes (*K. Avasthi, D. Devaprabhakara and A. Suzuki*). Allyl derivatives of the Group IVA metals and mercury (*J. A. Mangravite*). Silyl-mercurials in organic synthesis (*W. P. Neumann and K. Reuter*). Organosiliciumverbindungen des Schwefels, Selens und Tellurs (*D. Brandes*). Ferrocenyl-carbocations and related species (*W. E. Watts*). The chemistry of cobaltocene, cobalticinium salts and other cobalt sandwich compounds (*J. E. Sheats*).

1979 viii + 522 pages US \$109.75/Dfl. 225.00 ISBN: 0-444-41788-5

Volume 6: Organometallic Chemistry Reviews (1976); Annual Surveys: Silicon - Germanium - Tin - Lead

1978 viii + 550 pages US \$97.50/Dfl. 200.00 ISBN: 0-444-41698-6

Volume 5: Organometallic Chemistry Reviews

1977 viii + 320 pages US \$87.75/Dfl. 180.00 ISBN: 0-444-41633-1

Volume 4: Organometallic Chemistry Reviews (1975); Annual Surveys - Silicon - Tin - Lead

1977 viii + 548 pages US \$87.75/Dfl. 180.00 ISBN: 0-444-41591-2

Volume 3: Organometallic Chemistry Reviews

1977 viii + 342 pages US \$87.75/Dfl. 180.00 ISBN: 0-444-41538-6

Volume 2: Organometallic Chemistry Reviews: Organosilicon Reviews

1976 viii + 404 pages US \$87.75/Dfl. 180.00 ISBN: 0-444-41488-6

Volume 1: New Applications of Organometallic Reagents in Organic Synthesis Out of Print



ELSEVIER

The Dutch guildler price is definitive. US \$ prices are subject to exchange rate fluctuations.

P.O. Box 211,
1000 AE Amsterdam
The Netherlands

52 Vanderbilt Ave
New York, N.Y. 10017

NEW

First Issue Scheduled for January 1981

Editor-in-chief: B. DELMON,
Louvain-la-Neuve, Belgium.

Editors: J. A. CUSUMANO, Santa
Clara, CA, U.S.A., L. GUCZI,
Budapest, Hungary, D. L. TRIMM,
Kensington, Australia and
D. A. WHAN, Edinburgh, Scotland.

The editors will be supported by an
international Editorial Board.

APPLIED CATALYSIS

**An International Journal
Devoted to
Catalytic Science and its
Applications.**

The scope will include:

- Catalytic phenomena occurring in industrial processes or in processes in the stage of industrial development and in conditions similar to those of industrial processes. Both heterogeneous and homogeneous catalysis are included, together with aspects of industrial enzymatic catalysis;
- Scientific aspects of the preparation and characterization of industrial or practical catalysts;
- Activation, start up transient effects, aging, poisoning, rejuvenation, regeneration of catalysts as well as steady state phenomena;
- Aspects of chemical engineering relevant to the science of catalysis;
- New catalytic reactions of potential practical interest.

A *News Brief* section, provided by correspondents, will contain information gathered from patents, technical journals etc., on new catalytic reactions, catalysts and processes, new methods of catalyst preparation, and on new scientific facts related to the application of catalysis.

Further information on APPLIED CATALYSIS is available from the publishers.

Subscription Information

1981: Volume 1 (in 6 issues) –
US \$ 88.75 / Dfl. 173.00 including
postage.



ELSEVIER

P.O. Box 211,
1000 AE Amsterdam,
The Netherlands,

52 Vanderbilt Ave,
New York, N.Y. 10017.

*The Dutch guilder price is definitive. US \$ prices are
subject to exchange rate fluctuations.*

Euroanalysis III

edited by **D. M. CARROLL**, *Institute for Industrial Research and Standards, Dublin, Ireland*

6 × 9" (15.5 × 23 cm). xvi + 428 pages. 137 illus. 1979.

This book contains the plenary and keynote lectures presented at the Third European Conference on Analytical Chemistry, Euroanalysis III, held in Dublin in August 1978, organised by the Institute of Chemistry of Ireland on behalf of the Working Party on Analytical Chemistry of the European Federation of Chemical Societies.

It provides a comprehensive review of the present situation and future prospects in chemical, pharmaceutical and environmental analysis as well as the role of analytical chemistry in the earth sciences and the analysis of solid surfaces.

CONTENTS: 1. Irish contributions to European analytical chemistry. 2. Stable free radicals—electron spin resonance—analytical chemistry. 3. Are you still eating? Chemical food analysis—fact and fiction. 4. Clinical laboratory reference materials and methods—present status and future prospects. 5. Atomic spectrochemical analysis in soil science research. 6. *In-situ* microanalysis and surface analysis by electron probe techniques. 7. Computers in spectroscopy. 8. Reference materials: Their production, certification and use in compatible measurement networks. 9. Ion-selective electrodes—application in flowing systems. 10. Modern polarographic and voltammetric techniques. 11. Recent developments in high performance liquid chromatography. 12. Infrared spectroscopy of biocontact surfaces. 13. Analytical chemistry in the dairy industry. 14. Electron spectroscopy for chemical analysis. 15. Analytical chemistry in the earth sciences. 16. Conformational analysis: An account of experimental and theoretical methods applied to the analysis of mixtures and of constituent structures. 17. Hydrocarbon analysis. 18. Environmental analysis—air quality evaluation. 19. Pharmaceutical analysis. 20. Clinical biochemical analysis. Index.



APPLIED SCIENCE PUBLISHERS Ltd

Ripple Road, Barking, Essex, England

(continued from opposite page)

Dosage simultané par chromatographie liquide à haute performance de l'acide benzoïque et de l'acide sorbique A. Collinge et A. Noirfalise (Liège, Belgique)	337
An automatic spectrophotometric method for the determination of uranium(VI) extracted into a liquid ion-exchanger medium S. J. Lyle and M. Tamizi (Canterbury, Gt. Britain)	341
Purge vessel design in determinations of volatile organic compounds T. Ramstad and T. J. Nestrick (Midland, MI, U.S.A.)	345
<i>Author Index</i>	349
<i>Information for Authors</i>	353

© Elsevier Scientific Publishing Company, 1980.

All rights reserved. No part of this publication may be reproduced, stored in a retrieval system or transmitted in any form or by any means, electronic, mechanical, photocopying, recording or otherwise, without the prior written permission of the publisher, Elsevier Scientific Publishing Company, P.O. Box 330, 1000 AH Amsterdam, The Netherlands.

Submission of an article for publication implies the transfer of the copyright from the author to the publisher and is also understood to imply that the article is not being considered for publication elsewhere.

Submission to this journal of a paper entails the author's irrevocable and exclusive authorization of the publisher to collect any sums or considerations for copying or reproduction payable by third parties (as mentioned in article 17 paragraph 2 of the Dutch Copyright Act of 1912 and in the Royal Decree of June 20, 1974 (S. 351) pursuant to article 16 b of the Dutch Copyright Act of 1912) and/or to act in or out of court in connection therewith.

Printed in The Netherlands

Determination of soluble/insoluble tungsten compounds as discrete entities in industrial hygiene samples	
R. D. Hull and J. C. Haartz (Cincinnati, OH, U.S.A.)	187
Determination of phosphorus in waste-waters by inductively-coupled plasma atomic emission spectrometry	
T. Ishizuka, K. Nakajima (Nagoya, Japan) and H. Sunahara (Hiroshima, Japan)	197
Molekülabsorptionsspektrometrie bei elektrothermischer Verdampfung in einer Graphitrohr-küvette. Teil 6. Bestimmung von Chloridspuren durch die Molekülabsorption von AlCl_3 , GaCl_3 und InCl_3 -Molekülen	
K. Dittich und P. Meister (Leipzig, E. Germany)	205
Breakdown of organic mercury compounds by hydrochloric acid—permanganate or bromine monochloride solution for the determination of mercury by cold-vapour atomic absorption spectrometry	
O. Szakács, A. Lásztity and Zs. Horváth (Budapest, Hungary)	219
Synthesis and analytical properties of an N-phenylhydroxamic acid resin	
R. J. Phillips and J. S. Fritz (Ames, IA, U.S.A.)	225
Determination of total sulphur in fuel oils by ion chromatography	
M. J. McCormick (E. Melbourne, Victoria, Australia)	233
The separation of rhodium and iridium by ion flotation	
E. W. Berg and D. M. Downey (Baton Rouge, LA, U.S.A.)	239
Description of liquid—liquid extraction equilibria in exchange extractions of chelates. Part 1. Exchange equilibria of diethyldithiocarbamates in chloroform—water and carbon tetrachloride — water systems	
D. Vančo and F. Macásek (Bratislava, Czechoslovakia)	249
Gaseous catalysts for end-point indication in titrimetric analysis in the microgram range	
H. Weisz and J. Schlipf (Freiburg, W. Germany)	257
New metallochromic indicators for compleximetric titration of calcium	
H. Wada and G. Nakagawa (Nagoya, Japan)	265
Asymmetrically substituted diphenylcarbazones as chelate formers	
N. Czech, B. Fries and F. Umland (Münster, W. Germany)	275
Flow injection determinations of polyphosphates based on colored metal complexes of xylenol orange and methylthymol blue	
N. Yoza, Y. Kurokawa, Y. Hirai and S. Ohashi (Fukuoka, Japan)	281
Phosphorimetric assay for β -glucuronidase in biological materials	
M. Yamaguchi, S. Miyamoto, K. Kohashi and Y. Ohkura (Fukuoka, Japan)	289
A fluorimetric method for the determination of traces of gallium	
J. J. Laserna, A. Navas and F. Garcia-Sanchez (Malaga, Spain)	295
The fluorescence properties of metal complexes of alkyl derivatives of aromatic Schiff bases	
K. Morishige (Higashi-Osaka, Japan)	301

Short Communications

Spurenanalyse von Huminstoffen im Trinkwasser	
H. Sohr und K. Wienhold (Leipzig, E. Germany)	309
Polarographic study of adsorbed tellurium at the hanging and dropping mercury electrodes in 1 M hydrochloric or perchloric acid solutions	
O. Vittori (Villeurbanne, France)	315
Dosage mercurimétrique des thioethers en milieu acétique anhydre	
M. Hamon et P. Epifanoff (Chatenay-Malabry, France)	321
Measurement of calcium and titanium from ^{47}Sc by instrumental neutron activation analysis	
J. Yellin, I. Perlman and S. Tandy (Jerusalem, Israel)	327
Determination of trace elements in sea water by inductively-coupled plasma emission spectrometry	
A. Sugimae (Osaka, Japan)	331

CONTENTS

<i>Special Report: The analytical performance of direct current, normal pulse and differential pulse polarography with static mercury drop electrodes</i>	
A. M. Bond and R. D. Jones (Wairn Ponds, Victoria, Australia)	1
Theoretical considerations on the performance of electrochemical flow-through detectors	
H. B. Hanekamp and H. J. van Nieuwkerk (Amsterdam, The Netherlands)	13
The continuous removal of oxygen from flowing solutions	
A. Trojánek and K. Holub (Prague, Czechoslovakia)	23
Electrochemistry in fluosol-43, a perfluorinated blood substitute. The influence of pluronic F-68 surfactant on some polarographic electrode processes	
J. Georges (Villeurbanne, France)	29
An evaluation of differential pulse anodic stripping voltammetry at a rotating glassy carbon electrode for the determination of cadmium, copper, lead and zinc in Antarctic snow samples	
M. P. Landy (Cambridge, Gt. Britain)	39
Voltammetric on-line analysis for some sulphur-containing drugs	
A. Ivaska (Åbo, Finland), Y. Vaneesorn (Ching Mai, Thailand), I. E. Davidson (Maidenhead, Gt. Britain) and W. Franklin Smyth (Cork, Eire)	51
Automated potentiometric determination of glucose oxidase activity with a gas-sensing sulphur dioxide probe	
P. W. Alexander and P. Seegopaul (Kensington, N.S.W., Australia)	61
Reductive potentiometric stripping analysis for elements forming sparingly soluble mercury compounds with amalgamated metal as the reducing agent	
J. K. Christensen, L. Kryger, J. Mortensen and J. Rasmussen (Aarhus, Denmark)	71
The determination of molybdenum in high-nickel alloys by potentiometric titration with cerium(IV) solutions	
E. L. Montgomery, Jr. (Huntington, WV, U.S.A.)	85
Determination of pharmaceutical compounds containing covalently-bound halogen by means of ion-selective electrodes	
F. Rakiás, K. Toth and E. Pungor (Budapest, Hungary)	93
Monohydrogenphosphate-sensing electrode formulations	
G.-S. Ihn, C. F. Nash and R. P. Buck (Chapel Hill, NC, U.S.A.)	101
Enzyme electrode system from oxalate determination utilizing oxalate decarboxylase immobilized on a carbon dioxide sensor	
R. K. Kobos and T. A. Ramsey (Richmond, VA, U.S.A.)	111
Enhancement of selectivity of a benzoate-sensitive liquid membrane electrode by alkylphenol	
H. Hara, S. Okazaki and T. Fujinaga (Kyoto, Japan)	119
Fixed-time kinetic enthalpimetry: improved sensitivity for enthalpimetric enzyme activity determinations in homogeneous and heterogeneous systems	
J. K. Grime and E. D. Sexton (Denver, CO, U.S.A.)	125
A catalimetric thermochemical unsegmented flow system based on the iodide-catalyzed cerium(IV)-arsenic (III) reaction	
J. M. Elvecrog and P. W. Carr (Minneapolis, MN, U.S.A.)	135
The determination of boron in zirconium and zircaloy by proton activation analysis based on the $^{10}\text{B}(p, \alpha)^7\text{Be}$ reaction	
R. Mortier, C. Vandecasteele and J. Hoste (Gent, Belgium)	147
Multi-element determinations of trace elements in glass by instrumental photon activation analysis	
Y. Kanda, T. Oikawa and T. Niwaguchi (Tokyo, Japan)	157
Reduction of spectral interferences in flame emission spectrometry by selective spectral-line modulation	
S. W. Downey, J. G. Shabushnig and G. M. Hieftje (Bloomington, IN, U.S.A.)	165
Optimisation of sulphur emission in molecular emission cavity analysis. Effects of variation in cavity position and phosphate addition	
T. J. Cardwell, P. J. Marriott and D. J. Knowles (Bundoora, Victoria, Australia)	175

(continued on inside page of cover)